超分子システム内での１分子機能・分子間協調の顕微画像化と解析

（研究課題番号　10308030）

平成 10 年度～平成 13 年度科学研究費補助金

基盤研究(A)(2)研究成果報告書

平成 15 年 3 月

研究代表者　石渡　信一

（早稲田大学・理工学部・教授）

はしがき

この報告書は、平成１０年度（1998年4月）から１４年度（2002年3月）にわたる４年間で行った文部省（文部科学省）科学研究費基盤研究Ａ（２）「超分子システム内での１分子機能・分子間協調の顕微画像化と解析（課題番号 10308030)」の研究成果をまとめたものである。本報告書は、本来研究が終了した昨年春に発行すべきであったが、引き続く研究課題のスタートなどで遅れてしまった。そこで、昨年の2002年4月以降に発表した論文については掲載していないか、あるいは未発表、論文作成中としてその内容を概要の中で簡単に説明することとした。

また、本研究と並行して平成１１年度と１２年度に、科学研究費基盤Ｂ（２）展開「遺伝子ハンドリング技術を用いた単一細胞内調節タンパク質の機能解析法の開発」(課題番号：11559016）を推進したが、そこで得られた研究業績についても簡単に触れ（本冊子とは別に編集した研究成果報告書を参照)、研究発表リストもここに併せて掲載してある。さらに、本研究と並行して、CREST研究「一方向性反応のプログラミング基盤（代表、木下一彦）（平成８年１１月から平成１３年１１月まで)」に参加したが、その終了の際にそれまでの研究成果をまとめた。ここに掲載する報告は、そこでまとめたものが中心となっていることをお断りしておく。本研究を通じて得られた成果のほとんどは、口頭発表したものだが、未だに論文として公表していないものもある。それを含めて、「研究成果の概要」としてまとめた。

本研究の研究目標として当初記載した文章を以下に掲載する。
「生体機能の分子メカニズムの研究は、今や工学や物理学からも大きな注目を集めている。しかし、その機能を分子レベルで自由に操作出来るような生体システムはほとんど存在しない。そこで我々は、生体（細胞）運動機能の担い手であるアクトミオシンと微小管キネシン分子モーター系、それに（心筋・骨格筋）培養細胞系を取り上げる。生体分子モーター系は、近年の顕微解析・顕微操作技術の進歩によって、その機能を分子レベルで操作できる数少ない生体システムの一つである。単一分子モーターとその集合体に固有の、1 nm からサブμmスケールの動きを、構成タンパク質にラベルした蛍光分子を通して捉え、同時にＡＴＰ分解活性などの化学反応を時間・空間的に顕微（蛍光）画像化することができる。さらに、レーザー光ピンセットを組み合わせることによってpNオーダーの発生力を定量できる。我々は、このような１分子操作技術を駆使し、新たに開発した温度パルス顕微鏡法を用いて分子モーター機能の力学・熱力学を明らかにする。分子モーターにおける力学過程（力発生・滑り運動など）と化学過程（酵素作用、濃度勾配形成など)、それに構成タンパク質の構造との間の連関を明らかにする。我々の研究の特徴は、一分子レベルの（熱）力学、生理学を明らかにするだけでなく、分子集合体及び細胞内にみられる協同現象（分子シンクロナイゼーション）に着目し、独自に開発したタンパク質集合体の再構築法や細胞操作法を用いて、超分子システム内における標的分子の機能と動的構造を明らかにしようとするところにある。」

本研究には多くの大学院生たちが関与している。特に川口憲治（1999.3 修士了、2003.3 博士号取得：現、全日空)、斎藤素子（1999.3 修士了：現、(株) 三共)、熊木雄一（1999.3 修士了：現、NTT)、藤原郁子（2000.3 修士了、2003.3 博士号取得)、鈴木団（1999.3 修士了：現、早大理工助手)、佐々木大輔、上村想太郎（現、D２)、瀬尾隆造（2001.3 修士了：現、川崎製鉄)、島本勇太、井手純一、奈良郁子（現、M2）らの寄与が大きい。筋生理については、藤田英明（2000.3 博士号取得：現、ワシントン州立大）を中心とする研究が多い。1998.10 からは船津高志氏が物理学科教員として赴任したことにより、助手の多田隈尚史氏（1997.3 修士了）らとともに、光学顕微鏡技術をはじめ様々な面で協力をえた。また、2000.4 からは東條正（1992 学部卒：東大医科研にて博士号取得）を博士研究員として迎え、遺伝子組換え技術や細胞操作法を導入することができた。さらに、幾つかのグループと共同研究を行った。福田紀男、栗原敏（慈恵医大)、安田賢二（日立基礎研：現、東大総合文化研究科)、岡野和宣（日立中研)、豊島陽子研（東大総合文化研究科)、末次志郎、竹縄忠臣（東大医科研)、河合正隆（アイオワ大）の諸氏との研究は、幸い論文としてまとめることができた。岡崎国立共同研究機構・統合バイオサイエンスセンター（2001.3 まで慶応義塾大学・理工学部・物理学科）木下一彦研究室とは、変わらぬ研究交流を続けている。CREST 研究の当初から、数ヶ月に一度、木下研、吉田賢右研（東工大）と SKY セミナーを開催してきた。また、20 年近くに亘って、慈恵医大馬詰良樹研とは毎年一度の合宿ゼミを開いている。このような多くの方々との交流を通じて、特に学生間の情報交換や共同研究が自由に出来るようになったことは、私のグループだけでなく、この分野の活性化にとって大きな力になっているものと信じる。こうして本研究の成果を、2002 年度から 2006 年度までの文部科学省特別推進研究「タンパク質機能の１分子デザインとシステム構築」へと発展することができた。この機会に、記して皆様に感謝します。

平成 15 年 3 月　　研究代表者　石渡信一

研　究　組　織

研究代表者

石渡　信一　　（早稲田大学理工学部・教授）

研究分担者

船津　高志　　（早稲田大学理工学部・助教授）
平成14年10月1日より教授

藤田　英明　　（日本学術振興会・特別研究員）

交付決定額（配分額）　　（金額単位：千円）

	直接経費	間接経費	合　計
平成10年度	17,400	0	17,400
平成11年度	5,600	0	5,600
平成12年度	6,100	0	6,100
平成13年度	5,200	1,560	6,760
総　計	34,300	1,560	35,860

研究業績

研究成果の概要

1）微小管・キネシン分子間結合の1分子計測－キネシン分子モーターの仕組み（文献16）：

キネシン分子モーターは神経細胞内に存在して、ヌクレオチドATPをADPと無機リン酸に加水分解しつつ微小管の表面を“歩く”。その“歩く”仕組みについて、hand-over-handモデル（キネシンは双頭構造をもつが、単頭結合と双頭結合とを繰り返しつつ歩くというモデル）が提唱されている。ところが、この仕組みについて直接的な証拠を提出すべき電子顕微鏡観察の結果が互いに矛盾しており、新たな証拠が求められていた。そこで我々は、キネシン分子と微小管との1分子結合力（結合破断力）を顕微計測することによって、各ヌクレオチド結合状態におけるキネシン分子の結合様式（単頭結合か双頭結合か）を決定すること、そのことによってhand-over-handモデルを検証することを企てた。平均1個のキネシン分子（ウシ脳から調製）を結合した直径1μmのポリスチレンビーズを光ピンセットで顕微操作し、カバーガラス表面に吸着した微小管（ブタ脳から調製）に接触させることによって、キネシン分子を微小管に結合させる。そのようにして、（1）ATP非存在下、（2）ATPのアナログであるAMP-PNPとADPの共存下、そして、（3）AMP-PNP存在下という、hand-over-handモデルにおける3つの鍵状態でキネシン－微小管結合に負荷を加え、結合が破断するときの破断力を計測した。その結果、図1に示されたように、微小管の＋端方向に負荷を加えたときの、（1）と（2）状態での平均破断力が7pN、（3）状態での平均破断力が15pNと求められた。微小管の－端方向への負荷に対しては、平均破断力はそれぞれ45%大きかった。さらに、各条件下でのキネシン分子の弾性率を見積もり、負荷の方向に関わらず、それぞれ約0.4pN/nmと約0.8pN/nmと見積もった。

これらのことから我々は、前者では単頭結合、後者では双頭結合であると結論することができた。この結果は、hand-over-handモデルを強く支持するものである。ATPの結合と加水分解に応じて一歩一歩交互に歩くためには、キネシン分子内部の双頭間に“分子協調性”が備わっていることを強く示唆する。

さらに最近のデータ（Nature Struct. Biol. 2003. 4 発表予定）によれば、上記の“分子協調性”の中に、“力と酵素活性との共役”、すなわち、力学酵素の酵素活性→力発生→分子歪み→酵素活性の変調というフィードバックループが、存在する可能性が強く示唆されている。この性質こそ力学酵素の本質であると考え、研究を集中している。

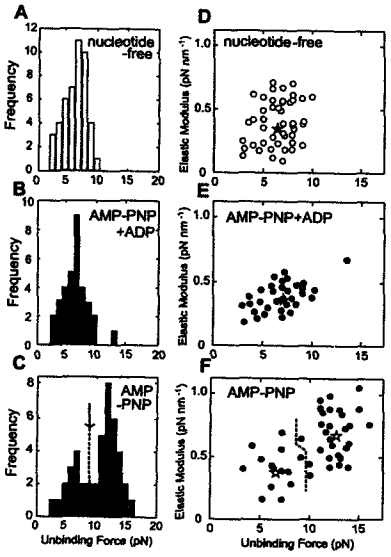

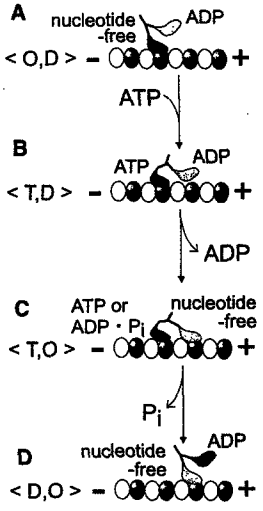

図1．ヌクレオチドなし、AMPPNP+ADP 共存、AMPPNP 存在の３状態における天然キネシン・微小管結合の破断力分布と、破断する直前の複合体の弾性率との相関。この結果から、キネシン分子は、ヌクレオチドなし状態と AMPPNP＋ADP 共存状態では単頭結合、AMPPNP 存在状態では双頭結合をしていると結論できる（文献１６：Kawaguchi & Ishiwata, *Science*, 2001）。

２）温度パルス顕微鏡（ＴＰＭ）法の開発（文献６）：我々の開発した温度パルス顕微鏡（TPM）法には、光学顕微鏡の試料面上に撒かれた金属粉末の塊（5μm 程度の大きさ）に赤外レーザー光を照射し、これを熱源として直径数十μm にわたって同心円状の温度分布を得る「金属粉末法（図２）」と、ガラス表面上に直径 10μm の円状に蒸着したアルミ金属面を熱源とする「金属蒸着法」との２種類がある。温度の空間分布と時間変化は、アクチンフィラメントに結合した蛍光物質 rhodamine-phalloidin の蛍光強度が温度上昇に伴って減少する性質（熱消光）を画像化することによって行った。この結果、１本のアクチンフィラメント上の温度分布を画像化することができ、約２℃/μm の温度勾配を、「金属粉末法」の場合には 6ms の立ち上がり・立ち下がり時間で可逆的に作り出すことが出来るようになった。

「金属蒸着法」は温度分布の再現性は高いが、温度変化の緩和時間は数十 ms と遅かった。TPM 法の最大の長所は、短時間の可逆的な温度上昇と下降が出来ることにある。そのことによって、分子機能が熱変性する前に、通常法では得られないような高温における分子機能を研究することが出来ることである。

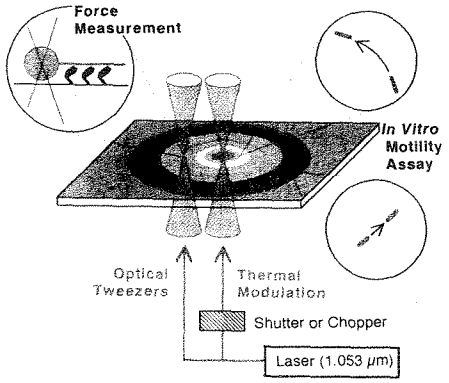

図２．温度パルス顕微鏡法の模式図
（文献６：Kato et al., *Proc. Natl. Acad. Sci. USA*, 1999）

３）キネシン分子モーター機能の熱変調・熱励起（文献１２、１７）：TPM 法を、微小管－キネシン系に応用した。まずキネシン分子をガラス表面に吸着させ、ATP 存在下で、そのガラス表面上における微小管の滑り運動を観察した。18℃から約 50℃に上昇すると、微小管の滑り速度は約 0.4μm/s から約 4.0μm/s（これはキネシンの歩行運動速度としては最高記録である）へと上昇した（図３）。50℃という、平衡状態では変性するといわれるような高温であっても、短時間（１秒程度）であれば、ATP 加水分解機能は促進され、運動速度も上昇することがわかった。

ところでキネシン分子の場合には、一分子での滑り機能を解析することが出来る。

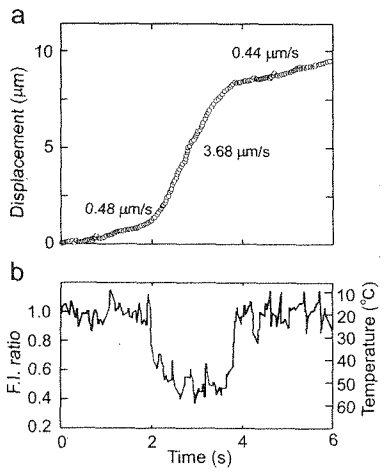

図３．TPM によって短時間温度上昇させたときのキネシン分子モーターの変位。この直線の傾きが運動速度を与える（文献１７；Kawaguchi & Ishiwata, *Cell Motil. & Cytoskel.*, 2001）。

ポリスチレンビーズの表面にキネシン分子を吸着し、ガラス基板に結合した微小管の上でビーズの滑り運動を行わせるのである。その結果、キネシン一分子でも、上の結果と同程度に熱励起されることが確認された。この研究の過程で、キネシン分子の滑り運動機能が熱に対して弱い（高温にさらすと、滑り運動速度が不可逆的に減少する）ことが分かった。従って、キネシン分子モーター機能の熱変調・熱励起の研究にとってTPM法は最適である。

1分子のキネシンが発生する力、歩く速度、一度に歩く距離、の3つの特性に対する温度の影響を検討した(この場合はTPM法の他に、通常の温度制御方式も用いた)。その結果、意外なことに発生力は15-35℃の範囲で温度に依存せず約7pNであった（図4）。すなわち、力発生ステップは温度に依存しない分子機構によるものであることがわかった。

一方、歩く速度と歩く距離は温度の上昇とともに増大した。図5に示されるように、15-50℃の広い温度範囲にわたってアーレニウス活性化エネルギーは50kJ/molであり、従ってこの温度範囲において、同一の酵素活性化機構が働いていることが強く示唆された。歩く速度はATP加水分解のサイクル速度を反映している。これらの結果は、歩く仕組みの解明に示唆を与えるものである。

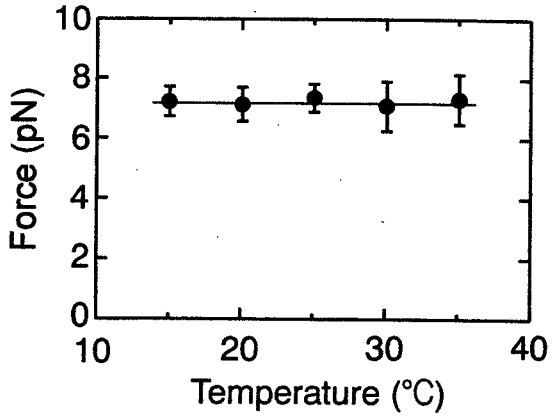

図4．キネシン1分子が発生する力の温度依存性。
（文献12；Kawaguchi & Ishiwata, BBRC, 2000）

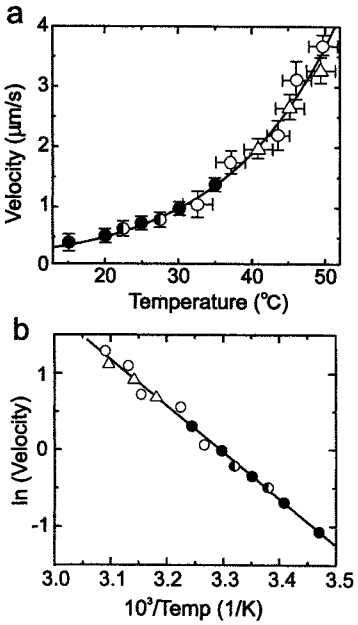

図5．キネシン分子モーターの歩行速度の温度依存性。
（文献12；Kawaguchi & Ishiwata, BBRC, 2000）

4）TPM法によるミオシン分子モーター機能の熱変調・熱励起（文献6）：「金属粉末法」を用いて，HMM分子上でのアクチンフィラメントの滑り運動速度と滑り力の温度依存性を研究した。その結果、温度上昇に約6ms遅れて滑り運動が始まることが分かった。さらに、18℃から約45℃への温度上昇に伴って、滑り速度は約4μm/sから約30μm/sへと可逆的に上昇することが分かった。滑り力も同様に約7倍に上昇した（ただし、この滑り力上昇は、in vitro滑り運動系に特徴的な性質、つまり、分子モーターの特性そのものを反映していない可能性がある)。これらは通常用いられているイオン環境下（25mM KCl）で計測されたが、50mM KCl存在下では、滑り速度は筋肉から精製したミオシン分子モーターとしては最高の50μm/s（約45℃）を記録した。

5）ミオシン分子モーター滑り運動に対するヌクレオチド分子種の影響（未発表）：通常の in vitro 滑り運動系を用いて ATP 以外のヌクレオチド（GTP, UTP, ITP, CTP）の作用を検討した。アクチンフィラメントの滑り速度と、1μmあたりの滑り力については、ATP、CTP、UTP、ITP、GTP の順番に減少した。特に GTP について、ミオシン分子の滑り運動速度と発生力を、温度を変えて検討した。その結果、ATP と比べて GTP の場合には滑り速度は 1/5 程度に減少するが、発生力は 1/2 程度にしか減少しなかった。つまり、滑り速度と発生力とは必ずしも 1:1 には対応していないことが明らかになった。

6）アクチンフィラメント・ミオシン分子間結合の破断力（文献１３、未発表）： アクチンフィラメントの後端に結合した直径 1μm のポリスチレンビーズを、レーザー光ピンセットによって顕微操作し、アクチンフィラメントとアクチン結合性タンパク質との間の分子間結合に一定の負荷を加え、結合の破断力などを繰り返し顕微計測することができる方法を、この数年の研究によって確立した。この方法を用いて、ATP 非存在下におけるアクチンフィラメントと HMM（ウサギ天然ミオシン分子をキモトリプシン処理によって調製した双頭 HMM、あるいは、パパイン処理によって調製した単頭 HMM、あるいはキモトリプシン処理で調製した S1）分子の硬直結合について、破断力の１分子計測を行った。その結果、単頭HMM・アクチン硬直結合の破断力分布は約 7pN にピークを持つのに対して、双頭 HMM では数 pN から 20pN にわたって広く分布し、7pN と 10 数 pN に２つのピークを持った。即ち、アクチン・双頭 HMM 分子の結合破断力は、単頭と双頭とで約２倍異なっていた。

7）アクチンフィラメント・ミオシン分子間硬直結合の寿命（未発表）：無負荷で熱平衡の状態にあるアクチンフィラメント・ミオシン分子間の硬直結合の寿命について、単頭 HMM 分子と双頭 HMM 分子、それにＳ１分子について比較検討した。非常にまばらにミオシン分子をガラス表面に吸着し、それに一点で結合したアクチンフィラメント（一点で結合しているかどうかは、アクチンフィラメントがその点の周りで旋回ブラウン運動するかどうかで判定した）が時間的に解離していく様子を観察・計測した。その結果、硬直結合の平均寿命は、双頭 HMM 分子の場合には 1000 数百秒であるのに対して、単頭 HMM 分子とＳ１分子の場合には約 100 秒であった。これは溶液系の実験で得られていた値にほぼ一致する。

8）アクチンフィラメント・ミオシン分子間硬直結合の寿命に対する負荷の影響（文献１３）：アクチン・ミオシン分子（S1、HMM）間の硬直結合に対して、光ピンセットを用いて瞬時に（ビデオレート内に）一定の負荷を加え、結合の寿命を１分子ごとに計測した（図６Ａ；２つの矢印の間の時間を計測）。こうして多数の分子についてデータを集めた（図６Ｂ；60s の点線上のデータは、負荷を加えてから 60s 以内には結合が解離しなかったものを表す；▼は HMM 分子、◇印は S1 分子）。

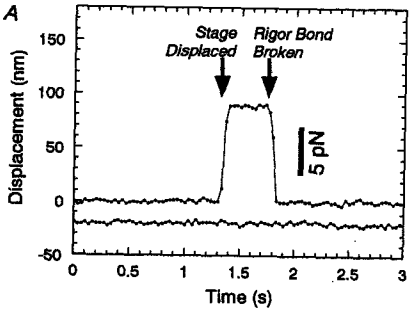

図６A. アクチン・HMM 硬直結合に一定の負荷を加え、結合が破断するまでの時間を計測。

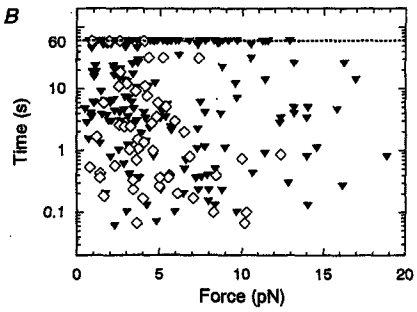

図６B. 負荷と結合寿命との関係。
（文献１３；Nishizaka et al., *Biophys. J.*, 2000）

解析の結果、図7のように、結合寿命τと負荷Fの関係が得られた。S1（◆印）については1つの指数関数$\tau(F) = \tau(0)\exp(-Fd/kT)$で表されたが（dは相互作用距離で約3nm）、HMMの場合には$\tau(F) = \tau_1(0)\exp(-Fd_1/kT)$（▲印）$+\tau_2(0)\exp(-Fd_2/kT)$（▼印）と、2つの指数関数の和で表された（$d_1$と$d_2$は相互作用距離で2と3nmと見積もられた。kとTは、それぞれボルツマン定数と絶対温度である）。そしてこの関係から得られた$\tau_1(0)$と$\tau_2(0)$はそれぞれ約1000数百秒と約100秒となり、無負荷のときの双頭結合と単頭結合の寿命に対応した。これらのことから、単頭結合と双頭結合との識別が可能になった。

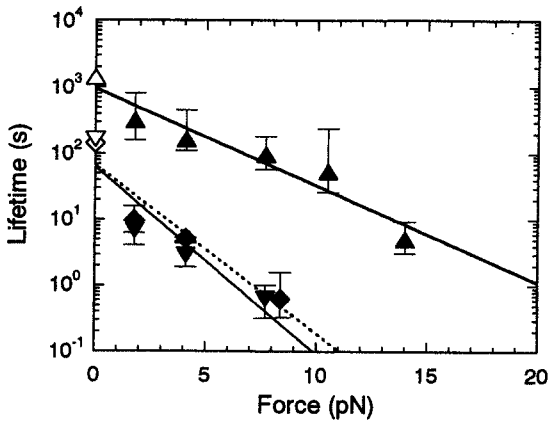

図7．結合寿命の負荷依存性。
（文献13；Nishizaka et al., *Biophys. J.*, 2000）

9）HMM分子の捻れ弾性率（文献13）：HMM1分子に硬直結合したアクチンフィラメントの旋回運動を通して見積もったHMM分子の捻れ弾性率は、平均で2×10^{-22}Nm/radであった。この値は、単頭HMMに比べて小さかった。ところが、双頭HMMの場合には旋回運動に幾つもの平衡角（互いに約2π離れた）が存在するように見え、各平衡角の周りで見積もった弾性率は、単頭HMMのものとほぼ一致した。即ち、双頭HMMの場合には、双頭結合（数十秒）→単頭結合（数秒）→双頭結合（数十秒）のように結合様式を変え、結合アクチンフィラメントの平衡角を変化させているように見えた。これは、アクチンフィラメント上でのミオシン分子モーターの滑り運動の様式を解明する上で、示唆に富んだ現象であると期待される。

10）単一アクチンフィラメントの直視による重合・脱重合メカニズムの解明（文献v）：　一本のアクチンフィラメントを蛍光顕微鏡下で直視し、フィラメント長の時間経過を計測することによって、アクチンの重合・脱重合ダイナミクスのメカニズムを解明しようとしている。従来、アクチンの研究は溶液系で行われてきたが、得られた値は溶液中に存在する全てのアクチンフィラメントの平均値であり、1本のアクチンフィラメントの性質を表してはいない。従って、アクチンの重合・脱重合ダイナミクスの分子メカニズムを解明することは、多種多様なアクチン結合・調節タンパク質の細胞調節作用を含む細胞骨格機能を理解する上で、最も重要な研究課題の一つになっている。そこで本研究の第一の目的を、1本の純粋なアクチンフィラメントの重合･脱重合ダイナミクスを可視化し、そのメカニズムを解明することにおく。次に、細胞内においてアクチン重合・脱重合ダイナミクスに関与している様々なアクチン調節タンパク質の調節機能を明らかにすることにおく。

（1）我々はまず、通常の蛍光顕微鏡法を用いて一本のアクチンフィラメントを可視化するために、Rhodamine-Phalloidin (Rh-Ph)存在下での重合過程のイメージングを行った。Phが存在するために脱重合過程は抑制されていたが、重合過程については溶液系で得られた結果と同様の平均重合速度（アクチン濃度依存性）が得られた（文献v）。

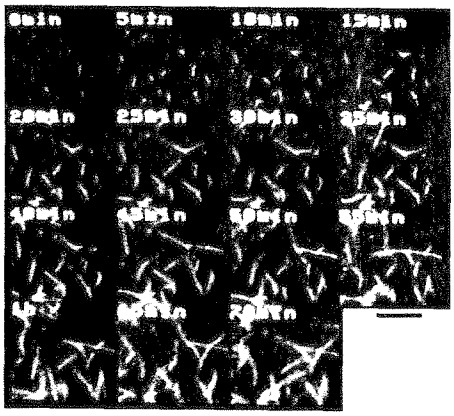

図8．アクチンフィラメントの重合過程を示す蛍光像。5分おきのビデオ画像。（文献v；Ishiwata et al., 2001）

（2）Ph 非存在下で、1本のアクチンフィラメントについて重合・脱重合過程を時間的に追跡しようとすると、直接蛍光ラベルしたアクチン分子をイメージング用のプローブとして加える必要がある。また、通常の重合・脱重合条件で行うためにアクチン濃度を高くする必要があり、蛍光アクチンに由来する背景光が大きく、従って通常の蛍光顕微鏡法を用いることはできない。そこで我々はエバネッセント照明法を用いることでこの問題を克服した。そうしてイメージングしたアクチンフィラメントの長さ揺らぎの解析から、重合・脱重合過程は、アクチン分子の結合・解離がフィラメントの両端で確率的に生じる拡散過程と見なせることが明らかになってきた（Nature Struct. Biol., 2002 発表）。さらに、1本のアクチンフィラメントの重合・脱重合のダイナミクスを、アクチンフィラメントの一部を強制的に退色させて両端を識別するという方法を用いて、B端（成長端）とP端を区別し記録・解析することを試みた。

11）「最小筋肉」システム－A帯滑り運動系－の開発（論文準備中）：1分子レベルの研究を進める一方で、我々は筋収縮系の構造と機能を明らかにする目的で、「最小筋肉」系を開発した。それはミオシンフィラメントの束（A帯）という、横紋筋の筋節構造を保ったものの中を、一本のアクチンフィラメントが滑り運動する実験系である（図9左）。この実験系でアクチンフィラメントに発生する張力とその揺らぎを、イオン強度を（25-150mM）mM KCl と変化させて計測したところ、同じ張力レベルのときには、イオン強度が高いほど張力揺らぎの幅が大きかった。また、この実験系でクロスブリッジ1個あたりに発生する張力は、約 1.6pN であった（図9右）。この実験系はいわゆる in vitro 滑り運動系とは異なって、筋収縮系本来の3次元的なフィラメント集合構造を保持しており、生理的な収縮機能を備えた最小のシステムだということが言える。今後はこの実験系を、従来からの筋生理学と1分子生理学とを繋ぐ実験系として育てたい。

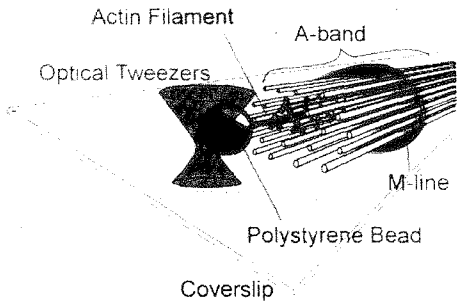

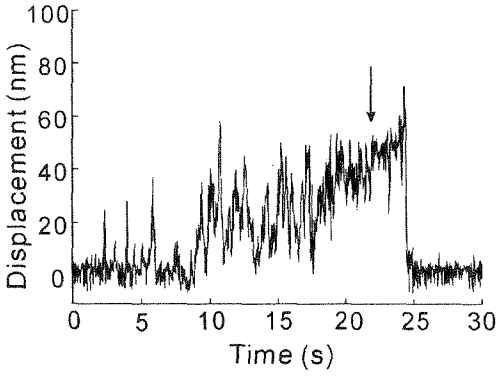

図9．A帯滑り運動系の模式図と、これを用いて得られた1本のアクチンフィラメントに発生する張力の計測。(未発表；M. Suzuki et al., MS in preparation)

12）単一筋原線維の、caged ATP による張力発生の初期過程高速画像化（未発表）：ガラス微小針にその両端を保持した単一(骨格筋)筋原線維の、硬直状態から収縮状態に至る力発生の時間経過を、caged ATP 存在下でのフラッシュ・フォトリシス法を用いて室温と低温とで比較検討した。張力の発生と、それに伴う筋節の形態変化の時間経過については、高速カメラを用いて計測・画像化した。その結果、低温では筋節構造を乱すことなく張力が発生するが、その際一過的に張力が減少する（弛緩する）相が存在することを見いだした。

13）心筋収縮系における SPOC（筋節長や張力が鋸波状に変動する自励振動現象）（論文準備中）：蛍光色素 Rhodamine-phalloidin でアクチンフィラメントを選択的にラベルしたグリセリン処理心筋線維束を用いて、ADP-SPOC 溶液（41 mM KCl, 14.2 mM $MgCl_2$, 2.2 mM ATP, 16.4 mM ADP, 10 mM Pi, 10 mM MOPS(pH 7.0), 2mM EGTA, 0.1mM AP_5A, 150 mM Ionic Strength, 1mM DTT, 酸素除去酵素系）中で SPOC 現象を誘起し、共焦点蛍光顕微鏡によってビデオレートで振動波形を観察記録した。ウシ、ブタ、イヌ、ウサギ、ラットの心筋から調製したグリセリン処理心筋収縮系の筋節長振動周期を計測した結果、ウシでは 20.8±1.4 s、ブタでは 16.7±2.6 s、ウサギでは 7.9±2.4 s（それぞれ平均値±SD、n=5）となり、心筋の由来する動物種の心拍数と強い正の相関を示した（図10）。このことは、ペースメーカー細胞からの電気パルスによる心拍の制御に加えて、心筋収縮系自体が(SPOC)自励振動系をなし、心臓が血液を効率よく送り出すためのポンプとして最適に機能するように構成されていることを示唆している。SPOC 周期が心拍の周期の約 20 倍と遅いことも、心拍の変動に収縮系が柔軟に適応するのに都合が良いと考えられる。

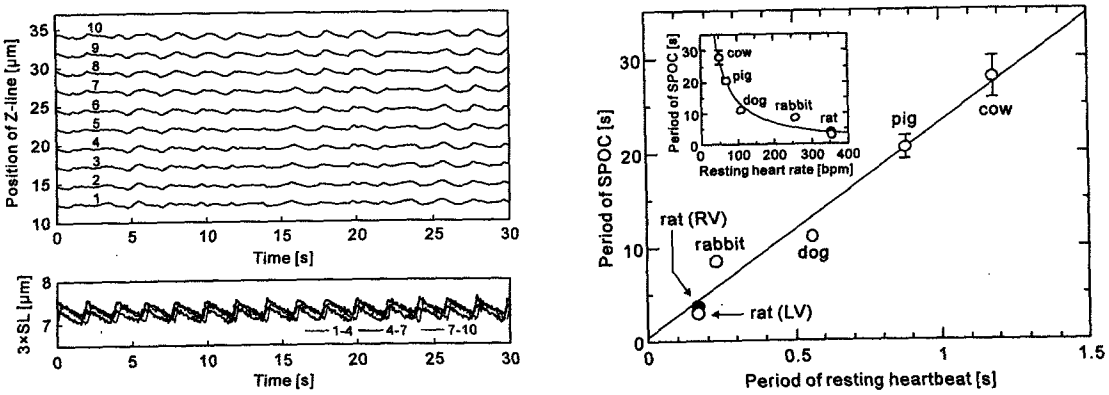

図10．SPOC 周期と静止時心拍周期との関係。

14）骨格筋筋原線維を用いた SPOC メカニズムの顕微鏡解析（未発表）：ウサギグリセリン処理骨格筋から調製した直径約 1 μm の筋原線維の両端をガラス微小針にからませ、位相差顕微鏡下で、SPOC 条件下における張力振動や筋節長振動を画像解析する。この研究は、SPOC 現象を発見した 15 年前から継続しているが、ごく最近、外力によって振動周期や振動そのものを制御できることが分かってきた。このことこそ我々が長年求めてきたことであり、その条件にやっと行き当たったということができる。この研究を通じて、分子モーター集合体のもつ未知の性質が明らかになるかもしれない。また、SPOC 現象の生理的意義についても決定的な実験ができるかもしれない。

１５）心筋再構成系を用いた研究（１）－制御タンパク質を含まない再構成アクチンフィラメント収縮系での自発的振動収縮（SPOC）（文献２）： 心筋収縮系（ウシ心筋から調製したグリセリン処理筋線維束）をゲルゾリン処理することにより細い（アクチン）フィラメントを選択的に除去した後、適当な温度とイオン環境下で精製アクチンを加えることによって、制御タンパク質を含まないアクチンフィラメントを再構築した。これを“心筋再構成収縮系”と呼ぶ。これを用いて、自発的振動収縮（SPOC）現象に制御タンパク質が必須の要素かどうかを検討した。SPOC 現象は、収縮と弛緩との中間の条件下で生じる。SPOC が安定に生じる条件は、具体的には ATP に、その加水分解産物である ADP と無機リン酸（Pi）を加え、収縮に必要な Ca イオンを除去（Ca イオンのキレート剤である EGTA を添加）するというものである。ところがこの条件では、Ca イオン感受性を必要とするために、制御タンパク質を必要とする。そこで、制御タンパク質の作用に替わるものとして、アクチン・ミオシン相互作用に直接作用するとされる筋弛緩剤 BDM を添加したところ、上記の心筋再構成収縮系で SPOC が生じることを発見した。このことは、SPOC 現象は、アクチンとミオシンという収縮要素それ自体に備わった特性であることを示している。分子モーターの新しい機能が見えてきた。この特性の本質は、アクチンやミオシン分子モーターの集合体としての“分子間協調性（分子シンクロナイゼーション）”にあるものと我々は期待している。

１６）心筋再構成系を用いた研究（２）－筋収縮特性におけるトロポミオシンの役割（文献７）： 心筋再構成収縮系を用いて、細いフィラメントを構成する制御タンパク質の一つであるトロポミオシンの役割を検討した。ところで、収縮力は酸性条件下で低下するが、その低下の程度は心筋に比べて骨格筋の方が大きい。そこで、この心筋再構成収縮系（制御タンパク質を含まず、純粋なアクチン分子によって再構築したもの）に、心筋由来のトロポミオシンを加えたところ、収縮力の酸性感受性は心筋のものに一致した。ところが、骨格筋由来のトロポミオシンで再構成したところ、収縮力の酸性感受性は骨格筋のものに一致した。この結果は、収縮力の酸性感受性の程度（収縮力の pH 依存性）をトロポミオシンが調節することを示している。酸性条件は心筋にとっては病的なものだが、心筋のトロポミオシンはこれを抑制するわけで、その生理的機能として理にかなっている。

これまで、制御タンパク質として重要なトロポミオシンの生理機能については、収縮系を用いた研究は不可能であった。我々が開発した“心筋再構成収縮系”は、これを初めて実現したものである。

１７）アクチンフィラメント・スペクトリン分子間結合の破断力（未発表）：赤血球から調製したスペクトリン分子を HMM 分子と同様にガラス表面上に吸着させ、アクチンフィラメントとの結合の破断力を１分子計測した。その結果、予備的実験ではあるが、平均 3pN という値を得た。これは、アクチン・ミオシン間の硬直結合力（平均 9pN）や、アクチンフィラメントとαアクチニンとの結合力（15pN）などと比べて有意に小さい。

１８）新しいレーザー熱励起方式によるマイクロチップからの DNA 回収法（文献９，１１，１８）： マイクロチップに結合した DNA 断片を DNA の熱変性を利用して回収する、新しい方法を考案した。マイクロチップ表面を Cr 蒸着し、そこに 1053nm のレーザービームを照射・吸収させることによって光を熱に変換する。Cr 蒸着面にはあらかじめシランカップリング反応で特定の DNA プローブを固定してあり、これとハイブリダイズした DNA 断片が DNA の熱変性によって遊離してくる。我々は、顕微鏡対物レンズによってレーザービームを絞ることによって、10μm の幅でチップ上の DNA を変性・遊離させること

ができた。また、遊離したところのDNAプローブは再びDNA断片を結合することができること、すなわち可逆的なDNAチップとして機能することを確認した。このように、本法では目的のDNA断片を順次回収できるので、DNAライブラリーを作り、必要に応じて、捕捉したDNAを回収・利用することができる。

１９）キネシン分子モーターの１分子力学と“歩く”仕組み（２００２年度発表）：

キネシンが微小管上を“歩く”仕組みについては、単頭・双頭結合とを繰り返すhand-over-hand（HoH）モデルが提唱されている。２０００年度には、双頭構造をもつキネシンと微小管との1分子結合力を、１）ATP非存在下、２）AMP-PNP（ATPアナログ）とADPの共存下、そして、３）AMP-PNP存在下という、HoHモデルにおける鍵となる３つのヌクレオチド状態で顕微計測した。２００１年度は、単頭構造をもつキネシン分子を用いて、とくにAMP-PNP存在下と、ADP結合状態で、結合破断力を計測した。その結果、ADP結合状態では弱結合であること、AMP-PNP結合状態は強結合であることが分かった（PNAS USAに論文発表, 2002）。

２０）ミオシンＶのアクチンフィラメントの周りでの回転歩行運動（２００２年度発表）：

２本足を使って歩くと考えられているミオシンVについて、アクチンフィラメント上の歩行に伴う回転の検出を試みた。2個の大きなビーズを橋渡しするようにアクチンフィラメントを張っておき、その上を小さな双子ビーズを結合させたミオシンVが動くところを観察した。双子ビーズは左ねじのように回転しながら進んでいった。右巻きらせんのアクチンフィラメント上を左回転したというこの結果は、ミオシンVがアクチンのらせんに沿って滑るのでなく、大股に歩くことを示す。そのときの歩幅は34.8nmと見積もられた（Nature Structure Biol.に論文発表, 2002）。

２１）筋収縮系の自励振動（SPOC）は外部力学刺激に同調する（論文準備中）：

骨格筋筋原線維の両端をガラス微小針に固定したのち、SPOC条件（ATP、ADP、無機リン酸（Pi）共存、Caイオン非共存）にし自発的な振動（SPOC）を生じさせる。一方のガラス針は柔らかく、これの撓みから発生張力とその振動を記録することができる。もう一方の硬い針にはピエゾ素子が装着されていて、任意の波形で筋原線維の長さを変えることができる。そこで、半筋節あたり10nm（分子モーターのサイズ）程度のステップで長さを変動したところ、これにシンクロして全ての筋節が一斉に伸びること、したがって外部力学刺激に対して長さ振動がシンクロすることが分かった。しかも、自発的には振動していない条件（SPOC溶液条件からPiを除去したもの）で硬い針を振動させたところ、これにシンクロして筋原線維が振動することも見出された。これらの結果は、分子モーターという力学酵素における力と酵素活性とのカップリングの本質を捉えたものと考えられる（論文準備中）。

２２）Arp2/3 Complexによるアクチンフィラメントの枝形成（２００２年度論文発表）：

アクチンフィラメントの重合・脱重合を１本のフィラメントレベルで画像解析するための手法を応用して、Arp2/3 Complexの作用を検討した。その結果、フィラメントの横腹だけでなく、B端近傍からもフィラメントの枝が形成されることが分かった。この成果は、細胞骨格のダイナミクスの素過程を明らかにするもので、細胞運動のみならず、細胞機能に果たす細胞骨格の役割りを解明する一つの手立てとなった（Biochem. Biophys. Res. Comm.に論文発表, 2002）。

２３）バイオナノゲージの開発（未発表）：

タンパク質線維状重合体として、アクチンフィラメントと微小管を取り上げ、これらの機能（ミオシンやキネシンなどの分子モーターの運動性への寄与）を解析するとともに、“生体ナノゲージ”として細胞生物学研究に利用することを企てている。その第一歩として、蛍光色素をラベルしたアクチン分子をアクチンフィラメントに組み込み、フィラメントの状態を蛍光画像化しモニターすることを試みた。１）蛍光性タンパク質GFPをfusionしたアクチンのプラスミドを、ニワトリの未分化筋芽細胞・マウス筋芽細胞株C2C12に導入し、その未分化細胞を筋管へと分化させることを試みた。まず、アクチン分子のN末端とC末端にそれぞれGFPを導入し培養心筋細胞に発現させたところ、細胞は正常に発達し、GFPアクチンはフィラメントに組み込まれた（共焦点蛍光顕微鏡により観察)。つぎに、アクチン分子を２つの部分に分割し、そこに、前後を入れ替えたGFPを導入した。そうすることによってGFPの構造を不安定化し、アクチン分子に加わる力によって生じる分子歪みに応じてGFPの蛍光性が変化することを期待した。これまで、分割する場所を２箇所検討したが、両方ともに大量発現させると、細胞は正常には発達しないことが分かった。現在、別の部位へのGFPの導入や、変異アクチンの発現量の制御、別タイプのGFP導入アクチンの調製を行っている。２）アクチン分子のCys374を蛍光ラベルし、これをフィラメントに導入することによってフィラメントの状態をモニターすることを試みた。ローダミンを導入するとミオシン分子モーターの運動性（運動速度、ATPase活性）が導入率に応じて減少することを見出した。今後は、フィラメントに負荷を加えることによる蛍光強度や蛍光スペクトルの変化、モーター機能への影響を、１本のフィラメントのレベルで検討したい。

２４）細いフィラメント再構成心筋を用いたクロスブリッジ動力学（文献２１）：

我々が開発した細いフィラメント再構成法を用いて、制御タンパク質を含まないアクチンフィラメント再構成心筋線維の動特性（張力、硬さの周波数分析など）を解析し、制御タンパク質を加えた再構成筋と比較検討した。その結果、制御タンパク質は、１個のクロスブリッジが発生する張力を増強する作用があることが明らかになった。

研 究 発 表

1．学会誌等

1) Kinosita,Jr., K., Yasuda, R., Noji, H., **Ishiwata, S.** and Yoshida, M. (1998). *Cell* **93**, 21-24. "F1-ATPase: A rotary motor made of a single molecule."

2) Fujita, H. and **Ishiwata, S.** (1998). *Biophys. J.* **75**, 1439-1445. "Spontaneous oscillatory contraction without regulatory proteins in actin filament-reconstituted fibers."

3) Fukuda, N., Fujita, H., Fujita, T. and **Ishiwata, S.**(1998). *J.Muscle Res.Cell Motil.* **19**, 909-921. "Regulatory roles of MgADP and calcium in tension development of skinned cardiac muscle."

4) Fukuda, N. and **Ishiwata, S.** (1999). *Pflugers Arch.* **438**, 125-132. "Effects of pH on spontaneous tension oscillation in skinned bovine cardiac muscle."

5) Kato, H., Nishizaka, T., Iga, T., Kinosita,Jr., K. and **Ishiwata, S.** (1999). *Proc. Natl. Acad. Sci. USA* **96**, 9602-9606. "Imaging of thermal activation of actomyosin motors."

6) Fujita, H. and **Ishiwata, S.** (1999). *Biophys. J.* **77**, 1540-1546. "Tropomyosin modulates pH dependence of isometric tension."

7) Fukuda, N., Kajiwara, H., **Ishiwata, S.** and Kurihara, S. (2000). *Circ. Res.* **86**, e1-e6. "Effects of MgADP on length dependence of tension generation in skinned rat cardiac muscle."

8) Yasuda, K., Okano, K. and **Ishiwata, S.** (2000). *Biotechniques* **28**, 1006-1011. "Focal extraction of surface-bound DNA from a microchip using photo-thermal denaturation."

9) Kawai, M., Kawaguchi, K., Saito, M. and **Ishiwata, S.** (2000). *Biophys. J.* **78**, 3112-3119. "Temperature change does not affect force between single actin filaments and HMM from rabbit muscles."

10) Okano, K., Yasuda, K. and **Ishiwata, S.** (2000). *Sensors & Actuators* B **64**, 88-94. "Position-specific release of DNA from a chip by using photothermal denaturation."

11) Kawaguchi, K. and **Ishiwata, S.** (2000). *Biochem. Biophys. Res. Comm.* **272**(3), 895-899. "Temperature dependence of force, velocity and processivity of single kinesin molecules."

12) Nishizaka, T., Seo, R., Tadakuma, H., Kinosita,Jr., K. and **Ishiwata, S.** (2000). *Biophys. J.* **79**(2), 962-974. "Characterization of single actomyosin rigor bonds - Load-dependence of lifetime and mechanical properties-."

13) 石渡信一 (2000). *トライボロジスト* **45,** 119-125. "筋収縮滑り運動機構とトライボロジー"

14) 藤田英明、佐々木大輔、石渡信一 (2000). *バイオサイエンスとインダストリー* **58,** 256-259. "生体分子モーター系における分子シンクロナイゼーションの研究"

15) Kawaguchi, K. and **Ishiwata, S.** (2001). *Science* **291**, 667-669. "Nucleotide-dependent single- to double-headed binding of kinesin."

16) Kawaguchi, K. and **Ishiwata, S.** (2001). *Cell Motil. Cytoskel.* **49**, 41-47. "Thermal activation of single kinesin molecules with temperature pulse microscopy."

17) 岡野和宣、陳鋼、小原賢信、梶山智晴、安田賢二、石渡信一 (2001). *電気学会論文誌* E **121-E**, 181-186. "DNA プローブアレイを用いた DNA 断片回収"

18) Fukuda, N., Ouchi, J., Kajiwara, H., Sasaki, D., **Ishiwata, S.** and Kurihara, S. (2001). *J. Physiol.* **536**, 153-160. "Acidosis and inorganic phosphate enhance length dependence of tension generation in skinned rat cardiac muscle."

19) Fukuda, N., Sasaki, D., **Ishiwata, S.** and Kurihara, S. (2001). *Circulation.* **104**, 1639-1645. "Length dependence of tension generation in rat skinned cardiac muscle. Role of titin in the Frank-Starling mechaism of the heart."

20) Fujita, H., Sasaki, D., **Ishiwata, S.** and Kawai, M. (2002). *Biophys. J.* **82**, 915-928. "Elementary steps of the cross-bridge cycle in bovine myocardium with and without regulatory proteins."

21) Harada, Y., **T. Funatsu**, K. Murakami, Y. Nonoyama, A. Ishihama, and T. Yanagida. **1999.** Single molecule imaging of RNA polymerase-DNA interactions in real time. *Biophysical J.* **76**: 709-715.

22) Ishii, Y. T. Yoshida, **T. Funatsu**, T. Wazawa, and T. Yanagida. 1999. Fluorescence resonance energy transfer between single fluorophores attached to a coiled-coil protein in aqueous solution. *Chemical Physics.* **247**:163-173.

23) Wazawa T., Y. Ishii, **T. Funatsu**, and T. Yanagida. 2000. Spectral Fluctuation of a Single Fluorophore Conjugated to a Protein Molecule. *Biophysical J.* **78**: 1561-1569.

24) Yamaguchi J., Nemoto, N., Sasaki, T., Tokumasu, A., Mimori-Kiyosue, Y., Yagi, T., and **Funatsu, T.** 2001. Rapid functional analysis of protein-protein interactions by fluorescent C-terminal labeling and single-molecule imaging. *FEBS Lett.* **502**: 79-83.

25) Taguchi, H., T. Ueno, H. Tadakuma, M. Yoshida, **T. Funatsu**. 2001. Single-molecule observation of protein-protein interactions in the chaperonin system. *Nature Biotechnol.* **19**: 861-865.

26) Tadakuma, H., Yamaguchi, J., Ishihama, Y., Funatsu, T. 2001. Imaging of Single Fluorescent Molecules Using Video-rate Confocal Microscopy. *Biochem Biophys*

Res Commun. **287**: 323-327.

27) Funatsu, T., Taniyama, T., Tajima, T., Tadakuma, H., and Namiki, H. 2002. Rapid and Sensitive Detection Method of A Bacterium Using GFP Reporter Phage. *Microbiol. Immuno.* **46**: 365-369.

2．出版物

1) Ishiwata, S., Funatsu, T. and Fujita, H. (1998). Adv. Exp. Med. Biol. 453, 319-329. "Contractile properties of thin (actin) filament-reconstituted muscle fibers." (eds. H. Sugi and G. Pollack) Plenum Press
2) Ishiwata,S., Tadashige,J., Masui,I., Nishizaka,T. and Kinosita,Jr.,K. (2001). In Molecular Interactions of Actin: Actin Structure and Actin-binding Proteins. (eds. C.G. dos Remedios and D.D. Thomas) Springer Verlag, Heidelberg, pp. 79-94. "Microscopic analysis of polymerization and fragmentation of individual actin filaments."
3) **船津高志**、多田隈尚史 1999.「1分子蛍光イメージング法」non-RI 実験の最新プロトコール（羊土社：栗原靖之、武内恒成、松田洋一編）pp. 165-166.
4) 「生命科学を拓く新しい光技術」1999.（総 186 ページ、共立出版：**船津高志**編）
5) **船津高志**、多田隈尚史 1999.「タンパク質の動き」顕微鏡フル活用術イラストレイテッド基礎から応用まで（秀潤社：稲沢譲治、津田均、小島清嗣 監修）pp. 171-174.
6) Tashiro, K., T. Sekiguchi, S. Shoji, **T. Funatsu**, W. Masumoto, H. Sato. 2000. Design and simulation of particles and biomolecules handling micro flow cells with three-dimensional sheath flow. Micro Total Analysis Systems 2000 (A. van den Berg et al. eds.): pp209-212.
7) Tashiro,K., S. Ikeda, T. Sekiguchi, H. Sato, S. Shoji, H. Makazu, K. Watanabe, T. Funatsu, and S.Tsukita. 2001. Micro Flow Switches Using Thermal Gelation of Methyl Cellulose for Biomolecules Handling. 11th International Conference on Solid-State Sensors and Actuators, (Transducers'01). pp932-935.
8) Tashiro,K., S. Ikeda, T. Sekiguchi, S. Shoji, H. Makazu, T. Funatsu, and S.Tsukita. 2001. A Particles and Biomolecules Sorting Micro Flow System Using Thermal Gelation of Methyl Cellulose Solution. Micro Total Analysis Systems 2001 (J.M.Ramsey and A.van den Berg eds.) Kluwer Academic Publishers. pp 471-473.
9) Y. Shirasaki, H. Makazu, K. Tashiro, S. Ikeda, T. Sekiguchi, S. Shoji, S. Tsukita, and T. Funatsu "A Novel Biomolecule Sorter Using Thermosensitve Hydrogel in Micro Flow System" Micro Total Analysis System 2002, pp925-927, (2002).

解説

1) 原田慶恵、**船津高志** 1998.「蛍光顕微鏡システムによる生体分子の1分子イメージング」細胞工学 vol.17(4月号) No.4 pp.626-633.
2) **船津高志** 1998.「1分子の生物分子モーターの動きと化学反応を観る」医用電子と生体

工学 vol.36 pp.228-234.

3) **船津高志** 1998.「蛋白質の運動と化学反応の１分子イメージング」 学術月報 vol.51 pp.1130-1133.

4) 齋藤究、**船津高志** 1999.「近接場光学の原理と生物科学への応用」 蛋白質核酸酵素 vol.44(5月号) No.6 pp.807-811.

5) 船津高志 1999.「1分子の生体高分子を観て操る」 高分子 vol. 48 pp.906-909.

6) 田口英樹、上野太郎、吉田賢右、船津高志 2000.「シャペロニンと GFP フォールディング」 生物工学会誌 vol. 78 pp. 384-386.

7) 多田隈尚史、船津高志 2001. 「生きた細胞の核内 mRNA の１分子蛍光イメージング」細胞工学 20: 672-677

8) 船津高志 新生物物理の最前線 2001. 第８章 一分子観測・一分子操作による生物の理解 pp. 239-269 (日本生物物理学会編)

9) 船津高志 2002 「１分子蛍光イメージング技術による生命現象の解析」可視化情報学会誌 vol. 22 pp. 18-21.

10) 座古保、船津高志 2002 「生体機能を１分子レベルで探る －１分子蛍光イメージングー」 分光研究 vol. 51 No.1 pp.3-14.

11) **船津高志** 2002 「１分子蛍光イメージング法」感覚器官と脳内情報処理 (共立出版： 御子柴克彦、清水孝雄 編) pp. 192-199.

3．口頭発表

【国内】

1) 福田紀男、石渡信一　「Effect of pH on spontaneous tension oscillation in skinned cardiac muscle」第７５回日本生理学会（金沢大学）1998. 3.
2) 多田隈尚史、西坂崇之、石渡信一　「単頭・双頭ミオシンを用いた単一硬直結合の確率的・力学的性質の顕微解析」第53回日本物理学会年会（東邦大学・習志野）1998. 4.
3) 川口 憲治、加藤 宏一、石渡信一　「温度パルス顕微鏡によるキネシン分子モーターの熱変調画像化」第53回日本物理学会年会（東邦大学・習志野）1998. 4.
4) H. Fujita and S. Ishiwata "Spontaneous oscillatory contraction (SPOC) without regulatory proteins: Investigation using thin filament-reconstituted cardiac muscle fibers" 第3回バイオメカニクス世界会議（札幌）1998. 8.
5) S. Ishiwata, H. Kato, Y. Kumaki, T. Nishizaka, H. Tadakuma, Y. Shindo, N. Terada, K. Yasuda, H. Fujita and K. Kinosita, Jr. "Mechanics and thermodynamics of single actomyosin motors and their assembly" 第3回バイオメカニクス世界会議　（札幌）1998. 8.
6) 藤田英明、石渡信一　「細いフィラメント再構成筋収縮系を用いた等尺張力への pH 作用の研究」日本生物物理学会第３６回年会（九州大学・福岡）1998. 10.
7) 川口憲治、石渡信一　「キネシン・微小管結合力の一分子顕微解析」日本生物物理学会第３６回年会（九州大学・福岡）1998. 10.
8) 川口憲治、加藤宏一、石渡信一　「温度パルス顕微鏡による分子モーター機能の熱変調」日本生物物理学会第３６回年会（九州大学・福岡）1998. 10.
9) 熊木 雄一、西坂 崇之、石渡 信一　「単一アクトミオシン硬直結合の破断力－異方性と負荷上昇速度依存性－」日本生物物理学会第３６回年会、1998. 10.（九州大学・福岡）
10) 斎藤 素子、石渡 信一　「アクトミオシン分子モーターに対する温度とヌクレオチドの作用」日本生物物理学会第３６回年会（九州大学・福岡）1998. 10.
11) 藤原 郁子、高橋 真、多田隈 尚史、石渡 信一　「エヴァネッセント光を用いた単一アクチンフィラメントの重合過程の直視」日本生物物理学会第３６回年会（九州大学・福岡）1998. 10.
12) 熊木雄一、西坂崇之、石渡信一　「アクトミオシン硬直結合の破断力と結合寿命」筋収縮・細胞運動研究会（帝京大学・東京）1998. 12.
13) 齋藤素子、石渡信一　「アクトミオシン分子モーター機能に対するヌクレオチド種と温度の作用」筋収縮・細胞運動研究会（帝京大学・東京）1998. 12.
14) 川口憲治、石渡信一　「Distinction of single- and double-head binding of kinesin with microtubule by unbinding force measurements」第7回 JST 国際シンポジウム　（東

京）1999. 2.

15) K. Okano, K. Yasuda and S. Ishiwata "Release of specific DNAS from a DNA chip by using photothermal denaturation" 固体センサ・アクチュエーター国際会議（仙台）1999. 6.

16) 川口憲治、上村想太郎、石渡信一　「キネシンの単頭-双頭結合変換」第３７回日本生物物理学会年会（和光市市民文化センター・埼玉）1999. 10.

17) 鈴木団、藤田英明、石渡信一　「A 帯中における単一アクチンフィラメントの張力発生」第３７回日本生物物理学会年会（和光市市民文化センター・埼玉）1999. 10.

18) 藤田英明、福田賢司、佐々木大輔、石渡信一　「MgADP 収縮におけるトロポニン C、ミオシン調節軽鎖の制御作用」第３７回日本生物物理学会年会（和光市市民文化センター・埼玉）1999. 10.

19) 佐々木大輔、藤田英明、石渡信一　「共焦点蛍光顕微鏡による心筋線維 SPOC の筋節長振動波形解析」　第３７回日本生物物理学会年会（和光市市民文化センター・埼玉）1999. 10.

20) 五嶋淳、加藤宏一、石渡信一　「アクチンフィラメントのリング形成」第３７回日本生物物理学会年会（和光市市民文化センター・埼玉）1999. 10.

21) 藤原郁子、高橋真、多田隈尚史、船津高志、石渡信一　「単一アクチンフィラメントの重合ダイナミクスの顕微解析」第３７回日本生物物理学会年会（和光市市民文化センター・埼玉）1999. 10.

22) 安田賢二、岡野和宣、五嶋淳、野崎貴之、石渡信一　「集束レーザー局所加熱による DNA チップからの DNA 選択回収」第３７回日本生物物理学会年会（和光市市民文化センター・埼玉）1999. 10.

23) 石渡信一　「生体分子モーター系にみる自励振動現象：1 分子から分子集団への機能構築」第７２回日本生化学会大会（パシフィコ横浜）1999. 10.

24) 石渡信一　「生体運動を担う分子モーターの仕組み」物性研短期研究会、1999. 11.

25) 岡野和宣、Li Tao、安田賢二、五嶋淳、野崎貴之、石渡信一　「レーザー熱誘起による DNA マイクロチップからの DNA 回収」分子生物学会（福岡）1999. 12.

26) 藤原郁子、高橋真、多田隈尚史、船津高志、石渡信一　「単一アクチンフィラメントの重合過程の実時間顕微鏡解析」筋収縮・細胞運動研究会（帝京大学・東京）1999. 12.

27) 佐々木大輔、藤田英明、石渡信一　「心筋線維ＳＰＯＣにおける筋節長振動の顕微鏡解析」筋収縮・細胞運動研究会（帝京大学・東京）1999. 12.

28) 藤原郁子、高橋真、多田隈尚史、船津高志、石渡信一　「Mg^{2+}-, Ca^{2+}-アクチンの重合ダイナミクスの単一アクチンフィラメント解析」生体運動研究合同班会議　（千里ライフサイエンスセンター・大阪）2000. 1.

29) 藤田英明、福田賢司、佐々木大輔、石渡信一　「MgADP 収縮におけるミオシン調節軽鎖のアロステリック制御」生体運動研究合同班会議（千里ライフサイエンスセンタ

一・大阪）2000. 1.

30) 福田紀男、佐々木大輔、石渡信一、栗原敏　「心筋の長さ－張力関係のメカニズム」日本生理学会、2000. 3.

31) M.Suzuki, H.Fujita and S.Ishiwata "Application of laser optical tweezers to force measurement in the minimum unit of muscle contractile system" 8th International Conference on Laser Application in Life Sciences（早稲田大学・東京）2000. 8.

32) I. Fujiwara, S. Takahashi, H. Tadakuma, T. Funatsu and S. Ishiwata "Real-time analysis of polymerization process of single actin filaments through fluorescence imaging with evanescent field illumination" 8th International Conference on Laser Application in Life Sciences（早稲田大学・東京）2000. 8.

33) 石渡信一　「Single molecular mechano-chemistry of motor proteins studied by laser optical tweezers」8th International Conference on Laser Application in Life Sciences　(早稲田大学・東京)　(Invited Talk)　2000. 8.

34) D. Sasaki and S. Ishiwata "Molecular synchronization in the myocardial contractile system that bears the rhythm of heartbeat" The 1st international symposium on molecular synchronization for design of new materials system,　2000. 9.

35) 石渡信一　「レールがレールでなくなる時」第 38 回日本生物物理学会（東北大学・仙台）（招待講演）2000. 9.

36) 新原岳雄、大沼清、石渡信一、安田賢二　「サイズ・パターン制御されたニワトリ胚培養心筋ネットワークの研究」　第 38 回日本生物物理学会（東北大学・仙台）2000. 9.

37) 藤原郁子、高橋真、多田隈尚史、船津高志、石渡信一　「重合・脱重合ダイナミクスにおける単一アクチンフィラメントの長さ揺らぎの顕微解析」第 38 回日本生物物理学会（東北大学・仙台）2000. 9.

38) 鈴木団、藤田英明、石渡信一　「最小筋収縮系に見られる単一アクチンフィラメントのステップ状の動きと力発生」第 38 回日本生物物理学会（東北大学・仙台）2000. 9.

39) 佐々木大輔、藤田英明、福田紀男、栗原敏、石渡信一　「心筋 SPOC 振動周期と心拍数との相関」第 38 回日本生物物理学会（東北大学・仙台）2000. 9.

40) 福田紀男、佐々木大輔、石渡信一、栗原敏　「心筋の長さ-張力関係のメカニズム」第 38 回日本生物物理学会（東北大学・仙台）2000. 9.

41) 五島淳、加藤宏一、石渡信一　「アクチンリングの形成メカニズム」第 38 回日本生物物理学会（東北大学・仙台）2000. 9.

42) 上村想太郎、川口憲治、石渡信一　「キネシン・微小管結合様式の 1 分子顕微解析」第 38 回日本生物物理学会（東北大学・仙台）2000. 9.

43) 瀬尾隆造、石渡信一　「キネシン・微小管結合の寿命とその負荷依存性」第 38 回日本生物物理学会（東北大学・仙台）2000. 9.

44) 藤原郁子、高橋真、多田隈尚史、船津高志、石渡信一　「単一アクチンフィラメント

重合・脱重合ダイナミクスの定量的解析」日本生化学会（横浜）2000. 10.

45) 藤原郁子、高橋真、多田隈尚史、船津高志、石渡信一　「エヴァネッセント場照明法を用いた単一アクチンフィラメント重合ダイナミクスの実時間顕微解析」レーザー顕微鏡研究会（東京）2000. 11.

46) S. Ishiwata "Role of actin in force generation" The 11th Takeda Science Foundation Symposium on Bioscience =COE International Conference=（淡路）(Invited Talk) 2000. 11.

47) S. Uemura, K. Kawaguchi and S. Ishiwata "Microscopic analysis of binding mode of single kinesin molecules with microtubule" The 11th Takeda Science Foundation Symposium on Bioscience =COE International Conference=（淡路）2000. 11.

48) M. Suzuki, H. Fujita and S. Ishiwata "Motility assay in the myosin filament lattice" The 11th Takeda Science Foundation Symposium on Bioscience =COE International Conference=（淡路）2000. 11.

49) I. Fujiwara, S. Takahashi, H. Tadakuma, T. Funatsu and S. Ishiwata "Direct observation of polymerization process of single actin filaments" 筋収縮・細胞運動研究会（帝京大学・東京）2000. 12.

50) 佐々木大輔、藤田英明、福田紀男、栗原敏、石渡信一　「心筋収縮系における SPOC 振動周期と心拍数との相関」生体運動研究合同班会議（早稲田大学・東京）2001. 1.

51) 鈴木団、藤田英明、石渡信一　「A 帯中における単一クロスブリッジあたりの発生張力」生体運動研究合同班会議（早稲田大学・東京）2001. 1.

52) 東條正、多田隈尚史、上野太郎、青木大輔、石渡信一、船津高志　「好中球走化性因子受容体の生細胞上での一分子計測」生体運動研究合同班会議（早稲田大学・東京）2001. 1.

53) 石渡信一　「分子モーターの生物理学」第 56 回日本物理学会　シンポジウム（中央大・八王子）2001. 3.

54) 石渡信一　「アクチンフィラメント：重合・脱重合ダイナミクスと内部運動」第 54 回日本細胞生物学会シンポジウム（岐阜）2001.5.

56) 藤原郁子、多田隈尚史、船津高志、石渡信一　「単一アクチンフィラメント重合・脱重合ダイナミクスの長さ揺らぎ顕微解析」第 54 回日本細胞生物学会（岐阜）2001. 5.

57) Sasaki, D., Fujita, H., Fukuda, N., Kurihara, S., Ishiwata,S. "Correlation between myocardial SPOC and heart rate" 4th International Conference on Biological Physics (Kyoto) 2001. 8.

58) Suzuki, M., Fujita, H. and Ishiwata, S. "Microscopic measurement of force generated on single actin filament in the A-band" 4th International Conference on Biological Physics (Kyoto) 2001. 8.

59) Fujiwara, I., Tadakuma, H., Funatsu T. & Ishiwata, S. "Microscopic analysis of polymerization and depolymerization dynamics occuring at each end of single actin

filaments" 4th International Conference on Biological Physics (Kyoto) 2001. 8.

60) Uemura, S., Kawaguchi, K., Yajima, J., Edamatsu, M., Toyoshima, Y., Ishiwata, S. "Two binding states in each head of kinesin as revealed by single-molecule mechanics" 4th International Conference on Biological Physics (Kyoto) 2001. 8.

61) Ali, M. Y., Uemura, S., Ishiwata, S., Kinosita, K. Jr. "Direct observation of the rotation of myosin-V around the axis of an actin filament" 4th International Conference on Biological Physics (Kyoto) 2001. 8.

62) 佐々木大輔、藤田英明、福田紀男、栗原敏、石渡信一 「心筋 SPOC の顕微解析－心拍との相関と振動波形－」 第 39 回日本生物物理学会（大阪）2001. 10.

63) 鈴木団、藤田英明、石渡信一 「最小筋収縮系―A 帯滑り運動系―から見たクロスブリッジの動作特性と筋収縮機構」 第 39 回日本生物物理学会（大阪）2001. 10.

64) 藤原郁子、多田隈尚史、船津高志、石渡信一 「両端識別した単一アクチンフィラメントにおける重合・脱重合過程の顕微解析」 第 39 回日本生物物理学会（大阪）2001. 10.

65) 上村想太郎、川口憲治、矢島潤一郎、枝松正樹、豊島陽子、石渡信一 「キネシン単頭内における２つの結合状態」 第 39 回日本生物物理学会（大阪）2001. 10.

66) 井手純一、新原岳雄、石渡信一 「サポニン処理培養心筋細胞ネットワークにおける SPOC の顕微解析」 第 39 回日本生物物理学会（大阪）2001. 10.

67) 島本勇太、鈴木団、安田賢二、石渡信一 「骨格筋収縮系 SPOC は力学的な外部刺激に同調する」 第 39 回日本生物物理学会（大阪）2001. 10.

68) 吉江方史、佐々木大輔、石渡信一 「心筋 SPOC 周期を決定する因子について」 第 39 回日本生物物理学会（大阪）2001. 10.

69) 奈良郁子、上村想太郎、藤原郁子、石渡信一 「キネシン歩行運動特性の温度依存性」第 39 回日本生物物理学会（大阪）2001. 10.

70) 東條正、青木大輔、多田隈尚史、石渡信一、船津高志 「G タンパク質共役型受容体・FPR1 はリガンド非依存的に多量体を形成する：一分子イメージングによる研究」 第 39 回日本生物物理学会（大阪）2001. 10.

71) 石渡信一 「生体分子モーターの１分子力学解析－バイオナノゲージの開発に向けて－」 大阪大学蛋白質研究所セミナー（大阪）2001. 12.

72) 鈴木団、藤田英明、石渡信一 "Contractile properties of single actin filaments in a newly developed A-band motility assay system" 筋収縮・細胞運動研究会 （東京）2001. 12.

73) 藤原 郁子、末次 志郎、上村 想太郎、竹縄 忠臣、 石渡 信一 「Arp2/3 complex によるアクチンの枝化形成過程の直視と解析」生体運動合同班会議（千葉）2002. 1.

74) 上村想太郎、石渡信一 「キネシン・微小管複合体への ADP 結合は負荷の方向に依存する」生体運動合同班会議（千葉）2002. 1.

75) M. Yusuf Ali、上村想太郎、足立健吾、石渡信一、伊藤博康、木下一彦　「Direct observation of the rotation of myosin-V around the axis of an actin filament」生体運動合同班会議（千葉）2002. 1.

76) 佐々木大輔、藤田英明、福田紀男、栗原敏、石渡信一　「心筋 SPOC の顕微解析－心拍との相関と振動波形－」筋生理の集い（東京）2002. 2.

77) 石渡信一　「分子モータのナノバイオロジー」　第１９回医用高分子研究会　（東京）2002. 2.

78) 石渡信一　「筋収縮を担う分子とシステム」　第５７回日本物理学会春季年次大会（草津）（招待講演）　2002. 3.

79) 石渡信一　「生体分子モーターを見て操作する：１分子酵素力学、分子間協調そしてシステム機能構築」日本動物学会・関東支部公開シンポジウム、2002. 3.

80) 新原岳雄、石渡信一　「周期的電気刺激に対するニワトリ胚培養心筋細胞の応用性」第５７回日本物理学会春季年次大会（草津）2002. 3.

81) 野崎貴之、東條正、石渡信一　「actin 内部への蛍光性タンパク質 GFP 挿入の効果」第５７回日本物理学会春季年次大会（草津）2002. 3.

82) 島本勇太、鈴木団、安田賢二、石渡信一　「力学刺激による骨格筋収縮系自励振動の制御」第５７回日本物理学会春季年次大会（草津）2002. 3.

83) 船津高志　1998.　生命現象の1分子イメージング　Optics Japan '98　講演予稿集 95-96.

84) 多田隈尚史、田口英樹、上野太郎、吉田賢右、船津高志　1998.　GroELとGroESの相互作用の1分子蛍光イメージング　日本生物物理学会第 36 回年会　生物物理 38: S159.

85) 多田隈尚史、船津高志　1998.　細胞内蛍光1分子観察技術の開発　日本生物物理学会 36 回年会　生物物理 38: S207.

86) 船津高志　1998.　1分子生化学　—*in vitro* から *in vivo* へ—　第 71 回日本生化学会大会　生化学 70:659.

87) 田口英樹、多田隈尚史、吉田賢右、船津高志　1998. シャペロニン GroEL と GroES の結合解離の1分子イメージング 生化学 70:743.

88) 船津高志、田口英樹、多田隈尚史、上野太郎、吉田賢右　1999. シャペロニン機能の1分子イメージング　細胞生物学会

89) 上野太郎、田口英樹、多田隈尚史、吉田賢右、船津高志　1999. シャペロニンによるタンパク質折れ畳みの1分子蛍光イメージング　日本生物物理学会第 37回年会　生物物理 39: S131.

90) 多田隈尚史、阿藤淳一郎、石浜陽、羽原靖晃、谷時雄、船津高志　1999. 核内における mRNA の運動の1分子イメージング　日本生物物理学会第 37回年会　生物物理 39: S207.

91) 船津高志　1999.　1分子蛍光イメージング法による生化学・生物物理学　第 72 回日本生化学会大会　生化学 71:592.

92) 田口英樹、上野太郎、多田隈尚史、吉田賢右、船津高志 1999. シャペロニンによるタンパク質折れ畳みの1分子イメージング 第72回 日本生化学会大会 生化学 71:964.
93) 多田隈尚史、阿藤淳一郎、羽原 靖晃、谷 時雄、船津高志 1999. mRNAの核内運動の1分子蛍光イメージング 第72回 日本生化学会大会 生化学 71:788. 1999年
94) 船津高志、多田隈尚史、羽原 靖晃、谷 時雄 1999. mRNAの核内運動の1分子蛍光イメージング 第22回 日本分子生物学会年会 講演要旨集 pp.263.
95) 船津高志 シャペロニン機能と細胞内mRNA運動の一分子蛍光イメージング 日本生化学会東北支部シンポジウム「細胞機能制御系のネットワーク」. 2000年
96) 多田隈尚史、山口淳一、上野太郎、石浜陽、船津高志 2000. 1分子蛍光イメージング法を用いた生体分子の観察 日本生物物理学会第38回年会 生物物理 40: S14.
97) 多田隈尚史、渋谷利治、石浜陽、谷時雄、船津高志 2000. 細胞核内のmRNA1分子の動きを観察する 日本生物物理学会第38回年会 生物物理 40: S77.
98) 田口英樹、上野太郎、多田隈尚史、吉田賢右、船津高志 シャペロニン機能の1分子イメージング 日本生物物理学会第38回年会 生物物理 40: S160. 2000年
99) 上野太郎、田口英樹、多田隈尚史、吉田賢右、船津高志. 1分子蛍光イメージング法を用いたシャペロニン反応サイクルの解析 日本生物物理学会第38回年会 生物物理 40: S177. 2000年
100) 船津高志、多田隈尚史、石浜陽、渋谷利治、谷時雄 細胞核内mRNAの1分子蛍光イメージング レーザー顕微鏡研究会第26回講演会 2000年
101) Takashi Funatsu. Imaging of single bio-molecules in vitro and in vivo. 第5回東洋大学バイオ・ナノエレクトロニクス研究センター・シンポジウム講演集 pp.64-74. 2000年
102) T.Funatsu, H.Taguchi, T.Ueno, H.Tadakuma, M.Yoshida. Single-molecule analysis of chaperonin function. The 12-th Nagoya Conference "Problems of Protein Folding". 2000年
103) 山口淳一、香月康孝、船津高志 2000. ネイティブキネシンの運動の蛍光一分子イメージング 第9回日本バイオイメージング学会学術集会
104) H. Tadakuma, T. Shibuya, Y. Ishihama, T. Tani, and T. Funatsu. Imaging of single mRNA molecules moving within a nucleous of a living cell. The 6-th International Symposium. The Graduate University for Advanced Studies (SOKEN-DAI). Genome Science in the 21st Century: Information of the Higher-Order Structure beyond the Primary Sequence. March 14-16 at Hayama, Kanagawa, Japan. 2001年
105) 船津高志、多田隈尚史、渋谷利治、石浜陽、谷時雄 生きた細胞の核内mRNAの1分子蛍光イメージング 日本電子顕微鏡学会第57回学術講演会(シンポジウム指名講演)2001年
106) 田口英樹、上野太郎、多田隈尚史、吉田賢右、船津高志 シャペロニン機能の1分子蛍光イメージング 第1回日本蛋白質科学会年会 要旨集 pp.107 2001年
107) 山口淳一、根本直人、佐々木亨、徳増亜古、船津高志 蛍光ピューロマイシンと1分子蛍

光イメージング法を用いた蛋白質間相互作用の新しい機能解析法 第1回日本蛋白質科学会年会 要旨集 pp.414 2001 年

108) 船津高志、田口英樹、多田隈尚志、上野太郎、吉田賢右 2001. シャペロニン機能の 1 分子蛍光イメージング 単一(超)分子系研究ミニシンポジウム

109) Y. Ishihama, H.Tadakuma, T.Shibuya, T.Tani, and T.Funatsu. Imaging of single mRNA molecules moving within a nucleous of living cells. 4th International Conference on Biological Physics.. Kyoto International Conference Hall, Kyoto, Japan. Abstracts p41. 2001 年 7 月 30 日～8 月 3 日

110) N.Nemoto, Yamaguchi J., Sasaki, T., Tokumasu, A., Mimori-Kiyosue, Y., Yagi, T., and Funatsu, T. Rapid functional analysis of protein-protein interactions by fluorescent C-terminal labeling and single-molecule imaging. 4th International Conference on Biological Physics. Kyoto International Conference Hall, Kyoto, Japan. Abstracts p64. 2001 年 7 月 30 日～8 月 3 日

111) 船津高志 生物分子機械システムから学んだこと 第 39 回生物物理学会年会 要旨集 pp.S2 2001 年

112) 多田隈尚志、船津高志 生体分子の1分子機能解析 第 39 回生物物理学会年会 要旨集 pp.S28 2001 年

113) 石浜陽、渋谷利治、多田隈尚志、座古保、谷時雄、船津高志 2001. mRNA スプライシングの1分子蛍光分光イメージング 第 39 回生物物理学会年会 要旨集 pp.S94

114) 山口淳一、根本直人、佐々木亨、徳増亜古、船津高志 2001. 蛍光ピューロマイシンと1分子蛍光イメージング法を用いた蛋白質間相互作用の新しい機能解析法 第 39 回生物物理学会年会 要旨集 pp.S108

115) 東條正、青木大輔、多田隈尚志、石渡信一、船津高志 G タンパク質共役型受容体—FPRI はリガンド非依存的に多量体を形成する:1分子イメージングによる研究 第 39 回生物物理学会年会 要旨集 pp.S121 2001 年

116) 真一弘士、白崎善隆、田代浩一、池田晋吾、庄司習一、月田承一郎、船津高志 マイクロシステムによる分子・オルガネラ・セルソーターの開発 第 39 回生物物理学会年会 要旨集 pp.S155 2001 年

117) 船津高志、谷山忠義、田島貴司、並木秀男 GFP ファージによる特定の細菌の高感度検出法 第 39 回生物物理学会年会 要旨集 pp.S156 2001 年

118) 渡辺健二郎、弓場俊輔、亀井保博、青木大輔、船津高志 . 単一細胞を局所加熱する赤外線レーザー顕微鏡システムの開発 第 39 回生物物理学会年会 要旨集 pp.S157 2001 年

119) 上野太郎、田口英樹、多田隈尚志、吉田賢右、船津高志 1分子蛍光イメージング法を用いた GroEL・GroES 結合時間と GFP folding の温度依存性の解析 第 39 回生物物理学会年会 要旨集 pp.S167 2001 年

120) 小池理恵子、上野太郎、田口英樹、吉田賢右、船津高志 「基質タンパク質と GroEL の結

合解離時間の測定」第39回生物物理学会年会 要旨集 pp.S168 2001年

121) **船津高志**、多田隈尚志、渋谷利治、石浜 陽、谷 時雄 「生きた細胞の核内 mRNA の1分子蛍光イメージング」第24回日本分子生物学会年会 要旨集 pp.W3pJ-6 2001

122) 船津高志 「1分子の蛍光観察とポストゲノム時代」日本電子顕微鏡学会関東支部第26回講演会イメージングの最先端とその技術 要旨集 pp.12-17 2002年3月16日(土) 日本女子大学八十年館

123) 船津高志 「mRNA の核内運動の1分子蛍光イメージング」第107回日本解剖学会総会全国学術集会抄録号 SJ2－2 2002年3月29日(金)～31日（日）アクトシティー浜松（静岡県浜松市）

124) **船津高志**「1分子蛍光イメージング法による生体分子機能解析」
日本化学会第81回春季年会 2002年3月28日 早稲田大学西早稲田キャンパス

【海外】

1) N. Fukuda, H. Kajiwara, S. Ishiwata and S. Kurihara "Effects of MgADP on sarcomere length (SL)-dependent changes of pCa-tension relation in skinned rat myocardium" 米国生理学会 1998. 6.
2) N. Fukuda, S. Kurihara and S. Ishiwata "Effects of pH on spontaneous tension oscillation in skinned bovine cardiac muscle" Gordon Conference, 1998. 7.
3) M. Kawai, K. Kawaguchi, M. Saito and S. Ishiwata "The effect of temperature on sliding force and velocity of actin filaments and HMM" 43nd Annual Meeting of the Biophysical Society, Baltimore (USA), 1999. 2.
4) K. Kawaguchi and S. Ishiwata "Single-head and double-head binding of kinesin with microtubule as revealed by unbinding force measurements" 43nd Annual Meeting of the Biophysical Society, Baltimore (USA), 1999. 2.
5) H. Fujita and S. Ishiwata "Tropomyosin suppresses tension decline due to reduced pH" 43nd Annual Meeting of the Biophysical Society, Baltimore (USA), 1999. 2.
6) S. Ishiwata "Regulation mechanism as revealed using a thin filament-reconstituted contractile system" Gordon Research Conference, Colby-Sawyer College (USA) (Invited Talk) 1999. 6.
7) H. Fujita and S. Ishiwata "Modulation of pH-tension relation by tropomyosin in thin filament-reconstituted cardiac muscle fibers" Gordon Research Conference, Colby-Sawyer College (USA) 1999. 6.
8) K. Kawaguchi and S. Ishiwata "Single-molecule analysis of single-headed and double-headed binding of kinesin with a microtuble" Gordon Research Conference, Colby-Sawyer College (USA) 1999. 6.
9) H. Fujita, S. Ishiwata "Modulation of pH-tension relation by tropomyosin:

Investigation using thin filament-reconstituted cardiac muscle fibers" XIII International Biophysics Congress, New Delhi (India) 1999. 9.

9) M. Kawai, K. Kawaguchi, M. Saito and S. Ishiwata "Temperature change does not affect the force measured between single actin filaments and heavy meromyosin molecules prepared from rabbit skeletal muscles" European Muscle Conference (United Kingdom) 1999. 9.

10) S. Ishiwata and K. Kawaguchi "Nucleotide- and loading rate-dependent switching of single- to double-headed binding of kinesin" 44th Annual Meeting of the Biophysical Society, New Orleans (USA) 2000. 2.

11) K. Kawaguchi and S. Ishiwata "Effect of temperature on force generation and velocity of single kinesin molecule" 44th Annual Meeting of the Biophysical Society, New Orleans (USA) 2000. 2.

12) M. Kawai, K. Kawaguchi, M. Saito and S. Ishiwata "Temperature change does not affect the force measured between single actin filaments and heavy meromyosin molecules prepared from rabbit skeletal muscles" 44th Annual Meeting of the Biophysical Society, New Orleans (USA) 2000. 2.

13) N. Fukuda, D. Sasaki, S. Ishiwata and S. Kurihara "Understanding of sarcomere length (SL)-dependent tension generation in skinned cardiac muscle" 44th Annual Meeting of the Biophysical Society, New Orleans (USA) 2000. 2.

14) J. Goshima, H. Kato and S. Ishiwata "Ring formation of actin filaments in an *in vitro* motility assay" 3rd East Asian Biophysics Symposium, 慶州 (Korea) 2000. 5.

15) M. Suzuki, H. Fujita and S. Ishiwata "Microscopic measurements of force generation by single actin filaments in the A-band" 3rd East Asian Biophysics Symposium, 慶州 (Korea) 2000. 5.

16) I. Fujiwara, S. Takahashi, H. Tadakuma, T. Funatsu and S. Ishiwata "Analysis of polymerization - depolymerization dynamics of single actin filaments -Comparison between Mg^{2+}- and Ca^{2+}- actin-" 3rd East Asian Biophysics Symposium, 慶州 (Korea) 2000. 5.

17) S. Ishiwata "Single molecular characterization of protein motors" International Workshop on signaling neuropeptides and conformation of macromolecules (Moscow) (Invited Talk) 2000. 9.

18) S. Ishiwata "Single-molecular mechanics of motor proteins" Aspen Workshop on Single Molecule Biophysics, Aspen (USA) 2001. 1.

19) I. Fujiwara, S. Takahashi, H. Tadakuma, T. Funatsu and S. Ishiwata "Microscopic analysis of polymerization process of single actin filaments" 45th Annual Meeting of the Biophysical Society, Boston (USA) 2001. 2.

20) M. Suzuki, H. Fujita and S. Ishiwata "Force generation on single actin filaments in the A-band motility assay system" 45th Annual Meeting of the Biophysical Society, Boston (USA) 2001. 2.

21) N. Fukuda, J. O-uchi, H. Kajiwara, S. Ishiwata and S. Kurihara "Effect of Acidosis on length dependence of tension generation in skinned cardiac muscle" 45th Annual Meeting of the Biophysical Society, Boston (USA) 2001. 2.

22) S. Ishiwata "" The Molecular Motors workshop, Alpbach (Austria) 2001. 4.

23) Ishiwata, S. "Molecular Synchronization Observed in Protein Motors" Seminar in Curie Institute, Paris (France) 2001. 4.

24) S. Ishiwata "Actomyosin Interaction Studied by Single Molecule Mechanics and A-band Motility Assay" International Workshop, Actin filament from structure to mechanism (Aioi) (Invited Talk) 2001. 11.

25) Sasaki, D., Fujita, H., Fukuda, N., Kurihara, S., Ishiwata, S. "Correlation between myocardial SPOC and heartbeat" International Workshop, Actin filament from structure to mechanism (Aioi), 2001. 11.

26) Suzuki, M., Fujita, H. and Ishiwata, S. "A-band motility assay system: Microscopic analysis of force generated on a single actin filament" International Workshop, Actin filament from structure to mechanism (Aioi), 2001. 11.

27) Fujiwara, I., Suetsugu, S., Miki, H., Takenawa, T. & Ishiwata, S. "Direct observation of branching in actin filaments triggered by Arp2/3 complex" International Workshop, Actin filament from structure to mechanism (Aioi), 2001. 11.

28) Sasaki, D., Fujita, H., Fukuda, N., Kurihara, S., Ishiwata S. "Relationship between myocardial SPOC and heartbeat" 46th Annual Meeting of the Biophysical Society, (San Francisco), 2002. 2.

29) Suzuki, M., Fujita, H., Ishiwata, S. "New aspects of muscle contraction from the A-band motility assay system" 46th Annual Meeting of the Biophysical Society, (San Francisco), 2002. 2.

30) Fujiwara, I., Suetsugu, S., Uemura, S., Miki, H., Takenawa, T. and Ishiwata, S. "Direct observation of branching in actin filaments triggered by Arp2/3 complex" 46th Annual Meeting of the Biophysical Society, (San Francisco), 2002. 2.

31) Uemura, S., Ishiwata, S. "Binding of ADP to Kinesin-Microtubule Complex Depends on Loading Direction" 46th Annual Meeting of the Biophysical Society, (San Francisco), 2002. 2.

32) Ali, M. Y., Uemura, S., Adachi, K., Ishiwata, S., Itoh, H., Kinosita, K. Jr. "Direct Observation of The Rotation of Myosin-V Around an Actin Filament" 46th Annual Meeting of the Biophysical Society, (San Francisco), 2002. 2

33) Yokota, H., Y. Ishii, Y., T. Wazawa, **T. Funatsu**, and T. Yanagida. 1998. Dynamic structure of single actin molecules revealed by FRET imaging. 42nd annual meeting of the biophysical society. *Biophysical J.* **74**: A46.

34) Harada, Y., T. Funatsu, Y. Nonoyama, and T. Yanagida. 1998. Single molecule imaging of RNA polymerase-DNA interactions in real time. 42nd annual meeting of the biophysical society. *Biophysical J.* **74**: A69.

35) Iwane, A.H., **T. Funatsu**, Y. Harada, M. Tokunaga, O. Ohara, and T. Yanagida. 1998. Single molecular assay of the individual ATP turnovers by a myosin-GFP fusion protein expressed *in vitro*. 42nd annual meeting of the biophysical society. *Biophysical J.* **74**: A260.

36) Tadakuma, H., T. Nishizaka, T. Funatsu, and S. Ishiwata. 1998. Direct measurement of lifetime and torsional stiffness of single acto-myosin rigor complex. 42nd annual meeting of the biophysical society. *Biophysical J.* 74: A265.

37) Ishijima, A., H. Kojima, H. Tanaka, **T. Funatsu**, H. Higuchi, M. Tokunaga, and T. Yanagida. 1998. Simultaneous observation of individual ATPase and mechanical events by a single myosin molecule during interaction with actin. 42nd annual meeting of the biophysical society. *Biophysical J.* 74: A265.

38) **Funatsu, T. 1998. Imaging and nano-manipulation of single biomolecules. RIES Symposium. Single Molecule Observation in Bioscience: Detection and Diagnosis (SMDD98)**

39) Funatsu, T., Y. Harada, M. Tokunaga, K. Saito, R.D. Vale, A. Ishijima, H. Kojima, H. Higuchi, and T. Yanagida. 1998. Imaging and nano-manipulation of single bio-molecules. The 2nd International Symposium on Electrochemical Micro system Technologies. Abstract pp.126.

40) Funatsu, T. 1999. Imaging of single bio-molecules *in vitro* and *in vivo*.
The 7th JST International Symposium. Molecular Processes and Biosystems. Abstract pp.28.

41) Funatsu, T. 1999. Imaging of single bio-molecule dynamics in vitro and in vivo.
Second Annual Symposium on Japanese-American Frontiers of Science.

42) Taguchi H., H. Tadakuma, T. Ueno, M. Yoshida, and T. Funatsu. Single Molecule Imaging of the Chaperonin GroEL-BroES Function. *Biophysical J.* 78: 36A.
2000 年

43) H. Tadakuma, T. Shibuya, Y. Ishihama, J. Atoh, Y. Habara, T. Tani, and T. Funatsu. Imaging of single mRNA molecules moving within a nucleus of living cells.
8th International conference on laser applications in life sciences. 2000 年

44) H. Tadakuma, T. Shibuya, Y. Ishihama, J. Atoh, Y. Habara, T. Tani, and T. Funatsu. 2001.

Imaging of single mRNA molecules moving within a nuclear of living cells.
45th Annual meeting of Biophysical Society, U.S.A.. *Biophysical J.* 80: 148a.

45) T. Funatsu Single molecule Imaging of Biological Functions in vitro and in vivo.
Fluor 2001 Asia-Pacific Workshop Fluorescence Spectroscopy and Imaging. April 18-21 at University of Sydney. 2001 年

46) K.Tashiro, S.Ikeda, T.Sekiguchi, H.Sato, S.Shoji, H.Makazu, K.Watanabe, T.Funatsu, and S.Tsukita. "Micro Flow Switches Using Thermal Gelation of Methyl Cellulose for Biomolecules Handling" 11th International Conference on Solid-State Sensors and Actuators, (Transducers'01). pp932-935, 2001 年

Cell, Vol. 93, 21–24, April 3, 1998, Copyright ©1998 by Cell Press

F_1-ATPase: A Rotary Motor Made of a Single Molecule

Minireview

Kazuhiko Kinosita, Jr.,*† Ryohei Yasuda,*† Hiroyuki Noji,† Shin'ichi Ishiwata,‡† and Masasuke Yoshida§†
*Department of Physics
Faculty of Science and Technology
Keio University
Yokohama 223-8522
Japan
†CREST (Core Research for Evolutional Science and Technology)
"Genetic Programming" Team 13
Teikyo University Biotechnology Research Center 3F
Nogawa, Kawasaki 216-0001
Japan
‡Department of Physics
School of Science and Engineering
Waseda University
Tokyo 169-8555
Japan
§Research Laboratory of Resources Utilization
Tokyo Institute of Technology
Yokohama 226-8503
Japan

The bacterial flagellar motor (DeRosier, 1998) has long been the sole rotary mechanism known in the biological world. While we might call some movements in the body "rotation", the continuous nature of our joints does not allow true rotation, which requires separation of the two parts in order to achieve sliding of one part against the other over all angles. At the level of molecules, however, sliding is commonly encountered, and repeated use of identical subunits often leads to formation of helical structures, including cylinders and rings, which can support rotational motions. A helical actin filament sliding past myosin, for example, has been shown to rotate (Nishizaka et al., 1993), albeit inefficiently (Sase et al., 1997). It is quite possible that rotating molecular machines have simply been overlooked, due to the technical difficulties of detecting molecular rotations. Recently, a new face has joined the class of circularly rotating machines, second to the bacterial flagellar motor. A single molecule of F_1-ATPase, a portion of ATP synthase, is by itself a rotary motor in which a central rotor, made of a γ subunit, rotates over unlimited angles against a surrounding stator cylinder of an $\alpha_3\beta_3$ hexamer (Noji et al., 1997; Figure 1). At a size of ~10 nm, it is the smallest rotary motor ever found.

ATP Synthase

ATP, a major currency of energy, is synthesized by ATP synthase. This enzyme is composed of a membrane-embedded, proton-conducting portion, F_0, and a protruding portion, F_1 (Figure 1). When protons flow through F_0, ATP is synthesized in F_1. The synthase is fully reversible in that hydrolysis of ATP in F_1 drives reverse flow of protons through F_0. Isolated F_1 catalyzes only hydrolysis of ATP, and hence is called the F_1-ATPase.

How is the proton flow through F_0 coupled to the synthesis/hydrolysis of ATP in F_1? Almost 20 years ago Paul Boyer made a radical proposal that the two reactions are mechanically coupled by rotation of a common shaft penetrating F_0 and F_1 (see Boyer, 1997). Part of his reasoning was that F_1 contains three catalytic sites, one on each β, which participate on average equally in ATP synthesis/hydrolysis. The γ subunit, known to be adjacent to β, lacks 3-fold symmetry. For γ to touch the three β's impartially, therefore, it has to rotate. F_0 may also be a rotary motor if likened to the bacterial flagellar motor which is driven by the flow of protons. In this view, the ATP synthase comprises two motors, one ATP-driven and the other proton-driven, with a common shaft of which γ is a major part. Rotation in one direction produces ATP, and ATP hydrolysis causes reverse rotation.

Boyer's model gained support when a crystal structure of F_1 was solved by John Walker and colleagues (Abrahams et al., 1994). Importantly, the three β's carried different nucleotides in the crystal, AMPPNP (an ATP analog), ADP, and none in the clockwise order when viewed from the F_0 side (Figure 1, bottom). If hydrolysis were to proceed, the order in the next step would be ADP, none, and ATP. A face of γ opposing the empty β, for example, would thus turn counter-clockwise. In the crystal, the conformation of empty β was noticeably different from those bearing a nucleotide.

Cross-linking and spectroscopic studies have since given strong evidence favoring rotation of γ (Junge et al., 1997, and references therein): a residue on γ could be cross-linked to different β's only when ATP was hydrolyzed/synthesized, and an optical probe attached to

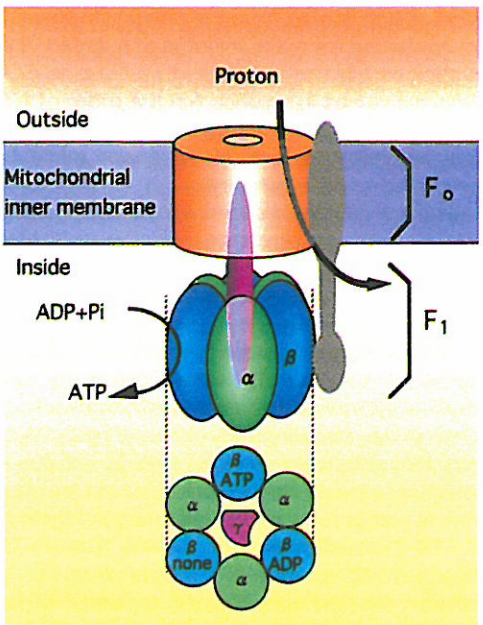

Figure 1. Simplified Structure of ATP Synthase

F_1 consists of $\alpha_3\beta_3\gamma\delta\epsilon$ (δ and ϵ are not shown), and the simplest composition of F_0 (not mitochondrial) is $ab_2c_{9\text{-}12}$. The gray portion indicates a suggested location of δab_2.

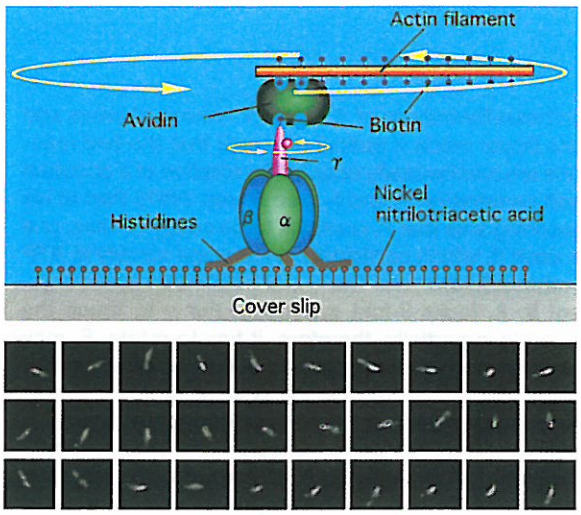

Figure 2. Observation of F_1 Rotation
Video images of a rotating actin filament at intervals of 133 ms are shown at the bottom.

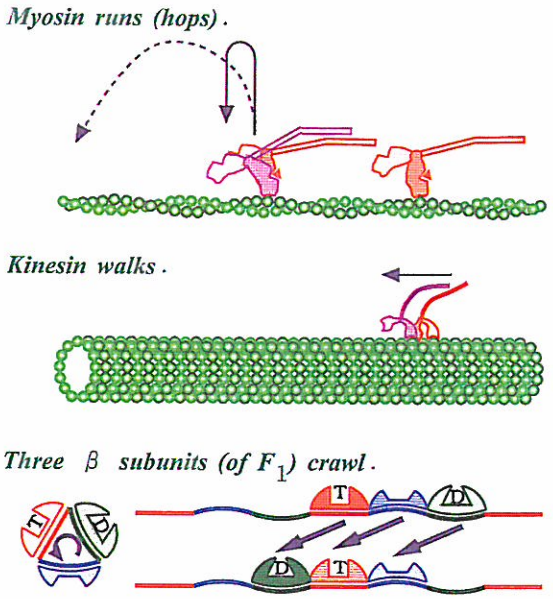

Figure 3. Mode of Operation of Various Molecular Motors
See text for further description. T, ATP; D, ADP. The β subunits of F_1 slide across unrolled γ with the forefoot in front and the hindfoot at back. Note that the different colors of the three β's indicate differences in the bound nucleotide and their nucleotide-dictated conformations (and not their identity). The surfaces of γ that would match the three β's conformations are colored accordingly. The heavy, medium, and light stippling of the β subunits indicate their respective identity. All three β's move simultaneously as shown by the arrows. The scheme here is simplified and the bound nucleotides on the three β's may not change simultaneously. In addition to its bound nucleotide, the conformation of each β should depend on the surface of γ it faces (and indirectly the conformations of the other two β's).

γ underwent large-amplitude rotations. However, the questions of whether γ continues to rotate in one direction, and, if so, its direction, were not addressed in these studies.

Rotation of F_1 Has Been Videotaped

One way of detecting molecular rotation is to attach a large tag that is readily visible under an optical microscope. Noji et al. (1997) attached a fluorescently labeled actin filament to the γ subunit of F_1 (lacking δ and ε subunits) through a streptavidin-biotin link (Figure 2). The β subunits were bound to a glass surface through histidine tags engineered at the N termini. When ATP was added, the filament rotated, invariably counterclockwise as anticipated from the crystal structure. The rotation continued for many minutes at a speed of several revolutions per second. Based on the rate of ATP hydrolysis measured in solution (on the order of 10^2/s), and the assumption of the hydrolysis of three ATP molecules per revolution, the rotational speed might have been predicted to be much higher.

The observed rotational speed was, in fact, quite high when taking into account the hydrodynamic friction against the rotating actin filament. If F_1 were scaled to the size of a person, the person would be standing at the bottom of a large swimming pool rotating an ~500 m rod at several revolutions per second! The F_1 was really working at full throttle. The torque the molecular F_1 produced to overcome the friction amounted to ~40 pN · nm over a broad range of rotational speed (Noji et al., 1997). This torque times $2\pi/3$ (=120°), ~80 pN · nm, is the mechanical work done in one third of a revolution. This work is comparable to the free energy of hydrolysis of one ATP molecule of ~80 pN · nm. If one ATP is consumed per 120° as one may anticipate from the make of this motor, the efficiency of our F_1 is nearly 100%, far superior to a Honda V6. A model by Oosawa and Hayashi (1986) has predicted such a high efficiency.

F_0 Awaits Experimental Proof of Rotation

Relatively little is known about the putative proton-driven motor F_0. In *E. coli*, the subunit composition of F_0 is believed to be ab_2c_{9-12} (the number of c subunits is yet uncertain). Models have been proposed (Junge et al., 1997; Elston et al., 1998) in which a ring of c_{9-12} is attached to γ and the two together constitute the common shaft; ab_2, bound to $\alpha_3\beta_3$ through δ, extends to the c ring and serves as the stator for ring rotation (Figure 1, gray part). Supportive (but not yet conclusive) evidence exists, but the models detract from the elegance in the Boyer's proposal in that the presumably symmetric ring of c's is attached to the asymmetric γ, and δab_2 rests on one side of the symmetric $\alpha_3\beta_3$. Whether the c ring really rotates with γ remains to be seen (videotaped?).

Comparison of Nucleotide-Driven Molecular Motors

In Figure 3, we compare the different ways that molecular motors use their multiple "feet." Myosin is a linear motor that "runs" along actin, in that its two feet (the two globular parts of myosin usually referred to as "heads") are detached from actin for most of the time (Sase et al., 1997). In fact, myosin can run, skipping many actin monomers in a step, if other myosin molecules pull the actin filament while the first one is detached. If only one myosin molecule interacts with actin, it simply hops and will not move relative to actin while detached (except for random diffusion). Kinesin, on the other hand, appears to "walk" along a microtubule, without detaching its two feet simultaneously and probably using

Table 1. Comparison of Nucleotide-Driven Motors

Motor/Rail	Step Size	Max. force	Max. Efficiency	Processivity	Mode
Myosin/Actin	variable	3–5 pN	~20%	none–poor	runs (hops)
Kinesin/Microtubule	8 nm	5 pN	~50%	good	walks
RNA polymerase/DNA	0.34 nm?	14 pN	~20%	excellent	crawls?
$F_1\beta/F_1\gamma$	120°	40 pN · nm	~100%	perfect	crawls
(at the radius of 1 nm)	(2 nm)	(40 pN)			

its two feet in an alternate fashion (Block, 1998, and references therein). F_1 could be unrolled, conceptually, to make it a linear motor (Figure 3). The three β's (and α's) then "crawl" on repeats of unrolled γ in that they never detach from γ (they would slide on γ by pushing and/or pulling actions) and, in contrast to the presumed walking of kinesin, the forefoot always remains in front and the hindfoot at the back. (If unrolled γ is considered to slide along repeats of unrolled $\alpha_3\beta_3$, the γ would "walk" in that it uses the three feet alternately. Figure 3 conforms to the prevailing custom of regarding only the molecule that hydrolyzes a nucleotide as the "motor" and its partner a passive rail.)

The three motors above and another linear motor, RNA polymerase (Gelles and Landick, 1998), are compared in Table 1. The F_1 motor most likely makes 120° steps, because the asymmetric conformations of the three β's, presumably dictating the orientation of γ, are stable in the crystal structure. Short pauses at 120° orientations were not resolved in the video images of Noji et al. (1997) at the resolution of 33 ms; however, measurements at low ATP concentrations could reveal such steps. RNA polymerase is expected to step by 0.34 nm, the distance between base pairs. Kinesin's 8 nm steps have been measured. All these step sizes represent intervals of the structural repeats. Myosin's so-called "unitary step" measured in vitro is a different quantity, in most cases representing movement made while a foot of myosin is attached to actin. It is believed by many to be related to the size of a conformational change that occurs in attached myosin (Goldman, 1998). Genuine steps of running myosin are expected to be multiples of 5.5 nm, the distance between neighboring actin monomers.

The four motors differ in efficiency, the mechanical work divided by the free energy of nucleotide hydrolysis. Because the motors can move without an external load (efficiency 0%), maximal efficiencies are quoted in Table 1. The near 100% efficiency of F_1 accords with the fully reversible nature of this motor; net synthesis of nucleotide triphosphate has not been reported for the other motors. The efficiency of the myosin/actin system quoted here is the work produced in a "unitary step" divided by the free energy of ATP hydrolysis. The myosin efficiency appears low in vitro, the quoted value being on the higher end in the literature (Ishijima et al., 1995), although the efficiency of intact muscle is generally considered to be higher.

Motor Mechanism: Bending versus Binding

Nucleotide-driven motors, including F_1, share common structural motifs near the nucleotide-binding site (Vale, 1996; Noji et al., 1996), suggesting that these motors might employ common principles in some aspects of their mechanisms. As a general principle, we propose that the distinction between bending and binding is important.

Bending (conformational change) of a motor protein alone could produce motion and force relative to its rail, the latter serving merely as a base that securely holds the "sole" of the "foot" of the motor. Myosin is considered to bend its leg forward when attached to actin, producing the "unitary step" (Figure 3, pink myosin on the left; Goldman, 1998). The machinery for bending could all be in myosin, because isolated myosin changes its conformation depending on the bound nucleotide (Gulick and Rayment, 1997). The free-energy changes associated with myosin ATPase, however, indicate that myosin alone would be unable to produce a large amount of work. Moreover, when myosin interacts with actin, as much as half of the free energy of ATP hydrolysis is used for unbinding of myosin from actin. Subsequent rebinding thus liberates energy. If myosin is to work at high efficiency, it should convert the energy gained during rebinding to mechanical output, by cooperation with actin.

A model by A. F. Huxley (1957) is on the other extreme: that binding alone produces motion and force. Myosin fluctuates thermally, and when it fluctuates in the correct direction, it binds to actin resulting in displacement and pull. In binding-alone models, thermal diffusion brings the motor and rail close to the binding configuration, and binding energy is used to stabilize that configuration. Work has to be done in the diffusion process, and can be done as shown below. Diffusive displacement of a particle of diameter d over a distance L takes a time of the order of $(L^2/2) \cdot (3\pi\eta d/k_BT)$, which is ~1 μs for $L = d = 10$ nm at room temperature (thermal energy $k_BT \approx 4$ pN · nm) in water (the viscosity $\eta \approx 10^{-3}$ N · s · m^{-2}). If this displacement is to produce work W (against a load), the time for displacement is multiplied by $\sim\exp(W/k_BT)$, which is 2×10^4 for $W = 10\ k_BT \approx 40$ pN · nm and 5×10^8 for $W = 20\ k_BT \approx 80$ pN · nm. Thus, work below $10\ k_BT$ can be done if the frequency of motor operation is below $\sim 10^2$/s. Binding models also require a mechanism that ensures correct choice of a binding site, or proper directional biasing of diffusion. The mechanism is not specified in the Huxley model.

An elegant interplay between bending and binding has been proposed for kinesin and its cousin ncd (Hirose et al., 1996). When one foot of kinesin (or ncd) is bound to a microtubule (rail), the other foot is unbound and undergoes thermal motion. They have shown that the unbound foot of kinesin, which walks toward the plus end of a microtubule, swings toward the plus end presumably by bending of the bound leg (Figure 3, pink

kinesin), and the unbound foot of minus-directed ncd swings toward the minus end. The bending biases the Brownian search of the unbound foot for the next binding site, for the plus direction for kinesin, and minus for ncd. The 8 nm step of kinesin (yet unresolved for ncd), and associated force, are produced when the foot lands on the binding site. A substep(s) and partial force may be produced by the bending, but the major mechanical output of this motor likely comes from the binding of the motor to its rail.

The three-foot F_1 (Figure 3) could in principle operate by binding alone, stepping among the three stable configurations with the correct direction being dictated by the bound nucleotide. ("Binding" for the case of F_1 should be interpreted as a transition to the most stable configuration between β's and γ, and might involve repulsive rather than attractive interactions.) The large mechanical output of $\sim 20\ k_BT$ per step, however, cannot be achieved by a purely diffusive process because it would be too infrequent to account for the observed rate of rotation. Probably, the effective potential between β's and γ is downhill toward the next stable configuration, thus assisting the diffusion against an external load. The work per step would be determined by the total height of the potential slope, which is not dependent on the rotational speed. Bending of the three β's alone is unlikely to rotate γ by 120° because of the obstruction by intervening α subunits.

Of course the distinction between bending and binding becomes less obvious as one inquires more deeply into the mechanism. What we wish to stress here is that molecular motors must work through close cooperation of the two partners. The rail, in particular, is not a simple support, and binds and unbinds its nucleotide-hydrolyzing partner, supplying binding energy and controlling hydrolysis. The two aspects, bending and binding, should be useful in analyzing the mechanism of cooperation. The F_1 motor in which the two partners never detach from each other provides a wonderful opportunity to explore the details of the cooperation experimentally.

Selected Reading

Abrahams, J.P., Leslie, A.G.W., Lutter, R., and Walker, J.E. (1994). Nature *370*, 621–628.

Block, S.M. (1998). Cell *93*, this issue, 5–8.

Boyer, P.D. (1997). Annu. Rev. Biochem. *66*, 717–749.

DeRosier, D.J. (1998). Cell *93*, this issue, 17–20.

Elston, T., Wang, H., and Oster, G. (1998). Nature *391*, 510–513.

Gelles, J., and Landick, R. (1998). Cell *93*, this issue, 13–16.

Goldman, Y.E. (1998). Cell *93*, this issue, 1–4.

Gulick, A.M., and Rayment, I. (1997). Bioessays *19*, 561–569.

Hirose, K., Lockhart, A., Cross, R.A., and Amos, L.A. (1996). Proc. Natl. Acad. Sci. USA *93*, 9539–9544.

Huxley, A.F. (1957). Progr. Biophys. Biophys. Chem. *7*, 255–318.

Ishijima, A., Harada, Y., Kojima, H., Funatsu, T., Higuchi, H., and Yanagida, T. (1995). Biochem. Biophys. Res. Commun. *199*, 1057–1063.

Junge, W., Lill, H., and Engelbrecht, S. (1997). Trends Biochem. Sci. *22*, 420–423.

Nishizaka, T., Yagi, T., Tanaka, Y., and Ishiwata, S. (1993). Nature *361*, 269–271.

Noji, H., Amano, T., and Yoshida, M. (1996). J. Bioenerg. Biomemb. *28*, 451–457.

Noji, H., Yasuda, R., Yoshida, M., and Kinosita, K., Jr. (1997). Nature *386*, 299–302.

Oosawa, F., and Hayashi, S. (1986). Adv. Biophys. *22*, 151–183.

Sase, I., Miyata, H., Ishiwata, S., and Kinosita, K., Jr. (1997). Proc. Natl. Acad. Sci. USA *94*, 5646–5650.

Vale, R.D. (1996). J. Cell Biol. *135*, 291–302.

Spontaneous Oscillatory Contraction without Regulatory Proteins in Actin Filament-Reconstituted Fibers

Hideaki Fujita* and Shin'ichi Ishiwata*#§¶

*Department of Physics, School of Science and Engineering, #Advanced Research Institute for Science and Engineering, and §Materials Research Laboratory for Bioscience and Photonics, Waseda University, Shinjuku-ku, Tokyo 169-8555, Japan; and ¶Core Research for Evolutional Science and Technology, Genetic Programming Team 13, Nogawa, Kawasaki 216-0001, Japan

ABSTRACT Skinned skeletal and cardiac muscle fibers exhibit spontaneous oscillatory contraction (SPOC) in the presence of MgATP, MgADP, and inorganic phosphate (P_i), but the molecular mechanism underlying this phenomenon is not yet clear. We have investigated the role of regulatory proteins in SPOC using cardiac muscle fibers of which the actin filaments had been reconstituted without tropomyosin and troponin, according to a previously reported method (Fujita et al., 1996. *Biophys. J.* 71:2307–2318). That is, thin filaments in glycerinated cardiac muscle fibers were selectively removed by treatment with gelsolin. Then, by adding exogenous actin to these thin filament-free cardiac muscle fibers under polymerizing conditions, actin filaments were reconstituted. The actin filament-reconstituted cardiac muscle fibers generated active tension in a Ca^{2+}-insensitive manner because of the lack of regulatory proteins. Herein we have developed a new solvent condition under which SPOC occurs, even in actin filament-reconstituted fibers: the coexistence of 2,3-butanedione 2-monoxime (BDM), a reversible inhibitor of actomyosin interactions, with MgATP, MgADP and P_i. The role of BDM in the mechanism of SPOC in the actin filament-reconstituted fibers was analogous to that of the inhibitory function of the tropomyosin-troponin complex ($-Ca^{2+}$) in the control fibers. The present results suggest that SPOC is a phenomenon that is intrinsic to the actomyosin motor itself.

INTRODUCTION

Muscle is generally in one of two possible states, relaxation or contraction, depending on the Ca^{2+} concentration in the presence of MgATP (Ebashi and Endo, 1968; Weber and Murray, 1973). On the other hand, skinned cardiac muscle fibers are in an oscillatory state at intermediate Ca^{2+} concentrations (Fabiato and Fabiato, 1978; Sweitzer and Moss, 1990; Linke et al., 1993; Fukuda et al., 1996). This is also the case in slow-type skeletal muscle (Iwazumi and Pollack, 1981; Stephenson and Williams, 1981), but not in fast-type skeletal muscle (Ishiwata and Yasuda, 1993).

Nearly 10 years ago, we established a new autooscillation condition, that is, the coexistence of MgATP and its hydrolytic products, MgADP and P_i, in myofibrils (Okamura and Ishiwata, 1988; Ishiwata et al., 1991; Anazawa et al., 1992; Yasuda et al., 1996) and skinned muscle fibers (Shimizu et al., 1992; Ishiwata et al., 1993; Fukuda et al., 1996). We termed this phenomenon spontaneous oscillatory contraction (SPOC). SPOC was classified into ADP-SPOC, which occurs under the coexistence of MgATP, MgADP, and P_i in the absence of Ca^{2+}, and Ca-SPOC, which occurs in the presence of micromolar concentrations of Ca^{2+} under normal activating conditions. Under SPOC conditions, isometric tension oscillates spontaneously. When myofibrils are observed under a phase contrast microscope, repetition of rapid lengthening followed by a slow shortening of sarcomeres occurs reproducibly, resulting in an oscillation of sarcomere length with a sawtooth waveform. SPOC conditions are sandwiched between relaxation and contraction conditions, indicating that SPOC is a third state of muscle, occurring between the two major states (Ishiwata and Yasuda, 1993; Ishiwata et al., 1993; Fukuda et al., 1996).

Although the chemical and mechanical properties of SPOC have been studied for nearly a decade, the molecular mechanism of SPOC is not yet clear. In the present study, to clarify the role of regulatory proteins in SPOC, we investigated tropomyosin-troponin complex-free actin filament-reconstituted cardiac muscle fibers. Thin filaments in skeletal and cardiac muscle fibers can be selectively removed using calf plasma gelsolin, an actin filament-severing protein (Funatsu et al., 1990, 1993; Yasuda et al., 1995). By adding exogenous actin to the thin filament-free cardiac muscle fibers under polymerizing conditions, actin filaments can be fully reconstituted (Fujita et al., 1996). Because of the lack of regulatory proteins, these actin filament-reconstituted fibers generate active tension in a Ca^{2+}-insensitive manner, and tension oscillation was not observed under standard SPOC conditions. Herein we have succeeded in generating spontaneous tension oscillation in actin filament-reconstituted fibers by adding 2,3-butanedione 2-monoxime (BDM), an inhibitor of actomyosin interactions (Li et al., 1985; Horiuti et al., 1988). These results indicate that regulatory proteins are not necessarily required for autooscillation of the contractile system and that the actomyosin motor itself has autooscillatory properties.

Received for publication 11 August 1997 and in final form 28 May 1998.

Address reprint requests to Dr. Shin'ichi Ishiwata, Department of Physics, School of Science and Engineering, Waseda University, 3-4-1 Okubo, Shinjuku-ku, Tokyo 169-8555, Japan. Tel.: +81-3-5286-3437; Fax: +81-3-3200-2567; E-mail: ishiwata@mn.waseda.ac.jp.

0006-3495/98/09/1439/07 $2.00

MATERIALS AND METHODS

Muscle fibers and proteins

Bovine cardiac muscle bundles (~5 mm in diameter) were excised from a straight portion of left ventricular papillary muscle while the muscle was

still warm. Both ends of the muscle bundle were tied to a glass rod and incubated overnight in glycerol solution composed of 50% (v/v) glycerol, 0.5 mM $NaHCO_3$, 5 mM EGTA, and 2 mM leupeptin at 0°C. Fibers were then stored in fresh glycerol solution at −20°C. Glycerinated fibers were used between 2 and 8 weeks after storage. Bovine plasma gelsolin was prepared according to the method of Kurokawa et al. (1990). Actin was extracted from acetone powder (Kondo and Ishiwata, 1976) of bovine cardiac muscle according to the method of Spudich and Watt (1971). Purified G-actin was stored at 0°C and used within 2 weeks.

Solutions

The solutions used were rigor solution (170 mM KCl, 1 mM $MgCl_2$, 1 mM EGTA, 10 mM 3-(*N*-morpholino)propanesulfonic acid (MOPS) (pH 7.0)); relaxing solution (117 mM KCl, 5 mM $MgCl_2$, 4 mM ATP, 1 mM EGTA, 10 mM MOPS (pH 7.0), 20 mM 2,3-butanedione 2-monoxime (BDM)); contracting solution (117 mM KCl, 4.25 mM $MgCl_2$, 2.2 mM ATP, 2 mM EGTA, 20 mM MOPS (pH 7.0), 1.9 mM $CaCl_2$); and standard SPOC solution (41 mM KCl, 14.2 mM $MgCl_2$, 2.2 mM ATP, 16.4 mM ADP, 2 mM EGTA, 10 mM MOPS (pH 7.0), 10 mM P_i, 0.1 mM P^1,P^5-di(adenosine-5′)pentaphosphate (AP_5A)). ATP (Na-salt), ADP (K-salt), and AP_5A were purchased from Boehringer Mannheim (Mannheim, Germany); EGTA and MOPS were from Dojindo Laboratories (Kumamoto, Japan). Other chemicals were of reagent grade. The concentrations of free Mg^{2+}, MgATP, MgADP, P_i, and other chemicals were calculated by computer, using the published values for stability constants (Horiuti, 1986).

Tension measurement

For the experiments, a glycerinated thin bundle (~1 mm in length, ≤60 μm in diameter) was carefully stripped from a glycerinated fiber with a pair of forceps with the aid of a stereomicroscope just before use. To prepare a suitably thin bundle, dissection was carried out in glycerol solution at around −10°C (Fukuda et al., 1996). Both ends of the muscle bundle were fixed to thin tungsten wires with enamel, one of which was attached to a tension transducer (AE-801; SensoNor a.s, Holten, Norway). The muscle was then immersed in rigor solution containing 1% Triton X-100 for 20 min to remove residual portions of the membrane system. After the Triton X-100 was washed out with rigor solution, the muscle was immersed in relaxing solution. Active tension was measured by immersing the muscle bundle in activating solution, and the measurements were recorded with a pen recorder (VP-6533A; National, Tokyo). Tension was first measured in the standard solution and then, after immersion in the relaxing solution, in the assay solution. The tension was then measured again in the standard solution. The relative tension was estimated from the ratio of the tension measured in the assay solution to the average of the standard tension before and after the assay measurement. The measurement chamber used was a silicon-coated aluminum block (10 cm × 10 cm × 1 cm) with several small holes (5 mm in diameter) filled with ~0.4 ml of various solutions, designed for tension measurements (Horiuti, 1986). The muscle was immersed in the piled-up portion of the solution, such that only 1–2 s was required for transfer of the muscle from one solution to another.

Removal and reconstitution of actin filaments

Fig. 1 schematically illustrates the process of removal and reconstitution of thin filaments in a sarcomere. Cardiac muscle fibers were immersed in contracting solution containing 20 mM BDM (to suppress tension development during gelsolin treatment) and 0.3 mg/ml gelsolin at 2°C for 80 min to remove thin filaments. We confirmed that no active tension developed after the gelsolin treatment in contracting solution. Fibers were then immersed in actin-polymerizing solution (80 mM KI, 4 mM $MgCl_2$, 4 mM ATP, 4 mM EGTA, 20 mM BDM, and 20 mM K-phosphate, pH 7.0) containing 1 mg/ml purified G-actin that had been mixed just before use. The polymerizing solutions containing actin were newly prepared and exchanged every 7 min. The actin polymerizing treatment was applied for

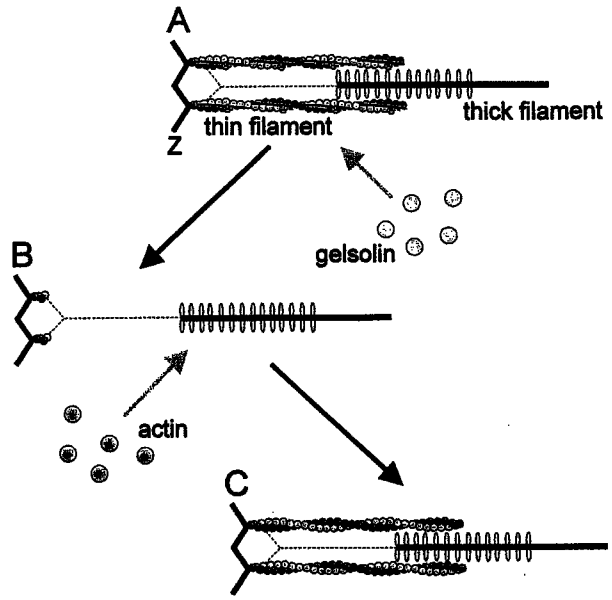

FIGURE 1 Schematic diagram illustrating how to remove and reconstitute actin filaments in a half-sarcomere of muscle fibers. Thin filaments in glycerinated cardiac muscle fibers (*A*) can be removed by gelsolin, yielding thin filament-free muscle fibers (*B*). (*C*) Actin filaments can be reconstituted by adding exogenous G-actin under polymerizing conditions. The actin filament-reconstituted fibers do not have regulatory proteins in reconstituted actin filaments and thus generate active tension in a Ca^{2+}-insensitive manner. Dotted lines schematically show connectin/titin that connects the thick filament and the Z line.

a total of 28 min (7 min × 4), shorter than the 42 min (7 min × 6) reported in our previous paper (Fujita et al., 1996), so that the average tension developed in the actin filament-reconstituted fibers was nearly equal to that in the control fibers. All procedures were carried out at 2°C. Relaxation of the actin filament-reconstituted fibers was achieved by immersing the fibers in relaxing solution containing 20 mM BDM. We confirmed that Ca^{2+} sensitivity was not observed in actin filament-reconstituted fibers.

Laser scanning confocal microscopy

Both ends of glycerinated fibers (~2 mm in length, ≤60 μm in diameter) were attached, via double-sided adhesive tape, to a glass slide so that fibers were suspended in solution without touching the glass surface. Fibers were stained with 8 μM rhodamine-phalloidin (RhPh) (Molecular Probes, Eugene, OR) in relaxing solution for 2 h at 0°C, and then free RhPh was washed out with relaxing solution. For microscopic observation, 20 mM dithiothreitol, 0.22 mg/ml glucose oxidase, 0.036 mg/ml catalase, and 4.5 mg/ml glucose were added to the solution. The preparation was observed with an inverted microscope (TMD-300; Nikon, Tokyo) equipped with a real-time confocal scanning unit (CSU10; Yokogawa Electric Co., Tokyo), and fluorescence images were recorded on a videotape recorder.

RESULTS

Effects of MgADP on isometric tension development

We first examined the effects of MgADP on the tension developed by actin filament-reconstituted cardiac muscle fibers, because SPOC observed in the absence of Ca^{2+} is a phenomenon that occurs under activation by MgADP. As

previously reported (Fukuda et al., 1996), skinned cardiac muscle fibers (control) generated isometric tension with the addition of MgADP under relaxing conditions (Fig. 2, *open circles*), suggesting that MgADP functions as an activator, probably because the AMADP (A, actin; M, myosin) complex acts as a desuppressor of the inhibitory state of thin filaments (Shimizu et al., 1992). In Ca^{2+}-activated fibers, tension augmentation up to ~20% occurred with the addition of low concentrations of MgADP (0.5–3 mM), reaching a maximum at ~1 mM (Fig. 2, *filled circles*). Active tension was decreased by further addition of MgADP up to 10 mM, and was below the original level. These results are consistent with those previously reported (Cooke and Pate, 1985; Kawai, 1986). In the actin filament-reconstituted fibers, active tension developed irrespective of the presence or absence of Ca^{2+} when MgATP was present, because of the lack of regulatory proteins. Tension augmentation was not observed in the actin filament-reconstituted fibers at low concentrations of MgADP; rather, only monotonous inhibition was observed regardless of the Ca^{2+} concentration. Active tension decreased by ~10% with the addition of 10 mM MgADP in both the presence and absence of Ca^{2+} (Fig. 2, *triangles*).

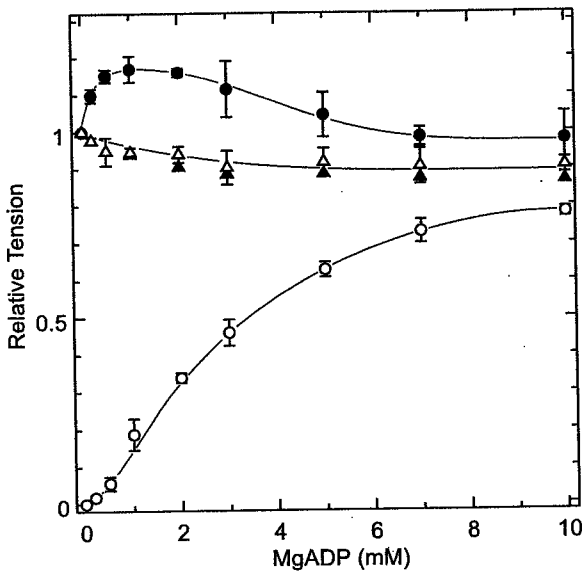

FIGURE 2 Effects of MgADP on active tension in control (○, ●) and actin filament-reconstituted (△, ▲) fibers. ●, ▲, With (pCa < 5) Ca^{2+}; ○, △, without (pCa > 8) Ca^{2+}. Active tension was measured at 20°C. Relaxation of actin filament-reconstituted fibers was obtained by the addition of 20 mM BDM. Tension was normalized to that of Ca^{2+}-activated fibers without MgADP. The ratio of the normalized tension level between control and actin filament-reconstituted fibers was nearly 1. Vertical bars show SD calculated from three to five data points. Solvent conditions: 4.25–15.6 mM $MgCl_2$ (2 mM free Mg^{2+}), 2.2 mM ATP (2 mM MgATP), 2 mM EGTA, 10 mM MOPS (pH 7.0), 0.1 mM AP_5A, ±2 mM $CaCl_2$ ($+Ca^{2+}$: pCa < 5; $-Ca^{2+}$: pCa > 8), and various MgADP concentrations (0–15.6 mM ADP). Ionic strength (I.S.) was maintained at 150 mM by the addition of KCl (61–120 mM KCl).

Effects of P_i on isometric tension in the presence of MgADP

Next we examined the effects of P_i on the isometric tension developed in the presence of 10 mM MgADP. In the control fibers, the tension was decreased by the addition of P_i and reached a plateau at ~50% of the initial tension (Fig. 3, *open circles*). SPOC was observed when more than 3 mM P_i was added, as previously reported (Fukuda et al., 1996). On the other hand, in the actin filament-reconstituted fibers, no tension decrease was observed in the 1–10 mM range of P_i (Fig. 3, *triangles*). This result was indistinguishable from that of the control fibers in the presence of Ca^{2+} (pCa < 5.0) (Fig. 3, *filled circles*). SPOC was not observed in either the actin filament-reconstituted fibers or the control fibers with Ca^{2+}.

Effects of BDM on isometric tension and SPOC

In the actin filament-reconstituted fibers, not only SPOC but also tension suppression did not occur with the addition of P_i in the presence of MgADP and MgATP. We therefore examined the inhibitory effects of BDM in combination with or instead of P_i. Fig. 4 *A* shows the effects of BDM on isometric tension in the presence of 10 mM MgADP and 10 mM P_i. In control fibers (Fig. 4 *A*, *open circles*), when BDM was added under SPOC conditions, active tension decreased in a dose-dependent manner and became undetectable in the

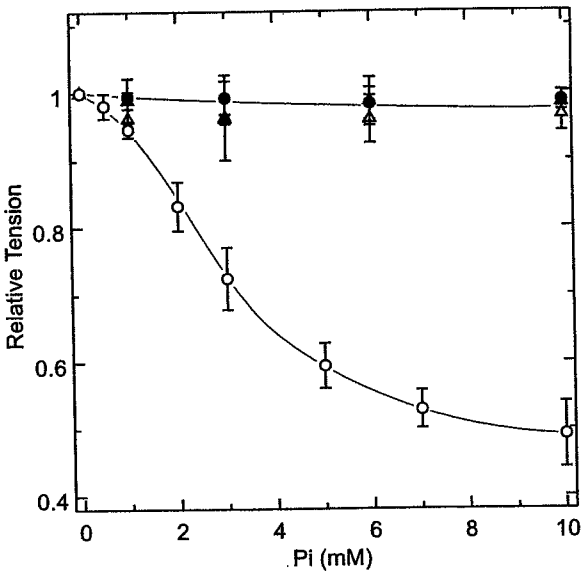

FIGURE 3 Effects of P_i on MgADP-induced tension in control (○, ●) and actin filament-reconstituted (△, ▲) fibers. ●, ▲, With (pCa < 5) Ca^{2+}; ○, △, without (pCa > 8) Ca^{2+}. Active tension was measured at 20°C. Tension was normalized to that obtained at 0 mM P_i. Vertical bars show SD calculated from three to five data points. Solvent conditions: 15.6 mM $MgCl_2$ (2 mM free Mg^{2+}), 2.2 mM ATP (2 mM MgATP), 15.6 mM ADP (10 mM MgADP), 2 mM EGTA, 10 mM MOPS (pH 7.0), 0.1 mM AP_5A, ±2 mM $CaCl_2$ ($+Ca^{2+}$: pCa < 5; $-Ca^{2+}$: pCa > 8), and various P_i concentrations. I.S. was maintained at 150 mM by the addition of KCl (38–58 mM KCl).

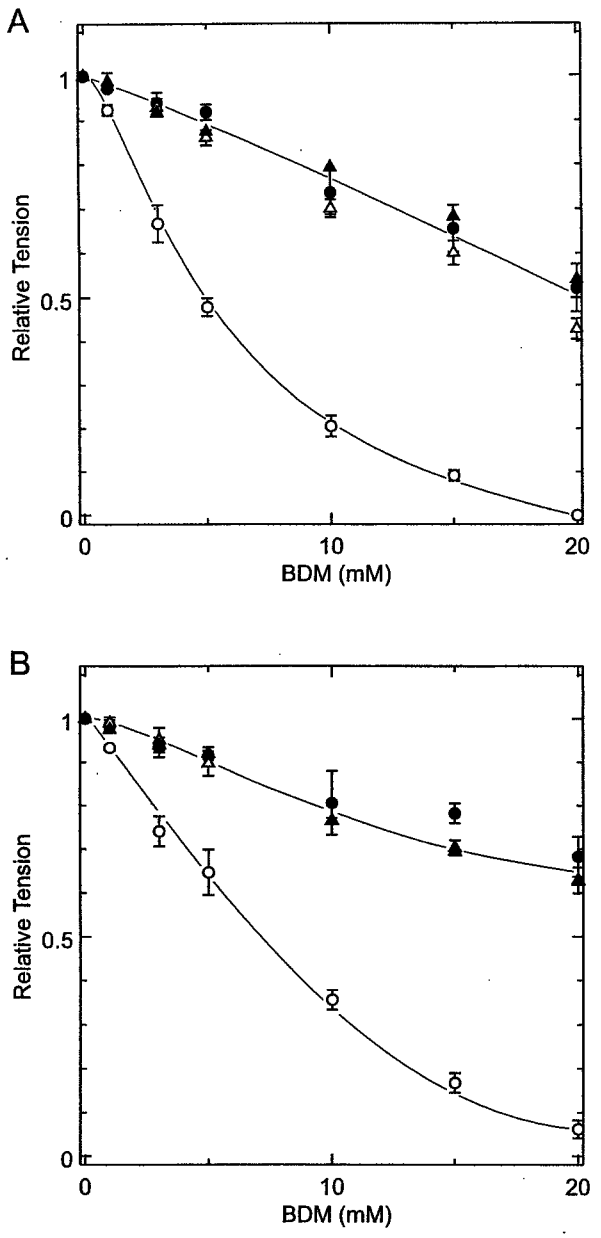

FIGURE 4 Effects of BDM on MgADP-induced tension in control (○, ●) and actin filament-reconstituted (△, ▲) fibers in the presence (*A*) and absence (*B*) of P_i. ●, ▲, With (pCa < 5) Ca^{2+}: ○, △, without (pCa > 8) Ca^{2+}. Active tension was measured at 20°C. Tension was normalized to that obtained in the absence of BDM. Vertical bars are SD calculated from three to five data points. Solvent conditions: 15.6 mM $MgCl_2$ (2 mM free Mg^{2+}), 2.2 mM ATP (2 mM MgATP), 15.6 mM ADP (10 mM MgADP), 2 mM EGTA, 10 mM MOPS (pH 7.0), 0.1 mM AP_5A, ±10 mM P_i, ±2 mM $CaCl_2$ (+Ca^{2+}: pCa < 5; -Ca^{2+}: pCa > 8), and various BDM concentrations. I.S. was maintained at 150 mM by the addition of KCl (39–61 mM KCl).

presence of 20 mM BDM; tension oscillation was observed between 0 and 10 mM BDM but, with further addition of BDM, became undetectable because of the minimal tension. In both control fibers with Ca^{2+} and actin filament-reconstituted fibers, the tension decreased with the addition of BDM, but the degree of the decrease was much smaller, only 50–60%, even at 20 mM BDM.

Surprisingly, in both the control fibers with Ca^{2+} and the actin filament-reconstituted fibers, tension oscillation occurred when 10–20 mM BDM was added. An example of recordings of this tension oscillation is shown in Fig. 5. The period of tension oscillation was ~20 s. The amplitude and frequency of oscillation were almost the same as those of SPOC observed in the control fibers without BDM, i.e., under standard SPOC conditions. These results show that SPOC occurs even without regulatory proteins when the chemical conditions are met.

Next we examined the effects of BDM on isometric tension in the presence of MgADP without P_i (Fig. 4 *B*). With the addition of BDM, MgADP-activated tension decreased monotonously, falling below 10% at 20 mM BDM in the control fibers without Ca^{2+}. In the control fibers with Ca^{2+} and the actin filament-reconstituted fibers, the tension decrease was smaller than that in the presence of P_i (Fig. 4 *A*). The degree of the tension decrease was 30–40% at 20 mM BDM. The smaller tension suppression, as compared to that in the presence of P_i, is attributable to a small population of non-force-generating complexes, such as $AMADPP_i$, stabilized by BDM (Higuchi and Takemori, 1989; Mckillop et al., 1994). When P_i was absent, tension oscillation was not observed, even when active tension was partially suppressed by BDM, indicating that the presence of P_i is essential for SPOC.

Sarcomere length oscillation inside actin filament-reconstituted fibers

To determine the sarcomere length oscillation within fibers, which is one of the characteristics of SPOC, actin filaments were stained with fluorescent rhodamine-phalloidin and observed under a laser-scanning confocal fluorescence microscope.

Fig. 6 *A* shows the internal structure of actin filament-reconstituted fibers under SPOC conditions produced by 10 mM BDM. As shown in a series of micrographs in Fig. 6 *B*, the Z lines moved back and forth, a phenomenon confirmed to last for 5–10 min. The period of this translational movement of sarcomeres was ~20 s, which is consistent with the

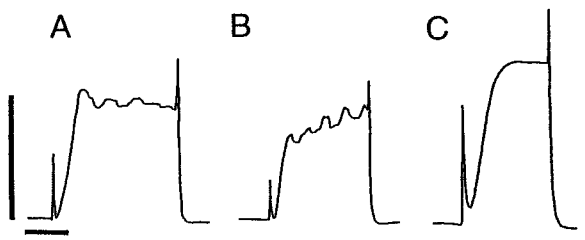

FIGURE 5 Recordings of SPOC in control (*A* and *C*) and actin filament-reconstituted (*B*) fibers. Solvent conditions: (*A*) standard SPOC solution; (*B*) standard SPOC solution with 10 mM BDM; (*C*) standard SPOC solution without 10 mM P_i and with 20 mM BDM. Vertical and horizontal bars indicate 5 × 10^{-5} N and 30 s, respectively.

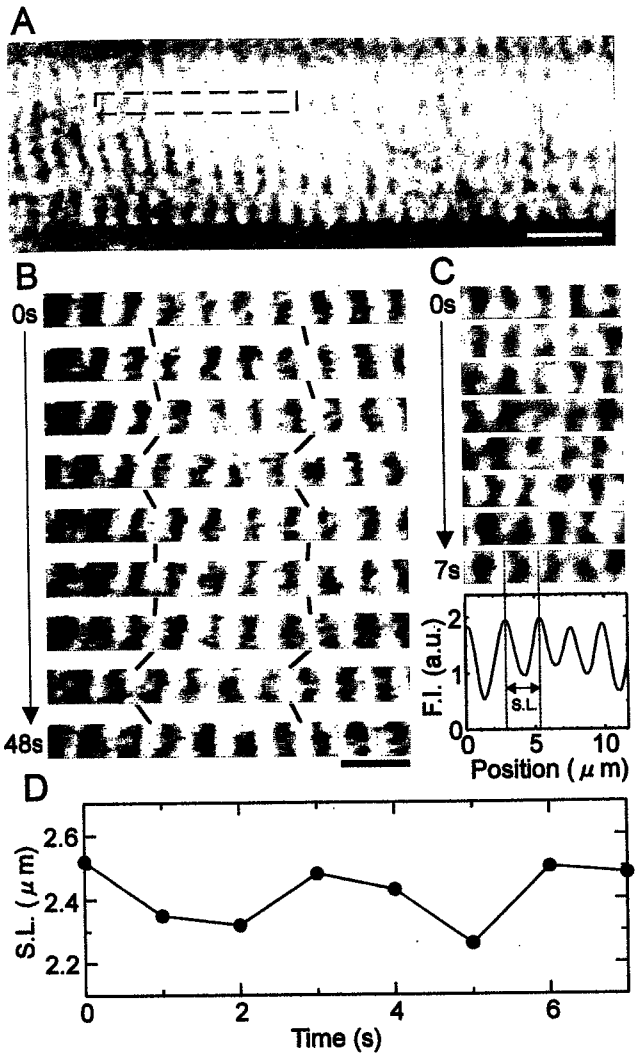

FIGURE 6 Confocal fluorescence image of actin filament-reconstituted fibers stained with rhodamine-phalloidin under SPOC conditions. (*A*) Micrograph of the internal structure of actin filament-reconstituted fibers in standard SPOC solution with 10 mM BDM. The width and thickness of the fibers were ~40 μm and 30 μm, respectively. White scale bar, 10 μm. (*B*) Series of micrographs taken every 6 s of the sarcomeres located in the box surrounded by dashed lines in *A*. The centers of the I-Z-I brushes corresponding to the Z lines are connected by thin lines, allowing observation of the translational movement of sarcomeres. Black scale bar, 5 μm. (*C*) Series of micrographs taken every second, arbitrarily chosen within the box of *A*. *Bottom*: Fluorescence intensity (F.I.) profile of sarcomeres. (*D*) Time course of length change of one sarcomere; the sarcomere length (S.L.) was measured from the separation between two adjacent peaks of the F.I. profile shown in *C*.

period of tension oscillation in fibers. On the other hand, each sarcomere length oscillated in shorter periods (~3 s), as shown in Fig. 6, *C* and *D*, consistent with the period of sarcomere length oscillation observed in myofibrils under standard SPOC conditions. We confirmed that neither periodic translational movement of sarcomeres nor sarcomere length oscillation was observed under either relaxing or contracting conditions (data not shown).

DISCUSSION

Effects of MgADP and P_i

In control fibers, tension augmentation of up to ~20% occurred with the addition of MgADP (Fig. 2). This tension augmentation can be explained as follows. In the control fibers, Ca^{2+} binding is not adequate to fully desuppress the inhibitory function of the regulatory system; desuppression due to strong binding of the AMADP complex is also required to attain full activation of the thin filaments. The decrease in active tension with further addition of MgADP is attributable to competitive binding of MgADP to the MgATP binding site (Shimizu et al., 1992; Seow and Ford, 1997). The above interpretation is supported by the present observation that only a monotonous decrease, without augmentation of tension by MgADP, was observed in the actin filament-reconstituted fibers (Fig. 2); actin filaments without regulatory proteins are considered to be in a fully activated state under the conditions we examined. This is consistent with the previous result that the active tension of the actin filament-reconstituted fibers decreased to some extent (~20%) after the incorporation of regulatory proteins (Figure 8 *a* in Fujita et al., 1996, the vertical scale in which should read "5×10^{-5} N"). These results are also consistent with the binding of myosin subfragment 1 (S1) with the reconstituted F-actin-tropomyosin-troponin complex (Green and Eisenberg, 1980) or thin filaments in myofibrils (Swartz et al., 1996), in the absence of ATP, being cooperative even in the presence of Ca^{2+}. That is, the apparent binding constant increases sigmoidally with the addition of S1, which indicates that the thin filaments are not in a fully activated state, even in the presence of Ca^{2+}.

The tension decrease in response to P_i (Fig. 3), observed in MgADP-activated control fibers (-Ca^{2+}), can be interpreted based on the kinetic scheme of actomyosin ATPase. In the MgADP-activated fibers (-Ca^{2+}), thin filaments are considered to be activated by the AMADP (strong-binding) complex formed by the association of MgADP with the AM complex. When P_i is added, the population of AMADPP_i complexes increases, whereas that of AMADP complexes decreases, resulting in the deactivation of thin filaments. In the presence of both MgADP and Ca^{2+} in the actin filament-reconstituted fibers, P_i did not act as a deactivator, probably because the AMADP complex described above is not the main factor in activation.

Effects of BDM

Although the inhibitory effects of P_i and BDM on tension development are apparently similar and additive, significant differences exist between the effects of these two substances: 1) P_i is essential for SPOC, whereas the role of BDM in SPOC can be played by the tropomyosin-troponin complex (-Ca^{2+}). 2) The inhibitory effects of BDM (Fig. 4 *B*) on tension development with MgADP of both control fibers and actin filament-reconstituted fibers are larger than

those of P_i (Fig. 3). Furthermore, under normal activating conditions without MgADP, BDM can completely relax the fibers, whereas P_i cannot. These differences between the actions of P_i and BDM in the SPOC mechanism and tension development can be explained as follows. If the $AMADPP_i$ complex is composed of at least two isoforms as previously reported (Dantzig et al., 1992), i.e., non-force-generating ($AMADPP_i(I)$) and force-generating ($AMADPP_i(II)$), P_i must attach to the second isoform, whereas BDM may stabilize the first so as to relax the muscle. Thus the minimum requirements for SPOC, which we previously proposed (Ishiwata et al., 1993; Ishiwata and Yasuda, 1993), that a weak binding (non-force-generating) actomyosin complex (e.g., $AMADPP_i(I)$) and a strong binding (force-generating) actomyosin complex (e.g., AMADP and $AMADPP_i(II)$) coexist over a certain threshold proportion, may be met by the addition of BDM. This explanation is consistent with the idea that the relaxing mechanism of BDM is similar to that of the tropomyosin-troponin complex ($-Ca^{2+}$). The possibility remains that the binding sites of P_i essential for SPOC are not only on myosin catalytic sites, but also on actin nucleotide binding sites. This awaits investigation.

Period of tension and sarcomere length oscillation in SPOC

The period of tension oscillation of actin filament-reconstituted fibers under SPOC conditions with BDM, 10–20 s (Fig. 5 *B*), was consistent with that of control fibers under standard SPOC conditions (~10 s for skeletal muscle: see Shimizu et al., 1992; 10–20 s for cardiac muscle: see Fukuda et al., 1996). On the other hand, the average period of sarcomere length oscillation observed under a confocal fluorescence microscope was much shorter than that of tension oscillation, i.e., 3–4 s, as observed in Fig. 6, *C* and *D*. Such a short period of sarcomere length oscillation is consistent with the period of oscillations of sarcomere length and tension observed in single (or a thin bundle of) myofibrils under a microscope, which is 1–7 s (for skeletal muscle, see Okamura and Ishiwata, 1988; Yasuda et al., 1996; for cardiac muscle, see Fabiato and Fabiato, 1978; Linke et al., 1993).

As for the apparent discrepancy between the long period of tension oscillation in muscle fibers and the short period of sarcomere length oscillation, we suggested in the previous paper (Fukuda et al., 1996) that the long period of tension oscillation may be the effect of interference of a number of oscillations with different periods of sarcomere length oscillation. In fact, a domain consisting of hundreds of sarcomeres showed a translational movement with a period of ~20 s (see the movement of connected thin lines in Fig. 6 *B*). Such a long period of movement of large domains in the fibers coincides with a long period of tension oscillation of fibers. On the other hand, the waveform of sarcomere length oscillation (Fig. 6 *D*) was not so regular as observed in myofibrils, in which the distinct sawtooth waveform of each sarcomere length oscillation was usually observed. We confirmed that the above properties were also the case for control cardiac fibers under standard SPOC conditions (data not shown). Thus the SPOC observed in the actin filament-reconstituted fibers in the presence of BDM was indistinguishable from that observed in the control fibers under standard SPOC conditions.

CONCLUSIONS

We have shown that SPOC occurs even in fibers without regulatory proteins, i.e., tropomyosin-troponin complexes, when the chemical requirements are met, indicating that SPOC is a phenomenon that is inherent to the actomyosin motor itself. In this respect, Jülicher and Prost (1997) showed theoretically that spontaneous oscillation, the waveform of which is similar to that of SPOC, can occur in a system of collective molecular motors elastically coupled to each other, in which regulatory mechanisms are not taken into account. The present results and these theoretical considerations strongly suggest that molecular motor itself (or its assembly) possesses autooscillatory properties, such that SPOC may occur in an in vitro motility assay system consisting of molecular motors and pure actin filaments when an external load is imposed under appropriate conditions.

This research was partly supported by Grants-in-Aid for Scientific Research, for Scientific Research on Priority Areas and for the High-Tech Research Center Project from the Ministry of Education, Science, Sports, and Culture of Japan, and by Grants-in-Aid from CREST. HF is the recipient of a Research Fellowship from the Japan Society for the Promotion of Science for Young Scientists.

REFERENCES

Anazawa, T., K. Yasuda, and S. Ishiwata. 1992. Spontaneous oscillation of tension and sarcomere length in skeletal myofibrils. Microscopic measurement and analysis. *Biophys. J.* 61:1099–1108.

Cooke, R., and E. Pate. 1985. The effects of ADP and phosphate on the contraction of muscle fibers. *Biophys. J.* 48:789–798.

Dantzig, J. A., Y. E. Goldman, N. C. Millar, J. Lacktis, and E. Homsher. 1992. Reversal of the cross-bridge force-generating transition by photogeneration of phosphate in rabbit psoas muscle fibres. *J. Physiol. (Lond.).* 451:247–278.

Ebashi, S., and M. Endo. 1968. Calcium ions and muscle contraction. *Prog. Biophys. Mol. Biol.* 18:123–183.

Fabiato, A., and F. Fabiato. 1978. Myofilament-generated tension oscillation during partial calcium activation and activation dependence of the sarcomere length-tension relation of skeletal cardiac cells. *J. Gen. Physiol.* 72:667–699.

Fujita, H., K. Yasuda, S. Niitsu, T. Funatsu, and S. Ishiwata. 1996. Structural and functional reconstitution of thin filaments in the contractile apparatus of cardiac muscle. *Biophys. J.* 71:2307–2318.

Fukuda, N., H. Fujita, T. Fujita, and S. Ishiwata. 1996. Spontaneous tension oscillation in skinned bovine cardiac muscle. *Pflügers Arch.* 433:1–8.

Funatsu, T., H. Higuchi, and S. Ishiwata. 1990. Elastic filaments in skeletal muscle revealed by selective removal of thin filaments with plasma gelsolin. *J. Cell Biol.* 110:53–62.

Funatsu, T., E. Kono, H. Higuchi, S. Kimura, S. Ishiwata, T. Yoshioka, K. Maruyama, and S. Tsukita. 1993. Elastic filaments in situ in cardiac

muscle: deep-etch replica analysis in combination with selective removal of actin and myosin filaments. *J. Cell Biol.* 120:711–724.

Greene, L. E., and E. Eisenberg. 1980. Cooperative binding of myosin subfragment-1 to the actin-troponin-tropomyosin complex. *Proc. Natl. Acad. Sci. USA.* 77:2616–2620.

Higuchi, H., and S. Takemori. 1989. Butanedione monoxime suppresses contraction and ATPase activity of rabbit skeletal muscle. *J. Biochem.* 105:638–643.

Horiuti, K. 1986. Some properties of the contractile system and sarcoplasmic reticulum of skinned slow fibers from *Xenopus* muscle. *J. Physiol. (Lond.).* 373:1–23.

Horiuti, K., H. Higuchi, Y. Umazume, M. Konishi, O. Okazaki, and S. Kurihara. 1988. Mechanism of action of 2,3-butanedione 2-monoxime on contraction of frog skeletal muscle. *J. Muscle Res. Cell Motil.* 9:156–164.

Ishiwata, S., and K. Yasuda. 1993. Mechano-chemical coupling in spontaneous oscillatory contraction of muscle. *Phase Transitions.* 45: 105–136.

Ishiwata, S., N. Okamura, H. Shimizu, T. Anazawa, and K. Yasuda. 1991. Spontaneous oscillatory contraction (SPOC) of sarcomeres in skeletal muscle. *Adv. Biophys.* 27:227–235.

Ishiwata, S., T. Anazawa, T. Fujita, T. Fukuda, H. Shimizu, and K. Yasuda. 1993. Spontaneous tension oscillation (SPOC) of muscle fibers and myofibrils. Minimum requirements for SPOC. *In* Mechanism of Myofilament Sliding in Muscle Contraction. H. Sugi and G. Pollack, editors. Plenum, London. 545–556.

Iwazumi, T., and G. H. Pollack. 1981. The effect of sarcomere nonuniformity on the sarcomere length-tension relationship of skinned fibers. *J. Cell. Physiol.* 106:321–337.

Jülicher, F., and J. Prost. 1997. Spontaneous oscillations of collective molecular motors. *Phys. Rev. Lett.* 78:4510–4513.

Kawai, M. 1986. The role of orthophosphate in cross-bridge kinetics in chemically skinned rabbit psoas fibres as detected with sinusoidal and step length alterations. *J. Muscle Res. Cell Motil.* 7:421–434.

Kondo, H., and S. Ishiwata. 1976. Uni-directional growth of F-actin. *J. Biochem.* 79:159–171.

Kurokawa, H., W. Fujii, K. Ohmi, T. Sakurai, and Y. Nonomura. 1990. Simple and rapid purification of brevin. *Biochem. Biophys. Res. Commun.* 168:451–457.

Linke, W. A., M. L. Bartoo, and G. H. Pollack. 1993. Spontaneous sarcomeric oscillations at intermediate activation levels in skinned isolated cardiac myofibrils. *Circ. Res.* 73:724–734.

Li, T., N. Sperelakis, R. E. Teneick, and J. Solaro. 1985. Effects of diacetyl monoxime on cardiac excitation-contraction coupling. *J. Pharmacol. Exp. Ther.* 232:688–695.

Mckillop, D. F. A., N. S. Fortune, K. W. Ranatunga, and M. A. Geeves. 1994. The influence of 2,3-butanedione 2-monoxime (BDM) on the interaction between actin and myosin in solution and in skinned muscle fibers. *J. Muscle Res. Cell Motil.* 15:309–318.

Okamura, N., and S. Ishiwata. 1988. Spontaneous oscillatory contraction of sarcomeres in skeletal myofibrils. *J. Muscle Res. Cell Motil.* 9:111–119.

Seow, C. Y., and L. E. Ford. 1997. Exchange of ATP for ADP on high-force cross-bridges of skinned rabbit muscle fibers. *Biophys. J.* 72:2719–2735.

Shimizu, H., T. Fujita, and S. Ishiwata. 1992. Regulation of tension development by MgADP and P_i without Ca^{2+}. Role in spontaneous tension oscillation of skeletal muscle. *Biophys. J.* 61:1087–1098.

Spudich, J. A., and S. Watt. 1971. The regulation of rabbit skeletal muscle contraction. I. Biochemical studies of the interaction of the tropomyosin-troponin complex with actin and the proteolytic fragments of myosin. *J. Biol. Chem.* 246:4866–4871.

Stephenson, D. G., and D. A. Williams. 1981. Calcium-activated force response in fast- and slow-twitch skinned muscle fibres of the rat at different temperatures. *J. Physiol. (Lond.).* 317:281–317.

Swartz, D. R., R. L. Moss, and M. L. Greaser. 1996. Calcium alone does not fully activate the thin filament for S1 binding to rigor myofibrils. *Biophys. J.* 71:1891–1904.

Sweitzer, N. K., and R. L. Moss. 1990. The effect of altered temperature on Ca^{2+}-sensitive force in permeabilized myocardium and skeletal muscle. *J. Gen. Physiol.* 96:1221–1245.

Weber, A., and J. M. Murray. 1973. Molecular control mechanisms in muscle contraction. *Physiol. Rev.* 53:612–673.

Yasuda, K., T. Anazawa, and S. Ishiwata. 1995. Microscopic analysis of the elastic properties of nebulin in skeletal myofibrils. *Biophys. J.* 68:598–608.

Yasuda, K., Y. Shindo, and S. Ishiwata. 1996. Synchronous behavior of spontaneous oscillations of sarcomeres in skeletal myofibrils under isotonic conditions. *Biophys. J.* 70:1823–1829.

Journal of Muscle Research and Cell Motility **19**, 909–921 (1998)

Regulatory roles of MgADP and calcium in tension development of skinned cardiac muscle

NORIO FUKUDA[1], HIDEAKI FUJITA[1], TAKASHI FUJITA[1] and SHIN'ICHI ISHIWATA[1,2,3,4,*]

[1] *Department of Physics, School of Science and Engineering,* [2] *Advanced Research Institute for Science and Engineering, and* [3] *Materials Research Laboratory for Bioscience and Photonics, Waseda University, 3-4-1 Okubo, Shinjuku-ku, Tokyo 169-8555, Japan*
[4] *Core Research for Evolutional Science and Technology (CREST), Genetic Programming Team 13, Kawasaki 216-0001, Japan*

Received 23 May 1998; revised 22 July 1998; accepted 23 July 1998

Summary

We investigated the regulatory roles of MgADP and free Ca^{2+} in isometric tension development in skinned bovine cardiac muscle. We found that, in the relaxed state without free Ca^{2+}, MgADP elicited a sigmoidal increase in active tension, as is the case in skeletal muscle (ADP-contraction). The critical MgADP concentration, at which the tension increment became half-maximal, increased in proportion to MgATP concentration, with a slope of approximately 1 for cardiac and 4 for skeletal muscle. Raising the free Ca^{2+} concentration decreased the critical MgADP concentration in proportion to the free Ca^{2+} concentration. In addition, the apparent Ca^{2+} sensitivity of tension development increased with MgADP, while decreasing with inorganic phosphate (Pi); MgADP suppressed the Ca^{2+}-desensitizing effect of Pi in a concentration-dependent manner. These activating effects of MgADP were quantitatively assessed by means of a model based upon the kinetic scheme of actomyosin ATPase. These experimental results and model simulation suggest that the state of thin filaments is synergistically regulated by both the binding of Ca^{2+} to troponin and the formation of the actomyosin–ADP complex.

Introduction

Muscle contraction is triggered by micromolar concentrations of free Ca^{2+} released from the inner membrane system (Ebashi & Endo, 1968). In striated muscle, Ca^{2+}-activated contraction is regulated by the thin filament proteins troponin and tropomyosin. The increased Ca^{2+} in the myoplasm binds to troponin, which leads to conformational changes amongst the regulatory proteins on thin filaments, allowing actin and myosin to interact with each other. It is also accepted that the state of thin filaments is regulated not only by the binding of Ca^{2+} to troponin (Ebashi & Endo, 1968), but also by the formation of strongly-binding cross-bridges (Bremel & Weber, 1972; Weber & Murray, 1973; Nagashima & Asakura, 1982; Lehrer & Morris, 1982; Williams *et al.*, 1988; McKillop & Geeves, 1993; Swartz *et al.*, 1996). Bremel and Weber (1972) first reported that, upon reduction in MgATP concentration, rigor cross-bridges (actomyosin linkages free of bound nucleotides) could 'turn on' adjacent actin molecules in a cooperative manner, making them receptive to myosin binding just as if Ca^{2+} were bound to troponin; this can allow neighbouring ATP-bound cross-bridges to interact cyclically with thin filaments. In addition, the Ca^{2+} sensitivity of tension is increased upon lowering the MgATP concentration in activating ($+Ca^{2+}$) solutions (Brandt *et al.*, 1972; Godt, 1974; Best *et al.*, 1977). Güth and Potter (1987) found an increase in the fluorescence of dansylaziridine-labelled troponin-C due to myosin binding to thin filaments.

We found, on the other hand, that exogenously added MgADP elicited active tension to a level nearly comparable to that brought about by Ca^{2+} in fast skeletal (rabbit psoas) muscle (Shimizu *et al.*, 1992), and increased the Ca^{2+} sensitivity of the contractile element in cardiac (bovine ventricular) muscle (Fukuda *et al.*, 1996). These results are in agreement

Abbreviations used: AP_5A, P^1,P^5-di(adenosine-5′)pentaphosphate; CP, creatine phosphate; CPK, creatine phosphokinase; IS, ionic strength; MOPS, 3-(N-morpholino)propanesulphonic acid; SPOC, spontaneous oscillatory contraction.

*To whom correspondence should be addressed at:
Department of Physics, School of Science and Engineering, Waseda University, 3-4-1 Okubo, Shinjuku-ku, Tokyo 169-8555, Japan.
E-mail: ishiwata@mn.waseda.ac.jp

0142–4319/98

with Hoar and colleagues (1987), in which they obtained substantially the same result using slow skeletal (rabbit soleus) muscle. Therefore, it is reasonable to assume that the actomyosin–ADP complex formed by exogenously added MgADP has the same function as the rigor complex in the regulation of the contractile system, and consequently influences the contractile performance of muscle.

It is well known that, under conditions of ischaemia or hypoxia, the ATP concentration decreases in cardiac cells, while ADP and inorganic phosphate (Pi) accumulate (Kammermeier *et al.*, 1982; Allen *et al.*, 1985; Kusuoka *et al.*, 1986; Allen & Orchard, 1987; Marban & Kusuoka, 1987). Pi has been reported to exert an inhibitory effect on the contractile performance of skinned cardiac muscle (Kentish, 1986; Godt & Nosek, 1989; Fukuda *et al.*, 1996), whereas, since few systematic investigations have been conducted, especially under Ca^{2+}-free conditions, the role of ADP in the cross-bridge interaction are not fully understood. It has been pointed out that, during ischaemia or hypoxia, the local MgADP concentration around cross-bridges could be markedly increased (Yamashita *et al.*, 1994), and so MgADP may have some role in modulating the cross-bridge interaction under pathological states. Therefore, it is important to investigate the effects of MgADP on the cardiac muscle contractile system.

In the present study, we systematically investigated the effects of MgADP on isometric tension development in skinned bovine cardiac muscle at various free Ca^{2+} concentrations, in order to clarify the regulatory roles of MgADP and Ca^{2+} in isometric tension development. The results showed that MgADP induces active tension despite the absence of free Ca^{2+}, with the sensitivity of MgADP relative to that of MgATP being approximately four times higher in cardiac (bovine ventricular) than in fast skeletal (rabbit psoas) muscle. MgADP markedly increases the Ca^{2+} sensitivity of myofilaments, irrespective of the presence or absence of Pi. We also attempted to elucidate the regulatory roles of MgADP and Ca^{2+} in isometric tension development using a modified version of our previous model (Ishiwata & Yasuda, 1993), which was constructed based upon the accepted kinetics of actomyosin ATPase (Goldman, 1987; Goldman & Brenner, 1987). The present model of regulation is complementary to the three state models proposed to date (e.g. Geeves, 1991; Palmer & Kentish, 1994) and an allosteric model (e.g. Lehrer & Geeves, 1998).

A preliminary report on this investigation has appeared in abstract form (Fukuda *et al.*, 1991).

Materials and methods

Solutions

The chemical compositions of solutions used in this study were as described previously (Fukuda *et al.*, 1996). The isometric tension was measured in solutions containing 1–3 mM MgATP, 0–10 mM MgADP (for cardiac muscle; 0–15 mM for skeletal muscle) and various concentrations of free Ca^{2+} (pCa = 4.7 ($+Ca^{2+}$), pCa = 5.15–6.9, and +EGTA ($-Ca^{2+}$)). The concentration of free Mg^{2+} was maintained at 2 mM. The ionic strength (*IS*) was maintained at 0.15 ± 0.01 M by adjusting the KCl concentration. The concentrations of ATP (Na-salt, Boehringer Mannheim GmbH, Mannheim, Germany), ADP (K-salt, Boehringer Mannheim GmbH), $MgCl_2$, Pi (K-salt), EGTA (Dojindo, Kumamoto, Japan) and other chemicals were calculated with a computer program using the published values for stability constants (Horiuti, 1986). The pH value for each solution was finally adjusted to 7.00 ± 0.02 with 1 M KOH or HCl in the presence of 10 mM 3-(N-morpholino)propanesulphonic acid (MOPS; Dojindo) at 25°C. To inhibit the rephosphorylation of ADP to ATP by myokinase (Lienhard & Secemski, 1973), 0.1 mM P^1,P^5-di(adenosine-5')pentaphosphate (AP_5A; Boehringer Mannheim GmbH) was added. When required, an ATP-regenerating system composed of 1.0 mg/ml^{-1} creatine phosphokinase (CPK; Sigma Chem. Co., St Louis, MO, USA) and 10 mM creatine phosphate (CP; Boehringer Mannheim GmbH) was used. We used the following rigor and relaxing solutions: rigor, 1 mM EGTA, 5 mM $MgCl_2$, 10 mM MOPS (pH 7.0), 120 mM KCl; high (or low)-EGTA relaxing solutions, 4 (or 0.4) mM EGTA, 3.8 mM ATP (MgATP = 3.0 mM), 3.9 mM $MgCl_2$ (free Mg^{2+} = 0.9 mM), 120 mM KCl. All chemicals were of reagent grade.

Preparation of skinned muscle

Skinned cardiac muscle (left ventricular papillary muscle of bovine heart) was prepared according to a previously reported procedure (Fukuda *et al.*, 1996). Briefly, a glycerinated bundle (40–80 μm wide, 20–40 μm thick and 1.5 mm long) was carefully stripped off just before use; we took special care to make the bundle as thin as possible, because the higher the ATPase activity and the thicker the bundle, the greater the possibility of ATP depletion while ADP and Pi accumulate inside the muscle (Cooke & Pate, 1985; Shimizu *et al.*, 1992). To prepare a suitably thin bundle of glycerinated cardiac muscle, the dissection was done with the preparation in glycerol solution below 0°C, at approximately −10°C (Fukuda *et al.*, 1996).

Single glycerinated skeletal muscle fibres were prepared from rabbit psoas muscle according to a previously described procedure (Shimizu *et al.*, 1992).

Measurement of tension development

Tension development was measured according to a previously described protocol (Fukuda *et al.*, 1996). In brief, both ends of the muscle bundle (or the single muscle fibre) were attached to thin tungsten wires, one of which was connected to a tension transducer (AE-801, SensoNor a.s, Holten, Norway) and the other to a micromanipulator (Narishige, Tokyo, Japan) with enamel. After removal of the glycerol, the residual portion of the membrane system was removed in rigor solution containing 0.3% (v/v) Triton X-100 for 90 s. After the muscle had been washed with rigor solution, it was immersed in a high-EGTA relaxing solution, in which the muscle length was adjusted to a sarcomere length of

approximately 2.0 μm. Then, the muscle was transferred to a low-EGTA relaxing solution; the EGTA concentration was set low enough that the muscle responded rapidly to activating conditions. All procedures were done at room temperature (25°C).

The tension measurement was initiated by immersing the muscle bundle (fibre), prepared as described above, in an appropriate activating solution. The relative tension was estimated from the ratio of the tension developed in an assay solution to the average of those obtained under standard solvent conditions (see figure legends) before and after the assay measurement. The data were used only when the ratio of the tension after to that before the assay measurement exceeded 85%, and the final tension measured in the standard solution was more than 70% of the initial tension. One to four data points were obtained from each bundle (fibre).

The measurement chamber used was a silicon-coated aluminium block (10 cm × 10 cm × 1 cm), with several small holes filled with 0.4 ml of various solutions (Horiuti, 1986). The solution was stirred vigorously with a spherical, Teflon-coated magnetic stirrer 3 mm in diameter. The chamber temperature was maintained at 25.0 ± 0.2°C.

Model explaining the effects of MgADP and Ca^{2+} on tension development

The effects of MgADP and Ca^{2+} on tension development were analysed based upon a kinetic model of actomyosin ATPase (Fig. 1; Goldman, 1987; Goldman & Brenner, 1987). We adopted a modified version of a previously proposed model (Ishiwata & Yasuda, 1993), in which regulation occurs not only at the attachment step of actin (A) and myosin–ADP–Pi (MADPPi) complex, but also at the Pi-release step of the actomyosin–ADP–Pi complex (AMADPPi). In Fig. 1, AM1ADP is a species that contributes to isometric tension (F) and AM2ADP is an isomer of AM1ADP. Both AM2ADP and AM (rigor complex) may also contribute to tension development, but their contributions are ignored in the present simulation, mainly because, even if we take into account the contribution of these species as being 20% of that of AM1ADP, the extent of the increase in isometric tension was only a few per cent within the concentration range of MgADP examined. (The contribution of AM to tension must be taken into account at low concentrations of ATP.) Specifically, we assumed that:

(1) the transition of thin filaments from the *off* state to the *intermediate* state occurs not only by the binding of Ca^{2+} to troponin, but also by the formation of AM2ADP, such that the proportion of *intermediate*-state thin filaments, [A*], is determined according to the Hill equation (or a simple absorption equation when the Hill coefficient is 1) for the concentration of free Ca^{2+} ([Ca]) and the proportion of AM2ADP ([AM2ADP]); here, the contribution of AM was negligible because the proportion of AM was quite small under the present conditions (Ishiwata & Yasuda, 1993);
(2) [A*] determines the proportion of *on*-state thin filaments, $[A_{on}]$, according to the Hill equation with a Hill coefficient larger than 1;
(3) both k_{5a}, the kinetic constant for the Pi-release step (Chalovich & Eisenberg, 1982), and k_{4+}, the kinetic constant for attachment of actin and MADPPi, are regulated by $[A_{on}]$, such that the regulatory functions of Ca^{2+} and MgADP apparently become cooperative.

In this model, the essential point is that the equilibrium at both steps is non-linearly regulated by [A*]. It is not essential that either forward or backward kinetic constant is regulated. Even if the reverse kinetic constants are assumed to be regulated by $[A_{on}]$ instead of those assumed in the present work, the experimental data must be similarly simulated. Thus, we formulated the following equations:

$$[A^*] = C \cdot [Ca]^l/([K_{Ca}]^l + [Ca]^l) + (1 - C) \cdot [AM2ADP]^m/\{[K_f]^m + [AM2ADP]^m\} \quad (1)$$

$$[A_{on}] = [A^*]^n/([K_{on}]^n + [A^*]^n) \quad (2)$$

$$k_{4+} = 10^6 \cdot [FA_0] \cdot [A_{on}] \quad (3)$$

$$k_{5a} = 40 \cdot [A_{on}] \quad (4)$$

where C is constant, l, m and n are Hill coefficients, $[FA_0]$ is an effective total concentration of actin in the contractile system, K_{Ca} is a dissociation constant for the Ca^{2+}-binding site on troponin, and K_f and K_{on} are the apparent equilibrium constants. To estimate F (i.e. [AM1ADP]), under various conditions, we calculated the proportion of each species in the kinetic model under steady-state conditions (d[**]/dt = 0, where [**] indicates the proportion of each species in Fig. 1 to the total concentration of myosin, $[M_0]$; cf. Ishiwata & Yasuda, 1993).

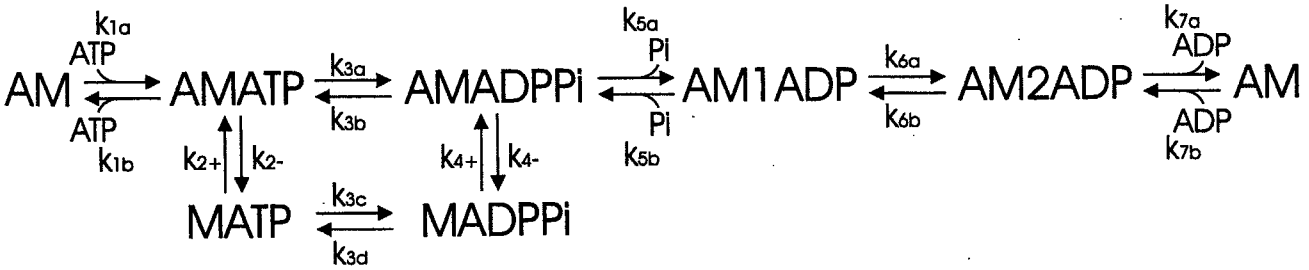

Fig. 1. Kinetic model of actomyosin (AM) ATPase adopted to analyse the experimental results of the present study. In this model, k_{5a} and k_{4+} are assumed to be regulated by the proportion of the *on* state of thin filaments ($[A_{on}]$), which depends on the concentration of free Ca^{2+} (pCa) and the proportion of AM2ADP.

Results

Effects of MgADP on isometric tension: comparison between cardiac and skeletal muscle

We examined the effects of MgADP on isometric tension development in cardiac muscle, in the presence of 2 mM MgATP and in the absence of free Ca^{2+} (+EGTA; pCa > 8), for comparison with those of skeletal muscle. As shown in Fig. 2, tension developed in a sigmoidal manner as the MgADP concentration increased (ADP-contraction) and reached approximately 70% of that obtained under normal contracting conditions in the absence of MgADP (+Ca^{2+}, data shown below). These features were qualitatively the same as those of skeletal muscle but differed quantitatively (cf. Shimizu *et al.*, 1992). In cardiac muscle, tension developed at a lower MgADP concentration than in skeletal muscle.

The critical MgADP concentration ($MgADP_{50}$) at which a 50% tension increase was attained, indicating

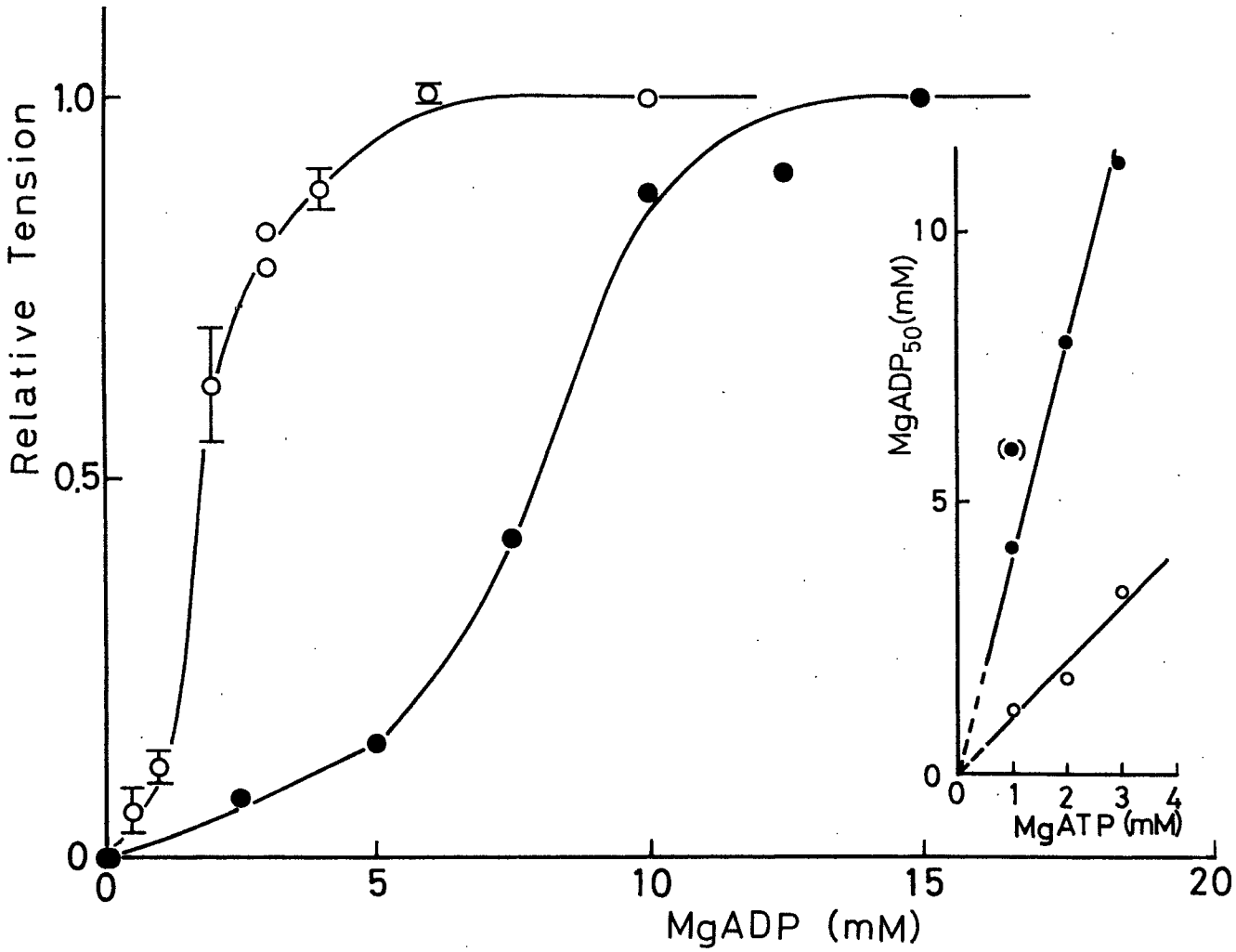

Fig. 2. Effects of MgADP on tension development in cardiac and skeletal muscle in the presence of MgATP and the absence of free Ca^{2+}. Standard solvent conditions for cardiac muscle: 61 mM KCl, 2.2 mM ATP (2.0 mM MgATP), 16.4 mM ADP (10 mM MgADP), 14.2 mM $MgCl_2$ (2 mM free Mg^{2+}), 10 mM MOPS (pH 7.0), 2 mM EGTA, 0.1 mM AP_5A and *IS* (ionic strength) of 0.15 ± 0.01 M. Standard solvent conditions for skeletal muscle: the same as those for cardiac muscle except the concentrations of added KCl, ADP and $MgCl_2$ were 30 mM, 24.5 mM (15 mM MgADP) and 19.0 mM (2 mM free Mg^{2+}) respectively. Other conditions: the same as standard conditions except that the MgADP concentration was changed so as to maintain *IS* at 0.15 ± 0.01 M. Tension was normalized with respect to that at 10 mM MgADP (standard conditions; (1–2) × 10^{-4} N) for cardiac muscle (○) or at 15 mM MgADP (standard conditions; (2–3) × 10^{-4} N) for skeletal muscle (●). For chart recordings of tension development, see Fig. 1 of Fukuda *et al.* (1996) for cardiac muscle, and Fig. 3 of Shimizu *et al.* (1992) for skeletal muscle. Vertical bars: SD for 3 to 7 data points obtained at each concentration of MgADP. Temperature: 25 ± 0.2°C. Insert: relationship between the critical MgADP concentration ($MgADP_{50}$) that produced half-maximal tension increment, and the concentration of MgATP (○, cardiac; ●, skeletal); the closed circle in parentheses represents a previously reported data point (Shimizu *et al.*, 1992).

the apparent effectiveness of MgADP, was examined at different MgATP concentrations (1–3 mM). As summarized in the Fig. 2 insert, both cardiac and skeletal muscle showed a linear relationship between $MgADP_{50}$ and MgATP concentration. The slopes of these linear relationships differed, however, being approximately 1 and 4 for cardiac and skeletal muscle, respectively. The Hill coefficient, an indicator of cooperativity, of the relationship between tension and the MgADP concentration shown in Fig. 2 was approximately 2 for cardiac and 3 for skeletal muscle (for how to obtain the Hill coefficient, see Fukuda *et al.*, 1996).

The maximal tension obtained at 10 (or 15) mM MgADP was nearly the same at all MgATP concentrations examined in cardiac (and skeletal) muscle; this rules out the possibility that the muscles used were in rigor; had the tension developed with MgADP been ascribable to rigor tension, the maximal tension would presumably have decreased as the MgATP concentration increased.

It is noteworthy that no tension oscillations were observed under any of the conditions used, in either cardiac or skeletal muscle. This is consistent with our previous observation that tension oscillation (SPOC) occurs only when ATP coexists with ADP and Pi (Ishiwata & Yasuda, 1993; Fukuda *et al.*, 1996; Fujita & Ishiwata, 1998)

Effects of MgADP at various free Ca^{2+} concentrations

As shown in Fig. 3A, as pCa decreased to 6.0, the sigmoidal tension development curve shifted to a lower MgADP concentration. More precisely, the critical MgADP concentration ($MgADP_{50}$) for ADP-contraction decreased in proportion to the free Ca^{2+} concentration (Fig. 3B). When pCa was so low that the muscle contracted without MgADP (see upper three curves in Fig. 3A), the tension increased slightly (ca 15%) with MgADP; thereafter, a gradual decrease was seen as the MgADP concentration increased further. These potentiating effects of MgADP at low pCa were qualitatively similar to those observed in skeletal muscle (Cooke & Pate, 1985; Shimizu *et al.*, 1992).

The tension v. MgADP relationship at various free Ca^{2+} concentrations (Fig. 3A) was replotted as the tension v. pCa relationship at various MgADP concentrations. As shown in Fig. 3C, as the MgADP concentration increased, the tension–pCa curve shifted to the left (in other words, the pCa_{50} value indicated by arrowheads, i.e. the pCa at which the tension increment became half-maximal, reflecting Ca^{2+} sensitivity, was increased) and the tension level in the absence of free Ca^{2+} was increased, whereas that in the presence of free Ca^{2+} was somewhat decreased.

All experiments described thus far were performed in the absence of the ATP-regenerating system so as to maintain the ratio of the concentration of MgATP to that of MgADP. Herein, we assessed whether the ATP-regenerating system had an effect on the developed tension, in the presence of free Ca^{2+} and the absence of MgADP, but none was observed (data not shown). Moreover, we previously confirmed that MgADP at only 0.1 mM shifted the tension–pCa relationship towards higher pCa (cf. Fig. 4 in Fukuda *et al.*, 1996). These results suggest that accumulation of ADP in the centre of the muscle is minimal.

Effects of MgADP on Pi-induced changes in the tension–pCa relationship

The characteristics of Pi-induced changes in the tension–pCa relationship in the presence of MgADP clearly differed from those observed in the absence of MgADP. In the absence of MgADP (Fig. 4A), pCa_{50} (indicated by arrowheads) monotonically decreased towards lower pCa, as reported by others (e.g. Kentish, 1986); this pCa_{50} shift occurred even at 1 mM Pi, and saturation occurred at less than 10 mM Pi. However, the Ca^{2+}-desensitizing effect of Pi was markedly suppressed in the presence of 10 mM MgADP (Fig. 4B).

Figure 5 summarizes the Ca^{2+}-desensitizing effect of Pi at various concentrations of MgADP (0, 2, 4, and 10 mM). In the absence of MgADP, pCa_{50} decreased from 5.9 to 5.5 with 0–20 mM Pi; in the presence of MgADP, on the other hand, pCa_{50} increased from 5.9 to 6.1 with more than 2 mM MgADP (see Fig. 3C), showing a slight further increase with less than 2 mM Pi, and thereafter began to decrease and ultimately recovered to the initial value. A 50% recovery was attained at approximately 2, 5 and 10 mM Pi for 2, 4 and 10 mM MgADP, respectively. MgADP and Pi therefore function as a promoter and a suppressor, respectively, in modulating the Ca^{2+} sensitivity of the contractile system. These properties manifest independently when the concentration of Pi is higher than 2 mM, a condition in which MgADP and Pi compete. However, it is of interest that, at low concentrations of Pi, Ca^{2+} sensitivity was apparently increased.

Model calculation

The tension–MgADP relationship at various concentrations of free Ca^{2+}, especially the decrease in the critical MgADP concentration with an increase in the concentration of free Ca^{2+} (Fig. 3A), could be explained by means of our model assuming the multi-step regulation of the thin filaments (Fig. 6A). The agreement between the experimental data and the simulated curve was satisfactory as a whole, except in the intermediate pCa region. The disagreement may

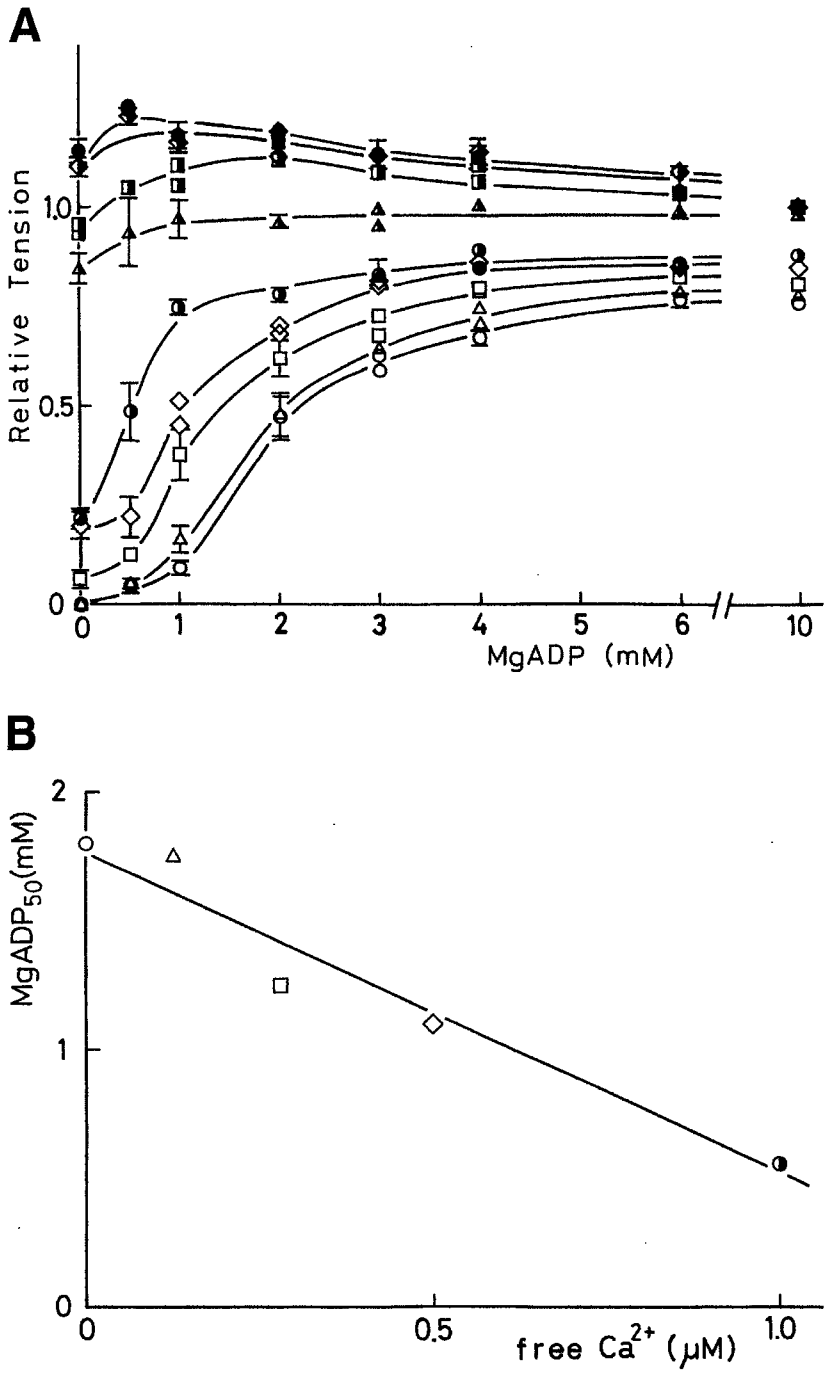

be attributable to an experimental error that occurred in a region of steep transition.

In our previous study (Ishiwata & Yasuda, 1993), we assumed that only the Pi-release step was regulated by the state of thin filaments. We found that the nearly 40% tension augmentation by Ca^{2+} at high concentrations of MgADP (Fig. 3A) could not be explained unless the two steps are assumed to be regulated by the state of thin filaments.

Next, we tried to explain the apparent differences between cardiac and skeletal muscle (Fig. 2), firstly, in the critical concentration ratio, [MgADP]/[MgATP], needed to induce ADP-contraction (Fig. 2 insert), and secondly in the Hill coefficient in the tension–MgADP relationship. The former difference seems to be explained by the difference in the binding constant of AM and MgADP; in fact, the values of $MgADP_{50}$, about 2 mM (cardiac muscle) and about 8 mM (skeletal muscle) for 2 mM MgATP, could be simulated by k_{7a} = 500 and 1500, respectively. However, the Hill coefficient for skeletal muscle was too small to simulate the data. Alternatively, we

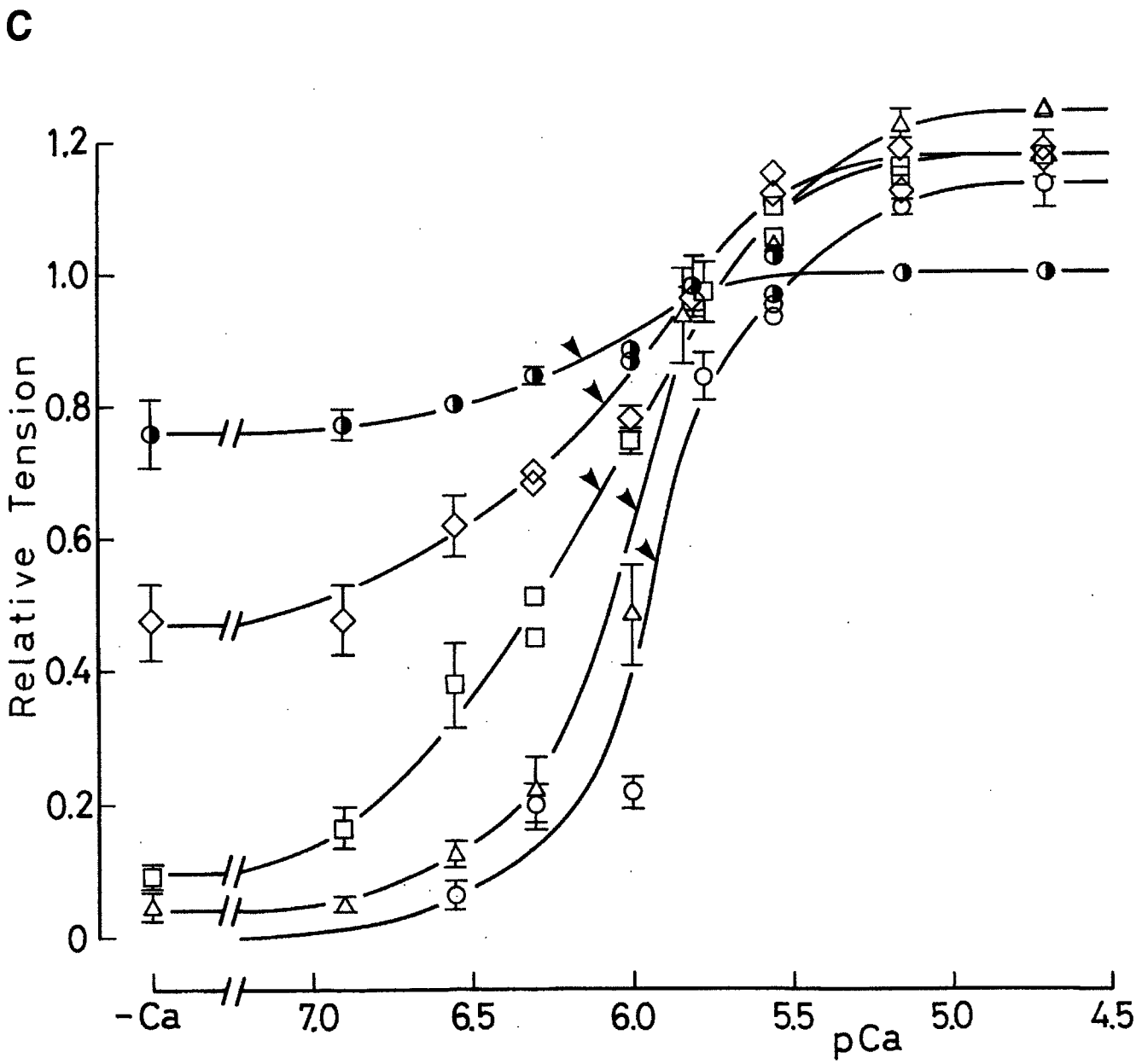

Fig. 3. Effects of MgADP on tension development in cardiac muscle under various pCa conditions. Conditions: the same as in Fig. 2 except that the free Ca^{2+} concentration was adjusted with Ca^{2+}-EGTA buffer, i.e. Ca^{2+}(0–1.9 mM)/EGTA(2.0 mM) buffer to obtain pCa > 5.15, or Ca^{2+}(3.95 mM)/EGTA(4.0 mM) buffer to obtain pCa = 4.7 (+Ca^{2+}) in 2.2 mM ATP (2.0 mM MgATP), 0–16.4 mM ADP (0–10 mM MgADP), 2 mM free Mg^{2+}, 10 mM MOPS (pH 7.0) and 0.1 mM AP_5A, and *IS* was maintained by addition of KCl at 0.15 ± 0.01 M. (A) Relative tension v. MgADP concentration (○, –Ca^{2+}, as in Fig. 2; pCa = 6.9 (△), 6.55 (□), 6.3 (◇), 6.0 (◑), 5.8 (◭), 5.55 (◧) and 5.15 (◈); ●, +Ca^{2+}). (B) The critical MgADP concentration ($MgADP_{50}$) that produced a half-maximal increment in tension (ordinate) at each free Ca^{2+} concentration (abscissa) obtained from (A) (symbols the same as in A). (C) Relative tension v. pCa relation at various MgADP concentrations (replot of A; MgADP (mM), 0 (○), 0.5 (△), 1 (□), 2 (◇) and 10 (◑)). Tension was normalized with respect to that at 10 mM MgADP and +Ca^{2+} (standard condition). Arrowheads indicate pCa_{50}, i.e., pCa at which the tension increment becomes half-maximal. Vertical bars: SD for 3 to 10 data points.

examined whether these differences could be explained by the difference in the values of m and/or n without changing the binding constant. However, the resultant curves were too steep to simulate the data. Thus, we finally found that, as shown in the dotted and dashed curves in Fig. 6B, both the increase in the value of k_{7a} from 500 to 1000 and the increase in the value of m from 1 to 2 were best for explaining the higher $MgADP_{50}$ and Hill coefficient for skeletal muscle.

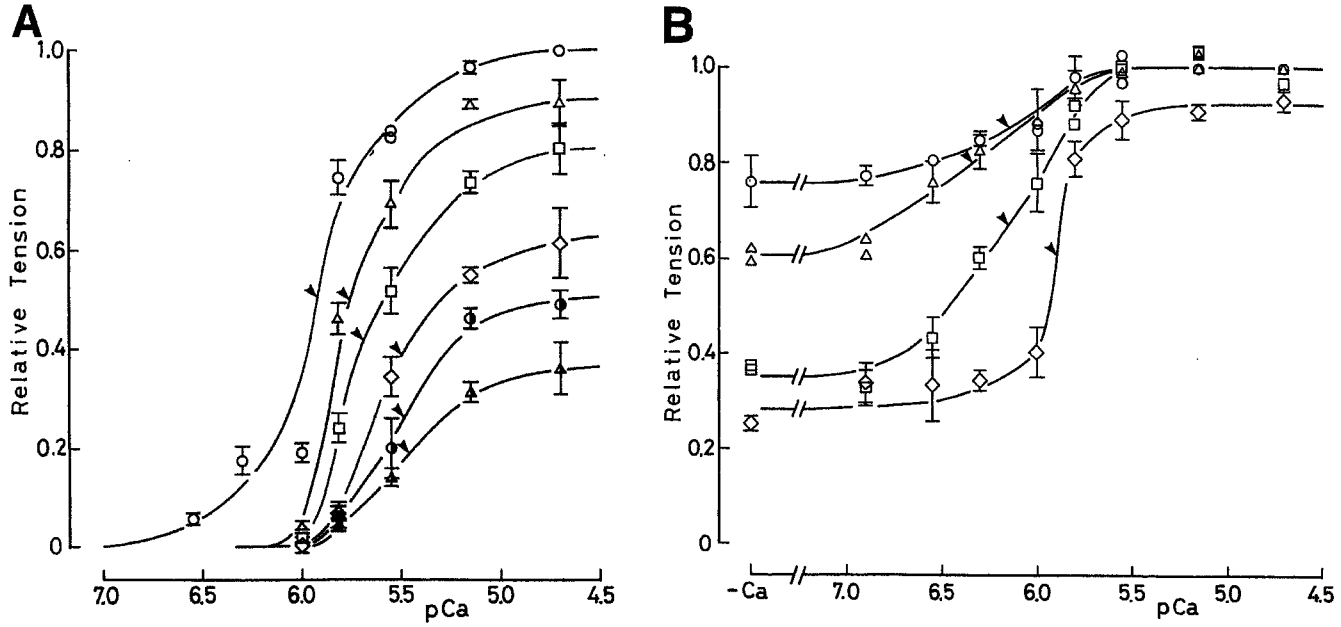

Fig. 4. Effects of Pi on tension v. pCa relationship in the absence (A) and presence (B) of 10 mM MgADP. Conditions: the same as in Fig. 2 except that the free Ca^{2+} concentration was adjusted with Ca^{2+}-EGTA buffer, i.e. Ca^{2+}(0–1.9 mM)/EGTA(2.0 mM) buffer to obtain pCa > 5.15 or Ca^{2+}(3.95 mM)/EGTA(4.0 mM) buffer to obtain pCa = 4.7 (+Ca^{2+}) in 2.2 mM ATP (2.0 mM MgATP), 0 mM (A) or 16.4 mM (B) ADP (10 mM MgADP), 2 mM free Mg^{2+}, 10 mM MOPS (pH 7.0), 0–20 mM Pi and 0.1 mM AP_5A, and *IS* was maintained by addition of KCl at 0.15 ± 0.01 M. Symbols in (A): ○, –Pi (the same data as circles in Fig. 3C); △, □, ◇, ◑ and ◭, 1, 2, 5, 10 and 20 mM Pi, respectively. Note that no ATP-regenerating system was present. Symbols in (B): ○, –Pi (the same data as half-filled circles in Fig. 3C); △, □ and ◇, 2, 10 and 20 mM Pi, respectively. For both A and B, tension was normalized with respect to that at –Pi and +Ca^{2+} (standard conditions). The arrowheads indicate pCa_{50}, i.e. the pCa at which the tension increment becomes half-maximal. Vertical bars: SD for 3 to 10 data points.

In the present simulation, we tried to achieve a significant figure of the kinetic constants of usually one digit and at most two digits; also, we tried to find out the best-fit values of the Hill coefficient among integers. Therefore, the set of values of kinetic constants and the Hill coefficients we present here may not be the best, although they are good enough to explain the experimental data.

Discussion

Activating effect of MgADP in absence of free Ca^{2+}

We found that, albeit in the absence of free Ca^{2+}, the isometric tension of skinned cardiac muscle increased along a sigmoidal curve as the MgADP concentration increased (Fig. 2); this phenomenon was designated ADP contraction (Shimizu *et al.*, 1992). For ADP-contraction to occur, it is not the MgADP concentration itself but the ratio of the MgADP concentration to the MgATP concentration that is essential for generating tension (Fig. 2 insert). The linear relationship shown in Fig. 2 (insert) suggests that exogenously added MgADP competes for MgATP-binding sites on the myosin molecule (Seow & Ford, 1997). In a previous study using skeletal muscle, we interpreted the activating effect of MgADP as being due to the positive feedback effect of the actomyosin–ADP (AMADP) complex on the Pi-release step of the cross-bridge cycle (Shimizu *et al.*, 1992). The results shown in Fig. 2 strongly suggest that a similar mechanism operates in the contractile system of cardiac muscle. However, cardiac muscle apparently has a higher affinity for MgADP than skeletal muscle.

The binding affinity of MgADP to myofibrils (Johnson & Adams, 1984) or actomyosin-S1 (Siemankowski & White, 1984) is reportedly approximately ten times higher in bovine cardiac than in rabbit skeletal muscle. In the present study, we found the ratios of the critical MgADP concentration to the MgATP concentration to be approximately 1 and 4 for cardiac and skeletal muscle, respectively. This may simply reflect the aforementioned results (Johnson & Adams, 1984; Siemankowski & White, 1984). However, our model calculation, in which the cooperativity of the cardiac muscle thin filament was assumed to be lower than that of skeletal muscle, suggests that the apparent difference in MgADP affinity between cardiac and skeletal muscle must be partly attributable to a difference in the cooperativity of the thin filament. It has, in fact, been reported that thin filament activation by Ca^{2+} is less cooperative in

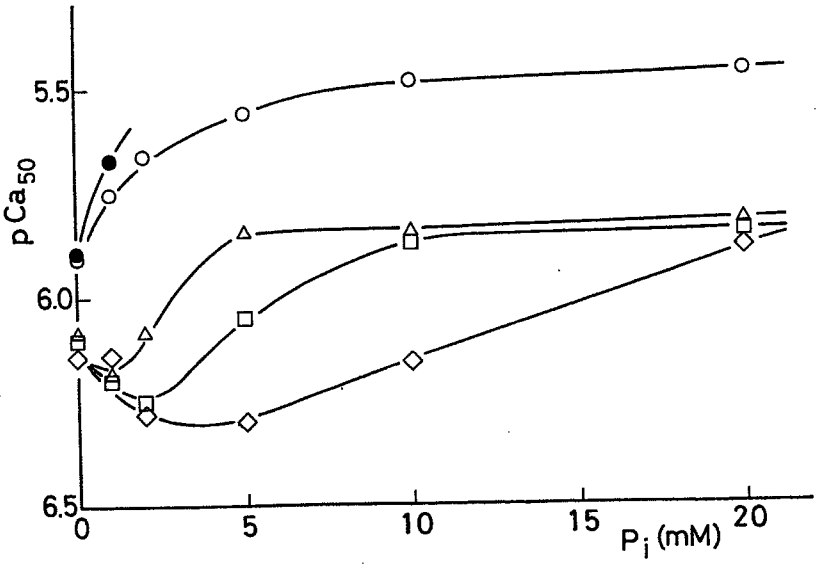

Fig. 5. Effects of MgADP on the Ca^{2+}-desensitizing effect of Pi. The value of pCa at which the tension increment became half-maximal (pCa_{50}) was obtained at each Pi concentration in the absence of MgADP (○; cf. Fig. 4A) and in the presence of 2 (△), 4 (□) and 10 (◇; cf. Fig. 4B) mM MgADP. Tension v. pCa relationships for 2 and 4 mM MgADP similar to those in Fig. 4 were obtained, but are not shown. ●, a previously reported data point in the presence of the ATP-regenerating system (Fukuda *et al.*, 1996).

cardiac than in skeletal muscle, probably because the number of Ca^{2+} binding sites of cardiac troponin-C is smaller than that of skeletal troponin-C (Sweitzer & Moss, 1990; Fukuda *et al.*, 1996); therefore, thin filament cooperativity may play an important role in determining the *apparent* MgADP affinity observed in the tension–MgADP relationship.

Metzger (1995) examined the tension–pMgATP relationship at low concentrations of MgATP in cardiac and skeletal muscle and reported that: (1) the rigor tension in the absence of free Ca^{2+} was generated at a lower concentration of MgATP in cardiac muscle than in skeletal muscle, suggesting that the binding affinity of MgATP for cardiac muscle is higher than that for skeletal muscle; and (2) the cooperativity of rigor tension development was apparently higher for cardiac muscle than for skeletal muscle. The former property is similar to that of MgADP mentioned above, whereas the latter appears to be the opposite to that observed in the tension development with either Ca^{2+} or MgADP.

In the present model simulation, we could simulate the difference of the tension–MgADP relationship between cardiac and skeletal muscle (Fig. 6B) by assuming that the binding constant of MgADP for cardiac actomyosin is twice that for skeletal actomyosin, while maintaining the same value for the binding constant of MgATP. If we take into account the above result, that the binding constant of MgATP for cardiac actomyosin is about three times that for skeletal actomyosin (Metzger, 1995), we must accordingly make the binding constant of MgADP $2 \times 3 = 6$ times larger to simulate the ratio of the *apparent* binding constant of MgADP to that of MgATP. Such a modification in our present simulation model may be able to explain the large difference in the binding constant for MgADP between cardiac and skeletal muscle reported previously (Johnson & Adams, 1984; Siemankowski & White, 1984).

The apparent discrepancy in the cooperativity of the rigor tension development of cardiac and skeletal muscle may imply that the feedback regulation due to the rigor (AM) complex has higher cooperativity than that due to the AMADP complex (the value of m in our model). Thus, the different set of data mentioned above seems to be consistently explainable according to the present model. More detailed examination is needed in the future.

Similarities and differences in effects of MgADP and Ca^{2+} on tension development

It has been reported that accumulation of ADP inside muscle modulates the mechano-chemical interaction of cross-bridges by inhibiting dissociation of the attached cross-bridges (and thus, the number of (strong-)force-generating cross-bridges will increase) (Siemankowski *et al.*, 1985; Cooke & Pate, 1985; Lu *et al.*, 1993) and allosterically increasing the Ca^{2+} affinity of troponin (Hoar *et al.*, 1987; Godt & Nosek, 1989; Ruff & Weissman, 1991). Our present results, on the other hand, suggest that MgADP has an activating function, apparently indistinguishable from that of

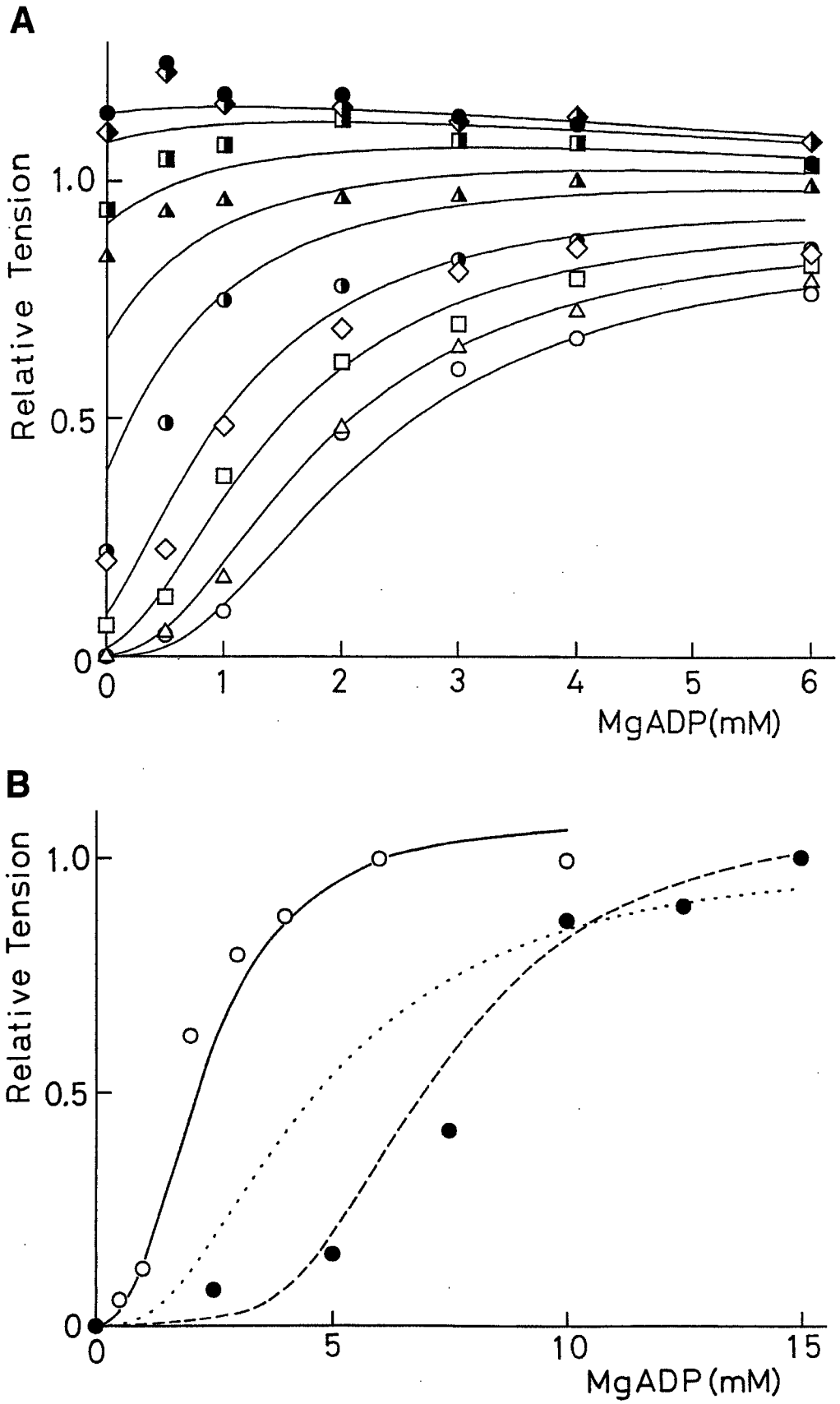
A
Relative Tension
1.0
0.5
0
0
1
2
3
4
5
6
MgADP(mM)
B
Relative Tension
1.0
0.5
0
0
5
10
15
MgADP (mM)

Ca^{2+}, as demonstrated by MgADP and Ca^{2+} inducing a similar level of tension (Fig. 3A); that is, ADP-contraction may be an intrinsic property of the cardiac muscle contractile system. This speculation is supported by the observation that the activating effects of MgADP at various concentrations of free Ca^{2+} were simulated by our computer analysis, in which both MgADP and Ca^{2+} were assumed to produce *independently* the *intermediate* state of thin filaments (defined as [A*]) and then *cooperatively* produce the *on* state of thin filaments (defined as $[A_{on}]$), and the two key steps (i.e. 4 and 5) in the actomyosin ATPase scheme (Fig. 1) were regulated by $[A_{on}]$. The non-linearity present in the regulatory mechanism could simulate the apparent cooperativity observed between the concentrations of free Ca^{2+} and MgADP.

The multi-step regulatory mechanism assumed here implies that the structural change of actin from the *off* state to the *intermediate* state ([A*]) occurs through the binding of Ca^{2+} to troponin and the formation of the actomyosin–ADP complex, independently. Then, the proportion of the *on* state of thin filaments, $[A_{on}]$, is allosterically regulated by [A*] (here, we arbitrarily assumed that this regulation occurs according to the Hill equation). Thus, the key steps in the actomyosin ATPase cycle are regulated by $[A_{on}]$.

It should be noted that there was a difference between ADP-contraction and Ca^{2+}-contraction in terms of the kinetic properties of tension development; the rising rate of tension development in ADP-contraction (2 mM MgATP, 10 mM MgADP, and $-Ca^{2+}$), $t_{1/2} \sim 10$ s (see Fig. 1A in Fukuda *et al.*, 1996, for chart recording), was slower than that in Ca^{2+}-contraction (2 mM MgATP, –MgADP, and $+Ca^{2+}$), $t_{1/2} \sim 2$ s (chart recording, not shown). The slow rate of tension development in ADP-contraction may be attributable to: (1) the time required to achieve the *on* state of thin filaments (one reason for this may be differences in diffusion coefficients of MgADP and Ca^{2+}/CaEGTA/EGTA inside the muscle bundles); and (2) disturbance of the sliding movement of myofilaments by the AM2ADP complex.

Suppression of Ca^{2+}-desensitizing effect of Pi by MgADP

Pi reverses the Pi-release step of the cross-bridge cycle by shifting the distribution of cross-bridges towards a state with a full complement of bound products (ADP and Pi) and can decrease the number of (strong-) force-generating cross-bridges (Hibberd *et al.*, 1985). This could explain the well-known Ca^{2+}-desensitizing effect of Pi on the myofilament (Kentish, 1986; Godt & Nosek, 1989; Fukuda *et al.*, 1996), since (strong-)force-generating cross-bridges are thought to allosterically increase the Ca^{2+} sensitivity of the regulatory system on the thin filament (Bremel & Weber, 1972; Güth & Potter, 1987; Brozovich *et al.*, 1988; Swartz & Moss, 1992; for more detailed discussions, see Ashley *et al.*, 1991). In the present study, we found that the effect of Pi was markedly and concentration-dependently suppressed by the addition of MgADP (Figs 4 and 5). This finding favours the interpretation that (strong-) force-generating cross-bridges (e.g. the AMADP complex) allosterically promote the formation of the *on* state of thin filaments.

The apparent enhancement of the Ca^{2+}-sensitizing effect of MgADP in the presence of relatively low concentrations of Pi (less than 2 mM) (Fig. 5) appears to be difficult to explain. However, one possible explanation is as follows: the pCa_{50} values in the presence of MgADP and the absence of Pi may be underestimated because of the augmented tension levels under high pCa conditions (see Fig. 3C). Thus, true pCa_{50} values in the presence of ≥ 2 mM MgADP and the absence of Pi (on the ordinate in Fig. 5) may be 6.2–6.5, such that the apparent enhancement of Ca^{2+} sensitivity at low concentrations of Pi is abolished. This scenario is consistent with the

---

Fig. 6. Calculation of tension development based on the kinetic model of actomyosin. The following figures were chosen according to the experimental data reported to date (Ishiwata & Yasuda, 1993), but were slightly modified to simulate the present results: $k_{1a} = 2 \times 10^6 \times [ATP]/s$, $k_{1b} = 15/s$, $k_{2+} = 10^8 \times [FA_0]/s$, $k_{2-} = 10^4/s$, $k_{3a} = 10/s$, $k_{3b} = 10/s$, $k_{3c} = 200/s$, $k_{3d} = 15/s$, k_{4+} = (defined in the text), $k_{4-} = 10^3/s$, k_{5a} = (defined in the text), $k_{5b} = 1500 \times [Pi]/s$, $k_{6a} = 3/s$, $k_{6b} = 0.3/s$, $k_{7a} = 500(1000)/s$, $k_{7b} = 10^7 \times [ADP]/s$, $l = 1(2)$, $m = 1(2)$, $n = 2$, $K_{on} = 0.3$, $K_{Ca} = 2.5 \times 10^{-6}$ (1.0×10^{-6}) M, $K_f = 0.1$, $C = 0.5$, $[FA_0] = 0.9$ mM and $[M_0] = 0.3$ mM. Here, [ATP], [ADP] and [Pi] are, respectively, the concentrations of MgATP, MgADP and Pi; $[FA_0]$ and $[M_0]$ are, respectively, effective total concentrations of actin and myosin in the fibres. Isometric tension (F) was assumed to be proportional to [AM1ADP]. All figures are common to cardiac and skeletal muscles, except those in parentheses which represent skeletal muscle only. (A) and (B): the results of model calculations corresponding to Figs 3A and 2, respectively. The parameters used for simulating the data shown in (A) ($-Ca^{2+}$) and (B) of cardiac muscle are the same, but normalization of the tension level differed between the two, as explained in the legends of Fig. 3A for (A) and Fig. 2 for (B). (A) Symbols are the same as in Fig. 3A; thin lines show the results of simulation. (B) Symbols are the same as in Fig. 2; a thin line shows the result of simulation for cardiac muscle; dashed and dotted lines show the results of simulation for skeletal muscle (the values of parameters are the same as those in cardiac muscle except $k_{7a} = 1000$ and $m = 2$ for dashed line, and $k_{7a} = 1000$ for dotted line). Symbols in (A) and (B) represent the average values of data in Figs 3A and 2. The values of l and K_{Ca} for skeletal muscle, i.e. 2 and 1.0×10^{-6}, respectively, were not used in the present simulation.

above interpretation: that is, MgADP enhances Ca^{2+} sensitivity while Pi diminishes it.

Physiological significance of MgADP as an activator

It has been reported that, in the intracellular milieu of ischaemic or hypoxic cardiac muscle, the concentration of ADP increases, while that of ATP decreases (Kammermeier *et al.*, 1982; Allen *et al.*, 1985; Allen & Orchard, 1987). The estimated ratio of the myoplasmic concentration of ADP to that of ATP varies considerably depending on experimental conditions. Kammermeier and colleagues (1982), for example, showed that the [ADP]/[ATP] ratio markedly increased, approaching 0.2, in isolated rat heart after 2 min of anoxia (see their Appendix). The value of 0.2 appears to be too small to modulate cardiac muscle contraction substantially (see Figs 3A, 3C and 5). However, a previous report pointed out that the local concentration of MgADP in the vicinity of cross-bridges could be higher than that estimated because of slow diffusion of MgADP in the filament overlap zone, and limited buffering capacity of MgADP by the phosphocreatine circuit (Yamashita *et al.*, 1994). In addition, the local MgATP concentration may be lower than that estimated for the same reasons.

Our results indicate that, although the physiological role of MgADP as an activator remains unclear at present, if the ratio [MgADP]/[MgATP] increases in the vicinity of cross-bridges during ischaemia or hypoxia, MgADP may make a substantial contribution to steady-state tension and suppress the Ca^{2+}-desensitizing effect of Pi. Hence, activation produced by MgADP may be an adaptational cardiac muscle response which operates, albeit only in part, in opposition to the inhibitory effects of Pi on contractile performance during ischaemia or hypoxia.

Acknowledgements

This work was supported in part by Grants-in-Aid for Scientific Research, Grants-in-Aid for Scientific Research on Priority Areas and Grants-in-Aid for the High-Tech Research Center Project from the Ministry of Education, Science, Sports and Culture of Japan.

References

ALLEN, D. G., MORRIS, P. G., ORCHARD, C. H. & PIROLO, J. S. (1985) A nuclear magnetic resonance study of metabolism in the ferret heart during hypoxia and inhibition of glycolysis. *J. Physiol. (Lond.)* **361**, 185–204.

ALLEN, D. G. & ORCHARD, C. H. (1987) Myocardial contractile function during ischaemia and hypoxia. *Circ. Res.* **60**, 153–68.

ASHLEY, C. C., MULLIGAN, I. P. & LEA, T. J. (1991) Ca^{2+} and activation mechanisms in skeletal muscle. *Quart. Rev. Biophys.* **24**, 1–73.

BEST, P. M., DONALDSON, S. K. & KERRICK, W. G. L. (1977) Tension in mechanically disrupted mammalian cardiac cells: effects of magnesium adenosine triphosphate. *J. Physiol. (Lond.)* **265**, 1–17.

BRANDT, P. W., REUBEN, J. P. & GRUNDFEST, H. (1972) Regulation of tension in the skinned crayfish muscle fiber. *J. Gen. Physiol.* **59**, 305–17.

BREMEL, R. D. & WEBER, A. (1972) Cooperation within actin filament in vertebrate skeletal muscle. *Nature (New Biol.)* **238**, 97–101.

BROZOVICH, F. V., YATES, L. D. & GORDON, A. M. (1988) Muscle force and stiffness during activation and relaxation. Implications for the actomyosin ATPase. *J. Gen. Physiol.* **91**, 399–420.

CHALOVICH, J. M. & EISENBERG, E. (1982) Inhibition of actomyosin ATPase activity by troponin–tropomyosin without blocking the binding of myosin to actin. *J. Biol. Chem.* **257**, 2432–7.

COOKE. R. & PATE, E. (1985) The effects of ADP and phosphate on the contraction of muscle fibers. *Biophys. J.* **48**, 789–98.

EBASHI, S. & ENDO, M. (1968) Calcium ions and muscle contraction. *Prog. Biophys. Mol. Biol.* **18**, 123–83.

FUJITA, H. & ISHIWATA, S. (1998) Spontaneous oscillatory contraction without regulatory proteins in actin filament-reconstituted fibers. *Biophys. J.* **75**, 1439–45.

FUKUDA, N., FUJITA, T. & ISHIWATA, S. (1991) Effects of ADP, inorganic phosphate and calcium on spontaneous tension oscillation of glycerinated cardiac muscle. *J. Muscle Res. Cell Motil.* **12**, 304.

FUKUDA, N., FUJITA, H., FUJITA, T. & ISHIWATA, S. (1996) Spontaneous tension oscillation in skinned bovine cardiac muscle. *Pflügers Arch.* **433**, 1–8.

GEEVES, M. A. (1991) The dynamics of actin and myosin association and the crossbridge model of muscle contraction. *Biochem. J.* **274**, 1–14.

GODT, R. E. (1974) Calcium-activated tension of skinned muscle fibers of the frog. *J. Gen. Physiol.* **63**, 722–39.

GODT, R. E. & NOSEK, T. M. (1989) Changes of intracellular milieu with fatigue or hypoxia depress contraction of skinned rabbit skeletal and cardiac muscle. *J. Physiol. (Lond.)* **412**, 155–80.

GOLDMAN, Y. E. (1987) Kinetics of the actomyosin ATPase in muscle fibers. *Ann. Rev. Physiol.* **49**, 637–54.

GOLDMAN, Y. E. & BRENNER, B. (1987) Special topic: molecular mechanism of muscle contraction. *Ann. Rev. Physiol.* **49**, 629–36.

GÜTH, K. & POTTER, J. D. (1987) Effect of rigor and cycling cross-bridges on the structure of troponin C and on the Ca^{2+} affinity of the Ca^{2+}-specific regulatory sites in skinned rabbit psoas fibers. *J. Biol. Chem.* **262**, 13627–35.

HIBBERD, M. G., DANTZIG, J. A., TRENTHAM, D. R. & GOLDMAN, Y. E. (1985) Phosphate release and force generation in skeletal muscle fibers. *Science* **228**, 1317–9.

HOAR, P. E., MAHONEY, C. W., KERRICK, W. G. L. & MONTAGUE, D. (1987) MgADP increases maximum tension and Ca^{2+} sensitivity in skinned rabbit soleus fibers. *Pflügers Arch.* **410**, 30–36.

HORIUTI, K. (1986) Some properties of the contractile system and sarcoplasmic reticulum of skinned slow fibres from *Xenopus* muscle. *J. Physiol. (Lond.)* **373**, 1–23.

ISHIWATA, S. & YASUDA, K. (1993) Mechano-chemical coupling in spontaneous oscillatory contraction of muscle. *Phase Transitions* **45**, 105–36.

JOHNSON, R. E. & ADAMS, P. H. (1984) ADP binds similarly to rigor muscle myofibrils and to actomyosin-subfragment one. *FEBS Lett.* **174**, 11–14.

KAMMERMEIER, H., SCHMIDT, P. & JUNGLING, E. (1982) Free energy change of ATP-hydrolysis: a causal factor of early hypoxic failure of the myocardium? *J. Mol. Cell. Cardiol.* **14**, 267–77.

KENTISH, J. C. (1986) The effects of inorganic phosphate and creatine phosphate on force production in skinned muscles from rat ventricles. *J. Physiol. (Lond.)* **412**, 155–80.

KUSUOKA, H., WEISFELDT, M. L., ZWEIER, J., JACOBUS, W. E. & MARBAN, E. (1986) Mechanisms of early contractile failure during hypoxia in intact ferret heart: evidence for modulation of maximal Ca^{2+}-activated force by inorganic phosphate. *Circ. Res.* **59**, 270–82.

LEHRER, S. S. & GEEVES, M. A. (1998) The muscle thin filament as a classical cooperative/allosteric regulatory system. *J. Mol. Biol.* **277**, 1081–9.

LEHRER, S. S. & MORRIS, E. P. (1982) Dual effects of tropomyosin and troponin–tropomyosin on actomyosin subfragment 1 ATPase. *J. Biol. Chem.* **257**, 8073–80.

LIENHARD, G. E. & SECEMSKI, I. I. (1973) P^1, P^5-di(adenosine-5′) pentaphosphate, a potent multisubstrate inhibitor of adenylate kinase. *J. Biol. Chem.* **248**, 1121–3.

LU, Z., MOSS, R. L. & WALKER, J. W. (1993) Tension transients initiated by photogeneration of MgADP in skinned skeletal muscle fibers. *J. Gen. Physiol.* **101**, 867–88.

MARBAN, E. & KUSUOKA, H. (1987) Maximal Ca^{2+}-activated force and myofilament sensitivity in intact mammalian hearts. *J. Gen. Physiol.* **90**, 609–23.

MCKILLOP, D. F. A. & GEEVES, M. A. (1993) Regulation of the interaction between actin and myosin subfragment 1: evidence for three states of the thin filament. *Biophys. J.* **65**, 693–701.

METZGER, J. M. (1995) Myosin binding-induced cooperative activation of the thin filament in cardiac myocytes and skeletal muscle fibers. *Biophys. J.* **68**, 1430–42.

NAGASHIMA, H. & ASAKURA, S. (1982) Studies on cooperative properties of tropomyosin–actin and tropomyosin–troponin–actin complexes by the use of N-ethylmaleimide-treated and untreated species of myosin subfragment 1. *J. Mol. Biol.* **155**, 409–28.

PALMER, S. & KENTISH, J. C. (1994) The role of troponin C in modulating the Ca^{2+} sensitivity of mammalian skinned cardiac and skeletal muscle fibres. *J. Physiol. (Lond.)* **480**, 45–60.

RUFF, R. L. & WEISSMAN, J. (1991) Iodoacetate-induced contracture in rat skeletal muscle: possible role of ADP. *Am. J. Physiol.* **261**, C828–36.

SEOW, C. Y. & FORD, L. E. (1997) Exchange of ATP for ADP on high-force cross-bridges of skinned rabbit muscle fibers. *Biophys. J.* **72**, 2719–35.

SHIMIZU, H., FUJITA, T. & ISHIWATA, S. (1992) Regulation of tension development by MgADP and Pi without Ca^{2+}. Role in spontaneous tension oscillation of skeletal muscle. *Biophys. J.* **61**, 1087–98.

SIEMANKOWSKI, R. F. & WHITE, H. D. (1984) Kinetics of the interaction between actin, ADP, and cardiac myosin-S1. *J. Biol. Chem.* **259**, 5045–53.

SIEMANKOWSKI, R. F., WISEMAN, M. O. & WHITE, H. D. (1985) ADP dissociation from actomyosin subfragment 1 is sufficiently slow to limit the unloaded shortening velocity in vertebrate muscle. *Proc. Natl Acad. Sci. USA* **82**, 658–62.

SWARTZ, D. R. & MOSS, R. L. (1992) Influence of a strong-binding myosin analogue on calcium-sensitive mechanical properties of skinned skeletal muscle fibers. *J. Biol. Chem.* **267**, 20497–506.

SWARTZ, D. R., MOSS, R. L. & GREASER, M. L. (1996) Calcium alone does not fully activate the thin filament for S1 binding to rigor myofibrils. *Biophys. J.* **71**, 1891–1904.

SWEITZER, N. K. & MOSS, R. L. (1990) The effect of altered temperature on Ca^{2+}-sensitive force in permeabilized myocardium and skeletal muscle. Evidence for force dependence of thin filament activation. *J. Gen. Physiol.* **96**, 1221–45.

WEBER, A. & MURRAY, J. M. (1973) Molecular control mechanisms in muscle contraction. *Physiol. Rev.* **53**, 612–73.

WILLIAMS, D. L., GREENE, L. E. & EISENBERG, E. (1988) Cooperative turning on of myosin subfragment 1 adenosinetriphosphatase activity by the troponin–tropomyosin–actin complex. *Biochemistry* **27**, 6987–93.

YAMASHITA, H., SATA, M., SUGIURA, S., MOMOMURA, S., SERIZAWA, T. & IIZUKA, M. (1994) ADP inhibits the sliding velocity of fluorescent actin filament on cardiac and skeletal myosins. *Circ. Res.* **74**, 1027–33.

Pflügers Arch – Eur J Physiol (1999) 438:125–132

ORIGINAL ARTICLE

Norio Fukuda · Shin'ichi Ishiwata

Effects of pH on spontaneous tension oscillation in skinned bovine cardiac muscle

Received: 14 September 1998 / Received after revision: 23 February 1999 / Accepted: 10 March 1999

Abstract Skinned cardiac muscle preparations exhibit spontaneous tension oscillations (spontaneous oscillatory contractions; SPOCs) in the absence of Ca^{2+}, and in the presence of MgATP, MgADP and inorganic phosphate (Pi; ADP-SPOC). Similar oscillations occur in the presence of sub-micromolar concentrations of Ca^{2+} under normal activating conditions without MgADP and Pi (Ca-SPOC). In the study presented here, we investigated the effects of pH on both types of SPOC in skinned bovine cardiac ventricular muscle. First, a decrease in pH increased the MgADP concentration required to induce the half-maximal isometric tension that is obtained in the absence of Ca^{2+} and in the presence of MgATP (ADP-contraction). The inhibitory effect of Pi on ADP-contractions was not affected by pH. Second, ADP-SPOCs occurred upon the addition of Pi to the solution that resulted in ADP-contraction, and the relative amplitude and the period of the tension oscillation in the presence of 2 mM MgATP, 10 mM MgADP and 10 mM Pi were unchanged under all pH conditions examined (6.6, 7.0, 7.4). On the contrary, the relative amplitude and the period of the Ca-SPOCs were markedly diminished at pH 6.6. Finally, we constructed state diagrams showing the effects of pH on SPOC conditions. The state diagram shows that SPOCs occur less frequently under acidic conditions than at neutral pH. We suggest that the intermediate state of crossbridges that is required for SPOCs is more difficult to attain at a low pH.

N. Fukuda
Department of Physiology,
The Jikei University School of Medicine, Tokyo, Japan

S. Ishiwata
Department of Physics, School of Science and Engineering,
and Advanced Research Institute for Science and Engineering,
and Materials Research Laboratory for Bioscience and Photonics,
Waseda University, Tokyo 169-8555, Japan

S. Ishiwata (✉)
Department of Physics, School of Science and Engineering,
Waseda University, 3-4-1 Okubo, Shinjuku-ku,
Tokyo 169-8555, Japan
e-mail: ishiwata@mn.waseda.ac.jp
Tel.: +81-3-52863437; Fax: +81-3-32002567

Key words Cardiac muscle · Oscillation · Spontaneous tension oscillation · SPOC · State diagram of muscle

Introduction

Studies using skinned cardiac muscle preparations from which the sarcolemma is either chemically or mechanically removed, have provided evidence that H^+ acts directly to decrease the maximal Ca^{2+}-activated tension and Ca^{2+} sensitivity of the myofilaments [9, 14, 22, 33]. The mechanism by which H^+ suppresses Ca^{2+}-activated tension involves the direct competition between Ca^{2+} and H^+ for the Ca^{2+}-binding site on troponin C [5, 8, 37]. In addition, acidic pH suppresses rigor tension in cardiac muscle [9, 25, 36] and active tension in the absence of Ca^{2+} (elicited by partial removal of troponin from skeletal muscle) [26]. Therefore, the depressed tension development that occurs at low pH is, in part, attributable to a reduction in the number of (strong-)force-generating crossbridges, and/or to a reduction in the force that each crossbridge generates [26, 27, 34, 40].

In the relaxed state ($-Ca^{2+}$), spontaneous sarcomeric oscillation (spontaneous oscillatory contraction, SPOC), which is manifested as tension oscillation, occurs in skinned cardiac [12, 19] and fast-twitch skeletal muscles [2, 18, 19, 31, 35] in the presence of ADP and inorganic phosphate (Pi; ADP-SPOC). In previous studies using skinned bovine ventricular muscle [12] and fast skeletal (rabbit psoas) muscle [35], we demonstrated that Pi has an inhibitory effect on the active tension induced by the addition of MgADP in the absence of Ca^{2+} (ADP-contraction). In addition, skinned cardiac muscle (myofibrils) shows spontaneous tension and sarcomeric oscillation under partial Ca^{2+} activation, which is distinct from the oscillation due to the Ca^{2+}-induced Ca^{2+}-release mechanism (Ca-SPOC; see [10, 12, 19, 24, 38]). Neither ADP-SPOCs nor Ca-SPOCs are transitory processes, but occur in a steady state, as indicated by a state diagram of muscle [12, 17, 18, 19]. From our experimental results [12, 19] and computer analysis [17], we have concluded

that *the minimum requirement* for spontaneous tension oscillation, either ADP-SPOC or Ca-SPOC, is the coexistence of non (or weak) -force-generating and force-generating (strong) crossbridges beyond certain threshold proportions. It can therefore be considered that, despite different ionic conditions, the molecular mechanism is the same for both ADP-SPOCs and Ca-SPOCs. The previous studies were conducted under neutral pH, and the effects of pH on spontaneous tension oscillation have not been studied to date.

In the present study, we investigated systematically the effects of pH on spontaneous tension oscillation in skinned bovine ventricular cardiac muscle. The results show that with a decline of pH: (1) not only is the normal Ca-contraction suppressed, but the ADP-contraction is also suppressed, and (2) the ADP-SPOC region shifts to the higher MgADP concentration while the shape of the region is maintained, whereas the Ca-SPOC region shifts to the higher Ca^{2+} concentration and is diminished. Finally, we discuss the physiological significance of these results.

Materials and methods

Solutions

The chemical compositions of the solutions used in this study were as described previously [12]. The isometric tension was measured in solutions containing 2 mM MgATP, 0–10 mM MgADP, and various concentrations of Ca^{2+} [pCa=<5 (+Ca^{2+}), 5.15–6.9, and +ethyleneglycol-bis(oxonitrilo)tetraacetate (EGTA) (–Ca^{2+})]. The concentrations of ATP (Na-salt, Boehringer Mannheim, Mannheim, Germany), ADP (K-salt, Boehringer Mannheim), $MgCl_2$, EGTA (Dojindo, Kumamoto, Japan) and other chemicals were based on computer calculations using the published values for stability constants [16]. The pH value for each solution was adjusted to 6.6±0.02, 7.0±0.02 or 7.4±0.02 with either 1 N HCl or KOH in the presence of 10 mM 3-(*N*-morpholino)propanesulphonic acid (MOPS; Dojindo) at 25.0±0.2°C. P^1,P^5-di(adenosine-5')pentaphosphate (AP_5A; 0.1 mM, Boehringer Mannheim) was added to inhibit the rephosphorylation of ADP to ATP by adenylate kinase [23]. When required, an ATP-regenerating system composed of creatine phosphokinase (CPK; Sigma, St. Louis, Mo., USA) and creatine phosphate (CP; Boehringer Mannheim) was used. The following rigor and relaxing solutions were used: rigor, 1 mM EGTA, 5 mM $MgCl_2$, 10 mM MOPS (pH 7.0) and 120 mM KCl; high-EGTA or low-EGTA relaxing solutions, 4 mM (or 0.4 mM) EGTA, 3.8 mM ATP (MgATP=3.0 mM), 3.9 mM $MgCl_2$ (Mg^{2+}=0.9 mM) and 120 mM KCl. All chemicals were of reagent grade.

Preparation of skinned muscle

The skinned cardiac muscle bundles (left ventricular papillary muscle from the bovine heart) were prepared in glycerol according to the method described in a previous report [12]. Briefly, a small bundle (40–80 μm wide, 20–40 μm thick and 1.5 mm long) was dissected just before use. Special care was taken to make the bundle as thin as possible, since thick bundles are more prone to ATP depletion and accumulation of ADP and Pi inside the muscle [35].

Experimental protocol

Isometric tension was measured according to a protocol that has been described previously [12]. In brief, both ends of the muscle bundle were fixed to thin tungsten wires, one of which was attached to a tension transducer (AE-801, SensoNor, Holten, Norway). The residual portions of the membrane system were removed in rigor solution containing 0.3% (v/v) Triton X-100 for 90 s. After the muscle was washed with rigor solution, it was transferred to a high-EGTA relaxing solution in which the muscle length was adjusted so that the muscle became slack (sarcomere length, approximately 2.0 μm). The muscle was then transferred to a low-EGTA relaxing solution. All procedures were carried out at room temperature (25.0±0.2°C).

The relative tension was estimated from the ratio of the developed tension in an assay solution to the average of the tension developed in standard solutions (see figure legends) before and after the assay measurement. The data were used only when the ratio of the tension after the assay to that measured before the assay exceeded 85%, and the final tension measured in the standard solution was more than 70% of the initial tension.

The amplitude of tension oscillation was defined as the ratio of the peak-to-peak amplitude of tension oscillation (the largest one except for the initial spike of tension) to the average developed tension. Tension oscillation is termed "strong" or "weak" depending upon whether the amplitude was larger or smaller than 5%, respectively. The period of tension oscillation was defined simply as the averaged period of tension oscillation.

Analysis of experimental data

All experimental data are expressed as mean ±SD. For experiments on MgADP (or Ca^{2+})-induced tension, relative tension values were fitted to the linearized Hill equation: $\log[P/(1-P)]=n_H[pMgADP_{50}(or\ pCa_{50})-pMgADP(or\ pCa)]$, where P is the tension normalized to the maximum tension (at 10 mM MgADP or +Ca^{2+}) at each pH value, n_H is the Hill coefficient and $pMgADP_{50}$(or pCa_{50}) is –log[MgADP(or Ca^{2+})] ([ ], concentration) at P=0.5. We employed a linear regression analysis to derive the n_H and $MgADP_{50}$ (or pCa_{50}) values, of which statistical significance was estimated to be $p<0.01$. Only data points below 1.4 of $|\log[P/(1-P)]|$ were used.

Results

Effects of pH on ADP-induced tension

We examined the effects of pH on the isometric tension induced by MgADP in the absence of Ca^{2+} (ADP-contraction; see [13, 35]). As pH decreased from 7.4 to 6.6, the sigmoidal curve of the tension/MgADP relationship shifted to the right (i.e. to the higher MgADP concentration; Fig. 1A); concomitantly, the maximal tension obtained at the saturating concentration of MgADP (10 mM) decreased. In addition, the n_H value, an indicator of the cooperativity of thin-filament activation, increased from 1.9 at pH 7.4 to 2.7 at pH 7.0, and then to 3.1 at pH 6.6. As shown in Fig. 1B, there was a linear relationship between $MgADP_{50}$, the MgADP concentration at which 50% tension was attained, and the pH value, suggesting a decrease in the apparent affinity for MgADP with a decline of pH. It should be mentioned that at all of the pH values tested, spontaneous tension oscillation did not occur under any condition of ADP-contraction.

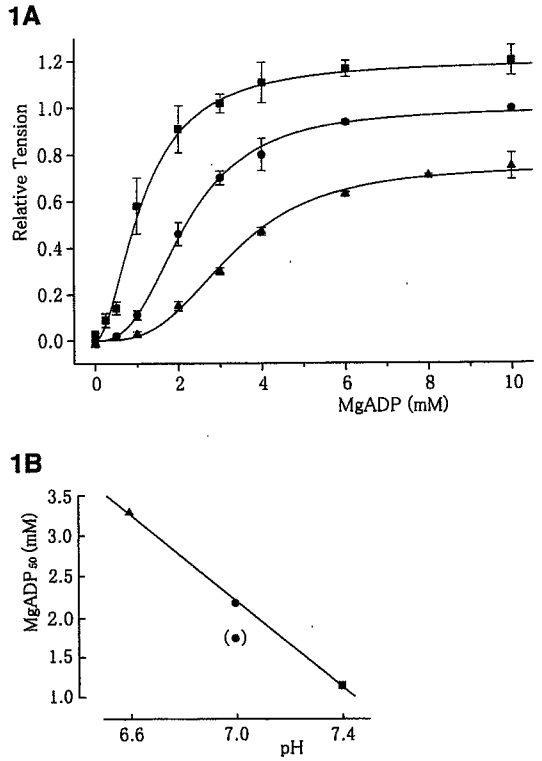

Fig. 1A, B Effects of pH on ADP-induced isometric tension. *Standard* solvent condition at values of pH 6.6, 7.0, 7.4 for ADP-induced contraction (ADP-contraction): 59±3 mM KCl, 2.2 mM ATP (maintained at 2.0 mM MgATP), ADP concentrations of 18.1, 16.4, and 16.1 mM, respectively (maintained at 10 mM MgADP), 14.2 mM $MgCl_2$ (maintained at 2 mM Mg^{2+}), 10 mM MOPS pH 6.6, 7.0 and 7.4, respectively, 2 mM EGTA, 0.1 mM AP_5A and ionic strength (IS) at 0.150±0.001 M. Solvent conditions: the same as in the *standard* condition except that the MgADP concentration was changed, maintaining IS at 0.150±0.001 M by changing the KCl concentration. **A** Relative tension versus MgADP concentration at different pH conditions (pH=7.4 *squares*, 7.0 *circles*, 6.6 *triangles*). Tension is given relative to that at 10 mM MgADP of pH 7.0. For a typical chart recording of ADP-induced tension (pH 7.0), see Fig. 1A in [12]. *Vertical bars*, SD of three data points. The *curves* represent the fit to the Hill equation with the values for n_H (see text) and $MgADP_{50}$ (see **B**) obtained by linear regression analysis, as described in Materials and methods. **B** The critical MgADP concentration that produced a half-maximal increment in tension ($MgADP_{50}$) at each pH (data were obtained from **A**, except the one in parentheses which was obtained previously [13]). Temperature, 25.0±0.2°C. An ATP-regenerating system was not used to maintain the ratio of [MgADP]/[MgATP]

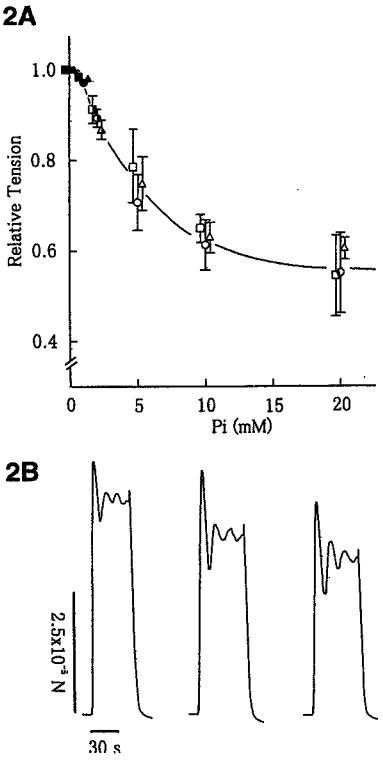

Fig. 2A, B Effects of inorganic phosphate (Pi) on the isometric tension induced by a saturating concentration of MgADP (10 mM) in the absence of Ca^{2+} under different pH conditions. Solvent conditions: the same as the *standard* condition described in Fig. 1 except that Pi was added up to 20 mM, maintaining IS at 0.150± 0.001 M. **A** Tension versus Pi concentration (pH=7.4 *squares*, 7.0 *circles*, 6.6 *triangles*). (*Filled symbols* Contraction without tension oscillation, *open symbols* strong tension oscillation, *half-filled symbols* weak tension oscillation.) Tension was normalized with respect to that in the absence of Pi. *Vertical bars* indicate the SD of three to seven data points. **B** Typical recordings of ADP-induced tension oscillation (ADP-SPOC) obtained at pH 7.4, 7.0 and 6.6 (from *left* to *right*) in the presence of 10 mM Pi. All recordings were taken from the same muscle bundle. The oscillation properties of ADP-SPOC were unaffected by ryanodine (30 μM; see chart recordings in Fig. 2B of [12])

Effects of pH on the inhibitory effects of Pi on ADP-induced tension

The inhibitory effects of Pi on ADP-contraction at 10 mM MgADP were examined at pH 7.4, 7.0 and 6.6. It has been reported that in fast-twitch skeletal muscle, the diprotonated form of Pi ($H_2PO_4^-$) is the molecular species responsible for the inhibitory effect of Pi under both ADP-contraction [35] and normal Ca-contraction conditions [29, 30, 41]. In contrast to our previous results on fast skeletal muscle [35], the inverse sigmoidal curves of isometric tension obtained under different pH conditions were overlapped up to 20 mM Pi, when they were normalized (Fig. 2A). Thus, it can be concluded that the total concentration of Pi is responsible for the inhibitory effect of Pi on ADP-contraction in cardiac muscle, consistent with previous reports conducted under normal conditions activated by Ca^{2+} [7, 22, 30].

Under all of the pH conditions tested, spontaneous tension oscillation (ADP-SPOC) was observed when Pi (≥2 mM) was added to the solution that results in ADP-contraction (Fig. 2A). As reported previously [12], it was the addition of Pi (not the degree of the decreased tension level) that was essential for the appearance of ADP-SPOC. Representative chart recordings of tension oscillation are shown in Fig. 2B. Note that the tension oscillation was seen clearly under all pH conditions, despite a decrease in the average level of tension of approximately 30% with a decline of pH from 7.4 to 6.6. Table 1 summarizes the effects of pH on the amplitude and period of

Table 1 Amplitude and period of tension oscillation (ADP-induced tension oscillations; ADP-SPOCs) at various pH values. Solvent conditions: 10 mM inorganic phosphate (Pi) was added to the *standard* solvent at different pH values, as described in Fig. 1, maintaining ionic strength at 0.150±0.001 M. Values are represented as the mean ±SD (n=4). There were no statistically significant differences compared with pH 7.0 in both parameters, as analysed by Student's t-test

	pH		
	7.4	7.0	6.6
Amplitude (%)	13.0±5.5	12.3±5.8	12.5±6.1
Period (s)	12.0±1.9	12.0±2.0	13.0±2.5

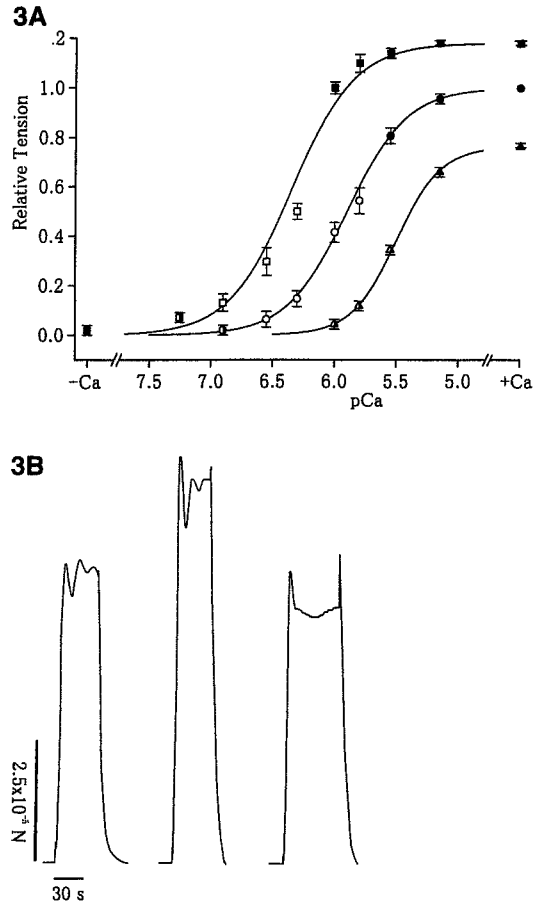

Fig. 3A, B Effects of pH on isometric tension under normal Ca-induced contraction (Ca-contraction) conditions. The conditions were the same as in Fig. 1 except that MgADP was absent and free Ca^{2+} concentrations were adjusted with Ca^{2+}-EGTA buffer [pCa=<5 (+Ca^{2+}), 5.15–6.9, and +EGTA (–Ca^{2+})]. An ATP-regenerating system composed of 1.0 mg/ml creatine phosphokinase and 10 mM creatine phosphate was present. **A** Relative tension versus pCa relationship (pH=7.4 *squares*, 7.0 *circles*, 6.6 *triangles*). Tension is given relative to that at +Ca^{2+} of pH 7.0. (*Filled symbols* Contraction without tension oscillation or relaxation, *open symbols* strong tension oscillation, *half-filled symbols* weak tension oscillation, *vertical bars* SD of four data points.) The *curves* represent the fit to the Hill equation, with the values for n_H (see text) and pCa_{50} (see text) obtained by linear regression analysis, as described in Materials and methods. **B** Typical chart recordings showing the effects of pH on Ca-induced tension oscillations (Ca-SPOCs). All recordings were taken from the same muscle bundle. From left to right, pH=7.4, 7.0 and 6.6 at pCa=6.55, 6.0 and 5.55, respectively. We have confirmed that the oscillation properties of Ca-SPOC were unaffected by ryanodine (30 μM; see [24])

Table 2 Amplitude and period of tension oscillation (Ca-induced tension oscillations; Ca-SPOCs) at various pH values. The experimental conditions are the same as in Fig. 3B. Note that at each pH, tension was approximately 40% of that obtained at +Ca^{2+} (see Fig. 3A). Values are represented as the mean ±SD (n=4).

	pH		
	7.4(pCa 6.55)	7.0(pCa 6.0)	6.6(pCa 5.55)
Amplitude (%)	9.5±2.3	10.3±2.4	2.3±1.5*
Period (s)	10.8±1.5	11.0±0.7	5.0±1.5*

*Statistically significant difference (p<0.05) compared with pH 7.0, as analysed by Student's t-test

ADP-SPOC in the presence of 10 mM Pi and 10 mM MgADP. Statistically significant differences were not detected for either parameter.

Effects of pH on spontaneous tension oscillation at intermediate concentrations of Ca^{2+}

Figure 3A shows the effects of pH on the tension versus pCa relationship under normal conditions, where the contraction was activated by Ca^{2+} without MgADP and Pi. As pH decreased, the tension/pCa curve shifted to the right (less Ca^{2+} sensitive), a result consistent with those of previous studies [9, 14, 33]; concomitantly, the maximal tension (+Ca^{2+}) decreased. The pCa_{50} values, at which the half-maximal tension was obtained, were 6.39, 5.90 and 5.50 for pH 7.4, 7.0 and 6.6, respectively. The n_H values increased: 1.7 (pH 7.4), 1.8 (pH 7.0), 2.4 (pH 6.6), but were smaller than the corresponding values for ADP-contraction.

Under partial activation, spontaneous tension oscillation (Ca-SPOC) was clearly observed at pH 7.0 and 7.4, with the extent of the oscillation region being nearly unchanged (Fig. 3A). At pH 6.6, however, the oscillation region was diminished. Figure 3B shows typical chart recordings of Ca-SPOC, obtained under all pH conditions at which relative tension was approximately 40% of the maximum tension (+Ca^{2+}) at pH 7.0 (see Fig. 3A). The amplitude and period of tension oscillation were nearly the same at pH 7.0 and 7.4, whereas the amplitude was significantly smaller and the period was significantly shorter at pH 6.6. These oscillation properties of Ca-SPOC are summarized in Table 2.

Effects of pH on maximal tension in ADP- and Ca-contraction

Figure 4 shows the effects of altered pH on the maximal tension elicited by either 10 mM MgADP or the saturating concentration of Ca^{2+}. Consistent with our previous report [13], the maximal absolute tension obtained with

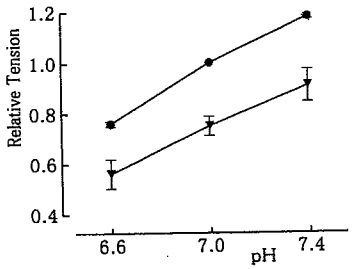

Fig. 4 Effects of varying pH on maximal tension in ADP-contraction and Ca-contraction. ●, Ca-contraction (+Ca^{2+}); ▼, ADP-contraction (10 mM MgADP). Data are from Fig. 1A and Fig. 3A for ADP-contraction and Ca-contraction, respectively. *Vertical bars* indicate the SD of three to four data points. Tension was normalized with respect to Ca-contraction at pH 7.0

MgADP in the absence of Ca^{2+} was approximately 75% of that obtained at +Ca^{2+} in the absence of MgADP at pH 7.0. It was found that the relative effect of pH on the maximal tension was nearly the same for ADP-contraction and Ca-contraction.

State diagrams of cardiac muscle under various pH conditions

We have summarized the above results in a three-dimensional (3-D) state diagram composed of the concentrations of MgADP and Pi, and pH (for ADP-SPOC; Fig. 5A), and a two-dimensional (2-D) state diagram composed of pCa and pH (for Ca-SPOC; Fig. 5B). As reported previously [12, 19], the cardiac muscle contractile system has three states: contraction (without oscillation), spontaneous oscillation (SPOC), and relaxation. The SPOC region is located in between the regions of contraction and relaxation. At each pH value, the ADP-SPOC and Ca-SPOC regions are connected through a single 3-D SPOC region in the state diagram composed of the concentrations of MgADP, Pi and Ca^{2+} [12, 19].

As shown in Fig. 5A, we defined the mid-point of the tension/MgADP relationship ($MgADP_{50}$; see Fig. 1B) as the triple point on the MgADP axis in the state diagram where the three states merge [31, 35]. With a decrease in pH, this triple point shifted to the higher MgADP concentration side (Fig. 1B), such that the ADP-SPOC region shifted to the same side.

The slope of the boundary between contraction and SPOC regions and that between relaxation and SPOC regions were unchanged over the range of pH values examined, since the same concentration of Pi (≥2 mM) was required for the induction of ADP-SPOC, and the degree of the inhibitory effect of Pi was identical under all of those pH values (Fig. 2A). Thus, the shape of the ADP-SPOC region hardly changed with the alteration in pH.

With a decline of pH, the Ca-SPOC region shifted to the higher Ca^{2+} concentration and was diminished at pH 6.6, at which point distinct tension oscillation was not observed (Fig. 5B). Thus, we conclude that the 3-D SPOC region, which includes the ADP-SPOC and Ca-SPOC regions, is smallest at pH 6.6.

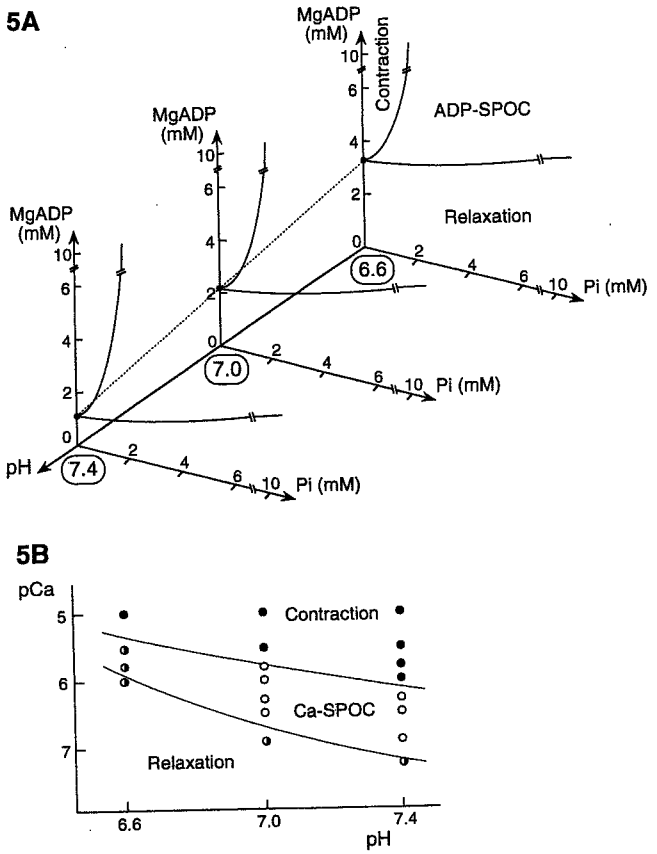

Fig. 5A, B State diagrams showing three states of cardiac muscle (i.e. contraction without tension oscillation, SPOC, and relaxation) at various pH values. **A** Three-dimensional state diagram composed of the concentrations of MgADP and Pi, and pH (6.6, 7.0 and 7.4, as shown by *ovals*); the concentration of MgATP was maintained at 2 mM and Ca^{2+} was absent. This diagram was constructed from Figs. 1 and 2A. The ADP-SPOC region is surrounded by two curved surfaces, the intersection of which is shown by a *dotted line*; the contraction region is surrounded by the MgADP-pH plane and the boundary surface between the contraction and ADP-SPOC regions; the relaxation region is surrounded by the Pi-pH plane and the boundary surface between the relaxation and ADP-SPOC regions. The *filled circles* on the MgADP axis show $MgADP_{50}$ values (see Fig. 1B), i.e. triple points at which the three states are merged. The triple point on the MgADP axis is shifted toward the higher MgADP concentration with a decrease in pH, as shown by a *dotted line*. Accompanying the shift of the triple point, both the contraction and ADP-SPOC regions are shifted upward, such that the relaxation region increases in size. **B** Two-dimensional state diagram composed of pCa and pH. This diagram was constructed from Fig. 3A (*filled circles* contraction without tension oscillation, *open circles* strong tension oscillation, *half-filled circles* weak tension oscillation). With a decline of pH, the Ca-SPOC region is diminished and is shifted towards the lower pCa. Clear tension oscillation was not observed at pH 6.6

Discussion

Effect of pH on isometric tension in ADP- and Ca-contraction

The molecular basis for the effect of H^+ in reducing Ca^{2+}-activated tension is complex and not fully understood. One mechanism for the depressed tension may involve the direct competition between Ca^{2+} and H^+ for the

Ca^{2+}-binding site on troponin C [5, 8, 37]. In addition, H^+ may have a direct action on the crossbridge cycle [25, 26, 27,28, 34, 39, 40].

H^+ is a product of ATP hydrolysis, hence it must be released during the crossbridge cycle. Kentish postulated that H^+ is released during the transition between the non (or weak)-force-generating states preceding the Pi release (force-generating) step [22, 33]. Consequently, an increased concentration of H^+ can reverse the H^+-release step, resulting in a decrease in the number of (strong-) force-generating crossbridges. Furthermore, it is possible that H^+ decreases the force produced by each crossbridge [26, 27, 34, 40], which is the case for rigor crossbridges [9, 25, 36]. These interpretations appear to account for the similar inhibitory effects of H^+ on ADP-contraction (Fig. 1) and Ca-contraction (Fig. 3A) seen in the present study (for summary, see Fig. 4).

In addition, Kardami et al. [20], in a solution study, provided evidence that the MgADP association constant in skeletal heavy meromyosin decreases with a decrease in pH (from 9.7 to 6.2). Therefore, the decreased myofibrillar MgADP sensitivity observed with a decrease in pH in ADP-contraction (Fig. 1) may be attributable to the decreased association constant of the myosin molecule for MgADP.

Cooperative activation of the thin filament

We found that the n_H value obtained for ADP-contraction is larger than that for Ca-contraction over the range of pH values from 7.4 to 6.6 (Figs. 1A and 3A); from this result we infer that the cooperativity in regulating the thin filament is higher with the addition of MgADP than with the addition of Ca^{2+}. This observation could be explained by our crossbridge model, in which MgADP, in contrast to Ca^{2+}, produces the turned-on thin filament state *indirectly* through the formation of actomyosin-ADP complexes [13, 17].

The mechanism by which n_H is increased in both ADP-contraction and Ca-contraction is unclear. To date, the action of pH on the cooperativity of thin-filament activation varies widely depending upon the experimental conditions. Metzger and Moss reported that the n_H value of the tension/pCa relationship is increased upon a decrease in pH from 7.0 to 6.2 in slow skeletal (rat soleus) muscle, but not in fast skeletal (rat vastus lateralis and rabbit psoas) muscles [28]. Recently, Hofmann et al. confirmed that the n_H of the tension/pCa relationship is significantly larger at pH 6.6 than at pH 7.0 in cardiac (rat ventricular) muscle [15]. Orchard and Kentish stated that acidic pH has no effect on the n_H of the tension/pCa relationship in guinea pig trabeculae [32]. However, Metzger reported that acidic pH decreases the cooperativity of rigor activation, (i.e. the n_H of the tension/pMg-ATP relationship) in rat ventricular cardiomyocytes [25]. These differences in the effect of pH on the cooperativity of thin-filament activation may have been due to differing ionic conditions, muscle differences, and species differences.

Effects of pH on spontaneous tension oscillation

We have reported that in fast skeletal muscle, in contrast to cardiac muscle, there is no Ca-SPOC region in the state diagram [12, 19], and that fast skeletal muscle shows about a four-fold lower affinity for MgADP than MgATP [13]. The oscillatory region of fast skeletal muscle is smaller than that of cardiac muscle, as illustrated schematically as a state diagram in our previous report [19]. In the present study, we found that acidic pH shifted the ADP-SPOC region to the higher MgADP concentration (Fig. 5A), and diminished the Ca-SPOC region (Fig. 5B). That is, with a decrease in pH, the oscillatory region of cardiac muscle approached that of fast skeletal muscle at pH 7.0.

Pi in solution exists mainly in the diprotonated form ($H_2PO_4^-$), the monoprotonated form without potassium (HPO_4^{2-}), and the monoprotonated form with potassium ($KHPO_4^-$). The ratio of the concentrations of HPO_4^{2-} and $H_2PO_4^-$ changes dramatically at near-neutral pH [22], according to the equation of $HPO_4^{2-}+H^+ \rightleftharpoons H_2PO_4^-$, where pKa is 6.8. In fast skeletal muscle, there is a strong correlation between the concentration of $H_2PO_4^-$ and the reduction of tension under conditions of both ADP-contraction [35] and normal Ca-contraction [29, 30, 41]. On the contrary, in cardiac muscle, the total concentration of Pi is responsible for its inhibitory effect on normal Ca-contraction [6, 21, 29, 30]. We found that this was also the case for the inhibitory effect of Pi on ADP-contraction (Fig. 2A). Thus, in contrast to fast skeletal muscle, all ionic species of Pi are active in cardiac muscle during ADP-SPOC. The Pi binding site on cardiac myosin may not distinguish $H_2PO_4^-$ from HPO_4^{2-} or $KHPO_4^-$. An alternative explanation is that more than one Pi binding site may be present. That is, the Pi binding sites on actin and/or the ATPase regulatory site on myosin [30, 42] may also play a crucial role in the generation of ADP-SPOC.

If $H_2PO_4^-$ is the sole molecular species of Pi that suppresses tension in fast skeletal muscle, then it follows that upon a decline of pH, the proportion of non(or weak)-force-generating crossbridges would increase, whereas the proportion of (strong-)force-generating crossbridges would decrease. This will result in the boundary between ADP-SPOC and relaxation regions moving upward (cf. Fig. 5A), and the ADP-SPOC region would become smaller [35]. In contrast, in cardiac muscle, the ADP-SPOC region shifts to the higher MgADP concentration, whereas the boundary between SPOC and relaxation regions are maintained almost horizontally (Fig. 5A). This can be explained by the fact that both the diprotonated and monoprotonated forms of Pi function as tension suppressors (Fig. 2B). This is the reason why the ADP-SPOC in cardiac muscle is resistant to reductions in pH.

As seen in the state diagram (Fig. 5), with a decrease in pH, the size of the relaxation region was increased and the ADP-SPOC region shifted to the higher MgADP concentration, the shape of the region being maintained

(Fig. 5A), whereas the Ca-SPOC region shifted to the higher Ca^{2+} concentration and was diminished (Fig. 5B). At pH 6.6, the amplitude and period of tension oscillation of Ca-SPOC were significantly diminished (Table 2). The reduction of the Ca-SPOC region at pH 6.6 was related to the increase in n_H in the tension/pCa relationship shown in Fig. 3A. The increase in the n_H value means a more abrupt transition from relaxation to contraction, so that the size of the intermediate SPOC region is reduced.

No tension oscillation was observed upon ADP-contraction (Fig. 1A); this may also be explained, at least in part, by the fact that the n_H value was larger with ADP-contraction than with Ca-contraction (cf. Figs. 1A and 3A). These results are consistent with our interpretation that the larger the n_H value, the more difficult it is for *the minimum requirements* for SPOC to be met (see Introduction; for more details, see [17, 19]).

It is interesting that as long as the minimum requirements for SPOC are *sufficiently* met, as in the 2-D ADP-SPOC region (Fig. 5A), the property of spontaneous tension oscillation in muscle fibres does not change when pH is changed (Figs. 2B and 3B; Tables 1 and 2). To clarify this point, it will be necessary to examine the relationship between sarcomere length oscillation and tension oscillation during SPOC at various pH values, using myofibrils in addition to muscle fibres.

Physiological significance

It is possible that spontaneous tension oscillation has a physiological role, such as stabilizing the dynamic properties of the rhythmic contraction of a cardiac cell. The apparent period of tension oscillation of the muscle bundles was approximately 10 s (Tables 1 and 2), being longer than the heartbeat period (1–2 s for bovine heart), but the period of sarcomere length oscillation was much shorter, a few seconds [11, 12]. In addition, the oscillation period tends to be shortened as the solvent conditions become unfavourable for tension development (Fig. 3 and Table 2; cf. [18]). The peak of the intracellular concentration of Ca^{2+} during twitch is within the range of 0.5–1.5 μM (i.e. the concentration that induces Ca-SPOC) [1, 3, 4]. In the present study, we have demonstrated that at acidic pH values, the intermediate state of crossbridges is difficult to attain due to high cooperativity, such that the size of the Ca-SPOC region is reduced and the amplitude of Ca-SPOC is attenuated (Fig. 3B and Table 2). Therefore, the inhibitory effect of acidosis on Ca-SPOC may, in part, underlie the contractile dysfunction that occurs during myocardial ischaemia, when the intracellular pH becomes acidic.

Acknowledgements We would like to thank Prof. S. Kurihara of The Jikei University School of Medicine for his continuing encouragement. We would also like to thank Professor M. Kawai of The University of Iowa for his critical reading of the manuscript. This research was supported partly by Grants-in-Aid for Scientific Research (No. 10308030 to S.I.), for Scientific Research on Priority Areas (No. 09279228 and No. 10175220 to S.I.) and for the High-tech Research Center Project from the Ministry of Education, Science, Sports and Culture of Japan, and by Grants-in-Aid from Core Research for Evolutional Science and Technology (CREST).

References

1. Allen DG, Kurihara S (1980) Calcium transients in mammalian ventricular muscle. Eur Heart J 1[Suppl A]:5–15
2. Anazawa T, Yasuda K, Ishiwata S (1992) Spontaneous oscillation of tension and sarcomere length in skeletal myofibrils. Microscopic measurement and analysis. Biophys J 61: 1099–1108
3. Berlin JR, Konishi M (1993) Ca^{2+} transients in cardiac myocytes measured with high and low affinity Ca^{2+} indicators. Biophys J 65:1632–1647
4. Beuckelmann DJ, Wier WG (1988) Mechanism of release of calcium from sarcoplasmic reticulum of guinea-pig cardiac cells. J Physiol (Lond) 405:233–255
5. Blanchard EM, Solaro RJ (1984) Inhibition of the activation and troponin Ca^{2+}-binding of dog cardiac myofibrils by acidic pH. Circ Res 55:382–391
6. Dawson MJ (1988) The relation between muscle contraction and metabolism: Studies by ^{31}P nuclear magnetic resonance spectroscopy. In: Sugi H, Pollack GH (eds) Molecular mechanism of muscle contraction. Plenum, New York, pp 433–448
7. Eisner DA, Elliott AC, Smith GL (1987) The contribution of intracellular acidosis to the decline of developed pressure in ferret hearts exposed to cyanide. J Physiol (Lond) 391:99–108
8. El-Saleh S, Solaro RJ (1988) Troponin I enhances acidic pH induced depression of Ca-binding to the regulatory sites in skeletal troponin C. J Biol Chem 263:3274–3278
9. Fabiato A, Fabiato F (1978) Effects of pH on the myofilaments and the sarcoplasmic reticulum of skinned cells from cardiac and skeletal muscles. J Physiol (Lond) 278:233–255
10. Fabiato A, Fabiato F (1978) Myofilament-generated tension oscillations during partial calcium activation and activation dependence of the sarcomere length-tension relation of skinned cardiac cells. J Gen Physiol 72:667–699
11. Fujita H, Ishiwata S (1998) Spontaneous oscillatory contraction without regulatory proteins in actin filament-reconstituted fibers. Biophys J 75:1439–1445
12. Fukuda N, Fujita H, Fujita T, Ishiwata S (1996) Spontaneous tension oscillation in skinned bovine cardiac muscle. Pflügers Arch 433:1–8
13. Fukuda N, Fujita H, Fujita T, Ishiwata S (1998) Regulatory roles of MgADP and calcium in tension development of skinned cardiac muscle. J Muscle Res Cell Motil 19:909–921
14. Godt RE, Nosek TM (1989) Changes of intracellular milieu with fatigue or hypoxia depress contraction of skinned rabbit skeletal and cardiac muscle. J Physiol (Lond) 412:155–180
15. Hofmann PA, Menon V, Gannaway KF (1995) Effects of diabetes on isometric tension as a function of $[Ca^{2+}]$ and pH in rat skinned cardiac myocytes. Am J Physiol 269:H1656–H1663
16. Horiuti K (1986) Some properties of the contractile system and sarcoplasmic reticulum of skinned slow fibres from *Xenopus* muscle. J Physiol (Lond) 373:1–23
17. Ishiwata S, Yasuda K (1993) Mechano-chemical coupling in spontaneous oscillatory contraction of muscle. Phase Transitions 45:105–136
18. Ishiwata S, Okamura N, Shimizu H, Anazawa T, Yasuda K (1991) Spontaneous oscillatory contraction (SPOC) of sarcomeres in skeletal muscle. Adv Biophys 27:227–235
19. Ishiwata S, Anazawa T, Fujita T, Fukuda N, Shimizu H, Yasuda K (1993) Spontaneous tension oscillation (SPOC) of muscle fibers and myofibrils. Minimum requirements for SPOC. In: Sugi H, Pollack GH (eds) Mechanism of myofilament sliding in muscle contraction. Plenum, New York, pp 545–556

20. Kardami E, De Bruin S, Gratzer W (1979) Interaction of ADP with skeletal and cardiac myosin and their active fragments observed by proton release. Eur J Biochem 97:547–553
21. Kawai M, Güth K, Cornacchia TW (1988) The role of monovalent phosphate anions in the crossbridge kinetics of chemically skinned rabbit psoas fibers. In: Sugi H, Pollack GH (eds) Molecular mechanism of muscle contraction. Plenum, New York, pp 203–217
22. Kentish JC (1991) Combined inhibitory actions of acidosis and phosphate on maximum force production in rat skinned cardiac muscle. Pflügers Arch 419:310–318
23. Lienhard GE, Secemski II (1973) P^1, P^5-di(adenosine-5')pentaphosphate, a potent multisubstrate inhibitor of adenylate kinase. J Biol Chem 248:1121–1123
24. Linke WA, Bartoo ML, Pollack GH (1993) Spontaneous sarcomeric oscillations at intermediate activation levels in single isolated cardiac myofibrils. Circ Res 73:724–734
25. Metzger JM (1996) pH dependence of myosin binding-induced activation of the thin filament in cardiac myocytes and skeletal fibers. Am J Physiol 270:H1008–H1014
26. Metzger JM, Moss RL (1988) Depression of Ca^{2+} insensitive tension due to reduced pH in partially troponin-extracted skinned skeletal muscle fibers. Biophys J 54:1169–1173
27. Metzger JM, Moss RL (1990) Effects of pH and stiffness due to reduced pH in mammalian fast- and slow-twitch skinned skeletal fibers. J Physiol (Lond) 428:737–750
28. Metzger JM, Moss RL (1990) pH modulation of the kinetics of a Ca^{2+}-sensitive cross-bridge state transition in mammalian single skeletal muscle fibres. J Physiol (Lond) 428:751–764
29. Nosek TM, Kimberly YF, Godt RE (1987) It is diprotonated inorganic phosphate that depresses force in skinned skeletal muscle fibers. Science 236:191–193
30. Nosek TM, Leal-Cardoso JH, Mclauhlin M, Godt RE (1990) Inhibitory influence of phosphate and arsenate on contraction of skinned skeletal and cardiac muscle. Am J Physiol 258:C967–C981
31. Okamura N, Ishiwata S (1988) Spontaneous oscillatory contraction of sarcomeres in skeletal myofibrils. J Muscle Res Cell Motil 9:111–119
32. Orchard CH, Kentish JC (1990) Effects of changes of pH on the contractile function of cardiac muscle. Am J Physiol 258:C967–C981
33. Palmer S, Kentish JC (1994) The role of troponin C in modulating the Ca^{2+} sensitivity of mammalian skinned cardiac and skeletal muscle fibres. J Physiol (Lond) 480:45–60
34. Renaud JM, Stein RB, Gordon T (1987) The effects of pH on force and stiffness development in mouse muscles. Can J Physiol Pharmacol 65:1798–1801
35. Shimizu H, Fujita T, Ishiwata S (1992) Regulation of tension development by MgADP and Pi without Ca^{2+}. Role in spontaneous tension oscillation of skeletal muscle. Biophys J 61:1087–1098
36. Smith GL, Steel DS (1994) Effects of pH and inorganic phosphate on rigor tension in chemically skinned rat ventricular trabeculae. J Physiol (Lond) 478:505–512
37. Solaro RJ, El-Saleh SC, Kentish JC (1989) Ca^{2+}, pH and the regulation of cardiac myofilament force and ATPase activity. Mol Cell Biochem 89:163–167
38. Sweitzer NK, Moss RL (1990) The effect of altered temperature on Ca^{2+}-sensitive force in permeabilized myocardium and skeletal muscle. Evidence for force dependence of thin filament activation. J Gen Physiol 96:1221–1245
39. Tonomura Y (1972) Muscle proteins, muscle contraction and cation transport. University of Tokyo Press, Tokyo
40. Ventura-Clapier R, Veksler V (1994) Myocardial ischemic contracture: metabolites affect rigor tension development and stiffness. Circ Res 74:920–929
41. Wilkie DR (1986) Muscular fatigue: effect of hydrogen ions and inorganic phosphate. Fed Proc 45:2921–2923
42. Yee DH, Wiendner H, Eckstein F (1980) Biphasic steady-state kinetics of myosin adenosine triphosphatase. Eur J Biochem 133:85–90

Proc. Natl. Acad. Sci. USA
Vol. 96, pp. 9602–9606, August 1999
Biophysics

Imaging of thermal activation of actomyosin motors

HIROKAZU KATO*†, TAKAYUKI NISHIZAKA‡, TAKASHI IGA†, KAZUHIKO KINOSITA, JR.‡§, AND SHIN'ICHI ISHIWATA†‡¶‖**

*Central Research Laboratory, Hitachi Ltd., Hatoyama, Saitama 350-0395, Japan; †Department of Physics, School of Science and Engineering, ¶Advanced Research Institute for Science and Engineering, ‖Materials Research Laboratory for Bioscience and Photonics, Waseda University, Tokyo 169-8555, Japan; ‡Core Research for Evolutional Science and Technology (CREST) "Genetic Programming" Team 13, Kawasaki 216-0001, Japan; and §Department of Physics, Faculty of Science and Technology, Keio University, Yokohama 223-8522, Japan

Communicated by Shinya Inoue, Marine Biological Laboratory, Woods Hole, MA, June 14, 1999 (received for review December 8, 1998)

ABSTRACT **We have developed temperature-pulse microscopy in which the temperature of a microscopic sample is raised reversibly in a square-wave fashion with rise and fall times of several ms, and locally in a region of approximately 10 μm in diameter with a temperature gradient up to 2°C/μm. Temperature distribution was imaged pixel by pixel by image processing of the fluorescence intensity of rhodamine phalloidin attached to (single) actin filaments. With short pulses, actomyosin motors could be activated above physiological temperatures (higher than 60°C at the peak) before thermally induced protein damage began to occur. When a sliding actin filament was heated to 40–45°C, the sliding velocity reached 30 μm/s at 25 mM KCl and 50 μm/s at 50 mM KCl, the highest velocities reported for skeletal myosin in usual *in vitro* assay systems. Both the sliding velocity and force increased by an order of magnitude when heated from 18°C to 40–45°C. Temperature-pulse microscopy is expected to be useful for studies of biomolecules and cells requiring temporal and/or spatial thermal modulation.**

Recent advances in optical microscopic techniques have made it possible to image single protein molecules in solution (1, 2) and investigate the dynamic nature of molecular motors (3–8). To introduce an additional dimension to this technology, we have developed temperature-pulse microscopy (TPM), in which a microscopic sample(s) in aqueous solution is heated reversibly.

There have been several reports on the effects of temperature jumps under an optical microscope: for example, on physiological functions of muscle fibers (9–12) and on phase transition phenomena in membranes of phospholipid vesicles and cells (13). To prevent thermal deterioration of biological samples, and to confirm the absence of the deterioration, it is highly desirable to restore the starting temperature as soon as the measurement is finished. In our TPM, temperature is elevated spatially and temporally by illuminating a lump of metal particles by IR laser; a concentric temperature gradient is created around the lump of metal particles. When the laser beam is shut off, the heat is rapidly dissipated into the surrounding medium. Thus, a square-wave temperature pulse with rise and fall times of less than 10 ms is generated. Exposure to high temperature is minimized, and repetitive thermal cycling is easily programmed. The local heating also permits simultaneous observation of the sample behaviors at various temperatures.

In the microscopic temperature-imaging techniques reported so far, the temperature was estimated either from the thermal quenching of fluorescence (14–16) or from the thermal shift of the fluorescence spectrum (13). Here, we applied the former technique. In our TPM, a concentric temperature gradient is formed around the metal aggregate, as assessed from thermal quenching of a fluorescent dye bound to actin filaments with a slope of 1–2°C/μm and extension out to 10–20 μm. The temperature distribution on single actin filaments also could be imaged.

We have applied this TPM technique to the thermal activation of sliding movement and tension development of actomyosin motors in an *in vitro* motility assay. We demonstrate that the motor functions can be thermally activated even at temperatures that are high enough to normally damage the proteins, if the duration of the temperature pulse is short enough.

MATERIALS AND METHODS

TPM. As schematically illustrated in Fig. 1, local heating was achieved by illuminating an aggregate of metal particles in the sample with an IR laser beam (1 W Nd:YLF laser, 1,053–1,000 p: λ = 1.053 μm; Amoco Laser, Naperville, IL; 50–100 mW on the sample plane). In most experiments we used aluminum (0.1 μmϕ; AL-014050, Nilaco, Tokyo), but gold (0.5 μmϕ; AU-174020, Nilaco), silver (0.07 μmϕ; AG-404050, Nilaco), and platinum (1.0 μmϕ; PT-354012, Nilaco) powders served equally well. The metal particles spontaneously formed aggregates in the sample and had irregular shapes. [Heat production by laser irradiation also can be achieved in other ways. For example, we have deposited, by vacuum evaporation, a thin layer of metal on a glass surface in the form of a regular array of μm-sized circles (not shown). This method allowed well-controlled and reproducible heating, whereas the use of amorphous metal aggregates described here is very simple. A magnetic bead also can be used (17).]

The presence of Al aggregates did not affect the *in vitro* motility for at least 2 h. The actin filament temperature was estimated from thermal quenching of the fluorescence of rhodamine phalloidin bound to the filament. The fluorescence images were taken with an image intensifier (KS1381; Video Scope International, Washington, DC) connected to a charge-coupled device camera (CCD-72; Dage MTI, Michigan City, IN) at the video rate of 30 frames/s. The decay lag in this camera system was well within one frame (33 ms). For the measurement of the rise and fall times of the temperature pulse, an image intensifier (ILS-3a; nac, Tokyo) connected to a high-speed camera (HSV-500DM; nac) was used at a rate of 500 frames/s.

The fluorescence image of labeled filaments at T°C was divided by that at 18°C (reference temperature) to yield the intensity ratio (r) in every pixel (18). r was related with T in a control experiment in which the temperature of the microscope stage was held at precise temperatures with the use of a thermal insulation chamber, which took about 45 min for

The publication costs of this article were defrayed in part by page charge payment. This article must therefore be hereby marked "*advertisement*" in accordance with 18 U.S.C. §1734 solely to indicate this fact.

PNAS is available online at www.pnas.org.

Abbreviation: TPM, temperature-pulse microscopy.

**To whom reprint requests should be addressed at: Department of Physics, School of Science and Engineering, Waseda University, Tokyo 169-8555, Japan. E-mail: ishiwata@mn.waseda.ac.jp.

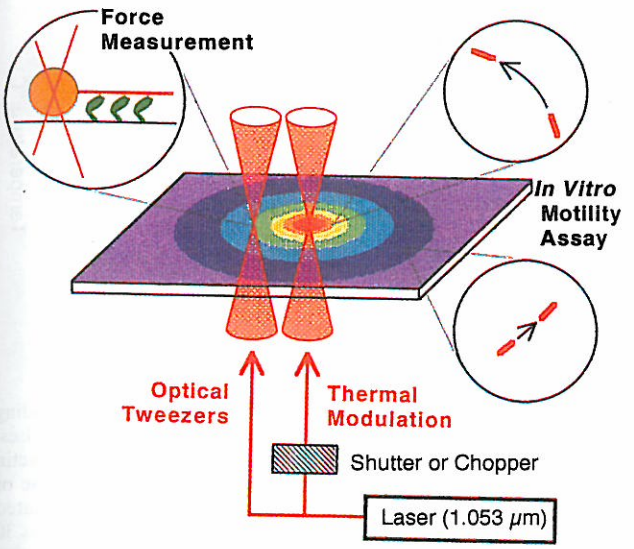

FIG. 1. Schematic illustration of TPM system. Metal aggregates of irregular shape and several to 10 μm in size, lumps of metal particles of 0.1–1.0 μm in diameter, are scattered on a glass coverslip in an *in vitro* motility assay system under an optical microscope. A peripheral, not the central, portion of one of the aggregates is illuminated by focusing an IR laser beam. If the central portion is illuminated, the aggregate is frequently blown off or the surrounding medium gets boiled. The metal aggregate that absorbs the laser light functions as a local heat source, around which a concentric temperature gradient is formed. Sliding movement of actin filaments occurs at temperature-dependent velocities, as illustrated by movement in circles. When tension is measured, the incident laser beam is split into two; one constitutes optical tweezers that hold a polystyrene bead attached at the rear end of an actin filament, and the other illuminates a metal aggregate. For repetitive temperature modulation, a chopper or shutter is used.

stabilization (Nikon). Room temperature was maintained at 18°C ± 1°C. We obtained the empirical equation $r = 1 - \alpha(T - T_0)$, where α and T_0 are, respectively, $0.018°C^{-1}$ and 18°C, in agreement with a spectroscopic measurement in a cuvette (fluorescence spectrophotometer F-4500, Hitachi, Tokyo). The temperature estimated from the fluorescence intensity averaged over a short (< a few μm) filament fluctuated from frame to frame, with a SD of ± 5°C over the duration of 0.5 s (15 frames). Spectroscopic studies in a cuvette (19) indicated that rhodamine phalloidin tended to detach from actin at high temperatures. We confirmed that the half-time for detachment under the solvent condition examined here was approximately 12 min at 35°C and 3 min at 45°C, which was much longer than the duration of the temperature pulse (<10 s). Photobleaching of rhodamine fluorescence was negligible within the period of time we examined. Thus, the linear relationship between relative fluorescence intensity and temperature, $r(T)$, is attributed solely to reversible thermal quenching of rhodamine.

Proteins. Actin and heavy meromyosin (a fragment of myosin prepared by chymotryptic digestion) were prepared from rabbit white skeletal muscle as described (20). Actin filaments were labeled with rhodamine phalloidin (Molecular Probes) according to Yanagida *et al.* (21).

***In Vitro* Motility Assay.** Details of the *in vitro* motility assay and tension measurement performed under an inverted microscope (TMD300; an oil-immersion objective lens with a phase ring, ×100 numerical aperture = 1.3 or ×60 numerical aperture = 1.4; Nikon) equipped with optical tweezers have been described (7, 8). The assay buffer used was 25 mM KCl/2.0 mM ATP/4.0 mM $MgCl_2$/25 mM imidazole-HCl, pH 7.4/1.0 mM EGTA/10 mM DTT with an oxygen-scavenger enzyme system (22); in one experiment where the highest sliding velocity was recorded, 50 mM KCl was used instead of 25 mM KCl, in which 1% (wt/vol) of methylcellulose was included to suppress the dissociation of actin filaments from the glass surface at high ionic strength. An *in vitro* motility cell was prepared by infusing 30 μg/ml heavy meromyosin in the assay buffer containing 0.5 mg/ml BSA. To measure the tension, a polystyrene bead of 1.0 μm in diameter was attached at the rear end of an actin filament through a barbed end capping protein, gelsolin, covalently attached to the bead (23), and the bead was trapped with optical tweezers (trap stiffness, 0.14 pN/nm). In this case, the laser beam was split into two by a polarizing beam splitter (Sigma Koki, Hidaka, Japan); one beam was used for optical tweezers and the other for heating. Movement of the bead in the trap was detected in a phase-contrast image under a dual-view microscope (18) and analyzed with sub-nm precision.

RESULTS AND DISCUSSION

A steady, concentric temperature gradient was produced within 10 ms around the metal after laser illumination was started, as monitored by the fluorescence intensity of the temperature-sensitive rhodamine phalloidin attached to actin filaments in the sample chamber (Fig. 2 *A–D*). Temperatures on a single actin filament could be imaged (Fig. 2*E*), even during sliding as shown below. A temperature difference as large as 40°C could be created across a high-magnification image, allowing simultaneous evaluation of sample behaviors over a wide range of temperatures. When the laser illumination was terminated, the sample cooled down to the original temperature within 10 ms, presumably because of the presence of a substance of large heat conductivity (glass and water) in contact with the small heat source. For a long actin filament, a temperature gradient around 2°C/μm was demonstrated (Fig. 2*E*).

First, we examined the effects of the temperature gradient on the sliding movement of a long actin filament. When the temperature of the front portion of a sliding filament was higher, the filament was straightened and sliding was smooth. However, when the temperature of the rear portion was higher, buckling occurred at the middle of the filament, the buckled portion being on the glass surface without looping out into the medium. In all likelihood, front motors can pull the whole filament, whereas rear motors cannot efficiently push the front portion because of the flexibility of the filament (20, 25, 26). When the rear part is faster, formation of a superhelix may be expected at the slow/fast junction, because a sliding actin filament has been shown to rotate as a right-handed screw (3, 20, 26). Indeed we observed a superhelix when the front part of an actin filament was completely fixed on a glass surface (20). In the present experiment, the temperature gradient in the running filament could not be maintained for a sufficiently long period to allow the buckled portion to loop out.

Then, we observed reversible acceleration of sliding movement by repetitive application of relatively long temperature pulses (0.5 to several seconds) by using a chopper. As shown in Fig. 3, sliding velocities reversibly reached two steady-state values within 1/30 s: the average velocities were 1.9, 19.3, 2.5, 20.7, and 2.2 μm/s, respectively, at 18°C, 41°C, 19°C, 40°C, and 15°C, which were estimated from the average fluorescence intensity of the sliding filament according to the relation, $r(T)$, described above. (Note that the coverslip temperature was maintained at 18°C ± 1°C.) On average, the sliding velocities at 25 mM KCl, the ionic strength usually used for *in vitro* motility assays (24), were 2.0 ± 0.1 (n = 6), 10 ± 1.5 (n = 6), and 20 ± 1.8 (n = 6) μm/s at 18°C, 30°C, and 40°C, respectively. For comparison, thermostatic regulation of the whole stage resulted in the average sliding velocities, respectively, of 2.0 ± 0.1 (n = 6), 8.0 ± 0.5 (n = 6), 13 ± 0.7 (n = 6), and 22 ± 2.1 (n = 6) μm/s at 18°C, 30°C, 40°C, and 50°C, consistent with previous reports (27–29). In this case, the

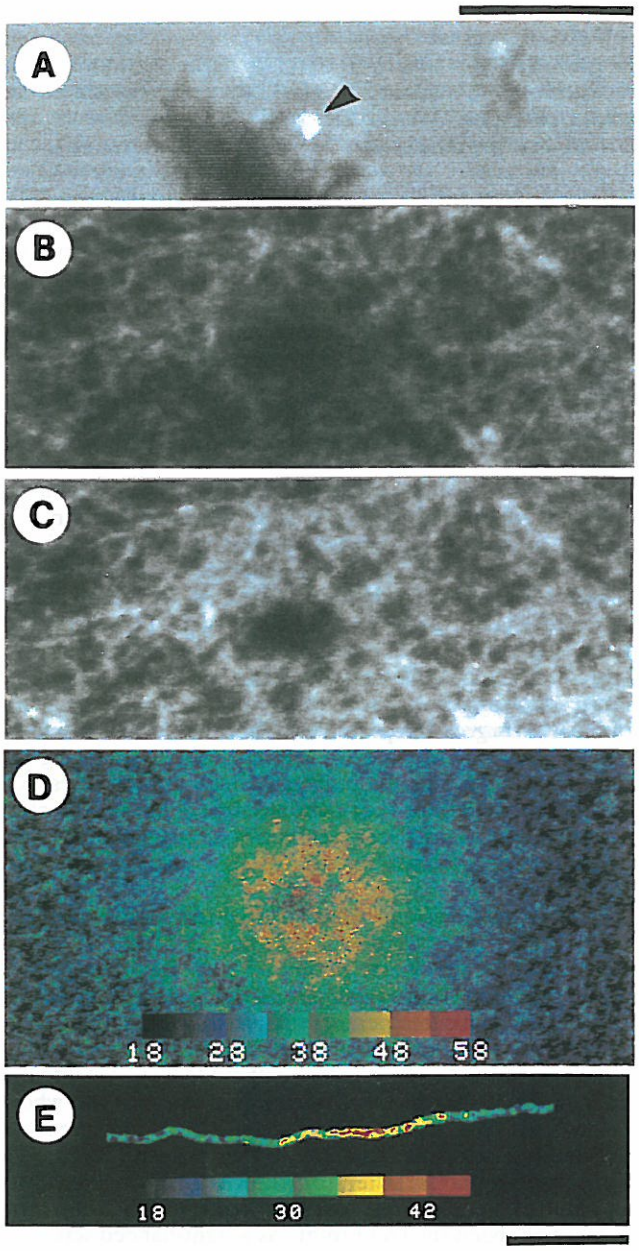

FIG. 2. Imaging of temperature distribution on actin filaments around the metal aggregate. (*A*) Phase-contrast image corresponding to the central part of fluorescence images (*B–D*). A laser beam was focused at a periphery (shown by an arrowhead) of a lump of Al particles of irregular shape. (*B–D*) Fluorescence images of a two-dimensional network of rhodamine phalloidin-labeled actin filaments (12 μg/ml) attached to heavy meromyosin molecules that adhered to the glass surface coated with nitrocellulose (24). Excess actin filaments were washed away, so that filaments were mostly in focus and thus within 1 μm of the glass surface. (*B*) Fluorescence image of the actin network taken in a single video frame coincident with laser illumination for 1/30 s under shutter control. A periphery of a ≈10-μm lump of Al particles observed in *A* was illuminated. Fluorescence under and close to the metal aggregate disappeared because of excessively high temperature. (*C*) A single-frame fluorescence image obtained two video frames after *B*; the image was indistinguishable from that obtained before laser illumination at 18°C ± 1°C, i.e., temperature of the coverslip. (*D*) Two-dimensional temperature distribution constructed from the ratio of the fluorescence intensities of the images *B* and *C*. (*E*) Temperature distribution on a single actin filament; only in this micrograph, the background fluorescence intensity was subtracted. In *D* and *E*, the temperature is scaled in pseudocolor as shown in color bars in °C unit. (Scale bars: upper one for *A–D*, lower one for *E*, 10 μm.)

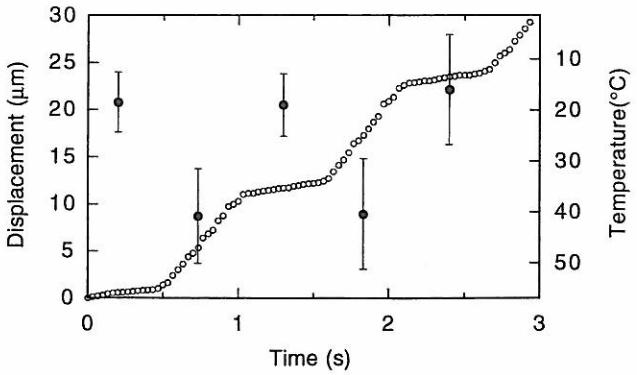

FIG. 3. Time course showing reversible changes in the sliding movement of an actin filament with repetitive temperature pulses. Displacement of the centroid of the fluorescence image of the actin filament (1.0 μm long) is shown by ○ every 1/30 s. A laser pulse of 0.53-s duration was given every 1.07 s. The temperature was estimated from the average intensity of the actin filament in each frame at 30 frames/s. ● and error bars show the average ± SD for 14 consecutive frames (0.47 s). The coverslip temperature was kept at 18°C ± 1°C.

sliding filaments tended to detach from the glass surface at higher temperatures, e.g., within 1 min at 50°C, suggesting gradual deterioration of motor functions. The higher velocities obtained with our TPM at 40°C demonstrate that the motors can be fully activated for a short period of time before thermally induced protein damage begins.

Next, we examined sliding movement of an actin filament during very short temperature pulses by using a shutter (Fig. 1). When illuminated with a laser pulse with a duration of 1/16 s, an abrupt displacement of the actin filament, by as much as 1.6 μm, occurred, corresponding to a sliding velocity of about 26 μm/s (Fig. 4 *A* and *B*). The average temperature during this 1/16-s illumination was estimated to be 45°C and the maximum temperature exceeded 60°C (Fig. 4*C*). On shortening the duration of the temperature pulse, the degree of abrupt displacement correspondingly decreased, i.e., 1 μm (average sliding velocity, 32 μm/s) for 1/32 s, 0.5 μm (32 μm/s) for 1/64 s, and 0.2 μm (26 μm/s) for 1/128-s illumination. The fact that the displacement was proportional to the duration of the temperature pulse implies that steady-state sliding at the high temperature already was achieved at the shortest duration of 1/128 s. In the Huxley scheme (30), the steady-state velocity of unloaded sliding is given by $hg_2/2$, where h is the maximal distance over which a myosin head attached to actin can exert positive tension (power stroke) and g_2 is the rate of unbinding for the head that has undergone a power stroke and is exerting a negative tension. The increase in the sliding velocity by more than an order of magnitude upon heating likely resulted from a corresponding increase in g_2 rather than in h. That is, the rate of unbinding, which is presumably coincident with the ADP release under the present condition where ATP was abundant, increases sharply with temperature. The rate of head binding is likely to also increase with temperature, because otherwise the actin filament would tend to float into the medium, and the tension, proportional to the number of heads attached to the filament, would be greatly reduced whereas our experiment showed the contrary (see below). The high temperature coefficient of the rate of ATP hydrolysis (22), a 5-fold increase from 22°C to 30°C, is consistent with these views. Kitamura *et al.* (31) have reported that the sliding distance per head per ATP can be as long as 30 nm, a value difficult to explain with a conventional power stroke model. Even so, the distance per ATP is not critically dependent on temperature (31), and thus the unbinding rate has to increase with temperature.

The sliding velocities, v, obtained under the long and short temperature pulses were fitted with an Arrhenius equation,

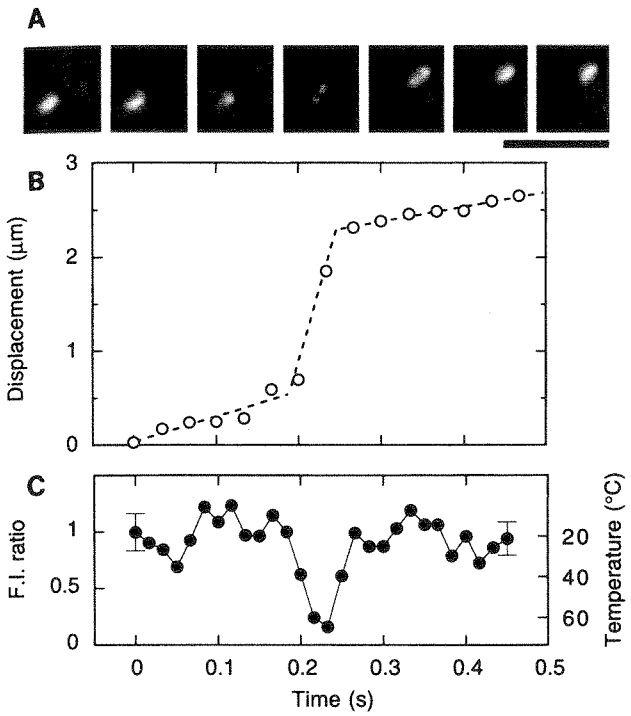

FIG. 4. Time course showing a reversible change in the sliding movement of an actin filament with a single temperature pulse. (*A*) Snapshots of a sliding actin filament (1.1 μm long) at 1/30-s intervals. A laser pulse of 1/16-s duration was given halfway at 0.19 s. (Scale bar, 5 μm.) (*B*) Time course of sliding movement of the actin filament; displacement of the centroid of the fluorescence image of the actin filament is shown by ○. (*C*) The temperature estimated from the average intensity of the filament at 1/60-s intervals. In this particular case, odd and even fields of interlaced images were analyzed separately. The coverslip temperature was kept at 18°C ± 1°C.

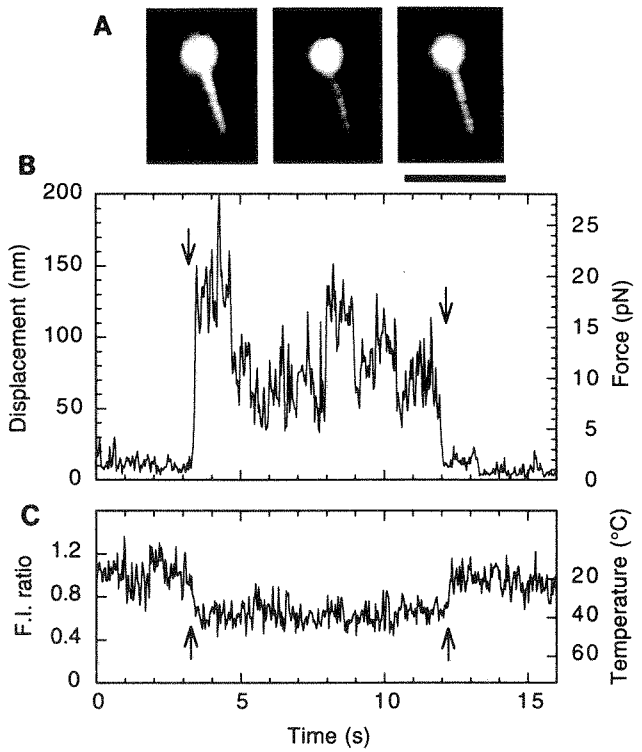

FIG. 5. Tension response of a single actin filament to a temperature pulse. (*A*) Fluorescence image of a bead-tailed actin filament (3.7 μm long) obtained by averaging 15 video frames for 0.5 s before, during, and after the temperature pulse, respectively, from left to right. The bead was coated with rhodamine-labeled BSA (23). The bead brightness is clipped in the central portion. (Scale bar, 5 μm.) (*B*) Time course of tension generation (displacement of the bead); a shutter for laser illumination was opened and closed at the times indicated by the left and right arrows, respectively. (*C*) Temperature was estimated from the fluorescence intensity profile obtained at the middle portion of the actin filament during the laser illumination and was 40°C ± 5°C (estimated by averaging the fluorescence intensity over 0.5 s). Only in this case, the fluorescence intensity gradually decreased with photobleaching because of prolonged laser illumination. The coverslip temperature was kept at 18°C ± 1°C.

$v(T) = v_0 \exp(-E_a/RT)$ where v_0 is a constant and R is the gas constant. The apparent activation energies, E_a, turned out to be 100 kJ/mol between 18°C and 30°C and 50 kJ/mol between 30°C and 45°C. These activation energies agree with those of prior reports (27–29), although the transition between the two temperature regions in the previous studies was at about 20°C rather than 30°C as shown here. The discrepancy could be the result of thermal deterioration that might have occurred at lower temperatures in the previous studies.

Next, to examine the potential of skeletal myosin for high sliding velocity, we used a higher ionic strength (50 mM KCl) (29), resulting in 52 ± 5 μm/s (n = 8) for a 0.5-s period at 46°C ± 7°C (n = 8) (estimated by averaging the fluorescence intensity over 0.5 s for each sample). The sliding velocity obtained here is the highest reported for skeletal myosin in a usual *in vitro* motility assay, although there is a report that the velocity of a large bead coated with myosin (65 μm in diameter) reached 500 μm/s at room temperature in a specially designed motility assay system (32). Faster sliding at higher ionic strength has been observed at lower temperatures (29). High salt may induce faster release of strongly bound heads (g_2 above) and/or the reduction of weakly binding interactions (33) that precede strong binding and that may impede sliding (34). The weakly binding interactions operate mainly at low ionic strengths (33).

We applied TPM to tension generation on single actin filaments. The tension record presented in Fig. 5 shows that an abrupt increase in tension (from 2 pN to 15–20 pN), in other words, sliding movement extending over a longer distance (10 nm to 100–150 nm) from the center of an optical trap, occurred after the temperature jump. A large tension fluctuation was observed around steady-state levels that were maintained for 1–2 s, during each of which the actin filament appeared to slide in one direction. The abrupt changes in the steady tension level, observed several times at 40°C in Fig. 5*B*, may be attributable to slight changes in the sliding direction resulting in a different number of heavy meromyosin molecules that can interact with the actin filament. The tension fluctuation did not correlate with the fluctuation of fluorescence intensity, indicating that the tension fluctuation is not attributable to temperature fluctuation. The average tension increased 5- to 10-fold with the increase in temperature from 18°C to 40°C and paralleled the increase in sliding velocity (Figs. 3 and 4).

In muscle fibers, it was reported that force rose by a factor of 2 to 3 (9, 11, 12, 35) between 5°C and 20°C but only by a factor of ≈1 (9, 12) or ≈1.5 (11) between 20°C and 40°C, much less than the 5- to 10-fold increase in our case. In principle, an increase in tension implies that each myosin head while attached to an actin filament exerts a larger force, and/or that a larger number of heads are attached at any instant. However, the former possibility, an increase in tension per attached head, is unlikely to be the major factor for the 5- to 10-fold increase in tension observed here. The number of attached heads must increase with temperature. Because the increase in the sliding velocity at no external load points to an increase in the rate of unbinding, as discussed above, the rate of head binding to actin has to increase with temperature more than the increase in the unbinding rate. This enormous increase in

binding rate is probably peculiar to the *in vitro* system. On the glass surface, unlike muscle interior, an actin filament tends to float into the medium by Brownian motion. Myosin heads cannot bind to the filament unless the filament happens to be close to the heads. The binding is thus cooperative in that binding of one head greatly facilitates the binding of neighboring heads. A slight increase in the affinity of myosin to actin, enough to account for the fiber data, will be amplified by this cooperativity.

As demonstrated by TPM, motor activity can be reversibly enhanced without denaturation upon raising the temperature above physiological levels (instantaneously, higher than 60°C). We can study the effects of various temperatures (and also the temperature gradient) at the same time for different molecules and different periods of time for the same molecules. The TPM described here can be improved to meet various applications. For example, the heat source of any size and shape can be made by microfabrication techniques. TPM in combination with real-time imaging of temperature on proteins should find broad applications in the studies of the energetics of protein–protein interactions and the response of cellular processes to thermal modulation, not only limited to cell motility but also on various aspects of cellular metabolism and signal transduction within and between cells.

This research was supported by Grants-in-Aid for Scientific Research, for Scientific Research on Priority Areas and for the High-Tech Research Center Project from the Ministry of Education, Science, Sports and Culture of Japan, by Core Research for Evolutional Science and Technology (CREST) of Japan Science and Technology Corporation and by a Waseda University Special Grant-in-Aid.

1. Funatsu, T., Harada, Y., Tokunaga, M., Saito, K. & Yanagida, T. (1995) *Nature (London)* **374,** 555–559.
2. Sase, I., Miyata, H., Corrie, J. E. T., Craik, J. S. & Kinosita, K., Jr. (1995) *Biophys. J.* **69,** 323–328.
3. Sase, I., Miyata, H., Ishiwata, S. & Kinosita, K., Jr. (1997) *Proc. Natl. Acad. Sci. USA* **94,** 5646–5650.
4. Ishijima, A., Kojima, H., Funatsu, T., Tokunaga, M., Higuchi, H., Tanaka, H. & Yanagida, T. (1998) *Cell* **92,** 161–171.
5. Svoboda, K., Schmidt, C. F., Schnapp, B. J. & Block, S. M. (1993) *Nature (London)* **365,** 721–727.
6. Finer, J. T., Simmons, R. M. & Spudich, J. A. (1994) *Nature (London)* **368,** 113–119.
7. Miyata, H., Hakozaki, H., Yoshikawa, H., Suzuki, N., Kinosita, K., Jr., Nishizaka, T. & Ishiwata, S. (1994) *J. Biochem.* **115,** 644–647.
8. Nishizaka, T., Miyata, H., Yoshikawa, H., Ishiwata, S. & Kinosita, K., Jr. (1995) *Nature (London)* **377,** 251–254.
9. Goldman, Y. E., McCray, J. A. & Ranatunga, K. W. (1987) *J. Physiol. (London)* **392,** 71–95.
10. Davis, J. S. & Harrington, W. F. (1987) *Proc. Natl. Acad. Sci. USA* **84,** 975–979.
11. Bershitsky, S. Y. & Tsaturyan, A. K. (1992) *J. Physiol. (London)* **447,** 425–448.
12. Ranatunga, K. W. (1996) *Biophys. J.* **71,** 1905–1913.
13. Liu, Y., Cheng, D. K., Sonek, G. J., Berns, M. W., Chapman, C. F. & Tromberg, B. J. (1995) *Biophys. J.* **68,** 2137–2144.
14. Kolodner, P. & Tyson, J. A. (1982) *Appl. Phys. Lett.* **40,** 782–784.
15. Romano, V., Zweig, A. D., Frenz, M. & Weber, H. P. (1989) *Appl. Phys. B* **49,** 527–533.
16. Zohar, O., Ikeda, M., Shinagawa, H., Inoue, H., Nakamura, H., Elbaum, D., Alkon, D. L. & Yoshioka, T. (1998) *Biophys. J.* **74,** 82–89.
17. Washizu, M., Kurosawa, O., Suzuki, S. & Shimamoto, N. (1996) *SPIE* **2716,** 133–143.
18. Kinosita, K., Jr., Itoh, H., Ishiwata, S., Hirano, K., Nishizaka, T. & Hayakawa, T. (1991) *J. Cell Biol.* **115,** 67–73.
19. De la Cruz, E. M. & Pollard, T. D. (1994) *Biochemistry* **33,** 14387–14392.
20. Nishizaka, T., Yagi, T., Tanaka, Y. & Ishiwata, S. (1993) *Nature (London)* **361,** 269–271.
21. Yanagida, T., Nakase, M., Nishiyama, K. & Oosawa, F. (1984) *Nature (London)* **307,** 58–60.
22. Harada, Y., Sakurada, K., Aoki, T., Thomas, D. D. & Yanagida, T. (1990) *J. Mol. Biol.* **216,** 49–68.
23. Suzuki, N., Miyata, H., Ishiwata, S. & Kinosita, K., Jr. (1996) *Biophys. J.* **70,** 401–408.
24. Kron, S. J., Toyoshima, Y. Y., Uyeda, T. Q. P. & Spudich, J. A. (1991) *Methods Enzymol.* **196,** 399–416.
25. Sellers, J. R. & Kachar, B. (1990) *Science* **249,** 406–408.
26. Tanaka, Y., Ishijima, A. & Ishiwata, S. (1992) *Biochim. Biophys. Acta* **1159,** 94–98.
27. Anson, M. (1992) *J. Mol. Biol.* **224,** 1029–1038.
28. Winkelmann, D. A., Bourdieu, L., Ott, A., Kinose, F. & Libchaber, A. (1995) *Biophys. J.* **68,** 2444–2453.
29. Homsher, E., Wang, F. & Sellers, J. R. (1992) *Am. J. Physiol.* **262,** C714–C723.
30. Huxley, A. F. (1957) *Prog. Biophys. Biophys. Chem.* **7,** 255–318.
31. Kitamura, K., Tokunaga, M., Hikikoshi-Iwane, A. & Yanagida, T. (1999) *Nature (London)* **397,** 129–134.
32. Suda, H. & Ishikawa, A. (1997) *Biochem. Biophys. Res. Commun.* **237,** 427–431.
33. Brenner, B. (1987) *Annu. Rev. Physiol.* **49,** 655–672.
34. Tawada, K. & Sekimoto, K. (1991) *J. Theor. Biol.* **150,** 193–200.
35. Bershitsky, S. Y., Tsaturyan, A. K., Bershitskaya, O. N., Mashanov, G. I., Brown, P., Burns, R. & Ferenczi, M. A. (1997) *Nature (London)* **388,** 186–190.

Tropomyosin Modulates pH Dependence of Isometric Tension

Hideaki Fujita* and Shin'ichi Ishiwata*#§¶

*Department of Physics, School of Science and Engineering, #Advanced Research Institute for Science and Engineering, and §Materials Research Laboratory for Bioscience and Photonics, Waseda University, Tokyo 169-8555, and ¶Core Research for Evolutional Science and Technology, "Genetic Programming" Team 13, Kawasaki 216-0001 Japan

ABSTRACT We investigated the effect of pH on isometric tension in actin filament-reconstituted and thin filament-reconstituted bovine cardiac muscle fibers in the pH range of 6.0–7.4. Thin filament was reconstituted from purified G-actin with either bovine cardiac tropomyosin (Tm) or rabbit skeletal Tm in conjunction with cardiac or skeletal troponin (Tn). Results showed that isometric tension decreased linearly with a decrease in pH. The slope of the pH-tension relation, $\Delta F/\Delta pH$ (Δrelative tension/Δunit pH), was 0.28 and 0.44 in control cardiac fibers and skeletal fibers, respectively. In actin filament-reconstituted fibers without regulatory proteins, $\Delta F/\Delta pH$ was 0.62, namely larger than that in cardiac or skeletal fibers. When reconstituted with cardiac Tm-Tn complex (nTm), $\Delta F/\Delta pH$ recovered to 0.32, close to the value obtained in control cardiac fibers. When reconstituted with skeletal nTm, $\Delta F/\Delta pH$ recovered to 0.48, close to the value for control skeletal fibers. To determine whether Tm or Tn is responsible for the inhibitory effects of nTm on the tension decrease caused by reduced pH, thin filament was reconstituted with cardiac Tm and skeletal Tn, or with skeletal Tm and cardiac Tn. When cardiac Tm was used, pH dependence of isometric tension coincided with that of control cardiac fibers. When skeletal Tm was used, the pH dependence coincided with that of control skeletal fibers. Furthermore, closely similar results were obtained in fibers reconstituted with actin and either cardiac or skeletal Tm without Tn. These results demonstrate that Tm but not Tn modulates the pH dependence of active tension.

INTRODUCTION

It is known that intracellular pH decreases when muscle fatigues, and in the onset of ischemia and hypoxia. A decrease in pH causes decreases in active tension, shortening velocity, and Ca^{2+} sensitivity in skinned muscle fibers (Dawson et al., 1978; Edman and Matiazzi, 1981; Donaldson and Hermansen, 1978; Fabiato and Fabiato, 1978; Robertson and Kerrick, 1979; Chase and Kushmerick, 1988; Cooke et al., 1988; Metzger and Moss, 1987). Moreover, ATPase activity increases when pH is reduced (Curtin et al., 1988), resulting in an increase in tension cost (Godt and Kentish, 1989; Potma et al., 1994).

The degree of the effect of reduced pH depends on the muscle type. For example, the rightward shift in the pCa-tension relationship is greater in cardiac than in skeletal muscle (Donaldson and Hermansen, 1978; Metzger et al., 1993). Furthermore, the decrease in maximum isometric tension is greater in skeletal muscle with predominantly fast twitch fibers than in soleus muscle, which has predominantly slow twitch fibers (Metzger and Moss, 1987; Potma et al., 1994). Because different isoforms of myofilament proteins are expressed in these fiber types (Nadal-Ginard and Mahdavi, 1989), this difference in pH dependence among different fiber types may be caused by a difference in their protein isoforms. It is known that different Tn isoforms are involved in the different pH effects on Ca^{2+} sensitivity (Solaro et al., 1986, 1989; Palmer and Kentish, 1994; Kawashima et al., 1995, Parsons et al., 1997). However, it is not known whether different Tm isoforms are involved in the difference in pH dependence on maximum isometric tension. It may be possible to examine this by using muscle fibers prepared from transgenic animals expressing Tm isoforms (Palmiter et al., 1996). In the present study, we investigated this possibility through the use of thin filament-reconstituted cardiac muscle fibers (Fujita et al., 1996; Fujita and Ishiwata, 1998).

The thin filament in skeletal or cardiac muscle fibers can be selectively removed using calf plasma gelsolin, an actin filament-severing protein (Funatsu et al., 1990, 1993; Yasuda et al., 1995). Actin filaments in such thin filament-removed cardiac muscle fibers can be fully reconstituted by adding exogenous actin (Fujita et al., 1996; Fujita and Ishiwata, 1998; Ishiwata et al., 1998). Furthermore, thin filament possessing full Ca^{2+} sensitivity can then be reconstituted by adding regulatory proteins Tm and Tn to the actin filament-reconstituted fibers. We found that, as in control muscle fibers, pH dependence of tension development in actin filament-reconstituted bovine cardiac muscle fibers in the absence of regulatory proteins was nearly linear in the pH range 6.0–7.4, but that the slope was steeper. The original slope was regained by reconstitution with bovine cardiac nTm (Tm and Tn). Furthermore, fibers reconstituted with rabbit skeletal nTm showed a pH dependence resembling that of rabbit skeletal muscle. Similar modulation of pH dependence of isometric tension was also observed in fibers reconstituted with actin and Tm but without Tn. These results demonstrate that $\Delta F/\Delta pH$ depends on the type of Tm isoform, such that Tm modifies the pH dependence of isometric tension.

Received for publication 9 February 1999 and in final form 7 June 1999.

Address reprint requests to Dr. Shin'ichi Ishiwata, Department of Physics, School of Science and Engineering, Waseda University, 3-4-1 Okubo, Shinjuku-ku, Tokyo 169-8555, Japan. Tel.: +81-3-5286-3437; Fax: +81-3-3200-2567; E-mail: ishiwata@mn.waseda.ac.jp.

0006-3495/99/09/1540/07 $2.00

MATERIALS AND METHODS

Solutions

The solutions used were as follows: rigor solution, 170 mM KCl, 1.0 mM $MgCl_2$, 1.0 mM EGTA, and 10 mM 3-(*N*-morpholino)propanesulfonic acid (MOPS) (pH 7.0); relaxing solution, 117 mM KCl, 5.0 mM $MgCl_2$, 4.0 mM ATP, 1.0 mM EGTA, 10 mM MOPS (pH 7.0), and 20 mM 2,3-butanedione 2-monoxime (BDM); contracting solution, 117 mM KCl, 4.25 mM $MgCl_2$ (2.2 mM free Mg^{2+}), 2.2 mM ATP (2.0 mM $MgATP^{2-}$), 2.0 mM EGTA, 20 mM MOPS (pH 6.6–7.4) or 2-(*N*-morpholino)ethanesulfonic acid (MES) (pH 6.0–6.4), and 2.0 mM $CaCl_2$. ATP (disodium salt) was purchased from Boehringer Mannheim (Mannheim, Germany); EGTA, MOPS, and MES were from Dojindo Laboratories (Kumamoto, Japan). Tetramethyl rhodamine-5-iodoacetamide (Rh-IA) and fluorescein phalloidin (Fl-Ph) were purchased from Molecular Probes (Eugene, OR). Other chemicals were of reagent grade.

Muscle fibers and proteins

Glycerinated bovine cardiac muscle fibers and rabbit white skeletal muscle fibers were prepared in a solution composed of 50% (v/v) glycerol, 0.5 mM $NaHCO_3$, 5.0 mM EGTA, and 2.0 mM leupeptin. Glycerinated fibers were stored at −20°C and used within 2–8 weeks. Bovine plasma gelsolin was prepared according to the method of Kurokawa et al. (1990). Actin was extracted from acetone powder (Kondo and Ishiwata, 1976) of bovine cardiac muscle according to the method of Spudich and Watt (1971). Purified G-actin was stored at 0°C and used within 1 week. Tm, Tn, and nTm were prepared from bovine cardiac muscle and from rabbit white skeletal muscle according to the method of Ebashi et al. (1968) and purified using DEAE Sephadex A-25 (Pharmacia, Sweden). Tm labeled with Rh-IA (9% labeled) was prepared according to the method of Ishii and Lehrer (1990).

Tension measurement

A thin muscle bundle (~1 mm in length, ≤60 μm in diameter) was carefully stripped from a glycerinated bovine cardiac muscle fiber with a pair of forceps under a stereomicroscope just before experiments. To prepare a suitably thin bundle, dissection was carried out in glycerol solution at about −10°C (Fukuda et al., 1996). Both ends of the bundle were fixed to thin tungsten wires with enamel (commercial nail polish for cosmetic use), one of which was attached to a tension transducer (AE-801; SensoNor a.s, Holten, Norway). The muscle bundle was then immersed in rigor solution containing 1% Triton X-100 for 20 min to remove residual portions of the membrane system. After Triton X-100 was washed out with rigor solution, the bundle was immersed in the relaxing solution. Active tension was measured with a pen recorder (VP-6533A; National, Japan) by immersing the muscle bundle in the contracting solution. Active tension of control cardiac muscle fibers were 60–80 kN/m^2 (cf. Fujita et al., 1996). The maximum activated tension in control and actin filament-reconstituted fibers did not change with the addition of creatine kinase (1.0 mg/ml)/creatine phosphate (10 mM), suggesting that ATP depletion within the muscle bundles did not occur, probably because the diameter of the muscle bundle was small (≤60 μm) and the solution was continuously stirred (Yamaguchi, 1998). The measurement chamber used was a silicon-coated aluminum block (10 cm × 10 cm × 1 cm) with several small wells (7 mm in diameter) filled with ~0.4 ml each of experimental solutions (Horiuti, 1986). The bundle was immersed just below the surface at the deepest part of the solution droplet in the well such that only 1–2 s was required for the transfer of the bundle from one solution to another. Measurements were carried out at 25°C.

Removal and reconstitution of actin filaments

Removal and reconstitution of the actin filament were performed as previously described (Fujita et al., 1996; Fujita and Ishiwata, 1998; Ishiwata et al., 1998). In brief, thin cardiac muscle bundles were immersed in contracting solution containing 20 mM BDM (to suppress tension development during gelsolin treatment, which requires Ca^{2+}) and 0.3 mg/ml gelsolin at 2°C for 80 min to selectively remove thin filament. We confirmed that no active tension developed after gelsolin treatment. The bundles were then immersed in actin-polymerizing solution (80 mM KI, 4.0 mM $MgCl_2$, 4.0 mM ATP, 4.0 mM EGTA, 20 mM BDM, and 20 mM K-phosphate, pH 7.0) containing 1 mg/ml purified G-actin, which was mixed just before use. G-actin in the polymerizing solution was freshly prepared just before use and exchanged every 7 min to avoid nucleation. Actin polymerization was performed for a total of 28 min (7 min × 4). Removal and reconstitution procedures were carried out at 2°C. Relaxation of the actin filament-reconstituted fibers was achieved by immersing the fibers in relaxing solution containing 20 mM BDM. Activation of actin filament-reconstituted fibers was achieved by washing out BDM relaxing solution with contracting solution. There was no Ca^{2+} sensitivity in actin filament-reconstituted fibers.

Reconstitution of thin filaments

To reconstitute the thin filament, actin filament-reconstituted fibers were immersed in relaxing solution containing 3 mg/ml nTm and 20 mM BDM at 2°C for 12 h. To reconstitute fibers with skeletal Tm and cardiac Tn, or with cardiac Tm and skeletal Tn (chimera nTm fibers), the fibers were first immersed in relaxing solution containing 1.5 mg/ml Tm and 20 mM BDM at 2°C for 12 h. The fibers were then immersed in relaxing solution containing 1.5 mg/ml Tn and 20 mM BDM at 2°C for 5 h. These thin filament-reconstituted fibers showed no active tension development in the absence of Ca^{2+}, but did develop tension when Ca^{2+} was added in the absence of BDM. Fibers that developed less than 70% of the tension obtained before reconstitution with regulatory proteins were not used.

To confirm the binding of Tm to the reconstituted actin filaments in the fibers, thin filaments were reconstituted with Rh-IA-labeled Tm instead of unlabeled Tm according to the same procedure as described above. The fibers were then fixed with relaxing solution containing 1% formaldehyde for 30 min and stained with 6.6 μM Fl-Ph in relaxing solution for 5 h at 2°C to visualize actin filaments. They were then mounted on a coverslip and washed with relaxing solution containing 4.5 mg/ml glucose, 0.22 mg/ml glucose oxidase, 0.036 mg/ml catalase, and 10 mM dithiothreitol. Preparations were observed under a laser scanning confocal microscope equipped with a 25-mW Ar laser at 488 nm (Fluoview-IX/AR; Olympus Co., Tokyo). No crossover between fluorescence images of rhodamine (>610 nm; red) and fluorescein (510–540 nm; green) was detectable. As shown in Fig. 1, *A* and *B*, the distribution of Rh-IA was identical to that of Fl-Ph except for the weak fluorescence at the Z line, showing that incorporated Tm was bound to actin filaments except at the Z line. Control cardiac muscle fibers were also incubated with Rh-IA-labeled Tm for 12 h at 2°C in BDM relaxing solution and then stained with Fl-Ph after formaldehyde fixation. As shown in Fig. 1, *C* and *D*, fluorescence of Rh-IA was not detectable, indicating that Tm was not incorporated into the thin filaments in control fibers.

RESULTS

pH dependence of isometric tension in actin filament-reconstituted and thin filament-reconstituted fibers

Fig. 2 shows pen traces of isometric tension measured at various pH values in actin filament-reconstituted fibers. First, glycerinated cardiac muscle fibers were treated with gelsolin (*arrow G* in Fig. 2). Removal of thin filaments was verified by measuring active tension, which was negligible after gelsolin treatment. The muscle bundles were then treated with actin-polymerizing solution (*arrow A* in Fig. 2),

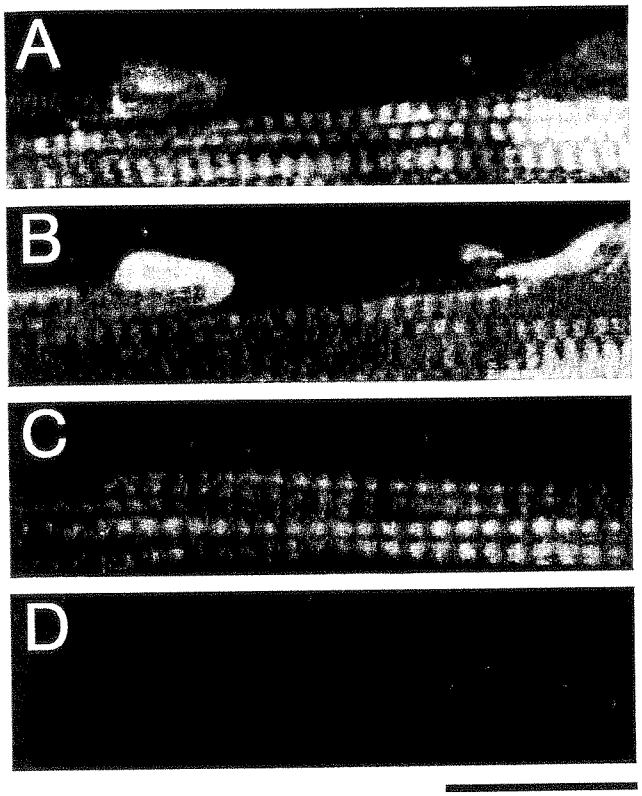

FIGURE 1 Confocal fluorescence micrographs showing the distribution of actin filaments labeled with Fl-Ph (*A, C*) and Tm labeled with Rh-IA (*B, D*) in thin filament-reconstituted (*A, B*) and control (*C, D*) cardiac muscle fibers. Bar, 20 μm.

and the pH dependence of active tension was measured. pH was increased stepwise from 6.0 to 7.0 at a 0.2 interval, and decreased again stepwise to 6.0. Active tension increased in proportion to the increase in pH and decreased in proportion to the decrease in pH. Relative tension was calculated by dividing average tension by that at pH 7.0. The stability and durability of the reconstituted muscle fibers with respect to contractile properties were indistinguishable from those of control fibers (Fig. 2).

The pH dependence of isometric tension in the actin filament- and thin filament-reconstituted fibers is shown in Fig. 3. In control bovine cardiac and rabbit skeletal muscle fibers, the pH-tension relation was nearly linear in the pH range 6.0–7.4. The slope of the pH-tension relation was greater in skeletal than in cardiac muscle fibers, with $\Delta F/\Delta$pH of 0.28 for cardiac (Fig. 3, *empty circles, thick line*) and 0.44 for skeletal muscle fibers (Fig. 3, *empty triangles, thin line*). $\Delta F/\Delta$pH in actin filament-reconstituted fibers without regulatory proteins was 0.62, the greatest value of all combinations tested (Fig. 3, *empty squares, dotted line*). When thin filament was reconstituted with bovine cardiac nTm, $\Delta F/\Delta$pH decreased to 0.32, close to the control value (Fig. 3, *filled circles, thick broken line*). The thin filament-reconstituted fibers did not develop active tension in the absence of Ca^{2+}. These results indicate that the regulatory proteins suppressed the decrease in tension caused by decreasing pH. In fibers reconstituted with rabbit skeletal nTm, $\Delta F/\Delta$pH was 0.48, close to that of the control skeletal fibers (Fig. 3, *filled triangles, thin broken line*).

pH-tension relation in fibers reconstituted with actin and chimera nTm

To determine whether Tm or Tn is responsible for the pH dependence, the pH-tension relation was examined in fibers reconstituted with chimera nTm, i.e., either cardiac Tm (cTm) and skeletal Tn (sTn), or skeletal Tm (sTm) and cardiac Tn (cTn). In fibers reconstituted with cTm + sTn, the relation resembled that in cardiac muscle fibers (Fig. 4, *half-filled circle*), with a $\Delta F/\Delta$pH value of 0.29, whereas in those reconstituted with sTm + cTn it resembled that in skeletal muscle fibers (Fig. 4, *half-filled triangle*), with a $\Delta F/\Delta$pH value of 0.44. These results indicate that the pH-tension relation is modified by Tm but not by Tn.

To confirm that the chimera nTm fibers were constructed successfully, the pCa-tension relation was examined. Fibers reconstituted with sTm + cTn showed a pCa-tension relation indistinguishable from that of control cardiac muscle fibers at pH 7.0 (Fig. 5 *A*) and pH 6.4 (Fig. 5 *B*). At pH 7.0, the Hill coefficient (n_H) for control cardiac and chimera nTm fibers was 1.9 and 2.0, respectively, and the pCa_{50} value, an indicator of Ca^{2+} sensitivity, was 6.05 and 6.1, respectively. The respective values at pH 6.4 were 2.0 and 2.0, and 5.6 and 5.55. A rightward shift in the pCa-tension relation by a decrease in pH was observed in control and chimera fibers to the same degree. The Hill coefficient did not change significantly with a decrease in pH from 7.0 to 6.4.

pH-tension relation in fibers reconstituted with actin and Tm

Next, we examined the pH-tension relation of fibers reconstituted with actin and Tm. Tm-reconstituted fibers generated active tension in a Ca^{2+}-insensitive manner because of the lack of Tn. In cTm-reconstituted fibers, $\Delta F/\Delta$pH was 0.33 (Fig. 6, *empty circle*), similar to that of control cardiac fibers, whereas in sTm-reconstituted fibers it was 0.49 (Fig. 6, *filled circle*), similar to that of control skeletal fibers. $\Delta F/\Delta$pH values for various types of muscle models thus obtained are summarized in Table 1. The difference in the pH-tension relation between different Tm isoforms was statistically significant, whereas there was no statistically significant difference between different Tn isoforms when the same Tm isoform was used.

DISCUSSION

Experiments using thin filament-reconstituted fibers

Actin polymerization was performed for only 28 min (7 min × 4) instead of the 42 min (7 min × 6) used in the

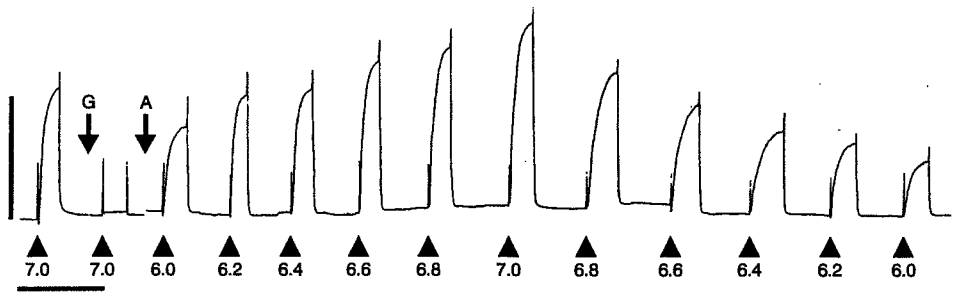

FIGURE 2 Recordings of isometric tension at varying pH in actin filament-reconstituted cardiac muscle fibers. After measurement of control tension, fibers were immersed in contracting solution containing 0.3 mg/ml gelsolin and 20 mM BDM for 80 min at 2°C (*arrow G*). After confirmation that fibers developed no active tension after gelsolin treatment, they were immersed in actin polymerizing solution containing 1 mg/ml G-actin for a total of 28 min (7 min × 4) at 2°C (*arrow A*). Arrowheads indicate solution change. pH values of contracting solutions are indicated below the arrowheads. Spikes are artifacts due to solution change. Active tension at varying pH was measured at 25°C. Relaxation was obtained by immersing the fiber in relaxing solution containing 20 mM BDM at 2°C. Vertical and horizontal bars, 2×10^{-4} N and 2 min, respectively.

original work (Fujita et al., 1996) to minimize fiber damage due to repeated high-tension developments. Consequently, the average tension developed in the actin filament-reconstituted fibers was closely similar to that in the control fibers. The only problem with this actin filament reconstitution method is that it was difficult to control the extent of tension recovery after reconstitution, which varied between preparations (Fujita et al., 1996). Because this variability makes it difficult to quantitatively analyze the difference between active tension of control fibers and actin filament-reconstituted fibers, experiments should have been designed to compare the properties of reconstituted and control fibers, using the same actual fiber. Here, the decrease in active tension with decreasing pH was compared between actin (thin) filament-reconstituted fibers and their controls. These properties were reproducible and reliable, as reported here.

In the present study, we succeeded in constructing chimera nTm fibers composed of either skeletal Tm and cardiac Tn or vice versa. To construct chimera nTm-reconstituted fibers, actin filament-reconstituted fibers were first

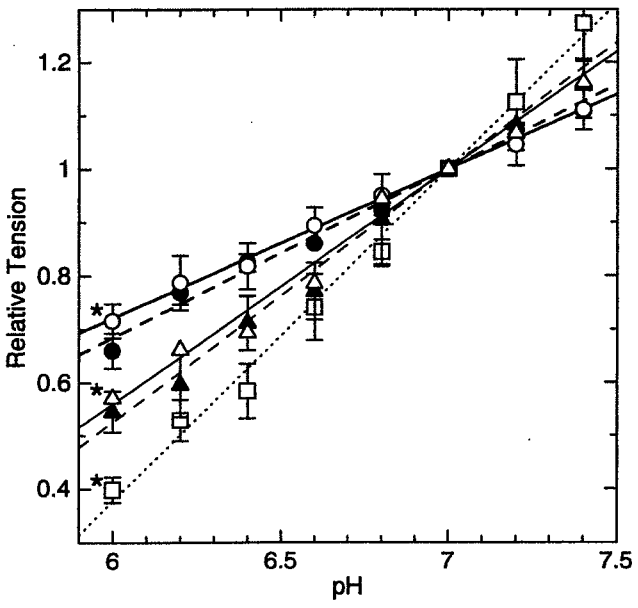

FIGURE 3 Effect of pH on isometric tension in control cardiac muscle fibers (*empty circles, thick line*), control skeletal muscle fibers (*empty triangles, thin line*), actin filament-reconstituted muscle fibers (*empty squares, dotted line*), thin filament-reconstituted fibers with cardiac nTm (*filled circles, thick broken line*), and thin filament-reconstituted fibers with skeletal nTm (*filled triangles, thin broken line*). Relative tension was normalized to that at pH 7.0. Lines are fitted by least-squares fit. Vertical bars show SD calculated from three to five data points. Active tension was measured at 25°C. The difference between any two data points marked with * at pH 6.0 was statistically significant ($p < 0.001$ by Student's *t*-test).

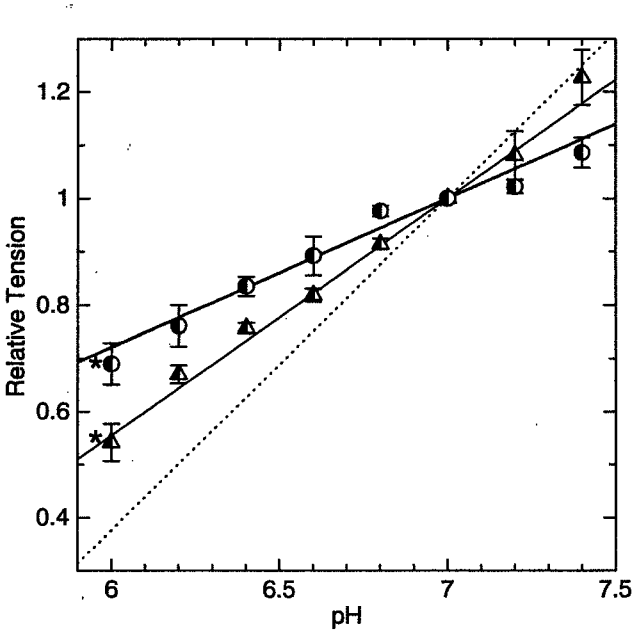

FIGURE 4 Effect of pH on isometric tension in fibers reconstituted with cTm and sTn (*half-filled circles*), and with sTm and cTn (*half-filled triangles*). Thick, thin, and dotted lines show, respectively, the fitted lines for control cardiac, control skeletal, and actin filament-reconstituted fibers obtained in Fig. 3. Relative tension was normalized to that at pH 7.0. Vertical bars show SD calculated from three to five data points. Active tension was measured at 25°C. The difference between two data points marked with * at pH 6.0 was statistically significant ($p < 0.01$ by Student's *t*-test).

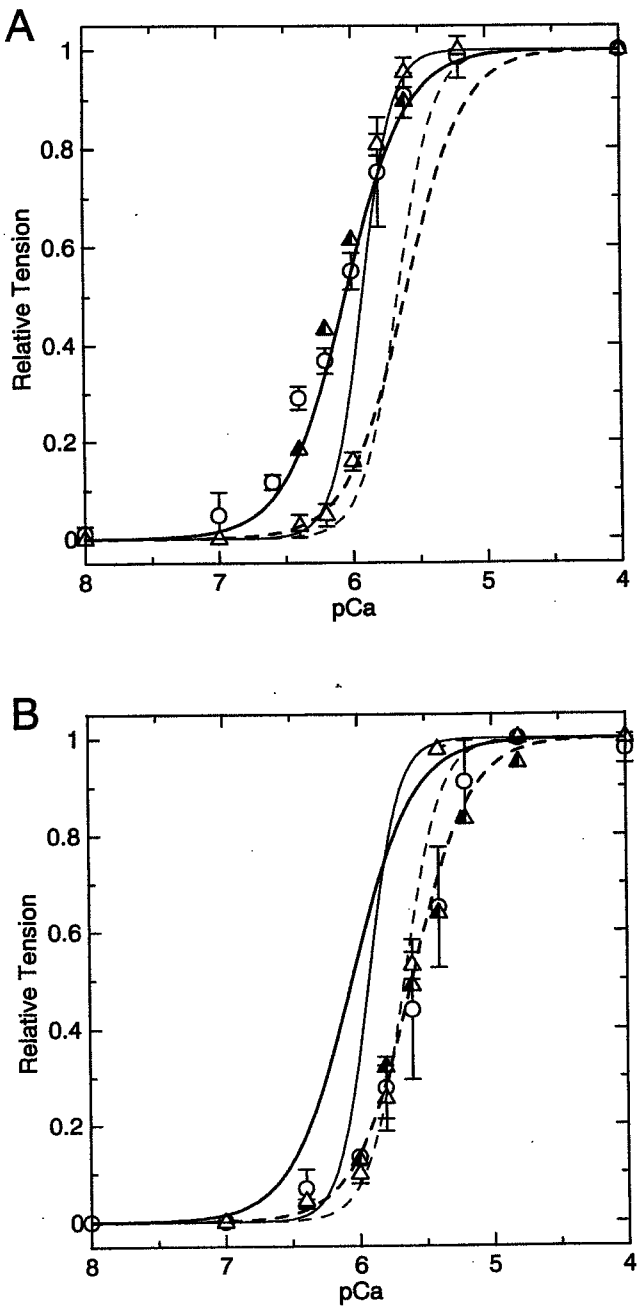

FIGURE 5 pCa-tension relation of control cardiac (*empty circles*), control skeletal (*empty triangles*), and (sTm + cTn)-reconstituted fibers (*half-filled triangles*) at pH 7.0 (*A*) and pH 6.4 (*B*). Thick and thin lines are the curves fitted for control cardiac and skeletal fibers (*solid line*, pH 7.0; *broken line*, pH 6.4), respectively. Relative tension was normalized to that at pCa 4.0. Vertical bars show SD calculated from three to five data points. Active tension was measured at 25°C.

reconstituted with Tm and then with Tn so that nonspecific binding of Tn to actin filaments was avoided (Ishiwata and Kondo, 1978). The purity of added proteins was confirmed by sodium dodecyl sulfate-polyacrylamide gel electrophoresis before reconstitution (data not shown), but the quality of reconstitution (e.g., the stoichiometry of actin, Tm, and Tn) in the reconstituted fibers could not be evaluated by sodium

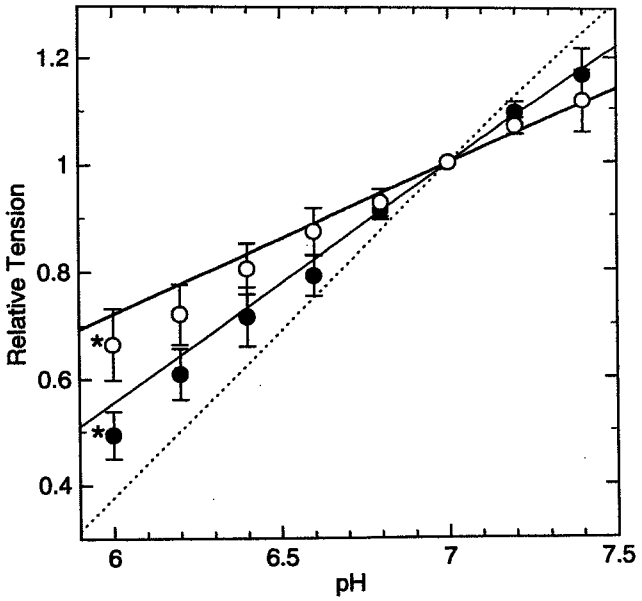

FIGURE 6 Effect of pH on isometric tension in fibers reconstituted with cTm (*empty circles*) and sTm (*filled circles*). Thick, thin, and dotted lines show, respectively, fitted lines for control cardiac, control skeletal, and actin filament-reconstituted fibers obtained in Fig. 3. Relative tension was normalized to that at pH 7.0. Vertical bars show SD calculated from three to five data points. Active tension was measured at 25°C. The difference between two data points marked with * at pH 6.0 was statistically significant ($p < 0.01$ by Student's *t*-test).

dodecyl sulfate-polyacrylamide gel electrophoresis because of the small amount of proteins. To confirm the reconstitution of thin filaments, the pCa-tension relation was therefore examined. On the basis that both the pCa_{50} value and the Hill coefficient in the chimera nTm fibers were determined by the type of Tn (Fig. 5), we conclude that the function of thin filaments was fully recovered.

Maximum decrease in active tension by decreased pH in actin filament-reconstituted fibers

In control cardiac muscle fibers, active tension decreased linearly with a decrease in pH in the range of pH 6.0–7.4 (Fig. 3, *empty circles*), which is consistent with the previous results (Metzger and Moss, 1987; Godt and Kentish, 1989; Solaro et al., 1989). Although a linear decrease in active

TABLE 1 $\Delta F/\Delta pH$ values for various types of muscle model

			Thin filament-reconstituted		
Control			cTn	sTn	no Tn
Cardiac	0.28*	cTm	0.32*	0.29#	0.33§
Skeletal	0.44*	sTm	0.44#	0.48*	0.49§
Actin reconstituted	0.62*				

*Taken from Fig. 3.
#Taken from Fig. 4.
§Taken from Fig. 6.

tension by reduced pH was also observed in actin filament-reconstituted fibers (Fig. 3, *empty squares*), $\Delta F/\Delta pH$ was more than twice that of control cardiac fibers. Because the only difference between control cardiac muscle fibers and actin filament-reconstituted fibers is the presence of regulatory proteins (Fujita et al., 1996), the difference in $\Delta F/\Delta pH$ should be related to regulatory proteins. Given that isometric tension is thought to be proportional to the population of attached cross-bridges, the decrease in active tension with reduced pH may be the result of cross-bridge detachment.

Several factors can be considered in the regulation of the number of attached cross-bridges. Myosin has a positively charged loop (called loop 2) in the upper 50-kDa domain, and actin has four corresponding negatively charged acidic residues located at the N-terminus in subdomain 1. These are assumed to make the initial contact in the actin-myosin interaction (Chaussepied and Van Dijk, 1999). Additionally, there are many histidine residues that have neutral pK values. In theory, a decrease in pH from 7.0 to 6.0 should decrease the proportion of negatively charged carboxyl groups (assume pK 4.7) by ~5% and increase that of positively charged imido groups (assume pK 6.5) by ~70%. The large decrease in active tension by reduced pH in the actin filament-reconstituted fibers may be primarily attributed to the effect of these changes in surface charge on the actin-myosin interaction. Changes in the charge distribution of actin, myosin, or both may also modulate secondary factors that affect the actin-myosin interaction, such as the distance between thick and thin filaments.

Modulation of the pH dependence of active tension by regulatory proteins

Given that the protein composition of skeletal nTm-reconstituted fibers is considered to be the same as that of cardiac muscle fibers with the exception of regulatory proteins, the results shown in Fig. 3 indicate that the differing pH dependency among muscle types is attributable to regulatory protein isoforms. We therefore conclude that the type of regulatory proteins modulates the pH dependence of active tension: the pH dependence of fibers reconstituted with sTm and cTn resembled that of the control skeletal muscle fibers (Fig. 4, *half-filled triangle*), whereas fibers reconstituted with cTm and sTn resembled that of control cardiac muscle fibers (Fig. 4, *half-filled circle*). These findings demonstrate that the pH dependence of active tension is modulated by Tm, and that Tn has no effect on this variable.

When Tm alone (cardiac or skeletal) was added to actin filament-reconstituted fibers, $\Delta F/\Delta pH$ decreased in both cases (Fig. 6). The effect was similar with nTm. These results support the conclusion that Tm alone modulates the pH dependence of active tension. It has been reported that the binding of Tm to actin is stabilized by lowering pH (Tanaka, 1972). The difference among Tm isoforms in modulating the pH dependence of active tension may be due to differences in the stability of Tm isoforms binding to actin filaments.

Three-dimensional modeling of thin filament showed that Tm does not cover the charged group on actin's surface in the presence or absence of Ca^{2+} (Lehman et al., 1995). However, because negative staining was used to visualize Tm, which may alter its location, the possibility remains that Tm is closer to the charged residues in vivo. In addition, the effect of Tm on the pH-tension relation may be attributable to allosteric regulation of charge distribution on actin filaments. That is, the presence of Tm may affect the accessibility of charged groups on actin, even though they are distant from the area covered by Tm.

Mammalian Tm has α and β subunits, which can be arranged as two isomers, $\alpha\alpha$ and $\alpha\beta$ (Eisenberg and Kielley, 1974). The amino acid sequence of these α and β subunits in rabbit skeletal and cardiac muscle is identical (Stone and Smillie, 1977; Lewis and Smillie, 1980). The subunits differ by 39 residues, including two residues, giving a more negative net charge on the β (Mak et al., 1979). Because the α:β ratio depends on muscle type (in general, the ratio of α to β in cardiac muscle is larger than that in skeletal muscle), the modulation of pH dependence of isometric tension in actin filament-reconstituted fibers may also be due to differences in charge distribution on Tm isoforms.

The present study used rabbit fast skeletal Tm and bovine cardiac Tm, both of which are a mixture of α and β Tm. It is not clear whether the difference in pH dependence of active tension between skeletal and cardiac Tm (Figs. 3 and 4) results from a difference in skeletal and cardiac Tm or in rabbit and bovine Tm. However, this ambiguity does not change our major conclusion that Tm modulates the pH dependence of active tension. The molecular basis of Tm's modulation of pH dependence of active tension may be clarified by reconstitution of thin filaments by the use of purified α and β Tm or mutant Tm with different charge distribution. This awaits further investigation.

The smaller decrease in active tension in an acidic environment in cardiac muscle than in skeletal muscle may have developed during the process of evolution. The ability to survive an acidic environment is of particular advantage for cardiac muscle cells, which are often subject to lowered pH induced by cardiac hypoxia and ischemia.

We thank Prof. M. Kawai of the University of Iowa for his critical reading of the manuscript.

This research was partly supported by Grants-in-Aid for Scientific Research, for Scientific Research on Priority Areas, and for the High-Tech Research Center Project from the Ministry of Education, Science, Sports, and Culture of Japan; and by Grants-in-Aid from Japan Science and Technology (CREST). HF is a recipient of a Research Fellowship from the Japan Society for the Promotion of Science for Young Scientists.

REFERENCES

Chase, P. B., and M. J. Kushmerick. 1988. Effects of pH on contraction of rabbit fast and slow skeletal muscle fibers. *Biophys. J.* 53:935–946.

Chaussepied, P., and J. Van Dijk. 1999. Role of charges in actomyosin interactions. *In* Molecular Interactions of Actin. C. G. dos Remedios and D. D. Thomas, editors. Springer-Verlag, Heidelberg, in press.

Cooke, R., K. Franks, G. B. Luciani, and E. Pate. 1988. The inhibition of rabbit skeletal muscle contraction by hydrogen ions and phosphate. *J. Physiol. (Lond.).* 395:77–97.

Curtin, N. A., K. Kometani, and R. C. Woledge. 1988. Effects of intracellular pH on force and heat production in isometric contraction of frog muscle fibres. *J. Physiol. (Lond.).* 396:93–104.

Dawson, M. J., D. G. Gadian, and D. R. Wilkie. 1978. Muscular fatigue investigated by phosphorus nuclear magnetic resonance. *Nature.* 274: 861–866.

Donaldson, S. K., and L. Hermansen. 1978. Differential, direct effects of H^+ on Ca^{2+}-activated force of skinned fibres from the soleus, cardiac and adductor magnus muscle of rabbits. *Pflügers Arch.* 367:55–65.

Ebashi, S., A. Kodama, and F. Ebashi. 1968. Troponin. I. Preparation and physiological function. *J. Biochem. (Tokyo).* 64:465–477.

Edman, K. A., and A. R. Matiazzi. 1981. Effects of fatigue and altered pH on isometric force and velocity of shortening at zero load in frog muscle fibers. *J. Muscle Res. Cell Motil.* 2:321–334.

Eisenberg, E., and W. W. Kielley. 1974. Troponin-tropomyosin complex. *J. Biol. Chem.* 249:4742–4746.

Fabiato, A., and F. Fabiato. 1978. Effects of pH on the myofilaments and the sarcoplasmic reticulum of skinned cells from cardiac and skeletal muscles. *J. Physiol. (Lond.).* 276:233–255.

Fujita, H., and S. Ishiwata. 1998. Spontaneous oscillatory contraction without regulatory proteins in actin filament-reconstituted fibers. *Biophys. J.* 75:1439–1445.

Fujita, H., K. Yasuda, S. Niitsu, T. Funatsu, and S. Ishiwata. 1996. Structural and functional reconstitution of thin filaments in the contractile apparatus of cardiac muscle. *Biophys. J.* 71:2307–2318.

Fukuda, N., H. Fujita, T. Fujita, and S. Ishiwata. 1996. Spontaneous tension oscillation in skinned bovine cardiac muscle. *Pflügers Arch.* 433:1–8.

Funatsu, T., H. Higuchi, and S. Ishiwata. 1990. Elastic filaments in skeletal muscle revealed by selective removal of thin filaments with plasma gelsolin. *J. Cell Biol.* 110:53–62.

Funatsu, T., E. Kono, H. Higuchi, S. Kimura, S. Ishiwata, T. Yoshioka, K. Maruyama, and S. Tsukita. 1993. Elastic filaments in situ in cardiac muscle: deep-etch replica analysis in combination with selective removal of actin and myosin filaments. *J. Cell Biol.* 120:711–724.

Godt, R. E., and J. C. Kentish. 1989. Effects of pH on isometric force, MgATPase, and tension-cost of skinned skeletal muscle fibres of the rabbit and cardiac muscles from rat. *J. Physiol. (Lond.).* 418:68P.

Horiuti, K. 1986. Some properties of the contractile system and sarcoplasmic reticulum of skinned slow fibers from *Xenopus* muscle. *J. Physiol. (Lond.).* 373:1–23.

Ishii, Y., and S. S. Lehrer. 1990. Excimer fluorescence of pyrenyliodoacetamide-labeled tropomyosin: a probe of the state of tropomyosin in reconstituted muscle thin filaments. *Biochemistry.* 29:1160–1166.

Ishiwata, S., T. Funatsu, and H. Fujita. 1998. Contractile properties of thin (actin) filament-reconstituted muscle fibers. *Adv. Exp. Med. Biol.* 453: 319–329.

Ishiwata, S., and H. Kondo. 1978. Studies on the F-actin-tropomyosin-troponin complex. II. Partial reconstitution of thin filaments by F-actin, tropomyosin and the tropomyosin binding component of troponin (TN-T). *Biochim. Biophys. Acta.* 534:341–349.

Kawashima, A., S. Morimoto, A. Suzuki, F. Shiraishi, and I. Ohtsuki. 1995. Troponin isoforms dependent pH dependence of the Ca^{2+}-activated myofibrillar ATPase activity of avian slow and fast skeletal muscles. *Biochem. Biophys. Res. Commun.* 207:585–592.

Kondo, H., and S. Ishiwata. 1976. Uni-directional growth of F-actin. *J. Biochem. (Tokyo).* 79:159–171.

Kurokawa, H., W. Fujii, K. Ohmi, T. Sakurai, and Y. Nonomura. 1990. Simple and rapid purification of brevin. *Biochem. Biophys. Res. Commun.* 168:451–457.

Lehman, W., P. Vibert, P. Uman, and R. Craig. 1995. Steric-blocking by tropomyosin visualized in relaxed vertebrate muscle thin filaments. *J. Mol. Biol.* 251:191–196.

Lewis, W. G., and L. B. Smillie. 1980. The amino acid sequence of rabbit cardiac tropomyosin. *J. Biol. Chem.* 255:6854–6859.

Mak, A. S., L. B. Smillie, and G. R. Stewart. 1979. A comparison of the amino acid sequences of rabbit skeletal muscle α- and β-tropomyosins. *J. Biol. Chem.* 255:3647–3655.

Metzger, J. M., and R. L. Moss. 1987. Greater hydrogen ion-induced depression of tension and velocity in skinned single fibres of rat fast than slow muscles. *J. Physiol. (Lond.).* 393:727–742.

Metzger, J. M., M. S. Parmacek, E. Barr, K. Pasyk, W. Lin, K. L. Cochrane, L. J. Field, and J. M. Leiden. 1993. Skelatal troponin C reduces contractile sensitivity to acidosis in cardiac myocytes from transgenic mice. *Proc. Natl. Acad. Sci. USA.* 90:9036–9040.

Nadal-Ginard, B., and V. Mahdavi. 1989. Molecular basis of cardiac performance. *J. Clin. Invest.* 84:1693–1700.

Palmer, S., and J. C. Kentish. 1994. The role of troponin C in modulating the Ca^{2+} sensitivity of mammalian skinned cardiac and skeletal muscle fibres. *J. Physiol. (Lond.).* 480:45–60.

Palmiter, K. A., Y. Kitada, M. Muthuchamy, D. F. Wieczorek, and R. J. Solaro. 1996. Exchange of β- for α-tropomyosin in hearts of transgenic mice induces changes in thin filament response to Ca^{2+}, strong cross-bridge binding, and protein phosphorylation. *J. Biol. Chem.* 271: 11611–11614.

Parsons, B., D. Szczesna, J. Zhao, G. van Slooten, W. G. L. Kerrick, J. A. Putkey, and J. D. Potter. 1997. The effect of pH on the Ca^{2+} affinity of the Ca^{2+} regulatory sites of skeletal and cardiac troponin C in skinned muscle fibres. *J. Muscle Res. Cell Motil.* 18:599–609.

Potma, E. J., I. A. van Graas, and G. J. M. Stienen. 1994. Effects of pH on myofibrillar ATPase activity in fast and slow skeletal muscle fibers of the rabbit. *Biophys. J.* 67:2404–2410.

Robertson, S. I., and W. G. L. Kerrick. 1979. The effects of pH on Ca^{2+}-activated skinned rabbit skeletal muscle fibres. *Pflügers Arch.* 380:41–45.

Solaro, R. J., S. C. El-Saleh, and J. C. Kentish. 1989. Ca^{2+}, pH and the regulation of cardiac myofilament force and ATPase activity. *Mol. Cell. Biochem.* 89:163–167.

Solaro, R. J., P. Kumar, E. M. Blanchard, and A. F. Martin. 1986. Differential effects of pH on calcium activation of myofilaments of adult and perinatal dog hearts. *Circ. Res.* 58:721–729.

Spudich, J. A., and S. Watt. 1971. The regulation of rabbit skeletal muscle contraction. I. Biochemical studies of the interaction of the tropomyosin-troponin complex with actin and the proteolytic fragments of myosin. *J. Biol. Chem.* 246:4866–4871.

Stone, D., and L. B. Smillie. 1977. The amino acid sequence of rabbit skeletal α-tropomyosin. *J. Biol. Chem.* 253:1137–1148.

Tanaka, H. 1972. The helix content of tropomyosin and the interaction between tropomyosin and F-actin under various conditions. *Biochim. Biophys. Acta.* 278:556–566.

Yamaguchi, M. 1998. Modulating factors of calcium-free contraction at low [MgATP]: a physiological study on the steady states of skinned fibres of frog skeletal muscle. *J. Muscle Res. Cell Motil.* 19:949–960.

Yasuda, K., T. Anazawa, and S. Ishiwata. 1995. Microscopic analysis of the elastic properties of nebulin in skeletal muscle myofibrils. *Biophys. J.* 68:598–608.

UltraRapid Communication

Effects of MgADP on Length Dependence of Tension Generation in Skinned Rat Cardiac Muscle

Norio Fukuda, Hidetoshi Kajiwara, Shin'ichi Ishiwata, Satoshi Kurihara

Abstract—The effect of MgADP on the sarcomere length (SL) dependence of tension generation was investigated using skinned rat ventricular trabeculae. Increasing SL from 1.9 to 2.3 μm decreased the muscle width by ≈11% and shifted the midpoint of the pCa-tension relationship (pCa_{50}) leftward by about 0.2 pCa units. MgADP (0.1, 1, and 5 mmol/L) augmented maximal and submaximal Ca^{2+}-activated tension and concomitantly diminished the SL-dependent shift of pCa_{50} in a concentration-dependent manner. In contrast, pimobendan, a Ca^{2+} sensitizer, which promotes Ca^{2+} binding to troponin C (TnC), exhibited no effect on the SL-dependent shift of pCa_{50}, suggesting that TnC does not participate in the modulation of SL-dependent tension generation by MgADP. At a SL of 1.9 μm, osmotic compression, produced by 5% wt/vol dextran (molecular weight ≈464 000), reduced the muscle width by ≈13% and shifted pCa_{50} leftward to a similar degree as that observed when increasing SL to 2.3 μm. This favors the idea that a decrease in the interfilament lattice spacing is the primary mechanism for SL-dependent tension generation. MgADP (5 mmol/L) markedly attenuated the dextran-induced shift of pCa_{50}, and the degree of attenuation was similar to that observed in a study of varying SL. The actomyosin-ADP complex (AM.ADP) induced by exogenous MgADP has been reported to cooperatively promote myosin attachment to the thin filament. We hereby conclude that the increase in the number of force-generating crossbridges on a decrease in the lattice spacing is masked by the cooperative effect of AM.ADP, resulting in depressed SL-dependent tension generation. The full text of this article is available at http://www.circresaha.org. **(*Circ Res.* 2000;86:e1-e6.)**

Key Words: MgADP ■ pimobendan ■ Ca^{2+} sensitivity ■ cardiac muscle ■ sarcomere length

An alteration in ventricular end-diastolic volume results in a marked change in cardiac output.[1,2] This intrinsic ability of the heart to alter cardiac output forms the basis for the Frank-Starling law of the heart. It is well established that twitch tension and Ca^{2+} responsiveness in cardiac muscle preparations are enhanced as muscle length (ie, sarcomere length [SL]) is increased within the normal physiological range (SL from ≈1.8 to ≈2.3 μm).[1–5] Although a number of studies have been conducted to account for the SL dependence of tension generation in living myocardium, its mechanism has not been completely elucidated.[6] However, at the myofilament level, there is an increasing amount of evidence suggesting that the SL dependence is primarily due to a change in the interfilament lattice spacing that accompanies the SL change.[7–9] A possible consequence of the decreased lattice spacing is an increase in the probability of myosin attachment to the thin filament, resulting in an increase in the number of force-generating crossbridges.[7,10,11] Ishiwata and Oosawa[12] proposed a model based on the Ca^{2+}-dependent flexibility of the thin filament, in which they assumed that (1) the muscle volume (ie, the lattice volume) remains constant on a change in SL and that (2) there is a critical distance between the thick and thin filaments for tension generation. This model quantitatively explains both the stretch-induced increase in the steady isometric tension and the slower (or faster) rate of tension development (or decline) at a shorter SL,[13,14] supporting the hypothesis that a change in the lattice spacing plays a pivotal role in determining the SL-dependent Ca^{2+} sensitivity of tension. Alternatively, it was proposed that the length-dependent change in myofilament activation is caused by cardiac troponin C (TnC), which acts as a "length sensor" in the cardiac muscle contractile system.[15,16] However, this idea has attained little experimental evidence from other groups, and it was challenged by McDonald et al,[17] who reported that the expression of skeletal TnC in ventricular myocytes of transgenic mice did not alter the SL dependence of Ca^{2+} sensitivity of tension in skinned myocytes. Thus, it is unlikely that TnC alone acts as a "length sensor" in cardiac muscle.

It is known that the degree of activation of the thin filament is regulated not only by the binding of Ca^{2+} to TnC but also

Received August 26, 1999; accepted November 17, 1999.

From the Department of Physiology (II) (N.F., H.K., S.K.), The Jikei University School of Medicine, Nishishinbashi, Minato-ku, Tokyo, Japan; Department of Physics (S.I.), School of Science and Engineering, Advanced Research Institute for Science and Engineering (S.I.), and Materials Research Laboratory for Bioscience and Photonics (S.I.), Waseda University, Okubo, Shinjuku-ku, Tokyo, Japan.

Previously published in abstract form (*Circulation.* 1998;98[suppl I]:I-258).

Address reprint requests to Dr Shin'ichi Ishiwata, Department of Physics, School of Science and Engineering, Waseda University, 3-4-1 Okubo, Shinjuku-ku, Tokyo 169-8555, Japan. E-mail ishiwata@mn.waseda.ac.jp

***Circulation Research* is available at http://www.circresaha.org**

by the formation of strong-binding crossbridges, such as the rigor[18,19] and crossbridges that bind ADP.[20–22] Fukuda et al[22] reported that the actomyosin-ADP complex (AM.ADP) induced by exogenous MgADP can "turn on" adjacent actin molecules in a cooperative manner so that the actin and myosin interaction becomes possible, just as if Ca^{2+} were bound to TnC. Consequently, upon the addition of MgADP, the pCa-tension relationship for skinned cardiac muscle is shifted to the left, showing greater Ca^{2+} sensitivity of tension.[21–23]

To investigate the influence of the formation of strong-binding crossbridges on SL-dependent tension generation in cardiac muscle, we measured the SL-dependent shift of the pCa-tension relationship in the presence of varying concentrations of MgADP using skinned rat ventricular trabeculae. The formation of strong-binding crossbridges is known to increase the affinity of TnC for Ca^{2+}.[3,5,24] Thus, to clarify whether the effect of MgADP is based on the increased affinity of TnC for Ca^{2+}, we examined the effect of pimobendan, a Ca^{2+} sensitizer, which promotes Ca^{2+} binding to TnC.[25,26] A preliminary report has been published in abstract form.[27]

Materials and Methods

Experimental Procedure

The heart was removed from male Wistar rats (250 to 300 g) anesthetized with sodium pentobarbital (50 mg/kg IP). The rats were supplied by Saitama Experimental Animals Supply (Saitama, Japan), and the present study conforms with the *Guiding Principles for the Care and Use of Animals* approved by the Council of the Physiological Society of Japan. Thin trabecula muscles with the diameter of 100 to 150 μm were dissected from the right ventricle in oxygenated Tyrode solution without Ca^{2+} at 30°C. The preparations were skinned by superfusion with 1% vol/vol Triton X-100 in the relaxing solution (in mmol/L: MgATP 4, MOPS 10, EGTA 10, free Mg^{2+} 1, and ionic strength 180 [pH 7.0]) for 60 minutes at ≈2°C. The ionic strength (IS) was adjusted with KCl. The preparations were then washed with the relaxing solution to remove Triton X-100 and stored at −20°C in the relaxing solution containing 50% vol/vol glycerol and 2 mmol/L leupeptin for 1 week or less.

Both ends of the preparation were tied to thin tungsten wires with a silk thread. One end was attached to a tension transducer (BG-10; Kulite Semiconductor Products, Inc, Leonia, NJ) and the other to a micromanipulator (Narishige, Tokyo, Japan). The SL was adjusted to either 1.9 or 2.3 μm by measuring laser light diffraction in the relaxing solution. Ca^{2+}-activated isometric tension was measured in activating solutions containing 4 mmol/L MgATP, 10 mmol/L MOPS, 1 mmol/L free Mg^{2+}, a varying concentration of free Ca^{2+} (adjusted with Ca/[10 mmol/L EGTA]), 0.1 mmol/L P^1,P^5-di(adenosine-5′)pentaphosphate (AP_5A), 15 mmol/L creatine phosphate (CP), 15 U/mL creatine phosphokinase (CPK), and 180 mmol/L IS [pH 7.0], at the two SLs with/without MgADP or pimobendan (donated by Nippon Boehringer Ingelheim; Kawanishi, Hyogo, Japan).

The control pCa-tension relationship without MgADP or pimobendan was first obtained at a SL of 1.9 μm and then at 2.3 μm. By using the same preparation, the pCa-tension relationships in the presence of MgADP or pimobendan were obtained at the two SLs. Each pCa-tension relationship was obtained by cumulatively raising the Ca^{2+} concentration from the relaxing condition. Because we noted a variation in n_H (and related parameters), depending on the preparation, paired experiments were carried out on the same preparation. Finally, maximal Ca^{2+}-activated tension (at pCa 4.8) was measured at the two SLs in the control condition without MgADP or pimobendan to examine the reproducibility of tension development. We only used the data in which the final tension values were greater than 70% of those measured at the beginning of the experiment.

The muscle width was measured under a microscope (Nikon SMZ645) at a magnification of ×225. The concentrations of chemicals in solutions were estimated by computer calculation.[28] All experiments were carried out at 20±0.2°C.

Data and Statistical Analyses

The pCa-tension relationship was fitted to the Hill equation: $\log[P/(100-P)]=n_H[pCa_{50}-pCa]$, where P is the relative tension expressed as a percentage of the maximum ($+Ca^{2+}$, pCa 4.8), n_H is the Hill coefficient, and pCa_{50} is $-\log[Ca^{2+}]$ at P=50. All data are expressed as mean±SEM. Paired Student's *t* test was used, and statistical significance was verified at $P<0.05$.

Results

Effect of MgADP on the Length Dependence of Ca^{2+} Sensitivity of Tension

Figure 1 shows the effect of MgADP on the SL dependence of Ca^{2+} sensitivity of tension. In the control condition without MgADP or pimobendan, maximal absolute Ca^{2+}-activated tension values were 52.5±4.7 and 77.9±4.1 mg (n=17; $P<0.001$) at SL 1.9 and 2.3 μm, respectively, and pCa_{50} was shifted leftward by about 0.2 pCa units by increasing SL from 1.9 to 2.3 μm. The degree of the SL-dependent shift of pCa_{50} was consistent with the result of a previous study using rat ventricular muscle strips.[29] In the absence of MgADP, the muscle width was reduced from 132±6 to 118±4 μm (n=4; $P<0.001$) on extension of SL during relaxation (ie, ≈11% reduction): The addition of MgADP (up to 5 mmol/L) did not change the muscle width at either SL (131±7 and 117±5 μm [n=4; $P<0.001$] at SL 1.9 and 2.3 μm, respectively, in the presence of 5 mmol/L MgADP).

Consistent with our previous studies using skinned bovine cardiac muscle,[22,23] MgADP shifted the pCa-tension relationship to the left in a concentration-dependent manner (Figure 1). Concomitantly, the SL-dependent shift of the pCa-tension relationship was diminished in a concentration-dependent manner; in the presence of 5 mmol/L MgADP, ΔpCa_{50} was decreased to ≈20% of the control value (Figure 1C, inset).

Change in Hill Coefficient With MgADP

	Figure 1A		Figure 1B		Figure 1C	
SL	Control	0.1 mmol/L	Control	1 mmol/L	Control	5 mmol/L
1.9 μm	5.81±0.28	5.78±0.40	4.77±0.45	4.74±0.32	4.96±0.55	2.43±0.08*
2.3 μm	5.10±0.29	5.03±0.56	4.17±0.14	3.97±0.07	5.31±0.31	2.21±0.10*

Values from left and right columns were obtained from Figures 1A, 1B, and 1C, respectively (mean±SEM [n=4 to 5]). *$P<0.05$ compared with corresponding control (−MgADP) values.

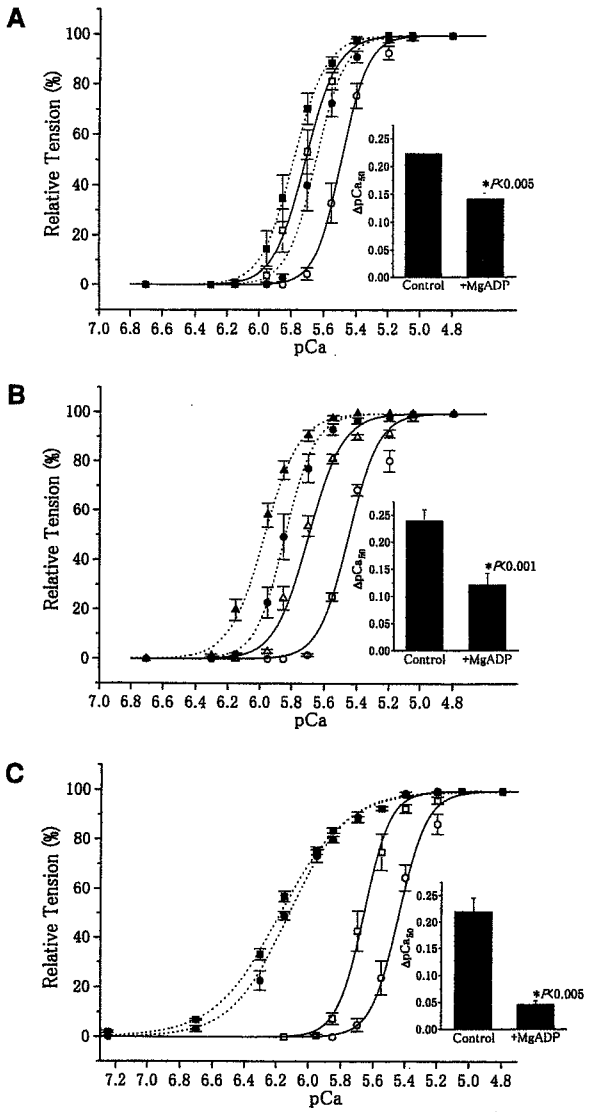

Figure 1. Effects of MgADP on pCa-tension relationships at different SLs. Solvent conditions: 4 mmol/L MgATP, 10 mmol/L MOPS (pH 7.0), 1 mmol/L free Mg^{2+}, varying [Ca^{2+}] (pCa adjusted by Ca/EGTA), 0.1 mmol/L AP_5A, 15 mmol/L CP, 15 U/mL CPK, and IS maintained at 180±1 mmol/L. MgADP was added to the above solution at a concentration of 0.1, 1, or 5 mmol/L. The ATP regenerating system (CP-CPK) was not added for experiments that used MgADP. Panels A, B, and C show the effects of MgADP at concentrations of 0.1, 1, and 5 mmol/L, respectively, on the pCa-tension relationships at SLs of 1.9 μm (circles) and 2.3 μm (squares); note that different muscle preparations were used. Solid lines and open symbols indicate pCa-tension relationships in the absence of MgADP; dotted lines and closed symbols, those in the presence of MgADP. Data obtained for each preparation were fitted to the Hill equation, and the results were simulated by the Hill equation with the mean values of pCa_{50} and n_H. Each inset represents ΔpCa_{50} (ie, difference between the values of pCa_{50} at long and short SLs) in the absence (control) and presence of MgADP. pCa-tension relationships were normalized by the maximum tension at pCa 4.8. Temperature was maintained at 20±0.2°C. Vertical bars indicate SEM of 4 to 5 data points.

The Table summarizes the n_H values of the pCa-tension relationships shown in Figure 1. MgADP at a concentration of 5 mmol/L significantly decreased n_H at both SLs,[23] whereas no significant changes were observed for 0.1 and 1 mmol/L MgADP.

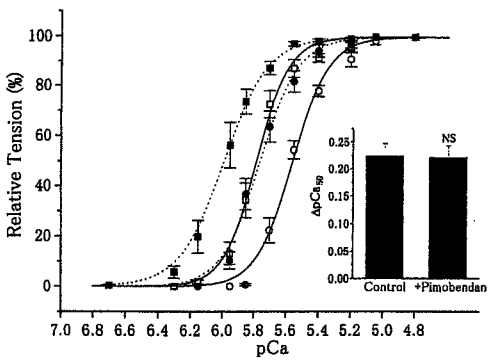

Figure 2. Effects of pimobendan on pCa-tension relationships at different SLs. Conditions are the same as in Figure 1 except that MgADP was absent and 10^{-4} mol/L pimobendan was present as well as CP and CPK. Pimobendan was initially dissolved in DMSO and diluted with the individual solutions. The final concentration of DMSO was 1%, having no effect on tension development. Symbols are the same as in Figure 1 except that dotted lines and closed symbols represent the pCa-tension relationships in the presence of pimobendan at SL 1.9 μm (circles) and at SL 2.3 μm (squares). Inset represents ΔpCa_{50} in the absence (control) and presence of pimobendan. NS indicates not significant compared with control. pCa-tension relationships were normalized with respect to the maximum tension at pCa 4.8. Vertical bars indicate SEM of 4 data points.

Because the ATP regenerating system (CP-CPK) was not used in the presence of MgADP, we estimated the concentration of contaminating MgADP inside the preparation. In the absence of MgADP, the pCa_{50} values obtained with and without CP-CPK were 5.45±0.05 and 5.53±0.05, respectively (n=4; $P<0.001$), at SL 1.9 μm. Thus, we estimated the contaminant MgADP to be ≈0.1 mmol/L under our experimental condition (see Figure 1A). This estimation is within the range of reported values for skinned cardiac and skeletal muscles.[30,31]

Effect of Pimobendan on the Length Dependence of Ca^{2+} Sensitivity of Tension

Pimobendan was reported to shift the pCa-tension relationship to the left with little influence on maximal Ca^{2+}-activated tension in skinned porcine ventricular muscle.[32] In the present study, 10^{-4} mol/L pimobendan substantially shifted the pCa-tension curve to the left at SLs of 1.9 and 2.3 μm, whereas in contrast to MgADP, pimobendan did not diminish the SL-dependent shift of the pCa-tension relationship (Figure 2).

The n_H values in the absence and presence of pimobendan were 4.01±0.27 and 3.93±0.15 (n=4; $P>0.1$), respectively, at SL 1.9 μm and 4.45±0.32 and 3.75±0.12 (n=4; $P>0.1$), respectively, at SL 2.3 μm. Pimobendan did not significantly change n_H at either SL.

Effect of MgADP or Pimobendan on Maximal Tension

Figure 3 summarizes the effect of MgADP or pimobendan on maximal Ca^{2+}-activated tension (pCa 4.8) at SLs of 1.9 and 2.3 μm. It has been reported that MgADP significantly potentiates maximal Ca^{2+}-activated tension in cardiac[22,23,33] and skeletal muscles.[20,33] We also found that MgADP augmented maximal tension in a concentration-dependent manner, and this potentiating effect was significantly less pro-

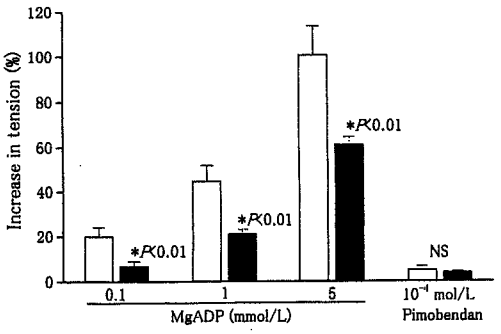

Figure 3. Effects of MgADP or pimobendan on maximal Ca^{2+}-activated tension. Conditions are the same as in Figures 1 and 2 for MgADP and pimobendan, respectively, except that pCa was fixed at 4.8. Open columns show SL 1.9 μm, and filled columns show SL 2.3 μm. NS indicates not significant. The degree of increase in tension was determined with respect to the maximal tension obtained without MgADP or pimobendan at each SL. Vertical bars indicate SEM of 4 to 5 data points for MgADP and 4 data points for pimobendan.

nounced at the longer SL ($P<0.01$). In contrast, pimobendan only minimally increased maximal tension at both SLs, and there was no significant difference in the increases in maximal tension between the two SLs.

Effect of MgADP on Dextran-Induced Shift of the pCa-Tension Relationship

Dextran (5% wt/vol) reduced the width of muscle from 135±5 to 117±4 μm (n=7; $P<0.001$) under the relaxing condition at SL 1.9 μm. The degree of reduction (≈13%) was similar to that observed when increasing SL to 2.3 μm without dextran (≈11%, see above).

In the absence of MgADP, dextran shifted pCa_{50} to the left by 0.19±0.03 pCa units (Figure 4). The degree of the shift of pCa_{50} was comparable, albeit slightly smaller, to what was observed when increasing SL to 2.3 μm (see Figures 1 and 2).

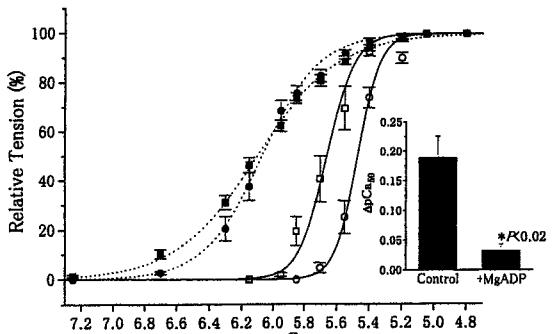

Figure 4. Effect of 5 mmol/L MgADP on pCa-tension relationships in the absence and presence of 5% wt/vol dextran at SL 1.9 μm. Solvent conditions are the same as in Figure 1 except that 5% wt/vol dextran (molecular weight ≈464 000; Sigma) was used to shrink the muscle volume instead of increasing SL to 2.3 μm. Circles indicate in the absence of dextran; squares, in the presence of dextran. Solid lines and open symbols indicate pCa-tension relationships in the absence of MgADP; dotted lines and closed symbols, pCa-tension relationships in the presence of MgADP. Inset represents ΔpCa_{50} (difference between the values of pCa_{50} with and without dextran) in the absence (control) and presence of MgADP. pCa-tension relationships were normalized with respect to the maximal tension at pCa 4.8. Vertical bars indicate SEM of 7 data points.

Maximal tension was also augmented by ≈15% in the presence of dextran as previously reported by other investigators using skinned skeletal[11] and cardiac muscles.[34]

It was found that in the presence of 5 mmol/L MgADP, the dextran-induced increase in apparent Ca^{2+} sensitivity was markedly diminished (Figure 4), and the degree of attenuation was similar to what was obtained in a study of varying SL (see Figure 1C).

The n_H values in the absence and presence of 5 mmol/L MgADP were 6.32±0.61 and 2.52±0.18 (n=7; $P<0.05$), respectively, without dextran and 5.29±0.31 and 1.68±0.06 (n=7; $P<0.05$), respectively, with dextran.

Discussion

We demonstrated that using skinned rat ventricular trabeculae, MgADP increases the Ca^{2+} sensitivity of tension and reduces the magnitude of SL-dependent changes in Ca^{2+} sensitivity. On the other hand, a simple increase in the Ca^{2+} binding affinity of TnC by pimobendan had no effect on the SL-dependent change in the Ca^{2+} sensitivity of tension. We discuss the implications of these results, focusing on the role of strong-binding crossbridges in the regulation of Ca^{2+} sensitivity of tension.

First, an increase in SL results in a decrease in the lateral separation between the thick and thin filaments in living cardiac muscle.[35] Similarly, the interfilament lattice spacing is decreased by increasing SL in skinned (glycerinated) muscle.[36] Although the latter study was conducted using skeletal muscle, it is reasonable to assume that the result can be extended to skinned cardiac muscle. In the present study, we observed that increasing SL from 1.9 to 2.3 μm produced about an 11% reduction in the width of muscle. Thus, it is suggested that there also occurred a corresponding reduction (ie, ≈11%) in the lattice spacing on extension of SL from 1.9 to 2.3 μm.

On the other hand, 5% wt/vol dextran decreased the muscle width by ≈13%. An X-ray diffraction study showed that a reduction in the width of skinned skeletal muscle produced by dextran reflects a proportional change in the lattice spacing.[37] Although an X-ray study has not been conducted with cardiac muscle, the conclusion made, on the basis of skeletal muscle, could be applicable to cardiac muscle.[38] It can thus be said that in the present study, 5% wt/vol dextran decreased the lattice spacing by ≈13%. Given the fact that both an increase in SL and osmotic compression produced a similar reduction in the muscle width and that both increased Ca^{2+} sensitivity of tension to a similar degree (Figures 1, 2, and 4), we consider that the decreased lattice spacing is the primary mechanism for length-dependent tension generation in skinned cardiac muscle.

There was, however, a slight mismatch between the effect of increasing SL and that of osmotic compression on Ca^{2+} sensitivity of tension and maximal Ca^{2+}-activated tension. Increasing SL to 2.3 μm resulted in about an 11% decrease in the muscle width, whereas osmotic compression decreased the width by ≈13%, yet the shift of pCa_{50} and the augmentation of maximal Ca^{2+}-activated tension were somewhat more pronounced by the lengthening. The exact reason(s) for this mismatch is unknown. However, it may be attributable to

some direct effect of dextran on the crossbridge cycle[39] and/or to the shape of the muscle being altered differently by mechanical stretch compared with osmotic compression.[7]

Although Ca^{2+} is a physiological activator of myocardium, it has been known that Ca^{2+} alone does not fully activate the thin filament[40] and that strong-binding crossbridges, such as the rigor complex, can further activate the thin filament.[18] We have reported that the formation of AM.ADP upon the addition of MgADP regulates the number of force-generating crossbridges, synergistically with Ca^{2+} binding to TnC.[20–22] In the present study, we found that MgADP, in addition to its apparent Ca^{2+} sensitizing effect, diminished the SL-dependent shift of the pCa-tension relationship in a concentration-dependent manner (Figure 1). Further, MgADP (5 mmol/L) attenuated the increase in Ca^{2+} sensitivity of tension produced by osmotic compression, to a similar degree observed when SL was increased (Figure 4). As discussed above, SL-dependent tension generation can be largely explained due to a decrease in the lattice spacing, which results in an increase in the number of force-generating crossbridges.[7,10,11] Therefore, it is realized that when force-generating crossbridges predominate inside the muscle through the cooperative effect of AM.ADP, the effect of lattice shrinkage becomes relatively small, leading to depressed SL-dependent tension generation. This interpretation is consistent with the fact that the potentiating effect of MgADP was significantly less pronounced at a longer SL (Figure 3).

Fitzsimons and Moss[9] reported that an application of *N*-ethylmaleimide–modified myosin subfragment 1 to single skinned rat ventricular myocytes diminishes the SL-dependent shift of the pCa-tension relationship. It is thus safe to conclude that when the number of force-generating crossbridges is increased through the cooperative effect of strong-binding crossbridges, the effect of increasing SL (ie, lattice shrinkage) to produce force-generating crossbridges is offset.

In skinned muscle preparations, strong-binding crossbridges promote Ca^{2+} binding to TnC.[24] If TnC acts as a "length sensor" in the cardiac contractile system,[15,16] then it follows that the SL dependence of tension generation would be modulated by a change in the affinity of TnC for Ca^{2+}, and the depressed shift of the pCa-tension relationship seen in the presence of MgADP may have been caused by the increased affinity of TnC for Ca^{2+}. However, pimobendan was found to have no effect on the SL-dependent shift of the pCa-tension relationship (Figure 2). Thus, it is unlikely that the increased affinity of TnC for Ca^{2+} is the major cause of the attenuation of SL-dependent tension generation by MgADP.

McDonald et al[41] hypothesized that the activation state of muscle with a higher cooperativity varies more dramatically as a result of length-induced variations in the number of force-generating crossbridges. However, in the presence of 0.1 or 1 mmol/L MgADP, the SL dependence was significantly diminished (Figures 1A and 1B), whereas n_H was not significantly changed (Table). Thus, it is unlikely that the attenuation of SL-dependent tension generation by MgADP underlies the decreased cooperative activation of the thin filament.

It should be stressed that MgADP as low as 0.1 mmol/L (or ≈0.2 mmol/L when contaminating MgADP is taken into account) augmented maximal and submaximal tension and diminished the SL dependence of tension generation (Figures 1A and 3). Because it has been known that cardiac contractile proteins are more sensitive to MgADP than skeletal muscle proteins,[22,42] it is possible that MgADP at ≈0.1 mmol/L significantly influences cardiac contractile performance, as in the in vitro motility assay system.[43] Recently, Tian et al[44] demonstrated that ≈0.1 mmol/L MgADP significantly increased the left ventricular end-diastolic pressure in intact rat heart. It has been pointed out that in the intracellular milieu of ischemic or hypoxic cardiac muscle, the concentration of ADP increases whereas that of ATP decreases.[45] Reportedly, an increase in the ratio of the concentration of ADP to that of ATP in the vicinity of crossbridges may elicit ischemic contracture.[46] The present results suggest that during ischemia or hypoxia, the accumulation of ADP may impair the Frank-Starling mechanism.

Acknowledgments

This work was supported in part by Grants-in-Aid for Scientific Research, for Scientific Research on Priority Areas, and for High-Tech Research Center Project from the Ministry of Education, Science, Sports and Culture of Japan, by Core Research for Evolutional Science and Technology (CREST) of Japan Science and Technology Corporation, and from the Vehicle Racing Commemorative Foundation. We would like to thank Nippon Boehringer Ingelheim for providing pimobendan, Prof Masataka Kawai of the University of Iowa for critical reading of the manuscript, and Naoko Tomizawa for technical assistance.

References

1. Allen DG, Kentish JC. The cellular basis for length-tension relation in cardiac muscle. *J Mol Cell Cardiol.* 1985;17:821–840.
2. Lakatta EG. Length modulation of muscle performance: Frank-Starling law of the heart. In: Fozzard HA, ed. *The Heart and Cardiovascular System.* New York, NY: Raven Press Publishers; 1991:1325–1352.
3. Allen DG, Kurihara S. The effect of muscle length on intracellular calcium transients in mammalian cardiac muscle. *J Physiol (Lond).* 1982; 327:79–94.
4. Kentish JC, ter Keurs HEDJ, Ricciardi L, Bucx JJJ, Noble MIM. Comparison between the sarcomere length-force relations of intact and skinned trabeculae from right ventricle. Influence of calcium concentrations on these relations. *Circ Res.* 1986;58:755–768.
5. Kurihara S, Komukai K. Tension-dependent changes of the intracellular Ca^{2+} transients in ferret ventricular muscles. *J Physiol (Lond).* 1995;489: 617–625.
6. Fuchs F. Mechanical modulation of the Ca^{2+} regulatory protein complex in cardiac muscle. *News Physiol Sci.* 1995;10:6–12.
7. McDonald KS, Moss RL. Osmotic compression of single cardiac myocytes eliminates the reduction in Ca^{2+} sensitivity of tension at short sarcomere length. *Circ Res.* 1995;77:199–205.
8. Fuchs F, Wang YP. Sarcomere length versus interfilament spacing as determinants of cardiac myofilament Ca^{2+} sensitivity and Ca^{2+} binding. *J Mol Cell Cardiol.* 1996;28:1375–1383.
9. Fitzsimons DP, Moss RL. Strong binding of myosin modulates length-dependent Ca^{2+} activation of rat ventricular myocytes. *Circ Res.* 1998; 83:602–607.
10. April EW, Maughan DW. Active force as a function of filament spacing in crayfish skinned cardiac muscle fibers. *Pflugers Arch.* 1986;407: 456–460.
11. Allen JD, Moss RL. Factors influencing the ascending limb of the sarcomere length-tension relationship in rabbit skinned muscle fibers. *J Physiol (Lond).* 1987;390:119–136.
12. Ishiwata S, Oosawa F. A regulatory mechanism of muscle contraction based on the flexibility change of the thin filaments. *J Mechanochem Cell Motil.* 1974;3:9–17.

13. Endo M. Stretch-induced increase in activation of skinned muscle fibres by calcium. *Nat New Biol.* 1972;237:211–213.
14. Endo M. Length dependence of activation of skinned muscle fibers by calcium. *Cold Spring Harbor Symp Quant Biol.* 1972;37:505–510.
15. Babu A, Sonnenblick E, Gulati J. Molecular basis for the influence of muscle length on myocardial performance. *Science.* 1988;240:74–76.
16. Gulati J, Sonnenblick E, Babu A. The role of troponin C in the length dependence of Ca^{2+}-sensitive force of mammalian skeletal and cardiac muscles. *J Physiol (Lond).* 1990;441:305–324.
17. McDonald KS, Field LJ, Parmacek MS, Soonpaa M, Leiden JM, Moss RL. Length dependence of Ca^{2+} sensitivity of tension in mouse cardiac myocytes expressing skeletal troponin C. *J Physiol (Lond).* 1995;483: 131–139.
18. Bremel RD, Weber A. Cooperation within actin filament in vertebrate skeletal muscle. *Nat New Biol.* 1972;238:97–101.
19. Weber A, Murray JM. Molecular control mechanisms in muscle contraction. *Physiol Rev.* 1973;53:612–673.
20. Shimizu H, Fujita T, Ishiwata S. Regulation of tension development by MgADP and Pi without Ca^{2+}. Role in spontaneous tension oscillation of skeletal muscle. *Biophys J.* 1992;61:1087–1098.
21. Ishiwata S, Yasuda K. Mechano-chemical coupling in spontaneous oscillatory contraction of muscle. *Phase Transitions.* 1993;45:105–136.
22. Fukuda N, Fujita H, Fujita T, Ishiwata S. Regulatory roles of MgADP and calcium in tension development of skinned cardiac muscle. *J Muscle Res Cell Motil.* 1998;19:909–921.
23. Fukuda N, Fujita H, Fujita T, Ishiwata S. Spontaneous tension oscillation in skinned bovine cardiac muscle. *Pflugers Arch.* 1996;433:1–8.
24. Guth K, Potter JD. Effect of rigor and cycling cross-bridges on the structure of troponin C and on the Ca^{2+} affinity of the Ca^{2+}-specific regulatory sites in skinned rabbit psoas fibers. *J Biol Chem.* 1987;262: 13627–13635.
25. Fujino K, Sperelakis N, Solaro RJ. Sensitization of dog and guinea pig heart myofilaments to Ca^{2+} activation and the inotropic effect of pimobendan: comparison with milrinone. *Circ Res.* 1988;63:911–22.
26. Nielsen-Kudsk JE, Aldershvile J. Will calcium sensitizers play a role in the treatment of heart failure? *J Cardiovasc Pharmacol.* 1995;26(suppl 1):S77–S84.
27. Fukuda N, Kajiwara H, Ishiwata S, Kurihara S. Effects of MgADP on sarcomere length (SL)-dependent changes of pCa-tension relation in skinned rat myocardium. *Circulation.* 1998;98(suppl I):I-258. Abstract 1345.
28. Horiuti K. Some properties of the contractile system and sarcoplasmic reticulum of skinned slow fibres from *Xenopus* muscle. *J Physiol (Lond).* 1986;373:1–23.
29. Hibberd MG, Jewell BR. Calcium and length-dependent force production in rat ventricular muscle. *J Physiol (Lond).* 1982;329:527–540.
30. Zhao Y, Kawai M. Inotropic agent EMD-53998 weakens nucleotide and phosphate binding to cross bridges in porcine myocardium. *Am J Physiol.* 1996;271:H1394–H1406.
31. Wang G, Kawai M. Effects of MgATP and MgADP on the cross-bridge kinetics of rabbit soleus slow-twitch muscle fibers. *Biophys J.* 1996;71: 1450–1461.
32. Beier N, Harting J, Jonas R, Klockow M, Lues I, Haeusler G. The novel cardiotonic agent EMD 53998 is a potent "calcium sensitizer." *J Cardiovasc Pharmacol.* 1991;18:17–27.
33. Godt RE, Nosek TM. Changes of intracellular milieu with fatigue or hypoxia depress contraction of skinned rabbit skeletal and cardiac muscle. *J Physiol (Lond).* 1989;412:155–180.
34. Wang YP, Fuchs F. Osmotic compression of skinned cardiac and skeletal muscle bundles: effects on force generation, Ca^{2+} sensitivity and Ca^{2+} binding. *J Mol Cell Cardiol.* 1995;27:1235–1244.
35. Matsubara I, Millman BM. X-ray diffraction patterns from mammalian heart muscle. *J Mol Biol.* 1974;82:527–536.
36. Rome E. Relaxation of glycerinated muscle: low-angle X-ray diffraction studies. *J Mol Biol.* 1972;65:331–345.
37. Kawai M, Wray JS, Zhao Y. The effect of lattice spacing change on cross-bridge kinetics in chemically skinned rabbit psoas muscle fibers, I: proportionality between the lattice spacing and the fiber width. *Biophys J.* 1993;64:187–196.
38. Roos KP, Brady AJ. Osmotic compression and stiffness changes in relaxed skinned cardiac myocytes in PVP-40 and dextran T-500. *Biophys J.* 1990;58:1273–1283.
39. Metzger JM. Effects of phosphate and ADP on shortening velocity during maximal and submaximal calcium activation of the thin filament in skeletal muscle fibers. *Biophys J.* 1996;70:409–417.
40. Swartz DR, Moss RL, Greaser ML. Calcium alone does not fully activate the thin filament for S1 binding to rigor myofibrils. *Biophys J.* 1996;71: 1891–1904.
41. McDonald KS, Wolff MR, Moss RL. Sarcomere length dependence of the rate of tension redevelopment and submaximal tension in rat and rabbit skinned skeletal muscle fibres. *J Physiol (Lond).* 1997;501:607–621.
42. Chase PB, Kushmerick MJ. Effect of physiological ADP concentration on contraction of single skinned fibers from rabbit fast and slow muscles. *Am J Physiol.* 1995;268:C480–C489.
43. Yamashita H, Sata M, Sugiura S, Momomura S, Serizawa T, Iizuka M. ADP inhibits the sliding velocity of fluorescent actin filaments on cardiac and skeletal myosins. *Circ Res.* 1994;74:1027–1033.
44. Tian R, Christe ME, Spindler M, Hopkins JCA, Halow JM, Camacho SA, Ingwall JS. Role of MgADP in the development of diastolic dysfunction in the intact beating rat heart. *J Clin Invest.* 1997;99:745–751.
45. Kammermeier H, Schmidt P, Jungling E. Free energy change of ATP-hydrolysis: a causal factor of early hypoxic failure of the myocardium? *J Mol Cell Cardiol.* 1982;14:267–277.
46. Ventura-Clapier R, Veksler V. Myocardial ischemic contracture. Metabolites affect rigor tension development and stiffness. *Circ Res.* 1994;74: 920–929.

Research Report

Focal Extraction of Surface-Bound DNA from a Microchip Using Photo-Thermal Denaturation

BioTechniques 28:1006-1011 (May 2000)

Kenji Yasuda, Kazunori Okano[1] and Shin'ichi Ishiwata[2]
The University of Tokyo, [1]Hitachi, Ltd. and [2]Waseda University, Tokyo, Japan

ABSTRACT

High-throughput, selective extraction of a particular DNA fragment from a mixture of DNA before PCR amplification is becoming increasingly important in the DNA analysis field. Although the latest microchip technology has enabled real-time DNA expression analysis using hybridization between surface-bound probe DNA and sample DNA, the potential of this technology in purification of a small amount of DNA has not been demonstrated. We report here a method for area-selective release and collection of specific DNA, in which an IR laser beam is focused onto surface-bound sample DNA at the target-spotted area to denature hybridized DNA. First, sample DNA labeled with a fluorescent dye was hybridized to a probe DNA immobilized on a chromium-coated chip. A 1053-nm IR laser beam with an intensity of 10–100 mW was then focused on the target area with a spatial resolution of 10 μm, causing the release of the fluorophore-labeled sample DNA as a result of photo-thermal denaturation. Confirmation of the amount of eluted DNA by PCR amplification after collection indicated that more than 10^{-20} mol DNA/μm² area was eluted from the microchip, representing more than 70% of the chip-bound sample DNA. These results indicate that this method can be applied to the highly sensitive purification of DNA in microchip technology.

INTRODUCTION

Purification and analysis of DNA from a mixture of cell extract are fundamental in molecular and cellular biology and molecular diagnosis. In purification, a DNA library constructed from cloned DNA is usually used. Although the cloning method is widely used and is suitable for the preparation of a large number of DNA, the cultivation step of this method is laborious and time consuming. Recently, molecular biology has moved rapidly towards the study of functional genomics (10) and proteomics. These studies require rapid selection and collection of the target parts of a gene and mRNA from crude samples (3,6). Although the latest chip technology is capable of simple, high-throughput analysis in distinguishing different sequences of DNA by hybridization detection between a chip-bound probe DNA and sample DNA (1,2,8,9), it has not yet been applied to high-throughput purification of DNA, in which a portion of the sample DNA having particular DNA segments is picked up for further analysis.

Here, we propose a new type of DNA purification method using a photo-thermal approach to extract specific DNA bound on a microchip surface. This method is based on the principle that a focused IR beam heats a spotted area on the metal-coated chip surface (4) and that the resulting increase in temperature leads to denaturation of the sample probe DNA. As shown in Figure 1, the method consists of the following four steps: (*i*) sample DNA are loaded onto a chip surface coated with a metal thin layer, on which a group of surface-bound probe DNA are immobilized; (*ii*) sample DNA is hybridized with probe DNA; (*iii*) the chip surface is washed, the hybridized sample DNA are observed and the plate is spot-heated to extract DNA from the spotted area; and (*iv*) the released sample DNA is collected. The advantages of this spot-heating method are that it provides non-contact, spatially distributed denaturation and faster relaxation time in the increase in temperature. It should thus prove highly suitable for extracting target DNA individually from a chip surface on which a crude DNA mixture has been loaded. Steps *i* and *ii* have already been realized in DNA chip technology (1,2,8,9), but steps *iii* and *iv* are not yet tested. Here, we focused on steps *iii* and *iv*, namely the technique for area-specific denaturation and release of surface-bound DNA and subsequent collection of the released DNA.

MATERIALS AND METHODS

Photo-Thermal Denaturation Microscopy System

Figure 2 shows a diagram of the photo-thermal denaturation microscopy system for area-specific extraction of surface-bound DNA. It consists of three different optical units for phase-contrast, fluorescence and 1053-nm IR laser irradiation, respectively (Nd:YLF laser, 1053-100p; Amoco Laser, Naperville, IL, USA; maximum power 100 mW at the focal point when a ×10 objective lens is used). Different probe DNA areas in the matrix are distinguished by phase-contrast microscopy. The amount of surface-bound sample DNA on the microchip was measured by fluorescence microscopy. Phase-contrast and fluorescence images were simultaneously acquired with a dual-view microscopy system (4,5,7): the former through a charge-couple device (CCD) camera and the latter through a CCD camera equipped with an image intensifier. The area of DNA denaturation was brought into focus using the

fluorescence image, and the IR laser beam irradiated the spotted area. The intensity of the IR laser beam can be controlled up to 100 mW at the focal position on the microchip.

Preparation of DNA Chip

Probe DNA was immobilized on a 6-nm-thick chromium-coated glass plate. The chromium surface was modified with an active residue having a glysidoxy group for coupling dsDNA (619 bp, 0.5 pmol, 0.5 µL) onto the surface by the following two reaction steps. First, the glass plate with a chromium surface (45 × 25 × 0.4 mm) was dipped into a solution of 3-glysidoxypropyltrimethoxysilane for 1 h at room temperature (25°C) and dried at 110°C for 30 min. Next, dsDNA was prepared with an amino residue at the 5′-terminus of one strand and sulforhodamine-101 fluorophore at the 5′-terminus of the other strand so as to immobilize the DNA through its amino residue with glysidoxy groups on the chip surface. The dsDNA was a product amplified from a cloned human DNA. The clone has M13 priming sites 5′-CATGACTG-GCCGTCGTT-3′ at both ends. It was amplified by PCR with *Taq* DNA polymerase (Amersham Pharmacia Biotech, Little Chalfont, UK) and two primers, 5′-fluorophore-AACGACGGCCAGT-CATGCG-3′ and 5′-NH2-AACGAC-GGCCAGTCATGTG-3′. Thermal cycling for PCR was carried out 35× at 94°C for 30 s, 60°C for 30 s, and 72°C for 60 s. A solution of the product (10 µM dissolved in 0.2 M sodium carbonate buffer, pH 9.5) was dropped onto the activated chip, incubated at 50°C for 45 min and kept at room temperature so that the 5′-terminus of the probe DNA was attached to the chip. The quantity of immobilized DNA was checked by fluorescence microscopy with a confocal scanning fluorescence microscope (LSM-200; Olympus, Tokyo, Japan).

Recovery of DNA Using Photo-Thermal Denaturation

The DNA chip was rinsed and overlaid with 5 µL 20 mM Tris-HCl (pH 7.4) containing 2 mM EDTA (2× TE buffer). A small area on the chip was heated with IR laser (10, 25, 50 and 100 mW on the surface of the chip) using the microscopy system. After IR irradiation, a 4-µL drop of solution from the heated spot was collected into a vessel.

The recovered DNA in the drop was amplified to check quantity. PCR amplification was carried out under the same conditions as described above. The products of this amplification were checked by electrophoresis using a 2% agarose gel followed by staining with 0.5 µg/mL ethidium bromide and analyzed with a fluorescence-image analyzer (FM-Bio® 100; Hitachi Software Engineering, Tokyo, Japan).

Rehybridization of Fluorophore-Labeled DNA with an ssDNA on the Microchip

A 60-nucleotide fluorophore-labeled oligomer ssDNA (60-nucleotide sample DNA) complementary to the 60 nucleotides from the 3′-end of the immobilized strand on the DNA chip was diluted to 2 µM. For rehybridization, the solution was dropped on the chip surface and incubated for 3 min at 60°C. After rehybridization, the chip was rinsed with 2× TE buffer at room temperature and analyzed using the microscopy system.

RESULTS AND DISCUSSION

The purpose of this study was to demonstrate the feasibility of denaturing and extracting sample DNA from a small area by a photo-thermal denaturation procedure. First, we examined the efficiency of denaturation of sample DNA from the chip surface with a conventional heating procedure using a heat block. When the chip was maintained at 95°C for 1 min, all of the sample DNA, which had been hybridized to the surface-bound probe DNA, was released from the chip surface (Figure 3, a and b). As shown in Figure 3b, more

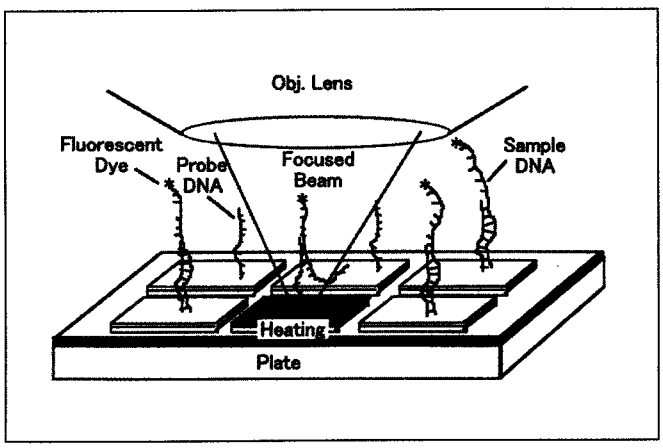

Figure 1. Schematic drawing of the photo-thermal denaturation method. First, the target DNA sample is captured by the immobilized probe DNA on the microchip surface. After the area for spot heating is selected by fluorescence microscopy, the area is heated by irradiation with an IR laser. The sample DNA released into the solution is collected and used for further analysis. The chosen DNA samples attached to the particular area on the chip surface are released by spot heating, which is controlled by the IR focused beam.

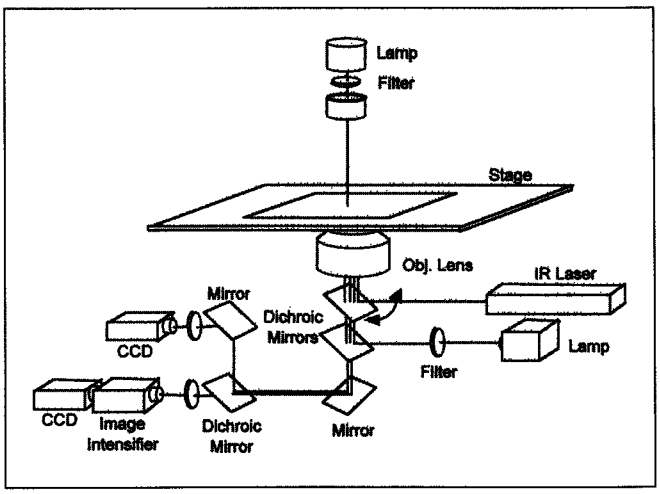

Figure 2. Schematic drawing of the photo-thermal denaturation microscopy system for area-specific extraction of surface-bound DNA. The microscope has three different optical units for phase-contrast, fluorescence and IR laser irradiation (5,7). Dichroic mirrors and band-pass filters direct the beams of the three different wavelengths of light.

than 95% of the fluorescent sample DNA was released from the chip surface. Next, a 2-μM 60-nucleotide sample DNA in 50 mM Tris-HCl (pH 7.5) was loaded onto the chip and successfully rehybridized with the surface-bound probe DNA (Figure 3c). The results indicate the following two facts. First, the integrity of the probe DNA remained intact, with the whole strands undamaged even after denaturation, as indicated by the 60-nucleotide sample DNA successfully attaching to the 3′-end (free end) of probe DNA. Second, the chromium-coated microchip served as a good substrate for the immobilized probe DNA and could release almost 100% of sample DNA, and 70% could be rehybridized on average through the thermal denaturation and renaturation steps. Note that the proportion of irreversibly attached sample DNA on the chromium-coated chip is negligibly small in contrast to the glass surface (Figure 3d). As shown in Figure 3d, the amount of undetached sample DNA on the glass surface was 90% after the denaturation process, in strong contrast to the case with the chromium-coated surface, which was less than 5%. This may

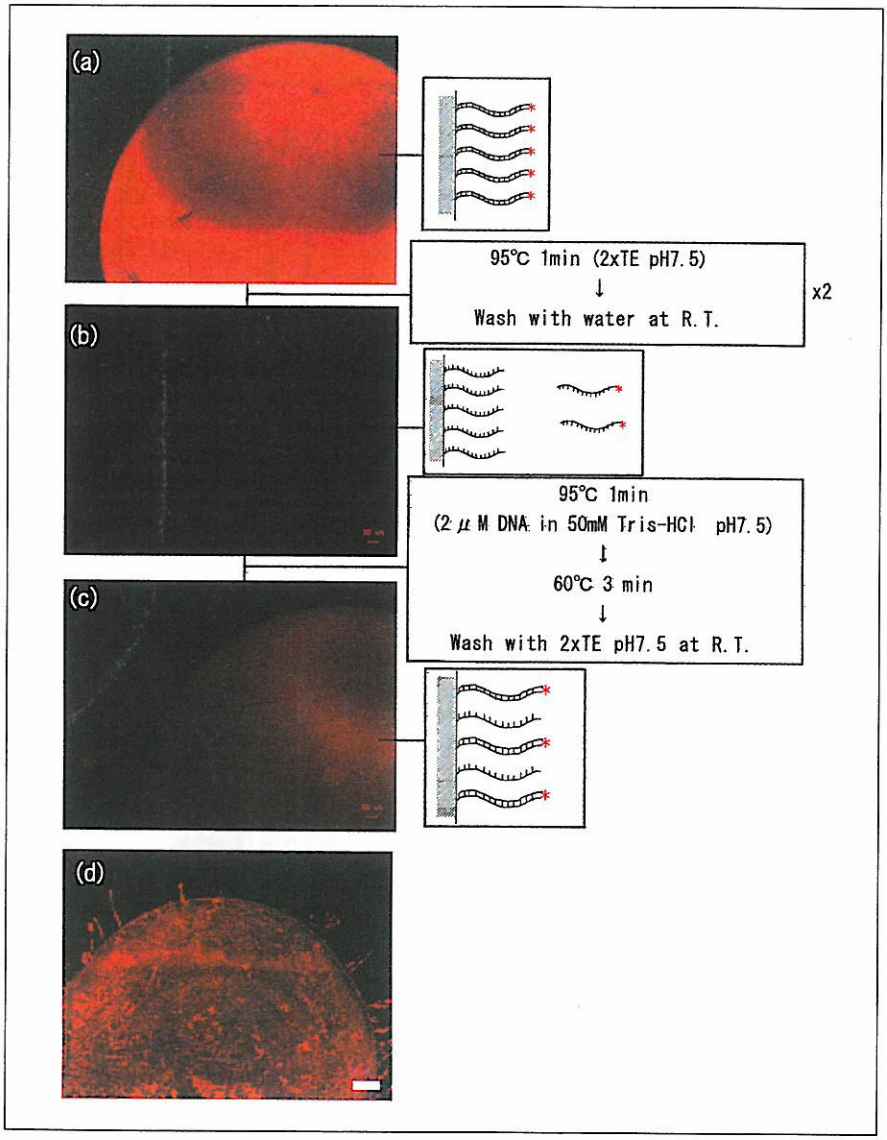

Figure 3. Fluorescence micrographs of the chromium-coated microchip surface and glass surface. (a) Fluorescence image of the chromium-coated microchip with attached fluorescent DNA; (b) the chip after the photo-thermal denaturation process; (c) the chip after rehybridization with the sample; and (d) the glass surface after the denaturation process. Bar, 200 μm.

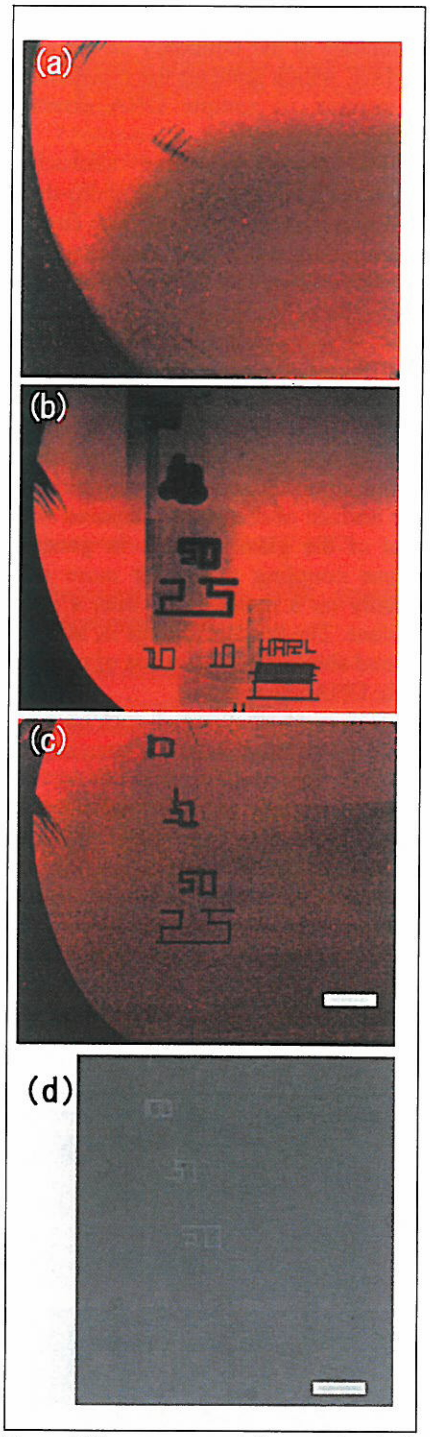

Figure 4. Fluorescence and phase-contrast micrographs of the microchip surface. Fluorescence image of the microchip surface before (a) and after (b) IR laser beam irradiation; (c) the chip after rehybridization with the sample DNA on the IR-irradiated microchip; and (d) phase-contrast micrograph of (c). The numbers traced on the surface of the chromium-coated microchip (100, 50, 25 and 10, respectively) indicate the power of IR laser irradiation for tracing, 100, 50, 25 and 10 mW. The word "HARL" was traced with a 10-mW IR laser beam. Bars, 100 μm.

be due to the charge of chromium (zeta potential) at the boundary of the chip surface, which prevents the nonspecific adsorption of sample DNA directly onto the chip surface.

The chromium-coated microchip has three advantages in the photo-thermal denaturation method. The first is its improvement of the absorbance of the IR laser on the surface of the chip during heating. While absorbance of a glass slide and water is negligibly small at 1053 nm, the 6-nm-thick chromium-coated surface achieved 40% absorption of the IR laser. The second advantage is the high efficiency of silane coupling on the oxydized chromium at the surface of the plate compared with that of the glass surface. In general, silane coupling works far more efficiently on a metal oxide than a glass surface. The third advantage is, as mentioned above, the prevention of nonspecific DNA adsorption.

Before photo-thermal spot heating, the fluorophore-labeled 619-nucleotide ssDNA (standard sample DNA), the complementary pair of whole-length probe DNA was hybridized onto the chromium-coated chip (Figure 4a). Importantly, although the whole area of the microchip was exposed to the standard sample DNA solution, the DNA attached only to the area coated with probe DNA. Next, the 1053-nm focused IR beam irradiated the surface of the chip and scanned it with varying laser power (10–100 mW) (Figure 4b). Bubbles generated by boiling water were sometimes observed at the irradiated area, indicating that the temperature of solution in the focused area exceeds boiling point. Figure 5a shows a magnified image of the area irradiated at 25 mW in Figure 4b. Figure 6a is the trace of fluorescence intensity along the line A-A in Figure 5a. As shown in Figures 5a and 6a, fluorescence intensity decreased in two steps, first to less than 30% in region P with a width of 30 μm and then to less than 5% in region Q with a width of 10 μm.

After photo-thermal extraction, we examined whether the probe DNA is maintained intact after IR irradiation by rehybridizing the 60-nucleotide sample DNA. Figure 4c shows the result of rehybridization between the 60-nucleotide sample DNA and the probe DNA after 10–100 mW IR laser irradiation. As analyzed in the 25-mW case (Figure 5b and Figure 6b), fluorescence intensity in region P recovered to the original level after the rehybridization procedure (width R), but the intensity in region Q did not. Thus, although all non-fluorescent lines traced by the IR beam

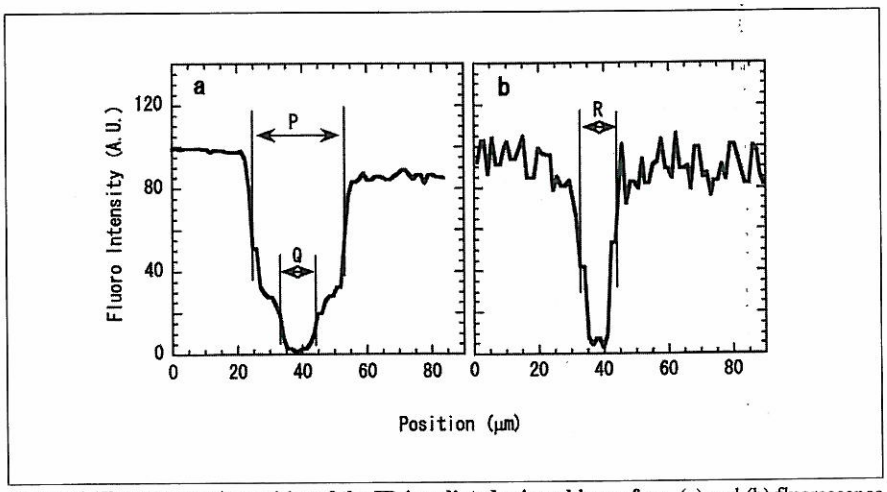

Figure 6. Fluorescence intensities of the IR-irradiated microchip surface. (a) and (b) fluorescence intensity profile along the A-A line in Figure 5, a and b, respectively.

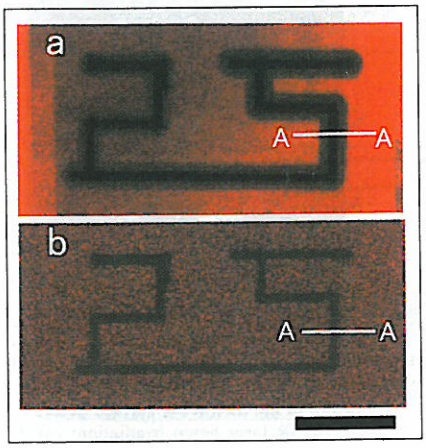

Figure 5. Fluorescence micrographs and intensity profiles of the 25-mW IR-irradiated microchip surface. (a) Fluorescence image of the microchip surface after 25 mW IR laser irradiation (magnified from Figure 4b); and (b) the chip after rehybridization with the sample DNA on the IR-irradiated microchip (magnified from Figure 4c). Bar, 100 μm.

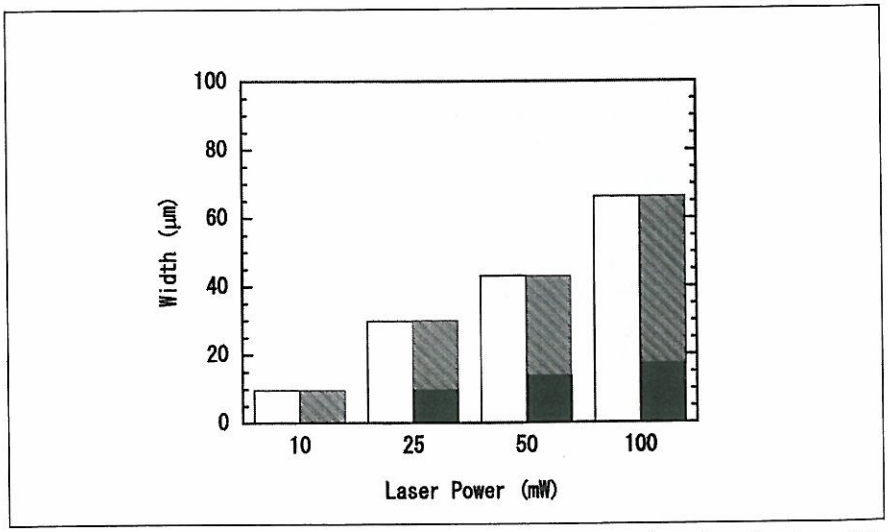

Figure 7. Laser power dependence of DNA denaturation on the microchip surface. Open box, width of the denatured area of the fluorophore-labeled sample DNA after IR irradiation; closed box, width of the damaged area on which no rehybridization occurred after rehybridization; hatched box, width of the rehybridized area after rehybridization.

at greater than 10 mW remained even after the rehybridization process, those traced at 10 mW were completely redecorated with fluorophores (Figure 4c). The width of the traced lines increased as laser power increased (Figure 7). A phase-contrast image (Figure 4d) shows that the chromium film was damaged by IR irradiation stronger than 10 mW. These results demonstrate that the probe DNA remains undamaged after IR irradiation unless the chromium coating has been damaged.

Finally, we measured the amount of sample DNA extracted from the chip after spot-heating a 100 × 10 μm area with a 10-mW IR focused beam. From fluorescence intensity analysis of the beam, more than 70% of the sample DNA was released from the chip surface after irradiation. As shown in Figure 8, the total amount of extract was in the order of 10^{-17} mol, on the basis that the fluorescence intensity of the extracted sample DNA was between that of the 1×10^{-16} mol and 1×10^{-17} mol reference samples after 15 cycles of PCR amplification. This result indicates that this photo-thermal denaturation extracted at least one DNA molecule from a 13 × 13 nm^2 area (10^{-17} mol/1000 μm^2) and further indicates that this method allows the area-specific extraction of a specified sample DNA.

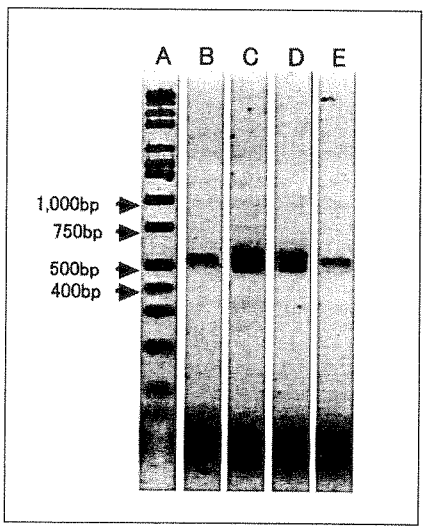

Figure 8. Agarose gel electrophoresis of PCR products amplified from the microchip extract. Five microliters of the DNA products were applied to a 2% agarose gel. Lane A, DNA molecular markers; lane B, sample DNA extracted from 10^3 μm^2 microchip surface; lanes C–E, concentration references, 1×10^{-15}, 10^{-16} and 10^{-17} mol of the same DNA, respectively.

The present study shows the potential of this DNA chip as a DNA purification apparatus. Spatial resolution of the denaturation spot size can be improved by increasing the objective lens magnification. We feel that this photothermal method will greatly enhance separation efficiency of different DNA from crude samples.

ACKNOWLEDGMENTS

We thank Drs. K. Miyauchi, T. Iwayanagi and T. Sakamoto of Hitachi, Ltd. for their support, and Dr. G. Harris for English editing. We also thank Prof. K. Kinosita, Jr. of Keio University and Dr. T. Nishizaka of Core Research for Evolutional Science and Technology (CREST) for their cooperation in consulting on the microscopy system. This research was partly supported by Grants-in-Aid for Scientific Research, for Scientific Research on Priority Areas and for the High-tech Research Center Project from the Ministry of Education, Science, Sports and Culture of Japan [grant no. 11559016 to S.I., no. 11878129 to S.I. and no. 11CE2006 (Komaba Complex Systems Life Science Project) to K.K.] and Grants-in-Aid from the Japan Science and Technology Corporation (CREST).

REFERENCES

1. **Burns, M.A., B.N. Johnson, S.N. Brahmasandra, K. Handique, J.R. Webster, M. Krishnan, T.S. Sammarco, P.M. Man et al.** 1998. An integrated nanoliter DNA analysis device. Science *282*:484-487.
2. **Cheng, J., E.L. Sheldon, L. Wu, A. Uribe, L.O. Gerrue, J. Carrino, M.J. Heller, and J.P. O'Connel.** 1998. Preparation and hybridization analysis of DNA/RNA from *E. coli* on microfabricated bioelectronic chips. Nat. Biotechnol. *16*:541-546.
3. **Kambara, H.** 1998. Recent progress in fluorescent DNA analyzers and methods. Curr. Topics Anal. Chem. *1*:21-36.
4. **Kato, H., T. Nishizaka, T. Iga, K. Kinosita, Jr. and S. Ishiwata.** 1999. Imaging of thermal activation of actomyosin motors. Proc. Natl. Acad. Sci. USA *96*:9602-9606.
5. **Kinosita, K., Jr., H. Itoh, S. Ishiwata, K. Hirano, T. Nishizaka and T. Hayakawa.** 1991. Double-view microscopy with a single camera: real-time imaging of molecular orientations and calcium. J. Cell Biol. *115*:67-73.
6. **Lockhart, D.J., H. Dong, M.C. Byrne, M.T. Follettie, M.V. Gallo, M.S. Chee, M. Mittmann, C. Wang et al.** 1996. Expression monitoring by hybridization to high-density oligonucleotide arrays. Nat. Biotechnol. *14*:1675-1680.
7. **Nishizaka, T., H. Miyata, H. Yoshikawa, S. Ishiwata and K. Kinosita, Jr.** 1995. Unbinding force of a single motor molecule of muscle measured using optical tweezers. Nature *377*:251-254.
8. **O'Donnell, M.J., K. Tang, H. Koster, C.L. Smith and C.R. Cantor.** 1997. High-density, covalent attachment of DNA to silicon wafers for analysis by MALDI-TOF mass spectrometry. Anal. Chem. *69*:2438-2443.
9. **Service, R.F.** 1998. Microchip arrays put DNA on the spot. Science *282*:396-398.
10. **Wang, D.G., J.-B. Fan, C.-J. Siao, A. Berno, P. Young, R. Sapolsky, G. Ghandour, N. Perkins et al.** 1998. Large-scale identification, mapping, and genotyping of single-nucleotide polymorphisms in the human genome. Science *280*:1077-1082.

Received 5 March 1999; accepted 1 December 1999.

Address correspondence to:
Dr. Kenji Yasuda
Department of Life Sciences
Graduate School of Arts and Sciences
The University of Tokyo
3-8-1 Komaba, Meguro
Tokyo 153-8902, Japan
Internet: cyasuda@mail.ecc.u-tokyo.ac.jp

Biophysical Journal Volume 78 June 2000 3112–3119

Temperature Change Does Not Affect Force between Single Actin Filaments and HMM from Rabbit Muscles

M. Kawai,* K. Kawaguchi,† M. Saito,† and S. Ishiwata†

*Department of Anatomy and Cell Biology, College of Medicine, University of Iowa, Iowa City, Iowa 52242 USA and †Department of Physics, School of Science and Engineering, Waseda University, Tokyo, Japan

ABSTRACT The temperature dependence of sliding force, velocity, and unbinding force was studied on actin filaments when they were placed on heavy meromyosin (HMM) attached to a glass surface. A fluorescently labeled actin filament was attached to the gelsolin-coated surface of a 1-μm polystyrene bead. The bead was trapped by optical tweezers, and HMM–actin interaction was performed at 20–35°C to examine whether force is altered by the temperature change. Our experiments demonstrate that sliding force increased moderately with temperature ($Q_{10} = 1.6 \pm 0.2$, ±SEM, $n = 9$), whereas the velocity increased significantly ($Q_{10} = 2.9 \pm 0.4$, $n = 10$). The moderate increase in force is caused by the increased number of available cross-bridges for actin interaction, because the cross-bridge number similarly increased with temperature ($Q_{10} = 1.5 \pm 0.2$, $n = 3$) when measured during rigor induction. We further found that unbinding force measured during the rigor condition did not differ with temperature. These results indicate that the amount of force each cross-bridge generates is fixed, and it does not change with temperature. We found that the above generalization was not modified in the presence of 1 mM MgADP or 8 mM phosphate.

INTRODUCTION

It has been known for some time that myosin cross-bridges generate force by interacting with actin molecules on the thin filament when they are placed in a solution that contains Ca^{2+} and $MgATP^{2-}$. It also has been known that the amount of force generation increases with an increase in the temperature in studies that used mammalian skeletal muscle fibers (Goldman et al., 1987; Zhao and Kawai, 1994; Ranatunga, 1996). To account for this temperature effect, two hypotheses are proposed. One hypothesis assumes that the force per cross-bridge does not change, but the number of force-generating cross-bridges increases with the temperature (Zhao and Kawai, 1994). The other hypothesis assumes that the force per cross-bridge increases with an increase in the temperature, but the number of cross-bridges does not change. In these experiments, force (F) is formulated in the following way:

$$F = \underbrace{N\sum_i f_i X_i}_{\text{(Fiber)}} = \underbrace{N f_1 X_1}_{\substack{\text{(In vitro} \\ \text{motility assay)}}}, \quad (1)$$

where N is the number of active cross-bridges that are involved in cycling. In fiber studies, f_i is the force associated with a cross-bridge at a state i, and X_i is the probability of the cross-bridge at the state i ($0 \leq X_i \leq 1$). The summation is over the all cross-bridge states (6–7 states were identified in fiber experiments) that are arranged in parallel in half sarcomere. Eq. 1 is modified from Kawai and Zhao (1993) to allow a change in the number of actively cycling cross-bridges (N). In the first hypothesis, X_i changes with temperature, and in the second hypothesis, f_i changes with temperature.

To obtain an insight on which one of the three parameters in Eq. 1 might change with temperature at the molecular level, we designed experiments using an in vitro motility assay, and studied sliding force between heavy meromyosin (HMM) molecules attached to a glass slide and an actin filament attached to a polystyrene bead that was clamped by a laser trap (optical tweezers). In the in vitro motility system, two cross-bridge states have been recognized. One is the attached state ($i = 1$) that generates force ($f_1 > 0$), and the other is the detached state ($i = 2$) that does not generate force ($f_2 = 0$). The fiber form of Eq. 1 can be applied to the in vitro motility system, if we assume that X_1 is the duty ratio (Howard, 1997) and f_1 is the unitary force. In this case, the product f_1X_1 is the average force/cross-bridge. Quite interestingly, our results demonstrate that, although force (F) increases with temperature, this increase is primarily based on the number of cross-bridges (N), but f_1X_1 remains approximately the same as the temperature is changed in the range 20–35°C. A preliminary account of the present work was reported in a recent Biophysical Society meeting (Kawai et al., 1999).

METHODS

Experimental apparatus

The experimental apparatus used here is the same as reported previously (Miyata et al., 1994, 1995; Nishizaka et al., 1995a; Nishizaka, 1996; Ishiwata, 1998). The entire apparatus is mounted on a pneumatic isolation table (Herz Kogyo KK, Tokyo, Japan). The optical system is based on an inverted microscope (TMD-300, Nikon, Tokyo, Japan). The light from an

Received for publication 25 June 1999 and in final form 28 February 2000.

Address reprint requests to Masataka Kawai, Department of Anatomy and Cell Biology, The University of Iowa, Iowa City, IA 52242. Tel.: 319-335-8101; Fax: 319-335-7198; E-mail: masataka-kawai@uiowa.edu.

0006-3495/00/06/3112/08 $2.00

Nd-YLF laser (1053 nm, 1W: Amoco Laser, Naperville, IL) is led through the oil-immersion objective lens (100×, n.a. = 1.3) from down below and traps a polystyrene bead in the flow cell to function as optical tweezers. The trap center of optical tweezers can be moved at a constant rate by controlling a mobile mirror with two DC-servo motors (Optmike-e; Sigma Koki, Hidaka, Japan). The light from a Halogen lamp, filtered at 380–520 nm, illuminates the flow cell, and its image is recorded by the CCD camera. The light from a Hg lamp is filtered at 550 nm and illuminates the flow cell from below. Accompanying fluorescent light (>590 nm) is led into the image intensifier (KS 1381, Video Scope, Washington, DC) before it is recorded by another CCD camera (CCD-72, Dage-MTI, Michigan City, IN). Phase contrast and fluorescence microscope images are combined and monitored on one screen. The combined image is videotaped (Hi8 Video, Sony Corp, Tokyo, Japan) for later analysis.

Flow cell

Both surfaces of a large coverslip (24 × 60 × 0.15 mm) were coated with collodion dissolved in 3-methylbutyl acetate. A small coverslip (20 × 20 × 0.15 mm) was glued to the large coverslip with double-stick tape at two sides. The gap between the two glass surfaces was about 0.1 mm. The total volume of the flow cell was about 25 μl. From one open side, 25 μl of HMM solution (1 μg/ml for rigor, else 60 μg/ml in solution HD) was applied and settled for 1 min to allow the HMM molecules to adsorb on the glass surface. Another 25 μl of HMM solution was applied from the other side. The cell was then washed by 25 μl of an experimental solution (CONT, +P, +ADP, or Rigor; Table 1). After 1 min, 25 μl rhodamine-phalloidin-labeled actin filaments in the same experimental solution were flowed in. Actin filaments were attached to polystyrene beads. The two open sides were then sealed by enamel (nail polish), and the flow cell was placed in the experimental apparatus.

Experimental solutions

Solutions used for the present studies are summarized in Table 1. Before mixing solutions, doubly distilled water was depressurized for 20 min by aspirator to minimize dissolved O_2. ATP was added as $Na_2H_2ATP{\cdot}2H_2O$, Pi as $H_{1.5}Na_{1.5}PO_4$, ADP as $KH_2ADP{\cdot}3H_2O$, EGTA as H_4EGTA, and pH was adjusted to 7.40.

Proteins, actin filaments, and polystyrene beads.

G-actin and HMM were purified from rabbit white skeletal muscles as described (Suzuki et al., 1996). Gelsolin was purified from bovine serum (Kurokawa, 1990). Polystyrene beads (1.0-μm diameter; Suzuki et al., 1996) were washed with carbonate and phosphate buffers, and coated with BSA and gelsolin. Actin was polymerized, rhodamine-conjugated phalloidin was bound, then F-actin was attached to polystyrene beads. Gelsolin binds to F-actin and serves as an anchor at the barbed end.

Temperature study

For experiments at 20 and 25°C, the room temperature was equilibrated to the respective temperatures. For experiments at 30 and 35°C, the inverted microscope, including the stage and the flow cell, was enclosed by a Nikon-plexiglass cover and its inside temperature was controlled. The temperature was measured by a thermister attached to the microscope stage near the flow cell, and regulated within ±1°C of the designated experimental temperature. The temperature in the flow cell was also estimated from thermal quenching of the fluorescence from rhodamine-maleimide conjugated to tubulin subunits of microtubule (Kawaguchi and Ishiwata, manuscript in preparation), a method similar to that reported earlier (Kato et al., 1999). For the purpose of Q_{10} calculation, Q_5 was first obtained and averaged, and then the Q_{10} was calculated as the square of Q_5. Q_5 is defined as the ratio of a parameter, which is measured at two temperatures that are 5°C apart.

RESULTS

Force on cross-bridges at different temperatures

A bead to which an actin filament is attached is placed 5 μm above the HMM-coated glass surface, which is moved to the left to align the filament parallel to the surface (Fig. 1 *A*). Then, the bead is lowered within 1.0 μm from the surface and filament–HMM interaction is performed in the presence of ATP (Fig. 1, *B* and *C*). From the video image (30 frames/sec), the displacement of the bead from the trap center is traced against time (Fig. 2). Sliding force is calculated as Force = k * Displacement, where k is the spring constant of the optical trap (k = 0.29 pN/nm). For detecting small force, the spring constant k was attenuated either to 50 or 30% of the value by inserting an appropriate neutral-density filter on the incident Nd-YLF laser beam. The length of actin filament was determined from the video image. Because the amount of force is proportionate to the length of actin filament (Kishino and Yanagida, 1988), the force value is divided by the length value to obtain force per unit length of the actin filament.

Figure 3 represents force plotted against the temperature for three experimental conditions (control, +Pi, +ADP).

TABLE 1 Solution compositions

	ATP (mM)	Pi (mM)	ADP (mM)	$MgCl_2$ (mM)	EGTA (mM)	KCl (mM)	DTT (mM)	Im-HCl (mM)	BSA (mg/ml)	GOC* (+/−)
AB†	–	–	–	4	1	25	–	25	–	–
HD	–	–	–	4	1	25	2	25	–	–
CONT	1	–	–	4	1	25	10	25	0.5	+
+Pi	1	8	–	4	1	8	10	25	0.5	+
+ADP	1	–	1	4	1	25	10	25	0.5	+
Rigor	–	–	–	3	1	28	10	25	0.5	+

*GOC represents 4.5 mg/ml glucose, 0.216 mg/ml glucose oxidase, and 0.036 mg/ml catalase to remove dissolved O_2 to minimize photo bleaching (Harada et al., 1990). In all solutions, pH was adjusted to 7.40.

†AB, actin buffer; HD, diluting solution for HMM; DTT, Dithiothreitol; Im-HCl, Imidazole-HCl.

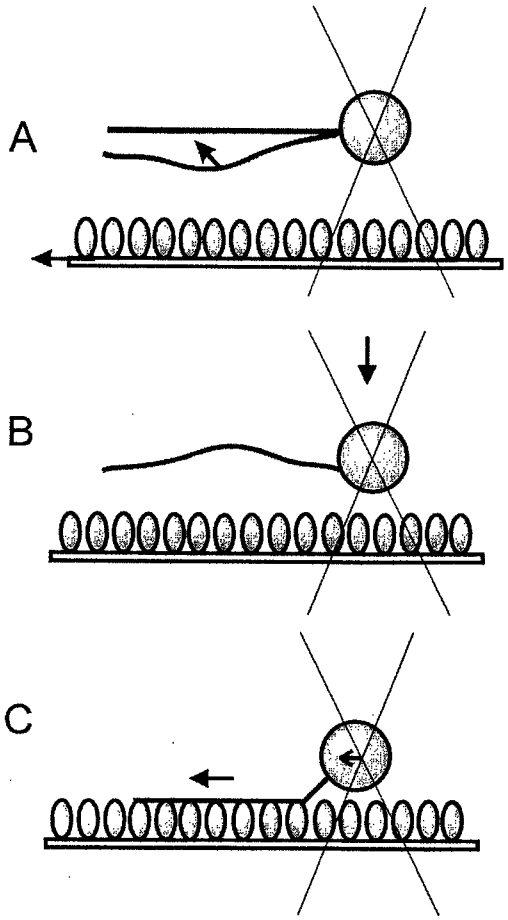

FIGURE 1 The method of measuring force on the single actin filament by optical tweezers. (*A*) An actin filament-attached bead (1 μm in diameter) is placed 5 μm above the HMM-coated glass surface, which is moved to the left (*lower arrow*) to line up the filament in parallel to the glass surface (*upper arrow*). (*B*) The bead is lowered within 1.0 μm from the glass surface (*arrow*). (*C*) The actin filament interacts with HMM to generate leftward force (*larger arrow*). This causes the bead displacement from the trap center indicated by the X mark. The displacement of the bead is measured (*small arrow*) and force is calculated by multiplying the spring constant of the optical tweezers.

Experiments were carried out in the presence of 1 mM ATP (Table 1). For these experiments, 60 μg/ml HMM was used to coat the glass surface. A proportionate relationship between force and the HMM concentration was demonstrated for 0–200 μg/ml HMM (Nishizaka, 1996) under similar experimental conditions. As shown in Fig. 3, a small increase in force was observed as the temperature was increased in the range of 20 to 35°C. This trend was not altered in the presence of 1 mM ADP or 8 mM Pi, except that force was slightly larger in the presence of ADP. From Fig. 3, we calculated Q_{10} for the control condition to be 1.6 ± 0.2 (±SEM, n = 3), Q_{10} in the presence of 8 mM Pi to be 1.8 ± 0.4 (n = 3), and Q_{10} in the presence of 1 mM ADP to be 1.4 ± 0.3 (n = 3). These values were not significantly different from the control condition. The averaged Q_{10} for all activating conditions tested was 1.6 ± 0.2 (n = 9).

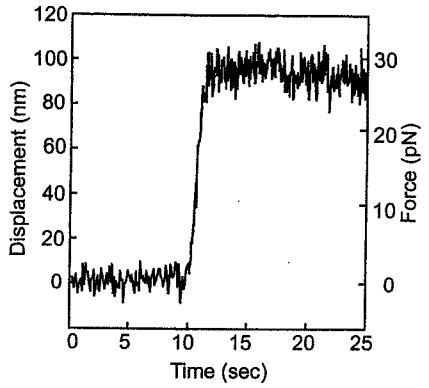

FIGURE 2 The time course to measure force on single actin filament. An actin filament-attached bead is placed within 1.0 μm above the HMM-coated surface, and filament-HMM interaction is performed in the presence of ATP (Fig. 1). The displacement (*left ordinate*) of the bead from the trap center is traced against time at the video rate (30 frames/sec). Sliding force (*right ordinate*) is calculated as Force = k * Displacement, where k is the spring constant of the optical trap (k = 0.29 pN/nm). The length of this particular actin filament was 4.8 μm.

Cross-bridge number per unit length of the actin filament

Because the total number of cross-bridges (N in Eq. 1) available for interaction with the actin filament may vary

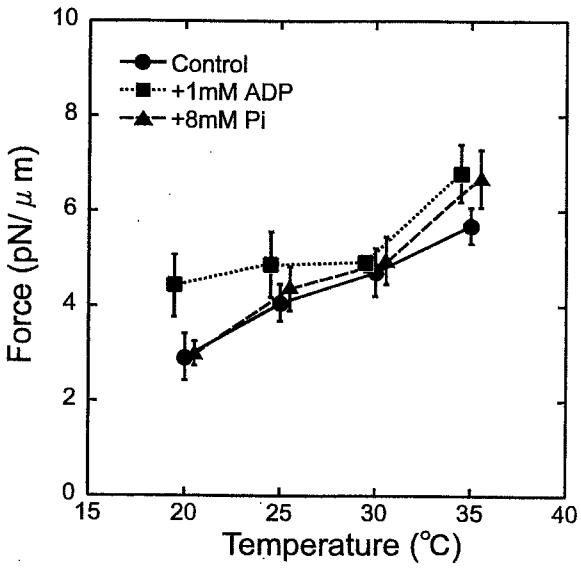

FIGURE 3 Force (pN) per unit length (μm) of actin filament is plotted against the temperature for three experimental conditions (control, +Pi, and +ADP) in the presence of 1 mM ATP. The error bars represent ±SEM. In the control experiment, n = 4, 5, 3, and 5 for 20, 25, 30, and 35°C, respectively. In the presence of Pi or ADP, n = 3 for 20°C, and n = 4 otherwise. Force was measured as shown in Figs. 1 and 2.

depending on the temperature, we counted the cross-bridge number during rigor induction, i.e., in the absence of ATP. For this series of experiments 1 μg/ml HMM was used to coat the glass surface. The method of counting the cross-bridge number and measuring unbinding force in the absence of ATP is depicted in Fig. 4 (see also Fig. 4 of Miyata et al., 1995; Fig. 2a of Nishizaka et al., 1995a; and Fig. 1 of Nishizaka et al., 1995b). The actin filament-attached bead is placed 2–3 μm above the HMM-coated surface, and filament–HMM interaction is performed. This height is necessary to count the cross-bridge number so that the unbound HMM does not rebind to the actin filament. From the video image, the displacement of the bead from the trap center is plotted against time (Fig. 4).

The gap on the trace represents unbinding of a single HMM molecule from the actin filament. The number of gaps is counted and divided by the filament length to obtain the number of cross-bridges per 1 μm of the actin filament. This method determines N in Eq. 1, the number of cross-bridges involved in cycling. A proportionate relationship between the number of cross-bridges and the HMM concentration was demonstrated for 0–15 μg/ml HMM under similar experimental conditions (Nishizaka, 1996, and manuscript in preparation). At a higher concentration, too many cross-bridges are formed, hence, counting the cross-bridge number becomes not possible. The results are plotted in Fig. 5. This figure demonstrates that the number of cross-bridges available for interaction with the actin filament increases with temperature. From Fig. 5, the averaged Q_{10} was calculated to be 1.5 ± 0.2 (n = 3).

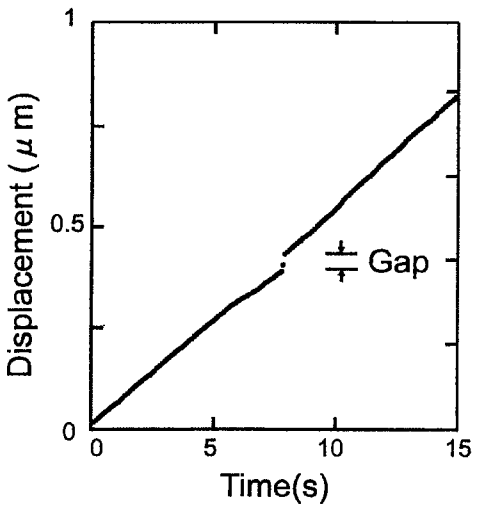

FIGURE 4 The time course to measure the number of cross-bridges and the unbinding force on single HMM molecules in rigor state. An actin filament-attached bead is placed 2–3 μm above the HMM-coated surface, and filament-HMM interaction is performed in the absence of ATP. The displacement of the bead from the trap center is traced against time. The gap on the trace represents unbinding of a single HMM molecule from the actin filament. The number of gaps is counted and divided by the actin filament length to obtain the number of cross-bridges per unit length. The unbinding force is calculated from the gap.

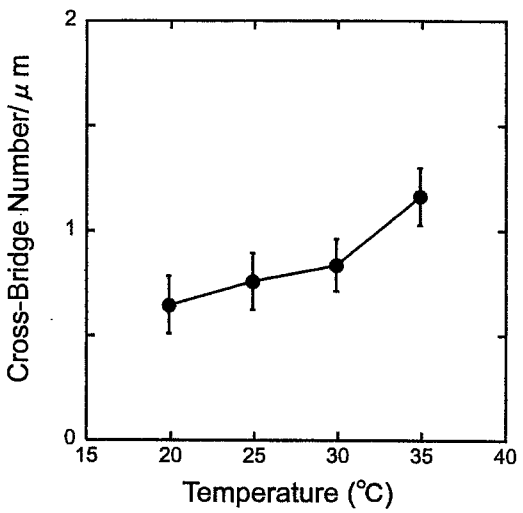

FIGURE 5 The cross-bridge number per unit length (μm) of actin filament in the absence of ATP is plotted against the temperature. The method of counting the cross-bridge number is shown in Fig. 4. The error bars represent ±SEM. n = 3, 4, 4, and 3 for the experiment at 20, 25, 30, and 35°C, respectively.

Corrected force on cross-bridges at different temperatures

Because the number of cross-bridges available for interaction with the actin filament increased with the temperature (Fig. 5), we divided the data of Fig. 3 with the data of Fig. 5, and plotted the results in Fig. 6. The errors in Figs. 3 and 5 were propagated and entered in Fig. 6 in a proper way (see figure legends). Figure 6 represents results from three experimental conditions (control, +1 mM ADP, and +8 mM Pi). Figure 6 demonstrates that the average force per cross-bridge (f_1X_1 in Eq. 1) remained approximately the same as the temperature was changed in the range 20–35°C in three experimental conditions.

Unbinding force

If the force generated by a cross-bridge changes with the temperature, this mechanism implies that a macromolecular change, such as in the shape of the myosin head, occurs when the temperature is elevated. If this is the case, then we expect that "unbinding force" also increases with the temperature. Unbinding force is the force at which a myosin cross-bridge detaches (unbinds) from actin when pulled away by external force, and measured by the "gap" in Fig. 4. The measurement is carried out in the absence of ATP, i.e., when rigor cross-bridges are formed. Unbinding force is plotted against the temperature in Fig. 7. As this figure

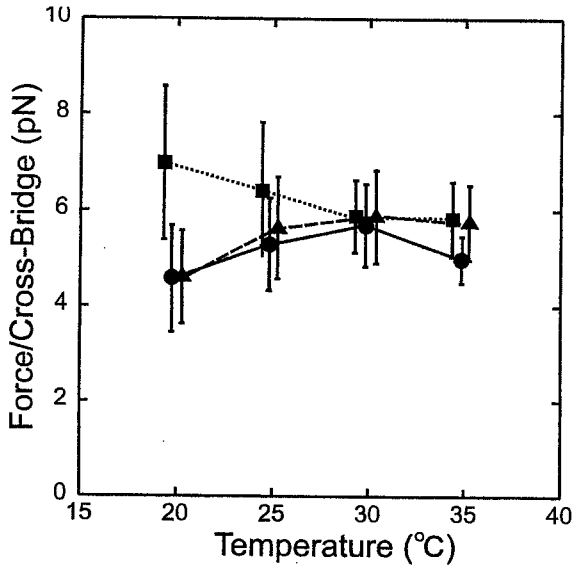

FIGURE 6 Corrected force is plotted against temperature. The data were obtained by dividing the values of force (Fig. 3) with the cross-bridge number (Fig. 5) to compensate for the artifact due to two-dimensional motility assay system, in which the number of HMM molecules within reach to the actin filament changes with the temperature. The same plotting nomenclatures as in Fig. 3 are used. The error bars E_z are calculated by $(E_z/Z)^2 = (E_x/X)^2+(E_y/Y)^2$ where X, Y, Z are the averaged values of Figs. 3, 5, 6, respectively ($Z = X/Y$), and E_x and E_y are SEM of Figs. 3 and 5, respectively.

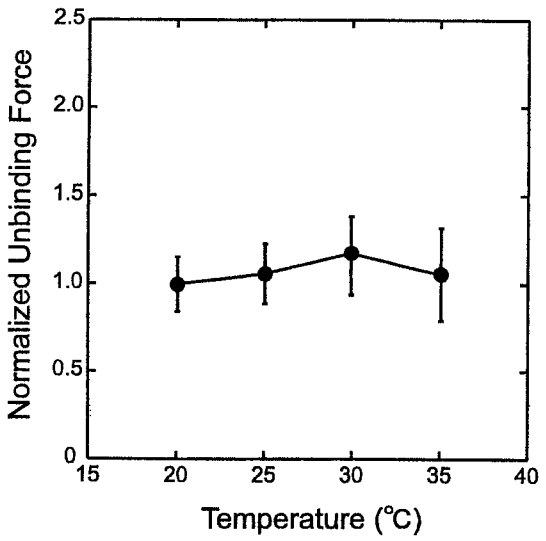

FIGURE 7 Unbinding force in the absence of ATP is plotted against the temperature after normalization at 20°C. The error bars represent ±SEM. n = 14, 17, 12, and 11 for experiments at 20, 25, 30, and 35°C, respectively. For these experiments, 1 μg/ml HMM was used to coat glass surface.

demonstrates, the unbinding force did not change much in the temperature range 20–35°C.

Sliding velocity

Unlike sliding force, the sliding velocity is expected to increase with temperature. To measure the velocity, actin filaments are placed on the HMM-coated surface, and the filaments are allowed to slide over the surface. From the video image (30 frames/sec), the position of the filament is obtained, and the sliding velocity is estimated from the time course in which the translation is linear over 5 μm. The results are plotted in Fig. 8 against the temperature for three experimental conditions (control, +Pi, and +ADP).

The experiments were carried out in the unloaded conditions and in the presence of 1 mM ATP. For this series of experiments, the standard 60 μg/ml HMM was used to coat the glass surface. As shown in Fig. 8, the velocity increased significantly with temperature with the average Q_{10} of 3.0 ± 0.7 (n = 4) in the control condition. The velocity was slightly faster in the presence of 8 mM Pi, and slower in the presence of 1 mM ADP. In this sense, the velocity behaves similar to the apparent rate constant of tension transients. The apparent rate constant $2\pi b$ (the rate constant of delayed tension) is faster in the presence of Pi and slower in the presence of ADP (Kawai and Zhao, 1993). From Fig. 8, Q_{10} in the presence of 8 mM Pi was calculated to be 3.0 ± 1.2 (n = 3), and Q_{10} in the presence of 1 mM ADP was 2.7 ± 0.9 (n = 3). These Q_{10} values were not significantly differ-

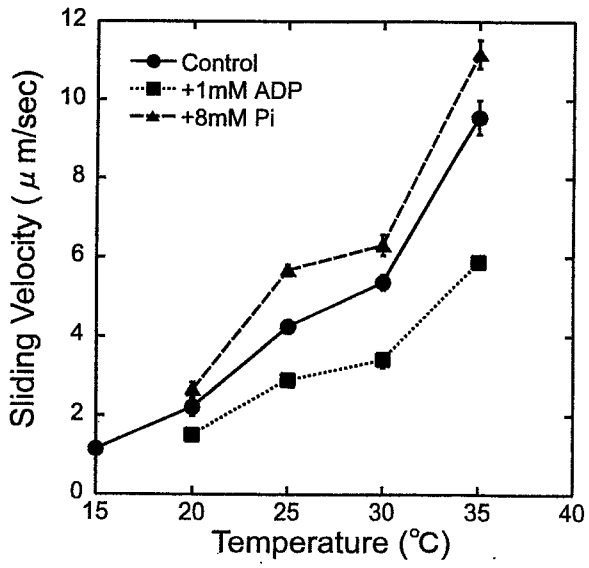

FIGURE 8 Sliding velocity is plotted against the temperature for three experimental conditions (control, +Pi, and +ADP) in the presence of 1 mM ATP. The error bars represent ±SEM. Error bars smaller than the symbol size cannot be seen. In the control experiment, n = 5, 4, 5, and 4 for 20, 25, 30, and 35°C, respectively. In the presence of Pi, n = 4, 3, 4, and 5 for experiments at 20, 25, 30, and 35°C, respectively. In the presence of ADP, n = 4, 5, 4, and 3 for experiments at 20, 25, 30, and 35°C, respectively.

ent from that of the control activating condition. The averaged Q_{10} for all conditions tested was 2.9 ± 0.4 (n = 10).

DISCUSSION

The purpose of the present study was to determine whether the isometric force on a cross-bridge increases with temperature using the in vitro motility assay system. For this purpose, we used synthetic actin filaments attached to polystyrene beads. The actin filaments were visualized by fluorescence as rhodamine-conjugated phalloidin was bound to the filament. HMM was attached to a collodion-coated glass surface. The position of the polystyrene beads were controlled by the laser trap (optical tweezers), and the interaction between HMM molecules and the actin filament was monitored.

We observed an increase in force as the temperature was elevated (Fig. 3; see also Kato et al., 1999). There are two possibilities to account for this increase: the cross-bridge number available for force generation (N in Eq. 1) may increase with temperature, and average force/cross-bridge (f_1X_1 in Eq. 1) may increase with temperature. We determined the cross-bridge number in the absence of ATP (rigor condition), because it is not possible to determine the number in the presence of ATP under the present set up. Interestingly, we found that the cross-bridge number increased with temperature (Fig. 5) just in the same way as force did. This increase may not be a physiological phenomenon, however, because the cross-bridge number is presumably maximized during the rigor induction, hence the number should not change with temperature in a physiological experiment. Therefore, the observed number increase may be specific to the in vitro motility system (Kato et al., 1999). One possibility is that the Brownian motion may release the head portion of HMM that are inadvertently stuck to the glass surface, but it leaves the C-terminus area of HMM attached to the glass surface, so that more HMM molecules become available to interact with the actin filament to generate more force at higher temperatures.

For this reason, we divided isometric force by the cross-bridge number to obtain corrected isometric force (f_1X_1, Fig. 6). We found that the corrected force does not change much with temperature in all three experimental conditions, from which we infer that the average force per cross-bridge does not change much with temperature in the in vitro motility assay system. The corrected force averaged 4.9 pN (range: 4.3–5.5 pN). This is not the unitary force, however, for this force value does not consider a 60× difference in the HMM concentration used in two sets of experiments. To obtain cross-bridge force, the ordinate values of Fig. 6 should be divided by the factor ~60, because the number of cross-bridges available for actomyosin interaction was 60× larger for the experiment of Fig. 3 than for the experiment of Fig. 5. Nishizaka (1996, and manuscript in preparation) demonstrated a proportionate relationship between the cross-bridge number and HMM for up to 15 μg/ml under the rigor condition, but no data are available for concentrations higher than 15 μg/ml. The factor must be >15, but ≤60, because the HMM concentration and the cross-bridge number may be nonlinear in this concentration range. Such nonlinearity is remote, however, because force and the HMM concentration are proportionally related for up to 200 μg/ml HMM under similar experimental conditions (Nishizaka, 1996). Thus, we calculate from our results that the force per cross-bridge (f_1X_1) is somewhere between 0.08 pN and 0.3 pN. The reason why this force value is less than unitary force (f_1) measured between actin and myosin molecules (1–6 pN, Finer et al., 1994; Miyata et al., 1995; Molloy et al., 1995; Ishijima et al., 1996) is because, in our measurement, force is the average over attachment and detachment cycle, whereas the unitary force (f_1) measures force during attachment. It is known that the duty ratio (X_1) is small in the in vitro motility assay system, and it is about 0.1 (Howard, 1997). What is important in this report is our conclusion that the average force per cross-bridge does not change much with temperature.

Although we could not examine the unitary force (f_1) and the duty ratio (X_1) independently, a possibility that both f_1 and X_1 change with temperature in a compensatory manner so that f_1X_1 remains the same is remote, because it is not likely that such compensation takes place at all temperatures we tested, and in all conditions (control, +Pi, and +ADP) we studied (Fig. 6). Furthermore, we measured unbinding force in the absence of ATP and studied the effect of temperature. We found that the unbinding force did not change much with temperature (Fig. 7). From results shown in Figs. 6 and 7, we infer that the HMM molecules do not change their shape much as the temperature is increased. A change in the shape would be necessary if force per cross-bridge or unbinding force were to change with the temperature, because force is presumably a result of the macromolecular architecture of the HMM and actin interrelationship. In this sense, it can be concluded that the result of Fig. 7 (unbinding force does not change with temperature) and the result of Fig. 6 (cross-bridge force does not change with temperature) are consistent.

In experiments using fast-twitch single skeletal muscle fibers, isometric force increases with temperature, and this increase was ascribed to an increase in the number (X_i in Eq. 1) of tension-generating cross-bridges (Zhao and Kawai, 1994), or to an increase in the force (f_i in Eq. 1) supported by an individual cross-bridge (Goldman et al., 1987; Kraft and Brenner, 1997). Both of these mechanisms result in an increase in the average force per cross-bridge (f_iX_i) with temperature. The total number of cross-bridges (N) involved in cycling is assumed not to change with temperature, because maximal activating condition with a saturating Ca^{2+} concentration was used in the fiber experiments. These experiments and mechanisms are primarily based on the temperature range ≤20°C. The effect of temperature is

smaller or absent when temperature is raised over 20°C (Bershitsky and Tsaturyan, 1992; Goldman et al., 1987; Zhao and Kawai, 1994; Ranatunga, 1996). Therefore, our results that the force/cross-bridge does not change much in the temperature range >20°C are consistent with the results on fiber experiments.

Sliding velocity is expected to increase with the temperature. This is because the velocity is limited by one or two steps in the cross-bridge cycle, and their rate constants almost invariably increase with the temperature (Goldman et al., 1987; Zhao and Kawai, 1994). In contrast, tension is determined primarily by the equilibrium constants (Kawai and Zhao, 1993), which may or may not be temperature sensitive. We found that the sliding velocity increased as the temperature was increased from 20 to 35°C (Fig. 8) with $Q_{10} = 3.0$ under the control-activating condition (Fig. 8). This quotient compares to 1.9 (Anson, 1992), 3.7 (calculated from Fig. 5 *B* of Winkelmann et al., 1995), 5.4 (calculated from Fig. 7 of Homsher et al., 1992), and 2.3–2.8 (calculated from the velocity data at 18°C and 40°C of Kato et al., 1999) under similar experimental conditions. Q_{10} in the presence of Pi (3.0) or ADP (2.7) is similar, but there is no previous work carried out in the presence of Pi or ADP.

It is interesting to point out that the sliding velocity decreases in the presence of ADP, much like in the case of the apparent rate constant. This observation can be explained by the mechanism that MgADP binds to the nucleotide binding site on myosin, and it competitively inhibits the ATP hydrolysis rate and work performance (Kawai and Zhao, 1993). It is also interesting to note that the velocity increases in the presence of Pi, as in the case of the apparent rate constant (Kawai and Zhao, 1993). This result may be consistent with the mechanism that Pi binding accelerates an approach to the steady state, and that the velocity behaves much like the apparent rate constant.

Although it may be difficult to carry out experiments on the actomyosin system because of the complexity of the myosin molecule, studying the temperature effect on the kinesin-microtubule system appears to be easier because kinesin is a smaller and simpler molecule than myosin. By using kinesin and microtubule isolated from bovine and porcine brains, respectively, Kawaguchi and Ishiwata (unpublished work) measured temperature dependence of force using optical tweezers. They found that the unitary force (f_1 in Eq. 1) produced by single kinesin molecules was about 7 pN, and this value did not differ in the temperature range between 20 and 35°C. Although the amino acid sequence of the motor domain of myosin and kinesin bears little homology, the tertiary structure of the motor domain bears a striking similarity in terms of the arrangement of α-helices and β-sheets; hence these two proteins are considered to have evolved from a common ancestor (Kull et al., 1998). It is interesting to know that the force that the two motor proteins generate does not differ at different temperatures, and this particular property was maintained throughout the process of evolution. This fact implies that the temperature insensitivity of the single molecular force is a fundamental property of a motor protein, and supports the idea that force is associated with a particular macromolecular architecture.

The results from single-molecule experiments, however, have to be applied to single-fiber experiments with caution, because there is a large difference in the solution composition in the two experimental systems. In particular, single-fiber experiments were carried out at or near physiological ionic strength (180–200 mM), whereas single-molecule experiments were carried out at a low ionic strength (about 50 mM). Because ionic interactions are weakened by increased ionic strength, single-molecule experiments become increasingly more difficult at higher ionic strength. Because the hydrophobic interaction is not affected by the ionic strength, the relative significance of the hydrophobic interaction is pronounced in single-fiber experiments, whereas the relative significance of the ionic interaction is pronounced in single-molecule experiments. As is well known, an increase in temperature facilitates hydrophobic interaction, because this interaction is endothermic (absorbs heat) and accompanies a large entropy increase (Zhao and Kawai, 1994). Similar temperature effect between a single-fiber system and a single-molecule system, in the temperature range of 20–35°C, suggests to us that the hydrophobic interaction may become saturated in this temperature range.

CONCLUSION

We found that force/cross-bridge does not change with temperature in in vitro assay in the temperature range 20–35°C.

This work was carried out during the tenure of a short-term fellowship to M.K. awarded by Japan Society for Promotion of Science in the summer of 1998. The work was also supported in part by grant IBN 96–03858 from the National Science Foundation and grant-in-aid 99–50437N from the American Heart Association National Center to M.K.; by grants-in-aid for Scientific Research (#10308030), for Scientific Research on Priority Areas (#11167280), for the High-Tech Research Center Project from the Ministry of Education, Science, Sports, and Culture of Japan, and by grants-in-aid for Japan Science and Technology, Core Research for Evolutional Science and Technology to S.I.

REFERENCES

Anson, M. 1992. Temperature dependence and Arrhenius activation energy of F-actin velocity generated in vitro by skeletal myosin. *J. Mol. Biol.* 224:1029–1038.

Bershitsky, S. Y., and A. K. Tsaturyan. 1992. Tension responses to Joul temperature jump in skinned rabbit muscle fibres. *J. Physiol. (Lond.)* 447:425–448.

Finer, J. T., R. M. Simmons, and J. A. Spudich. 1994. Single myosin mechanics: piconewton forces and nanometre steps. *Nature (Lond.)* 368:113–119.

Goldman, Y. E., J. A. McCray, and K. W. Ranatunga. 1987. Transient tension changes initiated by laser temperature jumps in rabbit psoas muscle fibers. *J. Physiol. (Lond.)* 392:71–95.

Harada, Y., K. Sakurada, T. Aoki, D. D. Thomas, and T. Yanagida. 1990. Mechanochemical coupling in actomyosin energy transduction studied by in vitro movement assay. *J. Mol. Biol.* 216:49–68.

Homsher, E., F. Wang, and J. R. Sellers. 1992. Factors affecting movement of F-actin filaments propelled by skeletal muscle heavy meromyosin. *Am. J. Physiol. Cell Physiol.* 262:C714–C723.

Howard, J. 1997. Molecular motors: structural adaptations to cellular functions. *Nature (Lond.)* 389:561–567.

Ishijima, A., H. Kojima, H. Higuchi, Y. Harada, T. Funatsu, and T. Yanagida. 1996. Multiple- and single-molecule analysis of the actomyosin motor by nanometer-piconewton manipulation with a microneedle: unitary steps and force. *Biophys. J.* 70:383–400.

Ishiwata, S. 1998. The use of fluorescent probes. In: *Current Methods in Muscle Physiology*, H. Sugi, editor. Oxford University Press, Oxford, U.K. 199–222.

Kato, H., T. Nishizaka, T. Iga, K. Kinosita, Jr, and S. Ishiwata. 1999. Imaging of thermal activation of actomyosin motors. *Proc. Natl. Acad. Sci. USA.* 96:9602–9606.

Kawai, M., K. Kawaguchi, M. Saito, and S. Ishiwata. 1999. The effect of temperature on sliding force and velocity of actin filaments and HMM. *Biophys. J.* 76:A35.

Kawai, M., and Y. Zhao. 1993. Cross-bridge scheme and force per cross-bridge state in skinned rabbit psoas muscle fibers. *Biophys. J.* 65: 638–651.

Kishino, A., and T. Yanagida. 1988. Force measurements by micromanipulation of a single actin filament by glass needles. *Nature (Lond.)* 334:74–76.

Kraft, T., and B. Brenner. 1997. Force enhancement without changes in cross-bridge turnover kinetics: the effect of EMD 57033. *Biophys. J.* 72:272–282.

Kull, F. J., R. D. Vale, and R. J. Fletterick. 1998. The case for a common ancestor: kinesin and myosin motor proteins and G proteins. *J. Muscle Res. Cell Motil.* 19:877–886.

Kurokawa, H., W. Fujii, K. Ohmi, T. Sakurai, and Y. Nonomura. 1990. Simple and rapid purification of brevin. *Biochem. Biophys. Res. Commun.* 168:451–457.

Miyata, H., H. Hakozaki, H. Yoshikawa, N. Suzuki, K. Kinosita Jr, T. Nishizaka, and S. Ishiwata. 1994. Stepwise motion of an actin filament over small number of heavy meromyosin molecules is revealed in an in vitro motility assay. *J. Biochem.* 115:644–647.

Miyata, H., H. Yoshikawa, H. Hakozaki, N. Suzuki, T. Furuno, A. Ikegami, K. Kinosita, Jr, T. Nishizaka, and S. Ishiwata. 1995. Mechanical measurements of single actomyosin motor force. *Biophys. J.* 68:S286–S290.

Molloy, J. E., J. E. Burns, J. Kendrick-Jones, R. T. Tregear, and D. C. S. White. 1995. Movement and force produced by a single myosin head. *Nature (Lond.)* 378:209–212.

Nishizaka, T. 1996. Microscopic analysis of function and mechanical properties of acto-myosin motor at single molecular level. Doctoral dissertation, Department of Physics, School of Science and Engineering, Waseda University, Tokyo, Japan.

Nishizaka, T., H. Miyata, H. Yoshikawa, S. Ishiwata, and K. Kinosita. Jr. 1995a. Unbinding force of a single motor molecule of muscle measured using optical tweezers. *Nature (Lond.)* 377:251–254.

Nishizaka, T., H. Miyata, H. Yoshikawa, S. Ishiwata, and K. Kinosita, Jr. 1995b. Mechanical properties of a single protein motor of muscle studied by optical tweezers. *Biophys. J.* 68:S75.

Ranatunga, K. W. 1996. Endothermic force generation in fast and slow mammalian (rabbit) muscle fibers. *Biophys. J.* 71:1905–1913.

Suzuki, N., H. Miyata, S. Ishiwata, and K. Kinosita, Jr. 1996. Preparation of bead-tailed actin filaments: estimation of the torque produced by the sliding force in an in vitro motility assay. *Biophys. J.* 70:401–408.

Winkelmann, D. A., L. Bourdieu, A. Ott, F. Kinose, and A. Libchaber. 1995. Flexibility of myosin attachment to surfaces influences F-actin motion. *Biophys. J.* 68:2444–2453.

Zhao, Y., and M. Kawai. 1994. Kinetic and thermodynamic studies of the cross-bridge cycle in rabbit psoas muscle fibers. *Biophys. J.* 67: 1655–1668.

ELSEVIER

Sensors and Actuators B 64 (2000) 88–94

SENSORS AND ACTUATORS B CHEMICAL

www.elsevier.nl/locate/sensorb

Position-specific release of DNA from a chip by using photothermal denaturation

Kazunori Okano [a,*], Kenji Yasuda [b], Shin'ichi Ishiwata [c,d,e,f]

[a] *Bio System Research Department, Central Research Laboratory, Hitachi Ltd., Kokubunji, Tokyo 185-8601, Japan*
[b] *Department of Life Sciences, Graduate School of Arts and Sciences, The University of Tokyo, Tokyo, Japan*
[c] *Department of Physics, School of Science and Engineering, Japan*
[d] *Advanced Research Institute for Science and Engineering, Japan*
[e] *Materials Research Laboratory for Bioscience and Photonics, Waseda University, Japan*
[f] *Core Research for Evolutional Science and Technology (CREST), "Genetic Programming" Team 13, Japan*

Abstract

A photothermal method to recover specific DNA fragments fixed in place on a DNA chip is described. This method uses infrared (IR) laser irradiation to thermally denature and release specific DNA immobilized in a specific area of a chip. A 1053-nm IR laser beam with an intensity of 10–100 mW is focused on the target area at a resolution of 10 μm, and the DNA fragments are released from the chip surface. We have demonstrated that DNA fragments containing different numbers of base pairs (231–799 bp) fixed in place on the DNA chip can be separately recovered. There are enough quantities of recovered DNA fragments that can be amplified by using polymerase chain reaction (PCR). The photothermal method coupled with the DNA chip can therefore be used in highly sensitive purification of DNA and will have many applications in the DNA chip technology.

Keywords: DNA chip; Photothermal denaturation; PCR; Infrared laser

1. Introduction

The purification of DNA fragments from living cells is a fundamental process in molecular biology and molecular diagnosis. We usually prepare a DNA library constructed from cloned DNA [1]. The cloning method is suitable for preparing a large number of DNA fragments, but is very laborious and time-consuming because of its cultivation processes. Nowadays, molecular biology is moving very rapidly towards the stage of functional genomics in which rapid preparation of different parts of genes will be required [2]. If a DNA library is constructed on a chip and any kind of DNA can be individually recovered from the chip, the DNA chip will become a very useful method and will change the way DNA-related experiments are done.

DNA chip technology in molecular biology has made rapid progress over the last 10 years [2–11]. Several approaches have been developed for producing DNA chips of different formats. In 1991, Fodor et al. [3] succeeded in making the microchips by photolithography on a solid surface. A chip containing 65,000 different 20-mer oligonucleotides of defined sequence in an area of 1.6 cm^2 was reported in 1996 [2], and it is now possible to assemble 150,000–300,000 oligonucleotides on one microchip [6]. Presynthesized oligonucleotides can be immobilized on a solid surface [5,7,8] or into a gel element fixed on a glass plate [9,10] by spotting the oligonucleotides. Any DNA produced by chemical syntheses, cloning, and polymerase chain reaction (PCR) can be immobilized on the microchip. The gel-fixed microchip has a high capacity for immobilizing oligonucleotides: 50 fmol of oligonucleotides is immobilized per microchip element of size 40 × 40 μm^2. This is more than 100 times higher than immobiliza-

* Corresponding author. Tel.: +81-423-23-1111; fax: +81-423-27-7833.
E-mail address: okano-k@crl.hitachi.co.jp (K. Okano).

0925-4005/00/$ - see front matter
PII: S0925-4005(99)00489-X

tion capacity of a plane glass surface, and this high capacity increases the hybridization velocity and the dynamic range. DNA microchips have been applied for gene expression analyses [5,11] and detection of single-nucleotide polymorphisms (SNPs) [6]. Matrix-assisted laser desorption/ionization time of flight (MALDI-TOF) mass spectrometry coupled with a DNA chip presents a new strategy for DNA analysis; it can analyze DNA extremely quick [12]. The oligonucleotide chip in reference [13] is very promising because the chip has a structure to control the hybridization by an electrode addressing each element of the chip. The DNA strands in a sample solution can quickly approach the probes immobilized on the chip surface. These DNA chip technologies, however, are mainly used in devices for analyzing a large number of DNA fragments, not for separating and preparing DNA fragments for further applications. A serious problem to be overcome in DNA separation applications is how to individually recover the DNA into aqueous solution from each small area on the microchip surface where DNA fragments are trapped.

Consequently, we developed a DNA preparation method that uses a photothermal approach to recover specific DNA fragments trapped on a chip surface. We found that the recovered DNA can be amplified by PCR and be subsequently characterized by further analysis. It is concluded that the developed method has a high potential for characterizing expressed genes and analyzing the differences between genes by using DNA chip.

2. Principle

The DNA preparation method is based on the fact that the stability of double-stranded DNA is highly dependent on temperature. As most double-stranded DNA fragments are denatured at 90–95°C, DNA hybridized with DNA probes fixed in place on the chip surface can be released by thermal denaturation. The temperature of the chip surface is locally elevated by irradiating a small metal-coated area with an infrared (IR) laser beam as schematically shown in Fig. 1 [14].

The method consists of five processes: (1) hybridizing reaction of sample DNA fragments with probe DNA fixed on the chip surface; (2) washing the chip surface to remove non-specific DNA species; (3) heating a small metal-coated area on the chip by IR laser irradiation to extract specific DNA from the chip surface; (4) collecting the released DNA; and (5) repeating of steps (3) and (4) in order to recover multiple DNA fragments fixed on the chip. This method of photothermal denaturation using an IR laser and a DNA chip rapidly extracts DNA fragments from the chip surface because it does not require any cloning procedure or electrophoretic separation.

3. Experimental

3.1. DNA samples preparation

The DNA samples were prepared by the method previously reported [15] as disclosed below. A half picomole of amplified human genome fragments (8.7 kb, supplied by the Human Genome Center, Institute of Medical Science, University of Tokyo, Japan) was digested with 40 units of *Hsp*92II (Promega, WI, USA). The restriction fragments (400 fmol) were treated with alkaline phosphatase and ligated by 1400 units of T4 DNA ligase (Takara) with 80 pmol of adaptor (5′-pACTGGCCGTCGTTT-3′) supported by 32 pmol of 5′-AAACGACGGCCAGTCATGp-3′. The phosphate residues were introduced into the 5′- and 3′-ends in order to prevent oligomer–oligomer ligation. The products ligated with the adaptor were purified with QIAquick

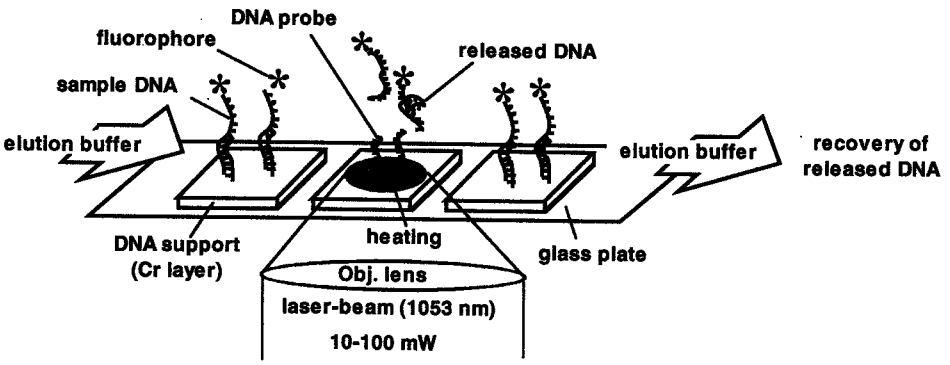

Fig. 1. Schematic illustration of DNA release from a DNA chip by using photothermal denaturation. The DNA hybridized with probe DNA fixed on a solid support can be released by a laser beam (1053 nm, 10–100 mW).

Spin Column (Qiagen, Hilden Germany) to eliminate free oligomers.

By using *Taq* DNA polymerase (0.625 units, Amersham Pharmacia Biotech, Amersham, UK) on a 50-μl scale, the fragments ligated with adaptor (50 amol) were selectively amplified by PCR with primer pairs (10 pmol). The primer pairs (from Sawady Technology, Tokyo, Japan) were 5′-(sulforhodamine-101)-AACGACGGCCAGTCACGNN-3′ and 5′-NH_2-AACGACGGCCAGTCACGNN-3′. Here, N is any one of the four deoxynucleotides for discriminating a complementary DNA fragment by PCR [15]. The thermal cycling reaction was carried out 35 times at 94°C (30 s), 62°C (30 s) and 72°C (60 s). The six products of this amplification were checked by electrophoresis using a 2% agarose gel followed by staining with 0.5 μg/ml ethidium bromide. They were analyzed by a FM-Bio 100 fluorescence image analyzer (Hitachi Software Engineering, Tokyo, Japan). The PCR product lengths were 779 bp (a pair of primers with discrimination sequences NN: AA and TC), 619 bp (NN: CG and TG), 411 bp (NN: GT and TA), 270 bp (NN: CA and TT), 231 bp (NN: CC and TT) and 179 bp (NN: AA and GT).

3.2. Preparation of the DNA chip

DNA was immobilized on a glass chip (45 × 25 × 0.4 mm^3) coated with 6-nm-thick chromium. The chip with the chromium surface was modified with 3-glysidoxypropyltrimethoxysilane to introduce the active residue and to fix double-stranded DNAs (PCR products) on the surface. The PCR products had an amino residue at a 5′-terminus of one strand and sulforhodamine-101 fluorophore at a 5′-terminus of the other strand, so that it was fixed on the chip surface through their amino residue. The chip was sonicated in 1 M KOH aqueous solution, washed with H_2O, and with 50% ethanol to clear the surface. After this pretreatment, the chip was dried for 30 min at 110°C, then dipped in neat 3-glysidoxypropyltrimethoxysilane for 15 min at 25°C followed by treating the same reagent (2%) diluted with 50% ethanol aqueous solution for 30 min. The chip was washed with 50% ethanol and dried at 110°C for 30 min to obtain a glysidoxy-activated chip. A solution of the DNA (10 μM) dissolved in 0.25 M carbonate buffer (pH 9.5) was dropped onto the glysidoxy-activated chip by a pin array coupled with Biomek 2000 Laboratory Automation Workstation (Beckman). Pipette was also used to make DNA chip; in that case, 0.2 μl of PCR products was dropped on the glysidoxy-activated chip. The chips are incubated at 50°C for 10 min in moisture atmosphere then kept at room temperature for 15 min. The remained active residues were blocked with Lys (0.1 M) dissolved in 0.25 M carbonate buffer (pH 9.5). The prepared DNA chips were stored in 20 mM of Tris–HCl (pH 7.5) containing 2 mM ethylenediaminetetraacetic acid (EDTA). The fixed DNA was easily detected by fluorescence imaging under a confocal scanning microscope (LSM-200, Olympus, Tokyo, Japan).

3.3. Recovery of DNA by photothermal denaturation

The DNA chip was overlaid with 25 μl of 20 mM Tris–HCl (pH 7.4) containing 2 mM EDTA. The laser (1053 nm, 10–100 mW on the surface of the DNA chip) was focused on the surface of the chip and about 20 μl drop of solution from the laser-irradiated area was collected in a vessel. A part of recovered DNA (3 μl) was amplified by PCR to check the DNA. The PCR was carried out using a primer (GTAAAACGACGGCCAGT). The amplified products were analyzed by electrophoresis using 2% agarose gel followed by staining with 0.5 μg/ml ethidium bromide. The electropherograms were visualized by a fluorescence image analyzer (FM-Bio 100, Hitachi Software Engineering, Tokyo, Japan).

4. Results and discussion

We made a DNA-arrayed chip as shown in Fig. 2. Each of the six different PCR products was immobilized along separate rows of a 6 × 6 grid. The photo shows a part of the DNA chip. The fluorescence from one spot clearly disappeared through IR laser irradiation, whereas the fluorescence from the untreated spots could be detected. This result indicates that the DNA from a small area was specifically released.

We then experimentally clarified the characteristics on how DNAs were released from the chip. As shown in the fluorescence image of Fig. 3, the fluorophore-labeled DNA (619 bp was immobilized at the fluorescent area on the chip) was removed from the irradiated region and the neighboring area. Bubbles were sometimes observed in the irradiated area, indicating that the solution temperature in the focused region could rise above the boiling point of water. The high temperature enabled the release of a DNA strand hybridized on its complementary strand fixed on the chip surface. It was possible to release the hybridized DNA from a 43-μm-wide denaturation area by 50 mW. However, the chip surface was partially damaged by the IR irradiation at this condition. The chromium came off the glass plate (the darkest area at the center on line a–a′ in Fig. 3), which could be easily observed by a phase-contrast microscope. Therefore, we optimized the laser power to release and recover the hybridized DNA from the chip surface. The fluorescence intensity at the small area of the laser-irradiated surface was measured in order to estimate the relative amount of denatured DNA. The hybridized DNA was released by the laser power ranging from 10 to 100 mW, as shown in Fig. 4 line A. More than 80% of the

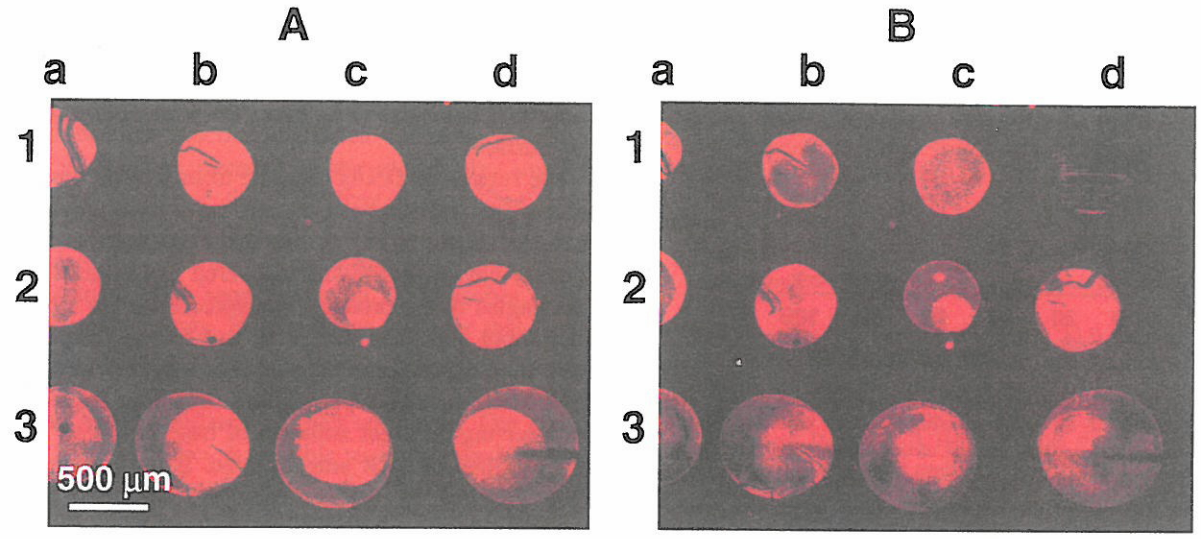

Fig. 2. Parts of fluorescence photographs of a DNA chip. The DNAs of 411, 270, and 231 bp were arrayed at lines 1–3 of each of column from a to d. Photograph A is the DNA chip before IR irradiation and photograph B is the same chip after IR irradiation at 10 mW. The IR laser-irradiated area was 1d.

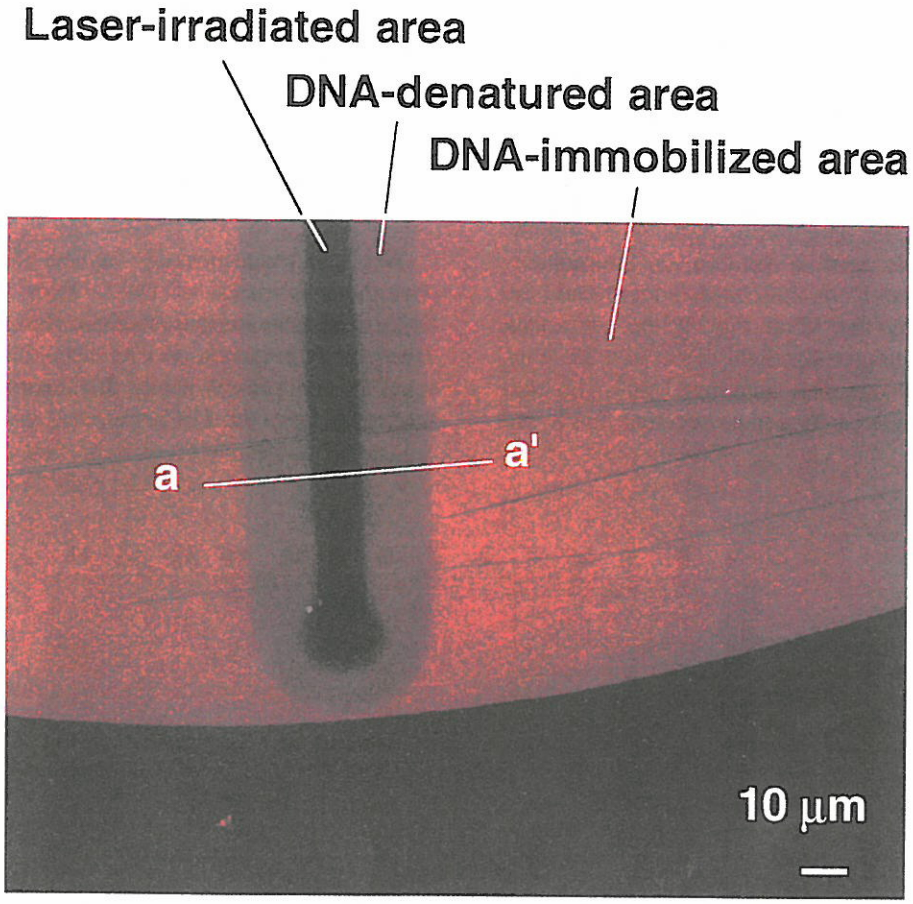

Fig. 3. Laser denaturation of a hybrid complex of sample DNA and probe DNA on chromium solid support (fluorescence image after laser irradiation). The fluorophore-labeled sample DNA disappeared from the small area on the solid support after laser irradiation. Intensity profiles at the a–a′ line under various laser powers are depicted in Fig. 4.

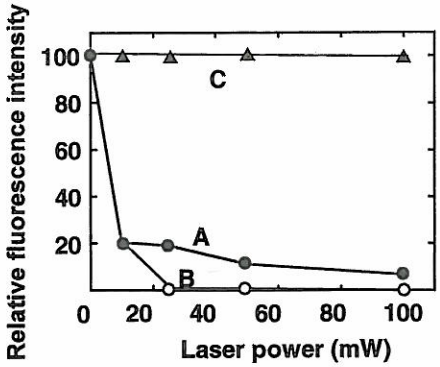

Fig. 4. Relative amounts of denatured DNA at different laser powers. The fluorescence intensity in the DNA-releasing area was measured from a fluorescence image as a relative amount of denatured DNA. The closed circles ● (line A) and open circles ○ (line B) show the fluorescence intensity in the DNA-denatured area and the chip-damaged area, respectively. The chip-damaged area, which was identified by phase-contrast microscopy, is the darkest area and the DNA-denatured area is the neighboring darkest area in Fig. 3. The same chip was treated with a fluorophore-labeled oligomer in order to rehybridize with the probe DNA on the chip surface, and the relative fluorescence intensity (▲, line C) was measured. The chip surface was not damaged at a laser power of 10 mW.

DNA was denatured and released from the chip surface by laser irradiation. It was possible to release the hybridized DNA by 10 mW light without damaging the chromium surface. However, the chip surface was partially damaged by the IR laser irradiation at a power of 25 mW or higher (line B). To prove that the DNA probe (or released DNA) was not damaged in the neighboring area of chromium-damaged area, we dropped a solution of fluorophore-labeled single-stranded DNA (60 base length) onto the surface. As shown by line C in Fig. 4, the previously denatured area was completely rehybridized with the fluorophore-labeled single-stranded oligomer DNA (60 base length), which hybridizes with a sequence near the 3′ end of the immobilized DNA strand. This shows that the DNA probe immobilized on the chip surface was not damaged after IR laser irradiation, because the 60 base length DNA could only hybridize to an intact DNA immobilized on the chip surface.

The recovered DNAs released from five different spots on one chip surface by a 10-mW laser were amplified by PCR. As shown in Fig. 5, one main product was detected in every electrophoresis of recovered DNA (lanes 9–13). The lengths of the products recovered from the DNA chip were about 800, 600, 420, 270, and 230 bp, respectively. They were the same as the intact immobilized DNA (lanes 2–6). Thus, the electropherograms show that the recovered DNA having different numbers of base pairs can be used as a template of PCR amplification. If the released DNA were damaged by the IR laser, the amplified products would not be obtained.

Some extra bands appeared in the electropherograms of recovered DNA. The immobilized DNA were prepared by the PCR using 5′-AACGACGGCCAGTCACGNN-3′ from a mixture of DNA fragments depicted in lane 7. All the fragments have the common sequence of AACGACGGCCAGT at both their 3′-termini. The PCR products in lanes 9–13 were amplified by using a common sequence primer. Since both the immobilized DNA and contaminants can be amplified with a common primer, there were some extra products in the electropherograms.

5. Conclusions

We have experimentally studied the characteristics of photothermal release of DNAs from a DNA chip. The DNA chip technology will allow separation of many different DNA fragments in one step. The procedure developed in the present study for releasing specific DNA fragments from the DNA chip has great potential in the

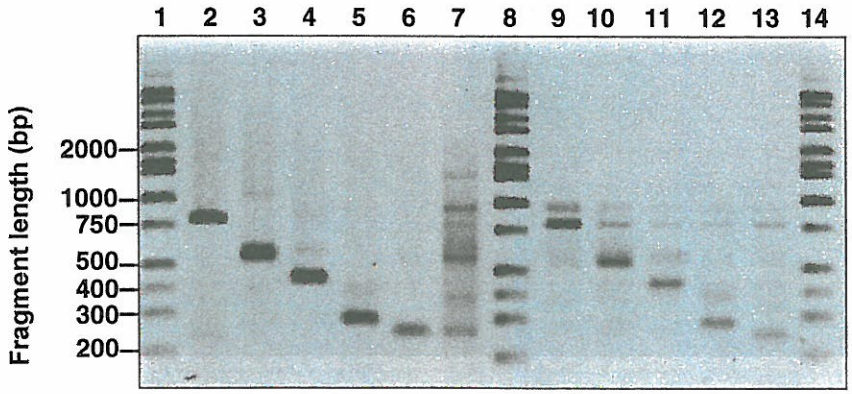

Fig. 5. Electropherograms of PCR products. The templates are DNA fragments recovered from the IR laser-irradiated chip (lanes 9–13), intact immobilized PCR products prepared from a mixture of DNA fragments (lanes 2–6), the mixture of DNA fragments (lane 7), and a marker (lanes 1, 8, and 14).

field of DNA preparation and purification. In general, hybridization reactions occur between not only complementary strands but also strands having similar sequences. The hybridization reaction is carried out at uni-condition because each probe element on the chip is too small to independently control the hybridization condition, e.g., annealing temperature and salt concentration. This is a drawback of the DNA chip because non-specific hybridization of similar DNA sequences with DNA probes on the chip frequently occurs. However, we consider that it will be a merit to analyze rapidly many kinds of DNA fragments because the chip elements can group the fragments according to the similarity of their sequences. Our photothermal method makes it possible to further analyze once the trapped DNA fragments on the chip elements. The DNA chip, coupled with photothermal denaturation, will work at searching DNA fragments of similar sequences (e.g., making a wholesale detection of DNA super family) to the best of its ability.

Molecular biology is rapidly approaching the stage of functional genomics. The screening of total gene expression profiles and the analysis of genome differentiation of species have become major research fields. A preparation method that enables separation of DNAs based on differences in expressed messages or in genomics will become more important. Our photothermal releasing procedure coupled with the DNA chip will have great potential in this field.

Acknowledgements

The authors thank Professor Sakaki for kindly supplying the human genome DNA. This research was partially supported by Grants-in-Aid for Scientific Research, for Scientific Research on Priority Areas and for the High-Tech Research Center Project from the Ministry of Education, Science, Sports and Culture of Japan.

References

[1] P.L. Deininger, Random subcloning of sonicated DNA: application to shotgun DNA sequence analysis, Anal. Biochem. 129 (1983) 216–223.

[2] D.J. Lockhart, H. Dong, M.C. Byrne, M.T. Follettie, M.V. Gallo, M.S. Chee, M. Mittmann, C. Wang, M. Kobayashi, H. Horton, E.L. Brown, Expression monitoring by hybridization to high-density oligonucleotide arrays, Nat. Biotechnol. 14 (1996) 1675–1680.

[3] S.P.A. Fodor, J.L. Read, M.C. Pirrung, L. Stryer, A.T. Lu, D. Solas, Light-directed, spatially addressable parallel chemical synthesis, Science 251 (1991) 767–773.

[4] A.C. Pease, D. Solas, E.J. Sullivan, M.T. Cronin, C.P. Holmes, S.P. Fodor, Light-generated oligonucleotide arrays for rapid DNA sequence analysis, Proc. Natl. Acad. Sci. U.S.A. 91 (1994) 5022–5026.

[5] M. Schena, D. Shalon, R.W. Davis, P.O. Brown, Quantitative monitoring of gene expression patterns with a complementary DNA microarray, Science 270 (1995) 467–470.

[6] D.G. Wang, J.-B. Fan, C.-J. Siao, A. Berno, P. Young, R. Sapolsky, G. Ghandour, N. Perkins, E. Winchester, J. Spencer, L. Kruglyak, L. Stein, L. Hsie, T. Topaloglou, E. Hubbell, E. Robinson, M. Mittmann, M.S. Morris, N. Shen, D. Kilburn, J. Rioux, C. Nusbaum, S. Rozen, T.J. Hudson, R. Lipshutz, M. Chee, E.S. Lander, Large-scale identification, mapping, and genotyping of single-nucleotide polymorphisms in the human genome, Science 280 (1998) 1077–1082.

[7] J.B. Lamture, K.L. Beattie, B.E. Burke, M.D. Eggers, D.J. Ehrlich, R. Fowler, M.A. Hollis, B.B. Kosicki, R.K. Reich, S.R. Smith et al., Direct detection of nucleic acid hybridization on the surface of a charge-coupled device, Nucleic Acids Res. 22 (1994) 2121–2125.

[8] M. Schena, D. Shalon, H. Heller, A. Chai, P.O. Brown, R.W. Davis, Parallel human genome analysis: microarray-based expression monitoring of 1000 genes, Proc. Natl. Acad. Sci. U.S.A. 93 (1996) 10614–10619.

[9] K.R. Khrapko, Yu.P. Lysov, A.A. Khorlyn, V.V. Shick, V.L. Florentiev, A.D. Mirzabekov, An oligonucleotide hybridization approach to DNA sequencing, FEBS Lett. 256 (1989) 118–122.

[10] G. Yershov, V. Barsky, A. Belgovskiy, E. Kirillov, E. Kreindlin, I. Ivanov, S. Parinov, D. Guschin, A. Drobishev, S. Dubiley, A. Mirzabekov, DNA analysis and diagnostics on oligonucleotide microchips, Proc. Natl. Acad. Sci. U.S.A. 93 (1996) 4913–4918.

[11] M.J. Marton, J.L. DeRisi, H.A. Bennett, V.R. Iyer, M.R. Meyer, C.J. Roberts, R. Stoughton, J. Burchard, D. Slade, H. Dai, D.E. Bassett Jr., L.H. Hartwell, P.O. Brown, S.H. Friend, Drug target validation and identification of secondary drug target effects using DNA microarrays, Nat. Med. 4 (1998) 1293–1301.

[12] M.J. O'Donnell, K. Tang, H. Koster, C.L. Smith, C.R. Cantor, High-density, covalent attachment of DNA to silicon wafers for analysis by MALDI-TOF mass spectrometry, Anal. Chem. 69 (1997) 2438–2443.

[13] J. Cheng, E.L. Sheldon, L. Wu, A. Uribe, L.O. Gerrue, J. Carrino, M.J. Heller, J.P. O'Connell, Preparation and hybridization analysis of DNA/RNA from *E. coli* on microfabricated bioelectronic chips, Nat. Biotechnol. 16 (1998) 541–546.

[14] H. Kato, T. Nishizaka, T. Iga, K. Kinosita Jr., S. Ishiwata, Imaging of thermal activation of actomyosin motors, Proc. Natl. Acad. Sci. U.S.A. 96 (1999) 9602–9606.

[15] K. Okano, C. Uematsu, H. Matsunaga, H. Kambara, Characteristics of selective polymerase chain reaction (PCR) using two-base anchored primers and improvement of its specificity, Electrophoresis 19 (1998) 3071–3078.

Biographies

K. Okano is working for Central Research Laboratory, Hitachi as a Senior Research Scientist in research on methodology for analyzing DNA, i.e., DNA fingerprinting, sequencing, and DNA assay. He investigated characteristics of PCR and developed a method to eliminate the false-positive amplification reaction. Furthermore, he demonstrated that any unknown sequenced DNA fragment digested with a restriction enzyme can be grouped in 136 windows by using improved PCR with a library as small as 16 primers.

K. Yasuda is an Associate Professor at the University of Tokyo. He has been studying several fields such as the muscle contractile mechanism, basic and applications of acoustic radiation force, and biochip technologies. In the study, he proposed the non-contact handling method of biomaterials in the microchamber for the high-throughput, contamination-free analysis using acoustic radiation force.

S. Ishiwata is a Professor at Waseda University. He has been studying the mechanism of protein motors on a single molecular level, the molecular synchronization observed in motor assemblies, and the mechanism of formation of the organized structures in muscle. His groups used optical tweezers to successfully measure the mechanical properties of a single actomyosin complex. They demonstrated auto-oscillatory properties of actomyosin motors and reconstitution of thin actin filaments in the contractile apparatus of cardiac muscle.

Biochemical and Biophysical Research Communications 272, 895–899 (2000)
doi:10.1006/bbrc.2000.2856, available online at http://www.idealibrary.com on IDEAL®

Temperature Dependence of Force, Velocity, and Processivity of Single Kinesin Molecules

Kenji Kawaguchi* and Shin'ichi Ishiwata*,†,‡,§,[1]

*Department of Physics, School of Science and Engineering, †Advanced Research Institute for Science and Engineering, and ‡Materials Research Laboratory for Bioscience and Photonics, Waseda University, 3-4-1 Okubo, Shinjuku-ku, Tokyo 169-8555, Japan; and §Core Research for Evolutional Science and Technology, "Genetic Programming" Team 13, Kawasaki 216-0001 Japan

Received May 15, 2000

Using the bead assay in optical microscopy equipped with optical tweezers, we have examined the effect of temperature on the gliding velocity, force, and processivity of single kinesin molecules interacting with a microtubule between 15 and 35°C. The gliding velocity increased with the Arrhenius activation energy of 50 kJ/mol, consistent with the temperature dependence of the microtubule-dependent ATPase activity. Also, the average run length, i.e., a measure of processivity of kinesin, increased on increasing temperature. On the other hand, the generated force was independent of temperature, 7.34 ± 0.33 pN (average ± S.D., n = 70). The gliding velocities decreased almost linearly with an increase in force irrespective of temperature, implying that the efficiency of mechanochemical energy conversion is maintained constant in this temperature range. Thus, we suggest that the force generation is attributable to the temperature-insensitive nucleotide-binding state(s) and/or conformational change(s) of kinesin-microtubule complex, whereas the gliding velocity is determined by the ATPase rate. © 2000 Academic Press

Key Words: **kinesin; microtubule; motor proteins; processivity; temperature effect; single molecule analysis; force generation; gliding velocity; Arrhenius activation energy.**

In nerve cells, organelles such as mitochondria and synaptic vesicles travel distances as long as several micrometers at a rate of 2–4 μm/s at physiological temperature (1–3). This movement has been classified as fast axonal transport and appears to be similar to the vesicular movement observed in other cells. Kinesin is a homodimer motor protein that bears such intracellular movements along a microtubule in an anterograde manner as a fast axonal transporter and requires the energy of ATP hydrolysis (4). An important property of kinesin is that it is a processive motor: an individual molecule can move continuously for long distances along the surface of the microtubule. Kinesin moves along the microtubule with 8 nm steps and generates force of 5–8 pN at 25°C (5–9).

In general, chemical reaction proceeds faster at higher temperatures. It has been known that the gliding velocity of microtubule interacting with kinesin molecules increases with an increase in temperature (10, 11). However, this property has not yet been examined by single molecular experiments. Because kinesin functions as a single molecule, single molecular experiments are indispensable. Here, to investigate the temperature effect on single kinesin molecules, we examined single-molecular bead assay under an optical microscope. A single native kinesin molecule purified from bovine brain was attached to a polystyrene bead, and the bead was trapped by optical tweezers and then brought onto a microtubule which was attached to a coverslip (7, 9). As expected from the Arrhenius law on temperature dependence of chemical reactions, the gliding velocity of single kinesin molecules measured by the displacement of the bead increased steadily up to 35°C, and the corresponding Arrhenius plot was linear. The distance over which kinesin molecules continue moving along a microtubule without detachment (run length) was longer at higher temperatures, which is reasonable as a property of kinesin that is an intracellular transporter. Also, we investigated the effect of temperature on the force generation. Interestingly, the force generated by a single kinesin molecule did not change when the temperature was increased from 15 to 35°C. This result suggests that the force generation of kinesin might be programmed to perform the same efficiency irrespective of

[1] To whom correspondence and reprints requests should be addressed at Department of Physics, School of Science and Engineering, Waseda University, 3-4-1 Okubo, Shinjuku-ku, Tokyo 169-8555, Japan. Fax: +81-3-3200-2567. E-mail: ishiwata@mn.waseda.ac.jp.

0006-291X/00 $35.00

temperatures. A preliminary report of this investigation was presented previously (12).

MATERIALS AND METHODS

Proteins. Kinesin was prepared from bovine brain according to the method of Kojima *et al.* (13). Tubulin was purified from porcine brain and labeled with tetramethylrhodamine succinimidyl ester (C-1171, Molecular Probes, Eugene, OR) according to Hyman (14). Microtubules were stabilized with 40 μM taxol.

Bead assay. Kinesin-coated beads were prepared according to Kojima *et al.* (13) with slight modifications. We used fluorescent latex beads (1.0 μm in diameter, carboxylate-modified latex; yellow-green, F-8823; Molecular Probes). The number of kinesin molecules attached to the bead that can interact with a microtubule was estimated by statistical methods (15). All the experiments were performed with beads on which the average number of kinesin molecules was one.

Flow chamber for beads assay. The fluorescent microtubules were introduced into a flow chamber and incubated for 2 min to allow binding of the microtubule to the glass surface of the chamber. The chamber was washed with an assay buffer containing 2 mM $MgCl_2$, 80 mM PIPES (piperazine-1,4-bis(2-ethanesulfonic acid), pH 6.8), 1 mM EGTA and 0.7 mg/ml filtered casein (0.73-19, Nacalai Tesque, Kyoto) to remove unattached microtubules and left for 2 min to coat the glass surface with casein. The chamber was then filled with an assay solution containing the kinesin-coated beads and an oxygen scavenging enzyme system (16) [approximately 0.1 pM kinesin-coated beads, 2 mM $MgCl_2$, 80 mM PIPES (pH 6.8), 1 mM EGTA, 0.7 mg/ml filtered casein, 1 mM ATP (127531, Boehringer Mannheim, Mannheim, Germany), 10 μM taxol (T-1912, Sigma, St. Louis, MO), 10 mM dithiothreitol (DTT), 4.5 mg/ml glucose, 0.22 mg/ml glucose oxidase (G-2133, Sigma), 0.036 mg/ml catalase (C-10, Sigma)], and sealed with enamel. Other chemicals were of reagent grade.

Microscope. A microscopy system used for measuring the interaction of kinesin and microtubule was previously described by Nishizaka *et al.* (17). An inverted microscope (TMD-300; an oil-immersion objective lens with a phase ring, ×100 NA = 1.3; Nikon, Tokyo) was equipped with optical tweezers with 1W Nd: YLF laser (1053-1000p: λ = 1.053 μm; Amoco Laser, IL). The centroid of the phase-contrast image of polystyrene beads was calculated with a frame memory computer (DIPS-C2000; Hamamatsu Photonics, Hamamatsu, Japan) and a fluorescence image of a microtubule was simultaneously acquired with a modified dual-view fluorescence microscope system (18, 19). Stiffness of the optical trap was estimated to be 0.087 pN/nm by the method of Nishizaka *et al.* (17).

Temperature control. For experiments at 15, 20, and 25°C, the room temperature was equilibrated by an air conditioner to each temperature. For experiments at 30 and 35°C, the stage of the inverted microscope that contained the flow cell was covered by a thermal insulation chamber (Nikon, Tokyo) and the temperature of the cell was controlled. The temperature was measured by a thermistor on the microscope stage near the flow chamber and regulated within ±1°C of the designated experimental temperature. We confirmed that the local temperature around the bead trapped by the laser beam did not increase by measuring thermally quenched fluorescence intensity of tetramethyl-rhodamine which was attached to a microtubule (12, 20). The single-molecular bead assay was done after keeping the flow cell for 1 min at each temperature.

Gliding velocity of single kinesin-coated bead. A bead, to which a single kinesin molecule was attached, was manipulated with optical tweezers onto a microtubule adsorbed to a coverslip. After the attachment of the bead to the microtubule was confirmed in the assay solution, the laser beam for optical tweezers was shut off. Then the movement of the bead occurred towards the plus end of a microtubule. From the video image (30 frames/s), the time course of displacement of the bead was obtained. Because the displacement was nearly linear with time, the average gliding velocity could be determined from the slope of the displacement vs. time relationship.

Force generated by single kinesin. A bead, to which a single kinesin molecule was attached, was manipulated onto a microtubule in the assay solution by using optical tweezers. When the bead was placed in contact with a microtubule, the bead was displaced from the trap center, gradually decreasing its displacement velocity until it reached a plateau. The bead stayed at the plateau level for some period of time and then returned to the trap center. On some occasions, however, the bead returned to the trap center before reaching the plateau. These data were not used for the data analyses. From the video image, the displacement of the bead from the trap center was traced against time. Force was calculated from (stiffness of optical trap) × (displacement).

Measurement of the force-velocity curves. To determine the relation between velocity and force, 7 raw data showing the time course of the bead displacement were averaged at each temperature (cf. Fig. 2c). The gliding velocities at various forces were determined from the slope of the average time course of bead displacement in the range of 1-2, 2-3, 3-4, 4-5, 5-6 and 6-7 pN. The velocities at zero force were obtained without applying an external load by an optical trap. To determine the velocity of kinesin molecules under an external load, the velocity of the bead must be corrected by multiplying the factor, 1 + (stiffness of optical tweezers)/(stiffness of kinesin-microtubule complex) (13). But, the stiffness of the kinesin-microtubule complex has been estimated to be larger than approximately 0.4 pN/nm (21), being several times larger than that of optical tweezers, 0.087 pN/nm, so that the correction was not done. Thus, the velocities we estimated may have been a little underestimated except those at no load.

RESULTS AND DISCUSSION

Temperature Effect on Gliding Velocity

First, we examined the effect of temperature on the gliding velocity of the bead without external load (Fig. 1a). The result was similar to the previous results obtained by microtubule gliding assay (10, 11). The Arrhenius plot was linear in this temperature range as shown in Fig. 1b. The activation energy was estimated as 50 kJ/mol from the slope of the Arrhenius plot, consistent with the temperature dependence of the microtubule-dependent ATPase activity (11). The Arrhenius activation energy thus obtained is comparable to that determined in the actomyosin in vitro motility assay (21–24). At temperatures higher than 40°C, however, we could not measure the gliding velocities of beads in the present experimental setup because the beads tended to detach during incubation for 1 min which was required for stabilizing the temperature of the cell in the thermal insulation chamber.

Recently, Böhm *et al.* (10) reported that the Arrhenius plot of microtubule gliding velocity revealed a break at 27°C, resulting in the activation energies of 65 kJ/mol for <27°C and 9 kJ/mol for >27°C. They concluded that the break in the Arrhenius plot results from conformational changes of kinesin and/or microtubule (25). On the contrary, there seemed to be no break at around 27°C in our data (Fig. 1). Besides, a preliminary result (12) of the microtubule gliding as-

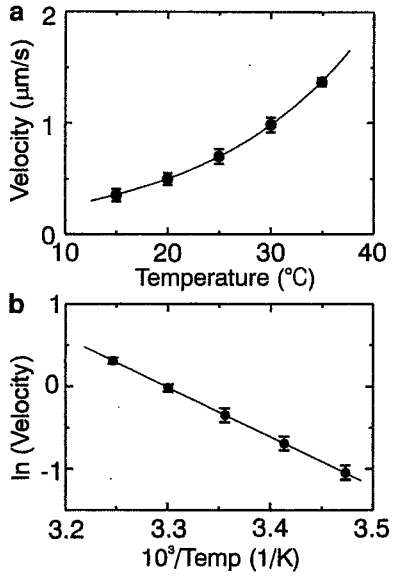

FIG. 1. Temperature dependence of gliding velocity of a single kinesin molecule attached to a bead. (a) Gliding velocity vs temperature. (b) Arrhenius plot of a. The error bars represent ± S.D. for 7 measurements. The velocities of the bead (average ± S.D.) were, 0.35 ± 0.04, 0.50 ± 0.05, 0.71 ± 0.07, 0.99 ± 0.07 and 1.36 ± 0.04 μm/s, respectively, at 15, 20, 25, 30, and 35°C. Solvent conditions, an assay buffer containing 2 mM $MgCl_2$, 80 mM PIPES (pH 6.8), 1 mM EGTA, 0.7 mg/ml filtered casein, 10 mM DTT, 1 mM ATP and an oxygen scavenging enzyme system.

say examined between 35 and 50°C by temperature pulse microscopy (TPM) technique (21) showed that there are no breaks between 15 and 50°C with a unique activation energy of about 50 kJ/mol. As the previous experiments (10) were not a single molecular assay but a multi-molecular one, there is a possibility that kinesin molecules may be thermally damaged due to long incubation at high temperatures might have prevented smooth movement of microtubule. Actually, we confirmed that we could not obtain reliable data when the incubation time of the flow cell was longer than 10 min at 30°C, and even for 1 min at 40°C, because of a gradual deterioration of motility of kinesin.

Temperature Effect on Processivity

From the same data as used for measuring the gliding velocity, we could estimate the run length (= the number of steps times the step size), a measure of processivity, over which kinesin molecules continued moving on a microtubule without detachment. Although the number of data was not large enough to confirm the exponential distribution of the run length (6, 8), we could find that the average run length monotonously increased from approximately 0.7 to 1.5 μm on increasing temperature from 15 to 35°C. This implies that a probability of detachment at every step of kinesin becomes smaller on increasing temperature, suggesting that the hydrophobic interaction is important to stabilize the attached state of kinesin. It is to be noted, however, that the average duration of continuous running decreased with increasing temperature, i.e., approximately 2 s at 15°C and 1 s at 35°C. In any case, such a temperature dependence of run length is important for the physiological function of kinesin as an intracellular transporter that needs to carry an organella for long distances at body temperature.

Temperature Effect on Force Generation

Next, external load was applied to a bead by trapping the bead with optical tweezers. Figures 2a and b, respectively, show examples of raw data for the bead moving away from the trap center at 20 and 35°C. Figure 2c shows the average displacement of the kinesin-coated bead at 20 and 35°C. Seven traces of the

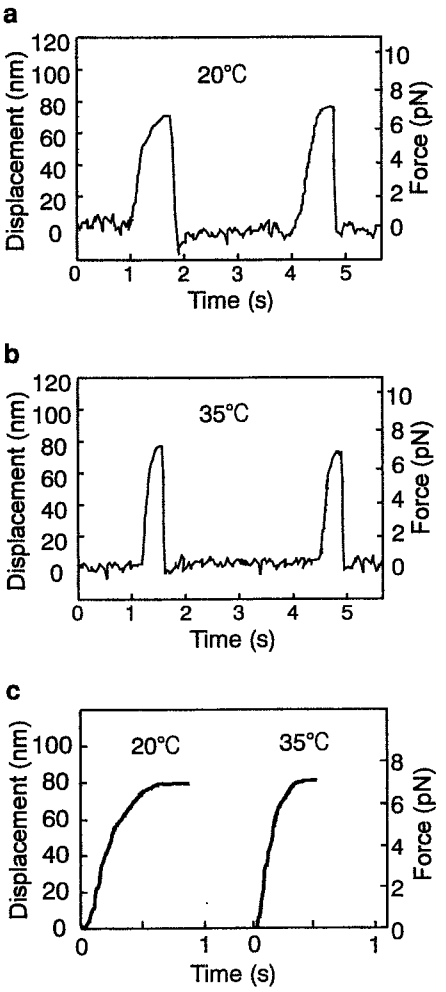

FIG. 2. Time course of force generation of a single kinesin molecule attached to a bead. (a and b) Examples of raw data for the bead moving away from the trap center at 20 (a) and 35 (b) °C. (c) Average (n = 7) of the above data at 20 and 35°C. Force calculated from the bead displacement is shown on the right ordinate. Solvent conditions are the same as in Fig. 1.

displacement of a bead, in which the bead stayed at a plateau level for a period longer than 0.1 s, were superimposed and averaged at each temperature. The gliding velocity gradually decreased with the increase in the external load. The clear difference at these two temperatures was the velocity of the rising phase. Also, we found that the duration between the beginning of tension generation and its end was shorter at higher temperatures. The duration obtained by averaging 7 data (see Figs. 2a and b) was 1.03 ± 0.25 (average ± S.D.), 0.82 ± 0.18, 0.73 ± 0.12, 0.69 ± 0.21 and 0.58 ± 0.18 s, respectively, at 15, 20, 25, 30 and 35°C. Thus, the lifetime of the attached state became shorter by imposing external load.

As summarized in Fig. 3, the steady forces at the plateau level were independent of temperature between 15 and 35°C, i.e., 7.34 ± 0.33 pN (average ± S.D., n = 70). Based on the above results, we suggest that the force generation in kinesin molecules is attributable to the temperature-insensitive nucleotide-binding state(s) and/or conformational change(s) of kinesin-microtubule complex, whereas the gliding velocity is coupled with the temperature-sensitive ATPase rate. It was recently reported that the maximum force generated by acto-myosin (heavy meromyosin) complex is independent of temperature in the same temperature range as examined here (26), although their data were not obtained by single molecular experiments. Thus, it is suggested that the temperature-insensitive force generation and the temperature-sensitive gliding velocity may be common to molecular motors.

Temperature Effect on Force-Velocity Relation

The force-velocity curves for single kinesin molecules at several temperatures shown in Fig. 4 were obtained from the slope of the averaged time course of the bead displacement (force development) as shown in Fig. 2c

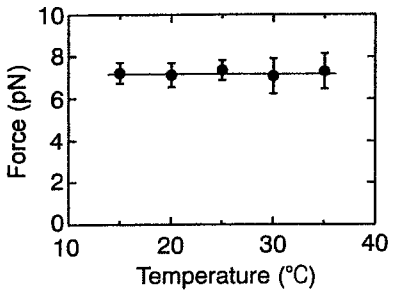

FIG. 3. Temperature dependence of maximum force generated on a single kinesin molecule attached to a bead. The maximum forces (average ± S.D.; data, of which duration at a plateau level was shorter than 0.1 s, were also included for this calculation) were 7.38 ± 0.45 (n = 12), 7.21 ± 0.57 (n = 16), 7.50 ± 0.47 (n = 25), 7.16 ± 0.83 (n = 10) and 7.43 ± 0.83 (n = 7) pN, respectively, at 15, 20, 25, 30, and 35°C. Solvent conditions are the same as in Fig. 1.

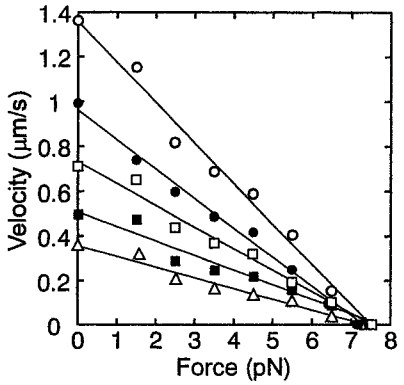

FIG. 4. Temperature dependence of force-velocity relation. From bottom to top, open triangles, 15°C; closed squares, 20°C; open squares, 25°C; closed circles, 30°C; open circles, 35°C. Velocities at various forces were estimated from the average slope of the bead displacement shown in Fig. 2c in the range of 1-2, 2-3, 3-4, 4-5, 5-6 and 6-7 pN. The velocities at zero load on the ordinate were obtained from Fig. 1 and the maximum forces on the abscissa were from Fig. 3. Solvent conditions are shown in Fig. 1.

in the range of 1-2, 2-3, 3-4, 4-5, 5-6 and 6-7 pN. The data on the ordinate and the abscissa of Fig. 4 were, respectively, obtained from Figs. 1a and 3. As seen in Fig. 4, the force-velocity curve was nearly linear in the whole temperature range we examined from zero to the maximum force. Such a linear relationship between force and velocity has previously been reported around room temperature (13, 15, 27).

The maximum work (= force × working distance) that a motor can perform is bounded by the free energy decrease associated with the hydrolysis of one ATP molecule, ~25 kT or ~100 × 10^{-21} J. In the case of kinesin of which step size is 8 nm, the force must be ≤12 pN. Our data showed that a single kinesin molecule is able to generate a force of 7 pN irrespective of temperature (Fig. 3). Thus, provided that each step is associated with the hydrolysis of just one ATP molecule, the efficiency of energy conversion is estimated to be less than 60% because the maximum work performed is 7 pN × 8 nm = 56 × 10^{-21} J. Besides, because both gliding velocity and ATPase activity changed in parallel with the increase in temperature (at least without external load), the efficiency of mechanochemical energy conversion, which is proportional to (external load = force) × (gliding velocity)/(ATPase activity), seems to be independent of temperature. Motor molecules may be programmed so as to perform the biological movement at a fixed efficiency at any temperatures.

ACKNOWLEDGMENTS

We thank Dr. K. Kinosita, Jr., of Keio University for his critical reading of the manuscript. This research was partly supported by Grants-in-Aid for Scientific Research, for Scientific Research on Priority Areas and for the High-Tech Research Center Project from the

Ministry of Education, Science, Sports, and Culture of Japan, and by Grants-in-Aid from Japan Science and Technology Corporation (CREST). This was also supported by a grant from the Mitsubishi Foundation.

REFERENCES

1. Brady, S. T. (1985). A novel brain ATPase with properties expected for the fast axonal transport motor. *Nature* **317,** 73–75.
2. Grafstein, B., and Forman, D. S. (1980). Intercellular transport in neurons. *Physiol. Rev.* **60,** 1167–1283.
3. Lasec, R. J., Garner, J. A., and Brady, S. T. (1984). Axonal transport of the cytoplasmic matrix. *J. Cell Biol.* **101,** 2181–2193.
4. Howard, J., Hudspeth, A. J., and Vale, R. D. (1989). Movement of microtubules by single kinesin molecules. *Nature* **342,** 154–158.
5. Howard, J. (1996). The movement of kinesin along microtubules. *Annu. Rev. Physiol.* **58,** 703–729.
6. Block, S. M., Goldstein, L. S. B., and Schnapp, B. J. (1990). Bead movement by single kinesin molecules studied with optical tweezers. *Nature* **348,** 348–352.
7. Svoboda, K., Schmidt, C. F., Schnapp, B. J., and Block, S. M. (1993). Direct observation of kinesin stepping by optical trapping interferometry. *Nature* **365,** 721–727.
8. Vale, R. D., Funatsu, T., Pierce, D. W., Romberg, L., Harada, Y., and Yanagida, T. (1996). Direct observation of single kinesin molecules moving along microtubules. *Nature* **380,** 451–453.
9. Higuchi, H., Muto, E., Inoue, Y., and Yanagida, T. (1997). Kinetics of force generation by single kinesin molecules activated by laser photolysis of caged ATP. *Proc. Natl. Acad. Sci. USA* **94,** 4395–4400.
10. Böhm, K. J., Stracke, R., Baum, M., Zieren, M., and Unger, E. (2000). Effect of temperature on kinesin-driven microtubule gliding and kinesin ATPase activity. *FEBS Lett.* **466,** 59–62.
11. Mazumdar, M., and Cross, R. A. (1998). Engineering a lever into the kinesin neck. *J. Biol. Chem.* **273,** 29352–29359.
12. Kawaguchi, K., and Ishiwata, S. (2000). Effect of temperature on force generation and velocity of single kinesin molecule. *Biophys. J.* **78,** 122A (Abstract).
13. Kojima, H., Muto, E., Higuchi, H., and Yanagida, T. (1997). Mechanics of single kinesin molecules measured by optical trapping nanometry. *Biophys. J.* **73,** 2012–2022.
14. Hyman, A. A. (1991). Preparation of marked microtubules for the assay of the polarity of microtubule-based motors by fluorescence. *J. Cell Sci. Suppl.* **14,** 125–127.
15. Svoboda, K., and Block, S. M. (1994). Force and velocity measured for single kinesin molecules. *Cell* **77,** 773–784.
16. Harada, Y., Sakurada, K., Aoki, T., Thomas, D. D., and Yanagida, T. (1990). Mechanochemical coupling in actomyosin energy transduction studied by in vitro movement assay. *J. Mol. Biol.* **216,** 49–68.
17. Nishizaka, T., Miyata, H., Yoshikawa, H., Ishiwata, S., and Kinosita, Jr., K. (1995). Unbinding force of a single motor molecule of muscle measured using optical tweezers. *Nature* **377,** 251–254.
18. Miyata, H., Hakozaki, H., Yoshikawa, H., Suzuki, N., Kinosita, Jr., K., Nishizaka, T., and Ishiwata, S. (1994). Stepwise motion of an actin filament over a small number of heavy meromyosin molecules is revealed in an *in vitro* motility assay. *J. Biochem.* **115,** 644–647.
19. Kinosita, Jr., K., Ito, H., Ishiwata, S., Hirano, K., Nishizaka, T., and Hayakawa, T. (1991). Dual-view microscopy with a single camera: Real-time imaging of molecular orientations and calcium. *J. Cell Biol.* **115,** 67–73.
20. Kato, H., Nishizaka, T., Iga, T., Kinosita, Jr., K., and Ishiwata, S. (1999). Imaging of thermal activation of actomyosin motors. *Proc. Natl. Acad. Sci. USA* **96,** 9602–9606.
21. Ishiwata, S., and Kawaguchi, K. (2000). Nucleotide- and loading rate-dependent switching of single- to double-headed binding of kinesin. *Biophys. J.* **78,** 278A (Abstract).
22. Anson, M. (1992). Temperature dependence and arrhenius activation energy of F-actin velocity generated in vitro by skeletal myosin. *J. Mol. Biol.* **224,** 1029–1038.
23. Homsher, E., Wang, F., and Sellers, J. R. (1992). Factors affecting movement of F-actin filaments propelled by skeletal muscle heavy meromyosin. *Am. J. Physiol.* **262,** C714–C723.
24. Winkelmann, D. A., Bourdieu, L., Ott, A., Kinose, F., and Libchaber, A. (1995). Flexibility of myosin attachment to surfaces influences F-actin motion. *Biophys. J.* **68,** 2444–2453.
25. De Cuevas, M., Tao, T., and Goldstein, L. S. B. (1992). Evidence that the stalk of *Drosophila* kinesin heavy chain is an α-helical coiled coil. *J. Cell Biol.* **116,** 957–965.
26. Kawai, M., Kawaguchi, K., Saito, M., and Ishiwata, S. (2000). Temperature change does not affect force between single actin filaments and HMM from rabbit muscles. *Biophys. J.* **78,** in press.
27. Mayhöfer, E., and Howard, J. (1995). The force generated by a single kinesin molecule against an elastic load. *Proc. Natl. Acad. Sci. USA* **92,** 574–578.

Characterization of Single Actomyosin Rigor Bonds: Load Dependence of Lifetime and Mechanical Properties

Takayuki Nishizaka,*† Ryuzo Seo,* Hisashi Tadakuma,* Kazuhiko Kinosita, Jr.,†‡ and Shin'ichi Ishiwata*†§¶
*Department of Physics, School of Science and Engineering, Waseda University, Tokyo169-8555; †Core Research for Evolutional Science and Technology, Genetic Programming Team 13, Kanagawa 216-0001; ‡Department of Physics, Faculty of Science and Technology, Keio University, Yokohama 223-8522; §Advanced Research Institute for Science and Engineering, Waseda University, Tokyo; and ¶Materials Research Laboratory for Bioscience and Photonics, Waseda University, Tokyo, Japan

ABSTRACT Load dependence of the lifetime of the rigor bonds formed between a single myosin molecule (either heavy meromyosin, HMM, or myosin subfragment-1, S1) and actin filament was examined in the absence of nucleotide by pulling the barbed end of the actin filament with optical tweezers. For S1, the relationship between the lifetime (τ) and the externally imposed load (F) at absolute temperature T could be expressed as $\tau(F) = \tau(0)\cdot\exp(-F\cdot d/k_BT)$ with $\tau(0)$ of 67 s and an apparent interaction distance d of 2.4 nm (k_B is the Boltzmann constant). The relationship for HMM was expressed by the sum of two exponentials, with two sets of $\tau(0)$ and d being, respectively, 62 s and 2.7 nm, and 950 s and 1.4 nm. The fast component of HMM coincides with $\tau(F)$ for S1, suggesting that the fast component corresponds to single-headed binding and the slow component to double-headed binding. These large interaction distances, which may be a common characteristic of motor proteins, are attributed to the geometry for applying an external load. The pulling experiment has also allowed direct estimation of the number of myosin molecules interacting with an actin filament. Actin filaments tethered to a single HMM molecule underwent extensive rotational Brownian motion, indicating a low torsional stiffness for HMM. From these results, we discuss the characteristics of interaction between actin and myosin, with the focus on the manner of binding of myosin.

INTRODUCTION

Recent developments in microscopic techniques have opened up opportunities of studying "single-molecule physiology," which enables us to elucidate protein-protein interactions and their various biological functions under living circumstances in aqueous media. For molecular motors, their individual behaviors have been successfully studied at the single molecule level. Nanometer steps and piconewton forces generated by single molecular motors have been measured under an optical microscope (Svoboda et al., 1993; Finer et al., 1994; Ishijima et al., 1994, 1998; Miyata et al., 1994, 1995; Molloy et al., 1995; Mehta et al., 1999). Single-fluorophore imaging (Funatsu et al., 1995; Sase et al., 1995a) has revealed individual ATP turnovers by myosin and rotational movement between actin and myosin (Sase et al., 1997), suggesting a hopping character for myosin (Kinosita et al., 1998). The mechanisms of motor operation, however, are still unclear. During one cycle of ATP hydrolysis, molecular motors are considered to form different conformations with different affinities for their substrate filaments and to alternate binding and unbinding. Here we focus on the characteristics of unbinding between myosin and actin.

In general, binding and unbinding interactions of proteins are essential for many biological functions, e.g., adhesion between cells, migration of cells on substratum (Nishizaka et al., 2000), recognition between ligands and receptors, processive movement of molecular motors, and so on. Several techniques have been developed to measure forces of protein bonds in the range from the subpiconewton level to a nanonewton. Glass microneedles were first applied to measure the sliding force generated between a microtubule and dynein motors (Kamimura and Takahashi, 1981) and then successfully used to measure the sliding force and the tensile strength of single actin filaments (Kishino and Yanagida, 1988; Tsuda et al., 1996). Individual ligand-receptor binding has been extensively characterized by atomic force microscopy (Nakajima et al., 1997; Fritz et al., 1998). The interaction between avidin and biotin has been examined in detail, and its molecular dynamics has been simulated (Florin et al., 1994; Moy et al., 1994; Grubmuller et al., 1996; Izrailev et al., 1997; Merkel et al., 1999). In the present study we used optical tweezers to characterize single actomyosin rigor bonds.

Optical tweezers, formed by focusing a laser beam, capture a particle of micrometer size without direct contact (Ashkin et al., 1986, 1990). In our previous studies (Nishizaka et al., 1995b), we measured the force required to unbind a rigor bond formed between an actin filament and a single heavy meromyosin (HMM) molecule in the absence of ATP using optical tweezers under a dual-view (fluorescence and phase-contrast) microscope (Kinosita et al., 1991; Sase et al., 1995b; Arai et al., 1999). The average unbinding force was ~9 pN, which is 2–5 times larger than the sliding force (Finer et al., 1994; Ishijima et al., 1994; Miyata et al., 1995) and an order of magnitude smaller than other intermolecular forces (Florin et al., 1994; Tsuda et al., 1996; Fritz et al., 1998). Unbinding under a constant force was a

Received for publication 28 February 2000 and in final form 26 April 2000.

Address reprint requests to Dr. Shin'ichi Ishiwata, Department of Physics, School of Science and Engineering, Waseda University, 3-4-1 Okubo, Shinjuku-ku, Tokyo 169-8555, Japan. Tel.: 81-3-5286-3437; Fax: 81-3-3200-2567; E-mail: ishiwata@mn.waseda.ac.jp.

0006-3495/00/08/962/13 $2.00

stochastic process, and an increase in the load by 10 pN decreased the lifetime of the rigor bond by a factor of 10^2 to 10^3. Interestingly, two types of HMM molecules were found, one with a large (long) and the other with a small (short) unbinding force (lifetime), suggesting "molecular individualism."

In this study, we measured the lifetime of single actomyosin (either HMM or subfragment-1 of myosin (S1)) rigor bonds under various external loads and could formulate the relationship between the lifetime and the load. The stochastic properties of the rigor bonds have been demonstrated. We developed a microscopic way to count the number of myosin molecules attached to the glass surface. Based on the number density of myosin molecules interacting with an actin filament thus measured, we estimated the minimum number of myosin molecules needed to slide actin filaments continuously. Furthermore, the torsional stiffness of single myosin molecules was estimated by observing the rotational Brownian motion of a short actin filament attached to myosin. Throughout the present study, we tried to characterize the interaction with actin of double-headed HMM molecules compared with that of single-headed S1 molecules.

MATERIALS AND METHODS

Dual-view imaging microscopy and optical tweezers system

Fig. 1 shows a schematic diagram of a dual-view (phase-contrast and fluorescence) video microscope imaging system (Kinosita et al., 1991; Nishizaka et al., 1995a,b; Sase et al., 1995b; Arai et al., 1999) equipped with optical tweezers. The inverted microscope (TMD-300; Nikon Co., Tokyo) with a 100× objective with a phase-contrast plate (NA 1.3, fluor 100 Ph; Nikon) was used on an optical bench (HG-LM; Herz Co., Kanagawa, Japan). The optical system included dichroic mirrors (DM 550, DM infrared, Sigma Koki Co., Saitama, Japan; DM 530, Asahi Spectra Co., Tokyo), filters (F 380–520, F 550, F 590; Asahi Spectra), and mirrors. The beam from the sample, which consisted of two components, the phase-contrast image of the bead (wavelength 380–520 nm, the *once-broken* line in Fig. 1) and the fluorescence image of actin filaments (excitation 550 nm and emission > 590 nm; the *dashed line* in Fig. 1), was separated by a beam separator (DM > 530 nm). Colorless filters (HA-30; Hoya Co., Tokyo, and Asahi Spectra) were placed behind the Hg lamp and before the image intensifier to cut off the infrared light. The field stop was positioned between the microscope and the beam separator, and lenses (DLB-50–150PM; Sigma Koki) were positioned before each camera to focus images clearly. The bead image, acquired with a CCD camera (CCD-72; Dage-MTI, Michigan City, IN), was stored in a digital frame memory (DIPS-C2000; Hamamatsu Photonics K. K., Hamamatsu, Japan). The position of the bead was determined by calculating the centroid of its intensity profile with a spatial resolution of nanometer scale (Fig. 2; Miyata et al., 1994; Nishizaka et al., 1995b). The data were analyzed with a personal computer (Apple Japan, Tokyo).

The sample stage of the microscope was replaced with the custom-made stage, on which the position of the objective along the z direction could be controlled by using a piezoelectric microscope positioner (P-720.00; Physik Instrumente GmbH and Co., Waldbronn, Germany) with a power supply (BWS 1202.5; Takasago, Tokyo). Because the drift between the commercial sample stage and the objective is mainly caused by deformation of the gear(s) sustaining a nose piece, the nose piece was removed and the objective was fixed directly to the sample stage to suppress the drift during measurements. Large displacement of the stage (as much as >40 nm) was achieved with the use of high-resolution actuators (HPA-10; Sigma Koki), their controller (Mark-8; Sigma Koki), and a personal computer (Apple Japan, Tokyo) with GPIB (NI488.2; National Instruments Co., Austin, TX). The small displacement (nanometer scale) was adjusted with a piezoelectric substage (p-770.10; Physik Instrumente GmbH and Co.) with a function generator (1915; NF Electronic Instruments, Yokohama, Japan) and an amplifier (BWS 120–2.5; Takasago). The temperature of the microscopic system was stabilized by allowing it to sit for 4–6 h before the measurements.

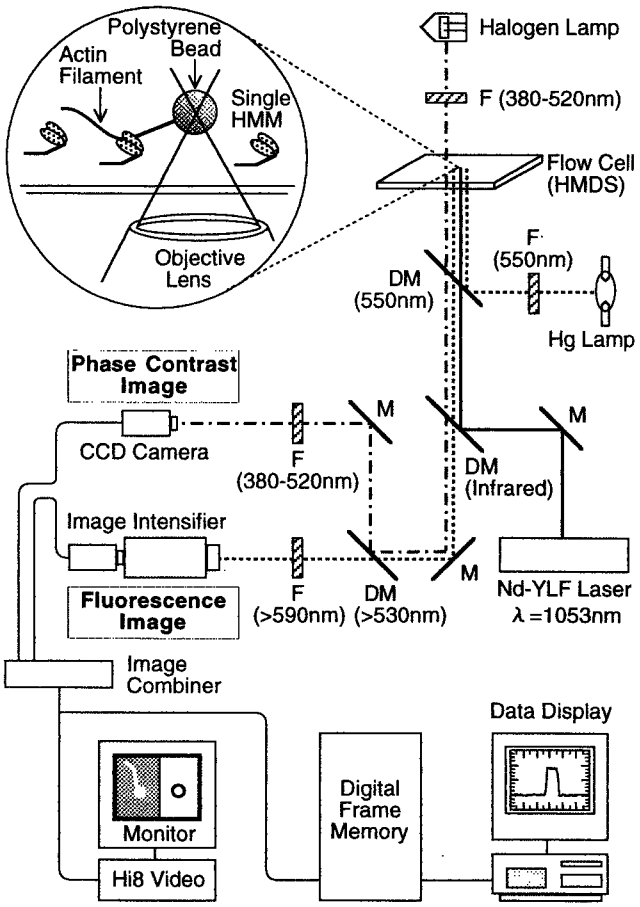

FIGURE 1 Schematic diagram of optical tweezers and dual-view imaging video microscope system. The once-broken lines and the dashed lines represent phase-contrast and fluorescence imaging optical paths, respectively, and the solid lines represent the optical tweezers optical path. The microscope system includes dichroic mirrors (DM) (the wavelength in parentheses shows the wavelength of the reflected light, and the wavelength with the > sign shows the range of wavelength passing through DM), filters (F) (the wavelength in parentheses shows the wavelength of light passing through F), and mirrors (M).

The spatial resolution of the system and the performance of the sample stage were examined by the method shown in Fig. 2. Fig. 2 *A* gives an example showing the position fluctuation of a bead trapped by optical tweezers with a stiffness of 0.27 pN/nm. The standard deviation (SD) of the displacement of the bead trapped for 1 min was 0.84 nm for the x direction and 0.93 nm for the y direction (n = 5). Here these values are considered to be the spatial resolution of our system, with 1/30 s time resolution. In

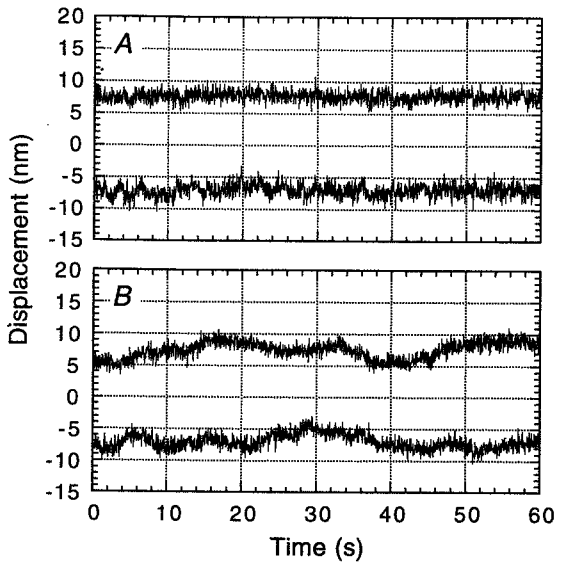

FIGURE 2 Performance of the image analysis system and the sample stage. (*A*) Time course of the displacement of the bead that was trapped in the medium by optical tweezers with a stiffness of 0.27 pN/nm. The displacement reflects both the stability of the trap center and the spatial resolution of our analysis system. (*B*) Displacement of the bead that was fixed to the glass surface. The glass surface was covered with nitrocellulose over the bead, so that the bead was fixed between the nitrocellulose membrane and the glass surface. Thus the displacement of the bead reflects the movement of the sample stage. Upper and lower traces in each figure respectively represent the displacements along the x and y axes.

contrast, to check the drift of the stage, we measured the displacement of the bead fixed to a glass surface by covering it with nitrocellulose (Fig. 2 *B*). The SD of the displacement of the bead for 1 min was 2.1 nm for the x direction and 2.0 nm for the y direction (n = 10). They were larger than the spatial resolution of our system, indicating the drift of the microscopic stage or the vibration of the system.

The actin filaments labeled with a fluorescent probe were visualized using another CCD camera equipped with an image intensifier (KS1381; Video Scope International, Washington, D.C.). To observe a phase-contrast image of beads simultaneously, the focus of the phase-contrast image plane was displaced ~0.5 μm (the radius of the bead) higher than the focus of the fluorescence image plane by moving the lenses in front of the camera. Two images were electronically combined (MV24-c; For. A Co., Tokyo) on the same screen to compare the behavior of the actin filament against the displacement of the bead at the same time.

The 1 W Nd:YLF laser (1053–1000p: λ = 1.053 μm; Amoco Laser Co., Naperville, IL) was coupled with an optical fiber, and the laser was not placed on the optical bench, to avoid a vibration. The position of the optical fiber could be moved along three directions (x, y, and z) and tilted in two directions (xy plane). The laser beam was set parallel with the objective (YTL-25-20PY1; Sigma Koki) and then focused with a custom-made optical apparatus (Nikon and Sigma Koki). The laser beam was led into the microscope from the right-hand side to the position just below the dichroic mirror for fluorescence excitation, which was originally designed to set an analyzer of a DIC microscope. The linear polarization of the laser light was changed to a circular polarization with a quarter wave plate. The laser light could be split into two beams with a set of beam splitters (PBN-20-16040; Sigma Koki) if needed. The trap stiffness we used, 0.1–0.3 pN/nm, was calibrated as described before (Nishizaka et al., 1995b).

In vitro assay system and preparation of bead-tailed F-actin

Actin and myosin were prepared from rabbit skeletal white muscle according to a standard procedure (Kondo and Ishiwata, 1976). HMM prepared by chymotryptic digestion, and s1 by papin digestion of myosin was stored in liquid N_2 (Nishizaka et al., 1993). A bead-tailed actin filament was prepared as previously reported (Suzuki et al., 1996). Bovine plasma gelsolin (Kurokawa et al., 1990) was cross-linked to the carboxylated polystyrene bead (1-μm diameter; Polysciences, Warrington, PA) with 1-ethyl-3-(3-dimethyl-aminopropyl)-carbodiimide (Nacalai Tesque Co., Kyoto), such that the barbed end (B-end) of an actin filament, which corresponds to the rear end when the filament slides, was attached to the bead. The average number of actin filaments attached to the bead was controlled by cross-linking an appropriate amount of bovine serum albumin (BSA) to the bead (BSA/gelsolin = 20:1 w/w). BSA labeled with rhodamine X maleimide (Molecular Probes, Eugene, OR) was also attached to the bead surface to visualize the bead as a fluorescence image (cold BSA/labeled BSA = 19:1). The bead was washed with F-buffer (0.1 M KCl, 2 mM $MgCl_2$, 2 mM 3-(*N*-morpholino)propanesulfonic acid (pH 7.0), 1.5 mM NaN_3, 1 mM dithiothreitol (DTT)) and mixed with 0.2 mg/ml actin filament labeled with rhodamine phalloidin (Molecular Probes) (Yanagida et al., 1984). Before infusion to the flow cell, bead-tailed actin filaments were diluted in F-buffer containing 1 mg/ml BSA to avoid adsorption of the bead to the glass surface. The in vitro assay system was prepared according to the report by Toyoshima et al. (1987), with slight modifications (Nishizaka et al., 1995b). The coverslip, cleaned in a sonicator with neutral detergent, was silanized with hexamethyl disilazane (Nacalai Tesque) (Nishizaka et al., 1995b). HMM and S1 were diluted in an assay buffer (AB) (25 mM KCl, 4 mM $MgCl_2$, 25 mM imidazole-HCl (pH 7.4), 1 mM EGTA, 1 mM DTT) and infused with the flow cell from one side and then from the other side after 60 s. The cell was washed with AB-buffer containing 0.5 mg/ml BSA, 10 mM DTT, 0.22 mg/ml glucose oxidase, 0.036 mg/ml catalase, and 4.5 mg/ml glucose. The bead-tailed actin filament, which was a mixture of 20 nM actin and 0.05% (w/v) bead, was infused. After washing with 3 volumes of AB-buffer containing 0.5 mg/ml BSA and the oxygen scavenger system, the edges of the flow cell were sealed with grease (Toray Dow Corning Silicone, Tokyo). All experiments were done at 30–32°C, except the S1 measurement at 27–32°C.

RESULTS

Direct counting of the number of HMM molecules

First we developed a method for directly counting the number of HMM molecules interacting with actin filaments. Our previous studies showed that the location of each HMM molecule attaching to a glass surface could be determined (Nishizaka et al., 1995a,b). When an actin filament was pulled and taut, HMM molecules could be recognized as a nodal point of the fluctuation of actin filament. By imposing the external load, we broke the nodal point and loosened the filament again (figure 1 *A* of Nishizaka et al., 1995a). Although this technique was useful for determining the location of HMM molecules, it was restricted to a very low density of HMM molecules, because the loosened part of the actin filament immediately attached to adjacent HMM molecules when the distance between adjacent molecules was less than ~1 μm. To solve this difficulty, the bead was manipulated not in the direction parallel to the glass surface but perpendicular to the surface (Figs. 3 and 4). This tech-

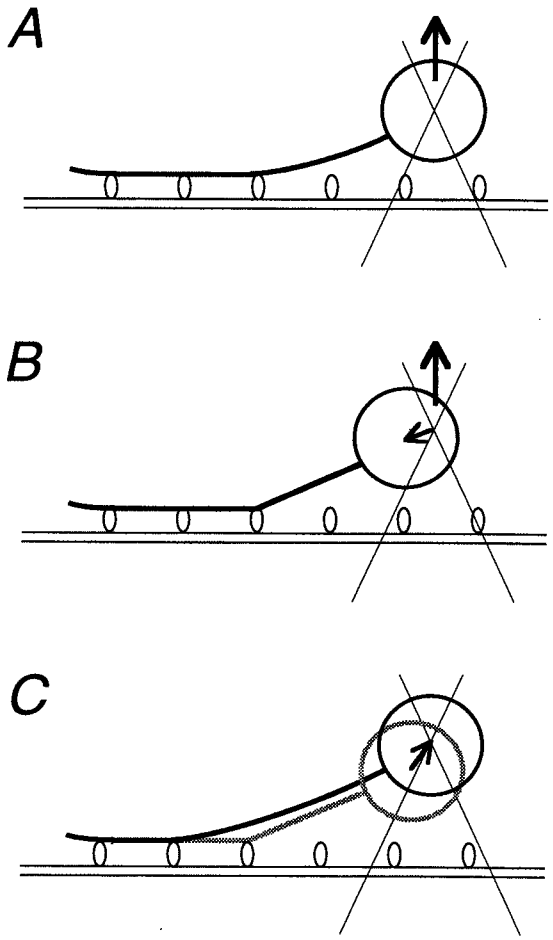

FIGURE 3 Schematic illustration of the technique used to count the number of motor molecules attached to the glass surface. The bead-tailed actin filament bound to HMM molecules was manipulated in the upward (z) direction at a constant rate (A). The filament was pulled taut from the HMM molecule (B), so that the bead was displaced from the trap center in the direction of the HMM. The bead returned to the trap center when the cross-bridge was broken, and subsequently the actin filament was loosened (C).

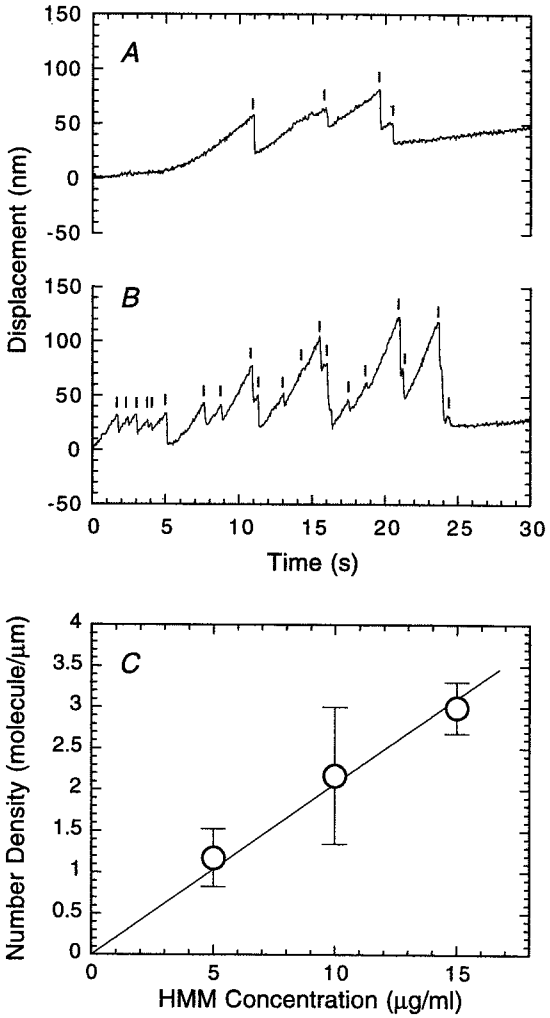

FIGURE 4 (A and B) Examples of the time course of the bead displacement projected onto the xy plane of the glass surface. The objective was moved in the upward (z) direction at a constant rate, 100 nm/s. The glass surface was precoated with 5 and 15 μg/ml HMM in A and B, respectively. The small bar indicates the moment at which the cross-bridge was broken (cf. Fig. 3 C). (C) The relation between the concentration of HMM infused into the flow cell and the number density of HMM. Bars indicate the standard deviation (n = 4–5). The slope of a linear approximation is 0.21 molecules/((μg/ml)·μm actin filament).

nique could be used to avoid overcounting the number of molecules.

Fig. 4, A and B, shows examples of the time course of the bead movement projected onto the xy plane with this technique. The trapped bead was manipulated in the upper z direction at a constant rate of 100 nm/s by moving the objective with a piezoelectric positioner (Fig. 3 A). After the part of the actin filament closest to the bead became taut, the bead began to deviate from the trap center (*sawtooth pattern* in Fig. 4, A and B; cf. Fig. 3 B). Then, after a while, the bead returned to the trap center accompanying the unbinding of the rigor bond. Thus each peak in Fig. 4, A and B, indicated by a small bar corresponds to the moment at which the cross-bridge was broken (Fig. 3 C). Finally, the filament was completely detached from the glass surface (at 21 s in Fig. 4 A and 24 s in Fig. 4 B). In 0–5 s and 21–30 s in Fig. 4 A, the trapped bead was displaced to the x direction at a rate of ~2 nm/s, which was accompanied by the upward motion of the objective. This movement is attributable to a slight misalignment between the laser beam and the optical center axis of the objective.

We applied the above method to the HMM solution in the range of 5–15 μg/ml (Fig. 4); at higher HMM concentrations, actin filaments were severed at a nodal point by pulling. The maximum trapping force of our system was estimated to be ~60 pN, indicating that an actin filament can be broken by applying a force less than 60 pN when the

filament is bent at an acute angle (cf. Arai et al., 1999). As shown in Fig. 4 *C*, the average number of HMM molecules that attached to a unit length of an actin filament was proportional to the concentration of infused HMM, and its slope was 0.21 molecules/((μg/ml)·μm actin filament).

We also examined the minimum concentration of HMM needed to achieve smooth sliding movement of actin filaments in the presence of 1 mM ATP. On the glass surface coated with HMM lower than 20 μg/ml, actin filaments could not slide and became detached from the glass surface. At 30 μg/ml HMM, actin filaments ~10 μm in length slid continuously at a speed of 9.3 ± 0.7 μm/s (n = 5), whereas short actin filaments slid intermittently and sometimes became detached. Under these conditions (1 mM ATP and 30 μg/ml HMM), the minimum length of actin filaments that slid continuously for 10 s was 1.4 μm.

Swiveling motion of actin filaments tethered to HMM

On a glass surface that was coated with a low concentration of HMM in the absence of ATP, short actin filaments (1–2 μm long) showed swiveling Brownian motion around a single point over a range of more than 360° (Nishizaka et al., 1995a,b). An example of this swiveling motion is shown in Fig. 7. This observation is analogous to the case of a microtubule tethered by a single kinesin molecule (Hunt and Howard, 1993). By analyzing the swiveling motion of actin filaments, we estimated the torsional stiffness of the flexible part, which is probably located in a HMM molecule.

The direction of a rotating actin filament was estimated from the centroid of its fluorescence image. We chose those actin filaments tethered to the glass surface by a single point that was slightly deviated from the center of the filament. When the filament swiveled around the tether point, the centroid of its fluorescence image also swiveled, showing the direction of the filament (Noji et al., 1997; Yasuda et al., 1998). Before the centroid calculation, noise in the video images was reduced by recording by averaging over 4 consecutive video frames. Actin filaments 1–3 μm long were selected for calculation to avoid the effect of their bending motion in calculation.

Fig. 5 *A* is an example showing the time course of the rotation of the short actin filament. The direction of the filament fluctuated with time. This fluctuation was assumed to be caused by thermal energy, and the torsional stiffness could be estimated as follows: the direction was divided every 1-rad partition, and the probability that the filament existed in each direction of 1 rad width, $P(\theta)$ (θ = torsion angle), was calculated. The energy $E(\theta)$ was thus obtained by the equation $E(\theta) = -k_B T \cdot \ln(P(\theta))$ as shown in Fig. 5 *B*, where k_B is the Boltzmann constant and T is the absolute temperature. The approximation of $E(\theta)$ to a spring shape function, $E(\theta) = \frac{1}{2} k \theta^2$ (k is the spring constant), is shown as a thin line in Fig. 5 *B*. The value of k was estimated to be

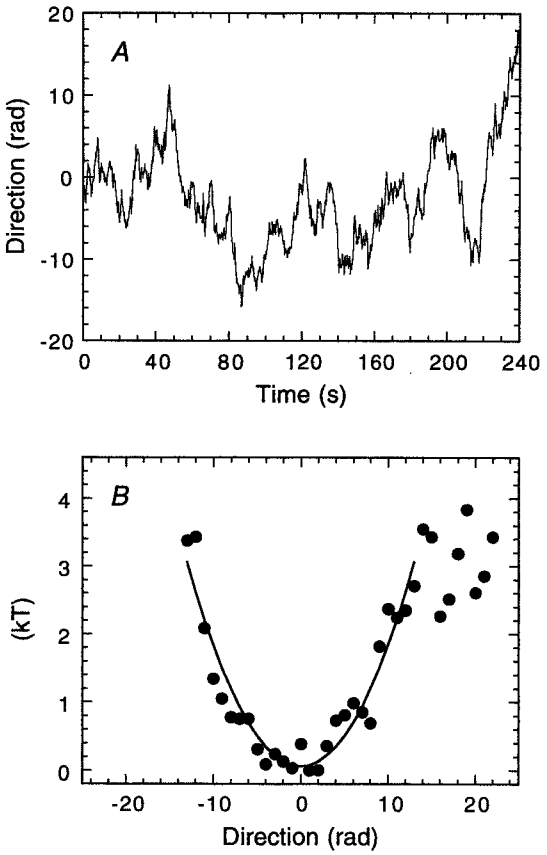

FIGURE 5 (*A*) An example showing the time course of swiveling of a short actin filament tethered to the glass surface through a single HMM molecule (see the short actin filament in Fig. 7, indicated by an *arrow*). (*B*) The energy profile showing the torsional stiffness of the single HMM molecule estimated from *A*. The thin line is an approximation with a spring shape function ($E(\theta) = 1/2 \cdot k\theta^2$, where $E(\theta)$ is energy, k is the spring constant, and θ is the torsion angle), in which the spring constant is 0.074×10^{-21} N · m/rad in the range of ±12 rad.

$2.3 \pm 1.9 \times 10^{-22}$ (± SD, n = 5) N·m/rad. Actin filaments rotated 6.4 times at maximum and 3.8 times on average.

Lifetime of single rigor bonds

In our previous studies (Nishizaka et al., 1995a,b), the unbinding force was measured by moving the trap center with a movable mirror. In the present study, the optical stage was displaced by using a piezoelectric substage, while the trap center was fixed. The advantage of this method is that the imposed load can be precisely determined at any moment. Fig. 6 illustrates how to examine the load dependence of the lifetime of single rigor bonds formed between a single actin filament and a single myosin (HMM or S1) molecule that attached to the glass surface. First the bead attached to the B-end of an actin filament is trapped by optical tweezers (Fig. 6 *A*). When the optical stage is displaced stepwise so as to make the actin filament taut, the

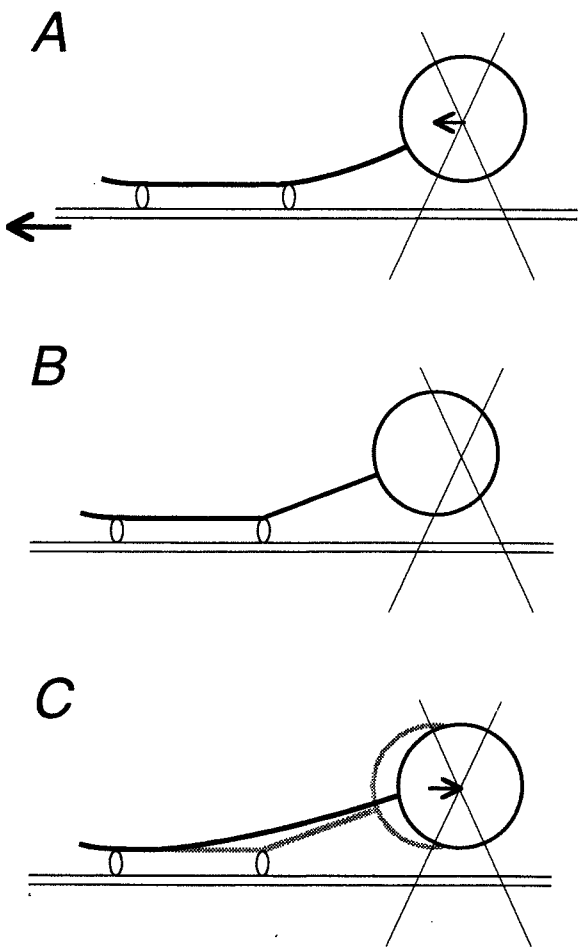

FIGURE 6 Schematic illustration of the procedure to measure the lifetime of the rigor bond between a single actin filament and a single HMM (or S1) molecule. (*A*) The bead-tailed actin filament bound to a motor protein is trapped by optical tweezers, and then the piezoelectric substage is displaced stepwise. (*B*) The filament is pulled taut from the motor protein, and the bead is displaced from the trap center, so that a sudden constant load is imposed on the rigor bond. (*C*) Finally, the bead returns to the trap center accompanying the breakage of the rigor bond, and the filament is loosened again. The time that elapsed between *B* and *C* corresponds to the lifetime of rigor bond.

bead is subsequently displaced from the trap center (Fig. 6, *A* and *B*). Thus a constant load is imposed stepwise on the rigor bond within a video frame, 1/30 s. After a while, the rigor bond is broken, and the bead is returned to the trap center (Fig. 6 *C*). The actin filament is loosened and shows bending Brownian motion again between the bead and the adjacent myosin molecule.

Fig. 7 is a series of fluorescence micrographs showing how to impose an external load on single rigor bonds. An actin filament was first trapped with optical tweezers (Fig. 7 *A*) and tautened by stepwise displacement to the left by the piezoelectric substage (Fig. 7 *B*) because the bead had located to the right of the HMM molecule. In this example, there were two HMM molecules that tethered the actin filament to the glass surface as identified as a nodal point (*arrowheads*), and the actin filament was pulled taut from the first HMM molecule. After a while, the bond was broken (Fig. 7 *C*), such that the lifetime of the rigor bond under a constant load could be directly measured. The actin filament was immediately loosened and showed bending Brownian motion again. When the stage was moved further, the filament was pulled taut from the next HMM molecule (Fig. 7 *D*). The stage was displaced stepwise again, and the second rigor bond was subsequently broken. Thus the actin filament was completely dissociated from the glass surface and the fluorescence image became out of focus (Fig. 7 *E*). Note that in Fig. 7, there is a short actin filament swiveling around a single point (indicated by a *small arrow*), at which a single HMM molecule is considered to be attached. The data in Fig. 5 were obtained from such a fluorescence image.

Fig. 8 *A* is an example of a record showing the time course of the displacement of the bead after stepwise imposition of an external load. When the stage was displaced stepwise (at 1.3 s, as shown by an *arrow*), the actin filament became taut (cf. Fig. 7, *B* and *D*), and the bead was displaced from the trap center. In this example, the external load imposed on the rigor bond was estimated to be 10.6 pN (we could not determine the external load beforehand, because the degree of loosening of an actin filament before applying the load could not be controlled), and the rigor bond was broken 0.43 s after the load was imposed. This observation showed that the lifetime of the actin-HMM rigor bond at no load, ~1000 s, was decreased to 0.43 s by imposing a load of 10.6 pN.

In the case of acto-S1 rigor bonds, spontaneous unbinding occurred, on the average, in ~100 s (Tadakuma et al., manuscript in preparation). Because of this short lifetime, measurement of the load dependence of the lifetime was technically difficult. To solve this problem, we prepared a flow cell coated with a higher density of S1 as compared with HMM, and actin filament was pulled at an acute angle to avoid the possibility of stretching two rigor bonds simultaneously.

Fig. 8 *B* is a summary showing the relationship between the imposed load and the lifetime. While the lifetime of HMM rigor bonds was distributed over a wide range of imposed loads, that of S1 rigor bonds was limited to a narrower range. In the case where a bond was broken within 66 ms (two video frames), we could not precisely determine the imposed load, so that these data (~5% of measurements) were omitted from Fig. 8 *B*. In the case of S1, there were four exceptional cases in which rigor bonds did not break for 60 s over 20 pN. We judge that they are attributable to the aggregation of S1, and thus they are not included in Fig. 8 *B*.

To elucidate the load dependence of the lifetime, we divided loads on the abscissa of Fig. 8 *B* into 3-pN partitions and replotted the time course of the unbinding occurrence of HMM and S1 rigor bonds in each partition, as shown in Fig. 9. The error bars indicate $N^{1/2}$, corresponding to the stan-

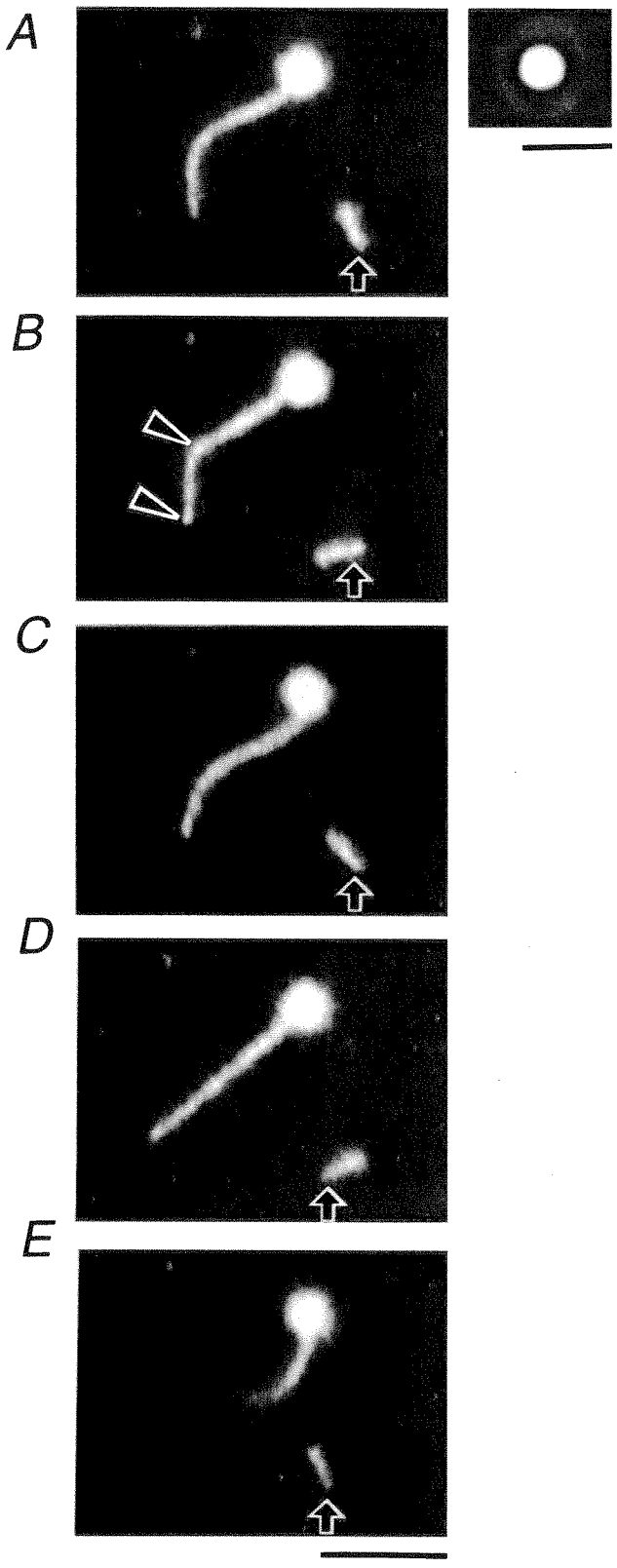

FIGURE 7 A series of fluorescence micrographs showing how to measure the lifetime of single rigor bond(s). (*A*) The bead attached to the B-end of an actin filament was trapped by optical tweezers. (*B*) The flow cell was moved (within 1/30 s) ~200 nm stepwise, using a piezoelectric substage, so that the actin filament was pulled taut from an HMM molecule (*arrowheads*). (*C*) After a while, the rigor bond was broken and the lifetime of the single rigor bond was measured. (*D*) The substage was moved further leftward and displaced stepwise again, such that the filament became nearly straight. (*E*) The filament was detached completely from the glass surface and showed Brownian motion. Note that a short actin filament, tethered to the glass surface through probably only one HMM molecule (indicated by an *arrow*), swiveled in each micrograph. Scale bar, 5 μm. (*upper right*) Phase-contrast image of the bead of *A–E*. Scale bar, 2 μm. The two images were simultaneously observed using the optics of Fig. 1.

dard deviation for events that stochastically occur N times. For S1, and for 9.0–12.0 pN and 12.0- pN of HMM, plots were approximated with the equation of a single exponential decay, $N(t) = N(0)\cdot\exp(-t/\tau)$, where τ is a lifetime of the rigor bond. Deviations of τ were estimated from fitted curves with maximum and minimum τ so as not to deviate from error bars by more than one data point in Fig. 9, and then they were expressed as error bars in Fig. 10. For 0.0–3.0, 3.0–6.0, and 6.0–9.0 pN of HMM, the data were approximated with the sum of two exponential decays, i.e., $N(t) = N_f(0)\cdot\exp(-t/\tau_f) + N_s(0)\cdot\exp(-t/\tau_s)$, where τ_f and τ_s are, respectively, a fast and a slow component of the lifetime, and $N_f(0) + N_s(0) = N_0$ is the total number of data at each region. After an optimum set of τ_f, τ_s, and $N_f(0)$ values was determined, deviations in τ_f and τ_s were independently estimated from fitted curves with maximum and minimum values so as not to deviate from the error bars of all data points. These maximum and minimum values of τ_f and τ_s were expressed as error bars in Fig. 10. The lifetimes thus obtained are summarized in Table 1.

Fig. 10 is a semilogarithmic plot of the data summarized in Table 1. As for the slow component of HMM, the relation between the lifetime, $\tau(F)$, and the imposed load, F, was closely approximated by the equation $\tau(F) = \tau(0)\cdot\exp(-F\cdot d/kT)$ (*thick solid line*). The relations for S1 and for the fast component of HMM were also approximated by this equation, as shown by a dashed line and a thin solid line, respectively. Note that the relation for S1 coincided with that for the fast component of HMM. From these approximation lines, d and $\tau(0)$ were estimated as summarized in Table 2.

DISCUSSION

Minimum number of HMM molecules needed to slide actin filaments continuously

The estimation of the number of myosin molecules interacting with an actin filament is essential for describing the sliding movement of an actin filament in an in vitro motility assay. Unlike myosin V (Mehta et al., 1999) or kinesin (Howard et al., 1989; Vale et al., 1996), the skeletal myosin (myosin II) molecule is not a processive motor, such that multiple motors are required for smooth and continuous

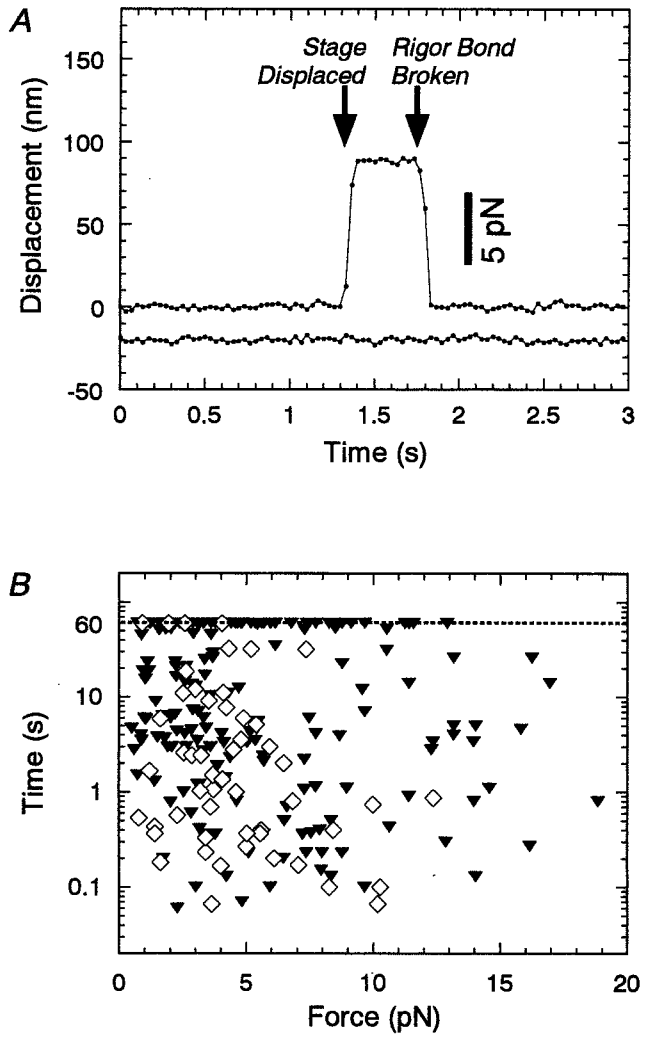

FIGURE 8 Load dependence of the lifetime of single rigor bonds. (*A*) An example of the time course of the displacement of the bead (cf. Figs. 6 and 7). Upper and lower plots show, respectively, the displacement of the bead along and perpendicular to the actin filament. Each dot was plotted every 1/30 s. The stage was displaced stepwise at 1.3 s so as to impose a constant external load, and then the bond was broken after 0.43 s in this example. (*B*) Relationship between the imposed load and the lifetime of rigor bonds of HMM (▼) and S1 (◇). For the rigor bonds not broken within 60 s, the lifetimes are plotted on the dashed line indicating 60 s.

sliding of actin filaments without dissociation. Although we could not directly count the number of HMM molecules during the sliding movement, the number required for smooth sliding of an actin filament could be estimated from our results (Fig. 4). The lowest concentration of HMM required for continuous sliding motion of actin filaments was 30 μg/ml in our method, so that the minimum line density of HMM molecules is estimated to be 30 (μg/ml) $\times$ 0.21 (molecules/μm/(μg/ml)) = 6.3 (molecules/μm actin filament). Furthermore, the minimum length of the filament showing the sliding movement was ~1.4 μm under the same conditions. Thus we obtain the minimum number of molecules required for smooth sliding without dissociation, 6.3 (molecules/μm) $\times$ 1.4 (μm) = 8.8 (molecules).

We can assume that one ATP hydrolysis of the actomyosin system takes (10–100) ms, as in an in vitro motile system (Harada et al., 1990) and in solution (cf. Goldman, 1987). On the other hand, the probability that at least one myosin head binds to an actin filament is given by $P = 1 - \{(N - n)/N\}^N$, where N is the total number of myosin heads that can interact with the filament and n is the average number of heads that bind to the filament at one time. Therefore, $(1 - P) \times$ (10–100) ms is the dissociation period during which no myosin heads interact with the filament. The diffusion coefficient perpendicular to the filament axis for a 1.4-μm actin filament is calculated to be 1.4×10^{-8} cm^2/s from the equations $D = k_BT/\Gamma_\perp$ and $\Gamma_\perp = 4\pi\eta L/(\ln(L/2r) + \gamma_\perp)$, where $L = 1.4$ μm, $r = 5$ nm, $\eta = 0.010$ g/cm·s, $\gamma_\perp = 0.89$ (Hunt et al., 1994) and $T = 300$ K. Thus the time required for actin filaments 1.4 μm long to diffuse as far as δx, ~17 nm (the size of myosin heads) to 34 nm (its doubled size), within which the filaments can maintain a sliding motion, is calculated to be 0.1–0.4 ms according to the equation $\delta x = (2Dt)^{1/2}$. To make $(1 - P) \times$ (10–100) ms shorter than 0.1–0.4 ms, P should be larger than 0.96–0.999. Together, n should be larger than 3.0–5.8 under $N = 17.6$ ($= 8.8 \times 2$) heads to keep P as 0.96–0.999 ($1 - \{(N - n)/N\}^N = 1 - \{(17.6-3.0)/17.6\}^{17.6} > 0.96$, $1 - \{(17.6-5.8)/17.6\}^{17.6} > 0.999$), suggesting that at least (3.0–5.8)/17.6 ≅ 17–30% of myosin heads always bind to the filament during sliding motion. If all n heads are in a state of producing the active force, the value 17–30% corresponds to the "duty ratio," which is the proportion of the period in which a single head produces the force in one ATPase cycle. However, because some head is only capable of holding the filament without producing active force (Goldman, 1987; Ishiwata and Yasuda, 1993), 17–30% could be an overestimation of the duty ratio.

Torsional stiffness of a single HMM molecule

By analysis of the rotational Brownian motion of a short actin filament tethered to a single HMM molecule, the torsional stiffness has been estimated to be $(2.3 \pm 1.9) \times 10^{-22}$ N·m/rad. The flexible part responsible for this small stiffness must be located at the joint between the S1 and S2 regions, and/or within the S2 region of the HMM molecule (Kinosita et al., 1984; Ishiwata et al., 1987, 1988). Note that this stiffness is so small that the thermal fluctuation energy, k_BT (4.1×10^{-21} N·m), can twist myosin 2.8 times ($(4.1 \times 10^{-21})/(2.3 \times 10^{-22})/2\pi = 2.8$). This small stiffness can explain the following mechanical properties of myosin previously reported: myosin can interact with an actin filament under various orientations (Toyoshima et al., 1989; Molloy et al., 1995), although it modifies the motor functions, such as the sliding velocity and force (Yamada et al., 1990; Sellers and Kachar, 1990; Ishijima et al., 1996). The unbinding

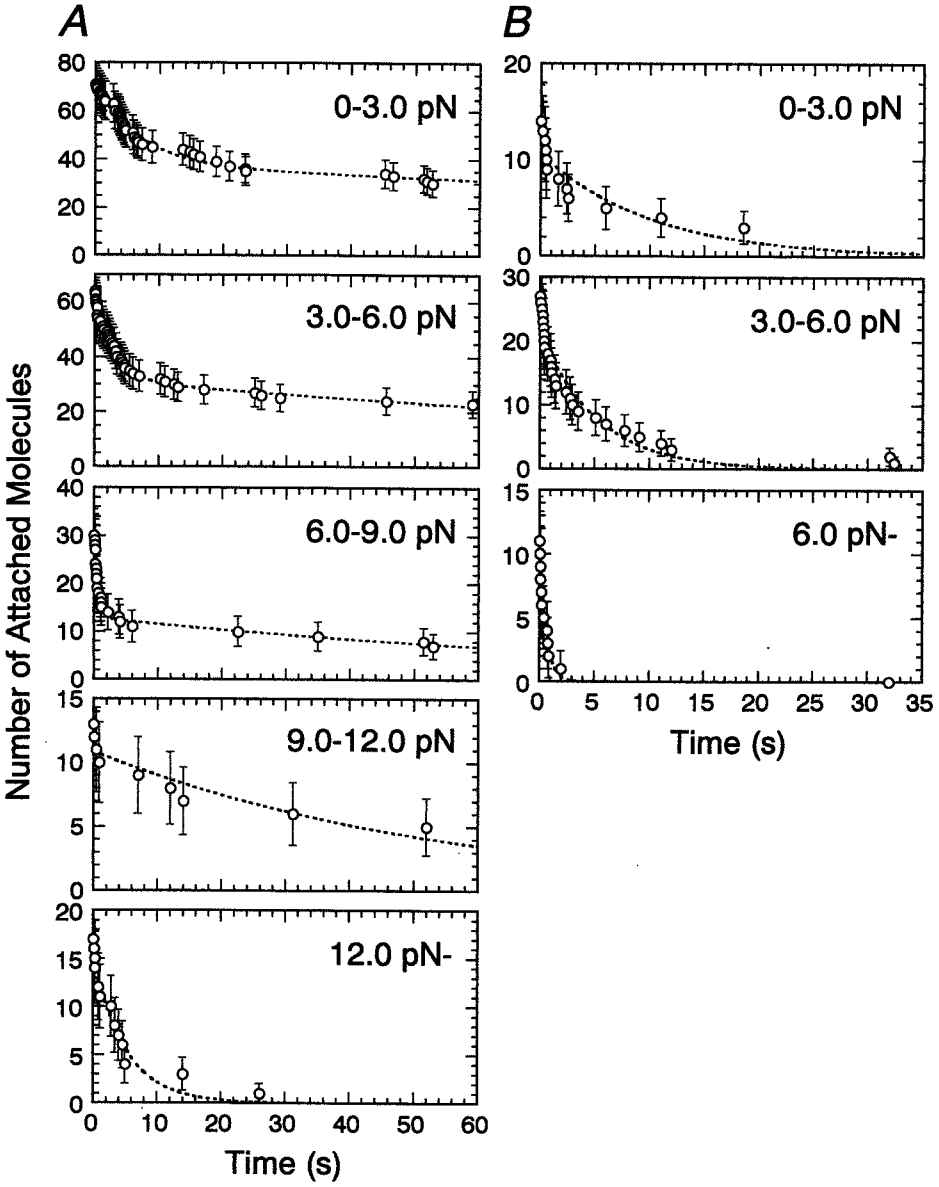

FIGURE 9 Time course of the decrease in the number of attached molecules, N, under various imposed loads, replotted from the data of Fig. 8 *B*. Error bars show standard deviation, which is simply determined as the square of the number of measurements at each point ($\pm N^{1/2}$). (*A*) HMM. Dashed lines indicate the approximation by $N(t) = N(0)\cdot\exp(-t/\tau)$ or $N(t) = N_f(0)\cdot\exp(-t/\tau_f) + N_s(0)\cdot\exp(-t/\tau_s)$ (for details see Results). (*B*) S1. Dashed lines indicate the approximation by $N(t) = N(0)\cdot\exp(-t/\tau)$.

force of rigor bonds is independent of the direction of external load, at least within ±90° (Nishizaka et al., 1995b). Because of the small stiffness, the geometrical relationship of the actin-myosin binding interface is probably maintained.

As for kinesin, the stiffness was estimated to be 1.2×10^{-22} N·m/rad by observing the rotational Brownian motion of an attached microtubule (Hunt and Howard, 1993), which is comparable to that of HMM. Thus such a small torsional stiffness may be common to motor proteins. Surprisingly, kinesin could be twisted more than 30 times by manipulation with optical tweezers without breaking the bond between kinesin and a microtubule (Kuo et al., 1995). This result may not be explainable by twisting of a head-rod junction; thus we alternatively assume that detachment and reattachment occur on one head while the other head binds to a filament. The twisting distortion in the attached head will be released during unbinding, and then the head can bind again without large distortion. If the two heads repeat this process alternately, the filament can rotate in one direction without limitation. We favor this model as an explanation of how protein can rotate more than 30 times without dissociation. If this process also occurred in our actin-HMM complex, the estimated value is an underestimation as a torsional stiffness of single HMM molecules.

Load dependence of lifetime of rigor bonds and binding manner of HMM

In our previous study, we repeatedly measured the load dependence of the lifetime of rigor bonds on the same

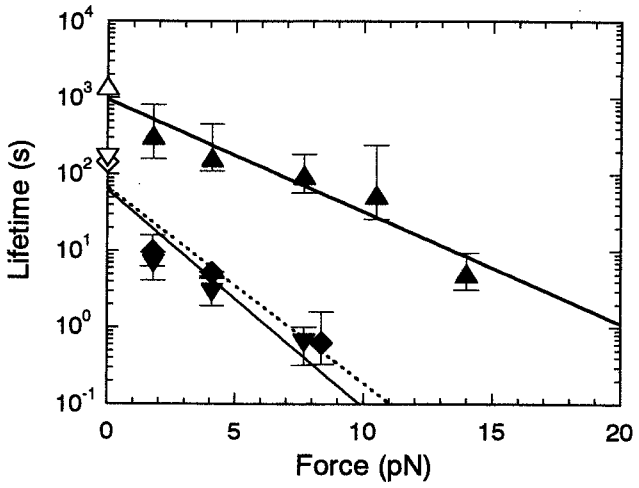

FIGURE 10 Relation between imposed load and lifetime of HMM and S1 rigor bonds. Triangles and inverted triangles show the slow and fast components of HMM, respectively. Squares show the lifetime of S1. Filled symbols were determined from Fig. 9, and open symbols are experimental data obtained without load (Tadakuma et al., manuscript in preparation). Fitted lines show the approximation by the equation $\tau(F) = \tau(0)\cdot\exp(-F\cdot d/k_BT)$. The thick and thin solid lines show the approximation of slow and fast components of HMM, respectively. The dashed line shows the approximation for S1.

acto-HMM rigor complexes (figure 4 in Nishizaka et al., 1995b). In the present study, we improved the mechanical stability of the microscopy apparatus to realize more accurate measurements, especially for longer times. As a result, the spatial resolution became less than 1 nm, and the drifting movement of the stage was restricted to within ~2 nm for 1 min. Such an improvement was essential for quantitatively investigating the relationship between the lifetime and the load.

TABLE 1 Lifetimes of HMM and S1 rigor bonds estimated from the approximation with exponential decay shown in Fig. 9

Load (pN)	Ratio, fast/total	Lifetime (s) τ_f	Lifetime (s) τ_s
A. HMM			
No load	(0.41)	(170)	(1400)
0–3	0.47	6.9	320
3–6	0.51	2.9	160
6–9	0.57	0.64	97
9–12	—	—	53
12+	—	—	5.1
	Lifetime (s)		
B. S1			
No load	(150)		
0–3	9.9		
3–6	5.2		
6–9	0.63		

The data were approximated by the equation of single exponential decay, $N(t) = N(0)\cdot\exp(-t/\tau)$, or the sum of two exponential decays, $N_f(0)\cdot\exp(-t/\tau_f) + N_s(0)\cdot\exp(-t/\tau_s)$. Ratio, $N_f(0)/(N_f(0) + N_s(0))$, means the proportion of cross-bridges having the fast component. Both ratio and lifetimes without load shown in parentheses were determined by the microscopic observation of spontaneous detachment from a glass surface of swiveling short actin filaments (Tadakuma et al., manuscript in preparation).

TABLE 2 Interaction distance, d, and lifetime without external load, $\tau(0)$, for, respectively, single rigor bonds of HMM and S1, estimated from the slope and the extrapolation of the solid and dashed lines in Fig. 10

	d	$\tau(0)$
HMM (fast)	2.7	62
HMM (slow)	1.4	950
S1	2.4	67

We found that the time course of the decrease in the number of attached S1 molecules under an external load nearly followed a single exponential decay (Fig. 9 *B*). In contrast, the decay for HMM was not expressed by a single exponential, except for a large applied force (Fig. 9 *A*), but could be approximated by the sum of two exponentials with different lifetimes. As shown in Table 1, *A* and *B*, the fast component of the lifetime of HMM nearly coincided with the lifetime of S1. One plausible explanation for this result is that HMM molecules that attached to the glass surface are classified into two groups: one having the slow component of lifetimes in which double-headed binding occurs, and another having the fast component in which only single-headed binding is possible, probably because of the adsorption of either head to the glass surface. This explanation will be examined in the future by using single-headed myosin (Harada et al., 1987) or single-headed HMM. The ratio between single-headed and double-headed molecules in our HMM assay is estimated to be nearly 1:1 (Table 1 *A*). We previously suggested the presence of "molecular individualism" in each HMM, based on the fact that each HMM molecule showed the individual load dependence of the lifetime (Nishizaka et al., 1995b). The difference in the number of active heads may be the main reason for this "individuality."

The lifetime, τ, is generally related to the activation energy for unbinding, $\Delta G^{\ddagger}$, through $\tau \propto \exp(\Delta G^{\ddagger}/k_BT)$. This could be extended to a fundamental property of the binding between a ligand and a receptor under an external load, i.e., $\tau(F) = \tau_0\cdot\exp((\Delta G^{\ddagger} - F\cdot d)/k_BT) = \tau(0)\cdot\exp(-F\cdot d/k_BT)$, where $\tau(F)$ is the lifetime under the load F and d is defined as the distance of an intermolecular interaction beyond which the intermolecular bond is ruptured (Bell, 1978; Erickson, 1994). The value of d is generally assumed to be less than a nanometer. Note that even though there is no load, the intermolecular bonds in an aqueous solution break with a lifetime of $\tau(0)$ in a stochastic manner under thermal equilibrium. This aspect is essential for understanding the unbinding force of the bond between proteins. The unbinding force between proteins was previously estimated to be

larger than 100 pN (Kishino and Yanagida, 1988; Florin et al., 1994; Tsuda et al., 1996; Fritz et al., 1998); however, it has been predicted that these values depend on the rate of the increase in the applied load. The unbinding force could be smaller when the external load is applied slowly, e.g., at a rate comparable to the dissociation rate constant. This was confirmed for actin-HMM rigor complex (cf. Fig. 4 in Nishizaka et al., (1995b)) and for avidin-biotin complex: the unbinding force increases from several piconewtons to hundreds of piconewtons as the velocity is increased by 10^6 (Merkel et al., 1999). In the case of P-selectin, the unbinding force was confirmed to increase logarithmically with the increase in the pulling velocities of ligand against receptor (figure 5 in Fritz et al., 1998). Thus the difference in the pulling velocity is considered to be the main reason why the average unbinding force of actin-HMM rigor complex obtained by AFM (Nakajima et al., 1997), ~14 pN, was larger than that obtained with optical tweezers (Nishizaka et al., 1995b), ~9 pN.

The exponential dependence of lifetime on the external load, which was predicted before (Bell, 1978; Erickson, 1994), fits well with our results as shown in Fig. 10. From the slope of the straight lines in Fig. 10, we obtained the values of d: 1.4 nm for the slow component of HMM, 2.7 nm for the fast component of HMM, and 2.4 nm for S1 (Table 2). The value of d for slow HMM components, which corresponds to the double-headed binding, was nearly one-half of those of d for fast HMM components, corresponding to the single-headed binding, and for S1. This difference by a factor of 2 suggests that the external load (F) is evenly shared on each attached head of HMM, such that the external load imposed on each head effectively becomes a half. This suggests that d for the interaction between single-head myosin and actin is ~2.5 nm.

It is expected that the large d value is attributable to the geometry of application of an external load. In fact, regarding the interaction between actin monomers in a filamentous actin, the tensile strength depends on the direction of the applied load to the molecular interface. Tsuda et al. (1996) reported that 600 pN was required for the breakage of the actin filament by straight pull, whereas Arai et al. (1999) reported that the actin filament broke when they applied 1 pN after tying a knot in it. In both measurements, the process of unbinding was observed at a video rate, so that the duration required for breakage was similar. Thus the apparent value of d for the latter may be an order of magnitude larger than that for the former.

In our system, the load was always imposed toward the long axis of an actin filament. The value of d could be decreased when the external load is applied in the direction parallel to the coordinate axis of the interaction potential, which may usually be the direction perpendicular to the intermolecular interface. The proposed structure of myosin head is longitudinally thin, and the actin-binding site is not located at the tip of the head but relatively at the side of the catalytic domain of the head, such that myosin heads bind to an actin filament at an acute angle (Rayment et al., 1993a,b). As a result, the myosin is being pulled from an angle, which would tend to tilt it out of the interface rather than pulling it out perpendicularly. The applied load could induce the distortion of the myosin head around the binding interface, then the activation energy for unbinding is efficiently decreased by a small load, as shown in Fig. 10, which results in the large value of d. In contrast, in the case of avidin-biotin unbinding force measurement by AFM (Florin et al., 1994; Moy et al., 1994), a symmetrical avidin molecule was sandwiched between an AFM cantilever and an agarose bead that was biotinylated (the 50-μm-diameter agarose bead versus the 6-nm-diameter avidin). It is expected that the load was imposed nearly perpendicularly to the interface of the avidin-biotin bond (Grubmuller et al., 1996; Evans and Ritchie, 1997; Izrailev et al., 1997), so that the small value of d was obtained.

X-ray crystallography showed that the myosin head consists of two domains, i.e., a catalytic domain that contains ATP- and actin-binding sites, and a neck domain. One possible hypothesis for how myosin heads generate force is that the neck domain tilts against the catalytic domain like a lever arm and induces a power stroke accompanied by the release of P_i (Rayment et al., 1993a,b; Corrie et al., 1999; Taylor et al., 1999). This structural dynamic is thought to be coupled with the change in the binding affinity between the myosin head and actin (Goldman and Brenner, 1987), although this hypothesis seems to have difficulty explaining the results showing their uncoupling (Ishijima et al., 1998) and multiple unitary displacements of single myosin head per ATP hydrolysis (Kitamura et al., 1999). In general, it is believed that the post-power stroke state has higher binding affinity for actin, and the pre-power stroke state has relatively lower affinity. In our experiments, the actin filament was always pulled in the direction of the reversal of the power stroke of myosin because the bead was attached to the B-end of an actin filament. In other words, we imposed the load so as to change the state of myosin from a post-power stroke state to a pre-power stroke state. If the structure of the myosin head changes from a high-affinity form to a low-affinity form with the application of an external load, the unbinding that occurs very efficiently with an imposed load can also be explained by this mechanism. In this relation, the following experiment is interesting: measurement of the lifetime by pushing the myosin head, which is in the pre-power stroke state with ATP analogs, toward the post-power stroke state along the direction of the power stroke. In this case, the lifetime may become longer because of the transition from the low-affinity state to the high-affinity state.

Finally, we would like to point out that the geometry for applying an external load in our system is similar to that in muscle fibers. The gradual change in the binding affinity, which is assumed in the Huxley and Simmons model (Hux-

ley and Simmons, 1971), may accompany the change in the number of intermolecular bonds at the actomyosin interface. Thus a large value of d may be a feature common to motor proteins.

We thank Drs. Naoya Suzuki, Hidetake Miyata, Ichiro Sase, and Ryohei Yasuda of Keio University and Mr. Madoka Suzuki of Waseda University for their technical support and advice. This research was partly supported by grants-in-aid for Scientific Research, for Scientific Research for Priority Areas, and for the High-Tech Research Center Project to SI from the Ministry of Education, Science, Sports and Culture of Japan, and by grants-in-aid from the Japan Science and Technology Corporation. TN was a Research Fellow of the Japan Society for the Promotion of Science.

REFERENCES

Arai, Y., R. Yasuda, K. Akashi, Y. Harada, H. Miyata, K. Kinosita, Jr., and H. Itoh. 1999. Tying a molecular knot with optical tweezers. *Nature.* 399:446–448.

Ashkin, A., J. M. Dziedzic, J. E. Bjorkholm, and S. Chu. 1986. Observation of a single-beam gradient force optical trap for dielectric particles. *Optics Lett.* 11:288–290.

Ashkin, A., K. Schutze, J. M. Dziedzic, U. Euteneuer, and M. Schliwa. 1990. Force generation of organelle transport measured in vivo by an infrared laser trap. *Nature.* 348:346–348.

Bell, G. I. 1978. Models for the specific adhesion of cells to cells. *Science.* 200:618–627.

Corrie, J. E., B. D. Brandmeier, R. E. Ferguson, D. R. Trentham, J. Kendrick-Jones, S. C. Hopkins, U. A. van der Heide, Y. E. Goldman, C. Sabido-David, R. E. Dale, S. Criddle, and M. Irving. 1999. Dynamic measurement of myosin light-chain-domain tilt and twist in muscle contraction. *Nature.* 400:425–430.

Erickson, H. P. 1994. Reversible unfolding of fibronectin type III and immunoglobulin domains provides the structural basis for stretch and elasticity of titin and fibronectin. *Proc. Natl. Acad. Sci. USA.* 91: 10114–10118.

Evans, E., and K. Ritchie. 1997. Dynamic strength of molecular adhesion bonds. *Biophys. J.* 72:1541–1555.

Finer, J. T., R. M. Simmons, and J. A. Spudich. 1994. Single myosin molecule mechanics: piconewton forces and nanometre steps. *Nature.* 368:113–119.

Florin, E. L., V. T. Moy, and H. E. Gaub. 1994. Adhesion forces between individual ligand-receptor pairs. *Science.* 264:415–417.

Fritz, J., A. G. Katopodis, F. Kolbinger, and D. Anselmetti. 1998. Force-mediated kinetics of single P-selectin/ligand complexes observed by atomic force microscopy. *Proc. Natl. Acad. Sci. USA.* 95:12283–12288.

Funatsu, T., Y. Harada, M. Tokunaga, K. Saito, and T. Yanagida. 1995. Imaging of single fluorescent molecules and individual ATP turnovers by single myosin molecules in aqueous solution. *Nature.* 374:555–559.

Goldman, Y. E. 1987. Kinetics of the actomyosin ATPase in muscle fibers. *Annu. Rev. Physiol.* 49:637–654.

Goldman, Y. E., and B. Brenner. 1987. Special topic: molecular mechanism of muscle contraction. General introduction. *Annu. Rev. Physiol.* 49:629–636.

Grubmuller, H., B. Heymann, and P. Tavan. 1996. Ligand binding: molecular mechanics calculation of the streptavidin-biotin rupture force. *Science.* 271:997–999.

Harada, Y., A. Noguchi, A. Kishino, and T. Yanagida. 1987. Sliding movement of single actin filaments on one-headed myosin filaments. *Nature.* 326:805–808.

Harada, Y., K. Sakurada, T. Aoki, D. D. Thomas, and T. Yanagida. 1990. Mechanochemical coupling in actomyosin energy transduction studied by in vitro movement assay. *J. Mol. Biol.* 216:49–68.

Howard, J., A. J. Hudspeth, and R. D. Vale. 1989. Movement of microtubules by single kinesin molecules. *Nature.* 342:154–158.

Hunt, A. J., F. Gittes, and J. Howard. 1994. The force exerted by a single kinesin molecule against a viscous load. *Biophys. J.* 67:766–781.

Hunt, A. J., and J. Howard. 1993. Kinesin swivels to permit microtubule movement in any direction. *Proc. Natl. Acad. Sci. USA.* 90: 11653–11657.

Huxley, A. F., and R. M. Simmons. 1971. Proposed mechanism of force generation in striated muscle. *Nature.* 233:533–538.

Ishijima, A., Y. Harada, H. Kojima, T. Funatsu, H. Higuchi, and T. Yanagida. 1994. Single-molecule analysis of the actomyosin motor using nano-manipulation. *Biochem. Biophys. Res. Commun.* 199: 1057–1063.

Ishijima, A., H. Kojima, T. Funatsu, M. Tokunaga, H. Higuchi, H. Tanaka, and T. Yanagida. 1998. Simultaneous observation of individual ATPase and mechanical events by a single myosin molecule during interaction with actin. *Cell.* 92:161–171.

Ishijima, A., H. Kojima, H. Higuchi, Y. Harada, T. Funatsu, and T. Yanagida. 1996. Multiple- and single-molecule analysis of the actomyosin motor by nanometer-piconewton manipulation with a microneedle: unitary steps and forces. *Biophys. J.* 70:383–400.

Ishiwata, S., K. Kinosita, Jr., H. Yoshimura, and A. Ikegami. 1987. Rotational motions of myosin heads in myofibril studied by phosphorescence anisotropy decay measurements. *J. Biol. Chem.* 262: 8314–8317.

Ishiwata, S., K. Kinosita, Jr., H. Yoshimura, and A. Ikegami. 1988. Optical anisotropy decay studies of the dynamic structure of myosin filaments. *Adv. Exp. Med. Biol.* 226:267–276.

Ishiwata, S., and K. Yasuda. 1993. Mechano-chemical coupling in spontaneous oscillatory contraction of muscle. *Phase Transitions.* 45: 105–136.

Izrailev, S., S. Stepaniants, M. Balsera, Y. Oono, and K. Schulten. 1997. Molecular dynamics study of unbinding of the avidin-biotin complex. *Biophys. J.* 72:1568–1581.

Kamimura, S., and K. Takahashi. 1981. Direct measurement of the force of microtubule sliding in flagella. *Nature.* 293:566–568.

Kinosita, K., Jr., S. Ishiwata, H. Yoshimura, H. Asai, and A. Ikegami. 1984. Submicrosecond and microsecond rotational motions of myosin head in solution and in myosin synthetic filaments as revealed by time-resolved optical anisotropy decay measurements. *Biochemistry.* 23:5963–5975.

Kinosita, K., Jr., H. Itoh, S. Ishiwata, K. Hirano, T. Nishizaka, and T. Hayakawa. 1991. Dual-view microscopy with a single camera: real-time imaging of molecular orientations and calcium. *J. Cell Biol.* 115:67–73.

Kinosita, K., Jr., R. Yasuda, H. Noji, S. Ishiwata, and M. Yoshida. 1998. F_1-ATPase: a rotary motor made of a single molecule. *Cell.* 93:21–24.

Kishino, A., and T. Yanagida. 1988. Force measurements by micromanipulation of a single actin filament by glass needles. *Nature.* 334:74–76.

Kitamura, K., M. Tokunaga, A. H. Iwane, and T. Yanagida. 1999. A single myosin head moves along an actin filament with regular steps of 5.3 nanometres. *Nature.* 397:129–134.

Kondo, H., and S. Ishiwata. 1976. Uni-directional growth of F-actin. *J. Biochem.* 79:159–171.

Kuo, S. C., K. Ramanathan, and B. Sorg. 1995. Single kinesin molecules stressed with optical tweezers. *Biophys. J.* 68:74s.

Kurokawa, H., W. Fujii, K. Ohmi, T. Sakurai, and Y. Nonomura. 1990. Simple and rapid purification of brevin. *Biochem. Biophys. Res. Commun.* 168:451–457.

Marston, S. B. 1982. The rates of formation and dissociation of actin-myosin complexes. Effects of solvent, temperature, nucleotide binding and head-head interactions. *Biochem. J.* 203:453–460.

Mehta, A. D., R. S. Rock, M. Rief, J. A. Spudich, M. S. Mooseker, and R. E. Cheney. 1999. Myosin-V is a processive actin-based motor. *Nature.* 400:590–593.

Merkel, R., P. Nassoy, A. Leung, K. Ritchie, and E. Evans. 1999. Energy landscapes of receptor-ligand bonds explored with dynamic force spectroscopy. *Nature.* 397:50–53.

Miyata, H., H. Hakozaki, H. Yoshikawa, N. Suzuki, K. Kinosita Jr, T. Nishizaka, and S. Ishiwata. 1994. Stepwise motion of an actin filament

over a small number of heavy meromyosin molecules is revealed in an in vitro motility assay. *J. Biochem.* 115:644–647.

Miyata, H., H. Yoshikawa, H. Hakozaki, N. Suzuki, T. Furuno, A. Ikegami, K. Kinosita, Jr., T. Nishizaka, and S. Ishiwata. 1995. Mechanical measurements of single actomyosin motor force. *Biophys. J.* 68:286s–290s.

Molloy, J. E., J. E. Burns, J. Kendrick-Jones, R. T. Tregear, and D. C. White. 1995. Movement and force produced by a single myosin head. *Nature.* 378:209–212.

Moy, V. T., E. L. Florin, and H. E. Gaub. 1994. Intermolecular forces and energies between ligands and receptors. *Science.* 266:257–259.

Nakajima, H., Y. Kunioka, K. Nakano, K. Shimizu, M. Seto, and T. Ando. 1997. Scanning force microscopy of the interaction events between a single molecule of heavy meromyosin and actin. *Biochem. Biophys. Res. Commun.* 234:178–182.

Nishizaka, T., H. Miyata, H. Yoshikawa, S. Ishiwata, and K. Kinosita, Jr. 1995a. Mechanical properties of single protein motor of muscle studied by optical tweezers. *Biophys. J.* 68:75s.

Nishizaka, T., H. Miyata, H. Yoshikawa, S. Ishiwata, and K. Kinosita, Jr. 1995b. Unbinding force of a single motor molecule of muscle measured using optical tweezers. *Nature.* 377:251–254.

Nishizaka, T., Q. Shi, and M. P. Sheetz. 2000. Position dependent linkages of fibronectin-integrin-cytoskeleton. *Proc. Natl. Acad. Sci. USA.* 97: 692–697.

Nishizaka, T., T. Yagi, Y. Tanaka, and S. Ishiwata. 1993. Right-handed rotation of an actin filament in an in vitro motile system. *Nature.* 361:269–271.

Noji, H., R. Yasuda, M. Yoshida, and K. Kinosita, Jr. 1997. Direct observation of the rotation of F_1-ATPase. *Nature.* 386:299–302.

Rayment, I., H. M. Holden, M. Whittaker, C. B. Yohn, M. Lorenz, K. C. Holmes, and R. A. Milligan. 1993a. Structure of the actin-myosin complex and its implications for muscle contraction. *Science.* 261: 58–65.

Rayment, I., W. R. Rypniewski, K. Schmidt-Base, R. Smith, D. R. Tomchick, M. M. Benning, D. A. Winkelmann, G. Wesenberg, and H. M. Holden. 1993b. Three-dimensional structure of myosin subfragment-1: a molecular motor. *Science.* 261:50–58.

Sase, I., H. Miyata, J. E. Corrie, J. S. Craik, and K. Kinosita, Jr. 1995a. Real time imaging of single fluorophores on moving actin with an epifluorescence microscope. *Biophys. J.* 69:323–328.

Sase, I., H. Miyata, S. Ishiwata, and K. Kinosita, Jr. 1997. Axial rotation of sliding actin filaments revealed by single- fluorophore imaging. *Proc. Natl. Acad. Sci. USA.* 94:5646–5650.

Sase, I., T. Okinaga, M. Hoshi, G. W. Feigenson, and K. Kinosita, Jr. 1995b. Regulatory mechanisms of the acrosome reaction revealed by multiview microscopy of single starfish sperm. *J. Cell Biol.* 131: 963–973.

Sellers, J. R., and B. Kachar. 1990. Polarity and velocity of sliding filaments: control of direction by actin and of speed by myosin. *Science.* 249:406–408.

Suzuki, N., H. Miyata, S. Ishiwata, and K. Kinosita, Jr. 1996. Preparation of bead-tailed actin filaments: estimation of the torque produced by the sliding force in an in vitro motility assay. *Biophys. J.* 70:401–408.

Svoboda, K., C. F. Schmidt, B. J. Schnapp, and S. M. Block. 1993. Direct observation of kinesin stepping by optical trapping interferometry. *Nature.* 365:721–727.

Taylor, K. A., H. Schmitz, M. C. Reedy, Y. E. Goldman, C. Franzini-Armstrong, H. Sasaki, R. T. Tregear, K. Poole, C. Lucaveche, R. J. Edwards, L. F. Chen, H. Winkler, and M. K. Reedy. 1999. Tomographic 3D reconstruction of quick-frozen, Ca^{2+}-activated contracting insect flight muscle. *Cell.* 99:421–431.

Toyoshima, Y. Y., S. J. Kron, E. M. McNally, K. R. Niebling, C. Toyoshima, and J. A. Spudich. 1987. Myosin subfragment-1 is sufficient to move actin filaments in vitro. *Nature.* 328:536–539.

Toyoshima, Y. Y., C. Toyoshima, and J. A. Spudich. 1989. Bidirectional movement of actin filaments along tracks of myosin heads. *Nature.* 341:154–156.

Tsuda, Y., H. Yasutake, A. Ishijima, and T. Yanagida. 1996. Torsional rigidity of single actin filaments and actin-actin bond breaking force under torsion measured directly by in vitro micromanipulation. *Proc. Natl. Acad. Sci. USA.* 93:12937–12942.

Vale, R. D., T. Funatsu, D. W. Pierce, L. Romberg, Y. Harada, and T. Yanagida. 1996. Direct observation of single kinesin molecules moving along microtubules. *Nature.* 380:451–453.

Yamada, A., N. Ishii, and K. Takahashi. 1990. Direction and speed of actin filaments moving along thick filaments isolated from molluscan smooth muscle. *J. Biochem.* 108:341–343.

Yanagida, T., M. Nakase, K. Nishiyama, and F. Oosawa. 1984. Direct observation of motion of single F-actin filaments in the presence of myosin. *Nature.* 307:58–60.

Yasuda, R., H. Noji, K. Kinosita, Jr., and M. Yoshida. 1998. F_1-ATPase is a highly efficient molecular motor that rotates with discrete 120° steps. *Cell.* 93:1117–1124.

解 説　特集・生体の運動機構とバイオトライボロジー

筋収縮滑り運動機構とトライボロジー

石　渡　信　一
早稲田大学 理工学部物理学科
(〒169-8555　東京都新宿区大久保3丁目4-1)

原稿受付　1999年10月12日
"トライボロジスト" 第45巻 第2号 (2000) 119～125

1. はじめに

われわれの体の中で，筋肉ほど身近な生体組織（臓器）は他にない．何しろ手で触ることができる．しかも指圧をして思いきり押したり，ゴリゴリと揉みほぐしたりすることさえできる．そんなことをしても筋肉としての収縮機能は損なわれないし，むしろ硬さがほぐれて気分がよくなりさえする．思えば不思議な臓器である．手指の先でその硬さや状態を感知することができるこの臓器が，分子モータと呼ばれる数十ナノメートル（nm）の大きさのタンパク質が無数に集まったタンパク質集合体であることを思うと，さらにその不思議さは倍加する（サイコロ程度の大きさの筋肉片には，1兆の，そのまた1兆倍個もの分子モータが詰まっている！）．

筋肉，特に骨格筋は非常に細長い細胞で，長軸方向に張力を発生して収縮する（図1の階層構造参照）．われわれの手足を動かす骨格筋の場合，単位断面積（1 cm²）あたりに発生する最大収縮力は数kg重，数十ニュートン（N）となる．この事実と，筋肉の微細構造から求めたミオシン分子モータの数密度から，分子モータ1個が発生する平均の力を数ピコニュートン（pN）と見積もることができる．最近の1分子顕微鏡計測でもほぼ同じ値が得られている[1,2]．

筋収縮は2種類の筋フィラメント，すなわちミオシン分子の繊維状重合体である太いフィラメントと，アクチン分子の繊維状重合体である細いフィラメントが，互いに"滑り合う"ことによって生じる（滑り運動機構）．この"滑り運動機構"は，1954年に2人のハックスレー（A. F. HUXLEYとH. E. HUXLEY）とその共同研究者達によってNature誌上に並んで発表された．

ところでトライボロジストがもし筋収縮運動の

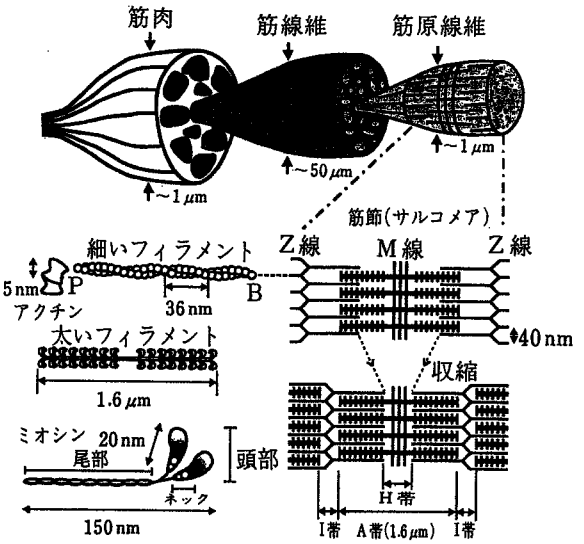

図1　筋線維，筋原線維から単一アクトミオシン分子モータに至る横紋筋収縮系の階層構造（このような階層性は，横紋筋である骨格筋，心筋に共通のものである．横紋構造をもつ筋収縮系の最小構造単位は，筋節（サルコメア）と呼ばれる．筋節は，ミオシン分子の繊維状重合体である太いフィラメントと，アクチン分子がらせん状に重合した細いフィラメントが，スメクチック液晶のように整然と配列した格子構造からなっている．ミオシン分子は，アクチンとの結合部位とATP結合部位を含む"頭部"と"尾部"，そして頭部と尾部をつなぐ"首部（ネック）"からなる）〔出典：文献1)〕

Sliding Mechanism of Muscle Contraction and Tribology

By Shin'ichi ISHIWATA, Department of Physics, School of Science and Engineering, Waseda University (4-1, Okubo 3-chōme, Shinjuku-ku, Tokyo 169-8555, *E-mail*: ishiwata@mn.waseda.ac.jp)

Key Words: *sliding mechanism, molecular friction, muscle contraction, actomyosin interaction, cross-bridge cycle, tribology, SPOC*

仕組みに関心を寄せるとすれば，その理由の第一は“滑り運動”と呼ばれていることにあるのではないか，と推測する．タンパク質繊維が互いに滑り合うという．そうであるならば，そこには摩擦があるはずだ．しかし，筋収縮機構の研究において“分子摩擦”という概念が登場し，滑り運動機構における生理的な意義が認められるようになったのはごく最近のことである（本号特集掲載：太和田らの解説参照）．

“滑り運動”と名づけられた理由は，筋収縮研究の歴史にある．“滑り運動機構”が実験的な証拠を得た当時，筋収縮は筋タンパク質分子が折りたたまれることによって生じる，とする説が強かった．それに対して，筋収縮は2種類の筋フィラメントがその長さを変えることなく（タンパク質の折りたたみではなく），互いに位置をずらすことによって生じる，という意味で“滑る”と表現したのである．“滑り運動機構”が広く受け入れられるようになるまでには紆余曲折があったが，現在ではこの機構自体に意義を申し立てる研究者はいない．滑り運動機構が認められるようになって以来，この分野では，滑り運動をもたらす“分子機構”の研究に重心が移った．そして50年近い研究の歴史を積み重ね，やっと一つの解答が得られようとしている[1,2]．

（1）アクチンとミオシン頭部の立体構造が，それぞれ1990年と1993年にX線結晶構造解析によって解明されたこと，（2）1分子解析・操作のための顕微鏡法が開発され，モータ1分子の素機能，素過程が解明されつつあること，そして（3）遺伝子解析により，ミオシン分子モータファミリーには15種類もの多くの分子モータが存在し，その運動特性に想像以上の多様性が見出されつつあることなどから，滑り運動機構が文字通り分子レベルで明らかにされつつある．この数年間に，いくつもの驚くべき発見があり，見事な実験が行なわれた．たとえば，この原稿を書いている最中にも，これまで知られていたすべてのミオシン分子モータとは逆向き（P端の向き）に滑り運動をするミオシン分子モータ（myosin VI型；筋収縮系のミオシンはmyosin II型）が発見されたとの報告が，Nature誌上に掲載された[3]．

この小論では，筆者の注目する“滑り運動”機構に関する最近の知見を述べ，さらに筆者の研究室で得られた研究成果を紹介することを通して，筋収縮滑り運動の分子機構の一側面について述べることにしよう．

2. クロスブリッジサイクルと滑り運動機構

まず，アクトミオシン分子モータによるATP（アデノシン3リン酸）加水分解反応のスキームと，各反応ステップにおけるミオシン分子モータ（頭部とネック領域）の構造を模式的に示したのが図2である[4,5]．この図はクロスブリッジサイクルとも呼ばれる．クロスブリッジとは，図1に見られるように，細いフィラメントと太いフィラメントを“架橋”するミオシン頭部を指す．クロスブリッジサイクルの詳細は，ATP加水分解反応と力発生の素過程を結びつけようとする試みの中から，繰り返し繰り返し実験的に検証されてきたものである．特に力発生の分子機構としてミオシン分子の“首振り運動”（クロスブリッジが角度を変える運動）を捉える目的で，スピンラベルや蛍光ラベルをミオシン頭部の先端部あるいはネック領域に導入し，ラベルの向きが“滑り運動”あるいは力発生に伴って変化するか否かが調べられた．

このようなアプローチの一つの集大成が，最近米英の共同研究チームによって報告された[5]．このグループは，分子構造から予測されたミオシンネックの角度変化（Lever-arm-model）を検証することに精力を注いだ．ミオシンネックの角度が変化することを示すためには，適当な部位に選択的に蛍光ラベルを導入したい．ところがこれまでの研究では，導入したラベルがタンパク質に対してブラウン運動する自由度があったために，ラベルの向きはタンパク質の向きを正確には反映していなかった．そこで彼らはタンパク質表面の2箇所に結合する2架橋性蛍光色素を合成した．そして，ネック領域に結合しているミオシン軽鎖LC2（図1のミオシン頭部に記した二つの丸印のうちの下の丸印）の適当な2箇所をシステイン残基で置換し，この色素をラベルした．もちろん，

このラベルを導入することによって分子モータとしての機能が損なわれないことを確認した．こうして，再構成された筋線維が力を発生する際に，蛍光色素の向きがどのように変化するかを時間分解計測した．得られた結果を解釈したものが図2の模式図にまとめられている．注目すべき点は，力発生のステップにおいて，ネック領域の向きが，アクチンフィラメントの長軸に対して鈍角から直角へ，そして鋭角へと変化することを示したことである．このことは，Lever-arm-model を支持する．

ミオシン頭部の分子変形は，結晶構造解析やX線溶液散乱，それに電子顕微鏡解析などによっても捉えられている[1]．しかも，上記のミオシンVI型の場合には，ネックが逆側に折れ曲がっている電子顕微鏡像が得られている[3]．ところで，力発生との時間的な関係が明らかになっているのは，上で紹介した筋線維を用いた蛍光（あるいはスピン）ラベル法による研究のみである．しかし筋線維を用いる実験には，得られる蛍光色素の配向度が多数分子の平均値であるためか，期待値に比べて角度変化が小さいという弱点がある．今後期待されるのは，蛍光顕微鏡による1分子解析であろう．1分子レベルで，力発生のタイミングと分子の向きとの関係が明らかになれば，何が原因で，何が副産物であるかがよりいっそう明確になるだろう．

以上の成果をまとめたモデル（図2）によれば，一つのクロスブリッジサイクルは，(1)解離したミオシン頭部（M）内でのATP分子のADP（アデノシン2リン酸）と無機リン酸（Pi）への加水分解（MADPPi）と，その後のミオシン頭部のアクチン（A）への結合（AMADPPi複合体；結合が弱いために，ネック領域が揺らいでいる），(2)PiやADPの解離に伴うミオシン・アクチン強結合の形成と，ミオシンネック領域の変形による数pNの力発生，そして10 nmの滑り運動（AMADPからAMへの転移），(3)ATP分子の再結合によるミオシン頭部のアクチンフィラメントからの解離（ミオシン頭部のブラウン運動；A+MATP），そしてこの過程が再び(1)に戻る，というものである．1回の化学サイクル

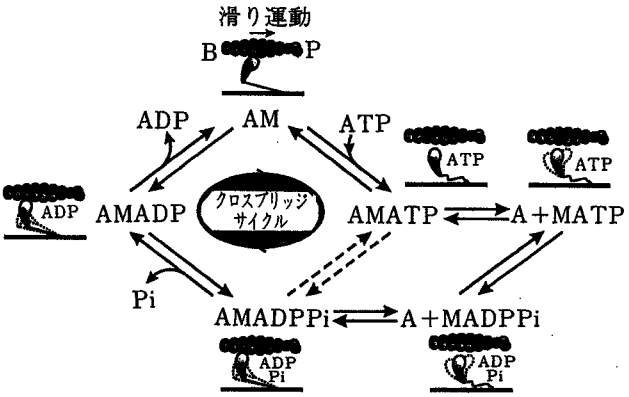

図2　アクトミオシン分子モータのATPaseサイクルと分子間結合様式の模式図（クロスブリッジサイクル）（ミオシンネックに結合しているLC2と呼ばれるミオシン軽鎖に蛍光色素をラベルし，その向きを時分割計測することによって，各状態におけるアクチンフィラメントに対するミオシンネックの傾きが求められる[4,5]）

（ATP加水分解）に伴って1回の力学過程（力発生と滑り運動）が生じる．

ところがこのような研究成果がある一方で，化学サイクルと力学過程とが必ずしも1：1に対応していないことを示す実験結果も存在する[2,6]．まず，ATPがミオシンから遊離するタイミングと，力発生のタイミングとを1分子解析した結果，力発生はATP（ADP）が解離した後に生じることがあるという[6]．これは，図2で示したものと相矛盾する．また，図2で示されたような機構であるならば，1個のATPが加水分解することによる“滑り運動の大きさ”は高々ミオシン頭部の大きさ，あるいはネックの長さ程度のはずである．ところが，1個のATPが加水分解される間にミオシン頭部の大きさの何倍も滑り運動することを示唆する実験結果が報告されている[2]．しかもその滑り運動の間には，アクチン分子の大きさ（約5 nm）に等しいステップを何歩もつづけて踏むという[7]．力学素過程は何か，が問われている．

また，遺伝子組換え技術を用いてミオシンネックの長さを数倍に変えたところ，滑り速度がネックの長さに比例して数倍になった，という実験結果が存在する（これは図2のモデルを支持する[1]）．その一方で，ネックの長さに応じてATP分解速度が上昇する，それが滑り速度が上昇した理由であるとする報告もある（図2のモデルを否

定するものではないが，残念ながらこの手の実験が図2のモデルの決定的証拠にならないことを示唆している)．未だにこのようなどんでん返しの実験結果が報告されている状態である．図2のモデルだけでは，滑り運動分子機構の全貌を説明しきれないのかもしれない．アイデアの飛躍と，決定的実験が求められる所以である．

ところでミオシン分子は，ATPが結合するとアクチンから直ちに解離する．したがってミオシン分子モータは1分子だけでは長距離に渡ってアクチンフィラメントの上を“滑る”ことができない．それに対して，キネシンと呼ばれる分子モータは微小管から容易に解離せず，解離しないままに何回もATP加水分解サイクルをまわる．この性質により，キネシン分子は微小管上を，単頭-双頭結合を交互に繰り返しつつ“歩く”．1分子で機能し，神経細胞の末端に向かって1分子で小胞を運ぶことができる．ミオシン分子はアクチンフィラメント上で“ジャンプする”[8]．しかし，三段跳びのように右・左と交互に単頭結合を繰り返すのか，途中でケンケンのように同じ頭部で結合するのか，などのジャンプの仕方はまったくわかっていない．ただ，単頭ミオシンに比べて双頭ミオシンの方が滑り速度が大きいので，二つの頭部間に何らかの協同性が働いている可能性はある．いずれにしても，筋フィラメントを滑らかに動かすためにはミオシン分子は多数個で機能せざるをえない．このことは筋肉に限らず，II型のミオシン分子モータが働いているすべての細胞運動系に共通する性質である．

3．1分子モータの機能解析

ここで，必ずしも“滑り運動分子機構”に直結するものではないが，1分子レベルでの機能解析を目指すわれわれの研究を紹介しよう[9~12]．われわれは，アクチン・ミオシン間の結合（破断）力や結合寿命を光学顕微鏡下で1分子計測している．その計測法の模式図[9,10]と計測結果の一部[12]を図3に示す．アクチンフィラメントのB端（滑り運動の後ろ端）に結合したプラスチックビーズをレーザ光ピンセットで捕捉する．次に光ピンセットの捕捉中心をB端方向に一定速度で移動することによって，一定の上昇速度で負荷を加える．こうして得られたアクチン・ミオシン硬直結合の破断力分布は，二つのピークからなっていた．負荷上昇速度が小さいときには〔図3(a)〕，それぞれのピークの平均破断力は，約7 pNと15 pNであった．負荷上昇速度が大きくなると〔図3(b)〕，それぞれ約9 pNと18 pNとなり，しかもピークの大きさの比が変化した．このように，負荷の上昇速度が大きいほど，破断力分布は破断力の大きい側に移動した．一般に負荷を加えるとタンパク質間結合の寿命は短くなるが，負荷の上昇速度が大きいほど結合寿命の間に加わる負荷が大きくなる．その結果破断力は大きくなることが，単純なタンパク質間結合について原子間力顕微鏡(AFM)を用いて示されている[13]．この性質は，アクチン・ミオシン硬直結合の場合にもみられたことになる．

ところが，ミオシン分子は2個の頭部をもち，それぞれアクチン分子とほぼ等価に結合しうるという特徴をもつ．この特徴が，破断力ヒストグラムに現われている．まず二つのピークは，それぞれミオシン単頭と双頭の結合破断に対応している．しかも，この二つのピークの大きさの比が負荷上昇速度に依存するということは，ミオシン分子の硬直結合が，単頭結合と双頭結合との間を行き来する平衡関係にあることを示唆する．無負荷の条件下ではこの平衡は双頭結合側に大きく片寄っている．ところが，負荷が加わっている間に双頭結合から単頭結合への変換が生じ，したがって単頭破断の頻度が増すものと推測される．

図2に示したクロスブリッジサイクルの中では，数mMのATPが存在するために硬直結合(AM)の寿命は非常に短い．しかし，硬直結合に関する上記の性質は，クロスブリッジサイクル中の他の分子種にも共通するものであろう．つまり，結合破断の負荷依存性とその速度論は，多数のミオシン分子が集団として一斉に滑り運動する際に重要な意味をもつであろう．

そもそもタンパク質間結合は，熱平衡状態では結合と解離の間を行き来している．そこで分子間結合定数Kは，結合の速度定数k_+と解離定数k_-の比k_+/k_-で与えられ，k_-の逆数がタンパク質

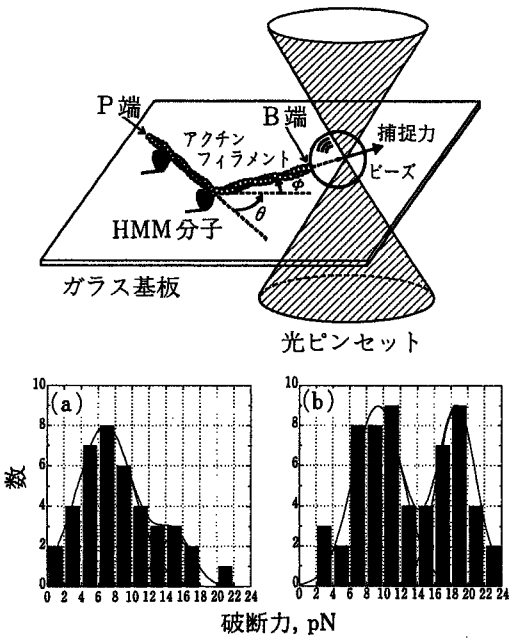

図3　アクチン・ミオシン分子間結合力（破断力）の1分子計測法〔上図：分子間結合力を計測するための模式図[9~11]．アクチンフィラメントのB端（滑り運動の後ろ端）を，B端キャップタンパク質であるゲルゾリンを介して直径1 μmのプラスチックビーズに固定し，ビーズをレーザ光ピンセットによって捕捉・操作する．一方ミオシン分子（実験では，双頭構造を保ち尾部を欠損したミオシンII型の酵素活性断片HMM分子を使用)は，長さ1 μmのアクチンフィラメントあたり約1個の線密度で，ガラス表面にまばらに吸着させてある。レーザ光を集束した光ピンセットによって一方のビーズを捕捉し，ガラス基板あるいは光ピンセットの捕捉中心を，ガラス基板に平行に，一方向に一定速度で動かすことにより，分子間結合に一定速度で負荷を加え続ける．また，変性ミオシンを表面に吸着したビーズを調製し，それをP端側に結合することによって，アクチンフィラメントのP端方向に負荷を加えることもできる．同じミオシン分子について何度でも，様々な角度θで結合・破断を繰り返すことができる．角度ϕは，アクチンフィラメントとガラス基板のなす角度で，10度程度である．ある大きさの負荷で分子間結合が破断すると，ビーズは再び光ピンセットの捕捉中心の位置にもどる．破断する際のビーズの位置（重心）と捕捉中心との距離を求めることによって，破断力を見積もることができる．下図：ATP非存在下で形成されるアクチン・ミオシン（HMM）硬直結合の破断力のヒストグラム[12]．負荷はB端の方向に加えられた．平均約7 pNのピークと，その倍の大きさのピークからなる．(a)と(b)の違いは，負荷上昇速度だけである(a)：5 pN/s，(b)：36 pN/s〕

間結合の平均寿命に相当する．たとえば無負荷のアクチン・ミオシン硬直結合の場合には約1 000秒である．アクチン・ミオシン硬直結合の寿命とその負荷依存性を，顕微鏡下で1分子解析した結果，結合寿命τと負荷Fとの間に

$$\tau=\tau_0\exp(-Fd/k_BT)$$

の関係が成り立つことがわかった[9,11]．ここでτ_0は無負荷時の結合寿命（双頭構造をもつHMM分子の場合には約1 000秒，1個の頭部に相当するS1分子の場合には約100秒），dはタンパク質分子間の相互作用距離，k_Bはボルツマン定数，Tは絶対温度である．

ここで，硬直結合のdの値は約3 nmと見積もられた．この値は分子間結合ポテンシャルの有効距離にしては1桁大きい．dを求める1分子計測は，アビジン-ビオチンなどの単純なタンパク質について主にAFMを用いて研究されているが，1桁小さな値が報告されている．そこでわれわれは，dが大きいことはモータ分子の特徴ではないかと想像する．ミオシン・アクチン間結合部位には多くの分子間力が関与している．そのすべてが一度に外れるのであれば，相互作用距離は1桁小さくなるであろう．しかしミオシン・アクチン間結合の場合には片側から徐々に外れるので，見掛け上dの値が大きくなるのではないか．逆にいえば，破断が徐々に生じるような方向に負荷が加えられたのだ，ということもできる．ところで負荷と滑り力とは，方向が同じで向きが逆，という関係にある．そうであるならば，滑り力発生時のミオシン分子のアクチンへの結合は，分子間結合の数を徐々に増すように，破断の過程と逆の過程をたどるのではないか．化学エネルギー源であるATPが存在しない場合でも，ミオシン・アクチン結合それ自体にこのような性質が備わっている．ATPは分子モータに備わったこの性質を制御するという役割を担っているのかもしれない[9]．このような分子間結合と分子間解離の性質こそ，分子モータの運動性に直結するものではないか，とわれわれは期待している．

4. 分子モータ集団の運動特性

図1にみるように，筋収縮系の最小単位である(半)筋節では，多くのミオシン分子が直列，並列に連結して働いている．もしミオシンがキネシン

のような“歩く”分子モータであったなら，多くのモータは互いに運動を妨げあい，がちがちに動かなくなるのではなかろうか．つまり，動くタイミングがよほど揃っていない限り，あるモータがフィラメントの上を進もうとすると，別のモータはまだ力発生の状態に移行していなかったり，あるいは力を出し終わった状態で結合しているだろう．このような状態にある分子モータは“分子摩擦”の原因となる．その結果，多数のモータはまったく無駄な内部仕事をすることになり，ATPの加水分解エネルギーはひたすら熱発生に費やされることになるだろう．骨格筋ミオシン（II型）の場合には，ATP加水分解の1サイクルに占める，力発生状態にある分子種（図2のAMADP複合体など）の寿命の割合は，10％程度と小さいことが知られている．一方，単に結合しているだけの弱結合状態（図2で，AMADPPi複合体など）も存在するが，いずれにしても多数個の分子モータが働くには都合が良い，“走るモータ”という特徴を備えている．

筋収縮滑り運動機構においては，多数分子が並列に相互作用することによる分子摩擦が存在する．では分子摩擦の筋生理における意味は何か．第一に，分子摩擦に伴う熱発生は，温血動物にとって体温の維持に役立っている．収縮特性に関しては，力を発生している状態にある分子モータと，単に結合しているだけで滑り運動の抵抗となっている分子モータが共存し，（収縮力）—（摩擦力）によって（最大の滑り運動速度）が決まる．さらに，分子摩擦の原因となるであろうミオシン・アクチン結合状態（たとえばAM結合やAMADP結合）が，アクチンフィラメントを通じて分子モータ機能の協同性，協調性を生み出しているという証拠がある．分子間協同性・協調性は，自励振動（SPOC）現象などの多分子筋収縮系に特徴的な現象において，特に重要な役割を担っていることが期待される[1,14]．今後は，単一分子モータの素機能・素過程の解明とともに，多分子モータ系固有の高次機能の解明が待たれる．

5. おわりに

トライボロジーの視点から生体運動の分子メカニズムにアプローチしようとすると，ミオシン・アクチン結合部位における原子（団）レベルでのタンパク質間結合の動的特性（上で述べたような結合寿命の負荷依存性や，さらに一歩進んで，アミノ酸残基間の分子間結合ポテンシャルの特性など）を取り込む必要があるだろう．そのうえで，多分子運動系の運動特性・運動機構をトライボロジーの視点から捉え，生体運動の分子機構にとって新たな視点が与えられることを期待したい．

文 献

1) 石渡信一編：生体分子モーターの仕組み，シリーズ・ニューバイオフィジックス4，共立出版（1997）pp. 214.
2) 柳田敏雄・石渡信一編：ナノピコスペースのイメージング—生物分子モーターのメカニズムを見る—，シリーズ・生物物理から見た生命像3，吉岡書店（1997）pp. 164.
3) A. L. WELLS et al.: Myosin VI Is an Actin-based Motor that Moves Backwards, Nature, **401** (1999) 505.
4) Y. E. GOLDMAN: Wag the Tail: Structural Dynamics of Actomyosin, Cell, **93** (1998) 1.
5) J. E. T. CORRIE, B. D. BRANDMEIER, R. E. FERGUSON, D. R. TRENTHAM, J. KENDRICK-JONES, S. C. HOPKINS, U. A. van der HEIDE, Y. E. GOLDMAN, C. SABIDO-DAVID, R. E. DALE, S. CRIDDLE & M. IRVING: Dynamic Measurement of Myosin Light-chain-domain Tilt and Twist in Muscle Contraction, Nature, **400** (1999) 425.
6) A. ISHIJIMA, H. KOJIMA, T. FUNATSU, M. TOKUNAGA, H. HIGUCHI, H. TANAKA & T. YANAGIDA: Simultaneous Observation of Individual ATPase and Mechanical Events by a Single Myosin Molecule during Interaction with Actin, Cell, **92** (1998) 161.
7) K. KITAMURA, M. TOKUNAGA, A. HIKIKOSHI-IWANE & T. YANAGIDA: A Single Myosin Head Moves along an Actin Filament with Regular Steps of ~5.3 nm, Nature, **397** (1999) 129.
8) K. KINOSITA Jr., R. YASUDA, H. NOJI, S. ISHIWATA & M. YOSHIDA: F 1-ATPase: A Rotary Motor Made of a Single Molecule, Cell, **93** (1998) 21.
9) T. NISHIZAKA, H. YOSHIKAWA, H. MIYATA, S. ISHIWATA & K. KINOSITA Jr.: Unbinding Force of a Single Motor Molecule of Muscle Measured Using Optical Tweezers, Nature, **377** (1995) 251.
10) 西坂崇之・石渡信一：分子モーターの力学・機能特性を見る，生物物理，**36** (1996) 15.
11) 西坂崇之：アクトミオシン分子モーターの機能と力学特性の一分子顕微解析，早稲田大学理工学部博士論文（1996）pp. 160.
12) 熊木雄一：アクトミオシン硬直結合の1分子顕微解析，早稲田大学理工学部修士論文（1999）.
13) R. MERKEL, P. NASSOY, A. LEUNG, K. RITCHIE & E. EVANS: Energy Landscapes of Receptor-ligand Explored with Dynamic Force Spectroscopy, Nature,

397 (1999) 50.
14) 石渡信一：生体系材料の分子シンクロナイゼーション，ポリファイル，**34** (1997) 25.

著者プロフィール

石渡　信一　1945年生まれ．東京大学理学部物理学科卒業．名古屋大学理学系大学院修了．理学博士．現在，早稲田大学理工学部物理学科教授．専門は，生物物理学．生体分子モーターの1分子・多分子機能解析，筋収縮系の構造と機能の再構築，自励振動(SPOC)現象のメカニズム解析，1分子から分子集合体，そして細胞とその集団の機能構築を目指す．日本生物物理学会，日本物理学会などに所属．

解　説

生体分子モーター系における分子シンクロナイゼーションの研究

Investigation of molecular synchronization in the assembly of molecular motors

超分子システム内における分子シンクロナイゼーション現象として、筋肉が短縮と伸張を繰り返す自励振動現象に着目し、人工的に細いフィラメントを再構築した生体分子モーター系を用いてその分子機構に迫る。

藤田英明
早稲田大学理工学部　佐々木大輔
石渡信一

はじめに

筋収縮は、アクチン分子が重合したアクチンフィラメントに制御タンパク質が結合した細いフィラメントと、主にミオシン分子が重合した太いフィラメントとの相互滑り運動によって起きる。筋肉は一般的に、生理的条件下で収縮か弛緩かの2状態をとる。即ち、筋小胞体からμM以上のCa^{2+}が放出されると制御タンパク質にCa^{2+}が結合し、細いフィラメントはOFF状態からON状態へと遷移する。ところが、除膜した心筋や骨格筋遅筋では、収縮・弛緩の中間濃度(μM程度)のCa^{2+}存在下で、自発的振動状態をとることが知られていた。筆者らは約10年前、Ca^{2+}非存在下であるにもかかわらず、ATPとADPに無機リン酸(Pi)が共存すると振動状態になることを、骨格筋速筋の筋(原)線維、および心筋筋線維で見いだし、この現象をSPontaneous Oscillatory Contraction (SPOC)と名付けた。SPOC現象の化学的性質と力学的性質についてはこの10年間で随分研究されたが、SPOC現象の分子メカニズムについてはいまだに明らかになっていない。そこで、細いフィラメントを人工的に再構成した心筋収縮系を用いてSPOC現象における制御タンパク質の役割を検討した。

1．筋収縮・制御のメカニズム

筋肉の収縮は、太いフィラメントと細いフィラメントが長さを変えずに、相互に滑り合うことによって生じる[1),2)](図1)。筋肉が力を発生するのはミオシン分子とアクチンフィラメントの相互作用によるものであるが、ミオシン分子が力を発生する分子的機構はいまだに解明されていない。ミオシンはATPを加水分解

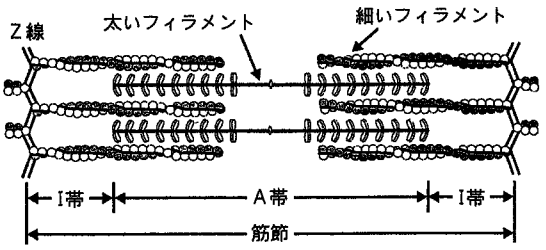

図1　横紋筋収縮系の模式図

筆者紹介：ふじた・ひであき(FUJITA, Hideaki)　早稲田大学理工学部(School of Science and Engineering, Waseda University)助手　1999年早稲田大学大学院理工学研究科博士課程修了　理学博士　専門：生物物理学　連絡先：〒169-8555 東京都新宿区大久保3-4-1　E-mail　fujitah@mn.waseda.ac.jp(勤務先)
ささき・だいすけ(SASAKI, Daisuke)　早稲田大学大学院理工学研究科(Graduate School of Science and Engineering, Waseda University)修士1年　専門：生物物理　連絡先：同　上　E-mail　6991 0513@mn.waseda.ac.jp(在学先)
いしわた・しんいち(ISHIWATA, Shin'ichi)　早稲田大学理工学部(School of Science and Engineering, Waseda University)物理学科教授　1974年名古屋大学大学院理学研究科博士課程単位取得満期退学　理学博士　専門：生物物理学　連絡先：同　上　E-mail　ishiwata@mn.waseda.ac.jp(勤務先)
キーワード：生体分子モーター、分子シンクロナイゼーション、心筋、SPOC、アクチンフィラメント再構成筋

するときに発生する化学エネルギーを仕事に変える分子モーターである。ミオシン単独でのATPase速度は遅いが、アクチンフィラメントと相互作用すると100倍程度加速される。また、力発生はPi放出とそれに続く段階で行われると考えられている。

筋収縮は細胞内Ca^{2+}濃度によって制御される[3]。神経からの信号が筋細胞膜からT管膜を通して内部膜系の筋小胞体に達すると、Ca^{2+}が筋小胞体から放出される。このCa^{2+}が制御タンパク質上のCa^{2+}結合部位に結合すると抑制が外れ、アクチンとミオシンが相互作用して筋肉は収縮する。遊離のCa^{2+}濃度がμM程度で最大張力の50％程度の張力を発生し、10μM程度で飽和に達する。

筋肉の活性化はCa^{2+}だけでなく、アクチンフィラメントに強く結合した(強結合状態)ミオシン頭部によっても生じることが知られている。BremelとWeberは1972年[4]、ATP濃度を下げることにより生成した硬直結合のクロスブリッジがアロステリック(遠隔作用的)に細いフィラメントをON状態にし、そこにほかのミオシン頭部が相互作用できるという制御機構を提唱した。また、硬直結合のクロスブリッジはCa^{2+}感受性を高めることがBrandtらによって示された[5]。一方、ADPが筋肉を活性化し、骨格筋[6,7]と心筋[8]においてCa^{2+}で活性化したときとほぼ同レベルの張力を発生することが分かった。このADPによる活性化もADPを結合した強結合クロスブリッジによるものと考えることができる[7,8]。

2．自励振動現象

通常の筋収縮系はCa^{2+}濃度によって収縮と弛緩の2状態をとるが、昆虫の飛翔筋などでは骨格や組織の弾性を巧みに利用しながら、筋肉自体は常にON状態のまま高速振動を繰り返す。一方、心臓の筋肉も振動を繰り返すが、これは神経系や特殊な細胞の指令によって周期的にCa^{2+}濃度を上げ下げして収縮と弛緩を繰り返させているものである。

弛緩状態(+ATP、$-Ca^{2+}$)にある筋収縮系(細胞膜がない収縮装置だけからなるモデル筋系)にADPを加えていくと張力が発生する(ADP収縮)。SPOC現象はこのADP収縮中の筋収縮系にPiを加えたときに生じる[9]。SPOCの溶液条件は弛緩と収縮の中間条件であり、筋収縮系の第三の状態と考えることができる。SPOC中の筋原線維を観察すると各筋節が遅い収縮と素早い伸長を繰り返し、鋸歯状の波形で振動していることが分かる(図2)。この振動の周期は数秒から20秒程度で、振幅は筋節長の15％程度にも及ぶ。また、ある筋節の振動が隣の筋節へとつぎつぎに伝搬する様子も観察される。さらに、加わる負荷を一定に保つと、筋節長振動が同調する[10]。一方、SPOC中の心筋線維の発生張力は、数秒～20秒程度の周期で振動した。この振動現象は新鮮な溶液が供給されていれば15分以上も安定に続くことからも、この現象が第三の生理状態であることが示唆される。

生理的環境ではATPの加水分解で生じたADPは、ATP再生系によって即座にATPに変換されるため、通常の状態でADP濃度がSPOC条件に達する事は考えにくい。しかし、心筋におけるSPOC条件は骨格筋と比較して低ADP濃度で起きることが分かっており、疲労時や虚血時にSPOC条件を満たす可能性がある。よって、振動そのものが生理的機能である心筋において、SPOCが生理的意味を持つ可能性は大

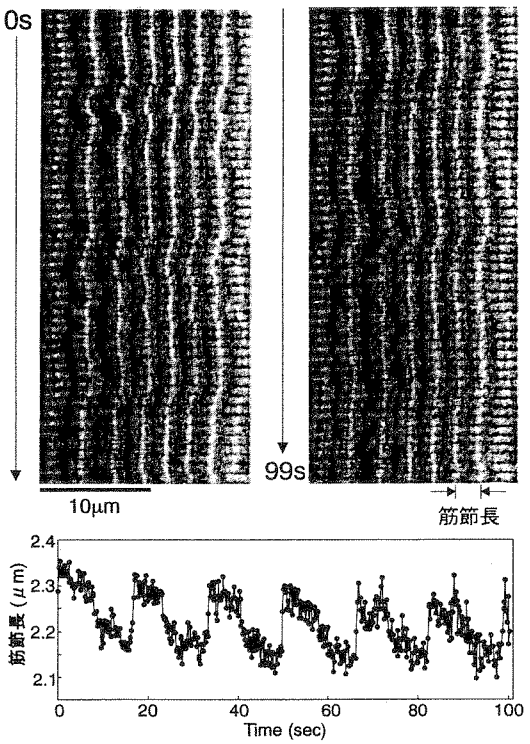

図2　SPOC条件下での心筋筋原線維のレーザー共焦点蛍光顕微鏡像と筋節長変化
上：SPOC中の心筋筋原線維の1秒おきの蛍光連続写真。細いフィラメントを蛍光色素で染色してある。
下：上図矢印部分の筋節長の時間変化を測定した。

きい。SPOCの分子メカニズムはいまだに十分には理解されていないが、コンピューターシミュレーションなどの結果から、AMADPPiのミオシン頭部とAMADPの頭部が、それぞれある一定以上の割合で存在していることが必要だと推測される。

また、Jülicher と Prost[11]は、多数の分子モーターが弾性要素でつながっているときに、たとえ制御系を考慮に入れなくてもSPOCのような振動が起きることを理論的に示した。光ピンセット法などを用いて分子モーター1個の特性が明らかになりつつある今、ミオシン分子モーターとアクチンフィラメントとの集合体が示すSPOC現象は、分子シンクロナイゼーション(分子間相互作用の協調性)を研究する系として非常に興味深いものである。

3．細いフィラメントの選択的解体と再構築

横紋筋の整った液晶構造がいかにして構築・維持されているのかについては不明な部分も多い。最近、筆者らは骨格筋と心筋において、細いフィラメントの選択的解体・再構築を行い、この問題の分子メカニズムを明らかにした[12),13)]。解体・再構築手法は、筋肉を構成する特定のタンパク質の機能を調べる手段としても有用である。

まず、除膜筋にアクチンフィラメント切断タンパク質であるゲルゾリンを作用させると、細いフィラメントを選択的に除去することができる。細いフィラメントの除去により、筋線維束は張力発生能を失う。この細いフィラメント除去筋に外部から精製したアクチンモノマーを重合条件下で加えることにより、アクチンフィラメントが再構築された。このとき自発的な核形成をできるだけ抑えるために、アクチン重合溶液は7分おきに新しいものと交換し、0℃に保つようにした。このことによって、Z線に残ったアクチンフィラメントの断片を重合核として働かせることができた。このアクチンフィラメント再構成筋は、制御タンパク質が存在しないため、Ca^{2+}濃度に依存せずに張力を発生した。したがって、弛緩はアクトミオシン相互作用の阻害剤である2,3-butanedione 2-monoxime (BDM)を用いて行った。アクチンフィラメント再構成後の張力は、骨格筋では元の張力の30％程度であったが、心筋では135％にも達した。心筋再構成筋における張力増強効果は、アクチンフィラメントの平均長が伸びたためと考えられる。アクチンフィラメントの解体と再構築は、細いフィラメントを蛍光色素で染色し、レーザー走査型共焦点顕微鏡で観察することによって確認された。また、再構成された細いフィラメントの長さ分布と筋フィラメントの格子内での位置を、電子顕微鏡を用いて確認することができた。さらに、制御タンパク質を含む弛緩溶液にアクチンフィラメント再構成筋を12時間浸すことにより、最大発生張力に影響を与えずにCa^{2+}感受性を回復させることに成功した。

以上の結果から、適切な場所に重合核や鋳型構造体があれば、タンパク質の自己集合能によって筋肉のような高次生体構造が構造的にも機能的にも再構築されることが示された。細いフィラメント再構成心筋収縮系は、遺伝的に改変したアクチンや制御系の高次機能の解明に役立つものと考えられる。さらに、蛍光ラベルやスピンラベルしたタンパク質で細いフィラメントを再構成すれば、収縮－弛緩時のタンパク質の構造変化を捕らえることもできるだろう。

4．制御系なしでのSPOC現象

SPOC現象の化学的・力学的性質や発生張力については明らかになってきたが、SPOCの分子メカニズムについてはいまだに不明な点が多い。そこで、細いフィラメント再構成手法を用いてSPOCにおける制御タンパク質の役割を明らかにしようと試みた[14),15)]。

SPOC現象は弛緩状態にある収縮系がADPで活性化されたときに生じることから、まずアクチンフィラメント再構成筋におけるADPの作用を調べた。アクチンフィラメント再構成筋では制御タンパク質が存在しないために、ATPが存在しさえすればCa^{2+}濃度に依存せずに張力を発生した。そこにADPを加えても張力の上昇は見られず、張力の減少だけが観察された。また、ADP、Pi共存下でもSPOCは見られなかった。しかも、Piを添加しても張力の減少が見られなかった。そこで、さらにBDMの阻害作用を調べてみた。アクチンフィラメント再構成筋でも、BDM添加によって張力が減少したが、コントロール筋線維束よりも減少の程度は小さかった。しかし驚くべきことに、Pi存在下でアクチンフィラメント再構成筋にBDMを加えると、10～20 mMの範囲で張力振動が観察された。振動の周期と振幅は、コントロールの筋線維束(BDMなし)での標準SPOC条件のときとほとんど変わらなかった。SPOCの特徴の一つである筋節長振動を筋線維束中で観察するため、アクチンフィラメントを蛍

光色素で染色し、リアルタイム共焦点顕微鏡で蛍光観察した。10 mM BDM存在下でのSPOC中の筋節集団の大きな動きの周期は約20秒であり、これは張力振動の周期と一致した。一方、筋節長の振動の周期は約3秒程度と短く、筋原線維の標準SPOC状態の筋節長振動の周期と一致した。この結果は、制御系が存在しなくても溶液条件さえ満たせばSPOCが起きることを示している。また、Piが存在しないときはBDM添加によって張力を抑制しても、SPOCは見られなかった。このことは、SPOCにとってPiが必須因子であることを示している。

制御タンパク質が存在しなくても、条件さえ整えばSPOC現象は生じる。このことは、SPOCがアクトミオシン分子モーターに内在する現象であることを示している。一方、分子モーターの一種であるダイニン分子も微小管上で高速微小振動することが知られている[16]。自励振動現象は生体分子モーター系にとって一般的な現象である可能性がある。また分子モーター系に限らず、生体機能の多くの場面で自励振動現象が見られる。振動のメカニズムを分子レベルで、しかも分子集合体が示す分子シンクロナイゼーション(協調)という見方で捕らえることは、生体分子機械の高次機能とその仕組みを理解する上で重要なことである。

○参考文献

1) Huxley, A. F. and Niedergerke, R.：*Nature* (*Lond.*), 173, 971～973 (1954)
2) Huxley, H. E. and Hanson, J.：同上, 173, 973～976 (1954)
3) Ebashi, S. and Endo, M.：*Prog. Biophys. Mol. Biol.*, 18, 123～183 (1968)
4) Bremel, R. D. and Weber, A.：*Nature* (*New Biol.*), 238, 97～101 (1972)
5) Brandt, P. W., Reuben, J. P. and Grundfest, H.：*J. Gen. Physiol.*, 59, 305～317 (1972)
6) Hoar, P. E., Mahoney, C. W. and Kerrick W. G. L.：*Pflügers Arch.*, 410, 30～36 (1987)
7) Shimizu, H., Fujita, T. and Ishiwata, S.：*Biophys. J.*, 61, 1087～1098 (1992)
8) Fukuda, N., Fujita, H., Fujita, T. and Ishiwata, S.：*Pflügers Arch.*, 433, 1～8 (1996)
9) Okamura, N. and Ishiwata, S.：*J. Muscle Res. Cell Motil.*, 9, 111～119 (1988)
10) Yasuda, K., Shindo, Y. and Ishiwata, S.：*Biophys. J.*, 70, 1823～1829 (1996)
11) Jülicher, F. and Prost, H.：*Phys. Rev. Lett.*, 78, 4510～4513 (1997)
12) Funatsu, T., Anazawa, T. and Ishiwata, S.：*J. Muscle Res. Cell Motil.*, 15, 158～171 (1994)
13) Fujita, H., Yasuda, K., Niitsu, S., Funatsu, T. and Ishiwata, S.：*Biophys. J.*, 71, 2307～2318 (1996)
14) Fujita, H. and Ishiwata, S.：同上, 75, 1439～1445 (1998)
15) Fujita, H. and Ishiwata, S.：同上, 77, 1540～1546 (1999)
16) Kamimura, S. and Kamiya, R.：*Nature* (*Lond.*) 340, 476～478 (1989)

Nucleotide-Dependent Single- to Double-Headed Binding of Kinesin

Kenji Kawaguchi[1] and Shin'ichi Ishiwata[1,2,3,4]*

The motility of kinesin motors is explained by a "hand-over-hand" model in which two heads of kinesin alternately repeat single-headed and double-headed binding with a microtubule. To investigate the binding mode of kinesin at the key nucleotide states during adenosine 5′-triphosphate (ATP) hydrolysis, we measured the mechanical properties of a single kinesin-microtubule complex by applying an external load with optical tweezers. Both the unbinding force and the elastic modulus in solutions containing AMP-PNP (an ATP analog) were twice the value of those in nucleotide-free solution or in the presence of both AMP-PNP and adenosine 5′-diphosphate. Thus, kinesin binds through two heads in the former and one head in the latter two states, which supports a major prediction of the hand-over-hand model.

Kinesin is a molecular motor that transports membrane-bound vesicles and organelles toward the plus end of a microtubule in various cells including neurons (*1*, *2*). Kinesin takes hundreds of 8-nm steps (the size of tubulin heterodimers composed of α and β subunits) (*3*–*5*) before detachment, so that the run length reaches longer than 1 μm (*3*, *6*). Each step is associated with one cycle of ATP hydrolysis (*7*, *8*). Structural and biophysical evidence shows that stepping of kinesin is triggered by conformational changes in the ATP-bound head (*9*).

A "hand-over-hand" model has been proposed to explain the processive movement of kinesin (Fig. 1) (*5*, *9*–*16*). To substantiate the hand-over-hand model, it is essential to determine the binding mode—either single- or double-headed binding—at each nucleotide state, and the kinetic step at which the transi-

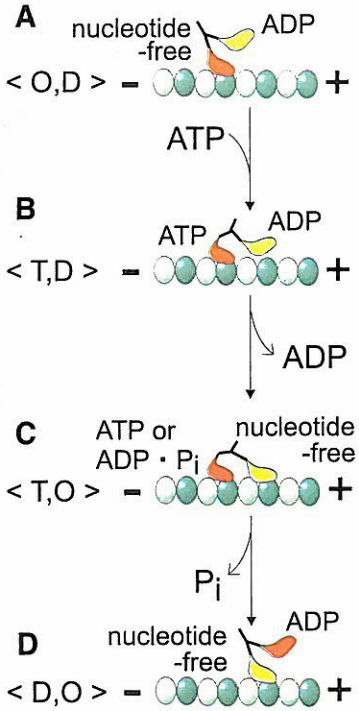

Fig. 1. A simplified version of the hand-over-hand model on the mechanism of kinesin motility proposed to date (*5*, *9*–*16*). O: nucleotide-free; D, T, and P_i: ADP, ATP, and inorganic phosphate, respectively.

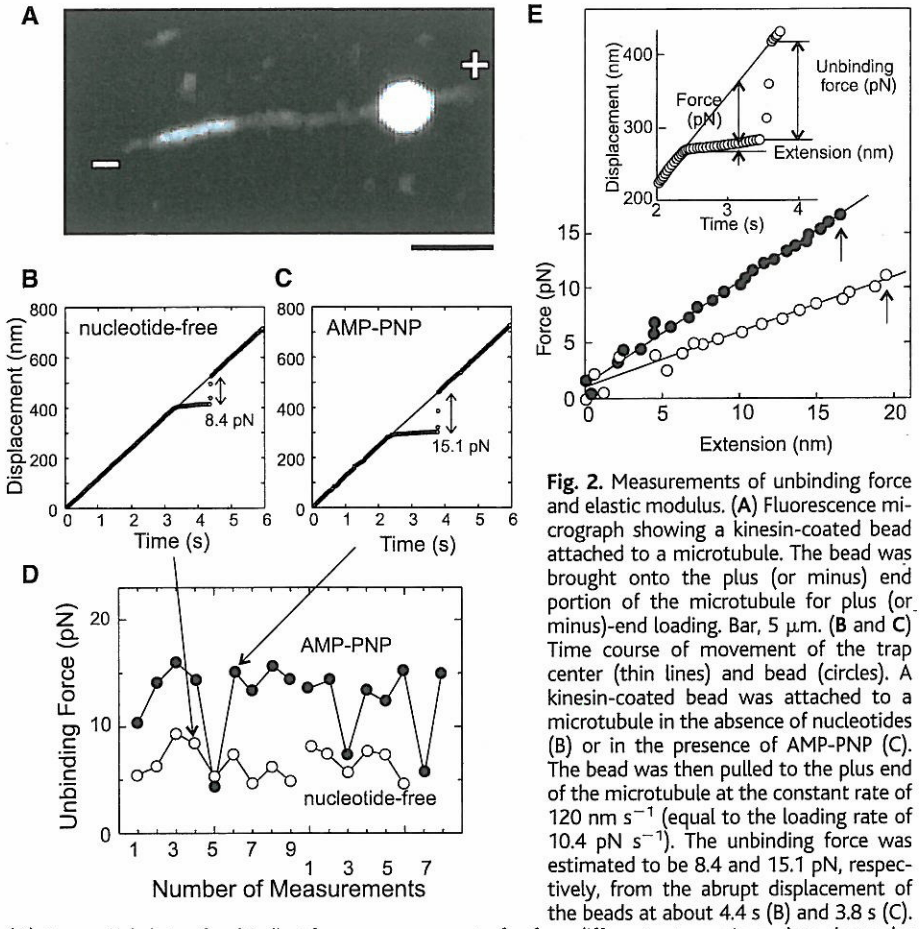

Fig. 2. Measurements of unbinding force and elastic modulus. (**A**) Fluorescence micrograph showing a kinesin-coated bead attached to a microtubule. The bead was brought onto the plus (or minus) end portion of the microtubule for plus (or minus)-end loading. Bar, 5 μm. (**B** and **C**) Time course of movement of the trap center (thin lines) and bead (circles). A kinesin-coated bead was attached to a microtubule in the absence of nucleotides (B) or in the presence of AMP-PNP (C). The bead was then pulled to the plus end of the microtubule at the constant rate of 120 nm s^{-1} (equal to the loading rate of 10.4 pN s^{-1}). The unbinding force was estimated to be 8.4 and 15.1 pN, respectively, from the abrupt displacement of the beads at about 4.4 s (B) and 3.8 s (C). (**D**) Sequential data of unbinding force measurements for four different preparations; data shown by arrows were taken from (B) and (C). Conditions: (B) and (○) in (D), nucleotide-free; (C) and (●) in (D), + AMP-PNP. (**E**) Examples of the force-extension relation (○, nucleotide-free; ●, + AMP-PNP). The relation was obtained from the time course of bead displacement as shown in the inset. To be strict, the force means the force component parallel to the glass surface, and the extension means the displacement of the bead in parallel to the glass surface (*27*). Arrows show the position of unbinding.

tion between the two binding modes occurs (*5*, *9*–*16*). Results of image analysis by cryo-electron microscopy on the dimeric kinesin-microtubule complex have been inconclusive; either single-headed (*13*, *14*) or double-headed (*15*, *16*) binding has been found to predominate both in the absence of nucleotides and in the presence of AMP-PNP. In solution the binding stoichiometry of the kinesin head and the tubulin heterodimer in a microtubule has a molar ratio of 2:1 in both the nucleotide-free state (*17*–*19*) and in the presence of AMP-PNP (*17*), implying a single-headed binding. In these studies, the microtubule was fully decorated by kinesin so that the conformation of kinesin may have been constrained (*16*). The intramolecular interhead distance of kinesin in the crystal structure is about 5 nm (*20*), considerably shorter than the size of the tubulin heterodimer. The kinetics of detachment in solution also suggests the single-headed binding not only in the nucleotide-free condition but also in the coexistence of AMP-PNP and adenosine 5′-diphosphate (ADP) (*21*). Overall, the evidence for the model remains indirect.

To obtain direct evidence for the binding mode at each nucleotide state, we measured the mechanical properties of single kinesin molecules attached to a microtubule in three different solvent conditions (*22*): in the absence of added nucleotides, in the presence of 0.5 mM AMP-PNP and 1 mM ADP, and in the presence of 1 mM AMP-PNP. The first condition corresponds to the ⟨O, O⟩ or ⟨O, D⟩ states (Fig. 1). Although apyrase was added, some proportion of heads may still have bound ADP because the kinesin was purified in the presence of ADP and the detachment rate of ADP is slow (*18*, *19*). The second condition mimics the ⟨T, D⟩ state. Under this condition, only one of the two heads is expected to bind AMP-PNP, while the other head is in the ADP state (*21*). The third condition is considered to represent the ⟨T, O⟩ state (*23*), because the binding ratio of AMP-PNP to kinesin molecules is reported to be 1:1 under the present condition (*23*).

An external load was imposed on a single kinesin-microtubule bead complex (Fig. 2A) (*24*, *25*) as it was moved toward the plus (or minus) end of a microtubule with optical tweezers (*26*, *27*). We repeated unbinding force measurements at nearly the same position on the same microtubule several times for the same bead, presumably for the same kinesin molecule (Fig. 2, B to D). Upon loading toward the plus end, unbinding force in the absence of nucleotides was about 7 pN (Fig. 2D), whereas that in the presence of AMP-PNP could apparently be classified into two components at about 14 pN (major) and 7 pN (minor), the latter corresponding to that in the absence of nucleotides. Using the same data, we obtained the force-extension relation on the kinesin-microtubule complex (Fig. 2E). This relation was almost linear, so that the elastic modulus could be estimated simply from the slope. The elastic modulus could also be classified into two components (compare Figs. 2E and 3, D to F). On the minus-end loading, the unbinding force for both components increased by 45% irrespective of the nucleotide states, keeping the elastic modulus unchanged. This shows that the binding is unstable

[1]Department of Physics, School of Science and Engineering; [2]Advanced Research Institute for Science and Engineering; [3]Materials Research Laboratory for Bioscience and Photonics, Waseda University, 3-4-1 Okubo, Shinjuku-ku, Tokyo 169-8555, Japan. [4]Core Research for Evolutional Science and Technology (CREST), "Genetic Programming" Team 13, Nogawa 907, Miyamae-ku, Kawasaki 216-0001, Japan.

*To whom correspondence should be addressed. E-mail: ishiwata@mn.waseda.ac.jp

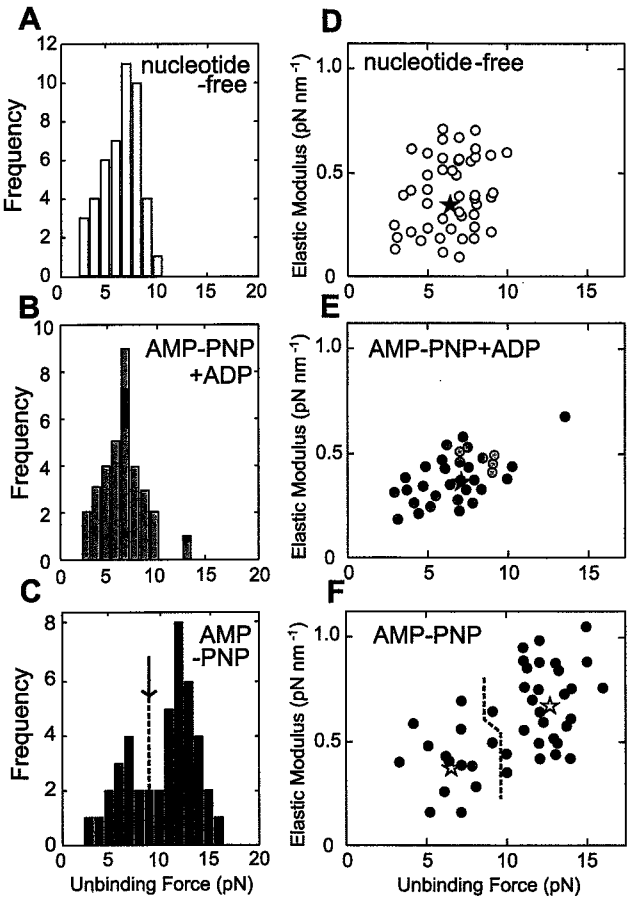

Fig. 3. Distribution of unbinding force (**A** to **C**) and relation between elastic modulus and unbinding force (**D** to **F**) at different nucleotide-binding states. The external load was applied toward the plus end. (A and D) Nucleotide-free (n = 46); (B and E) AMP-PNP + ADP (n = 33); (C and F) + AMP-PNP (n = 43). Unbinding force (pN) ± SD: 6.7 ± 1.8 (A), 7.2 ± 2.0 (B), and 6.6 ± 1.7 (n = 14), 12.8 ± 1.6 (n = 29) (C). Elastic modulus (pN nm^{-1}) ± SD: 0.35 ± 0.14 (D), 0.37 ± 0.16 (E), and 0.39 ± 0.17 (n = 14), 0.67 ± 0.21 (n = 29) (F). Loading rate (pN s^{-1}): 3.5 (A and D), 6.0 (B and E), and 4.3 (C and F). A single Gaussian distribution could simulate unbinding force distribution in (A) and (B). In contrast, the unbinding force distribution in (C) was simulated by the sum of two Gaussian distributions, with S- and L-components defined as the smaller and larger unbinding force, respectively. The boundary between the S- and L-components was determined by the junction of two Gaussian distributions [shown by an arrow (C)]; the boundary in (F) was determined according to that in (C). The average values for S- and L-components are shown by asterisks in (D) to (F).

for the plus-end loading compared with the minus-end loading.

The small (~7 pN; S-) and large (~14 pN; L-) components of unbinding force, respectively, correspond to those of the elastic modulus (Fig. 3). The finding that the unbinding force and the elastic modulus for the L-component were twice those for the S-component strongly suggests that the S- and L-components are attributable to the single- and double-headed binding of kinesin, respectively. Thus, each kinesin head contributes equally to the elastic modulus, such that each head equally shares the external load.

This interpretation shows that the binding mode in the ⟨O, D⟩ state (Fig. 1A) is single-headed. Assuming that AMP-PNP is an ATP analog, single-headed binding is also predominant in the ⟨T, D⟩ state (Fig. 1B). It is highly probable that the attached head binds AMP-PNP (ATP) (*9*), whereas the detached head binds ADP (*9*, *21*), because the attachment of the ADP-bound head was reported to be weak (*17*). In the ⟨T, O⟩ state (Fig. 1C), in contrast, double-headed binding is predominant. Here we find that, based on the bimodal distributions of unbinding force and elastic modulus at one loading rate (Figs. 2D and 3, C and F), both single- and double-headed binding exist. Additionally, we find that the proportion of the S-component decreased as the loading rate increased from 2 to 18 pN s^{-1} and, finally, disappeared at the highest loading rate we examined (18 pN s^{-1}), irrespective of the loading direction. This implies that double-headed binding predominates in the absence of external load. The finding that the unbinding force for the plus-end loading was smaller than that for the minus-end loading suggests that, in the "bridge" structure of double-headed binding (see Fig. 1C), the rear head is relatively unstable so that it tends to be detached. Such an asymmetry for the loading direction regarding the stability of the attached state is favorable for kinesin motors stepping forward.

References and Notes

1. R. D. Vale, in *Guidebook to the Cytoskeletal and Motor Proteins*, T. E. Kreis, R. D. Vale, Eds. (Oxford Univ. Press, Oxford, ed. 2, 1999), pp. 398–402.
2. N. Hirokawa, *Science* **279**, 519 (1998).
3. S. M. Block *et al.*, *Nature* **348**, 348 (1990).
4. K. Svoboda *et al.*, *Nature* **365**, 721 (1993).
5. J. Howard, *Annu. Rev. Physiol.* **58**, 703 (1996).
6. K. Kawaguchi, S. Ishiwata, *Biochem. Biophys. Res. Commun.* **272**, 895 (2000).
7. W. Hua *et al.*, *Nature* **388**, 390 (1997).
8. M. J. Schinitzer, S. M. Block, *Nature* **388**, 386 (1997).
9. S. Rice *et al.*, *Nature* **402**, 778 (1999).
10. R. D. Vale, R. A. Milligan, *Science* **288**, 88 (2000).
11. E. Mandelkow, K. A. Johnson, *Trends Biochem. Sci.* **23**, 429 (1998).
12. D. D. Hackney, *Proc. Natl. Acad. Sci. U.S.A.* **91**, 6865 (1994).
13. K. Hirose *et al.*, *Mol. Biol. Cell* **10**, 2063 (1999).
14. I. Arnal, R. H. Wade, *Structure* **6**, 33 (1998).
15. M. Thormählen *et al.*, *J. Mol. Biol.* **275**, 795 (1998).
16. A. Hoenger *et al.*, *J. Mol. Biol.* **297**, 1087 (2000).
17. A. Lockhart, I. M. Crevel, R. A. Cross, *J. Mol. Biol.* **249**, 763 (1995).
18. Y. Z. Ma, E. W. Taylor, *J. Biol. Chem.* **272**, 724 (1997).
19. S. P. Gilbert, M. L. Moyer, K. A. Johnson, *Biochemistry* **37**, 792 (1998).
20. F. Kozielski *et al.*, *Cell* **91**, 985 (1997).
21. Y. Vugmeyster, E. Berliner, J. Gelles, *Biochemistry* **37**, 747 (1998).
22. Kinesin and tubulin were prepared from bovine (*25*) and porcine (*28*) brains, respectively. Polarity-marked microtubules labeled with tetramethylrhodamine succinimidyl ester (Molecular Probes, Eugene, OR) were prepared according to Hyman (*28*) except that tubulin was not treated with *N*-ethylmaleimide (NEM) (Fig. 2A). Kinesin-coated beads and the flow cell were prepared as described (*6*, *25*). The final solvent condition was ~0.1 pM kinesin-coated beads, 2 mM $MgCl_2$, 80 mM Pipes (pH 6.8), 1 mM EGTA, 0.7 mg ml^{-1} filtered casein, 1 U ml^{-1} apyrase (nucleotide-free condition), 0.5 mM AMP-PNP with 1.0 mM ADP (AMP-PNP + ADP condition) (*21*) or 1 mM AMP-PNP (+ AMP-PNP condition), 10 μM taxol, 10 mM dithiothreitol, and an oxygen-scavenging enzyme system (*6*). All experiments were performed at 25° ± 1°C.
23. B. J. Schnapp *et al.*, *Proc. Natl. Acad. Sci. U.S.A.* **87**, 10053 (1990).
24. K. Svoboda, S. M. Block, *Cell* **77**, 773 (1994).
25. H. Kojima *et al.*, *Biophys. J.* **73**, 2012 (1997).
26. T. Nishizaka *et al.*, *Nature* **377**, 251 (1995).
27. A microscopy system equipped with optical tweezers was as previously described (*26*); the stiffness of the optical trap was estimated to be 0.087 pN nm^{-1}. The bead in the medium was first trapped by optical tweezers and placed in contact with a microtubule for 20 to 30 s, a period considered sufficient to realize the binding equilibrium between kinesin molecule and a microtubule. The trap center was then moved at a constant rate to the plus (or minus) end of the microtubule (Fig. 2A) until the unbinding event occurred. With a single-molecule attachment between the bead and the microtubule, it is possible for the bead to move some distance relative to the microtubule without deviating from the trap center. This is mainly because of the rotational movement of the bead in the trap. This rotational movement is not registered on the position detector. As observed in Fig. 2, B and C, for the first part of the movement of the bead, the kinesin may be attached to the microtubule but does not show in the displacement until the bead-kinesin-microtubule link pulls tight. On the basis of the size and geometry of the kinesin-tethered bead (*24*) (radius of bead, 0.5 μm; length of kinesin, 60 nm), we can estimate that the largest displacement required before the external load is imposed for the unbinding event is ~600 nm. In fact, this displacement was as large as 300 ± 140 nm (n = 122). Also, the actual extension of kinesin is estimated to be 8.3 ± 1 nm (Fig. 2E), which is approximated by 18 nm × cos(θ), where θ (1.1 ± 0.1 rad) is the angle between the kinesin tether and the glass surface. In our bead assay, the external force responsible for the extension of the kinesin-microtubule complex should also be multiplied by cos(θ). Thus, the elastic modulus is kept unchanged.
28. A. A. Hyman, *J. Cell Sci.* **s14**, 125 (1991).

29. We thank K. Kinosita Jr. and T. Nishizaka for continuous collaboration. We are grateful to Y. Y. Toyoshima and T. Yagi for suggestions on the preparation of kinesin and tubulin, and to H. Higuchi for the protocol for kinesin bead assay. We also thank J. Howard, K. Hirose, and W. Rozycki for critical reading of the manuscript. This research was partly supported by Grants-in-Aid for Scientific Research, for Scientific Research on Priority Areas, and for the High-Tech Research Center Project from the Ministry of Education, Science, Sports, and Culture of Japan; by Grants-in-Aid from CREST; and by the Mitsubishi Foundation.

28 September 2000; accepted 18 December 2000

Cell Motility and the Cytoskeleton 49:41–47 (2001)

Thermal Activation of Single Kinesin Molecules With Temperature Pulse Microscopy

Kenji Kawaguchi,[1] and Shin'ichi Ishiwata[1–4]*

[1]*Department of Physics, School of Science and Engineering, Waseda University, Tokyo, Japan*
[2]*Advanced Research Institute for Science and Engineering, Waseda University, Tokyo, Japan*
[3]*Materials Research Laboratory for Bioscience and Photonics, Waseda University, Tokyo, Japan*
[4]*Core Research for Evolutional Science and Technology, "Genetic Programming" Team 13, Kawasaki, Japan*

Conventional kinesin is a processive motor protein that keeps "walking" along a microtubule using chemical energy released by ATP hydrolysis. We previously studied the effects of temperature between 15° and 35°C on the moving velocity, force, and processivity of single kinesin molecules using a bead assay [Kawaguchi and Ishiwata, 2000b: *Biochem Biophys Res Commun* 272:895–899]. However, we could not examine the effects of temperature higher than 35°C because of the thermal damage to proteins. Here, using temperature pulse microscopy (TPM) [Kato et al., 1999: *Proc Natl Acad Sci USA* 96:9602–9606], we could examine the temperature dependence of the gliding velocity of single kinesin molecules interacting with a microtubule above 35°C up to 50°C (instantaneously, ~60°C), where the velocity reached 3.68 μm/s, the highest ever reported. The Arrhenius plot showed no breaks between 15° and 50°C with a unique activation energy of about 50 kJ/mol, suggesting that the molecular mechanism of kinesin motility is common over a broad temperature range including physiological temperature. Cell Motil. Cytoskeleton 49:41–47, 2001. © 2001 Wiley-Liss, Inc.

Key words: Arrhenius plot; motor protein; microtubule; temperature effect on kinesin; single molecule assay

INTRODUCTION

Kinesin is a motor protein that is responsible for the transport of various types of cargo along microtubules inside eukaryotic cells [Vale et al., 1985; Howard, 1996; Hirokawa, 1998; Vale, 1999]. The remarkable difference between myosin (except myosin V) and dynein is that a single kinesin molecule is sufficient for movement along a microtubule [Howard et al., 1989; Block et al., 1990; Vale et al., 1996] and nucleotide-dependent switching of single- to double-headed binding has been shown [Kawaguchi and Ishiwata, 2001]. Recently, we have reported the effect of temperature on the gliding velocity, processivity, and force generated by single kinesin molecules interacting with a microtubule between 15° and 35°C using a bead assay [Kawaguchi and Ishiwata, 2000b]. The Arrhenius plot was linear in the temperature range examined and the activation energy was estimated

Contract grant sponsor: Grants-in-Aid for Scientific Research; Contract grant sponsor: Ministry of Education, Science, Sports, and Culture of Japan; Contract grant sponsor: Grants-in-Aid from Japan Science and Technology Corporation (CREST).

*Correspondence to: Dr. Shin'ichi Ishiwata, Department of Physics, School of Science and Engineering, Waseda University, 3-4-1 Okubo, Shinjuku-ku, Tokyo 169-8555, Japan.
E-mail: ishiwata@mn.waseda.ac.jp

Received 30 October 2000; Accepted 7 February 2001

as 50 kJ/mol. At temperatures higher than 35°C, however, we could not obtain reliable values for the gliding velocities of beads because of thermal deterioration of motor functions.

In order to investigate the interaction between kinesin and microtubule at higher temperatures including physiological temperature, we have applied temperature pulse microscopy (TPM) described previously [Kato et al., 1999] to the gliding movement of a microtubule on kinesin molecules adhering a glass surface. In our TPM, temperature is elevated spatially and temporarily by illuminating a thin metal layer evaporated on the glass surface with infrared laser beam. The temperature of solution adjacent to the illuminated metal thin layer can be elevated even up to a boiling temperature and a concentric temperature gradient (1~2°C/μm) is created around the metal. When the laser beam is shut off, the heat is dissipated into the surrounding medium within 10 ms, so that it is expected that the protein function can be thermally activated beyond the physiological temperature. A preliminary report of this investigation was presented previously [Kawaguchi and Ishiwata, 2000a].

MATERIALS AND METHODS

Proteins

Bovine kinesin extracted from bovine brain was purified by using specific affinity with microtubule [Kojima et al., 1997] followed by DEAE chromatography and sedimentation. Tubulin was prepared from porcine brain and labeled with a fluorescent dye, tetramethylrhodamine succinimidyl ester (C-1171, Molecular Probes, Eugene, OR) according to Hyman et al. [1991]. Microtubules were prepared by polymerizing 20 μM tubulin (labeling ratio of the dye to tubulin heterodimers, about 1.0) in 80 mM PIPES (piperazine-1,4-bis(2-ethanesulfonic acid), pH 6.8), 1 mM EGTA, 5 mM $MgCl_2$, 1 mM GTP, and 36% glycerol at 37°C for 30 min. Microtubules thus prepared were stabilized with 10 μM taxol (T-1912, Sigma, St. Louis, MO).

Flow Chamber for Microtubule Gliding Assay and TPM

To make a heat source for TPM, aluminum was evaporated on a coverslip according to the following procedure [Kato et al., 1999; Yasuda et al., 2000]. First, a coverslip was cleaned by washing in 0.1 M KOH and then 100% ethanol. The cleaned surface was coated with photoresist (OFPR-800, Tokyo Ohka Kogyo Co. LTD., Kanagawa, Japan). The circular-shaped patterns were printed on the surface by irradiating UV light through a circular-shaped mask (diameter, 10 μm). The resist film was developed with NMD-3 (Tokyo Ohka Kogyo Co. LTD), and the irradiated area was removed. Then, the surface was coated with aluminum by vacuum evaporation. The aluminum protected by remaining resist was removed with exfoliation solution of resist. The coverslips thus obtained were then rinsed with distilled water.

Solution containing either 70 μg/ml (high density) or 50 ng/ml (low density) kinesin molecules was introduced into a flow chamber and incubated for 1 min to allow attachment of kinesin to the glass surface of the chamber. The chamber was washed two times with an assay buffer containing 2 mM $MgCl_2$, 80 mM PIPES (pH 6.8), 1 mM EGTA, and 0.7 mg/ml filtered casein (073-19, Nacalai Tesque, Kyoto, Japan) for 2 min each to coat the glass surface with casein and to remove free kinesin molecules. The solution containing fluorescent microtubules was then introduced into a flow chamber and incubated for 2 min to allow binding to kinesin molecules in the nucleotide-free state. The chamber was then filled with the assay buffer containing 1 mM ATP (127531, Boehringer Mannheim, Mannheim, Germany) and an enzymatic oxygen scavenging system (4.5 mg/ml glucose, 0.22 mg/ml glucose oxidase [G-2133, Sigma], 0.034 mg/ml catalase [C-10, Sigma], 10 mM dithiothreitol [DTT]), and sealed with enamel. Other chemicals were of reagent grade.

Temperature Pulse Microscopy (TPM)

Local heating was achieved by illuminating a thin aluminum layer circularly evaporated on a coverslip, 10 μm in diameter, with an infrared laser beam (1W Nd:YLF laser, 1053–1000p: λ = 1.053 μm; Amoco Laser, IL). The temperature of the microtubule was estimated from the degree of thermal quenching of the fluorescence of tetramethylrhodamine labeled with microtubules. The fluorescence images were taken with a CCD camera (CCD-72; Dage MTI, IN) connected to an image intensifier (KS1381; Video Scope International, Washington, DC) at the video rate of 30 frames/s. The decay lag of this camera system was within one frame (33 ms). According to Kato et al. [1999], the fluorescence intensity at each pixel of the image of labeled microtubule at T°C was divided by that at 20°C (reference temperature) to yield the intensity ratio (r) [Kinosita et al., 1991]. Room temperature was maintained at 20 ± 1°C. We obtained the relation $r = 1\text{-}\alpha(T\text{-}T_0)$, where α and T_0 were, respectively, 0.017°C^{-1} and 20°C (Fig. 1).

RESULTS

Effect of Temperature Pulse on Gliding Velocity of Microtubules

In order to investigate the interaction between kinesin and microtubules at higher than 35°C, we applied

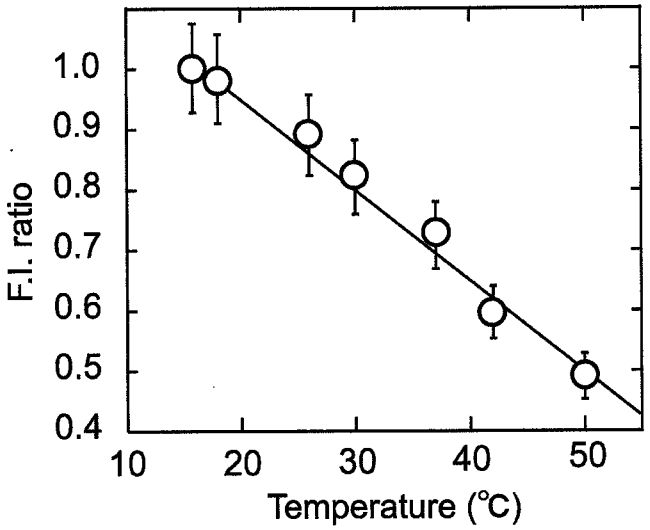

Fig. 1. Relation between fluorescence intensity and temperature. According to Kato et al. [1999], the fluorescence intensity of labeled microtubule at T°C was normalized with respect to that at 20°C (reference temperature) to yield the intensity ratio (r) in every pixel [Kinosita et al., 1991]. Temperature dependence of r was examined on the microscope stage of which temperature was controlled with the use of a thermal insulation chamber, which took about 45 min for stabilization. The reference (room) temperature was maintained at 20 ± 1°C. The data obtained were expressed by the linear relationship, $r=1-\alpha(T-T_0)$, where α and T_0 were, respectively, 0.017°C^{-1} and 20°C.

the TPM [Kato et al., 1999] to the microtubule gliding assay. We examined two densities of kinesin molecules, i.e., high (70 μg/ml) and low (50 ng/ml). At the low density, it was estimated that only one kinesin molecule could interact with each microtubule, such that the pivoting movement of microtubule could be observed [Howard et al., 1989]. The TPM method could thermally activate the motor function beyond the denaturation temperature determined at thermal equilibrium.

First, we examined the effects of temperature gradient on the gliding movement of a long microtubule (10 μm long) at a high density of kinesin. When the temperature of the front portion of a gliding microtubule was higher, the microtubule was straightened and gliding movement appeared to be smooth. However, when the temperature of the rear portion was higher (Fig. 2a), several bucklings were observed at the middle portion of microtubule. This implies that the kinesin motors working at the rear portion produced sufficient force to buckle a portion of microtubule 3μm long (Fig. 2b).

Then, we observed reversible acceleration and deceleration of gliding movement of the microtubule by repetitive application of temperature pulses (every two to several seconds) at high density of kinesin molecules. As shown in Figure 3a, gliding velocities reversibly reached two steady values within 1/30 s after the temperature change: the average velocities were 0.48, 3.65, 0.44, 2.71, 0.33, and 2.24 μm/s, respectively, at 20°, 50°, 22°, 50°, 18°, and 53°C. Here, the local temperature was estimated from the average fluorescence intensity of the gliding microtubule according to the relation, $r(T)$, described above (Fig. 3b). (Note that the coverslip temperature was maintained at 20 ± 1°C.) These data showed that the velocity of the microtubule was gradually decreased by repetitive thermal activation, suggesting that the thermally damaged kinesin molecules may have acted as an internal load for smooth movement of the microtubule. (We could not detect any photo-damage of gliding velocity during observation.) Thus, we considered that only the velocity initially obtained, 0.48 μm/s at 20°C and 3.65 μm/s at 50°C, represented a correct value at each temperature.

Second, we examined the gliding movement at a single molecular level (the low density of kinesin molecules). Before applying temperature pulse, the microtubules showing the pivoting movement were chosen at 20°C. When illuminated with a laser pulse with a duration of about 2 s, an abrupt displacement of the microtubule, by as much as 7.3 μm, occurred, corresponding to the gliding velocity of about 3.68 μm/s (Fig. 4). The average temperature during this 2-s illumination was estimated to be about 50°C. The gliding velocity obtained here (3.68 μm/s at 50°C) is the highest ever reported for single brain kinesin molecules in a normal in vitro motility assay. We confirmed that the gliding velocity obtained by the second temperature pulse was indistinguishable from that obtained by the first one within the experimental error (data not shown), although we succeeded with repetition of temperature pulses on the same *single* kinesin molecules only twice, partly because of the limited length (<10 μm) of microtubules and partly because of the thermal denaturation of proteins during the first temperature pulse. As pointed out by Howard et al. [1989], we found that the velocity was independent of the density of kinesin molecules, even at 50°C (compare 3.65 μm/s in Fig. 3 and 3.68 μm/s in Fig. 4).

Figure 5 summarizes the temperature dependence of gliding velocity of microtubules in the single-molecular assay between 15° and 50°C together with that in the multi-molecular assay between 40° and 50°C. The data shown by the filled circles in Figure 5 between 15° and 35°C were taken from those previously obtained by a single-molecular bead assay [Kawaguchi and Ishiwata, 2000b]. Interestingly, the result was represented by a single exponential curve against the inverse of absolute temperature (Fig. 5a), such that there were no breaks between 15° and 50°C with a unique activation energy of about 50 kJ/mol (Fig. 5b).

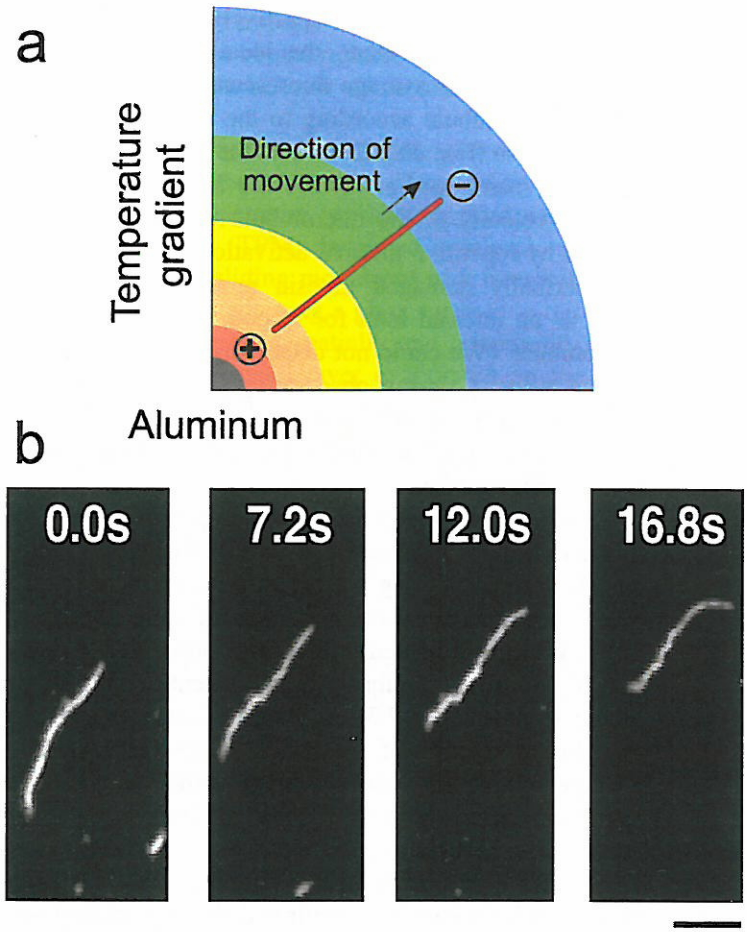

Fig. 2. Imaging of gliding microtubule under temperature gradient created by TPM. **a:** Schematic illustration of TPM system. The circularly aluminum-evaporated surface (10 μm in diameter) was illuminated by focused infrared laser light used for optical tweezers, so that the aluminum became a local heat source, creating concentric temperature gradient around the circle. Gliding movement of microtubule occurred at velocities depending on environmental temperatures. **b:** Effects of temperature gradient on a gliding microtubule (10 μm long). For this experiment, the glass cover was coated with 70 μg/ml kinesin, implying that this experiment was a multi-molecular assay. Bar = 5 μm.

DISCUSSION

Thermal Activation of Kinesins Using TPM

It has been known that the gliding velocity of microtubules interacting with kinesin molecules increases with an increase in temperature [Mazümdar and Cross, 1998; Böhm et al., 2000]. However, this property had not yet been examined by single molecular experiments until recently. In our previous study [Kawaguchi and Ishiwata, 2000b], we examined the temperature effect on single kinesin molecules using a single-molecular bead assay under an optical microscope between 15° and 35°C. In that report, we showed that the gliding velocity increased with the Arrhenius activation energy of 50 kJ/mol, consistent with the temperature dependence of ATPase activity, whereas the generated force was independent of temperature in the above temperature range, 7.34 ± 0.33 pN (n = 70) (Note that this was also the case in the actomyosin complexes) [Kawai et al., 2000]. However, we could not obtain reliable data above 35°C, probably because kinesin was denatured by incubation for 1 min, which was required for obtaining steady temperature in an insulation chamber.

In order to investigate the interaction between kinesin and microtubules at higher temperatures, especially around 40°C (physiological temperature), we applied the TPM described previously [Kato et al., 1999]. In our TPM, it is expected that the motor functions can be thermally activated even at temperatures higher than the denaturation temperature at equilibrium if the duration of the thermal activation is short enough. The gliding velocity thus obtained (Fig. 4) was the highest ever reported for single brain kinesin molecules in a normal in vitro motility assay. It is to be noted that the gliding velocity gradually decreased after each temperature pulse in a multi-molecular assay (Fig. 3), whereas, in a single-molecular assay (Fig. 4), it was kept unchanged, as far as the movement continued. The single-molecular experiments (Fig. 4) suggest that the thermal denaturation of motor function occurs in an all-or-none fashion.

For comparison, we confirmed that thermostatic regulation of the whole stage of microscope at 50°C resulted in the average gliding velocity of microtubules of 2.0 ± 0.1 (n = 7) μm/s at 70 μg/ml kinesin molecules (data not shown), about half of that obtained by TPM

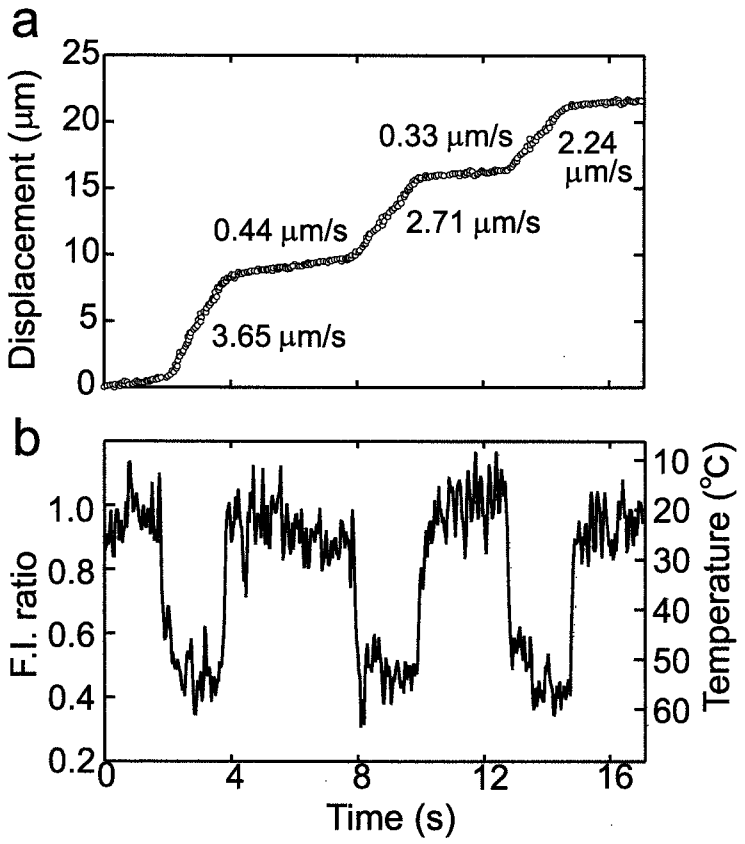

Fig. 3. Time course showing reversible change in the gliding movement of a microtubule with repetitive temperature pulses. **a:** Displacement of the centroid of the fluorescence intensity distribution of microtubule (1.0 μm long) is shown every 1/30 s. **b:** Temperature was estimated by averaging the fluorescence intensity of the image (every 1/30 s) of the microtubule. The temperature of coverslip was kept at 20 ± 1°C. For this experiment, 70 μg/ml kinesin was infused into a cell to perform a multi-molecular assay.

under the same conditions, consistent with the velocity obtained after applying several temperature pulses (see Fig. 3). The gliding motion of microtubules continued at least for 20 min at 50°C in spite of lowered gliding velocity. After incubation for 30 min at 50°C, few gliding microtubules were observed because of the detachment of microtubules from kinesin molecules as reported by Böhm et al. [2000], implying that almost all kinesin (and/or tubulin) molecules were denatured. On the other hand, in an actomyosin motility system, the sliding actin filaments tended to detach from the glass surface, on which heavy meromyosin molecules were adsorbed, within 1 min at 50°C [Kato et al., 1999]. This observation suggests that kinesin-microtubule complexes are more stable than actomyosin complexes against high temperature.

The temperature (T) dependence of gliding velocities (v) from 15° up to 50°C was expressed by a single Arrhenius equation, $v(T) = v_0 exp(-E_a/RT)$, where v_0 is a constant, E_a is an activation energy, and R is the gas constant. In this temperature range, the activation energy turned out to be 50 kJ/mol. Recently, Böhm et al. [2000] reported that the Arrhenius plot of microtubule gliding velocity revealed a break at 27°C, resulting in the activation energies of 65 kJ/mol for < 27°C and 9 kJ/mol for > 27°C. They concluded that the break in the Arrhenius plot results from conformational changes of kinesin and/or microtubule detected by circular dichroism [De Cuevas et al., 1992]. On the contrary, our data showed no break at around 27°C (Fig. 5). As the experiment by Böhm et al. [2000] was not a single-molecular assay but a multi-molecular one, we previously suggested that kinesin molecules that are thermally damaged due to prolonged incubation at high temperatures might have acted as an internal load for the movement of microtubules [Kawaguchi and Ishiwata, 2000b]. This suggestion was confirmed in the present study over the broader temperature range.

In the actomyosin motility system, Kato et al. [1999] reported that the two activation energies, i.e., 100 kJ/mol between 18° and 30°C and 50 kJ/mol between 30° and 45°C, exist in a multi-molecular assay [see also, Kawai et al., 2000]. If the single molecular assay can be performed for actomyosin at various temperatures by using TPM, the unique activation energy might be obtained. Further investigation is needed regarding the actomyosin system.

Temperature Effect on Processivity

In a previous report [Kawaguchi and Ishiwata, 2000b], we showed that the average run length monotonously increased on increasing temperature from 15° to

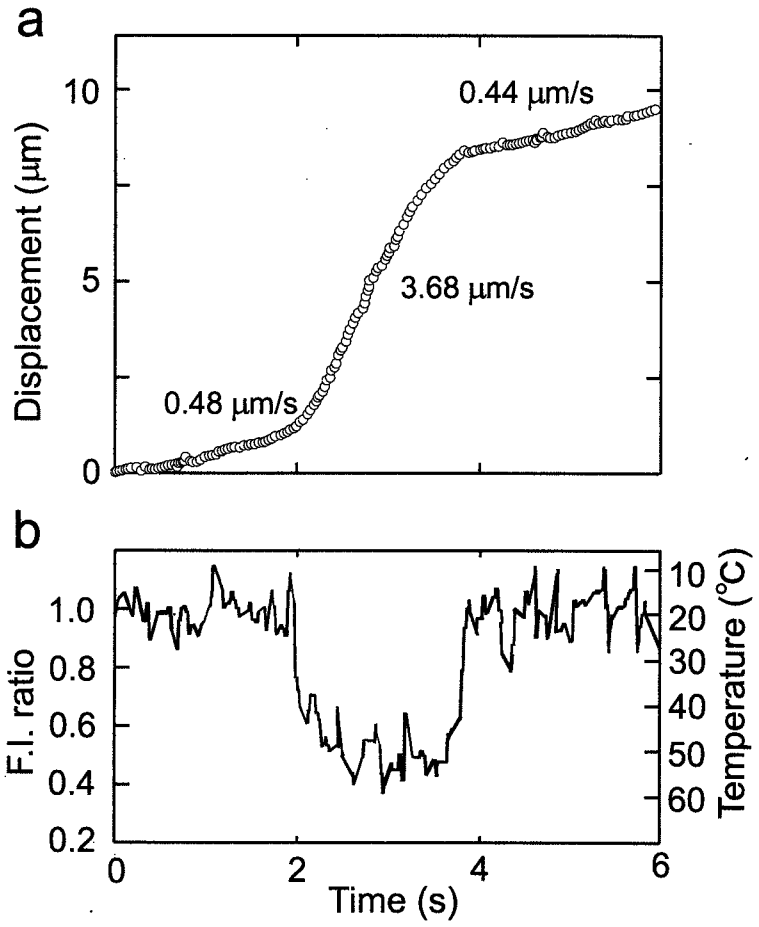

Fig. 4. Time course showing reversible change in the gliding movement of a microtubule on a single kinesin molecule with a single temperature pulse. **a:** Time course of gliding movement of microtubule. Displacement of the tip end of the microtubule (8.4 μm long) is shown every 1/30 s. **b:** Temperature was estimated by averaging the fluorescence intensity of the image (every 1/30 s) of the microtubule. The coverslip temperature was kept at 20 ± 1°C. For this experiment, 50 ng/ml kinesin was infused into a cell to perform a single-molecular assay.

35°C. Although the amount of data was not large enough to confirm the exponential distribution of run length [Block et al., 1990; Vale et al., 1996], we found in the present study that the average run length at around 50°C was approximately 9 ± 2 μm (e.g., Fig.4), 1.8 times longer than that (5 μm) at 20°C. This temperature dependence of run length is consistent with the previous one obtained in a single-molecular bead assay [Kawaguchi and Ishiwata, 2000b] except that the absolute value of run length obtained by the gliding assay was longer than that obtained by the bead assay. As pointed out by Block et al. [1990], the reason why the run length in the gliding assay (5 μm) [Howard et al., 1989] was longer than that in the bead assay (1.4 μm) at room temperature may be that the diffusion coefficient of a microtubule is smaller than that of a bead, so that rebinding of microtubule with kinesin preferably occurs in the gliding assay, apparently resulting in the longer run length [Kawaguchi and Ishiwata, 2000b].

The run length is considered to be proportional to the number of consecutive steps of kinesin along a microtubule. On increasing temperature, the rate limiting step(s) in the ATPase cycle is accelerated, so that the gliding velocity (stepping rate) coupled with the ATPase activity is also accelerated. Then, why was the ratio of run length at 20°C and 50°C only two, in contrast to seven in the gliding velocity (see Fig. 5a)? The run length must be determined by the stepping rate times the lifetime of attached state (probably, the lifetime of a single-headed binding state) of kinesin on the microtubule. Thus, the reason why the temperature dependence of run length is relatively small may be that the lifetime of the attached state decreases on increasing temperature. The temperature dependence of the lifetime of each nucleotide state of kinesin interacting with a microtubule, which is either in the single- or double-headed binding state, must be examined in the future.

CONCLUSION

Using temperature pulse microscopy (TPM), we have examined the gliding velocity at between 15° and 50°C of microtubules interacting with single or multiple kinesin molecules. The corresponding Arrhenius plot showed no breaks, with a unique activation energy (50

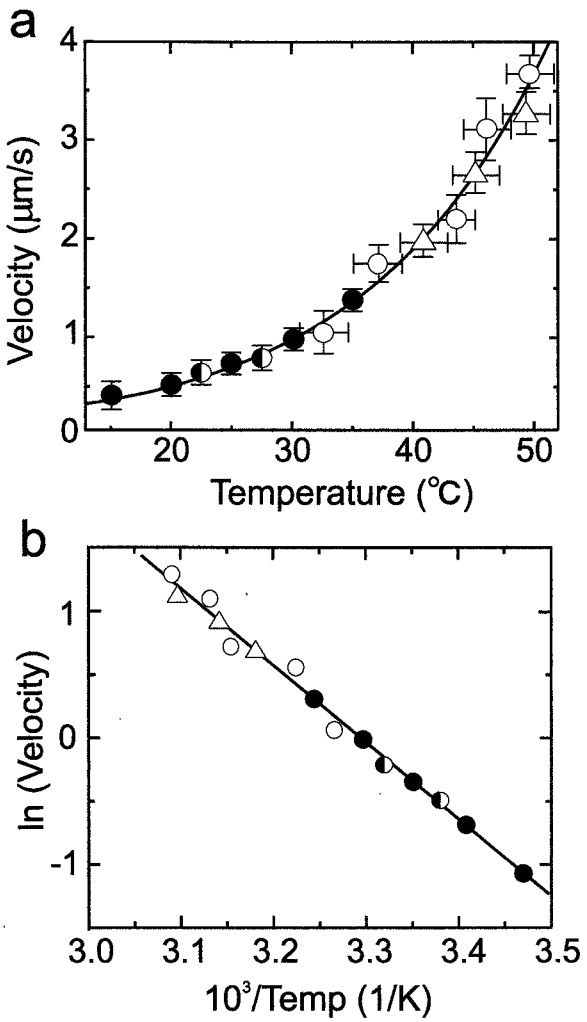

Fig. 5. Temperature dependence of gliding velocity of kinesin molecules. **a:** Gliding velocity vs. temperature. The data from 15° to 35°C (*closed circles*) were taken from the results of single kinesin-coated beads reported previously [Kawaguchi and Ishiwata, 2000b]. The data shown by *half-filled circles* at 22.5° and 27.5°C were taken from those obtained by using a temperature insulation chamber as reported previously [Kawaguchi and Ishiwata, 2000b], and from the pivoting movement of microtubules on single kinesin molecules. The data above 32.5°C were taken from the present results obtained by the single-molecular (*open circles*) and the multi-molecular (*triangles*) assays. The data obtained by the multi-molecular assay were taken only from those at the first temperature pulse because the velocity gradually decreased upon repetitive temperature pulses (Fig. 3). The error bars are standard deviations obtained from 4–6 data. b: Arrhenius plot of a. The error bars are omitted.

kJ/mol), suggesting a common molecular mechanism of kinesin motility over the broad temperature range.

ACKNOWLEDGMENTS

This research was partly supported by the Ministry of Education, Science, Sports, and Culture of Japan (Scientific Research on Priority Areas and the High-Tech Research Center Project).

REFFERENCES

Block SM, Goldstein LSB, Schnapp BJ. 1990. Bead movement by single kinesin molecules studied with optical tweezers. Nature (Lond) 348:348–352.

Böhm KJ, Stracke R, Baum M, Zieren M, Unger E. 2000. Effect of temperature on kinesin-driven microtubule gliding and kinesin ATPase activity. FEBS Lett 466:59–62.

De Cuevas M, Tao T, Goldstein LSB. 1992. Evidence that the stalk of *Drosophila* kinesin heavy chain is an α-helical coiled coil. J Cell Biol 116:957–965.

Hirokawa N. 1998. Kinesin and dynein superfamily proteins and mechanism of organelle transport. Science 279:519–526.

Howard J. 1996. The movement of kinesin along microtubules. Annu Rev Physiol 58:703–729.

Howard J, Hudspeth AJ, Vale RD. 1989. Movement of microtubules by single kinesin molecules. Nature (Lond) 342:154–158.

Hyman A, Drechsel D, Kellogg D, Salser S, Sawin K, Steffen P, Wordeman L, Mitchison T. 1991. Preparation of modified tubulins. Methods Enzymol 196:478–485.

Kato H, Nishizaka T, Iga T, Kinosita KJr, Ishiwata S. 1999. Imaging of thermal activation of actomyosin motors. Proc Natl Acad Sci USA 96:9602–9606.

Kawai M, Kawaguchi K, Saito M, Ishiwata S. 2000. Temperature change does not affect force between single actin filaments and HMM from rabbit muscles. Biophys J 78:3112–3119.

Kawaguchi K, Ishiwata S. 2000a. Effect of temperature on force generation and velocity of single kinesin molecule. Biophys J 78:122A (Abstract).

Kawaguchi K, Ishiwata S. 2000b. Temperature dependence of force, velocity and processivity of single kinesin molecules. Biochem Biophys Res Commun 272:895–899.

Kawaguchi K, Ishiwata S. 2001. Nucleotide-dependent single- to double-headed binding of kinesin. Science 291:667–669.

Kinosita K Jr, Ito H, Ishiwata S, Hirano K, Nishizaka T, Hayakawa T. 1991. Dual-view microscopy with a single camera: real-time imaging of molecular orientations and calcium. J Cell Biol 115:67–73.

Kojima H, Muto E, Higuchi H, Yanagida T. 1997. Mechanics of single kinesin molecules measured by optical trapping nanometry. Biophys J 73:2012–2022.

Mazümdar M, Cross RA. 1998. Engineering a lever into the kinesin neck. J Biol Chem 273:29352–29359.

Vale RD. 1999. Kinesin, conventional. In: Kreis TE, Vale RD, editors. Guidebook to the cytoskeletal and motor proteins, 2nd ed. Oxford: Oxford University Press. p 398–402.

Vale RD, Reese TS, Sheetz MP. 1985. Identification of a novel force-generation protein, kinesin, involved in microtubule-based motility. Cell 42:39–50.

Vale RD, Funatsu T, Pierce DW, Romberg L, Harada Y, Yanagida T. 1996. Direct observation of single kinesin molecules moving along microtubules. Nature (Lond) 380:451–453.

Yasuda K, Okano K, Ishiwata S. 2000. Focal extraction of surface-bound DNA from a microchip using photo-thermal denaturation. Biotechniques 28:1006–1011.

論　文

DNAプローブアレイを用いたDNA断片回収

正　員　岡野和宣（日立製作所）　非会員　陳　　鋼（日立製作所）
非会員　小原賢信（日立製作所）　正　員　梶山智晴（日立製作所）
非会員　安田賢二（東京大学　）　非会員　石渡信一（早稲田大学）

Recovery of DNA Fragment from a DNA Probe Array

Kazunori Okano, Member (Hitachi, Ltd)　Gang Chen, Non-member (Hitachi, Ltd)
Yoshinobu Kohara, Non-member (Hitachi, Ltd)　Tomoharu Kajiyama, Member (Hitachi, Ltd)
Kenji Yasuda, Non-member (the University of Tokyo)　Shin'ichi Ishiwata, Non-member (Waseda University)

Molecular biology is moving rapidly towards the stage of functional genomics in which rapid preparations of expressed messages (mRNA) will be required. If a DNA library is constructed on a solid support (DNA probe array) and any kind of expressed messages can be individually recovered from the probe array, DNA probe array will become a very useful method. Consequently, we developed a DNA preparation method using a DNA probe array that utilizes photo-thermal denaturation to recover specific DNA. The protocol for preparing DNA probe array was investigated to realize the stable immobilization of DNA probes on the surface of solid support. We used a glass plate coated with Cr (5-10 nm thick). The Cr surface was modified with 3-glysidoxypropyltrimethoxysilane to introduce active residues that can couple with amino residues at the 5' termini of DNA probes. The Cr surface acts as a photo-thermal transducer. The preparation method of DNA uses infrared (1053-nm) laser irradiation to thermally denature and release DNA immobilized in a specific area of a DNA probe array. Different DNA fragments fixed in place on the DNA probe array could be separately recovered. There were enough quantities of recovered DNA that can be amplified by using PCR.

キーワード：DNAプローブアレイ，レーザー，光熱変換法，PCR

Keywords: DNA probe array, laser, photo-thermal denaturation method, Polymerase Chain Reaction (PCR)

1．　はじめに

生命現象は多種類（ヒトでは約10万種）の遺伝子が相互に働きを調節し合って成立している。ゲノム計画[1-4]により，いろいろな生物のゲノム配列を解明することができる現在では，ゲノム配列の微細な変異が生体に与える影響や，生体機能を遺伝子の発現の総体として捕えることが重要な課題となっている[5]。多種類の遺伝子の量を同時に測定できる方法としてガラス基板表面に多種類のDNAプローブを種類毎に区画して並べたDNAプローブアレイが開発され，遺伝子発現解析に有効であることが示されている[6-7]。DNAプローブアレイの限界の一つは，遺伝子スーパーファミリー[8]やオルタナティブスプライシングのような類似配列を持つ遺伝子を分離検出することが困難な点にある[9]。実際に生体内の遺伝子発現をモニターし，遺伝子間の制御機能を調べるには，類似配列を持つ遺伝子でも分離して計測することが必要である。解決策としては，DNAプローブアレイ上の各プローブスポットにおけるハイブリダイゼーション温度を精密にコントロールすることで微妙な配列の違いを検出する試み[10]や，チップ上に捕捉した類似遺伝子

群を基板から回収し，他の分析手法で解析する方法[11-16]が提案されている。チップ上に捕捉した発現遺伝子群をマルチキャピラリーアレイ電気泳動装置で直接分析すれば，手間をかけずに個々の発現遺伝子の量を正確に知ることができると考えている。一般的なマルチキャピラリーアレイ電気泳動装置の検出感度は0.05～0.5 amol／バンドである[17]。これに対し，DNAプローブアレイの各スポットにハイブリダイズすることのできるDNA量は0.01 amol／μm^2なので[11]，0.1 mm径のスポットには最大75 amolの発現遺伝子をトラップできることになる。感度面で見る限り，実用的な分析が可能と考えられる。この原理に基づきDNAプローブアレイにハイブリダイズしたDNAをキャピラリーに電界注入して解析する一連の特許[13-16]が米国で成立しているので，実際にデバイス化されることが期待される。このためには，DNAプローブアレイの個々のプローブスポットにハイブリダイズしたDNAを遊離させる必要がある。

筆者らはレーザーで微小領域を過熱変性して各スポット上のDNA断片を回収する方法を報告してきた(図1)[11-12]。この方法に用いるDNAプローブアレイデバイスは，透明なガラス基板上に5-10 nm厚の光－熱変換層を持っている。

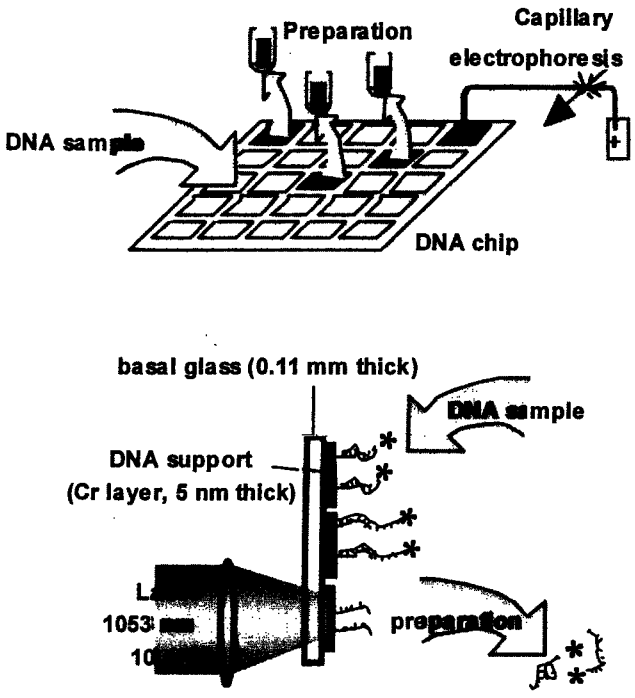

図1　分取用DNAマイクロアレイの概念

Fig. 1. Schematic illustration of preparative DNA probe array. The recovered DNA fragments can be used for the template of PCR and cloning.

DNAプローブはクロム表面に直接化学結合で強固に固定されている。回収したい配列のDNAプローブを固定したスポットにレーザーを当てると，クロム層がレーザー光を吸収して熱に変換する。レーザーは10 μmに絞られているので，特定のプローブスポットのみを過熱することができる。こうして特定プローブ上の発現遺伝子群のみを熱変性し溶液中に回収することができる。ここで問題となるのが，DNAプローブの固定法である。本報告では，光－熱変換層に用いる金属とプローブの固定法について検討し，実際にDNAを回収した結果について報告する。

2．　DNAプローブアレイの作成法

本研究のDNAプローブアレイは，光－熱変換層として金属蒸着面を持ち，その上にDNAプローブを固定した構造となっている。このため，1) 金属蒸着面が安定で，経時的に変化しない，2)均質で高密度のDNAプローブを固定できる，3)固定したDNAプローブが試料とのハイブリダイゼーションや洗浄操作で剥離しない，4) 光吸収によって局所発熱源として使用できる，5) 蛍光顕微鏡やレーザースキャナーで観測できるように半透明であるとの条件を満たす必要がある。光吸収体に金属を用いたのは，シランカップリング反応でDNAプローブを容易に固定できるからである。利用できるシランカップリング反応とそれに続くDNAプローブの固定法の一覧を図2に示す。

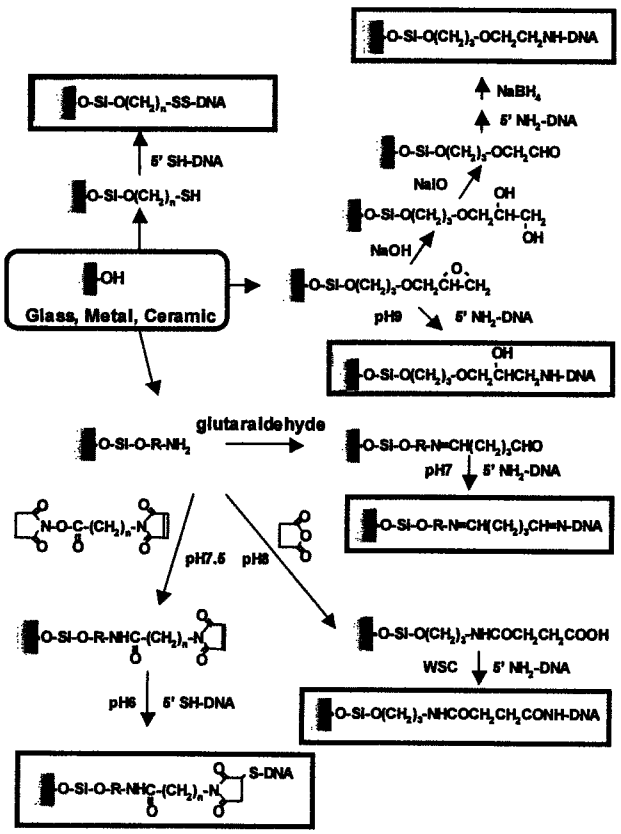

図2　無機質表面へのDNA固定

Fig. 2. Immobilization of DNA probe on the surface of inorganic materials.

一般的にハイブリダイゼーション反応においては，プローブDNA鎖の空間的な自由度を確保する必要があり，DNAプローブの末端を利用して固定する方がハイブリダイゼーシ

ョン反応において有利と考えられる。DNA プローブの 5' 末端に導入できる残基としては，アミノ基とスルフィッド基とリン酸基が一般的である。基板側に導入できる反応残基としては，アミノ基，スルフィッド基，グリシドキシ基（エポキシ基）がありうる。本報告では，3-グリシドキシプロピルトリメトキシシランを用いてアミノ基と反応するグリシドキシ基を基板表面に導入し，5' 末端をアミノ化した DNA をプローブとして固定した。グリシドキシ基とアミノ基の反応で得られる結合は安定な部類にはいる。

実際に，クロムとアルミニウムを 5 nm 厚に蒸着した基板にプローブ DNA を固定した結果について述べる。DNA プローブアレイでは，ハイブリダイゼーション反応における 95℃でのプローブと試料 DNA の変性と，室温から 55℃でのアニーリングの行程の間に，金属蒸着表面に固定したプローブが脱離しないことが条件となる。また，pH 条件や試料 DNA に含まれる化学物質に対して安定であることが必要である。クロムとアルミニウムを蒸着した基板で比較した結果，クロムでは安定に DNA プローブを固定することができた（図 3）。アルミニウムはハイブリダイゼーション溶液で溶解してしまうため，DNA プローブを固定することができなかった。

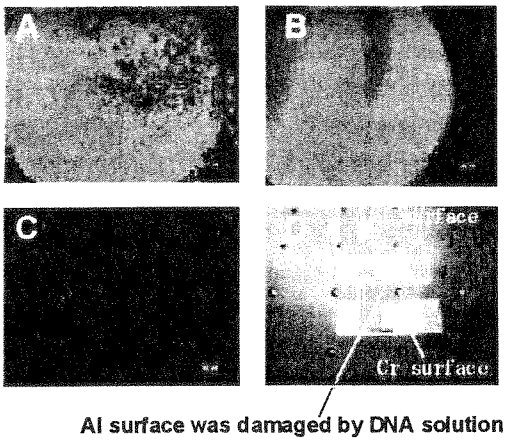

図 3　DNA 固定における金属材質の影響

Fig. 3. Surface effect of (A) glass plate, (B) chromium coated glass, and (C) aluminum coated glass on an immobilization of DNA. Each surface was treated with 3-glysidoxypropyltrimethoxysilane. The DNA having an amino residue at 5' terminus and a fluorophore at 3' terminus was coupled with glysidoxy residue on the surface of plate. Photographs (A), (B), and (C) were fluorescence images. Photograph (D) was a phase-contrast image of the chromium-coated glass and the aluminum coated glass. The aluminum was detached from the glass surface into buffer solution, whereas the chromium was remained.

クロム蒸着面に対する DNA プローブ固定反応の pH 依存性を図 4 に示す。グリシドキシ基とアミノ基の反応ではアミノ基の電子対がグリシドキシ基の炭素を攻撃することによるので，pH8.5～9 で良好な結果が得られた。pH=9.5～10 ではグリシドキシ基の加水分解が支配的になる。　以上の結果から，DNA プローブアレイの作成プロトコールを以下のように決定した。

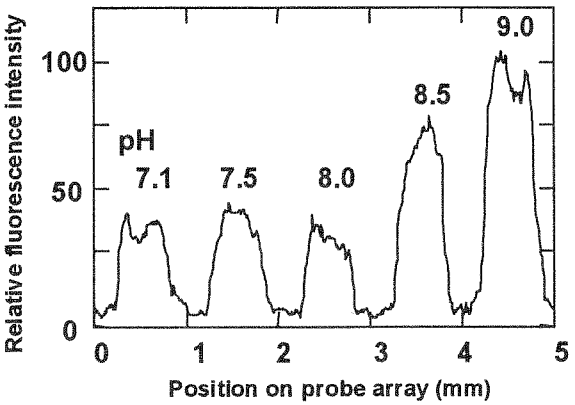

図 4　プローブ DNA 固定の pH 依存性

Fig. 4. Effect of pH on immobilization reaction of probe DNA on the surface of Cr-coated glass plate. A 10 μM of single stranded DNA (20 mer) having an amino residue at 5' terminus and a fluorophore at 3' terminus was coupled with glysidoxy residue on the surface of plate. The fluorescence intensity profile of the DNA immobilized plate was measured by scanning fluorescence microscope. The pH conditions were indicated in the figure.

1）DNA プローブ固定用基板の作成

①スライドガラス基板（24×60 mm）を 1 M の KOH で 10 分間超音波洗浄した後，超純水で十分に洗い，150℃で乾燥させる。

②クロムを 5～10 nm になるようにガラス表面に蒸着し，DNA プローブ固定用の基板とする。

③クロム蒸着した基板を 1%の 3-グリシドキシプロピルトリメトキシシランと酸触媒である 0.02%酢酸を含む 80%エタノール水溶液に 25 分間浸漬し，続いて反応を完結するために 5 分間超音波をかける。

④純水とエタノールで洗浄した後，120℃で 30 分間過熱する。

⑤直径 8 mm の穴をあけた厚さ 0.4 mm の半導体用発砲体両面テープ（東映工業）を表面に貼りつけてハイブリダイゼーション反応部を形成する。

2）DNA プローブの固定

①終濃度として 1×10^{-5} M の種々 DNA プローブを含む 7.5%グリセリン（乾燥防止用）と 0.15 M NaCl を含

む0.05 M ホウ酸緩衝液（pH8.5）30 nl をカルテシアン社のソレノイドバルブ式インクジェットアレイヤ（QUAD PixSys, Cartesian Technologies, USA）で1 mm間隔に滴下する。

②水をふくむガーゼを敷いた加湿チャンバ中で 25℃の条件で2時間放置する。

③未反応のグリシドキシ基をブロックし，過剰のDNAプローブを除去するために，10 mMのLysと0.01%のSDSと0.15 M NaClを含む0.05 M ホウ酸緩衝液（pH8.0）で5分間以上かけて洗浄する。続いて水洗しエアーブローで洗浄液を除去する。

④0.01%のSDSと0.3 M NaClを含む30 mM クエン酸ナトリウム緩衝液（2×SSC, pH7.0, 60℃）で洗浄し，非特異吸着したDNAプローブを除く。

3）ハイブリダイゼーション反応

①試料DNA溶液（条件検討には $2\sim50\times10^{-8}$ M を使用，0.01%のSDSと0.75 M NaClを含む75 mMクエン酸ナトリウム緩衝液（5×SSC, pH7）に溶解）20 μl をハイブリダイゼーション反応部にみたし，乾燥防止のためポリカーボネートフィルムでカバーする。

②95℃で30秒間加熱し，プローブと試料DNAを変性させる。

③45℃で30分間アニールさせ，DNAプローブアレイ上のプローブと試料DNAをハイブリダイズさせる。この行程は必要に応じ10分間から8時間の範囲で行う。

④未反応の試料DNAを0.01%のSDSを含む2×SSC pH7で洗浄して除く。

3．DNAプローブアレイ表面からのDNAの回収

作成したDNAプローブアレイを図5に示す。ここでは，観察を容易にするためにプローブ相補鎖DNAの5'末端にスルホローダミン101を標識してある。溶離回収液として2 mMのEDTAを含む20 mM Tris-HCl緩衝液（pH7.4）20 μlをチャンバー（8 mmφ×0.4 mm）に満たし，特定スポットに連続発振のYLFレーザー(1053 nm)を照射し熱変性させた。レーザーパワーは基板面で10 mWと高出力であるため，レーザー照射時にプローブアレイ表面から蛍光体が拡散する様子と，表面の蛍光が無くなるのが観測された。また，時々レーザー照射部から気泡が発生した。蛍光消失が起きるのは約10 μmの範囲であるので，この範囲でDNA変性温度（Tm）以上に溶液温度が上昇したと考えられる。レーザー径に対し，DNAプローブ固定範囲の方が広いので，レーザーをスキャンしてスポット全体を加熱した。レーザー照射した部分からの蛍光が観察されなかったことから，2本鎖DNAが熱変性してスルホローダミン101で標識した相補鎖DNAが溶離液中に拡散したと考えられる。このとき，隣接するDNAスポットに変化はなかった。

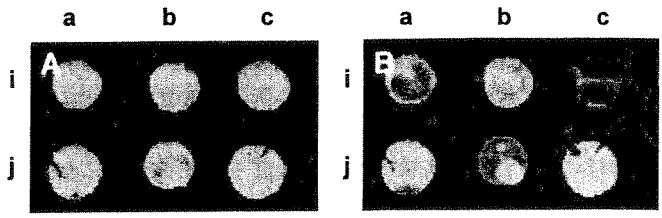

図5 DNAプローブアレイからのDNA回収

Fig. 5. Recovery of a DNA from a DNA probe array. Different DNA fragments were fixed in place on the DNA probe array. Photographs were the fluorescence images of the probe array surface before (photo A) and after (photo B) laser irradiation. The top of right spot (area i-c) was heated by 10 mW YLF laser (1053 nm).

回収した溶液は10～16 μlであった。回収液中のDNAをPCR増幅して，電気泳動を用いてDNAのサイズと純度を確かめた（図6）。PCRは擬陽性増幅を少なくするため，ホットスタート法を用いた(プラチナPCRスーパーミックス，GIBCO)。回収した溶液2 μlを25 μlスケールでPCR増幅した。反応サイクルは熱変性94℃30秒間，アニール62℃30秒間，ポリメラーゼ反応72℃60秒間のサイクルが35回であった。回収したDNAのサイズのメインピークは，各スポットに固定したDNAのサイズと一致していた。この結果は，クロム蒸着基板を用いたDNAプローブアレイの各スポットにレーザーを当てることでDNAの回収が実際にうまくいくことを示している。いくつかの擬陽性増幅産物由来のピークが観察されるため，メインピークの割合は60～67%であった。擬陽性増幅産物のうちa', b', c'はメインピークのDNAサイズと一致することから，隣接するスポットからのコンタミネーションと考えられる。ピークxとyはDNA固定試料中に増幅されるべきサイズのDNAが無いので，PCR時のプライマーミスマッチに由来する擬陽性産物と考えられる。近傍のスポットからの漏れこみに関しては，スポット間距離の最適化や，各スポット間の熱の伝達を防止する工夫をすることにより低減できると考えている。

4．まとめ

本報告では，クロム金属蒸着面をもつ半透明基板にDNAプローブを固定するプロトコールと，作成したDNAプローブアレイ表面に捕捉したDNAを利用する方法について述べた。クロム蒸着面を光—熱変換器として利用したが，電気伝導性のクロムは電極としても利用することができる。電極を持つDNAプローブアレイとしては，ナノジェン社が開発中の物が有名である[18]。報告によれば，電極表面に高分子の拡散層を設け，その表面にDNAプローブを固定した構造をしている。DNAはリン酸ジエステル結合でヌクレオチドが多数つながった構造をしているので，中性付近の水溶液中ではマイナスに荷電している。このため，DNAプロ

ーブアレイの表面電極をプラスに荷電させることでプローブスポット近傍に試料DNAを濃縮することができる。この技術は，固体表面でのハイブリダイゼーション速度を格段に早くすることができる。電極によるDNAハンドリングとレーザー照射による加熱を組み合わせることで，任意の発現遺伝子を分取することができるようになり，遺伝子発現の機能解析への利用が期待できる。

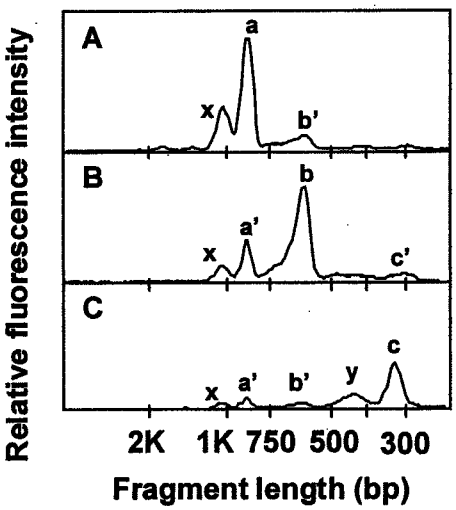

図6 DNAプローブアレイから回収したDNA断片の電気泳動パターン

Fig. 6. Electropherograms of DNA fragments recovered from DNA-probe-array. The DNA fragments recovered from different spot of A, B, and C on the DNA probe array were amplified with PCR and analyzed by electrophoresis. The different peaks a, b, and c were separated from DNA probe array. Peaks a', b', and c' were contamination of each other. The peaks x and y were false positive products of PCR.

謝辞

本研究の成果の一部は，文部省科学研究費（11559016（石渡），11878129（石渡），12206028（安田））の助成を受けて行われた。

（平成12年8月30日受付，平成13年1月4日再受付）

文 献

(1) Consortium TF: "The flybase database of the drosophila genome projects and community literature", *Nucleic Acids Res.* 27, 85-88 (1999).

(2) D.W. Meinke, J.M. Cherry, C. Dean, S.D. Rounsley, and M. Koornneef: "Arabidopsis thalinia: A model plant for genome analysis", *Science* 282, 679-682 (1998).

(3) M. Marra, L. Hillier, T. Kucaba, M. Allen, R. Barstead, C. Beck, A. Blistain, M. Bonaldo, Y. Bowers, L. Bowles, M. Cardenas, A. Chamberlain, J. Chappell, S. Clifton, A. Favello, S. Geisel, M. Gibbons, N. Harvey, F. Hill, Y. Jackson, S. Kohn, G. Lennon, E. Mardis, J. Martin, R. Waterston, et. al.: "An encyclopedia of mouse genomes", *Nature Genet.* 21, 191-194 (1999).

(4) F.S. Collins, A. Patrinos, E. Jordan, A. Chakravarti, R. Gesteland, L. Walters, and the members of the DOE and NIH planning groups: "New goals for the U.S. human genome project: 1998-2003", *Science* 282, 682-689 (1998).

(5) D.J. Lockhart, H. Dong, M.C. Byrne, M.T. Follettie, M.V. Gallo, M.S. Chee, M. Mittmann, C. Wang, M. Kobayashi, H. Horton, and E.L. Brown: "Expression monitoring by hybridization to high-density oligonucleotide arrays", *Nature Biotech.* 14, 1675-1680 (1996).

(6) M. Schena, D. Shalon, R.W. Davis, and P.O. Brown: "Quantitative monitoring of gene expression patterns with a complementary DNA microarray", *Science* 270, 467-470 (1995).

(7) M.J. Marton, J.L. DeRisi, H.A. Bennett, V.R. Iyer, M.R. Meyer, C.J. Roberts, R. Stoughton, J. Burchard, D. Slade, H. Dai, D.E. Jr. Bassett, L.H. Hartwell, P.O. Brown, and S.H. Friend: "Drug target validation and identification of secondary drug target effects using DNA microarrays", *Nature Medicine* 4 1293-1301 (1998).

(8) D.-K. Choi, T. Ito, Y. Mitsui, and Y. Sakaki: "Fluorescent differential display analysis of gene expression in apoptoptic neuroblastoma cell", *Gene*, 223, 21-31 (1998).

(9) P.T. Spellman, G. Sherlock, M.Q. Zhang, V.R. Iyer, K. Anders, M.B. Eisen, P.O. Brown, D. Botstein, B. Futcher: "Comprehensive identification of cell cycle-regulated genes of the yeast *Saccharomyces cerevisiae* by microarray hybridization", *Mol. Biol. Cell*, 9, 3273-97 (1998).

(10) 梶山智晴・村川克二・宮原裕二：平成12年 電気学会大会講演論文集 pp1263-1266.

(11) K. Yasuda, K. Okano, and S. Ishiwata: "Focal extraction of surface-bound DNA from a microchip using photo-thermal denaturation", *Biotechniques*, 28, 1006-1011 (2000).

(12) K. Okano, K. Yasuda, and S. Ishiwata: "Position-specific release of DNA from a chip by using photothermal denaturation", *Sensors and Actuators*

B, 64, 88-94 (2000).
(13) "Separation of polynucleotides using supports having a plurality of electrode-containing cells", USP 05434049.
(14) "Device for separating polynucleotides having a plurality of electrode-containing cells and movable collecting capillary", USP 05607646.
(15) "Polynucleotide capturing support for capturing, eluting and collecting polynucleotides in a sample solution", USP 05817506.
(16) "Polynucleotide separation method and apparatus therefore", USP 06093370.
(17) 神原秀記:「光による遺伝子解析」光アライアンス, 9, 1-6 (1998).
(18) J. Cheng, E. L. Sheldon, L. Wu, A. Uribe, L. O. Gerrue, J. Carrino, M. J. Heller, and J. P. O'Connell: "Preparation and hybridization analysis of DNA/RNA from *E. coli* on microfabricated bioelectronic chips", *Nature Biotech.*, 16, 541-546 (1998).

岡野　和宣

（正員）　1956年9月8日生まれ。1980年3月東京理科大学理学部化学科卒業。1982年3月東京工業大学理工学研究科化学専攻終了。同年（株）日立製作所中央研究所入社。タンパク質の二次元電気泳動解析手法，DNA断片高感度検出法，遺伝子発現プロファイルやDNA断片間の変異を網羅的解に解析する手法の研究，大規模全長cDNA配列解析に従事。

陳　鋼

（非会員）1961年11月30日生まれ。1984年7月中国延辺大学医学部卒業。1989年12月同大学大学院修士課程修了。1999年6月東京慈恵医科大学医学部医学博士課程修了。1999年11月より日立製作所中央研究所において難読DNA配列解析法の研究に従事。

小原　賢信

（非会員）　1969年5月24日生まれ。1992年3月東京大学工学部化学工学科卒業。1994年3月東京大学工学系研究科化学工学専攻修士課程修了。同年4月(株)日立製作所中央研究所入社。キャピラリーDNAシーケンサーの研究開発に従事後，現在DNAビーズアレイの研究に従事。

梶山　智晴

（正員）1966年10月2日生まれ。1992年3月筑波大学大学院修士課程理工学研究科終了。同年（株）日立製作所中央研究所入社。X線デジタルラジオグラフィー，生化学分析装置，遺伝子検出技術の研究開発に従事。現在，日立製作所計測器事業部にて新世代のDNAチップの研究開発に従事。

安田　賢二

（非会員）東京大学大学院総合文化研究科生命環境科学系助教授．筋収縮メカニズム，細胞内記憶のメカニズムの研究，生体物質ハンドリング法の研究などの生物物理，超音波物性の研究などに従事。

石渡　信一

（非会員）早稲田大学理工学部物理学科教授。生体分子モーターに関する一分子，分子集合体，細胞にわたる顕微解析，筋収縮構造と機能の解体と再構築，線維状重合体の形成機構，自励振動収縮機構などの生物物理学研究に従事。

Acidosis or inorganic phosphate enhances the length dependence of tension in rat skinned cardiac muscle

Norio Fukuda, Jin O-Uchi, Daisuke Sasaki*, Hidetoshi Kajiwara, Shin'ichi Ishiwata*†‡ and Satoshi Kurihara

*Department of Physiology (II), The Jikei University School of Medicine, 3-25-8 Nishi-shinbashi, Minato-ku, Tokyo 105-8461, *Department of Physics, School of Science and Engineering, † Advanced Research Institute for Science and Engineering, and ‡ Materials Research Laboratory for Bioscience and Photonics, Waseda University, Okubo, Tokyo 169-8555, Japan*

(Received 22 December 2000; accepted after revision 6 June 2001)

1. We investigated the effect of acidosis on the sarcomere length (SL) dependence of tension generation, in comparison with the effect of inorganic phosphate (P_i), in rat skinned ventricular trabeculae. The shift of the mid-point of the pCa–tension relationship associated with an increase in SL from 1.9 to 2.3 μm (ΔpCa_{50}) was studied.

2. Decreasing pH from 7.0 to 6.2 lowered maximal and submaximal Ca^{2+}-activated tension and increased ΔpCa_{50} in a pH-dependent manner (from 0.21 ± 0.01 to 0.30 ± 0.01 pCa units). The addition of P_i (20 mM) decreased maximal tension and enhanced the SL dependence, both to a similar degree as observed when decreasing pH to 6.2 (ΔpCa_{50} increased from 0.20 ± 0.01 to 0.29 ± 0.01 pCa units).

3. Further experiments were performed using 6% (w/v) Dextran T-500 (molecular weight ~500 000) to osmotically reduce interfilament lattice spacing (SL, 1.9 μm). Compared with that at pH 7.0, in the absence of P_i the increase in the Ca^{2+} sensitivity of tension induced by osmotic compression was enhanced at pH 6.2 (0.18 ± 0.01 *vs.* 0.25 ± 0.01 pCa units) or in the presence of 20 mM P_i (0.17 ± 0.01 *vs.* 0.24 ± 0.01 pCa units).

4. H^+, as well as P_i, has been reported to decrease the number of strongly binding cross-bridges, which reduces the co-operative activation of the thin filament and increases the pool of detached cross-bridges available for interaction with actin. It is therefore considered that during acidosis, the degree of increase in the number of force-generating cross-bridges upon reduction of interfilament lattice spacing is enhanced, resulting in greater SL dependence of tension generation.

5. Our results suggest that the Frank-Starling mechanism may be enhanced when tension development is suppressed due to increased H^+ and/or P_i under conditions of myocardial ischaemia or hypoxia.

It is well known that twitch tension in myocardium is enhanced as muscle length (i.e. sarcomere length, SL) is increased within the physiological range (SL from ~1.8 to ~2.3 μm), and is accompanied by an increase in the Ca^{2+} sensitivity of tension (Allen & Kurihara, 1982; Allen & Kentish, 1985; Lakatta, 1991). This, in part, is the basis for the Frank-Starling law of the heart. At the myofilament level, there is an increasing amount of evidence suggesting that length dependence is primarily caused by a change in interfilament lattice spacing (Harrison *et al.* 1988; McDonald & Moss, 1995; Fuchs & Wang, 1996; Fitzsimons & Moss, 1998; Fukuda *et al.* 2000). A possible consequence of decreased lattice spacing is an increase in the probability of myosin attaching to the thin filament, resulting in an increase in the number of force-generating cross-bridges (Ishiwata & Oosawa, 1974; McDonald & Moss, 1995; Fukuda *et al.* 2000).

An alternative hypothesis suggested that SL-dependent activation of the myofilament was caused by cardiac troponin C (TnC), which possibily acts as a 'length sensor' (Babu *et al.* 1988; Gulati *et al.* 1990). However, McDonald *et al.* (1995) demonstrated that the expression of skeletal TnC in ventricular myocytes of transgenic mice did not alter the SL dependence of the Ca^{2+} sensitivity of tension in skinned myocytes. Hence making it unlikely that

cardiac TnC acts as a length sensor (Moss *et al.* 1991; McDonald *et al.* 1995).

It is well known that contractile dysfunction is one of the earliest consequences of myocardial ischaemia/hypoxia, during which intracellular H^+ and inorganic phosphate (P_i) are markedly increased (for review see Allen & Orchard, 1987). The effects of acidosis on the contractile functions of cardiac muscle have been extensively studied (for review see Orchard & Kentish, 1990). Acidosis decreases both maximal Ca^{2+}-activated tension and the Ca^{2+} sensitivity of tension (Godt & Nosek, 1989; Orchard & Kentish, 1990; Komukai *et al.* 1998; Fujita & Ishiwata, 1999; Fukuda & Ishiwata, 1999). Acidosis also decreases maximum shortening velocity and lowers maximum power output (Ricciardi *et al.* 1994). In intact ventricular preparations, it has been reported that a reduction in extracellular pH results in a change in the length–tension relationship which is similar to that seen with a decrease in the extracellular Ca^{2+} concentration (Ricciardi *et al.* 1986; Orchard *et al.* 1991), exerting little influence on the slope of the length–tension relationship when normalized to peak tension (Orchard *et al.* 1991). In those studies, however, twitch contraction was used to examine the effects of acidosis at limited extracellular Ca^{2+} concentrations, and the degree of presumed pH reduction inside the cell was limited to within a narrow range. Therefore, a more systematic study is needed to clarify the effect of acidosis on the SL dependence of tension generation using skinned muscle preparations.

In the present report, we studied the SL-dependent shift of the pCa–tension relationship using skinned ventricular trabeculae over a large pH range to investigate the effects of acidosis on the SL dependence of tension generation. We compared the effect of acidosis with that of inorganic phosphate (P_i), which acts on the actin–myosin interaction, but not directly on TnC, resulting in a decrease in the number of attached cross-bridges (Hibberd *et al.* 1985; Kentish, 1986, 1991; Kawai *et al.* 1988; Fukuda *et al.* 1998). Our results demonstrate that acidosis, as well as P_i, enhances the SL dependence of tension generation.

METHODS

Experimental procedure

Male Wistar rats (250–300 g) were anaesthetized with sodium pentobarbitone (50 mg kg^{-1} I.P.) and the hearts were removed. The rats were supplied by Saitama Experimental Animals Supply (Saitama, Japan), and the present study conforms with the Guiding Principles for the Care and Use of Animals approved by the Council of the Physiological Society of Japan. Thin trabecula muscles (diameter 100–150 μm) were dissected from the right ventricle in oxygenated Tyrode solution without Ca^{2+} at 30 °C (135 mM Na^+, 5 mM K^+, 1 mM Mg^{2+}, 98 mM Cl^-, 20 mM HCO_3^-, 1 mM HPO_4^{2-}, 1 mM SO_4^{2-}, 20 mM acetate, 10 mM glucose, 5 i.u. l^{-1} insulin, pH 7.35 when equilibrated with 5% CO_2–95% O_2) (Komukai *et al.* 1998; Fukuda *et al.* 2000). The preparations were skinned by superfusion with 1% (v/v) Triton X-100 in relaxing solution (composition (mM): MgATP 4, Mops 10, EGTA 10, free Mg^{2+} 1, ionic strength 180 (pH 7.0)) for 60 min at about 2 °C. The ionic strength (IS) was adjusted with KCl. The preparations were stored at −20 °C in relaxing solution containing 50% (v/v) glycerol and 2 mM leupeptin for 1 week or less. Both ends of the preparation were tied to thin tungsten wires with silk threads (Fukuda *et al.* 2000). One end was attached to a tension transducer (BG-10; Kulite Semiconductor Products, Inc., Leonia, NJ, USA) and the other to a micromanipulator (Narishige, Tokyo). The SL was adjusted to either 1.9 or 2.3 μm by measuring laser light diffraction in the relaxing solution. Isometric tension was measured in solutions containing 4 mM MgATP, 10 mM Mops (or 10 mM Mes for pH 6.2), 1 mM free Mg^{2+}, various concentrations of free Ca^{2+} (adjusted with $CaCl_2$), 10 mM EGTA, 0.1 mM P^1,P^5-di(adenosine-5′)pentaphosphate (AP_5A), 15 mM creatine phosphate (CP), 15 IU ml^{-1} creatine phosphokinase (CPK) and 180 mM IS (adjusted with KCl). The pH of each solution was finally adjusted to within error of 0.02 of the desired pH.

The control pCa–tension relationship (at pH 7.0 without P_i) was first obtained at SL 1.9 μm and then at 2.3 μm. Subsequently, the pCa–tension relationships at a lower pH (6.8, 6.6 or 6.2) or in the presence of 20 mM P_i (pH 7.0) were obtained at the two SLs using the same preparation. In another series of experiments, the effect of acidosis or P_i on maximal Ca^{2+}-activated tension was measured at SLs of 1.9 and 2.3 μm according to a previously described procedure (Fukuda *et al.* 1998; Fukuda & Ishiwata, 1999). At the end of the experiments, maximal Ca^{2+}-activated tension was measured at the two SLs under control conditions (pH 7.0, no P_i). We only used data in which the final tension values were greater than 90% of those measured at the beginning of the experiment.

The muscle width was measured under a microscope (SMZ645, Nikon, Tokyo) at a magnification of ×225. The concentrations of ionic species in solutions were estimated by computer calculation (Horiuti, 1986). All experiments were carried out at 20 ± 0.2 °C.

Data and statistical analyses

The pCa–tension relationship was fitted to the Hill equation: $\log(P/(100-P)) = n_H(pCa_{50} - pCa)$, where P is the relative tension expressed as a percentage of the maximum, n_H is the Hill coefficient and pCa_{50} is $-\log[Ca^{2+}]$ at $P = 50$. All data are expressed as means ± S.E.M. Student's paired t test was used and significance verified at $P < 0.05$.

RESULTS

Effect of acidosis on the length dependence of the Ca^{2+} sensitivity of tension

The effect of acidosis on the SL dependence of the Ca^{2+} sensitivity of tension in the absence of P_i is shown in Fig. 1. The pH value was decreased from 7.0 to 6.8 (*A*), 6.6 (*B*) or 6.2 (*C*). At pH 7.0, maximal Ca^{2+}-activated tension values were 50.8 ± 4.0 and 83.1 ± 6.7 mg ($P < 0.001$, $n = 21$) at SL 1.9 and 2.3 μm, respectively, and the SL-dependent shift of pCa_{50} (ΔpCa_{50}) was ~0.2 pCa units (see Fukuda *et al.* 2000). The muscle width was decreased from 120.4 ± 7.2 to 107.1 ± 6.0 μm ($P < 0.001$, $n = 5$) when SL was increased from 1.9 to 2.3 μm during relaxation (i.e. ~11% decrease in the width). Acidosis did not change the muscle width (119.4 ± 7.3 and 105.8 ± 6.3 μm ($P < 0.001$, $n = 5$) at SL 1.9 and 2.3 μm, respectively, at pH 6.2). Consistent with previous studies using skinned cardiac muscle preparations (Godt &

Table 1. Change in the Hill coefficient with acidosis

	Fig. 1*A*		Fig. 1*B*		Fig. 1*C*	
SL	pH 7.0	pH 6.8	pH 7.0	pH 6.6	pH 7.0	pH 6.2
1.9 μm	5.81 ± 0.21	5.79 ± 0.28	5.49 ± 0.28	4.86 ± 0.30	5.48 ± 0.38	6.02 ± 0.52
2.3 μm	4.18 ± 0.29	4.38 ± 0.31	4.70 ± 0.19	4.80 ± 0.18	4.59 ± 0.21	5.70 ± 0.43*

Values were obtained from Fig. 1*A–C* (mean ± S.E.M.; $n = 5–6$). * $P < 0.05$ compared with the corresponding value of pH 7.0.

Nosek, 1989; Orchard & Kentish, 1990; Fujita & Ishiwata, 1999; Fukuda & Ishiwata, 1999), acidosis shifted the pCa–tension relationship to the right (Fig. 1). It was also found that the SL-dependent shift of the pCa–tension relationship was enhanced with acidosis in a pH-dependent manner ($P < 0.05$ and $P < 0.01$ for pH 6.6 and 6.2, respectively). At pH 6.8, ΔpCa_{50} was not significantly different from that at pH 7.0 (Fig. 1*A*, inset); however, it

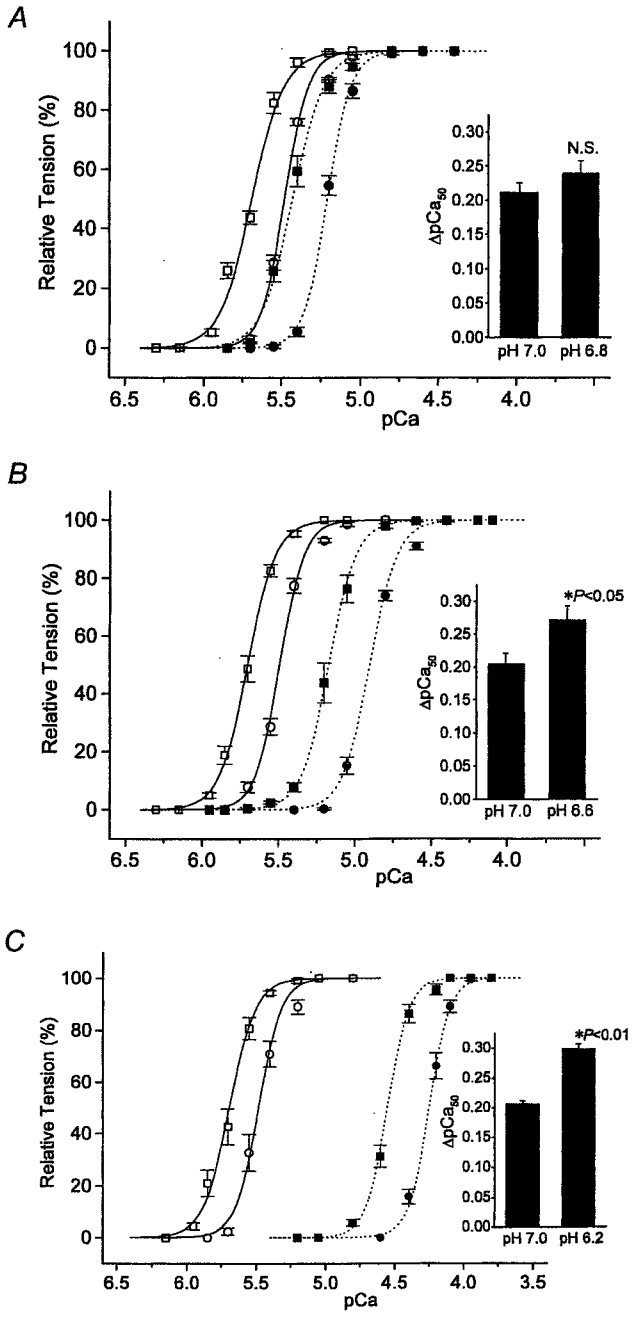

Figure 1. Effects of acidosis on pCa–tension relationships at different SLs

Solvent conditions: 4 mM MgATP, 10 mM Mops (or 10 mM Mes for pH 6.2), 1 mM free Mg^{2+}, various concentrations of free Ca^{2+} (pCa adjusted using Ca-EGTA), 0.1 mM AP_5A, 15 mM CP, 15 IU ml^{-1} CPK and IS maintained at 180 ± 1 mM. Temperature, 20 ± 0.2 °C. *A–C* show the effect of lowering pH from 7.0 to 6.8, 6.6 and 6.2, respectively, on the pCa–tension relationships at SLs of 1.9 μm (circles) and 2.3 μm (squares). Note that different preparations were used in *A*, *B* and *C*. Continuous lines and open symbols, pCa–tension relationships at pH 7.0; dotted lines and filled symbols, those at a lower pH. Data obtained for each preparation were fitted to the Hill equation, and the results were simulated by the Hill equation with the mean values of pCa_{50} and n_H. Each inset represents ΔpCa_{50} (difference between the values of pCa_{50} at long and short SLs) at pH 7.0 and at a lower pH. pCa–tension relationships were normalized to the maximal tension at pCa 4.8 for pH 7.0 and at 4.4, 4.1 and 3.8, respectively, for pH 6.8, 6.6 and 6.2. Error bars, S.E.M. of 5–6 data points. N.S., not significant compared with pH 7.0.

increased from 0.21 ± 0.01 to 0.30 ± 0.01 pCa units at pH 6.2 (Fig. 1*C*, inset).

Table 1 summarizes the n_H values of the pCa–tension relationships of Fig. 1. Decreasing pH to 6.2 significantly increased n_H at SL 2.3 μm. However, there was no definitive correlation between the magnitude of n_H at either SL and that of ΔpCa_{50} (i.e. at pH 6.6, ΔpCa_{50} was significantly increased with no significant change in n_H at either SL, Fig. 1*B* and Table 1) (see also Fukuda *et al.* 2000). The n_H values obtained here are relatively high in comparison with those reported in previous studies using rat skinned ventricular muscle (e.g. Kentish, 1986; Harrison *et al.* 1988; McDonald & Moss, 1995). One reason for this may lie in the different experimental conditions. It is also possible that the high n_H values came about because of our measurement protocol for the pCa–tension relationship. In accordance with our previous report (Fukuda *et al.* 2000), we measured the pCa–tension relationship by cumulatively raising the free Ca^{2+} concentration from the relaxing condition. It is thus possible that the thin filament is readily activated upon solution change, because of pre-activation at the preceding lower Ca^{2+}. This may result in enhanced co-operative activation of the thin filament (i.e. high n_H).

Effect of P_i on the length dependence of the Ca^{2+} sensitivity of tension

Figure 2 shows the effect of P_i (20 mM) on the SL dependence of the Ca^{2+} sensitivity of tension at pH 7.0.

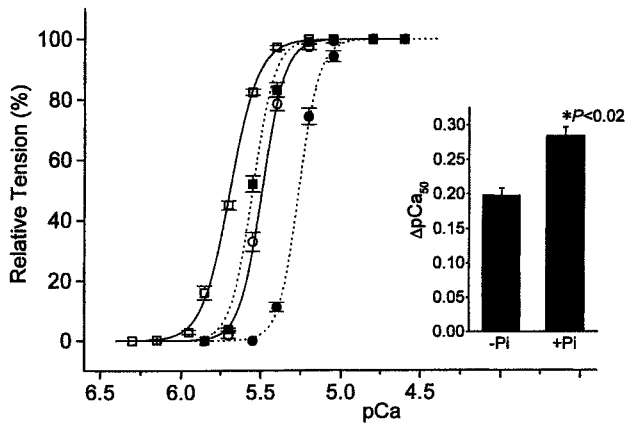

Figure 2. Effects of P_i on pCa–tension relationships at different SLs

Solvent conditions: the same as in Fig. 1 except that pH was maintained at 7.0 and 20 mM P_i was added, maintaining IS at 180 mM. Continuous lines and open symbols, pCa–tension relationships in the absence of P_i; dotted lines and filled symbols, those in the presence of P_i. Circles, SL 1.9 μm; squares, SL 2.3 μm. Inset represents ΔpCa_{50} in the absence (−P_i) and presence (+P_i) of P_i. pCa–tension relationships were normalized to the maximal tension at pCa 4.8 in the absence of P_i and at 4.6 in the presence of P_i. Error bars, S.E.M. of 5 data points.

Consistent with previous studies using skinned cardiac muscle (Godt & Nosek, 1989; Kentish, 1986; Fukuda *et al.* 1998), P_i shifted the pCa–tension relationship to the right. It was found that ΔpCa_{50} was significantly increased in the presence of P_i (0.20 ± 0.01 *vs.* 0.29 ± 0.01 pCa units), and the magnitude of increase was comparable to that

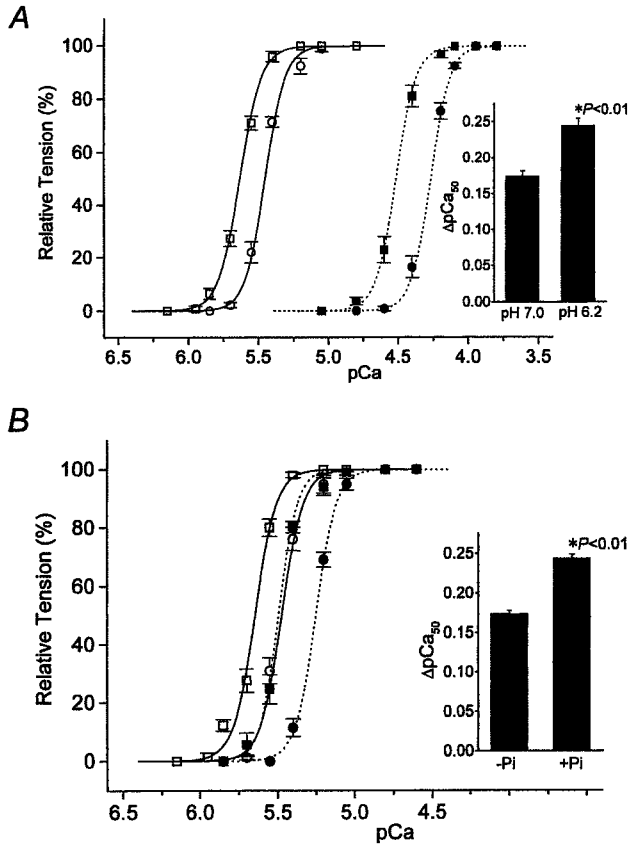

Figure 3. Effects of acidosis or P_i on pCa–tension relationships in the absence and presence of Dextran T-500

Solvent conditions: the same as in Figs 1*C* and 2 for acidosis and P_i, respectively, except that 6% (w/v) Dextran T-500 (molecular weight ~500 000, Amersham Pharmacia Biotech AB, Sweden) was used instead of increasing SL to 2.3 μm. Circles, in the absence of Dextran T-500; squares, in the presence of Dextran T-500. SL was fixed at 1.9 μm. *A*, effect of acidosis (pH 6.2). P_i was absent. Continuous lines and open symbols, pCa–tension relationships at pH 7.0; dotted lines and filled symbols, those at pH 6.2. Inset represents ΔpCa_{50} (difference between the values of pCa_{50} with and without Dextran T-500) at pH 7.0 and 6.2. *B*, effect of P_i (20 mM). pH was held at 7.0. Continuous lines and open symbols, pCa–tension relationships in the absence of P_i; dotted lines and filled symbols, those in the presence of P_i. Inset represents ΔpCa_{50} in the absence (−P_i) and presence (+P_i) of P_i. pCa–tension relationships in *A* and *B* were normalized to the maximal tension at the values of pCa shown in Figs 1*C* and 2, respectively. Error bars, S.E.M. of 5 data points.

obtained by lowering pH from 7.0 to 6.2 (see Fig. 1*C*), although the rightward shift of the pCa curve was smaller. The n_H values in the absence and presence of P_i were 6.26 ± 0.24 and 6.94 ± 0.36 ($P > 0.05$, $n = 5$), respectively, at SL 1.9 μm, and 5.08 ± 0.33 and 6.40 ± 0.43 ($P > 0.05$, $n = 5$), respectively, at SL 2.3 μm. Consistent with the work of Kentish (1986) using rat ventricular muscles, n_H did not change significantly with P_i.

Effects of acidosis and P_i on tension induced by osmotic compression

Dextran T-500 (6% w/v) reduced the muscle width from 129.3 ± 8.1 to 111.6 ± 6.8 μm ($P < 0.001$, $n = 10$) under relaxing conditions at SL 1.9 μm. The degree of reduction (~13.5%) was similar to that observed when increasing SL to 2.3 μm without Dextran T-500 (~11%). Osmotic compression shifted the pCa–tension relationship leftward (0.17–0.18 pCa units), similar to that observed when increasing SL to 2.3 μm (~0.2 pCa units) (Fukuda *et al.* 2000). Maximal tension was also increased by about 15% with compression, but this change was smaller than that obtained by lengthening (McDonald & Moss, 1995; Fukuda *et al.* 2000); in contrast, increasing SL from 1.9 to 2.3 μm in the absence of Dextran T-500 increased maximal tension by about 60% (see above). It was found that the Dextran-induced increase in the apparent Ca^{2+} sensitivity was significantly increased at pH 6.2 (0.18 ± 0.01 *vs.* 0.25 ± 0.01 pCa units) or in the presence of 20 mM P_i (0.17 ± 0.01 *vs.* 0.24 ± 0.01 pCa units) (Fig. 3). The n_H values at pH 7.0 and 6.2 were 6.12 ± 0.36 and 6.36 ± 0.40 ($P > 0.1$, $n = 5$), respectively, without Dextran T-500 and 5.63 ± 0.26 and 6.08 ± 0.54 ($P > 0.1$, $n = 5$), respectively, with Dextran T-500. Those in the absence and presence of P_i were 6.18 ± 0.54 and 6.43 ± 0.39 ($P > 0.1$, $n = 5$), respectively, without Dextran T-500 and 6.18 ± 0.38 and 7.08 ± 0.80 ($P > 0.1$, $n = 5$), respectively, with Dextran T-500.

Effects of acidosis and P_i on maximal Ca^{2+}-activated tension

Finally, we studied maximal Ca^{2+}-activated tension as functions of pH and P_i at SLs of 1.9 and 2.3 μm. As reported previously in skinned skeletal and cardiac muscle preparations (Godt & Nosek, 1989; Kentish, 1991; Fujita & Ishiwata, 1999; Fukuda & Ishiwata, 1999), maximal tension decreased almost linearly with the reduction of pH (Fig. 4*A*). We found that the inhibitory effect was SL dependent, and that the effect was weaker at the longer SL. The inhibitory effect of P_i on maximal tension was also SL dependent; the effect was less at the longer SL (Fig. 4*B*).

DISCUSSION

We found that in rat skinned ventricular trabeculae, both acidosis and P_i exhibited a similar inhibitory effect on maximal Ca^{2+}-activated tension and enhanced the magnitude of SL-dependent changes of the pCa–tension relationship. We discuss these results of the effects of interfilament lattice spacing, acidosis and P_i in relation to the formation of force-generating cross-bridges.

First, an increase in SL results in a decrease in the lateral separation between the thick and thin filaments both in living (Matsubara & Millman, 1974) and skinned (Irving *et al.* 2000) myocardium. A recent X-ray study using rat skinned ventricular trabeculae confirmed that inter-

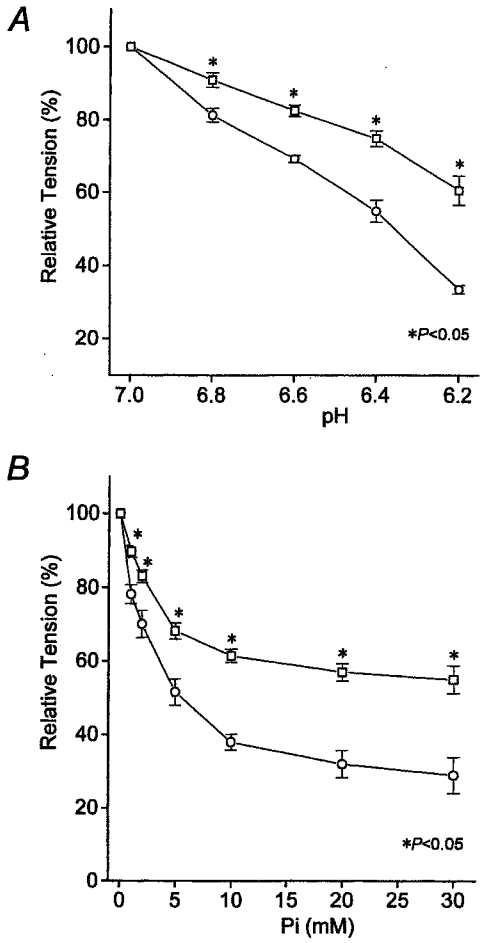

Figure 4. Effects of acidosis or P_i on maximal Ca^{2+}-activated tension at different SLs

Conditions: the same as in Figs 1 and 2 for acidosis and P_i, respectively. Circles, SL 1.9 μm; squares, SL 2.3 μm. *A*, effect of acidosis in the absence of P_i. The values of pCa at pH 7.0, 6.8, 6.6 and 6.2 for obtaining maximal Ca^{2+}-activated tension were set based on Fig. 1 (i.e. 4.8, 4.4, 4.1 and 3.8 for pH 7.0, 6.8, 6.6 and 6.2, respectively) and estimated to be 4.0 for pH 6.4 by drawing the pCa curve. Tension was normalized with respect to pH 7.0. *B*, effect of P_i. pH was held at 7.0. Tension was normalized with respect to 0 mM P_i. The value of pCa was held at 4.8 in all conditions, because there was little difference between the tension at pCa 4.8 and that at pCa < 4.8 in the presence of 30 mM P_i. Error bars, S.E.M. of 3–4 data points. *$P < 0.05$ compared with the corresponding values for SL 1.9 μm.

filament lattice spacing (d_{10}) decreases with an increase in SL, maintaining a nearly constant lattice volume over the physiological range of SL (i.e. from ~1.9 to ~2.4 μm) (Irving *et al.* 2000). Consistent with our previous study (Fukuda *et al.* 2000), an increase in SL from 1.9 to 2.3 μm produced a similar muscle width reduction as osmotic compression using 6% (w/v) Dextran T-500, and both procedures increased the Ca^{2+} sensitivity of isometric tension to a similar degree (Figs 1–3). Thus, we consider that the change in the lattice spacing is the primary cause of the modulation of the SL-dependent Ca^{2+} sensitivity of tension in the cardiac myofilament (McDonald & Moss, 1995; Fuchs & Wang, 1996; Fukuda *et al.* 2000).

A decrease in pH towards the isoelectric point of the myofilaments decreases the charge distribution on the filaments, causing a reduction of electrostatic repulsion force between filaments, which in turn causes inter-filament lattice spacing to shrink (Millman, 1998). In the present study, a decrease in pH from 7.0 to 6.2 did not significantly alter the muscle width at a SL of 1.9 or 2.3 μm. It is thus reasonable to consider that interfilament lattice spacing is not directly influenced by the change in pH in the range examined here, presumably because the isoelectric point is far below 6.2 (i.e. < 5.0; see Kawai *et al.* 1988; Millman, 1998).

The inhibitory effect of acidosis on Ca^{2+}-activated tension is in part attributable to a decrease in the number of force-generating cross-bridges (Metzger & Moss, 1988, 1990; Kentish, 1991; Fujita & Ishiwata, 1999; Fukuda & Ishiwata, 1999). Kentish (1991) postulated that H^+ is released during the transition between the non-force-generating states preceding the P_i release (force-generating) step. An increased concentration of H^+ will thus reverse the H^+ release step and decrease the number of force-generating cross-bridges (Kentish, 1991). P_i is believed to reverse the P_i release step in the cross-bridge cycle by shifting the distribution of cross-bridges toward a state with a full complement of bound products (ADP and P_i) (i.e. non-force-generating state) (Hibberd *et al.* 1985; Kentish, 1986, 1991; Kawai *et al.* 1988). It is thus realized that both acidosis and P_i reduce the co-operative activation of the thin filament by decreasing the number of strongly binding cross-bridges. In the present study, lowering pH to 6.2 and the addition of 20 mM P_i reduced maximal tension and enhanced the SL-dependent increase in the Ca^{2+} sensitivity of tension to a similar degree (Figs 1*C*, 2 and 4). However, the rightward shift of the pCa_{50}–tension curve was substantially larger for acidosis (Figs 1*C* and 2), which is reasonable because P_i decreases the number of force-generating cross-bridges with no direct effect on TnC, whereas acidosis reduces the affinity of TnC for Ca^{2+} in addition to its inhibitory effect on cross-bridges (Orchard & Kentish, 1990). It is therefore suggested that a change in the cross-bridge distribution, shown by a decrease in maximal tension, but not a reduced affinity of TnC for Ca^{2+}, underlies the mechanisms of enhanced SL-dependent tension generation by acidosis (see Fukuda *et al.* 2000). Once the number of strongly binding cross-bridges is decreased by either H^+ or P_i, co-operative activation of the thin filament will be reduced, resulting in an increase of detached cross-bridges that are available for interaction with actin. Consequently, the fraction of cross-bridges recruited to the force-generating state on lengthening (i.e. lattice shrinkage) will be increased, resulting in a greater SL dependence of isometric tension (Ishiwata & Oosawa, 1974). This interpretation is supported by the fact that both acidosis and P_i enhance the increase in the Ca^{2+} sensitivity of tension due to osmotic compression to a degree similar to that observed in the study of varying SL (Fig. 3). Also, this interpretation is consistent with the recent finding that SL-dependent tension generation is attenuated by an enhanced co-operative activation of the thin filament by strongly binding cross-bridges produced by the addition of *N*-ethylmaleimide-modified myosin subfragment 1 (Fitzsimons & Moss, 1998) or ADP (Fukuda *et al.* 2000).

We observed SL dependence in the inhibitory effects of acidosis and P_i (Fig. 4). Assuming that the formation of the force-generating cross-bridges is accelerated with an increase in SL, it is expected that the inhibitory effect of H^+ or P_i becomes less pronounced at a longer SL. Since maximal tension was dramatically increased by lengthening compared with osmotic compression (i.e. ~60% *vs.* ~15%) (see also McDonald & Moss, 1995; Fukuda *et al.* 2000), the reduction of interfilament lattice spacing may not fully account for the increase in maximal tension due to an increase in SL. There may be additional mechanisms modulating the SL-dependent activation in the cardiac myofilament, such as extension of titin/connectin (Fukuda *et al.* 2001), in addition to the reduction of the lattice spacing, and therefore the reduction of the lattice spacing alone may not be sufficient to produce force-generating cross-bridges. Alternatively, it is possible that osmotic compression and lengthening may not be precisely equivalent such that changes in lattice packing may differ in the two cases; the shape of the muscle may be altered differently by mechanical stretch compared with osmotic compression (McDonald & Moss, 1995; Fukuda *et al.* 2000).

Alterations of SL-dependent shift of the pCa–tension relationship are predicted to affect the relation between muscle length and tension production (Fuchs, 1995). The present finding that acidosis enhances the SL dependence of the Ca^{2+} sensitivity of tension (Fig. 1) leads us to conclude that as pH falls, the slope of the length–tension relationship at physiologically submaximal levels of Ca^{2+} is increased. This is in disagreement with an earlier finding that acidosis does not essentially change the slope of the length–tension relationship in intact myocardium (Ricciardi *et al.* 1986; Orchard *et al.* 1991). The difference

in the effect of acidosis on length-dependent tension generation may lie in the buffering capacity of pH by the cell membrane in intact preparations (Allen & Orchard, 1987; Ricciardi *et al.* 1994), resulting in values of intracellular pH between 6.6 and 6.8 in those studies (Ricciardi *et al.* 1986; Orchard *et al.* 1991), which are higher than that used in the present study (6.2). Other differences include ionic conditions and experimental protocols.

The manifestation of a change in the pCa–tension relationship in the ventricular volume–end-systolic pressure (ESP) relation of the intact ventricle is complex. However, a simplified prediction of how a change in SL-dependent activation may affect the slope of the volume–ESP relation can be made (Arteaga *et al.* 2000). Arteaga *et al* (2000) reported that the slope of the volume–ESP relation may depend on the degree of activation of the myofilament on SL. We have reported that the volume–ESP relation may be impaired during the late phase of myocardial ischaemia/hypoxia (Fukuda *et al.* 2000), in which the ratio of the intracellular concentration of ADP to that of ATP is dramatically increased and subsequently augments tension development (Kammermeier *et al.* 1982; Allen & Orchard, 1987; Ventura-Clapier & Veksler, 1994; Fukuda *et al.* 1998). In contrast, the present results indicate that during the early phase of myocardial ischaemia/hypoxia, in which accumulation of ADP is minimal and tension development is suppressed by the increased H^+ and/or P_i (Allen & Orchard, 1987; Ventura-Clapier & Veksler, 1994), the SL-dependent activation is enhanced. It can therefore be predicted that in the beating heart, the slope of the volume–ESP relation may be increased during the initial phase of myocardial ischaemia/hypoxia, thereby enhancing the Frank-Starling mechanism.

ALLEN, D. G. & KENTISH, J. C. (1985). The cellular basis for length-tension relation in cardiac muscle. *Journal of Molecular and Cellular Cardiology* **17**, 821–840.

ALLEN, D. G. & KURIHARA, S. (1982). The effect of muscle length on intracellular calcium transients in mammalian cardiac muscle. *Journal of Physiology* **327**, 79–94.

ALLEN, D. G. & ORCHARD, C. H. (1987). Myocardial contractile function during ischemia and hypoxia. *Circulation Research* **60**, 153–168.

ARTEAGA, G. M., PALMITER, K. A., LEIDEN, J. M. & SOLARO, R. J. (2000). Attenuation of length dependence of calcium activation in myofilaments of transgenic mouse hearts expressing slow skeletal troponin I. *Journal of Physiology* **526**, 541–549.

BABU, A., SONNENBLICK, E. & GULATI, J. (1988). Molecular basis for the influence of muscle length on myocardial performance. *Science* **240**, 74–76.

FITZSIMONS, D. P. & MOSS, R. L. (1998). Strong binding of myosin modulates length-dependent Ca^{2+} activation of rat ventricular myocytes. *Circulation Research* **83**, 602–607.

FUCHS, F. (1995). Mechanical modulation of the Ca^{2+} regulatory protein complex in cardiac muscle. *News in Physiological Sciences* **10**, 6–12.

FUCHS, F. & WANG, Y. P. (1996). Sarcomere length versus interfilament spacing as determinants of cardiac myofilament Ca^{2+} sensitivity and Ca^{2+} binding. *Journal of Molecular and Cellular Cardiology* **28**, 1375–1383.

FUJITA, H. & ISHIWATA, S. (1999). Tropomyosin modulates pH dependence of isometric tension. *Biophysical Journal* **77**, 1540–1546.

FUKUDA, N., FUJITA, H., FUJITA, T. & ISHIWATA, S. (1998). Regulatory roles of MgADP and calcium in tension development of skinned cardiac muscle. *Journal of Muscle Research and Cell Motility* **19**, 909–921.

FUKUDA, N. & ISHIWATA, S. (1999). Effects of pH on spontaneous tension oscillation in skinned bovine cardiac muscle. *Pflügers Archiv* **438**, 125–132.

FUKUDA, N., KAJIWARA, H., ISHIWATA, S. & KURIHARA, S. (2000). Effects of MgADP on length dependence of tension generation in skinned rat cardiac muscle. *Circulation Research* **86**, E1–6.

FUKUDA, N., SASAKI, D., ISHIWATA, S. & KURIHARA, S. (2001). Length dependence of tension generation in rat skinned cardiac muscle: Role of titin in the Frank-Starling mechanism of the heart. *Circulation* (in the Press).

GODT, R. E. & NOSEK, T. M. (1989). Changes of intracellular milieu with fatigue or hypoxia depress contraction of skinned rabbit skeletal and cardiac muscle. *Journal of Physiology* **412**, 155–180.

GULATI, J., SONNENBLICK, E. & BABU, A. (1990). The role of troponin C in the length dependence of Ca^{2+}-sensitive force of mammalian skeletal and cardiac muscles. *Journal of Physiology* **441**, 305–324.

HARRISON, S. M., LAMONT, C. & MILLER, D. J. (1988). Hysteresis and the length dependence of calcium sensitivity in chemically skinned rat cardiac muscle. *Journal of Physiology* **401**, 115–143.

HIBBERD, M. G., DANTZIG, J. A., TRENTHAM, D. R. & GOLDMAN, Y. E. (1985). Phosphate release and force generation in skeletal muscle fibers. *Science* **228**, 1317–1319.

HORIUTI, K. (1986). Some properties of the contractile system and sarcoplasmic reticulum of skinned slow fibres from *Xenopus* muscle. *Journal of Physiology* **373**, 1–23.

IRVING, T. C., KONHILAS, J., PERRY, D., FISCHETTI, R. & DE TOMBE, P. P. (2000). Myofilament lattice spacing as a function of sarcomere length in isolated rat myocardium. *American Journal of Physiology–Heart and Circulatory Physiology* **279**, H2568–2573.

ISHIWATA, S. & OOSAWA, F. (1974). A regulatory mechanism of muscle contraction based on the flexibility change of the thin filaments. *Journal of Mechanochemistry and Cell Motility* **3**, 9–17.

KAMMERMEIER, H., SCHMIDT, P. & JUNGLING, E. (1982). Free energy change of ATP-hydrolysis: a causal factor of early hypoxic failure of the myocardium? *Journal of Molecular and Cellular Cardiology* **14**, 267–277.

KAWAI, M., GUTH, K. & CORNACCHIA, T. W. (1988). The role of monovalent phosphate anions in the crossbridge kinetics of chemically skinned rabbit psoas fibers. In *Molecular Mechanism of Muscle Contraction*, ed. SUGI, H. & POLLACK, G. H., pp. 203–214. Plenum Publishing Corporation, New York, NY, USA.

KENTISH, J. C. (1986). The effects of inorganic phosphate and creatine phosphate on force production in skinned muscles from rat ventricle. *Journal of Physiology* **370**, 585–604.

KENTISH, J. C. (1991). Combined inhibitory actions of acidosis and phosphate on maximum force production in rat skinned cardiac muscle. *Pflügers Archiv* **419**, 310–318.

KOMUKAI, K., ISHIKAWA, T. & KURIHARA, S. (1998). Effects of acidosis on Ca^{2+} sensitivity of contractile elements in intact ferret myocardium. *American Journal of Physiology* **43**, H147–154.

LAKATTA, E. G. (1991). Length modulation of muscle performance: Frank-Starling law of the heart. In *The Heart and Cardiovascular System*, ed. FOZZARD, H. A., pp. 1325–1352. Raven Press Publishers, New York, NY, USA.

MCDONALD, K. S., FIELD, L. J., PARMACEK, M. S., SOONPAA, M., LEIDEN, J. M. & MOSS, R. L. (1995). Length dependence of Ca^{2+} sensitivity of tension in mouse cardiac myocytes expressing skeletal troponin C. *Journal of Physiology* **483**, 131–139.

MCDONALD, K. S. & MOSS, R. L. (1995). Osmotic compression of single cardiac myocytes eliminates the reduction in Ca^{2+} sensitivity of tension at short sarcomere length. *Circulation Research* **77**, 199–205.

MATSUBARA, I. & MILLMAN, B. M. (1974). X-ray diffraction patterns from mammalian heart muscle. *Journal of Molecular Biology* **82**, 527–536.

METZGER, J. M. & MOSS, R. L. (1988). Depression of Ca^{2+} insensitive tension due to reduced pH in partially troponin-extracted skinned skeletal muscle fibers. *Biophysical Journal* **54**, 1169–1173.

METZGER, J. M. & MOSS, R. L. (1990). Effects of pH and stiffness due to reduced pH in mammalian fast- and slow-twitch skinned skeletal fibers. *Journal of Physiology* **428**, 737–750.

MILLMAN, B. M. (1998). The filament lattice of striated muscle. *Physiological Reviews* **78**, 359–391.

MOSS, R. L., NWOYE, L. O. & GREASER, M. L. (1991). Substitution of cardiac troponin C into rabbit muscle does not alter the length dependence of Ca^{2+} sensitivity of tension. *Journal of Physiology* **440**, 273–280.

ORCHARD, C. H., HAMILTON, D. L., ASTLES, P., MCCALL, E. & JEWELL, B. R. (1991). The effect of acidosis on the relation between Ca^{2+} and force in isolated ferret cardiac muscle. *Journal of Physiology* **436**, 559–578.

ORCHARD, C. H. & KENTISH, J. C. (1990). Effects of changes of pH on the contractile function of cardiac muscle. *Americal Journal of Physiology* **27**, C967–981.

RICCIARDI, L., BOTTINELLI, R., CANEPARI, M. & REGGIANI, C. (1994). Effects of acidosis on maximum shortening velocity and force-velocity relation of skinned rat cardiac muscle. *Journal of Molecular and Cellular Cardiology* **26**, 601–607.

RICCIARDI, L., BUCX, J. J. J. & TER KEURS, H. E. D. J. (1986). Effects of acidosis on force-sarcomere length and force-velocity relations of rat cardiac muscle. *Cardiovascular Research* **20**, 117–123.

VENTURA-CLAPIER, R. & VEKSLER, V. (1994). Myocardial ischemic contracture. Metabolites affect rigor tension development and stiffness. *Circulation Research* **74**, 920–929.

Acknowledgements

We would like to thank Drs David Allen, Masataka Kawai, and Henk Granzier for critical reading of the manuscript, and Naoko Tomizawa for technical assistance. This work was supported in part by Grants-in-Aid for Scientific Research, for Scientific Research on Priority Areas, and for High-Tech Research Center Project from the Ministry of Education, Science, Sports and Culture of Japan, from Japan Heart Foundation, and from the Vehicle Racing Commemorative Foundation.

Corresponding author

N. Fukuda: Department of Physiology (II), The Jikei University School of Medicine, 3-25-8 Nishi-shinbashi, Minato-ku, Tokyo 105-8461, Japan.

Email: noriof@jikei.ac.jp

Length Dependence of Tension Generation in Rat Skinned Cardiac Muscle

Role of Titin in the Frank-Starling Mechanism of the Heart

Norio Fukuda, PhD; Daisuke Sasaki, MS; Shin'ichi Ishiwata, PhD; Satoshi Kurihara, MD, PhD

Background—At the basis of the Frank-Starling mechanism is the intrinsic ability of cardiac muscle to produce active tension in response to stretch. Titin, a giant filamentous molecule involved in passive tension development, is intimately associated with the thick filament in the sarcomere. Titin may therefore contribute to active tension development by modulating the thick filament structure when the muscle is elongated.

Methods and Results—Rat skinned right ventricular trabeculae were used. Passive tension at a sarcomere length (SL) of 2.0 to 2.4 μm was decreased after treatment of the preparation with trypsin (0.25 μg/mL) for 13 minutes in the relaxed state at 20°C. This mild trypsin treatment degraded titin without affecting other major contractile proteins. The sarcomere structure was little affected by brief contractions in the trypsin-treated preparations. When SL was adjusted to the slack SL (1.9 μm), active tension was unaffected by trypsin under partial (pCa 5.55) and maximal (pCa 4.8) activation. At longer SLs, however, active tension was significantly ($P<0.01$) decreased after trypsin treatment at either pCa. The increase in active tension on reduction of interfilament lattice spacing, produced by dextran T-500 (molecular weight ≈500 000), was not influenced by trypsin (SL 1.9 μm). In trypsin-treated preparations, the increase in active tension as a function of muscle diameter was nearly the same for lengthening and osmotic compression at the slack SL.

Conclusions—The length-dependent activation in cardiac muscle, an underlying mechanism of the Frank-Starling law of the heart, is at the myofilament level, predominantly modulated by titin and interfilament lattice spacing changes. (***Circulation.* 2001;104:1639-1645.**)

Key Words: myocardial contraction ■ myocardium ■ contractility

Isometric tension in isolated preparations of mammalian ventricular muscle increases dramatically when the muscle is stretched over the range of sarcomere length (SL; from ≈1.8 to ≈2.3 μm), which is observed in the intact heart.[1–3] This region of the length-tension relationship (the ascending limb) provides a useful model of the increase in myocardial performance that occurs as a result of increased diastolic filling of the heart.[1–3] Because length-dependent activation is seen in skinned cardiac muscle preparations from which the membrane system has been chemically removed, the steep variation of tension generation is due, at least in part, to variations in the activation of the contractile system with length.[1–3] The basis of this relationship in skinned muscle preparations is still not fully understood.

See p 1585

Recent articles,[4–6] however, indicate that SL dependence arises largely from a reduction of interfilament lattice spacing rather than from an increase in SL itself. A recent x-ray study with rat skinned ventricular trabeculae confirmed that the lattice spacing decreases as a function of SL, thereby maintaining a nearly constant lattice volume (SL from ≈1.9 to ≈2.4 μm).[7] A possible consequence of the decreased lattice spacing is an increase in the probability of myosin attachment to the thin filament.[6] We also found that SL dependence occurs during activation induced by lowering the ATP concentration in the absence of Ca^{2+}.[8] This finding does not support the proposal that the binding of Ca^{2+} to troponin C is the central player in SL-dependent activation[9] but suggests that structural changes within myofilaments during stretch are the basis of SL-dependent activation.

The giant muscle protein titin (also known as connectin), which spans from the Z-line to the M-line, is responsible for the elasticity of relaxed striated muscle, as well as acting as the molecular scaffold for thick filament formation.[10] The extensible I-band region of cardiac titin has a complex sequence with 3 distinct extensible segments: (1) a PEVK segment, (2) serially linked immunoglobulin-like domains that make up a proximal and a distal immunoglobulin segment, and (3) a unique sequence that is part of the N2B (or

Received May 14, 2001; revision received June 29, 2001; accepted July 2, 2001.

From the Department of Physiology II (N.F., S.K.), the Jikei University School of Medicine, Tokyo; and the Department of Physics (D.S., S.I.), School of Science and Engineering, the Advanced Research Institute for Science and Engineering (S.I.), and the Materials Research Laboratory for Bioscience and Photonics (S.I.), Waseda University, Tokyo, Japan.

Correspondence to Norio Fukuda, PhD, Department of Physiology II, the Jikei University School of Medicine, 3-25-8 Nishi-shinbashi, Minato-ku, Tokyo 105-8461, Japan. E-mail noriof@jikei.ac.jp

Circulation is available at http://www.circulationaha.org

N2BA) element.[10-12] Rat ventricular muscle predominately expresses N2B, having higher stiffness than either bovine or porcine ventricular muscle.[12] In the A-band, titin is composed primarily of super repeats of immunoglobulin- and fibronectin-like domains that interact with myosin at the rod portion of this molecule and C-protein.[13] Therefore, it is possible that the extension of titin imposes passive strain on the thick filament and that this strain modifies the actomyosin interaction by changing the position of the myosin heads.

In the current study, we studied the effect of degradation of the elastic segment of titin, by limited tryptic proteolysis, on the length-dependent activation in rat skinned ventricular trabeculae. A preliminary report has been published in abstract form.[14]

Methods

Experimental Procedure

The heart was removed from male Wistar rats (250 to 300 g) anesthetized with sodium pentobarbital (50 mg/kg IP). Cylinder-shaped, thin trabecular muscles (diameter, 100 to 150 μm) were dissected from the right ventricle in oxygenated Tyrode's solution without Ca^{2+} at 30°C.[6] The preparations were skinned in 1% (vol/vol) Triton X-100™ in the relaxing solution (in mmol/L: Mg-ATP 4, MOPS 10, EGTA 10, free Mg^{2+} 1, and ionic strength 180 [pH 7.0]) for 60 minutes at ≈2°C. The ionic strength was adjusted with KCl. The preparations were stored at −20°C in the relaxing solution containing 50% (vol/vol) glycerol and 2 mmol/L leupeptin for 1 week or less.

Isometric tension was measured in solutions containing 4 mmol/L Mg-ATP, 10 mmol/L MOPS, 1 mmol/L free Mg^{2+}, various concentrations of free Ca^{2+} (adjusted with Ca/[10 mmol/L EGTA]), 0.1 mmol/L P^1,P^5-di(adenosine-5′)pentaphosphate, 15 mmol/L creatine phosphate, 15 U/mL creatine phosphokinase, and 180 mmol/L ionic strength (adjusted with KCl).[6]

Protocols

SL was measured by laser diffraction.[6] Passive tension was measured at SL 2.0, 2.1, 2.2, 2.3, and 2.4 μm by slowly increasing SL (at ≈100 nm/s per sarcomere) from the slack SL (1.9 μm, no passive tension) in the relaxing solution. SL was then readjusted to 1.9 μm for trypsin treatment (see below). Thereafter, passive tension was measured at the above SLs.

Ca^{2+}-activated tension was measured according to a previously described procedure.[15] The preparation was bathed in the low-EGTA (1 mmol/L) relaxing solution for ≈15 seconds just before contraction to minimize the buffering effect of EGTA (the low-EGTA relaxing solution was used only for this purpose).[15] Contraction was stopped by transferring the preparation to the relaxing solution containing 10 mmol/L EGTA. SL was increased in the relaxing solution from 1.9 μm, and active tension was measured at SLs of 1.9, 2.0, 2.1, 2.2, 2.3, and 2.4 μm at the partial- (pCa 5.55) or full- (pCa 4.8) activation condition. Then, SL was readjusted to 1.9 μm for trypsin treatment; the active tension level was also checked before treatment. We used only those data in which the tension was >95% of that measured at the beginning of the experiment. After trypsin treatment, we measured active tension at the above SLs. Active tension was characterized as the total tension produced minus passive tension. Passive and active tension development were reproducible without trypsin treatment.

The control pCa-tension relationship was first obtained at SL 1.9 μm and then at 2.3 μm before trypsin treatment.[6] Then SL was readjusted to 1.9 μm for trypsin treatment. After trypsin treatment, the pCa-tension relationship was obtained at the 2 SLs. The muscle diameter was measured in the relaxing solution on a microscope at a magnification of ×225.[6] All experiments were performed at 20±0.2°C.

Trypsin Treatment

Leupeptin was removed from the skinned trabeculae by immersing the preparations in the relaxing solution, which was stirred for 10 minutes at 20°C. This washing procedure was repeated 7 times. Trypsin (Sigma, type I, ≈11 000 N-benzoyl-L-arginine ethyl ester [BAEE] units per milligram protein) was made up fresh in the leupeptin-free relaxing solution at 0.25 μg/mL.[16,17] The muscle preparation was immersed in this solution for 13 minutes at 20°C, and the reaction was stopped by immersing the preparation in the relaxing solution containing 2 mmol/L leupeptin for 10 minutes.[17]

Confocal Microscopy

Skinned preparations were stained with 3.3 μmol/L Alexa488 phalloidin (Molecular Probes) in the relaxing solution containing 20 mmol/L 2,3-butanedione monoxime for 7 hours at 4°C. Both ends of the preparation were fixed on the glass slide with double-sided adhesive tape and covered with a coverslip to make a solution-exchangeable flow cell. The preparation was activated under the microscope (IX70, Olympus Co) equipped with a real-time confocal scanning unit (CSU10, Yokogawa Electric Co). The confocal fluorescence image of the preparation was recorded on a videotape recorder. SL was calculated from the profile of fluorescence intensity by averaging the lengths of 25 sarcomeres. NIH Image software was used. Each solution contained 1 mmol/L dithiothreitol.

Gel Electrophoresis

Skinned preparations either before or after trypsin treatment were dissolved in lysis solution, heated for 3 minutes at 90°C, and electrophoresed on a 2.5% to 12% acrylamide gradient (or 10% acrylamide) gels.[18] The gels were stained with Coomassie Brilliant Blue. The lanes were scanned densitometrically, and peak areas were integrated geometrically (AE-6910CX, ATTO Co).

Data and Statistical Analyses

Significant differences were tested by the paired Student's *t* test. The unpaired *t* test was used for Figure 3 as well as for the analysis of internal shortening with laser diffraction. For protein content analysis, Tukey's multiple comparison was used. In all cases, statistical significance was verified at $P<0.05$. The pCa-tension relationship was fitted to the Hill equation.[6] Correlations between active tension and muscle diameter were evaluated by testing the correlation of these parameters. All data were expressed as mean±SEM, with n representing the number of muscles.

Results

Titin Degradation by Trypsin

Titin consisted of a doublet before trypsin treatment, T_1 and T_2, on SDS–polyacrylamide gel electrophoresis (Figure 1, left). T_2 is generally considered a degradation product of T_1 (intact titin).[16,17] After trypsin treatment, T_1 was degraded and a new band appeared on the gels below T_2 (T_3). Major thick and thin filament–based proteins other than titin were unaffected (Figure 1).[16,17]

Passive tension was exponentially increased with an increase in SL to a degree similar to that reported by Kentish et al[3] using rat skinned ventricular trabeculae (Figure 2 top). After trypsin treatment, passive tension was significantly (n=10, $P<0.05$) decreased (SL, 2.0 to 2.4 μm). A significant level of passive tension was, however, present in trypsin-treated preparations, particularly at long SLs. Trypsin treatment did not influence muscle diameter at SL 1.9 μm (130.1±7.9 and 131.9±7.7 μm, n=10, $P>0.05$, before and after trypsin, respectively). Highly correlated linear regression lines were obtained before and after trypsin treatment between (1/relative diameter)^2 and SL (Figure 2 bottom). Both regression lines were very close to the volume constant line.

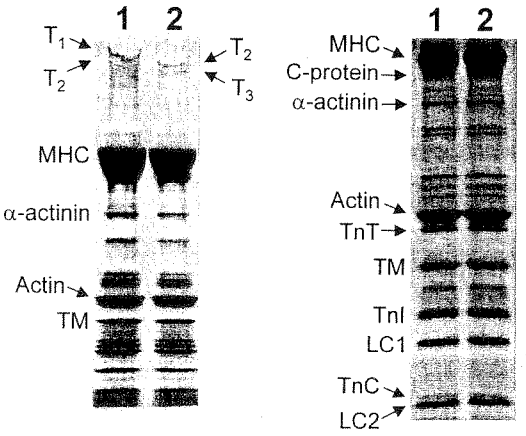

Figure 1. SDS analysis showing effect of trypsin treatment on myofibrillar proteins. Left, 2.5% to 12% acrylamide gradient gel. Right, 10% acrylamide gel. Lanes 1 and 2, untreated and trypsin-treated preparations, respectively. MHC, TnT, TM, TnI, LC1, TnC, and LC2 indicate electrophoretic bands of myosin heavy chain, troponin T, tropomyosin, troponin I, myosin light chain 1, troponin C, and myosin light chain 2, respectively.[16,19] Protein contents relative to actin obtained for trypsin-treated preparations were compared with those obtained for untreated preparations: titin (T_1), 0.08±0.02*; MHC, 1.02±0.05; C-protein, 1.02±0.08; α-actinin, 1.05±0.09; TnT, 0.97±0.05; TM, 1.04±0.05; TnI, 0.96±0.04; LC1, 1.01±0.02; TnC, 0.99±0.04; and LC2, 1.01±0.03. Data for titin and MHC were taken from 2.5% to 12% gels, whereas those for other proteins were from 10% gels. Only titin was significantly degraded ($P<0.01$). Number of experiments=3.

Reproducibility of Ca^{2+}-Activated Tension

The reproducibility of active tension development was checked (Figure 3). Brief contractions, sufficient for the estimation of peak active tension, were repeated 10 times at SL 1.9 or 2.4 μm (≈20 seconds and 5 to 7 seconds for SL 1.9 and 2.4 μm, respectively) at pCa 4.8. Then, a sustained contraction (1 minute) was induced, followed by a brief contraction. At SL 1.9 μm, we observed no differences in relative tension and time to half-maximal tension ($t_{1/2}$) between untreated and trypsin-treated preparations before, during, and after a sustained contraction. At SL 2.4 μm, the degree of tension reduction with repetitive brief contractions was almost the same in untreated and trypsin-treated preparations. During sustained contraction, however, tension was slightly (n=5, $P<0.05$) decreased in trypsin-treated preparations. In the subsequent brief contraction, tension was markedly depressed and $t_{1/2}$ was prolonged, indicating that the sarcomere structure had been disorganized during the preceding sustained contraction. We concluded that in trypsin-treated preparations, brief contractions could be induced at least 10 times with minimal damage to the sarcomere structure.

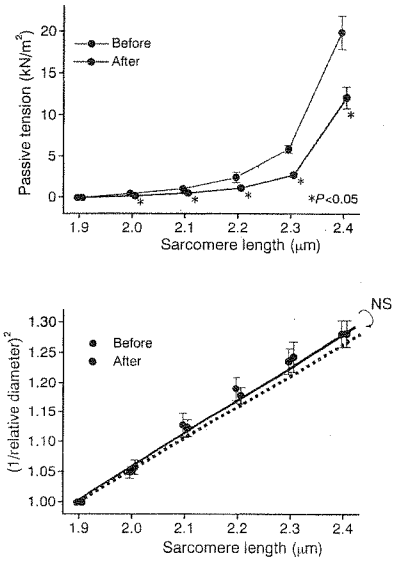

Figure 2. Effects of trypsin treatment on passive tension (top) and muscle diameter (bottom). Data were taken from same preparations for top and bottom panels. Bottom, Diameter was normalized by value at SL 1.9 μm for before and after trypsin treatment. Before trypsin, $y=0.581x-0.099$ ($R=0.89$, $P<0.0001$); after trypsin, $y=0.578x-0.099$ ($R=0.89$, $P<0.0001$). Slopes of 2 linear regression lines were not significantly different (NS). Dotted green line shows constant volume. Vertical bars are SEM of 10 data points.

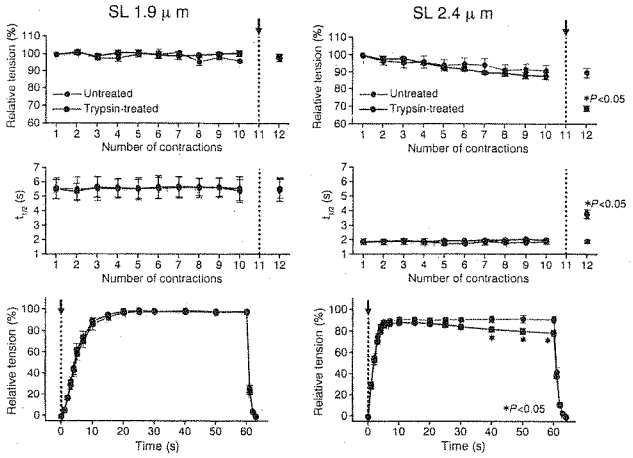

Figure 3. Reproducibility of active tension development at SL 1.9 and 2.4 μm. Top and middle, Changes in tension and $t_{1/2}$, respectively. Bottom, Time course of sustained contraction. Tension is given relative to that of first contraction. Absolute tension values of first contraction were 43.0±5.9 and 41.6±6.7 kN/m² (n=5, $P>0.05$), respectively, for untreated and trypsin-treated preparations at SL 1.9 μm and 94.1±8.6 and 69.4±5.6 kN/m² (n=5, $P<0.05$), respectively, for untreated and trypsin-treated preparations at SL 2.4 μm. Dotted lines indicate point at which sustained contraction was induced.

Effect of Trypsin on SL-Tension Relationship

Active tension was dramatically increased with SL before trypsin treatment, and the slope was steeper at partial activation than at full activation (Figure 4 left).[3] Trypsin treatment did not influence active tension at SL 1.9 μm.[16,17] Active tension was, however, significantly ($P<0.01$) decreased after trypsin treatment at SLs of 2.0 μm and longer under both activating conditions. We performed another series of experiments, maintaining SL at 2.4 μm (Figure 4 right). Active tension was markedly decreased after trypsin treatment. The degree of tension reduction was similar to that obtained when preparations were treated with trypsin at SL 1.9 μm: 93.2±8.4 and 64.2±8.1 kN/m² (n=6, $P<0.01$), respectively, at pCa 4.8 before and after trypsin and 75.0±5.1 and 51.3±7.1 kN/m² (n=6, $P<0.01$), respectively, at pCa 5.55 before and after trypsin.

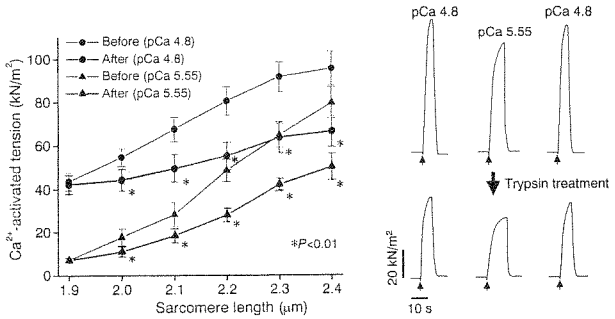

Figure 4. Effect of titin degradation on active tension. Left, SL–active tension relationships before and after trypsin treatment. Vertical bars are SEM of 6 and 7 data points, respectively, for pCa 5.55 and 4.8. Right, Typical chart recording showing effect of trypsin treatment on active tension at SL 2.4 μm. Note that trypsin treatment was performed at SL 2.4 μm in this experiment. Small arrows indicate point at which contraction was induced.

We measured average SL in the central region of the muscle during contraction (pCa 4.8) by laser diffraction. SLs set at 2.0, 2.1, 2.2, 2.3, and 2.4 μm in the relaxing condition (increased stepwise from 2.0 μm), respectively, were decreased to a similar degree in untreated and trypsin-treated preparations: 1.94±0.02 vs 1.93±0.02, 2.01±0.02 vs 2.00±0.02, 2.11±0.02 vs 2.10±0.03, 2.20±0.03 vs 2.19±0.02, and 2.29±0.02 vs 2.28±0.04 μm (n=4, $P>0.1$ for each comparison). The observed degree of internal shortening (ie, 3% to 5%) was consistent with that reported previously in rat skinned ventricular trabeculae.[3] If the degree of internal shortening is small enough, it can be concluded that titin-based passive tension is present during contraction in the preparations not treated with trypsin (see Figure 2 top).

Furthermore, we checked SL changes in the trypsin-treated preparation by using a confocal microscope. Figure 5 suggests that in the center of muscle, the resting SL of 2.33±0.01 μm was shortened to 2.25±0.07 μm during contraction (pCa 4.8) and returned to 2.32±0.01 μm on deactivation (internal shortening, ≈3.5%). Figure 5 also suggests that major deterioration does not occur in the sarcomere structure before, during, or after contraction after trypsin treatment.

Effect of Trypsin on the Increase in Active Tension by Osmotic Compression

It is well established that dextran T-500 osmotically decreases interfilament lattice spacing in skinned cardiac muscle[7] and consequently augments tension development.[5,6] When the muscle diameter was reduced by increasing the concentration of dextran T-500 (up to 6% wt/vol; Amersham Pharmacia Biotech), active tension was augmented, and significantly correlated linear regression lines were obtained between muscle diameter and active tension under partial and maximal activation conditions (Figure 6, SL 1.9 μm). The slope of the linear regression line was steeper under partial activation. The slope of the regression line under the partial or full activation condition was unaffected by trypsin treatment.

SL Change vs Osmotic Compression in Trypsin-Treated Preparations

Figure 7 compares the diameter–active tension relationships converted from the SL–active tension relationships (Figure 4 left) with those obtained by osmotic compression (Figure 6) for trypsin-treated preparations. At each pCa, the slope of the linear regression line obtained by SL change nearly overlapped that obtained by osmotic compression.

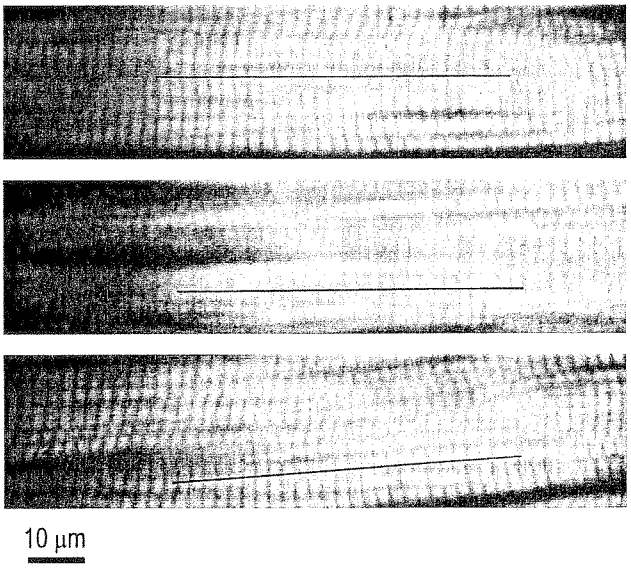

Figure 5. Typical confocal fluorescence images of sarcomeres in trypsin-treated preparation. Top, Relaxation before contraction; middle, during contraction at pCa 4.8; bottom, relaxation after contraction. Each image was taken from same preparation at video rate of 1/30 second, but it does not show precisely same region owing to movement of preparation on solution change. SL was measured along each thin line.

Effect of Trypsin on Ca^{2+} Sensitivity

Increasing SL from 1.9 to 2.3 μm caused a decrease in muscle diameter from 121.8±6.9 to 107.2±6.6 μm (≈12% reduction, n=5, $P<0.01$) and shifted the pCa-tension relationship to the left (Figure 8 top).[6] Dextran T-500 (6% wt/vol) reduced the diameter from 126.3±9.2 to 109.8±6.9 μm (≈13% reduction, n=4, $P<0.01$) at SL 1.9 μm and shifted the pCa curve leftward to a similar degree as that obtained by lengthening (Figure 8 bottom).[6] It was found that trypsin treatment did not affect the increase in Ca^{2+} sensitivity, as reflected by the shift of the midpoint of the pCa curve, by both lengthening (0.184±0.005 and 0.178±0.006 pCa units, $P>0.05$, before and after trypsin, respectively) and osmotic compression (0.163±0.013 and 0.162±0.017 pCa units, $P>0.05$, before and after trypsin, respectively).

The Hill coefficient values[6] for untreated and trypsin-treated preparations were 6.25±0.59 and 6.47±0.55 ($P>0.05$), respectively, at SL 1.9 μm and 5.97±0.56 and 5.74±0.15 ($P>0.05$), respectively, at SL 2.3 μm. Those for untreated and trypsin-treated preparations were 6.60±0.45 and 6.81±0.39 ($P>0.05$), respectively, without dextran T-500 and 5.58±0.44 and 5.40±0.29 ($P>0.05$), respectively, with dextran T-500. Trypsin treatment did not affect the cooperative activation of the thin filament as reflected by the Hill coefficient.

Discussion

We have demonstrated that the SL–active tension relationship in rat skinned ventricular trabeculae is primarily modulated

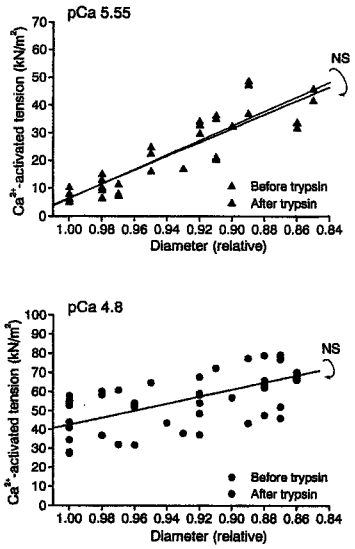

Figure 6. Plots of active tension vs muscle diameter. Preparations were compressed with dextran T-500 instead of increasing SL (SL fixed at 1.9 μm). Diameter was given relative to value without dextran T-500. pCa 5.55: before trypsin, $y=-261.7x+268.1$ ($R=-0.92$, $P<0.0001$); after trypsin, $y=-249.9x+256.4$ ($R=-0.92$, $P<0.0001$). pCa 4.8: before trypsin, $y=-183.9x+226.7$ ($R=-0.63$, $P<0.0001$); after trypsin, $y=-184.1x+226.5$ ($R=-0.66$, $P<0.0001$). Slopes of 2 linear regression lines were not significantly different in either pCa condition (NS). Data are pooled from 4 and 6 experiments, respectively, for pCa 5.55 and 4.8.

by 2 factors, 1 of which is related to titin extension and the other to a reduction of interfilament lattice spacing (Figures 4, 6, and 7). Consistent with earlier reports,[4–6] Ca^{2+} sensitivity was predominantly modulated by changes in interfilament lattice spacing but was unaffected by trypsin treatment (Figure 8). We now discuss these results, focusing on the role of titin in the regulation of the formation of force-generating cross-bridges.

Helms et al[16] found that the anti-titin antibody 9D10, which labels the PEVK segment of titin, failed to label the sarcomere after trypsin treatment in rat skinned cardiac cells. The authors concluded that passive tension was lowered after trypsin treatment due to degradation of the PEVK segment. In rat skinned ventricular trabeculae, titin and collagen are the most significant contributors to passive tension, with titin dominating at the shorter end of the working range of SL and collagen at longer SLs.[20] We therefore consider that the passive tension insensitive to trypsin (Figure 2 top) is predominantly attributable to collagen. It has also been pointed out that collagen could cause shrinkage of the lattice with increasing SL when the plasma membrane is absent.[7] Therefore, the lattice spacing may tend to remain unchanged on titin degradation in collagen-rich fibers, such as in rat ventricular trabeculae (Figure 2 bottom).

The results of Figure 3, as well as those of Figure 5, suggest that brief exposure of the trypsin-treated preparation to Ca^{2+} does not deteriorate the sarcomere structure. This appears to be contrary to the conclusion of a well-known earlier report.[21] That study, however, was conducted with rabbit fast skeletal muscle in the longer SL range (ie, 2.6 to 3.0 μm) under sustained contraction for electron microscopic observation.

We found that active tension was decreased at SLs beyond the slack SL after trypsin treatment (Figure 4). Because the degree of internal shortening was nearly the same for untreated and trypsin-treated preparations, it is unlikely that the decrease in active tension was due to excessive shortening of sarcomeres after trypsin treatment. Alternatively, it is possible that the decrease in active tension was due to the effect of trypsin on minor and/or unknown proteins. However, if one assumes that the mechanical as well as regulatory properties of the cardiac muscle contractile system are predominantly determined by the major contractile proteins examined in the current study, as is generally thought, it is reasonable to conclude that passive tension due to titin extension regulates active tension development, because the major proteins other than titin were not degraded (Figure 1) and major deterioration did not occur in the sarcomere structure on contraction (Figures 3 and 5) after trypsin treatment. Similar evidence for an interplay between passive and active tension generation has been obtained in earlier work on the role of minititin, a passive tension generator, in insect indirect flight muscle.[22] Active tension and active stiffness were increased with passive tension, and passive stiffness due to weak-binding cross-bridges increased linearly with passive tension.[22] Experiments were also performed in skeletal muscle,[23] and the authors concluded that the number of force-generating cross-bridges was increased with passive tension.[23]

Wakabayashi et al,[24] using synchrotron x-rays, found that in frog skeletal muscle, stretching the resting muscle from

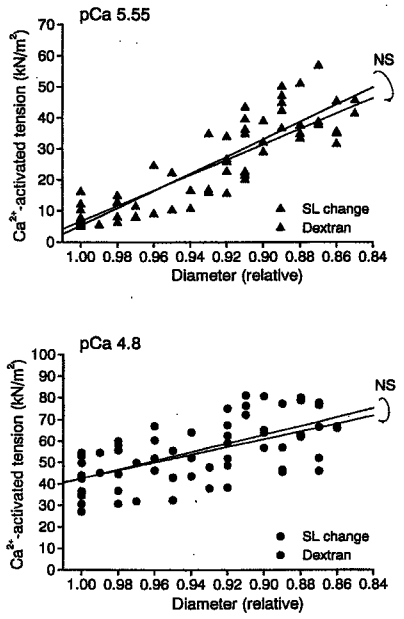

Figure 7. Comparison of effect of SL change with that of osmotic compression on active tension in trypsin-treated preparations. Data were taken from Figures 4 and 6. Diameter was given relative to value before lengthening or dextran T-500 addition. SL change: pCa 5.55, $y=-278.8x+284.1$ ($R=-0.87$, $P<0.0001$); pCa 4.8, $y=-203.5x+246.1$ ($R=-0.61$, $P<0.0001$). See Figure 6 for data of osmotic compression. Slopes of 2 linear regression lines were not significantly different (NS).

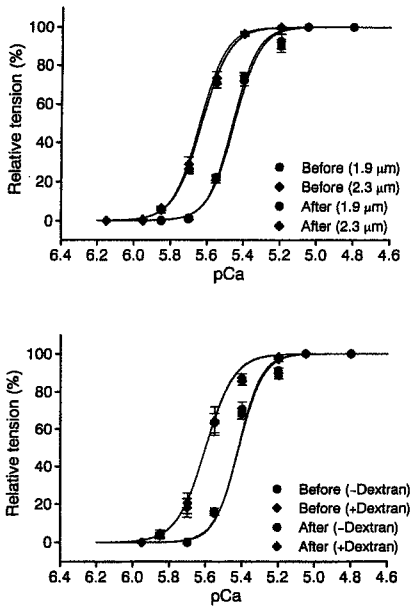

Figure 8. Effects of trypsin treatment on changes in Ca^{2+} sensitivity. Top, SL was changed from 1.9 to 2.3 μm in absence of dextran T-500. Bottom, 6% dextran T-500 was added instead of increasing SL to 2.3 μm (SL fixed at 1.9 μm). Vertical bars are SEM of 5 and 4 data points, respectively, for lengthening and osmotic compression.

full-overlap to nonoverlap length caused an increase in the myosin periodicity by ≈0.6%. This result suggests that passive tension due to extension of titin alters the thick filament structure. The authors also noted that stretching of the resting muscle caused loss of the characteristic resting order of myosin heads around the thick filament backbones.[24] It is thus reasonable to assume that a similar mechanism operates at a shorter SL range in cardiac muscle, which has a higher stiffness than skeletal muscle owing to different expressions of titin.[25]

Recent lines of evidence suggest that cross-bridge arrangement can vary in resting muscle, and cross-bridges are distributed in 3 populations: the cross-bridges that are ordered on the thick filament helix and those that are disordered; within the disordered population, some cross-bridges are detached and others are weakly bound to actin.[26,27] The apparent order-disorder transition is reportedly affected by temperature,[26,27] ionic strength,[28] and phosphorylation of myosin light chains[29] and C-protein.[30] It can therefore be predicted that when the disordered population is increased, the probability of myosin attachment to thin filaments is increased, enhancing the subsequent formation of force-generating cross-bridges under activating conditions. We therefore propose that passive tension due to extension of titin modulates the thick filament structure, increasing the disordered population, which enhances the interaction of myosin heads with thin filaments and consequently increases the number of force-generating cross-bridges.

A recent study showed that the magnitude of the SL-dependent shift of the pCa-tension relationship was diminished by trypsin treatment in rat skinned ventricular cells.[17] This finding is in disagreement with our results (Figure 8). Because those authors used cells that reportedly have lesser amounts of collagen than do trabecular preparations,[20] the constraint by collagen to maintain the lattice volume may have been lost. This may result in a decrease in Ca^{2+} sensitivity by expansion of interfilament lattice spacing, especially at long SLs. Other factors contributing to the difference in the effect of titin degradation on Ca^{2+} sensitivity are differing ionic conditions and experimental protocols.

More recently, Cazorla et al[31] presented evidence that titin-based passive tension affects Ca^{2+} sensitivity through changes in the lattice spacing in skinned cardiac muscle. The lattice spacing is under the influence of titin as well as of collagen.[7,31] Therefore, in preparations that have a low amount of collagen, such as in cardiac cells, titin-based passive tension likely influences the lattice spacing and subsequently, Ca^{2+} sensitivity. Our trabecular preparations, on the other hand, showed a constant volume behavior after titin degradation (Figure 2 bottom), leading us to propose that titin-based passive tension affects the thick filament structures.

It is well known that the SL dependence of tension generation is markedly attenuated in intact and skinned muscle preparations from the failing human heart.[32,33] It is also known that titin is downregulated in failing human myocardium.[33] The current study suggests that attenuation of the SL-dependent activation in failing myocardium may be due, at least in part, to the downregulation of titin. It would be interesting to investigate the correlation between the expression level of titin and the magnitude of SL-dependent activation in various animal models of heart failure.

Acknowledgments

This work was supported in part by Grants-in-Aid for Scientific Research, for Scientific Research on Priority Areas, and for High-Tech Research Center Project from the Ministry of Education, Science, Sports, and Culture of Japan; by the Japanese Heart Foundation; and by the Vehicle Racing Commemorative Foundation. We thank Naoko Tomizawa for technical assistance.

References

1. Lakatta EG. Length modulation of muscle performance: Frank-Starling law of the heart. In: Fozzard HA, ed. *The Heart and Cardiovascular System.* New York, NY: Raven Press Publishers; 1991:1325–1352.
2. Allen DG, Kentish JC. The cellular basis for length-tension relation in cardiac muscle. *J Mol Cell Cardiol.* 1985;17:821–840.
3. Kentish JC, ter Keurs HEDJ, Ricciardi L, et al. Comparison between the sarcomere length-force relations of intact and skinned trabeculae from right ventricle: influence of calcium concentrations on these relations. *Circ Res.* 1986;58:755–768.
4. Fuchs F, Wang YP. Sarcomere length versus interfilament spacing as determinants of cardiac myofilament Ca^{2+} sensitivity and Ca^{2+} binding. *J Mol Cell Cardiol.* 1996;28:1375–1383.
5. McDonald KS, Moss RL. Osmotic compression of single cardiac myocytes eliminates the reduction in Ca^{2+} sensitivity of tension at short sarcomere length. *Circ Res.* 1995;77:199–205.
6. Fukuda N, Kajiwara H, Ishiwata S, et al. Effects of MgADP on length dependence of tension generation in skinned rat cardiac muscle. *Circ Res.* 2000;86:e1–e6.
7. Irving TC, Konhilas J, Perry D, et al. Myofilament lattice spacing as a function of sarcomere length in isolated rat myocardium. *Am J Physiol.* 2000;279:H2568–H2573.
8. Kajiwara H, Morimoto S, Fukuda N, et al. Effect of troponin I phosphorylation by protein kinase A on length-dependence of tension activation in myocardium. *Biochem Biophys Res Commun.* 2000;272:104–110.

9. Babu A, Sonnenblick E, Gulati J. Molecular basis for the influence of muscle length on myocardial performance. *Science*. 1988;240:74–76.
10. Gregorio CC, Granzier H, Sorimachi H, et al. Muscle assembly: a titanic achievement? *Curr Opin Cell Biol*. 1999;11:18–25.
11. Labeit S, Kolmerer B. Titins: giant proteins in charge of muscle ultrastructure and elasticity. *Science*. 1995;270:293–296.
12. Cazorla O, Feiburg A, Helmes M, et al. Differential expression of cardiac titin isoforms and modulation of cellular stiffness. *Circ Res*. 2000;86:59–67.
13. Labeit S, Gautel M, Lakey A, et al. Towards a molecular understanding of titin. *EMBO J*. 1992;11:1711–1716.
14. Fukuda N, Sasaki D, Ishiwata S, et al. Understanding of sarcomere length (SL)-dependent tension generation in skinned cardiac muscle. *Biophys J*. 2000;78:141A. Abstract.
15. Fukuda N, Fujita H, Fujita T, et al. Spontaneous tension oscillation in skinned bovine cardiac muscle. *Pflugers Arch*. 1996;433:1–8.
16. Helms M, Trombitas K, Granzier H. Titin develops restoring force in rat cardiac myocytes. *Circ Res*. 1996;79:619–626.
17. Cazorla O, Vassort G, Garnir D, et al. Length modulation of active force in rat cardiac myocytes: is titin the sensor? *J Mol Cell Cardiol*. 1999;31:1215–1227.
18. Fujita H, Yasuda K, Niitsu S, et al. Structural and functional reconstitution of thin filaments in the contractile apparatus of cardiac muscle. *Biophys J*. 1996;71:2307–2318.
19. Trombitas K, Granzier H. Actin removal from cardiac myocytes shows that near Z line titin attaches to actin while under tension. *Am J Physiol*. 1997;273:C662–C670.
20. Granzier H, Irving TC. Passive tension in cardiac muscle: contribution of collagen, titin, microtubules, and intermediate filaments. *Biophys J*. 1995; 68:1027–1044.
21. Horowits R, Kempner ES, Bisher ME, et al. A physiological role for titin and nebulin in skeletal muscle. *Nature*. 1986;323:160–164.
22. Granzier H, Wang K. Interplay between passive tension and strong and weak binding cross-bridges in insect indirect flight muscle. *J Gen Physiol*. 1993;101:235–270.
23. Granzier H, Wang K. Passive tension and stiffness of vertebrate skeletal and insect flight muscles: the contribution of weak cross-bridges and elastic filaments. *Biophys J*. 1993;65:2141–2159.
24. Wakabayashi K, Sugimoto Y, Tanaka H, et al. X-ray diffraction evidence for the extensibility of actin and myosin filaments during muscle contraction. *Biophys J*. 1994;67:2422–2435.
25. Linke WA, Ivemeyer M, Olivieri N, et al. Towards a molecular understanding of the elasticity of titin. *J Mol Biol*. 1996;261:62–71.
26. Malinchik S, Xu S, Yu LC. Temperature-induced structural changes in the myosin thick filament of skinned rabbit psoas muscle. *Biophys J*. 1997;73:2304–2312.
27. Xu S, Malinchik S, Gilroy D, et al. X-ray diffraction studies of crossbridges weakly bound to actin in relaxed skinned fibers of rabbit psoas muscle. *Biophys J*. 1997;73:2292–2303.
28. Xu S, Kress M, Huxley HE. X-ray diffraction studies of the structural state of crossbridges in skinned frog sartorius muscle at low ionic strength. *J Muscle Res Cell Motil*. 1987;8:39–54.
29. Levine RJC, Yang Z, Epstein ND, et al. Structural and functional responses of mammalian thick filaments to alterations in myosin regulatory light chains. *J Struct Biol*. 1998;122:149–161.
30. Weisberg A, Winegrad S. Alteration of myosin cross bridges by phosphorylation of myosin-binding protein C in cardiac muscle. *Proc Natl Acad Sci U S A*. 1996;93:8999–9003.
31. Cazorla O, Wu Y, Irving TC, et al. Titin-based modulation of calcium sensitivity of active tension in mouse skinned cardiac myocytes. *Circ Res*. 2001;88:1028–1035.
32. Schwinger RHG, Bohm M, Koch A, et al. The failing human heart is unable to use the Frank-Starling mechanism. *Circ Res*. 1994;74:959–969.
33. Morano I, Hadicke K, Grom S, et al. Titin, myosin light chains and C-protein in the developing and failing human heart. *J Mol Cell Cardiol*. 1994;26:361–368.

Elementary Steps of the Cross-Bridge Cycle in Bovine Myocardium with and without Regulatory Proteins

Hideaki Fujita,* Daisuke Sasaki,† Shin'ichi Ishiwata,†‡ and Masataka Kawai*

*Department of Anatomy and Cell Biology, College of Medicine, The University of Iowa, Iowa City, Iowa 52242, USA; †Department of Physics, School of Science and Engineering, Waseda University, Shinjuku-ku, Tokyo 169-8555, Japan; and ‡Core Research for Evolutional Science and Technology (CREST) Team-13, Japan.

ABSTRACT The role of regulatory proteins in the elementary steps of the cross-bridge cycle in bovine myocardium was investigated. The thin filament was selectively removed by gelsolin and the actin filament was reconstituted without tropomyosin or troponin. Further reconstitution was achieved by adding tropomyosin and troponin. The effects of MgATP and phosphate (Pi) on the rate constants of exponential processes were studied in control, actin filament-reconstituted, and thin filament-reconstituted myocardium at pCa ≤4.66, pH 7.00, 25°C. In control myocardium, the MgATP association constant was 9.1 ± 1.3 mM^{-1}, and the Pi association constant 0.14 ± 0.04 mM^{-1}. The equilibrium constant of the cross-bridge detachment step was 2.6 ± 0.4, and the equilibrium constant of the force generation step was 0.59 ± 0.04. In actin filament-reconstituted myocardium without regulatory proteins, the MgATP association constant was approximately the same, and the Pi association constant increased to 2.8×. The equilibrium constant of cross-bridge detachment decreased to 0.2×, but the equilibrium constant of the force generation step increased to 4×. These kinetic constants regained control values after reconstitution of the thin filament. These results indicate that tension/cross-bridge in the presence of regulatory proteins is ~1.5–1.7× of that in the absence of regulatory proteins. These results further indicate that regulatory proteins promote detachment of cross-bridges.

INTRODUCTION

Striated muscle is a complex system that consists of impulse generation and propagation mechanisms, Ca^{2+} release and uptake mechanisms, Ca^{2+}-sensing and signal-transmission mechanisms, and actomyosin-force generation mechanisms. This complexity makes it difficult to interpret the experimental results when carried out in intact preparations, if the purpose was to understand the cross-bridge mechanisms of force generation. The introduction of chemically skinned (Szent-Györgyi, 1951) and mechanically skinned (Natori, 1954) fibers in which the sarcolemmal barrier was removed was a step forward to overcoming this problem. With the loss of the sarcolemmal barrier, chemical perturbation can be readily applied to the skinned fibers. In addition, the use of a detergent minimizes the Ca^{2+}-uptake mechanism of the sarcoplasmic reticulum and ATP-regenerating mechanism of mitochondria, thus further simplifying the system. The detergent-treated skinned fibers still possess the Ca^{2+}-regulatory system, tropomyosin (Tm) and troponin (Tn) (Endo et al., 1970), which is known to alter the actomyosin kinetics (Murray et al., 1975; Zhao et al., 1996). More recently, investigators have demonstrated with the in vitro motility assay that both gliding speed and force increase by the addition of the regulatory proteins (Gordon et al., 1998; Van Buren et al., 1999; Bing et al., 2000a, b; Homsher et al., 2000). It is desirable to demonstrate these points in physiological ionic strength in skinned fibers, in which force generation capability is maintained, because the in vitro assay is typically carried out at low ionic strength (~50 mM). The low ionic strength enhances the ionic interaction, whereas the major mechanism of force generation may rely on hydrophobic interaction (Kodama, 1985; Rayment et al., 1993; Zhao and Kawai, 1994). To study the influence of regulatory proteins on the cross-bridge kinetics in muscle fibers, it is necessary to modify the regulatory component of the contractile apparatus without interfering with the force-generating capability. However, the extraction-reconstitution method has been limited to small molecules, such as troponin C (Brandt et al., 1990; Zhao et al., 1996), troponin I (Hatanaka and Ohtsuki, 1992; Strauss et al., 1992), and myosin light chain 2 (Hofmann et al., 1990), that play accessory roles for contraction. A new approach using transgenic mice to generate tropomyosin rich in β-isoform (Palmiter et al., 1996) is a similar line of work.

Recently, Fujita et al. (1996) have developed a method that can completely remove the thin filament and reconstitute it in bovine myocardium. In this method, the thin filament in the myocardium was selectively removed by treatment with gelsolin, an actin-severing enzyme, to result in a loss of contractility. The actin filament was reconstituted from purified G-actin under the polymerizing condition. The resulting myocardium was capable of generating tension that was insensitive to Ca^{2+}. Further reconstitution with regulatory proteins Tm and Tn fully recovered the Ca^{2+} sensitivity and isometric tension. A parallel experiment was performed on skeletal muscles which resulted in a formation of the actin filament, but reproducibility of

Submitted December 11, 2000, and accepted for publication November 7, 2001.

Address reprint request to Dr. Masataka Kawai, Department of Anatomy, College of Medicine, The University of Iowa, Iowa City, IA 52242 USA. Tel.: 319-335-8101; Fax: 319-335-7198; E-mail: masataka-kawai@uiowa.edu.

0006-3495/02/02/915/14 $2.00

TABLE 1 Basic solutions

Solution Symbols	$K_2CaEGTA$ mM	K_2EGTA mM	Na_2MgATP mM	Na_2K_2ATP mM	$MgProp_2$ mM	Na_2CP mM	$K_{1.5}Pi$ mM	NaProp mM	Kprop mM	NaN_3 mM	MOPS mM	BDM mM	CK U/ml
Rigor (Rg)	—	—	—	—	—	—	8	55	122.0	—	10	—	—
Relax (Rx)	—	6	2.2	5.0	—	—	8	41	74.5	—	10	40	—
5S0P	6	—	5.83	1.36	—	15	0	0.6	91.7	10	10	—	320
5S32P	6	—	5.7	1.36	—	15	32	0.9	17.3	10	10	—	320
0S8P	6	—	—	—	0.85	15	8	15	87.6	10	10	—	320
5S8P	6	—	5.8	1.36	—	15	8	0.7	73.1	10	10	—	320
−Ca	—	6	5.95	1.13	—	15	—	0.6	91.7	10	10	—	320

Abbreviations: Prop = propionate, CP = creatine phosphate, and CK = creatine kinase. pH of all solutions was adjusted to 7.00.

isometric tension was not as large as in myocardium, presumably because of the presence of nebulin and weak Z-line (Funatsu et al., 1994). In this report, we have combined the actin filament-reconstitution technique with the sinusoidal analysis technique, and the effect of MgATP and Pi concentrations on the rate constants of exponential processes was studied in myocardium both with and without regulatory proteins. Our results indicate that the role of regulatory proteins is to augment force supported by each cross-bridge.

MATERIALS AND METHODS

Chemicals and solutions

Creatine phosphate (Na_2CP), adenosine 5′-triphosphate (Na_2H_2ATP), 3-[*N*-morpholino] propane sulfonic acid (MOPS), and ethylene glycol bis (2-aminoethyl ether)-*N,N,N′,N′* tetraacetic acid (H_4EGTA) were purchased from Sigma Chemical (St. Louis, MO); Triton-X100, (Fisher Scientific, Hanover Park, IL); $CaCO_3$, $Mg(OH)_2$, NaOH, KOH, KH_2PO_4, K_2HPO_4, NaN_3, and propionic (Prop) acid were from Fisher Scientific; and creatine kinase (CK) was from Boehringer Mannheim (Indianapolis, IN).

The compositions of each solution used are shown in Table 1. Experimental solutions are designated by *m*S*n*P, where *m* represents the millimolar concentration of $MgATP^{2-}$ (S), and *n* represents that of phosphate (P, Pi): for example, the 5S8P solution contained 5 mM $MgATP^{2-}$ and 8 mM Pi. The 5S8P solution is also called the standard activating solution. The pCa of all activating solutions was 4.35–4.66, pH was adjusted to 7.00, the Mg^{2+} concentration to 0.5 mM, the total Na to 55 mM, and ionic strength to 200 mM. All activating solutions contained 320 units/ml CK (0.64 mg/ml), and 10 mM NaN_3 to suppress mitochondrial ATPase. EGTA, CaEGTA, and Pi were added as neutral K salts; MgATP and CP as neutral Na salts; and free ATP as $Na_2K_{1.7}ATP$ (neutral salt). Individual concentrations of ionic species were calculated with our computer program using the following association constants (log values at pH 7.0): CaEGTA, 6.28; MgEGTA, 1.61; CaATP, 3.70; MgATP, 4.00; CaCP, 1.15; MgCP, 1.30.

Muscle bundles and proteins

Bovine hearts were obtained from a slaughterhouse and immediately cooled with crushed ice. The muscle bundles (~2 mm in diameter and 10 mm in length) were excised from a straight portion of left ventricular papillary muscles and incubated in the Na-skinning solution containing (mM) 2.0 dithiothreitol (DTT), 30 2,3-butanedione 2-monoxime (BDM), 10 Na_2H_2EGTA, 5.0 Na_2H_2ATP, 2.0 Na_2MgATP, 122 Na propionate (Prop), and 10 MOPS (pH 7.0) for 3 h at 0°C. The Na-skinning solution was used to minimize initial contraction. For further skinning, the solution was replaced with K-skinning solution containing (mM) 2.0 DTT, 30 BDM, 10 K_2H_2EGTA, 5.0 Na_2H_2ATP, 2.0 Na_2MgATP, 122 KProp, and 10 MOPS (pH 7.0), and stored overnight at 0°C. BDM and EGTA were used to minimize force generation. The solution was further replaced with a solution containing 50% (v/v) glycerol, 2.0 DTT, 30 BDM, 10 K_2H_2EGTA, 5.0 Na_2H_2ATP, 2.0 Na_2MgATP, 122 KProp, and 10 MOPS (pH 7.0) and stored at 0°C. The solution was replaced once again the next day, and the muscle bundles were stored in a freezer (−20°C).

Actin was extracted from acetone powder (Kondo and Ishiwata, 1976) of rabbit white skeletal muscles according to the method of Spudich and Watt (1971). We used rabbit skeletal actin for reconstitution because its sequence is almost identical to bovine cardiac actin with four minor substitutions (cardiac → skeletal: D2E, E3D, L298M, S357T) (Vandekerckhove and Weber, 1979). Purified G-actin was stored at 0°C and used within 2 weeks of extraction. The tropomyosin (Tm)-troponin (Tn) complex (nTm) was prepared from bovine cardiac muscle according to the method of Ebashi et al. (1968). Bovine plasma gelsolin was prepared according to the method of Kurokawa et al. (1990).

Selective removal and reconstitution of actin filament were performed as previously described (Fujita et al., 1996; Fujita and Ishiwata, 1998, 1999; Ishiwata et al., 1998). Particular care was taken to regulate the temperature and time of actin filament reconstitution protocol to prevent excessive elongation of the actin filament (Fujita and Ishiwata, 1998, 1999; Ishiwata et al., 1998) as seen in the initial report (Fujita et al., 1996).

Experimental procedure and deduction of kinetic constants

A strip of bovine myocardium was removed from the skinned muscle bundle and both ends were attached to a stainless steel wire (diameter: 210 μm) with nail polish, one end of which was attached to a tension transducer and the other to a length driver. The myocardium was stretched until a small passive tension was observed. At this point, the average sarcomere length was 2.0 μm, and it ranged 1.9–2.1 μm as determined by confocal microscopy after staining with rhodamine-conjugated phalloidin. The length (L_0 ~2 mm) of the myocardium was determined by measuring the end-to-end distance. The diameter was measured under a dissection microscope (20×). The diameter averaged 110 ± 2 μm (n = 73, ± SE). Myocardium was chemically skinned further in relaxing solution containing 1% (v/v) Triton-X100 for 20 min. Triton-X100 was washed by relaxing solution (Rx) before experiments.

Three muscle models (control, actin filament-reconstituted, and thin filament-reconstituted myocardium) were maximally activated in the presence of Ca^{2+} in a temperature-controlled bath at 25°C for subsequent experiments. The 0.25% L_0 peak-to-peak sinusoidal wave at 18 discrete frequencies (f: 0.13–100 Hz) was digitally synthesized in a personal computer with 386 CPU (Industrial Computer Source, San Diego, CA) that controlled the length driver via a 14-bit digital/analog converter. Tension and length signals were simultaneously digitized by two 16-bit analog/digital converters and complex modulus data $Y(f)$ were calculated as the ratio of force change and length change in the frequency domain. The

complex modulus data obtained during relaxation were subtracted to correct for the irrelevant pickup at high frequencies. The data were further corrected by using the rigor response. The complex modulus data were resolved into two exponential processes (B and C) by fitting the data to Eq. 1 (Kawai and Brandt, 1980; Wannenburg et al., 2000):

$$\text{Process B} \qquad \text{Process C}$$

$$Y(f) = H - B/(1 + b/fi) + C/(1 + c/fi) \qquad (1)$$

where $i = \sqrt{-1}$. Lowercase letters b and c represent the characteristic frequencies of the respective processes, and uppercase letters B and C represent their respective magnitudes. $2\pi b$ and $2\pi c$ are the apparent rate constants of the respective processes. Process B is a low-frequency exponential delay (b ~1 Hz) at which muscle generates oscillatory work. Process C is a high frequency exponential advance (c ~4 Hz) at which the muscle absorbs work from the length driver. Stiffness was calculated as $Y_\infty = H - B + C$. Process B corresponds to "phase 3," process C corresponds to "phase 2," and Y_∞ corresponds to "phase 1" of tension transients in response to a step-length change (Huxley and Simmons, 1971; Heinl et al., 1974). An implicit assumption of the transient analysis in response to step or sinusoidal length change is that the rate constants of elementary steps are strain-sensitive (Huxley and Simmons, 1971; Kawai and Brandt, 1980; Kawai and Zhao, 1993), so that a length change causes an instability in the cross-bridge cycle. A gradual transition to the new steady state is observed as tension transients in step analysis and exponential processes in sinusoidal analysis. In relaxed and rigor muscle fibers, these transients or exponential processes are absent, indicating that they are the results of cycling cross-bridges. Details of the sinusoidal analysis technique have been published (Kawai and Brandt, 1980).

Sodium dodecyl sulfate (SDS)-gel electrophoresis

Myocardium at each step of reconstitution was pooled and dissolved in a sample diluting buffer (2% SDS, 25% glycerol, 5% β-mercaptoethanol, 62.5 mM Tris-HCl, pH 6.8) and heated for 3 min at 90°C. SDS-polyacrylamide gel electrophoresis (PAGE) was carried out according to the method of Laemmli (1970) with an 8–16% linear gradient running gel and a 4% stacking gel (Bio-Rad, Hercules, CA). Protein was stained using Coomassie brilliant blue R-250.

RESULTS

Removal of the thin filament and reconstitution of the actin filament and the thin filament in myocardium

Fig. 1 shows a result from SDS-PAGE of control, gelsolin-treated, actin filament-reconstituted, and thin filament-reconstituted myocardium. In gelsolin treated myocardium (*lane 2*), the amount of actin, TnT, Tm, and TnI was markedly reduced or absent compared with the control myocardium (*lane 1*), whereas the amount of myosin heavy chain (HC), α-actinin (α-Ac), myosin light chain 1 (LC_1), myosin light chain 2 (LC_2) did not change much. A new band is seen in lane 2 below α-Ac, and this is gelsolin. In the actin filament-reconstituted myocardium (*lane 3*), actin recovery was nearly equal to that of the control, whereas Tm, TnI, and TnT are absent. After reconstitution with regulatory proteins (*lane 4*), the amount of Tm, TnI, and TnT recovered to a level similar to the control. The calculated density ratio of actin/LC_1 of gelsolin-treated myocardium was 14% of control myocardium, but this value is inflated because the actin band in control myocardium is saturated because of overloading. Thus, the amount of remaining actin in gelsolin-treated myocardium must have been <14%. The remaining actin is essential for subsequent elongation of the actin filament. We could not resolve the TnC band because cardiac TnC appears close to LC_2, and because the staining of TnC is weak compared with LC_2 with the method we used. There is a weak band between two light chains, but its origin is unknown.

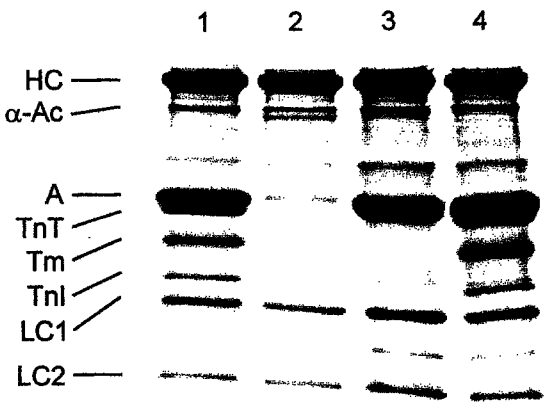

FIGURE 1 SDS-PAGE of control (*lane 1*), gelsolin-treated (*lane 2*), actin filament-reconstituted (*lane 3*), and thin filament-reconstituted (*lane 4*) myocardium. See Fig. 2 for detail of the treatments.

Fig. 2 shows a slow pen trace of isometric tension at each step of removal and reconstitution of the thin filament. Myocardium was initially tested by the Ca^{2+}-activating solution (5S0P) without Pi (Fig. 2 *A*). Then at G, the myocardium was treated by the solution that contained (mM) 117 KCl, 4.25 $MgCl_2$ (2.2 free Mg^{2+}), 2.2 Na_2H_2ATP (2.0 $MgATP^{2-}$), 2.0 H_4EGTA, 20 MOPS (pH 7.0), 2.0 $CaCl_2$, 40 BDM, and 0.3 mg/ml gelsolin at 2°C for 100 min to selectively remove the thin filament. BDM was used to suppress tension development during gelsolin treatment that requires Ca^{2+}. There was no active tension development when tested with the 5S0P solution (pCa 4.66) after gelsolin treatment (Fig. 2 *B*). At Ac, the myocardium was treated by the actin-polymerizing solution that contained (mM) 80 KI, 4.0 $MgCl_2$, 4.0 ATP, 4.0 EGTA, 40 BDM, 20 K-phosphate (pH 7.0), and 1.0 mg/ml G-actin at 2°C to reconstitute the actin filament. The actin-polymerizing solution was replaced every 7 min to avoid nucleation of actin. Similarly, KI was used to deter nucleation. After a total of 28 min (7 min × 4) of actin polymerizing treatment (Ac), this particular myocardium developed ~65% of the control tension (Fig. 2 *C*). Average active tension after reconstitution of the actin filament was 69 ± 5% (n = 26). In the actin filament-reconstituted myocardium, isometric tension developed in the solution that lacked Ca^{2+}, indicating the absence of regulatory proteins (Fujita et al., 1996).

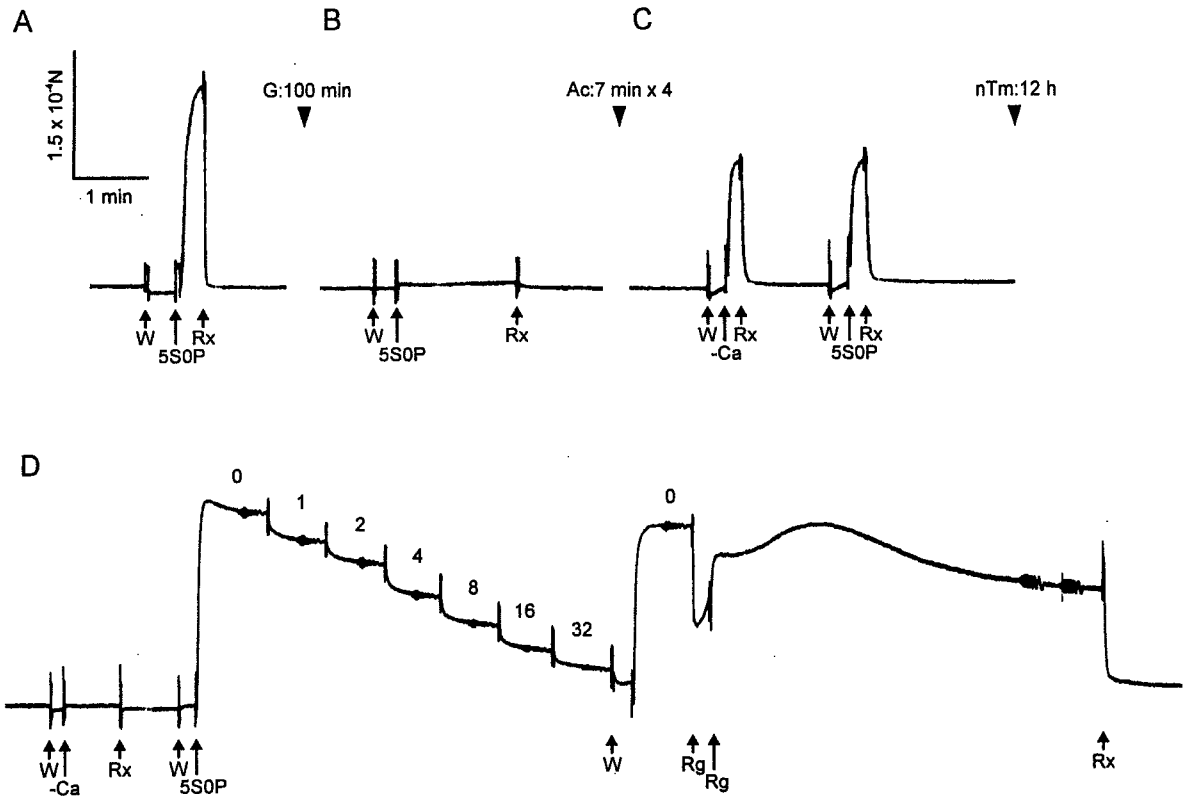

FIGURE 2 A slow pen trace of isometric tension at each step of removal and reconstitution of the thin filament. (*A*) Control myocardium; (*B*) After gelsolin treatment for 100 min (G); (*C*) After actin filament-reconstitution (Ac); (*D*) After thin filament-reconstitution (nTm). Control myocardium was first activated in 5S0P solution (pCa 4.66) at 25°C (*A*). Before activation, myocardium was immersed in the same 5S0P solution at 0°C to wash out BDM and Pi (W). Myocardium did not develop active tension in W because of the low temperature. After gelsolin treatment, myocardium was immersed in 5S0P solution at 25°C to confirm the removal of thin filament (*B*). After reconstitution of actin filament (Ac), myocardium was immersed in the solution without Ca^{2+} (−Ca) then the solution with Ca^{2+} (5S0P) at 25°C to confirm the absence of the regulatory system. The amount of isometric tension developed did not depend on Ca^{2+} (*C*). After reconstitution of regulatory proteins (nTm), active tension did not develop without Ca^{2+}, but it developed with Ca^{2+} (*D*). In *D*, the complex modulus data were collected at seven different Pi concentrations (0–32 mM), and the initial activation at 0 mM Pi was repeated to detect any deterioration in the preparation. The preparation was discarded when a >20% tension decrease was noticed. The relaxation was obtained in the solution containing 40 mM BDM (Rx) at 0°C. All activations including rigor were performed at 25°C. All records in this figure were taken sequentially from the same myocardium. Numbers above tension trace in (*D*) indicate the mM Pi concentration.

As seen in Fig. 2 *C*, isometric tension did not depend on Ca^{2+} in the actin filament-reconstituted myocardium. Relaxation was achieved by immersing the myocardium in the solution containing 40 mM BDM (Rx) at 0°C. To reconstitute the thin filament, the actin filament-reconstituted myocardium was then immersed in the Rx solution containing 4 mg/ml Tm-Tn complex for 12 h at 0°C (nTm). Care was taken so that the volume of the solution did not change because of evaporation or condensation. After reconstitution of regulatory proteins with nTm, the myocardium regained the Ca^{2+} sensitivity. It did not develop tension in the absence of Ca^{2+}, and did develop active tension in the presence of Ca^{2+} (Fig. 2 *D*). We infer from this observation that the reconstitution of the thin filament was complete. Isometric tension after reconstitution of regulatory proteins was 105% of that of the control in this particular myocardium (compare Fig. 2, *A* and *D*), and averaged 107 ± 4% (n = 26). In other words, the reconstitution of Tm and Tn augmented active tension by ~50%. Thus, it can be concluded that higher force is supported if Tm and Tn are present under the experimental conditions we examined.

Effect of MgATP on exponential process C

MgATP and Pi studies were performed to investigate whether the larger force, observed in the presence of Tm and Tn but not in their absence, is related to larger force/cross-bridge or to the larger number of cross-bridges in force-generating states. The effect of MgATP on exponential process C on control, actin filament-reconstituted, and thin filament-reconstituted myocardium (three muscle models) was studied in the range of 0.05–5.00 mM under the maximal Ca^{2+}-activating condition (pCa 4.35–4.66) in the presence of 8 mM Pi. The purpose was to characterize the elementary steps of MgATP binding and subsequent cross-

bridge detachment steps. 8 mM Pi was used because more cross-bridges are populated at AM, AMS, and Det states (scheme 1) than in its absence, hence characterization of transitions between these states is easier. The cross-bridge scheme is depicted in the following.

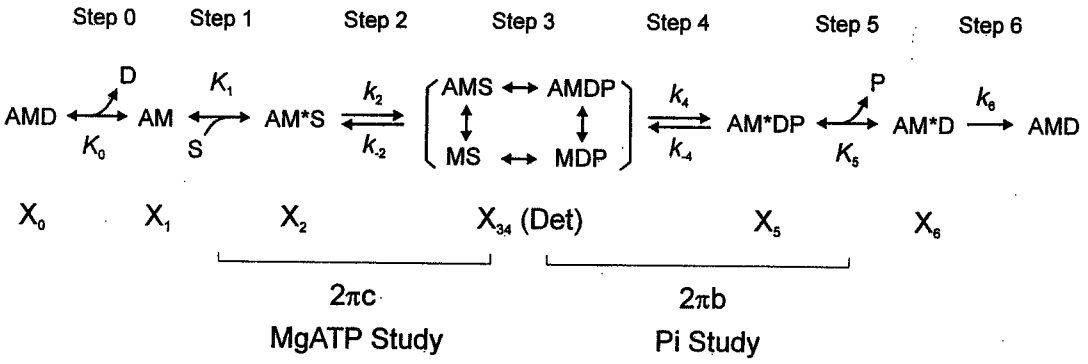

Scheme 1

where A = actin ± regulatory proteins, M = myosin, S = $MgATP^{2-}$, D = MgADP, and P = phosphate. Detached states (MS, MDP) and weakly attached states (AMS, AMDP) are lumped together and called the Det state. Two extreme MgATP solutions (0S8P and 5S8P, Table 1) were prepared and intermediate solutions were made by appropriately mixing the two solutions without affecting other ionic concentrations. Fig. 3 shows complex modulus $Y(f)$ in three muscle models activated at three different MgATP concentrations (0.1 mM, 0.5 mM, 5 mM). These plots are in general similar to those reported on other myocardial systems (Kawai et al., 1993; Zhao and Kawai, 1996, Wannenburg et al., 2000) in their shape and frequency response.

In cardiac muscles, there might be a concern that $2\pi b$ and $2\pi c$ are a part of the same process, because they are close together and only differ by the factor of ~3. A close examination of Fig. 3, *C*, *F*, and *I* indicates that there are at least two semicircles in the Nyquist plots: one going through the fourth quadrant, and the other going through the first quadrant. Note that, with an increase of frequency, the elastic modulus (Fig. 3, *A*, *D*, and *G*) decreases in the low-frequency range, and it increases at the high-frequency range. Also note that the viscous modulus (Fig. 3, *B*, *E*, and *H*) is negative in the low-frequency range, and it becomes positive at the high-frequency range. These shapes unambiguously justify the presence of two exponential processes and validate Eq. 1 as an approximation of the complex modulus data of activated myocardium.

The complex modulus data obtained were fitted to Eq. 1 to deduce the apparent rate constant $2\pi c$. The MgATP dependence on $2\pi c$ of control (○), actin filament-reconstituted (▲), and thin filament-reconstituted (□) myocardium is shown in Fig. 4 with SE error bars. The kinetic constants of elementary steps 1 and 2 of the cross-bridge cycle (scheme 1) were determined by fitting the MgATP dependence of $2\pi c$ to Eq. 2 (Kawai and Halvorson, 1991).

$$2\pi c = k_2K_1S/(1 + K_1S) + k_{-2} \quad (2)$$

where S denotes the concentration of $MgATP^{2-}$. When the three curves in Fig. 4 are compared, there is one obvious difference: the zero intercept (= k_{-2}) of ▲ is twice that of ○ and □. Other features of the curves, such as the half-saturation point (= $1/K_1$) and infinite ATP asymptote (= $k_2 + k_{-2}$) do not seem to be much different in the three curves. These features result in approximately $0.5 \times k_2$, $2 \times k_{-2}$, $0.25 \times K_2$, and little change in K_1 if regulatory proteins Tm and Tn are absent. The actual result of the data fitting is summarized in Table 2. As seen in Table 2, in control myocardium, the association constant of MgATP to cross-bridges (K_1) was 9.1 ± 1.3 mM^{-1} (± SE, n = 11). The forward rate constant of cross-bridge detachment step 2 (k_2) was 26.6 ± 1.2 s^{-1}. The backward rate constant (k_{-2}) was 12.1 ± 1.3 s^{-1}. The equilibrium constant K_2 (= k_2/k_{-2}) was 2.6 ± 0.4. In actin filament-reconstituted myocardium without regulatory proteins, K_1 slightly decreased to 0.95×; k_2 decreased to 0.50×; k_{-2} increased to 1.9×; and K_2 decreased to 0.23×. The kinetic constants of the thin filament-reconstituted myocardium were not different from the control myocardium (Table 2), indicating that the reconstitution was functionally complete.

Effect of phosphate (Pi) on exponential process B

To determine the kinetic constants associated with elementary steps 4 and 5, we studied the effect of Pi in the range of 0–32 mM on exponential process B in the three muscle models (Fig. 5). These studies were carried out under the maximal Ca^{2+}-activating condition (pCa 4.66) and in the presence of a saturating MgATP concentration (5 mM). Two Pi solutions, 5S0P and 5S32P, were initially prepared, and these were mixed appropriately to obtain intermediate

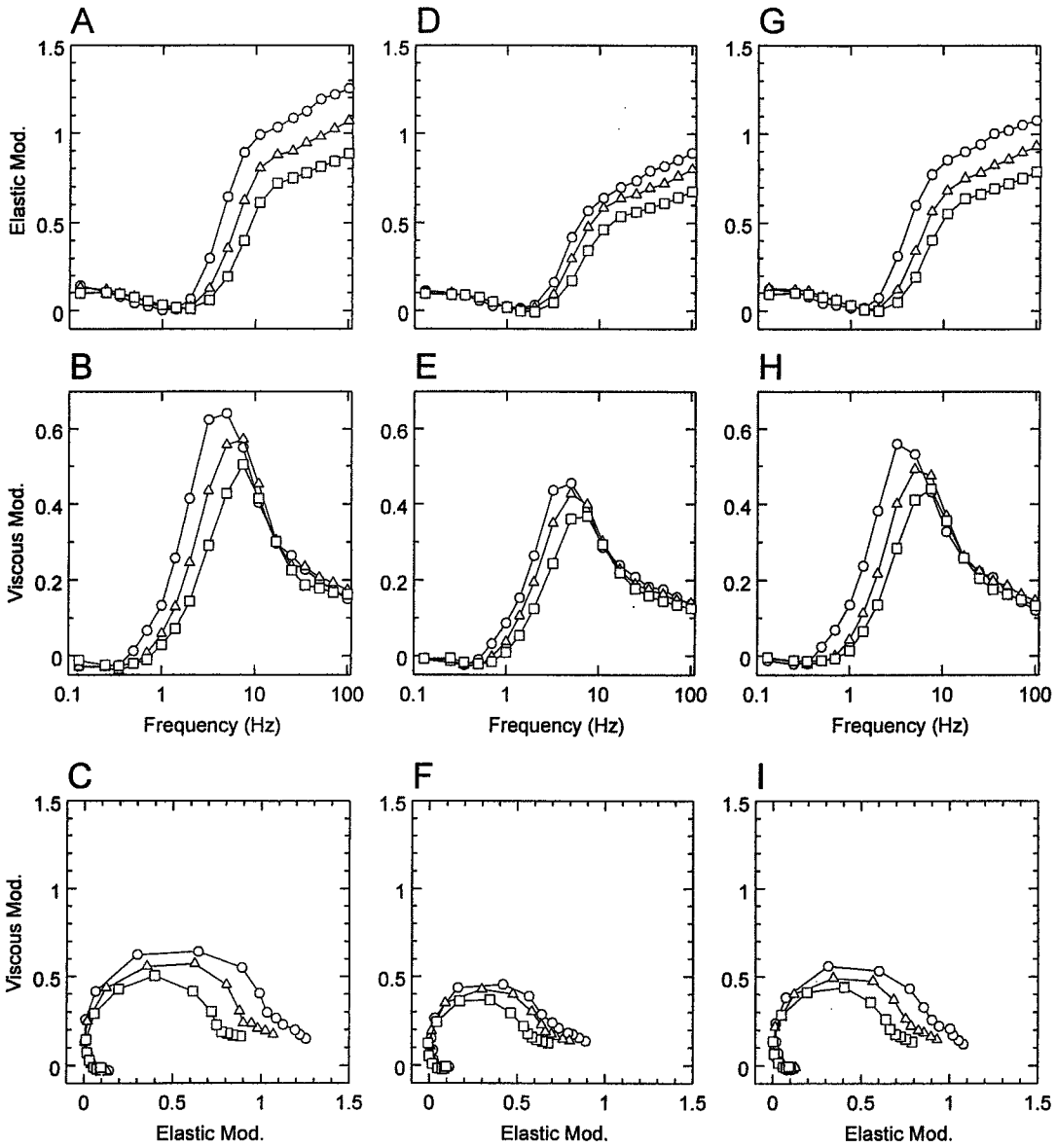

FIGURE 3 The effects of MgATP on the complex modulus $Y(f)$ in (*A–C*) control, (*D–F*) actin filament-reconstituted, and (*G–I*) thin filament-reconstituted myocardium. (*A*, *D*, and *G*) Elastic modulus vs. frequency. (*B*, *E*, and *H*) Viscous modulus vs. frequency. (*C*, *F*, and *I*) Data shown in Nyquist plot, which is a plot of elastic modulus (in abscissa) vs. viscous modulus (in ordinate). 0.1 mM MgATP (○), 0.5 mM MgATP (△), and 5 mM MgATP (□). The phosphate concentration was fixed to 8 mM. Peak-to-peak amplitude was 0.25% L_0. T_c (initial control tension) was 29 ± 3 kN/m^2 (n = 11) for control myocardium; 27 ± 3 kN/m^2 (n = 13) for actin filament-reconstituted myocardium; and 29 ± 3 kN/m^2 (n = 11) for thin filament-reconstituted myocardium. The units of elastic and viscous moduli are mN/m^2.

Pi solutions. The complex modulus data were fitted to Eq. 1 to obtain the apparent rate constant $2\pi b$. $2\pi b$ was then plotted against the Pi concentration and fitted to Eq. 3 (Kawai and Halvorson, 1991) to deduce the kinetic constants of elementary steps 4 and 5 of the cross-bridge cycle (Fig. 5).

$$2\pi b = \sigma k_4 + k_{-4}K_5P/(1 + K_5P) \quad (3)$$

where

$$\sigma = K_2K_1S/\{1 + (1 + K_2)K_1S\} \quad (4)$$

and P indicates the Pi concentration. K_1 and K_2 obtained from the MgATP study and S = 5 mM were used for calculation of σ. The results are summarized in Table 2. In the control myocardium, the rate constant of the force generation step (k_4) was 7.1 ± 0.6 s^{-1} (n = 10) and its reversal step (k_{-4}) was 12.6 ± 1.3 s^{-1}. The equilibrium

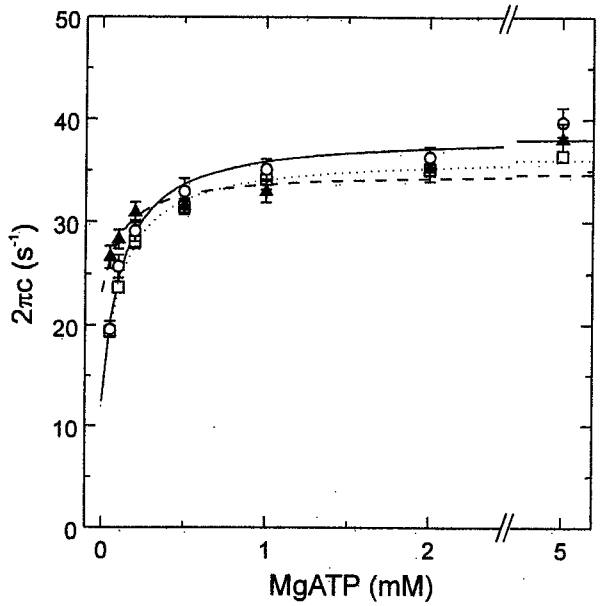

FIGURE 4 The rate constant $2\pi c$ is plotted as a function of MgATP concentration. (○ *and continuous line*) Bovine control myocardium (n = 11); (▲ *and dashed line*) actin filament-reconstituted myocardium (n = 7); (□ *and dotted line*) thin filament-reconstituted myocardium (n = 11). Error bars represent SE. Continuous curves are based on Eq. 2.

constant K_4 (= k_4/k_{-4}) of the force generation step was 0.59 ± 0.04, and the Pi association constant (K_5) was 0.14 ± 0.04 mM^{-1}. In actin filament-reconstituted myocardium, k_4 increased to 1.6×; k_{-4} decreased to 0.4×; K_4 increased to 4×; and K_5 increased to 2.8×. The kinetic constants of the thin filament-reconstituted myocardium were not significantly different from the control myocardium. Once again, this fact indicates that the reconstitution was functionally complete.

The endogenous Pi concentration in myocardium in the absence of added Pi

The Pi concentration in myocardium in the absence of added Pi is not zero. This is because Pi may be a contaminant in various phosphate compounds, particularly in Na_2CP, and because of continuous hydrolysis of ATP. One method of estimating the endogenous phosphate concentration (P_0) is to extrapolate $2\pi bB$ to the low Pi concentration, and to determine the Pi concentration in which $2\pi bB$ becomes zero (see Eq. 3 and Fig. 2 *C* of Kawai and Zhao, 1993). This is a negative value and equals $-P_0$. We found that there is no significant difference in the P_0 values for the three models of myocardium (control is 1.12 ± 0.25, n = 5; actin filament-reconstituted is 1.05 ± 0.26, n = 6; and thin filament-reconstituted is 1.08 ± 0.26, n = 15), and they averaged 1.08 ± 0.10 mM (n = 26). This endogenous Pi concentration has been taken into account in determining the kinetic constants of steps 4 and 5. This value compares with 0.6 mM in rabbit psoas fibers using the same method (Kawai and Halvorson, 1991), and 0.2 mM obtained using sucrose and the sucrose phosphorylase system to reduce the endogenous Pi (Pate and Cooke, 1989; Millar and Homsher, 1992).

Cross-bridge distribution

We calculated the steady-state distribution (probability) of cross-bridges in three muscle models by using Eq. 18 of Kawai and Halvorson (1991). The calculation was based on the equilibrium constants in Table 2 and on the standard activating condition (5 mM MgATP, 8 mM Pi). Fig. 6 shows the cross-bridge distribution obtained from the control (*white bars*), actin filament-reconstituted (*black bars*), and thin filament-reconstituted (*stippled bars*) myocardium. In all muscle models, the probability of cross-bridges in the AM state is ≤0.6% and not significantly populated. Cross-bridges are distributed by 13–44% in every other state. In the actin filament-reconstituted myocardium, both attached states AM*S and AM*DP increased to 1.8×, another attached state AM*D decreased to 0.7×, whereas the detached and weakly attached states (Det) decreased to 0.4×. In the thin filament-reconstituted myocardium, cross-bridge distributions regained the control values.

TABLE 2 The kinetic constants and the equilibrium constants of control, actin filament-reconstituted, and thin filament-reconstituted bovine myocardium

Kinetic Constants	Units	Control Myocardium	Actin Filament-Reconstituted Myocardium	Thin Filament-Reconstituted-Myocardium
K_1	mM^{-1}	9.1 ± 1.3 (11)	8.6 ± 2.5 (7)	9.9 ± 1.6 (11)
k_2	s^{-1}	26.6 ± 1.2 (11)	13.2 ± 1.1 (7)	25.6 ± 1.6 (11)
k_{-2}	s^{-1}	12.1 ± 1.3 (11)	23.0 ± 1.9 (7)	11.1 ± 1.5 (11)
K_2	—	2.64 ± 0.43 (11)	0.60 ± 0.08 (7)	3.47 ± 0.98 (11)
σ	—	0.72	0.37	0.77
k_4	s^{-1}	7.1 ± 0.6 (10)	11.4 ± 1.0 (13)	5.8 ± 0.3 (15)
k_{-4}	s^{-1}	12.6 ± 1.3 (10)	5.2 ± 0.6 (13)	11.1 ± 1.3 (15)
K_4	—	0.59 ± 0.04 (10)	2.58 ± 0.35 (13)	0.57 ± 0.04 (15)
K_5	mM^{-1}	0.14 ± 0.04 (10)	0.39 ± 0.08 (13)	0.18 ± 0.04 (15)

±SE. The number of observations is shown in parentheses.

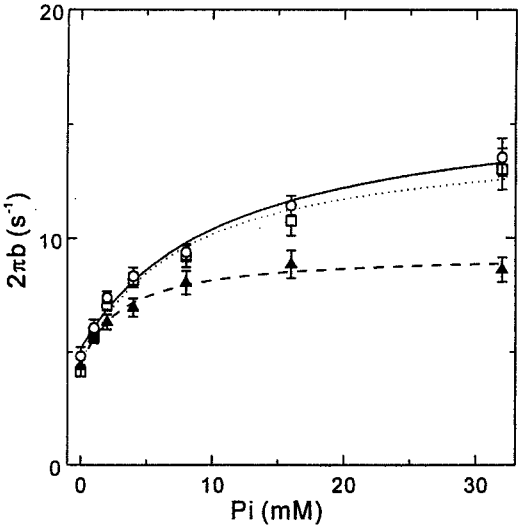

FIGURE 5 The rate constant $2\pi b$ is plotted as a function of Pi concentration. Bovine control myocardium (n = 10) (○ *and continuous line*); actin filament-reconstituted myocardium (n = 13) (▲ *and dashed line*); thin filament-reconstituted myocardium (n = 15) (□ *and dotted line*). Continuous curves are based on Eq. 3.

Isometric tension and stiffness

Fig. 7 shows isometric tension, stiffness, and isometric tension:stiffness ratio plotted against the MgATP concentration. In all muscle models, both isometric tension and stiffness decreased whereas tension/stiffness increased by the increase in the MgATP concentration. This result is in agreement with previous results in cardiac muscle fibers (Kawai et al., 1993) as well as in skeletal muscle fibers (Kawai and Zhao, 1993). In actin filament-reconstituted

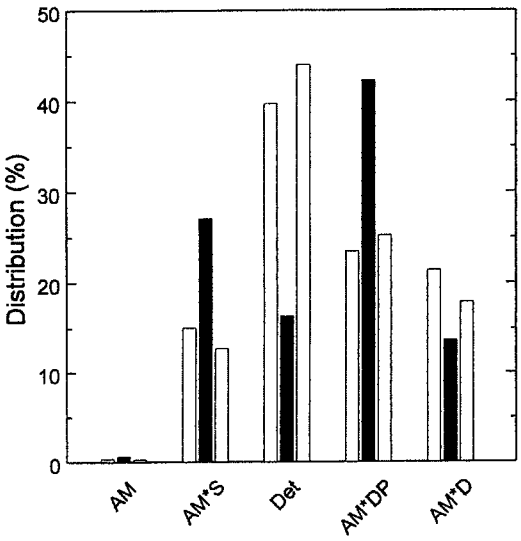

FIGURE 6 Calculated cross-bridge distribution in control (*white bars*), actin filament-reconstituted (*black bars*), and thin filament-reconstituted myocardium (*stippled bars*).

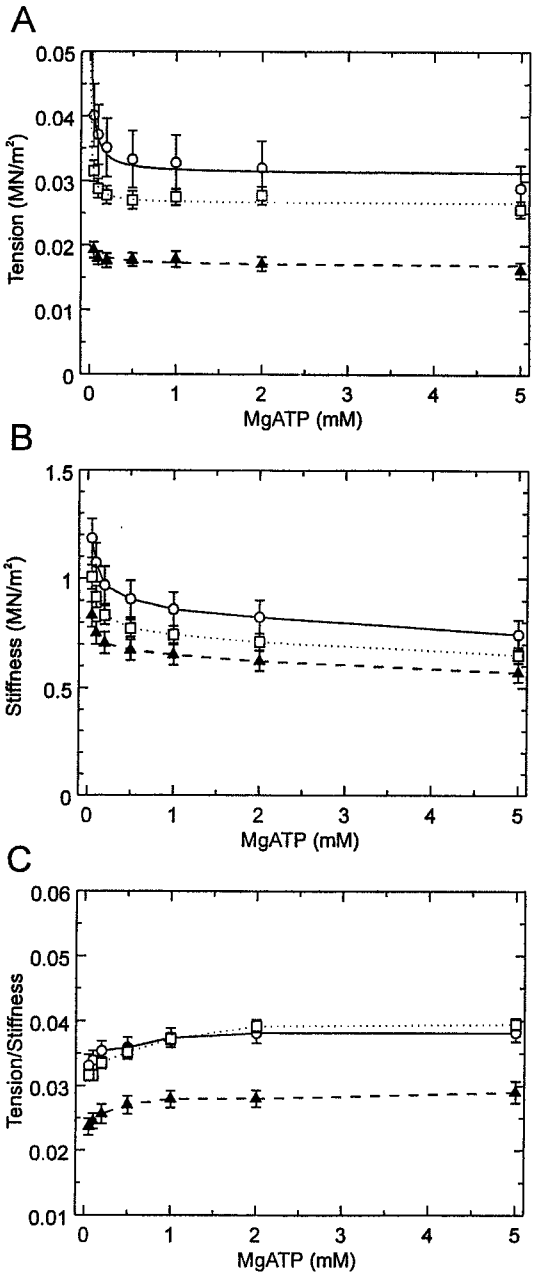

FIGURE 7 Isometric tension (*A*), stiffness (*B*), and tension/stiffness (*C*) are plotted against the MgATP concentration. Control myocardium (n = 11) (○ *and continuous line*); actin filament-reconstituted myocardium (n = 13) (▲ *and dashed line*); thin filament-reconstituted myocardium (n = 11) (□ *and dotted line*). Continuous lines in *A* are calculated based on Eq. 5 of Kawai and Zhao, 1993. Experiments were performed in the presence of 8 mM Pi.

myocardium, isometric tension was less than control in all MgATP concentrations tested. In thin filament-reconstituted myocardium, isometric tension regained that of control myocardium. The tension:stiffness ratio also decreased in actin filament-reconstituted myocardium (0.76 × at 5 mM MgATP) but regained the original value in thin filament-reconstituted myocardium.

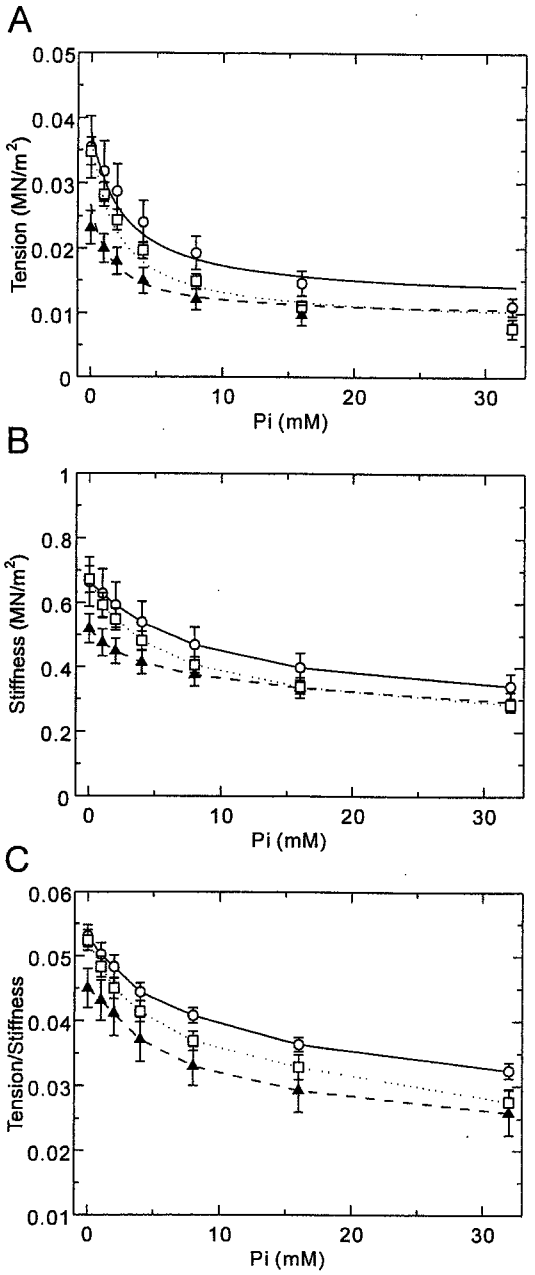

FIGURE 8 Isometric tension (*A*), stiffness (*B*), and tension/stiffness (*C*) are plotted against the Pi concentration. The same plotting nomenclatures were used as Fig. 7. Experiments were performed in the presence of 5 mM MgATP.

Fig. 8 shows isometric tension, stiffness, and the tension: stiffness ratio plotted against Pi concentration for the same experiments as shown in Fig. 5. In all muscle models, both isometric tension and stiffness decreased with the increase in the Pi concentration, which is in agreement with previous results in cardiac muscle fibers (Nosek et al., 1990; Kawai et al., 1993) and skeletal muscle fibers (Dantzig et al., 1992; Kawai and Zhao, 1993).

In thin filament-reconstituted myocardium, isometric tension regained that of control myocardium. The tension: stiffness ratio also decreased in actin filament-reconstituted myocardium (0.85× at no added Pi) but regained the original value in thin filament-reconstituted myocardium.

Isometric tension of accumulated data for MgATP and Pi studies at the standard activating condition (5 mM MgATP, 8 mM Pi) was T_c = 24.3 ± 2.4 kN/m^2 (n = 21) in control myocardium. T_c was used for the normalizing factor in rigor stiffness. This tension value is in agreement with the previous results on ferret myocardium (Saeki et al., 1991), rat myocardium (Wannenburg et al., 2000), rabbit myocardium (Nosek et al., 1990), and porcine myocardium (Zhao and Kawai, 1996). The tension:stiffness ratio of accumulated data for MgATP and Pi studies at the standard condition was 0.039 ± 0.001 (n = 21) in control myocardium, 0.031 ± 0.002 (n = 26) in actin filament-reconstituted myocardium, and 0.038 ± 0.001 (n = 26) in thin filament-reconstituted myocardium.

Adequacy of the ATP regenerating system

Although it can be argued that the CK concentration that we used (320 U/ml) would be adequate to buffer against ADP build up, which is known to slow down the cross-bridge kinetics (Cooke and Pate, 1985; Kawai and Halvorson, 1991; Thirlwell et al., 1994; Martin and Barsotti, 1994), it would be better to demonstrate this point experimentally. We chose 0.1 mM MgATP concentration for this purpose, because both $2\pi b$ and $2\pi c$ are sensitive to the change in MgATP at this concentration (Fig. 4). We then increased the CK concentration and the CP concentration by 50% each (ionic strength was maintained at 200 mM) and the rate constants were compared. After the increase, the ratio (after: before) for $2\pi b$ was 0.99 ± 0.06, and for $2\pi c$ was 1.01 ± 0.03 (n = 18). As these numbers indicate, there is hardly any change in the rate constants when CK and CP concentrations were increased, demonstrating that MgATP concentration was adequately buffered, and that the ADP concentration was kept minimal so as not to affect our results.

Rigor stiffness

It is possible that the decreased ability of force generation in the actin filament-reconstituted myocardium may have been caused by an increased compliance (= 1/stiffness) of the actin filament, because of the absence of Tm and Tn in this preparation. To test this possibility directly, the myocardium was brought into the rigor condition (such as shown in Fig. 2 *D*), and its stiffness at 100 Hz was compared in three muscle models. The rigor stiffness is approximately a constant of frequency (Kawai and Brandt, 1980), hence the choice of this frequency does not alter the results. We found that rigor stiffness was 50 ± 3 T_c (n = 21) for control, 61 ±

4 T_c (n = 26) for the actin filament-reconstituted myocardium, and 52 ± 3 T_c (n = 26) for the thin filament-reconstituted myocardium. These results were normalized to the initial control tension (T_c) to avoid errors because of the cross-sectional area estimation. Thus, we found that the rigor stiffness was 1.2× larger in the absence of the regulatory system than in its presence, although the effect is small. The rigor stiffness may depend on several factors: stiffness of the actin filament, presence/absence of regulatory proteins, presence/absence of Ca^{2+} when regulatory proteins are present, actomyosin interface, stiffness of the myosin head, and stiffness of the thick filament. With our present experiments, it is not possible to determine which one of these factors contributes to a small change observed in the rigor stiffness.

DISCUSSION

Reconstitution of the actin filament with/without the regulatory system

We have succeeded in selectively removing the thin filament from bovine myocardium using plasma protein gelsolin purified from bovine serum. We also have succeeded in reconstituting the thin filament first with G-actin, then with Tm and Tn. In the present study, these results are confirmed by SDS-PAGE, isometric tension, and the rate and association constants of the elementary steps of the cross-bridge cycle. In previous studies (Fujita et al., 1996; Fujita and Ishiwata, 1998, 1999; Ishiwata et al., 1998), the reconstitution was confirmed by SDS-PAGE, electron microscopy, fluorescence microscopy, and isometric tension. In the current report, the reproducibility of isometric tension averaged 107 ± 4% after thin filament reconstitution. This good reproducibility of the isometric tension was achieved by 1) good temperature regulation during actin filament reconstitution; 2) shorter duration of reconstitution of the actin filament; and 3) choosing similar diameter of the myocardium. Reproducibility of isometric tension varied more in an earlier report (Fujita et al., 1996), but reproducibility has been improved in our later reports (Fujita and Ishiwata, 1998, 1999; Ishiwata et al., 1998), because these factors were more tightly controlled.

The fact that the rate constants of elementary steps in the control myocardium and the thin filament-reconstituted myocardium are the same within an experimental error (Table 2) implies that the myocardium is not damaged by the extraction, and that functional reconstitution is complete. Therefore, we are at a stage to be able to compare the significance of the regulatory system (Tm and Tn) on the elementary steps of the cross-bridge cycle. It has been generally assumed that the addition of the regulatory system enhances the contractile function, based on the fact that the ATP hydrolysis rate increased in solution (Bremel and Weber, 1972) and both gliding speed and force increased on in vitro motility assay (Gordon et al., 1998; Van Buren et al., 1999; Bing et al., 2000a, b; Homsher et al., 2000). This report is the first to demonstrate the significance of the regulatory system of the thin filament in a skinned fiber system under the physiological ionic strength of 200 mM. Previous reports were based on a low ionic strength (~50 mM) where ionic interaction is relatively more significant than hydrophobic interaction. Because force generation is primarily based on hydrophobic interaction (Kodama, 1985; Rayment et al., 1993; Zhao and Kawai, 1994), we believe that it is important to observe these results at physiological ionic strength. In previous attempts on muscle fibers, TnC can be removed and reconstituted without disturbing the contractile function (Brandt et al., 1990; Moss, 1992; Zhao et al., 1996), but there have been difficulties in removing and replacing TnT or TnI (Strauss et al., 1992). Because Tm is a rod-like protein, its selective removal has been difficult despite several attempts (Yanagida and Oosawa, 1975). In the current method, these components can be removed completely and reconstituted with those from purified proteins (Fig. 1).

Comparison of the kinetic constants in the presence and absence of the regulatory proteins

The most significant finding in the current study is that the presence of the regulatory system promotes cross-bridge detachment by increasing K_2 and decreasing K_4 (Table 2). The effect is four- to sixfold and substantial. K_5 (Pi association constant) decreases to promote cross-bridge attachment in the presence of the regulatory system, but its effect (2×) is not as large. Thus, these findings imply that the addition of the regulatory system inhibits actomyosin interaction even in the presence of Ca^{2+}. It is not difficult to visualize this inhibitory effect, because the primary role of the regulatory system is to be placed between actin and myosin and to inhibit their interaction. The interaction may not be fully removed even if Ca^{2+} is introduced in the myofilament space and binds to TnC. The fact that the regulatory proteins modify the rate and association constants of the elementary steps demonstrates that cross-bridge kinetics are under the influence of the regulatory proteins, as shown previously with TnC (Zhao et al., 1996).

Comparison of the kinetic constants among mammalian cardiac muscles

We have analyzed the contractile function of ferret (Kawai et al., 1993), porcine (Zhao and Kawai, 1996), and bovine myocardium in terms of the elementary steps of the cross-bridge cycle. These results demonstrate that the equilibrium constant of the force generation step (K_4) is smallest in ferret myocardium (0.11), intermediate in porcine (0.32), and largest in bovine myocardium (0.59). The results also

demonstrate that the Pi-association constant (K_5) is smallest in ferret myocardium (0.06 mM^{-1}), intermediate in porcine (0.10 mM^{-1}), and largest in bovine myocardium (0.14 mM^{-1}). Thus, it can be concluded that the strongly attached AM*DP state is most significantly populated in bovine myocardium, and least significantly populated in ferret myocardium under the same ionic conditions. This trend is also evidenced in the tension versus Pi plot in which a tension decrease with an increase in the Pi concentration is least in ferret myocardium, followed by bovine and porcine myocardium. Therefore, resistance toward Pi accumulation is best in ferret, followed by bovine and porcine. This conclusion may be related to the fact that small animals readily accumulate Pi because of higher metabolic need, as shown by the higher heart rate. Conversely, the heart rate of large animals is slow, hence the metabolic need can be less stringent, and the Pi accumulation may not be significant. These differences are presumably related to a sequence difference of myosin HC as well as that of light chains among various mammals.

With respect to the MgATP binding step 1 and subsequent dissociation step 2, there is an order of magnitude agreement of the results among skinned myocardium data and solution biochemistry data on isolated myosin subfragment 1 (S1). The MgATP binding step (K_1) of this report (9×10^3 M^{-1}, Table 2) compares with 5×10^3 M^{-1} on bovine cardiac S1 (Taylor and Weeds, 1976). Taylor and Weeds measured fluorescence enhancement in the absence of actin. The corresponding value for porcine myocardium is 11×10^3 M^{-1} (Zhao and Kawai, 1996), and for ferret myocardium 1.0×10^3 M^{-1} (Kawai et al., 1993). The cross-bridge detachment step (k_2) of this report (27 s^{-1}) compares with 13 s^{-1} for porcine myocardium (Zhao and Kawai, 1996), and 48 s^{-1} for ferret myocardium (Kawai et al., 1993). The corresponding value for bovine cardiac S1 is 100 s^{-1} for the isomerization step that follows MgATP binding (Taylor and Weeds, 1976). Once again, there is a good agreement among the results of the solution study and those of skinned myocardium. The above results indicate that MgATP binds ~10× stronger in myocardium in large animals (porcine, bovine) than in a small animal (ferret).

Other investigators observed steps 1 and 2 by using NPE-caged ATP on guinea pig trabeculae muscles (Martin and Barsotti, 1994). Although this caged ATP has a slow photolysis reaction (~100 s^{-1}), this rate does not limit the steps of the actomyosin cycle in myocardium, because myocardial cross-bridge reactions (Table 2) are generally slower than the photolysis reaction of caged ATP. Martin and Barsotti reported that the second-order rate constant of MgATP binding was 0.084×10^6 $M^{-1}s^{-1}$ in the presence of Ca^{2+} and when rigor preparations were treated with apyrase to remove residual MgADP. Our corresponding value (K_1k_2) for the ferret is 0.05×10^6 $M^{-1}s^{-1}$ (Kawai et al., 1993); for the porcine is 0.14×10^6 $M^{-1}s^{-1}$ (Zhao and Kawai, 1996); and for the bovine is 0.11×10^6 $M^{-1}s^{-1}$ (Table 2). The value obtained from S1 of bovine cardiac muscle is 0.5×10^6 $M^{-1}s^{-1}$ (Taylor and Weeds, 1976). Again, a general agreement can be seen among the measurements. This agreement is striking when we realize that very different techniques and conditions were used in these measurements. The method that used caged ATP was not able to separate steps 1 and 2, presumably because the ATP concentration released by photolysis of caged ATP was limited to 2 mM (Martin and Barsotti, 1994), hence saturation of the rate constant could not have been observed. With our experience using ferret myocardium (which may be comparable with guinea pig myocardium), saturation of $2\pi c$ is barely visible at 2.5 mM but apparent at 5 mM MgATP (Kawai et al., 1993). This saturation is essential to characterize the ATP isomerization/cross-bridge detachment step.

The slowest step of the cross-bridge cycle

Step 6 is a transition from the AM*D state to AMD and/or to the AM state, and the slowest forward step in the cross-bridge cycle. The ATP hydrolysis rate is determined by k_6[AM*D] (Kawai and Zhao, 1993). Our result that the probability of the AM*D state being larger in the presence of Tm and Tn (Fig. 6) implies that the ATP hydrolysis rate would be larger if the actin filament is reconstituted with these regulatory proteins. This mechanism is consistent with an earlier observation (Bremel and Weber, 1972) that the ATP hydrolysis rate is larger in the presence of Tm and Tn in solution.

The rate constant of step 6 (k_6) may be relatively more significant in cardiac muscles than in skeletal muscles. This causes cross-bridges distributed in AM through AM*DP states even in the absence of added Pi. Our finding that the endogenous Pi concentration (P_0 ~1.1 mM) is higher than that of rabbit psoas fibers (0.6 mM; Kawai and Halvorson, 1991) implies that cross-bridges are indeed distributed in AM through AM*DP states in the absence of added phosphate, which is consistent with the hypothesis that the role of k_6 is more significant in cardiac muscles than in fast-twitch skeletal muscles.

Force supported by each cross-bridge

Fig. 6 demonstrates that, in the control and thin filament-reconstituted myocardium, ~44% of active cross-bridges are in the AM*DP and AM*D states that generate force. In contrast, in the actin filament-reconstituted myocardium, 56% of cross-bridges are attached in these states. Thus, ~1.3× (= 56/44) more cross-bridges are formed in the force generating states in the absence of the regulatory system. Fig. 2 *C* demonstrates that force is smaller and 0.7× compared with the control (Fig. 2 *A*). From these data, it can be concluded that force supported by strongly attached cross-bridges is 0.5× (= 0.7/1.3) in the absence of the

regulatory system. This argument is based on the hypothesis that the Pi release consists of steps 4 and 5, and that force is generated on step 4 (isomerization) and the same force is maintained after actual Pi release (step 5) based on lines of experimental evidence (Fortune et al., 1991; Kawai and Halvorson, 1991; Dantzig et al., 1992).

Although this hypothesis may appear in contradiction to a generally accepted assumption that force generation occurs with Pi release, it is not. This is because the general assumption was based on solution studies that did not recognize the strongly attached AM*DP state, but recognized that the Pi-release step was highly unidirectional, requiring 10–100 M Pi to reverse the equilibrium (Taylor, 1979). Because such a reaction accompanies a large, free-energy reduction, it has been generally assumed that this energy is used for force generation. In the muscle fiber system, it has been known that the Pi-release step is reversible with the millimolar Pi concentration (Bowater and Sleep, 1988; Kawai and Halvorson, 1991). In the fiber system, both a weakly attached AMDP state and a strongly attached AM*DP state have been recognized (Fortune et al., 1991; Kawai and Halvorson, 1991; Dantzig et al., 1992).

The above argument assumes that only the AM*DP and AM*D states are strongly attached force-generating states, but the argument is not much different if we include the AM and AMS states, because the cross-bridge distribution in the AM state is very small ($\leq$ 0.6%) (Fig. 6), and force supported by the AMS state is perhaps half of that supported by the AM*DP or AM*D state (Kawai and Zhao, 1993). Our observations, that in the absence of the regulatory system the tension:stiffness ratio is smaller by ~0.8×, and rigor stiffness is larger by 1.2×, also imply that the tension supported by each cross-bridge is smaller than in the presence of the regulatory system by ~0.7× (= 0.8/1.2). Although the two estimates (0.5× vs. 0.7×) do not match exactly, presumably because of errors associated with each estimate, the conclusion that the force supported by each cross-bridge is less in the absence of the regulatory system seems to be solid. The decrease in force-generating capacity in the actin filament-reconstituted myocardium is not attributable to an increased compliance of the filament, because our stiffness measurement during rigor induction demonstrates that the stiffness of actin filament-reconstituted myocardium is no less than that of the control or the thin filament-reconstituted myocardium. Our result on myocardium is consistent with recent results that used the in vitro motility assay, demonstrating that the gliding speed increased by 1.4–1.8× when Tm and Tn were added (Gordon et al., 1998; Bing et al., 2000a; Homsher et al., 2000), and demonstrating that force also increased by 1.5–3.0× when Tm and Tn were added (Homsher et al., 2000; Bing et al., 2000b). Geeves and Halsall (1986) showed actomyosin-binding affinity was increased in the presence of Tm and Tn in solution.

It is interesting to ask why force depends on the regulatory system. After the critical power stroke that takes place in step 4, the amount of force development must be a result of macromolecular architecture between actin and myosin molecules. If Tm is present together with Tn and Ca^{2+}, these molecules may either alter the conformation of actin, or intervene between actin and myosin to modify their relationship. The latter mechanism is less likely as a direct interaction between myosin and Tm has not been demonstrated, except that they are known to come close together. If the conformation of actin is altered by Tm, it is almost certain that this alteration affects the actin-myosin interaction surface, hence the amount of force generation.

A line of evidence suggests that Tm plays a role in the cross-bridge kinetics that result in force generation. Fujita and Ishiwata (1999) showed that the pH effect of isometric tension depends on a Tm isoform, demonstrating the significance of Tm in force generation. When Tm was added to the in vitro motility assay system, Van Buren at al. (1999) reported a 2× increase in force measured between single actin filament and myosin molecules coated on a glass surface, and Bing et al. (2000a) reported a 1.20–1.25× increase in sliding velocity. Another line of evidence suggests that the Tn complex plays a role in the cross-bridge cycling and concomitant force generation. It was shown that the phosphorylation of TnI increased relaxation and decreased Ca^{2+} sensitivity in the rabbit heart (Solaro et al., 1976; Zhang et al., 1995; Solaro and Van Eyk, 1996; Kajiwara et al., 2000). Sweeney et al. (1998) and Homsher et al. (2000) demonstrated that TnT mutant affected sliding speed in an in vitro motility assay. Zhao et al. (1996) showed that TnC removal resulted in a decrease in the rate constant of the force-generation step in rabbit psoas fibers.

The current study demonstrates that force per cross-bridge is enhanced by 1.5~1.7× in the presence of Tm and Tn in myocardium. These results imply that the signal transmission through TnC, TnI, TnT, Tm, actin, and myosin results in a conformational change at the interface of actin and myosin. A partial model consistent to this hypothesis was proposed by Tobacman and Butters (2000) based on actomyosin interaction in solution using internal deletion mutants of Tm, in which they showed that the interaction increased by sevenfold when Tm was present. The technique developed in this study would be useful to elucidate the role of molecular domains of contractile proteins by using mutants of thin filament proteins.

The authors thank Dr. Larry S. Tobacman for critical reading of the manuscript and useful suggestions. This work was supported by grant IBN 98–14441 from the National Science Foundation, and the Grant-in-Aid 99–50437N from the American Heart Association National Center. Dr. Fujita is a recipient of a Postdoctoral Fellowship award from Japan Society for Promotion of Science.

REFERENCES

Bing, W., A. Knott, and S. B. Marston. 2000b. A simple method for measuring the relative force exerted by myosin on actin filaments in the in vitro motility assay: evidence that tropomyosin and troponin increase force in single thin filaments. *Biochem. J.* 350:693–699.

Bing, W., A. Knott, C. Redwood, G. Esposito, I. Purcell, H. Watkins, and S. Marston. 2000a. Effect of hypertrophic cardiomyopathy mutations in human cardiac muscle α-tropomyosin (Asp175Asn and Glu180Gly) on the regulatory properties of human cardiac troponin determined by in vitro motility assay. *J. Mol. Cell Cardiol.* 32:1489–1498.

Bowater, R., and J. Sleep. 1988. Demembranated muscle fibers catalyze a more rapid exchange between phosphate and adenosine triphosphate than actomyosin subfragment 1. *Biochemistry.* 27:5314–5323.

Brandt, P. W., D. Roemer, and F. H. Schachat. 1990. Co-operative activation of skeletal muscle thin filaments by rigor crossbridges. The effect of troponin C extraction. *J. Mol. Biol.* 212:473–480.

Bremel, R. D., and A. Weber. 1972. Cooperation within actin filament in vertebrate skeletal muscle. *Nat. New Biol.* 238:97–101.

Cooke, R., and E. Pate. 1985. The effects of ADP and phosphate on the contraction of muscle fibers. *Biophys. J.* 48:789–798.

Dantzig, J. A., Y. E. Goldman, N. C. Millar, J. Lacktis, and E. Homsher. 1992. Reversal of the cross-bridge force-generating transition by photogeneration of phosphate in rabbit psoas muscle fibres. *J. Physiol.* 451:247–278.

Ebashi, S., A. Kodama, and F. Ebashi. 1968. Troponin. I. Preparation and physiological function. *J. Biochem.* 64:465–477.

Endo, M., M. Tanaka, and Y. Ogawa. 1970. Calcium induced release of calcium from the sarcoplasmic reticulum of skinned skeletal muscle fibres. *Nature* 228:34–36.

Fortune, N. S., M. A. Geeves, and K. W. Ranatunga. 1991. Tension responses to rapid pressure release in glycerinated rabbit muscle fibers. *Proc. Natl. Acad. Sci. U.S.A.* 88:7323–7327.

Fujita, H., and S. Ishiwata. 1998. Spontaneous oscillatory contraction without regulatory proteins in actin filament-reconstituted fibers. *Biophys. J.* 75:1439–1445.

Fujita, H., and S. Ishiwata. 1999. Tropomyosin modulates pH dependence of isometric tension. *Biophys. J.* 77:1540–1546.

Fujita, H., K. Yasuda, S. Niitsu, T. Funatsu, and S. Ishiwata. 1996. Structural and functional reconstitution of thin filaments in the contractile apparatus of cardiac muscle. *Biophys. J.* 71:2307–2318.

Funatsu, T., T. Anazawa, and S. Ishiwata. 1994. Structural and functional reconstitution of thin filaments in skeletal muscle. *J. Muscle Res. Cell Motil.* 15:158–171.

Geeves, M. A., and D. J. Halsall. 1986. The dynamics of the interaction between myosin subfragment 1 and pyrene-labelled thin filaments, from rabbit skeletal muscle. *Proc. Roy. Soc. Lond. Ser. B.* 229:85–95.

Gordon, A. M., Y. Chen, B. Liang, M. LaMadrid, Z. Luo, and P. B. Chase. 1998. Skeletal muscle regulatory proteins enhance F-actin in vitro motility. *Adv. Exp. Med. Biol.* 453:187–196.

Hatanaka, M., and I. Ohtsuki. 1992. Effect of removal and reconstitution of troponins C and I on the Ca^{2+}-activated tension development of single glycerinated rabbit skeletal muscle fibers. *Eur. J. Biochem.* 205: 985–993.

Heinl, P., H. J. Kuhn, and J. C. Ruegg. 1974. Tension responses to quick length changes of glycerinated skeletal muscle fibres from the frog and tortoise. *J. Physiol.* 237:243–258.

Hofmann, P. A., J. M. Metzger, M. L. Greaser, and R. L. Moss. 1990. Effects of partial extraction of light chain 2 on the Ca^{2+} sensitivities of isometric tension, stiffness, and velocity of shortening in skinned skeletal muscle fibers. *J. Gen. Physiol.* 95:477–498.

Homsher, E., D. M. Lee, C. Morris, D. Pavlov, and L. S. Tobacman. 2000. Regulation of force and unloaded sliding speed in single thin filaments: effects of regulatory proteins and calcium. *J. Physiol.* 524.1:233–243.

Huxley, A. F., and R. M. Simmons. 1971. Proposal mechanisms of force generation in striated muscle. *Nature.* 233:533–538.

Ishiwata, S., T. Funatsu, and H. Fujita. 1998. Contractile properties of thin (actin) filament-reconstituted muscle fibers. *Adv. Exp. Med. Biol.* 453: 319–329.

Kajiwara, H., S. Morimoto, N. Fukuda, I. Ohtsuki, and S. Kurihara. 2000. Effect of troponin I phosphorylation by protein kinase A on length-dependence of tension activation in skinned cardiac muscle fibers. *Biochem. Biophys. Res. Commun.* 272:104–110.

Kawai, M., and P. W. Brandt. 1980. Sinusoidal analysis: a high resolution method for correlating biochemical reactions with physiological processes in activated skeletal muscle of rabbit, frog and crayfish. *J. Muscle Res. Cell Motil.* 1:279–303.

Kawai, M., and H. R. Halvorson. 1991. Two step mechanism of phosphate release and the mechanism of force generation in chemically skinned fibers of rabbit psoas muscle. *Biophys. J.* 59:329–342.

Kawai, M., and Y. Zhao. 1993. Cross-bridge scheme and force per cross-bridge state in skinned rabbit psoas muscle fibers. *Biophys. J.* 65: 638–651.

Kawai, M., Y. Saeki, and Y. Zhao. 1993. Crossbridge scheme and the kinetic constants of elementary steps deduced from chemically skinned papillary and trabecular muscles of ferret. *Circ. Res.* 73:35–50.

Kodama, T. 1985. Thermodynamic analysis of muscle ATPase mechanisms. *Physiol. Rev.* 65:467–551.

Kondo, H., and S. Ishiwata. 1976. Uni-directional growth of F-actin. *J. Biochem.* 79:159–171.

Kurokawa, H., W. Fujii, K. Ohmi, T. Sakurai, and Y. Nonomura. 1990. Simple and rapid purification of brevin. *Biochem. Biophys. Res. Commun.* 168:451–457.

Laemmli, U. K. 1970. Cleavage of structural proteins during the assembly of the head of bacteriophage T4. *Nature.* 227:680–685.

Martin, H., and R. J. Barsotti. 1994. Activation of skinned trabeculae of the guinea pig induced by laser photolysis of caged ATP. *Biophys. J.* 67:1933–1941.

Millar, N. C., and E. Homsher. 1992. Kinetics of force generation and phosphate release in skinned rabbit soleus muscle fibers. *Am. J. Physiol.* 262:C1239–C1245.

Moss, R. L. 1992. Ca^{2+} regulation of mechanical properties of striated muscle. Mechanistic studies using extraction and replacement of regulatory proteins. *Circ. Res.* 70:865–884.

Murray, J. M., A. Weber, and R. D. Bremel. 1975. Could cooperativity in the actin filament play a role in muscle contraction? *In* Calcium Transport in Contraction and Secretion. E. Carafoli, F. Clementi, W. Drabikowski, and A. Margreth, editors. North-Holland Publishing Co., New York. 489–496.

Natori, R. 1954. The property and contraction process of isolated myofibrils. *Jikei. Med. J.* 1:119–126.

Nosek, T. M., J. H. Leal-Cardoso, M. McLaughlin, and R. E. Godt. 1990. Inhibitory influence of phosphate and arsenate on contraction of skinned skeletal and cardiac muscle. *Am. J. Physiol.* 259:C933–C939.

Palmiter, K. A., Y. Kitada, M. Muthuchamy, D. F. Wieczorek, and R. J. Solaro. 1996. Exchange of β- for α-tropomyosin in hearts of transgenic mice induces changes in the thin filament response to Ca^{2+}, strong cross-bridge binding, and protein phosphorylation. *J. Biol. Chem.* 271: 11611–11614.

Pate, E., and R. Cooke. 1989. Addition of phosphate to active muscle fibers probes actomyosin states within the powerstroke. *Pflügers Arch.* 414: 73–81.

Rayment, I., H. M. Holden, M. Whittaker, C. B. Yohn, M. Lorenz, K. C. Holmes, and R. A. Milligan. 1993. Structure of actin-myosin complex and its implications for muscle contraction. *Science.* 261:58–65.

Saeki, Y., M. Kawai, and Y. Zhao. 1991. Comparison of crossbridge dynamics between intact and skinned myocardium from ferret right ventricles. *Circ. Res.* 68:772–781.

Solaro, R. J., A. J. Moir, and S. V. Perry. 1976. Phosphorylation of troponin I and the entropic effect of adrenaline in the perfused rabbit heart. *Nature.* 262:615–617.

Solaro, R. J., and J. Van Eyk. 1996. Altered interactions among thin filament proteins modulate cardiac function. *J. Mol. Cell Cardiol.* 28: 217–230.

Spudich, J. A., and S. Watt. 1971. The regulation of rabbit skeletal muscle contraction. I. Biochemical studies of the interaction of the tropomyosin-troponin complex with actin and the proteolytic fragments of myosin. *J. Biol. Chem.* 246:4866–4871.

Strauss, J. D., C. Zuegner, J. E. Van Eyk, C. Bletz, M. Troschka, and J. C. Ruegg. 1992. Troponin replacement in permeabilized cardiac muscle. Reversible extraction of troponin I by incubation with vanadate. *FEBS Lett.* 310:229–234.

Sweeney, H. L., H. S. Feng, Z. Yang, and H. Watkins. 1998. Functional analyses of troponin T mutations that cause hypertrophic cardiomyopathy: insights into disease pathogenesis and troponin function. *Proc. Natl. Acad. Sci. U.S.A.* 95:14406–14410.

Szent-Györgyi, A. 1951. Chemistry of Muscular Contraction. 2nd ed. Academic Press, London.

Taylor, R. S., and A. G. Weeds. 1976. The magnesium-ion-dependent adenosine triphosphatase of bovine cardiac myosin and its subfragment-1. *Biochem. J.* 159:301–315.

Taylor, E. W. 1979. Mechanism of actomyosin ATPase and the problem of muscle contraction. *Crit. Rev. Biochem.* 6:103–164.

Thirlwell, H., J. E. Corrie, G. P. Reid, D. R. Trentham, and M. A. Ferenczi. 1994. Kinetics of relaxation from rigor of permeabilized fast-twitch skeletal fibers from the rabbit using a novel caged ATP and apyrase. *Biophys. J.* 67:2436–2447.

Tobacman, L. S., and C. A. Butters. 2000. A new model of cooperative myosin-thin filament binding. *J. Biol. Chem.* 275:27587–27593.

Van Buren, P., K. A. Palmiter, and D. M. Warshaw. 1999. Tropomyosin directly modulates actomyosin mechanical performance at the level of a single actin filament. *Proc. Natl. Acad. Sci. U.S.A.* 96:12488–12493.

Vandekerckhove, J., and K. Weber. 1979. The complete amino acid sequence of actins from bovine aorta, bovine heart, bovine fast skeletal muscle, and rabbit slow skeletal muscle. A protein-chemical analysis of muscle actin differentiation. *Differentiation.* 14:123–133.

Wannenburg, T., G. H. Heijne, J. H. Geerdink, H. W. Van den Dool, P. M. Janssen, and P. P. de Tombe. 2000. Cross-bridge kinetics in rat myocardium: effect of sarcomere length and calcium activation. *Am. J. Physiol.* 279:H779–H790.

Yanagida, T., and F. Oosawa. 1975. Effect of myosin on conformational changes of F-actin in thin filament in vivo induced by calcium ions. *Eur. J. Biochem.* 56:547–556.

Zhang, R., J. Zhao, A. Mandveno, and J. D. Potter. 1995. Cardiac troponin I phosphorylation increases the rate of the cardiac muscle relaxation. *Circ. Res.* 76:1028–1035.

Zhao, Y., and M. Kawai. 1994. Kinetic and thermodynamic studies of the cross-bridge cycle in rabbit psoas muscle fibers. *Biophys. J.* 67: 1655–1668.

Zhao, Y., and M. Kawai. 1996. Inotropic agent EMD-53998 weakens nucleotide and phosphate binding to cross bridges in porcine myocardium. *Am. J. Physiol.* 271:H1394–H1406.

Zhao, Y., P. M. Swamy, K. A. Humphries, and M. Kawai. 1996. The effect of partial extraction of troponin C on the elementary steps of the cross-bridge cycle in rabbit psoas fibers. *Biophys. J.* 71:2759–2773.

Microscopic Analysis of Polymerization and Fragmentation of Individual Actin Filaments

Shin'ichi Ishiwata[1,2,3,4], Junko Tadashige[1], Ichiro Masui[1], Takayuki Nishizaka[4], and Kazuhiko Kinosita, Jr[4,5]

Introduction

The dynamics of polymerization (and annealing of fragments) and depolymerization (and fragmentation) of actin filaments (F-actin) is a key process in diverse cellular functions, including cell motility. Up to the present, there have been many spectroscopic studies in solution, which have clarified time-dependent but averaged properties, as well as electron microscopic and other studies; but a single filament analysis, which is effective in clarifying not only time-dependent but also nonaveraged properties, has not yet been reported. Thus, direct observation of the polymerization-depolymerization dynamics of individual actin filaments is worthy of investigation.

The polymerization process consists of nucleation and growth phase, and at a steady state, annealing and fragmentation of polymerized filaments occur. The essential elements of these processes have been experimentally clarified and theoretically formulated (Oosawa and Kasai 1962; Oosawa and Asakura 1975). Actin filaments, like microtubules, have a structural polarity, such that the polymerization and depolymerization rates at the two ends of the filaments are different (Oosawa and Asakura 1975; Woodrum et al. 1975; Kondo and Ishiwata 1976; Hayashi and Ip 1976; Pollard and Cooper 1986). The end of the filaments at which the polymerization rate is larger is defined as the barbed (B-) end and the other is called the pointed (P-) end.

After the steady state of polymerization is attained, a treadmill process is expected to occur (Wegner 1976). The B-end of the filament is where filament assembly occurs, while depolymerization occurs at the P-end, such that the length of the filament is maintained nearly constant. The treadmill process has been experimentally demonstrated in solution (cf Wegner 1976; Korn et al. 1987). After actin monomers (G-actin) with ATP are polymerized, the bound

[1] Department of Physics, School of Science and Engineering
[2] Advanced Research Institute for Science and Engineering
[3] Materials Research Laboratory for Bioscience and Photonics, Waseda University, Tokyo 169-8555, Japan
[4] Core Research for Evolutional Science and Technology (CREST) Genetic Programming Team 13, Japan
[5] Department of Physics, Faculty of Science and Technology, Keio University, Yokohama 223-8522, Japan

Results and Problems in Cell Differentiation, Vol. 32
C. dos Remedios (Ed.): Molecular Interactions of Actin

ATP is hydrolyzed and inorganic phosphate (Pi) is released, leaving ADP attached.

When the rate of polymerization is greater than that of ATP hydrolysis, actin molecules with ATP should cap that end of the filaments. Depending on whether each end of the actin filaments is capped by either ATP-bound actin (ATP-cap) or ADP-bound actin (ADP-cap), dynamic instability of the filaments may occur (Korn et al. 1987; Carlier 1989). However, in contrast to microtubules, the dynamic instability has not yet been experimentally proved in actin filaments. Thus, the examination of whether this dynamic process occurs is a challenging problem.

About a decade ago, it became possible to visualize single actin filaments under a fluorescence microscope by labeling the filaments with rhodamine-phalloidin (Rh-Ph; Yanagida et al. 1984) or with fluorescein 5-isothiocyanate (FITC; Honda et al. 1986). In both studies, phallotoxins (Wieland et al. 1975) were added in order to suppress the depolymerization of actin filaments due to extremely low concentration (an order of nM) of actin, lower than the critical concentration for polymerization. Because the filament structure is stabilized, it became possible to visualize single filaments for a sufficiently long time to examine quantitatively not only the polymerization process but also the fragmentation process. Thus, the use of fluorescent-dye conjugated phallotoxins was very useful for stably and clearly visualizing the filament under a conventional fluorescence microscope without disturbance of background fluorescence (cf. Ishiwata 1998). The advantage of this technique is that Rh-Ph does not bind to G-actin and the fluorescence intensity of Rh-Ph increases several-fold upon binding to actin filaments (Harada et al. 1991; Huang et al. 1992).

In this chapter, we describe the properties of the polymerization and fragmentation processes of single actin filaments examined by direct observation through the fluorescence image of actin filaments in the presence of phallotoxins under a conventional fluorescence microscope (Tadashige et al. 1992; Masui et al. 1995).

We ask the reader to bear in mind that although the stabilization by phallotoxins is convenient for visualizing single actin filaments, there are several disadvantages to this method: (1) The greatest disadvantage is that spontaneous depolymerization is suppressed (Estes et al. 1981; Coluccio and Tilney 1984; Sampath and Pollard 1991), (2) The structure of actin filaments may be modified by the binding of phallotoxins (Drubin et al. 1993; Lorenz et al. 1993), so that the results may not represent polymerization properties of pure actin filaments. In this respect, however, this method can, conversely, be considered unique in studying the interaction of phallotoxins with actin filaments.

We have recently succeeded in visualizing polymerization and depolymerization of single actin filaments by using fluorescent dye(rhodamine)-labeled actin without using rhodamine-phallotoxins (phalloidin or phallacidin) under evanescent field illumination (Takahashi and Ishiwata 1998; Fujiwara et al. 1998). Thus it is now possible to visualize at a video rate both polymerization and depolymerization processes for every filament. The results will be published in more detail elsewhere.

How to Image the Polymerization (and Fragmentation) Process of Actin Filaments

To analyze polymerization and fragmentation of individual actin filaments under a fluorescence microscope, it is necessary to observe the same filaments at least for 30 min. Although single filaments are visualized in solution under a conventional fluorescence microscope, it is difficult to trace the polymerization process for each filament floating in solution because of its violent Brownian motion (Yanagida et al. 1984; Isambert et al. 1995).

To overcome this difficulty, we fixed short actin filaments to a glass surface through the cross-linked HMM molecules, as schematically illustrated in Fig. 1 [myosin easily adheres to a collodion(nitrocellulose)-coated glass surface], so that we can keep observing the same filaments. Thus, a short filament adhering to the glass surface was used as a nucleus for observing the polymerization process and as a tool to fix the long filaments so as to observe the fragmentation (severing) process.

To visualize the polymerization process at a constant concentration of G-actin, the actin solution was infused into a flow cell just after the addition

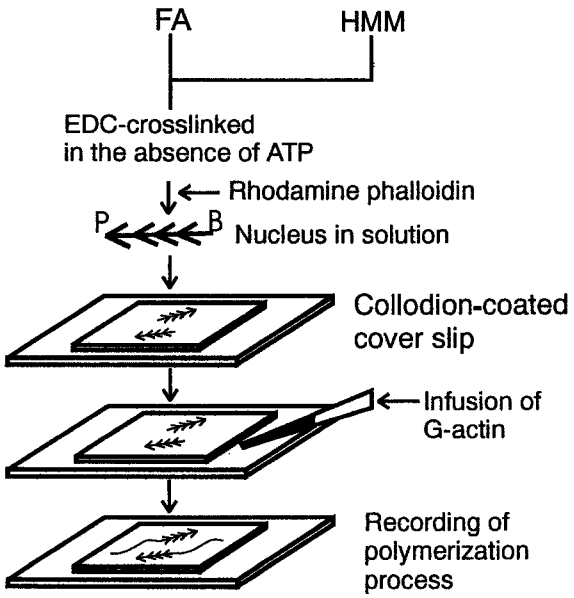

Fig. 1. Scheme showing how to measure the polymerization rate of actin on single actin filaments under a fluorescence microscope. Actin filaments decorated with HMM in the absence of ATP were cross-linked with 1-ethyl-3-(3-dimethyl-aminopropyl)-carbodiimide (EDC) and labeled with Rh-Ph to clearly identify the nuclei (Nishizaka et al. 1993). The EDC cross-linked acto-HMM complexes were mildly sonicated to make filaments short and used as nuclei for polymerization of actin. Immediately after the addition of salt, G-actin solution was infused into the flow cell sandwiched between a pair of coverslips, one of which was coated with nitrocellulose (collodion). The polymerization process was observed under an inverted fluorescence microscope and recorded on a videotape through a SIT camera (C1000; Hamamatsu Photonics). The length of the actin filaments was analyzed using a digital image processor (DIPS-C2000; Hamamatsu Photonics) (Nishizaka et al. 1995)

of salt to the G-actin solution, and the initial process of polymerization was recorded on a videotape at a rate of 30 frames s^{-1}. The length of actin filaments was determined by accumulating and averaging the images for 1 s every 5 (and 6, 7 or 10) min. Thus, the accuracy of the estimation of length change was less than 0.2 μm.

Visualization of the Polymerization Process of Actin Filaments

Figure 2 illustrates a series of fluorescence micrographs showing the polymerization process of individual actin filaments. The concentration of Rh-Ph was reduced to 15 nM, 1/7 that of phalloidin (or phallacidin), which was sufficiently high to image actin filaments. Under this condition, polymerization occurred only at one end of the actin nuclei, corresponding to the B-end.

Judging from the polymerization rate of actin (about 100 nm min^{-1} = 0.6 molecules s^{-1} assuming that the pitch of an actin monomer along the

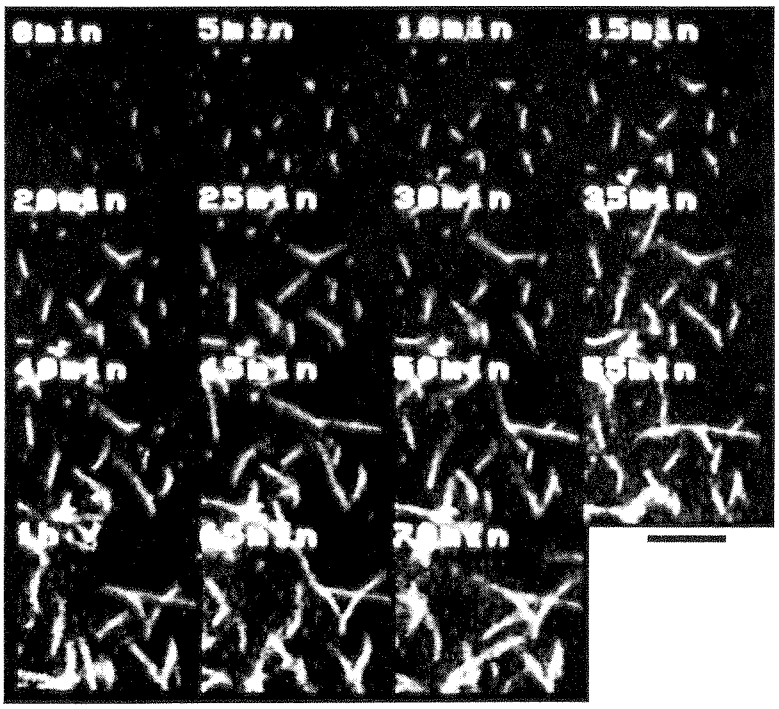

Fig. 2. Fluorescence images showing the time course of the polymerization on single actin filaments. Fluorescence images were recorded for several seconds every 5 min to minimize the photobleaching after the addition of the following actin solution. Condition: 5 μg ml^{-1} G-actin, 30 mM KCl, 1 mM $MgCl_2$, 4 mM ATP, 2 mM MOPS (pH 7), 105 nM phalloidin (Molecular Probes, Inc.), 15 nM Rh-Ph (Molecular Probes, Inc.) and oxygen scavenger system (Harada et al. 1991). The solvent was mixed with G-actin solution containing only ATP and MOPS immediately before the experiments, to minimize the spontaneous polymerization in solution. Temperature 25 °C. Bar, 5 μm

long-pitch helical strand of F-actin to be 5.5 nm) and the concentrations of nuclei and G-actin, the decrease in the concentration of G-actin can be neglected during initial observation (10 min) period. The polymerization rate (shown in Figs. 4 and 5 below) was estimated from the initial phase of elongation for 10 min (cf Fig. 3). We noticed that about one third of the nuclei among those attached to the glass surface did not elongate (see the upper left in each micrograph of Fig. 2). This is probably because G-actin was not accessible to the ends of the nuclei due to an obstacle such as nitrocellulose. Some filaments, which showed bending Brownian motion out of focus, were omitted from the length measurements.

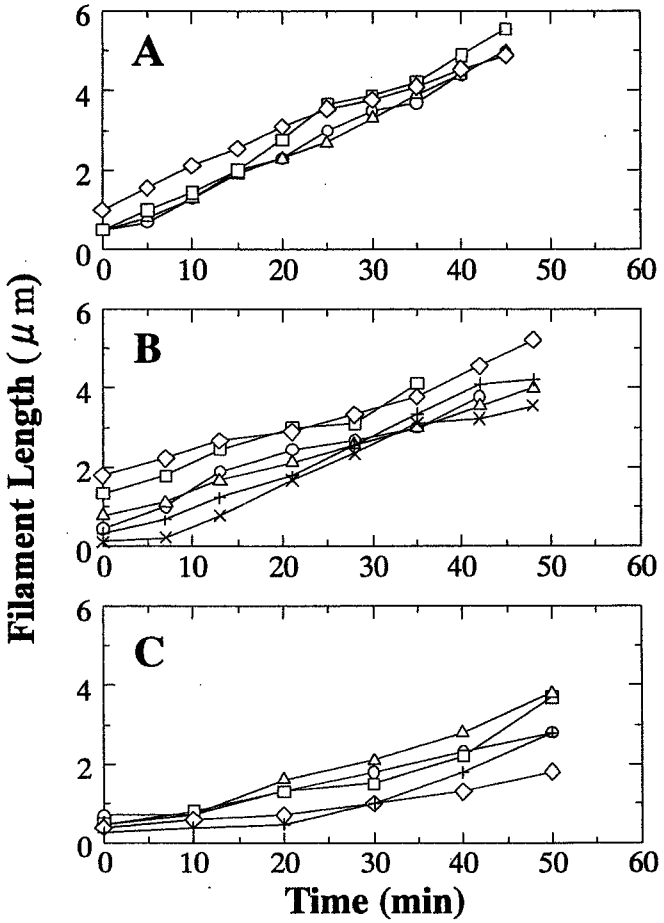

Fig. 3A–C. Time course of polymerization at the B-end of F-actin obtained under a fluorescence microscope at different actin concentrations. Conditions: G-actin, 5 $\mu g\,ml^{-1}$ (A, images are shown in Fig. 2), 4 $\mu g\,ml^{-1}$ (B) and 3 $\mu g\,ml^{-1}$ (C); other solvent conditions, the same as in Fig. 2 (the concentrations of phalloidin and Rh-Ph were maintained at 105 nM and 15 nM, respectively, irrespective of the concentrations of G-actin. Although the total concentration of phalloidin was less than the highest actin concentration examined, we estimated that it was high enough for the binding at the initial stage of polymerization). The filament length at time zero corresponds to the length of nucleus. Temperature 25 °C

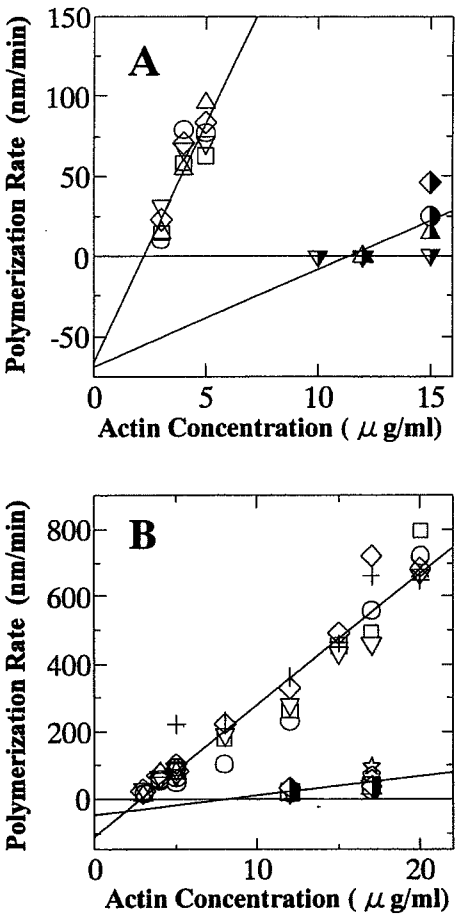

Fig. 4A,B. Initial rate of polymerization vs G-actin concentration in the presence of phalloidin. The polymerization rates at the B- and P-ends of F-actin were examined. When polymerization occurred at both ends of the filament, we decided the end elongated longer to be a B-end and that shorter to be a P-end. (A): polymerization at the B-end in the presence of 1 mM Mg^{2+} (open symbols) or 1 mM Ca^{2+} (half-filled symbols). Conditions as in Fig. 3, except that 1 mM $CaCl_2$ was added in half-filled symbols instead of 1 mM $MgCl_2$. (B) Polymerization at the B-end (open symbols and crosses) or the P-end (half-filled symbols, open star and pentagon) in the presence of Mg^{2+}. The data in A are also included. Different symbols show different preparations of actin. Temperature, 2 °C

Measurement of the Polymerization Process of Actin Filaments

Figure 3 shows an example of the time course of polymerization of individual actin filaments at three different concentrations of G-actin in the presence of phalloidin. The density of nuclei attached to the glass surface was common to all the experiments. On increasing the concentration of infused G-actin, the average rate of polymerization increased.

The polymerization rate varied from filament to filament (Fig. 3). Even in the same filament, the polymerization rate was not constant over 40–50 min but changed with time beyond the resolution of length determination. The accessibility of G-actin to the ends of the filaments may have fluctuated with time due to the adhesion to the nitrocellulose. Also, these results may be attributable to the nonhomogeneity of the local concentration of G-actin and/or the stochastic and cooperative properties of the polymerization process in the presence of phalloidin.

Depolymerization was suppressed by the presence of phalloidin, but there is a possibility that spontaneous fragmentation occurred. This could be one of the causes of length fluctuations during the polymerization process. In practice, however, we did not notice distinct fragmentation, at least in the middle of the filaments.

The rate of fragmentation in the absence of phalloidin was previously estimated in solution experiments to be $7 \times 10^{-7}\,s^{-1}$ (Kinosian et al. 1993), suggesting that in practice, fragmentation in the presence of phallotoxins does not occur within the period of measurements.

At low concentrations of G-actin, there was a tendency for the polymerization rate to increase with time (Fig. 3). The polymerization curve at $3\,\mu g\,ml^{-1}$ G-actin was convex downward, whereas the curve at $5\,\mu g\,ml^{-1}$ G-actin was nearly straight. This suggests that the polymerization kinetics change with the elongation of the filaments. The shorter the filament, the more the binding of G-actin may be disturbed.

Relation Between Polymerization Rate and Actin Concentration

The average rate of polymerization vs G-actin concentration relation is summarized in Fig. 4. In Fig. 4A, the relation observed at the B-end of F-actin in the presence of Mg^{2+} or Ca^{2+} is compared, while in Fig. 4B, the relation at the B- and P-ends is shown over a comparatively broader range of G-actin concentration.

These experiments were done in the presence of a constant concentration of phalloidin. Contrary to our expectation and differing from previous results obtained in solution (Estes et al. 1981; Coluccio and Tilney 1984; Sampath and Pollard 1991), the critical concentration of polymerization was not zero under all the conditions. This result was not changed even if the polymerization rates were estimated between 40 and 50 min in Fig. 3, where the polymerization rates were larger than the initial ones. However, when the same concentration of phallacidin was used instead of phalloidin, the result was as expected (Fig. 5). In both cases, the same concentration of Rh-Ph, one seventh that of phalloidin (or phallacidin), coexisted in order to visualize single actin filaments.

The relation between the polymerization rate (r) and G-actin concentration (c) can be expressed by:

$$r = k^{+}c - k^{-},$$

where k^{+} and k^{-} are the rate constants for polymerization and depolymerization, respectively. Thus, under the conditions examined in the presence of phalloidin, k^{+} was estimated to be $29.6\,(nm\,min^{-1})/(\mu g\,ml^{-1})$ $(= 7.5 \times 10^{6}\,M^{-1}\,s^{-1})$ and $6.2\ (nm\,min^{-1})/(\mu g\,ml^{-1})$ $(= 1.6 \times 10^{6}\,M^{-1}\,s^{-1})$ for the B-end in the presence of Mg^{2+} and Ca^{2+}, respectively (Fig. 4A), and $39.3\ (nm\,min^{-1})/(\mu g\,ml^{-1})$ $(= 1.0 \times 10^{7}\,M^{-1}\,s^{-1})$ and $5.9\ (nm\,min^{-1})/(\mu g\,ml^{-1})$ $(= 1.5 \times 10^{6}\,M^{-1}\,s^{-1})$ for the B-end and the P-end in the presence of Mg^{2+}, respectively (Fig. 4B). In calculating the values in the parentheses, we assumed that the molecular weight of actin is 42 kDa, and the number density of actin molecules along the filament is 2 molecules/5.5 nm.

On the other hand, in the presence of phallacidin, k^+ at the B-end was estimated to be 34.9 $(nm\,min^{-1})/(\mu g\,ml^{-1})$ $(= 8.9 \times 10^6 M^{-1} s^{-1})$ and 5.8 $(nm\,min^{-1})/(\mu g\,ml^{-1})$ $(= 1.5 \times 10^6 M^{-1} s^{-1})$ in the presence of Mg^{2+} and Ca^{2+}, respectively (Fig. 5).

The values of k^+ obtained above in the presence of Mg^{2+} (Figs. 4B, 5) were a little larger than, but consistent with, those obtained in solution under the same solvent conditions except for the absence of phallotoxins (the values of k^+ at the B- and P-ends were, respectively, $6.3 \times 10^6 M^{-1} s^{-1}$ and $1.1 \times 10^6 M^{-1} s^{-1}$; Suzuki and Mihashi 1989). This differs, however, from the results that the addition of phallotoxins reduced the value of k^+ by 20 to 50% (Coluccio and Tilney 1984; Wendel and Dancker 1987; Sampath and Pollard 1991). Such an apparent discrepancy may be attributable to the difference in experimental conditions. Note that the value of k^- was almost zero in the presence of phallacidin, consistent with the previous solution experiments (Estes et al. 1981; Coluccio and Tilney 1984; Sampath and Pollard 1991).

We found that the addition of 10 mM Pi in the presence of phallacidin slightly increased the value of k^+ to 39.0 $(nm\,min^{-1})/(\mu g\,ml^{-1})$ $(= 9.9 \times 10^6 M^{-1} s^{-1})$ and 6.9 $(nm\,min^{-1})/(\mu g\,ml^{-1})$ $(= 1.8 \times 10^6 M^{-1} s^{-1})$ in the presence of Mg^{2+} and Ca^{2+}, respectively, that is, by about 1.1 to 1.2 times (Fig. 5). This demonstrates that Pi does not significantly affect the polymerization rate but stabilizes the filament structure (Nonomura et al. 1975) through the decrease

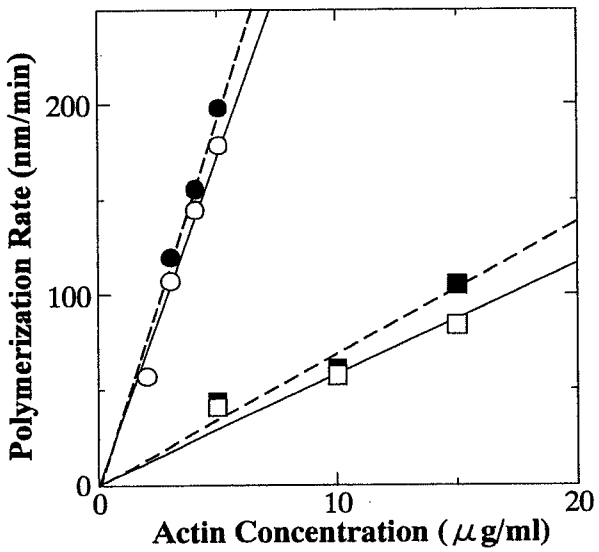

Fig. 5. Initial rate of polymerization at the B-end vs G-actin concentration in the presence of phallacidin. Effects of Pi and divalent cations (Mg^{2+} or Ca^{2+}) were examined. Conditions: various concentrations of G-actin, 30 mM KCl, 2 mM $MgCl_2$ (circles) or $CaCl_2$ (squares), 4 mM ATP, 2 mM MOPS (pH 7), 2 mg ml^{-1} BSA, 1.5 mM NaN_3, with (closed symbols) or without (open symbols) 1.5 mM Pi, 105 nM phallacidin, 15 nM Rh-Ph, 10 mM DTT, 0.3% (w/v) methylcellulose and oxygen scavenger system (Harada et al. 1991). The time course of polymerization of actin filaments was indistinguishable from that in the presence of phalloidin shown in Fig. 3, except that the polymerization curve was slightly convex upward at every G-actin concentration we examined

in the rates of both depolymerization (Rickard and Sheterline 1986, 1988; Funatsu 1986) and fragmentation as described below (Fig. 6).

It is also to be noted that, irrespective of the species of phallotoxins, in other words, independent of whether the critical concentration was zero (Fig. 5 for phallacidin) or not (Fig. 4 for phalloidin), the polymerization rate, k^+, was nearly the same under the same solvent conditions. On the other hand, the value of k^+ for Mg-actin was five-to-six times larger than that for Ca-actin (Figs. 4A, 5). This is in contrast to previous results obtained in solution that k^+ for Mg-actin was, at most, only two times larger than that for Ca-actin (see Estes et al. 1992). This apparent discrepancy may be attributable to the structural changes induced by the binding of phallotoxins and the difference in experimental conditions. Another possibility is that the HMM-cross linked nucleus may have amplified a small difference between the polymerization properties of Mg-actin and Ca-actin.

What is most notable in the above experiments is that the critical concentration for polymerization was practically zero in the presence of 105 nM phallacidin with 15 nM Rh-Ph (Fig. 5) but not zero in the presence of 105 nM phalloidin with 15 nM Rh-Ph (Fig. 4). At first sight, the reason for this difference appears to be attributable to the larger dissociation constant of phalloidin than that of phallacidin with F-actin. In practice, however, the dissociation constants of phalloidin and Rh-Ph with F-actin are, respectively, reported to be 67 and 40 nM (Molecular Probes Data Book; Huang et al. 1992), and those of fluorescent dye-conjugated phallotoxins such as coumarin-, NBD- and bodipy-phallacidin are, respectively, reported to be 24, 18 and 38 nM (Huang et al. 1992). Thus, although the dissociation constant of phallacidin has not yet been reported, there seems to be no large difference between phalloidin and phallacidin. If the dissociation constant itself is practically indistinguishable, the reason for the above difference may be attributable to the different rate constants.

The apparent association rate constant of Rh-Ph for F-actin is reported to be two-to-three orders of magnitude smaller than the rates of polymerization and depolymerization (De la Cruz and Pollard 1994, 1996; $6 \times 10^3 M^{-1} s^{-1}$ at 20 °C; and $5 \times 10^4 M^{-1} s^{-1}$ at 40 °C, Hotta and Ishiwata 1997). If this is also the case for the newly polymerized ends of the filaments, there would be an appreciable probability that the actin molecules once attached to the filament ends are detached, so that the apparent polymerization rate becomes reduced, resulting in the nonzero critical concentration.

This was not the case at least for phallacidin (as observed in Fig. 5), suggesting that the association rate constant of phallotoxins for the ends of the filaments is much larger than that for the bulk of the filaments. In fact, there is a report suggesting that phalloidin binds to the filament ends more rapidly than to the bulk of the filament (Cano et al. 1992). We infer that the rate constant of attachment to the filament ends of phalloidin may be still much slower than that of phallacidin.

Such a subtle difference may be produced by the structural change of actin molecules incorporated into the filament ends. The result shown in Fig. 4A,

that the apparent critical concentration for polymerization was larger in the presence of Ca^{2+} than of Mg^{2+}, can be ascribable to this mechanism, and may be related to the difficulty of nucleus formation for Ca-actin. That is, the association rate of phalloidin to the polymerized filament end may be slower for Ca-actin than for Mg-actin. This difference may be overcome in the presence of phallacidin, because the association rate constant of phallacidin at the polymerized ends is large enough to overcome the smaller association rate constant to Ca-actin. These mechanisms should be quantitatively examined in future.

Fragmentation of Actin Filaments: Effect of Anions at High Ionic Strength

Finally, the fragmentation of individual actin filaments was visualized using the same technique as described above. In this case, however, the long actin filaments polymerized beforehand in the presence of Rh-Ph were attached to the glass surface through the short fragments decorated with cross-linked HMM as shown in Fig. 6 (a similar technique has been used before: Bearer 1991; Maciver et al. 1991; Nishizaka et al. 1993). Various salt solutions were then infused into the cell and their effects on the fragmentation were examined under a continuous flow of the solutions.

As observed in a series of micrographs summarized in Fig. 6, shortening of the filaments in the presence of 3 M KSCN occurred mainly by severing with a lifetime of about 2 min (upper micrographs, –Pi) and 10 min (lower micrographs, +Pi), and finally all the filaments disappeared. Gradual depolymerization from the ends of the filaments was not detected. We examined various kinds of salts composed of K^+ as the cation, and Cl^-, I^-, SCN^-, etc as anions.

We found that the severing abilities were in the order of the Hofmeister series (lyotropic number) for anions, ie, the order according to which the hydrophobic interaction is destroyed: SCN^-, I^-, Cl^-, CH_3COO^-, SO_4^{2-}, etc (for the Hofmeister series, see Melander et al. 1984; Cacace et al. 1997). This is in spite of the fact that severing was largely retarded by phalloidin (for the effect of KI in the presence of phalloidin, see Dancker et al. 1975).

The present results are consistent with the previous results obtained by the phase-contrast image analysis of the dissociation process from the P-end of thin filaments in the I-Z-I brush of myofibrils (Funatsu and Ishiwata 1985; Funatsu et al. 1988), which was prepared by mildly etching the P-end of thin filaments with 0.5 M KCl treatment (Ishiwata and Funatsu 1985). The dissociation rate in the presence of 0.5 M salts in the absence of phallotoxins was in the order of SCN^-, I^-, NO_3^-, Cl^- and SO_4^{2-}, being consistent with the Hofmeister series (Funatsu 1986).

These results suggest that a hydrophobic interaction between actin molecules is important for the stabilization of the filament, even after the polymer structure is stabilized by the binding of phalloidin. However, we cannot completely eliminate the possibility that the interaction between phalloidin and

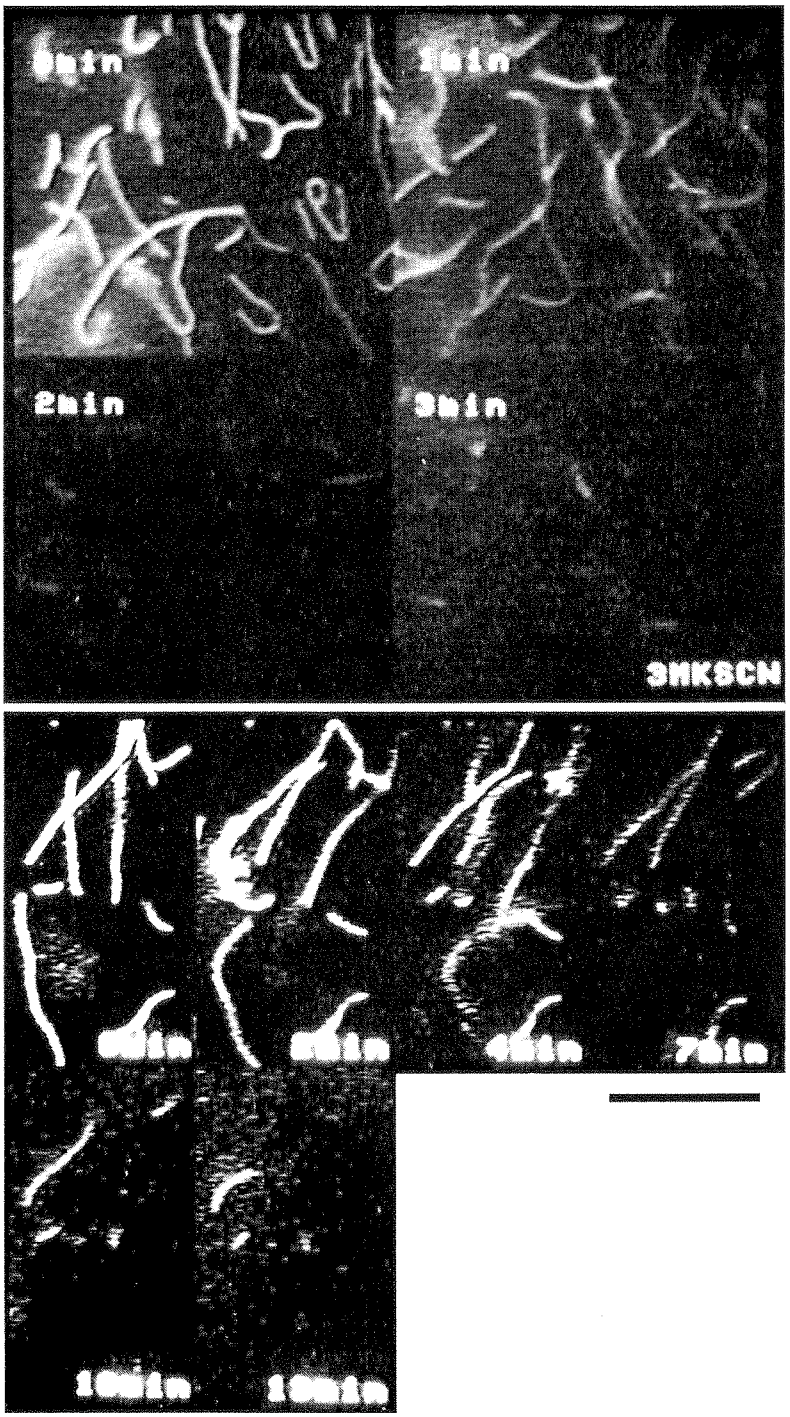

Fig. 6. Fluorescence images showing the time course of fragmentation of actin filaments in the presence of high concentrations of chaotropic anions. To record the time course of fragmentation of actin filaments, the filaments polymerized onto the nuclei of EDC-cross-linked acto-HMM complex in solution were infused into the cell, so that the filaments were attached to the glass surface through the short nuclei portion of the filaments and the polymerized portion of the filaments showed Brownian motion. The assay solvent was then infused. The time (min) after the infusion of the solvent is shown in each micrograph. Conditions as in Fig. 3, except that 3 M KSCN was added instead of 30 mM KCl and in the absence (upper micrographs) or presence (lower micrographs) of 10 mM Pi. Temperature 25 °C. Bars 5 μm

actin is weakened by the anions in the order of the Hofmeister series. It is to be noted that PO_4^{2-} was exceptional because it did not obey the Hofmeister series, ie, in practice, the shortening of the filaments did not occur in the presence of 0.5 M Pi.

The importance of hydrophobic interaction in the polymerization of actin has been recognized for many years (Oosawa and Asakura 1975). Nowadays, this discussion is based on the 3D atomic structure of G-actin (Kabsch et al. 1990) and the molecular model of F-actin (Holmes et al. 1990). These authors suggested that the hydrophobic loop located between subdomains 3 and 4 plays a role in stabilization of F-actin and this suggestion was supported by data from actin mutants or isoforms (Holmes et al. 1990; Allen et al. 1996b; Kuang and Rubenstein 1997).

Although we cannot add any information on the interaction between actin monomers on the atomic level, the results obtained here not only confirmed that the hydrophobic interaction is essential for maintaining the polymer structure but also demonstrated that other kinds of interactions exist between actin monomers, which are stabilized by phalloidin and Pi.

The manner in which phalloidin binds in the 3D structure of F-actin (Drubin et al. 1993; Lorenz et al. 1993; Steinmetz et al. 1998) suggests that phalloidin functions as a glue making connections among actin monomers in the filament. In practice, phalloidin can restore the polymerizability and also the ability of actin to activate myosin ATPase in monomers which have been impaired by chemical modifications of Lys 61 residue with FITC (Miki 1987), with several lysine residues with (m-maleimidobenzoyl)-N-hydroxysuccinimide ester (MBS) (Miki and Hozumi 1991), and by large hydrophobic probes at Cys-374 (Moens et al. 1994). Thus, actin filaments are stabilized by the cooperative nature of several kinds of molecular forces acting between actin and the regulators, ie, phallotoxins and Pi.

It is interesting that the addition of 10 mM Pi substantially lengthened the lifetime of F-actin in the presence of 3 M KSCN (Fig. 6), implying that Pi stabilized the structure of F-actin against the chaotropic effects of anions (for KI, see Dancker and Fischer 1989). For many years, the stabilizing effect of Pi has been well known. For example, with the addition of mM Pi: (1) the fragility of F-actin observed by negative staining in the electron microscope appeared to become stiffer (Nonomura et al. 1975); (2) the depolymerization rate observed in cuvette was slowed down (Rickard and Sheterline 1986, 1988; Carlier 1989); (3) subdomain 2 of the actin monomer in F-actin became oriented so as to interact strongly with the adjacent actin monomers (Orlova and Egelman 1992); and (4) severing activity of gelsolin (Allen et al. 1996a) and actophorin (Maciver et al. 1991) was reduced.

Pi does not greatly accelerate the polymerization rate, as seen in Fig. 5, and suppresses not only the depolymerization but also the fragmentation as observed in Fig. 6, such that Pi shifts the polymerization-depolymerization equilibrium to the polymerization side. The present results strongly suggest that Pi is a stabilizer of the hydrophobic interaction between actin monomers

which is essential for the polymerization of actin. On the other hand, phalloidin stabilizes the F-actin-ADP-Pi complex (Dancker and Hess 1990). Thus, phallotoxins and Pi function as allosteric effectors that synergistically stabilize the structure of actin filaments.

Conclusions

The polymerization and fragmentation processes of individual actin filaments can be visualized by imaging the polymerized filaments through binding of the fluorescent dye, Rh-Ph, under a conventional fluorescence microscope. Thus, the polymerization process at the B- and P-ends of actin filaments can be analyzed in the presence of Mg^{2+} or Ca^{2+}. By measuring the rate of polymerization at various G-actin concentrations, we confirmed that the depolymerization process was inhibited by the attachment of phallotoxins to the filaments (phallacidin was more effective than phalloidin), but the polymerization rate itself was not significantly affected, such that the critical concentration of polymerization was essentially zero. Also, the fragmentation process of filaments due to the addition of high concentrations of chaotropic salts such as KSCN and KI (except Pi) can be observed and stabilization of the hydrophobic interactions by Pi was confirmed. The present study demonstrates that the polymerization and fragmentation dynamics on single actin filaments can be examined quantitatively by fluorescence microscopy.

Acknowledgments. The authors would like to thank Dr JMQ Davies of Waseda University for his critical reading of the manuscript. The authors also thank Miss Ikuko Fujiwara for her assistance in preparing figures. This research was supported in part by Grants-in-Aid for Scientific Research, for Scientific Research on Priority Areas and for the HighTech Research Center Project from the Ministry of Education, Science, Sports and Culture of Japan, and Core Research for Evolutional Science and Technology (CREST) from the Japan Science and Technology Corporation (JST), and a Waseda University Special Grant-in-Aid.

References

Allen PG, Laham LE, Way M, Janmey PA (1996a) Binding of phosphate, aluminum fluoride, or beryllium fluoride to F-actin inhibits severing by gelsolin. J Biol Chem 271:4665–4670

Allen PG, Shuster CB, Kas J, Chaponnier C, Janmey PA, Herman IM (1996b) Phalloidin binding and rheological differences among actin isoforms. Biochemistry 35:14062–14069

Bearer EL (1991) Direct observation of actin filament severing by gelsolin and binding by gCap39 and CapZ. J Cell Biol 115:1629–1638

Cacace MG, Landau EM, Ramsden JJ (1997) The Hofmeister series: salt and solvent effects on interfacial phenomena. Q Rev Biophys 30:241–277

Cano ML, Cassimeris L, Joyce M, Zigmond SH (1992) Characterization of tetramethylrhodaminylphalloidin binding to cellular F-actin. Cell Motil Cytoskel 21:147–158

Carlier M-F (1989) Role of nucleotide hydrolysis in the dynamics of actin filaments and microtubules. Int Rev Cytol 115:139–170

Coluccio LM, Tilney LG (1984) Phalloidin enhances actin assembly by preventing monomer dissociation. J Cell Biol 99:529–535

Dancker P, Fischer S (1989) Stabilization of actin filaments by ATP and inorganic phosphate. Z Naturforsch C44:698–704

Dancker P, Hess L (1990) Phalloidin reduces the release of inorganic phosphate during actin polymerization. Biochim Biophys Acta 1035:197–200

Dancker P, Löw I, Hasselbach W, Wieland Th (1975) Interaction of actin with phalloidin: Polymerization and stabilization of F-actin. Biochim Biophys Acta 400:407–414

De la Cruz EM, Pollard TD (1994) Transient kinetic analysis of rhodamine phalloidin binding to actin filaments. Biochemistry 33:14387–14392

De la Cruz EM, Pollard TD (1996) Kinetics and thermodynamics of phalloidin binding to actin filaments from three divergent species. Biochemistry 35:14054–14061

Drubin DG, Jones HD, Wertman KF (1993) Actin structure and function: Roles in mitochondrial organization and morphogenesis in budding yeast and identification of the phalloidin-binding site. Mol Biol Cell 4:1277–1294

Estes JE, Selden LA, Gershman LC (1981) Mechanism of action of phalloidin on the polymerization of muscle actin. Biochemistry 20:708–712

Estes JE, Selden LA, Kinosian HJ, Gershman LC (1992) Tightly-bound divalent cation of actin. J Muscle Res Cell Motil 13:272–284

Fujiwara I, Takahashi S, Tadakuma H, Ishiwata S (1998) Visualization of polymerization process of single actin filaments under total reflection microscope. Biophysics (Japanese) 38:S63 (Abstr)

Funatsu T (1986) Structural stability and capping proteins of actin filaments. Doct Diss Waseda University

Funatsu T, Ishiwata S (1985) Characterization of β-actinin: A suppressor of the elongation at the pointed end of thin filaments in skeletal muscle. J Biochem 98:535–544

Funatsu T, Asami Y, Ishiwata S (1988) β-actinin: A capping protein at the pointed end of thin filaments in skeletal muscle. J Biochem 103:61–71

Harada Y, Sakurada K, Aoki T, Thomas DD, Yanagida T (1991) Mechanochemical coupling in actomyosin energy transduction studied by in vitro movement assay. J Mol Biol 216:49–68

Hayashi T, Ip W (1976) Polymerization polarity of actin. J Mechanochem Cell Motil 3:163–169

Holmes KC, Popp D, Gebhard W, Kabsch W (1990) Atomic model of the actin filament. Nature 347:44–49

Honda H, Nagashima H, Asakura S (1986) Directional movement of F-actin in vitro. J Mol Biol 191:131–133

Hotta M, Ishiwata S (1997) Temperature dependence of association and dissociation rate constants of rhodamine phalloidin with actin filaments. J Muscle Res Cell Motil 18:491 (Abstr)

Huang Z, Haugland RP, You W, Haugland RP (1992) Phalloidin and actin binding assay by fluorescence enhancement. Anal Biochem 200:199–204

Isambert H, Venier P, Maggs AC, Fattoum A, Kassab R, Pantaloni D, Carlier M-F (1995) Flexibility of actin filaments derived from thermal fluctuations. Effect of bound nucleotide, phalloidin, and muscle regulatory proteins. J Biol Chem 270:11437–11444

Ishiwata S (1998) The use of fluorescent probes. In: Current Methods in Muscle Physiology (ed by Sugi H) Oxford University Press, Oxford, UK, pp 199–222

Ishiwata S, Funatsu T (1985) Does actin bind to the ends of thin filaments in skeletal muscle? J Cell Biol 100:282–291

Kabsch W, Mannherz HG, Suck D, Pai EF, Holmes KC (1990) Atomic structure of the actin: DNase I complex. Nature 347:37–44

Kinosian HJ, Selden LA, Estes JE, Gershman LC (1993) Actin filament annealing in the presence of ATP and phalloidin. Biochemistry 32:12353–12357

Kondo H, Ishiwata S (1976) Uni-directional growth of F-actin. J Biochem 79:159–171

Korn ED, Carlier M-F, Pantaroni D (1987) Actin polymerization and ATP hydrolysis. Science 238:638–644

Kuang B, Rubenstein PA (1997) Beryllium fluoride and phalloidin restore polymerizability of a

mutant yeast actin (V266G, L267G) with severely decreased hydrophobicity in a subdomain 3/4 loop. J Biol Chem 272:1237–1247

Lorenz M, Popp D, Holmes KC (1993) Refinement of the F-actin model against X-ray fiber diffraction data by the use of a directed mutation algorithm. J Mol Biol 234:826–836

Maciver SK, Zot HG, Pollard TD (1991) Characterization of actin filament severing by actophorin from *Acanthamoeba castellani.* J Cell Biol 115:1611–1620

Masui I, Tadashige J, Nishizaka T, Ishiwata S (1995) Microscopic analysis of polymerization process on a single actin filament. Proc Annu Meet Phys Soc Jpn 29:pA3 (Abstr)

Melander WR, Corradini D, Horvath C (1984) Salt-mediated retention of proteins in hydrophobic-interaction chromatography. Application of solvophobic theory. J Chromatogr 317:67–85

Miki M (1987) The recovery of the polymerizability of Lys-61-labelled actin by the addition of phalloidin. Fluorescence polarization and resonance-energy-transfer measurements. Eur J Biochem 164:229–235

Miki M, Hozumi T (1991) Interaction of maleimidobenzoyl actin with myosin subfragment 1 and tropomyosin-troponin. Biochemistry 30:5625–5630

Moens PDJ, Yee D, dos Remedios CG (1994) Determination of the radial coordinate of Cys-374 in F-actin using fluorescence resonance energy transfer spectroscopy: Effect of phalloidin on random assembly. Biochemistry 33:13102–13108

Nishizaka T, Yagi T, Tanaka Y, Ishiwata S (1993) Right-handed rotation of an actin filament in an in vitro motile system. Nature 361:269–271

Nishizaka T, Miyata H, Yoshikawa H, Ishiwata S, Kinosita Jr K (1995) Unbinding force of a single motor molecule of muscle measured using optical tweezers. Nature 377:251–254

Nonomura Y, Katayama E, Ebashi S (1975) Effect of phosphates on the structure of the actin filament. J Biochem 78:1101–1104

Oosawa F, Asakura S (1975) Thermodynamics of the polymerization of proteins. Academic Press, New York

Oosawa F, Kasai M (1962) Theory of linear and helical aggregations of macromolecules. J Mol Biol 4:10–21

Orlova A, Egelman EH (1992) Structural basis for the destabilization of F-actin by phosphate release following ATP hydrolysis. J Mol Biol 227:1043–1053

Pollard TD, Cooper JA (1986) Actin and actin-binding proteins. A critical evaluation of mechanisms and functions. Annu Rev Biochem 55:987–1035

Rickard JE, Sheterline P (1986) Cytoplasmic concentrations of inorganic phosphate affect the critical concentration for assembly of actin in the presence of cytochalasin D or ADP. J Mol Biol 191:273–280

Rickard JE, Sheterline P (1988) Effect of ATP removal and inorganic phosphate on length redistribution of sheared actin filament populations. Evidence for a mechanism of end-to-end annealing. J Mol Biol 201:675–681

Sampath P, Pollard TD (1991) Effects of cytochalasin, phalloidin, and pH on the elongation of actin filaments. Biochemistry 30:1973–1980

Steinmetz MO, Stoffler D, Müller SA, Jahn W, Wolpensinger B, Goldie KN, Engel A, Faulstich H, Aebi U (1998) A correlative analysis of actin filament assembly, structure, and dynamics. J Mol Biol 276:1–6

Suzuki N, Mihashi K (1989) Subunit flow in F-actin under steady-state conditions. Application of a novel method to determination of the rate of subunit exchange of F-actin at the terminals. Biophys Chem 33:177–193

Tadashige J, Nishizaka T, Ishiwata S (1992) Direct observation of the dynamic process of polymerization and depolymerization on single actin filaments. Biophysics (Japanese) 32:S194 (Abstr)

Takahashi S, Ishiwata S (1998) Direct observation of polymerization process of single actin filaments under fluorescence microscope. Biophys J 74:A46 (Abstr)

Wegner A (1976) Head to tail polymerization of actin. J Mol Biol 108:139–150

Wendel H, Dancker P (1987) Influence of phalloidin on both the nucleation and the elongation phase of actin polymerization. Biochim Biophys Acta 915:199–204

Wieland T, de Vries JX, Schäfer AJ, Faulstich H (1975) Spectroscopic evidence for the interaction of phalloidin with actin. FEBS Lett 54:73–75

Woodrum DT, Rich SA, Pollard TD (1975) Evidence for biased bidirectional polymerization of actin filaments using heavy meromyosin prepared by an improved method. J Cell Biol 67:231–237

Yanagida T, Nakase M, Nishiyama K, Oosawa F (1984) Direct observation of motion of single F-actin filaments in the presence of myosin. Nature 307:58–60